

**Chiral Ligand and Transition Metal (Fe, Rh)
Complexes for Catalytic Alkoxylation,
Polymerization, Hydrosilylation and Hydrogenation**

by

**Anirban Sen
10CC15A26026**

A thesis submitted to the
Academy of Scientific & Innovative Research
For the Award of the Degree of
DOCTOR OF PHILOSOPHY
in
SCIENCE

Under the supervision of
Dr. Samir H. Chikkali



CSIR-National Chemical Laboratory, Pune



Academy of Scientific and Innovative Research
AcSIR Headquarters, CSIR-HRDC campus
Sector 19, Kamla Nehru Nagar,
Ghaziabad, U.P.–201 002, India

January-2023

Certificate

This is to certify that the work incorporated in this Ph.D. thesis entitled "**Chiral Ligand and Transition Metal (Fe, Rh) Complexes for Catalytic Alkoxylation, Polymerization, Hydrosilylation and Hydrogenation**" submitted by **Mr. Anirban Sen (Registration No. 10CC15A26026)** to Academy of Scientific and Innovative Research (AcSIR) in fulfilment of the requirements for the award of the Degree of Doctor of Philosophy, embodies original research work under my supervision. I further certify that this work has not been submitted to any other University or Institution in part or full for the award of any degree or diploma. Research material obtained from other sources has been duly acknowledged in the thesis. Any text, illustration, table etc., used in the thesis from other sources, have been duly cited and acknowledged.



(Signature of Student)

Anirban Sen

Date: 04-01-2023



(Signature of Supervisor)

Dr. Samir H. Chikkali

Date: 04-01-2023

STATEMENTS OF ACADEMIC INTEGRITY

I, Anirban Sen, a Ph.D. student of the Academy of Scientific and Innovative Research (AcSIR) with Registration No. 10CC15A26026 hereby undertake that, the thesis entitled “Chiral Ligand and Transition Metal (Fe, Rh) Complexes for Catalytic Alkoxylation, Polymerization, Hydrosilylation and Hydrogenation” has been prepared by me and that the document reports original work carried out by me and is free of any plagiarism in compliance with the UGC Regulations on “*Promotion of Academic Integrity and Prevention of Plagiarism in Higher Educational Institutions (2018)*” and the CSIR Guidelines for “*Ethics in Research and in Governance (2020)*”.



Signature of the Student

Date : 29-12-2022

Place : CSIR-NCL, Pune

It is hereby certified that the work done by the student, under my supervision, is plagiarism-free in accordance with the UGC Regulations on “*Promotion of Academic Integrity and Prevention of Plagiarism in Higher Educational Institutions (2018)*” and the CSIR Guidelines for “*Ethics in Research and in Governance (2020)*”.

NA

Signature of the Co-supervisor (if any)

Name :

Date :

Place :



Signature of the Supervisor

Name : Dr. Samir H. Chikkali

Date : 29-12-2022

Place : CSIR-NCL, Pune



Dedicated to
The Holy Feet of Lord Shiva

*“Faith is the bird
That feels the light
When the dawn is
Still dark.”*

–Rabindranath Tagore

Acknowledgement

The process of earning a doctorate and writing a dissertation is long and arduous and it is certainly not done singlehandedly. So, I am using this opportunity to express my gratitude to everyone who helped and supported me throughout the course of my research.

Firstly, I would like to express my special appreciation and thanks to my research supervisor **Dr. Samir Chikkali** for his valuable guidance and scholarly inputs. I have enjoyed the opportunity to watch and learn from his knowledge and experience. His enthusiasm, encouragement and faith in me throughout have been extremely helpful. He is the one who moulded me into a good researcher. He has given me full freedom in my research and I could not imagine to have a better mentor than him. I am also thankful to his family for the warm welcome offered to me on the auspicious occasion of “Eid Mubarak” with Sheer Khurma, Sweets and Snacks.

I wish to express my sincere thanks to the Doctoral Advisory Committee members, Dr. Benudhar Punji, Dr. Sakya Sen, Dr. Dhanasekaran Shanmugam and Dr. Ekambaram Balaraman whose contribution in stimulating suggestions and encouragement helped me to coordinate my work.

I am grateful to Prof. Ashish K. Lele, Director, NCL, Prof. A. K. Nangia and Prof. S. Pal (Former Directors, NCL), Dr. Asha S. K., Head, PSE Division, for giving me this opportunity and providing all necessary infrastructure and facilities. I also acknowledge the financial support of CSIR, New Delhi in terms of junior and senior research fellowships. I would also like to thank Mrs. B. Santhakumari, for HRMS analysis, Dr. Rajamohanam, Dr. Ajithkumar, Dr. Uday Kiran for NMR facilities.

I would like to thank all my collaborator colleagues **Dr. Vijay Koshti, Rohit Kumar, Tanuja Tewari, Kishor Khopade** for their valuable time and cooperation. I extend my thanks to our collaborators **Dr. Kumar Vanka** and **K. Vipin Raj** for DFT calculations, Dinesh Shinde for the timely help with NMR measurements.

I also want to thank my **all teachers from Jadavpur University and Maulana Azad College (Calcutta University)**, as well as **Dr. Nabakumar Bera** (Jhargram Raj College), **Dr. Chandan Saha** (School of Tropical Medicine, Kolkata), **Dr. Sanjib Ganguly** (St. Xavier’s College) for getting me interested in Chemistry and making me realize that I can take it further too.

Acknowledgement

My sincere thanks to the people in various parts of the institute and SAC office, X-ray single crystal analysis, NMR, Mass spectroscopy, Microanalysis, IR, Library, Administration and technical divisions of NCL for their assistance during the course of my work.

A special thanks goes to My lab seniors Dr. Vijay Koshti, **Dr. Shahaji Gaikwad**, **Dr. Bhausaheb Rajput**, Dr. Swechcha Pandey, Dr. Satej Deshmukh and Dr. Nilesh Mote for their valuable advice and help in lab practices which I greatly acknowledge and other lab seniors, colleagues and juniors Dr. Nagaraju, Dr. Seena, Dr. Ketan, Dr. Shilpi, Dr. Shailaja, Dr. Sandip, Dr. Dipa, **Dynaneshwar**, Ravi, Rohit, Amol, Kishor, Tanuja, Rajkumar, Poonam, Uday, Maulali, Nikhita, Rohan, Ganesh for the lively lab atmosphere and endless discussions. I am highly thankful and grateful to **Rohit** for his unconditional friendship and love throughout this journey which made every obstacle so easy to overcome. Also, I am thankful to Dr. Punji's lab members **Dr. Shrikant**, Dr. Hanuman, **Dr. Vineeta**, Dr. Ulhas, Dr. Dilip, Dr. Rahul, Dr. Dipesh, Shidheshwar, Vijay, Suryadev, Sadhna, Anand, Chandini, Rameshwar for their help.

A special thanks goes to all my friends from CSIR-NCL, **Dr. Santigopal**, **Dr. Tapas**, Dr. Manzur, **Dr. Sutanu**, Dr. Arghya, **Ashish**, Dr. Debranjana, Dr. Nirshad, Dr. Rohit, Dr. Kailash, Dr. Suman, **Dr. Sachin**, Dr. Govind, Rahul, **Dr. Prabhat**, **Dr. Krishanu**, **Dr. Anupam**, Dr. Sagar, Dr. Shrikant, Swapnil, Nittan, Kajal, Himanshu, Ankit, Umasharan, Sidharth, Pawan, Bharat, Viksit, Sphurti, Labanya, Vikas, Mahendra, Dharmendra, Prem for their help. Also I would like to take this opportunity to thank some of my childhood and college friends, Anku, Papan, Sumit, Ilu, Sanu, Jayanta, Banti, Vaiya, Soumik, Sayan, Swarup for their support and motivation.

I owe a lot to my beloved parents, **Arpita Sen** and **Rabindra Nath Sen**, who encouraged and helped me at every stage of my personal and academic life, and longed to see this achievement come true. My sincere thanks to my beloved sister **Anindita** for her endless support. I would also like to thank my grandparent **Arun Kumar Sen** and **Sandhya Sen**, for their tons of love and blessings. I am very much indebted to my whole **family**.....
Who supported me in every possible way to see the completion of this research work.

Above all, I owe it all to **Almighty God** for granting me the wisdom, health and strength to undertake this research task and enabling me to its completion.

-**Anirban**

Table of content

Chapter 1	Introduction	1-33
1.1	Introduction to catalysis	2
1.2	Introduction to hydrosilylation	4
1.2.1	Hydrosilylation by noble metals	6
1.2.2	Hydrosilylation by base metals	11
1.3	Introduction to alkoxylation of silanes	14
1.3.1	Alkoxylation of silanes by noble metals	15
1.3.2	Alkoxylation of silanes by base metals	17
1.4	Introduction to asymmetric hydrogenation	21
1.4.1	Asymmetric hydrogenation by noble metals	24
1.4.2	Asymmetric hydrogenation by base metals	25
1.5	Setting the goals	27
1.5.1	Statement of the problem	27
1.5.2	Objectives	28
1.6	References	29
Chapter 2	Radical iron breaks the myth: (E)-selective hydrosilylation of alkynes	34-82
2.1	Abstract	35
2.2	Introduction	35
2.3	Results and discussion	39
2.3.1	Rationale for iron complex	39
2.3.2	Reaction optimization	40
2.3.3	Substrate scope for hydrosilylation of alkynes	41
2.3.4	Application	43
2.3.5	Mechanistic aspects	43
2.3.5.1	Mechanistic experiments	44
2.3.6	Kinetic analysis	46
2.3.6.1	Rate law determination	46
2.3.6.2	Linear-free energy relationships	47
2.3.6.3	Eyring analysis	47

2.3.7	Proposed catalytic cycle	48
2.4	Experimental section	49
2.4.1	Methods and materials	49
2.4.2	Synthesis of Tricarbonyl(benzylideneacetone)iron complex	50
2.4.3	General procedure for iron catalysed hydrosilylation of alkynes	51
2.4.4	GC chromatogram of substrate scope	52
2.4.5	¹ H NMR of isolated compounds	59
2.4.6	Gram scale synthesis	66
2.4.7	Protodesilylation reaction	67
2.4.8	Chemoselective hydrosilylation	68
2.4.9	Test for homogeneity	69
2.4.10	Radical trap experiment	70
2.4.11	Control experiment	71
2.4.12	Synthesis of iron complex [Fe(CO) ₄ HSiPh ₃]	72
2.4.13	Hydrosilylation procedure	73
2.4.14	Rate order determination	73
	2.4.14.1 Rate order determination for [Fe-1]/L5	74
	2.4.14.2 Rate order determination for triethylsilane	75
	2.4.14.3 Rate order determination for diphenylacetylene	77
2.4.15	Rate determination for hydrosilylation of substituted alkynes with triethylsilane	78
2.4.16	Eyring analysis	80
2.5	Conclusion	81
2.6	References	81
Chapter 3	Catalytic alkoxylation, polymerization of silanes and tandem alkoxylation-hydrosilylation of alkynes: an iron blitzkrieg	83-138
3.1	Abstract	84
3.2	Introduction	84
3.3	Results and discussion	87
	3.3.1 Synthesis of iron complex (1)	87
	3.3.2 Alkoxylation of silanes	88
	3.3.3 Dehydrogenative polymerization of silanes	91
	3.3.4 Tandem alkoxylation-hydrosilylation of alkynes	93
3.4	Experimental section	97

3.4.1	Methods and materials	97
3.4.2	Synthesis of iron pre-catalyst [Fe(CO) ₄ HSiPh ₃] (1)	98
3.4.3	GC analysis for table 3.1	99
3.4.4	GC chromatogram for each entry of table3.1	100
3.4.5.1	General procedure for iron catalysed alkoxylation of silanes (GP-I)	102
3.4.5.2	General procedure for iron catalysed alkoxylation of silanes (GP-II)	103
3.4.6	GC chromatogram for substrate scope of alkoxylation of Silane	105
3.4.7	¹ H NMR for isolated compounds of alkoxylation of silanes	113
3.4.8	General procedure for iron catalysed synthesis of PSE	122
3.4.9	NMR spectrum for PSE-1	123
3.4.10	GC analysis for table 3.3	124
3.4.11	GC chromatogram for each entry of table3.3	124
3.4.12	General procedure for iron catalysed tandem Alkoxylation-hydrosilylation of alkynes	125
3.4.13	GC chromatogram for substrate scope of tandem Alkoxylation-hydrosilylation	127
3.4.14	¹ H NMR of isolated compounds for substrate scope of tandem Alkoxylation-hydrosilylation	130
3.5	Conclusion	135
3.6	References	136
Chapter 4	One pot synthesis of hybrid phosphine-phosphite ligand and its implication in asymmetric hydrogenation	139-201
4.1	Abstract	140
4.2	Introduction	140
4.3	Results and discussion	142
4.3.1	Ligand design, mechanistic understanding, synthesis and coordination	142
4.3.2	Rhodium catalyzed asymmetric hydrogenation	145
4.3.3	High TOF, TON and scale up experiments	148
4.3.4	Synthesis of DOPA	149
4.3.5	Synthesis of bis-phosphine (L2) and bis-phosphite (L3) ligand and comparison with L1	150
4.3.6	Comparison with literature reported hybrid phosphine-phosphite ligands and privileged ligands	152
4.4	Experimental section	154
4.4.1	Methods and materials	154
4.4.2	One pot synthesis of hybrid ligand L1	154

4.4.2.1	Investigating the reactivity of P-C versus P-O bond formation	154
4.4.2.2	Synthesis of phosphorchloridite	161
4.4.2.3	Synthesis of phosphine-phosphite ligand (L1)	161
4.4.3	Synthesis of bis-phosphine ligand (L2)	167
4.4.4	Synthesis of bis phosphite ligand (L3)	169
4.4.5	Investigating the coordination behavior of ligand L1	171
4.4.6	Synthesis of substrates	174
4.4.7	General procedure for asymmetric hydrogenation	176
4.4.8	High turn-over number experiment	193
4.4.9	DOPA synthesis	194
4.4.10	Establishing the enantiomeric excess after hydrolysis of 7n	195
4.5	Conclusions	197
4.6	References	198
Chapter 5	Summary and outlook	202-209
5.1	Summary	203
5.2	Outlook	207


ABREVIATIONS

Ac ₂ O	Acetic Anhydride
BINOL	1,1'-Bi-2-naphthol
CCDC	Cambridge Crystallographic Data Centre
CDCl ₃	Deuterated chloroform
cm	Centimeter
conv	Conversion
CSD	Cambridge Structural Database
d	Doublet
Da	Dalton
DCM	Dichloromethane
DEPT	Distortionless enhancement by polarization transfer
DFT	Density functional theory
DMF	Dimethylformamide
DMSO	Dimethyl sulfoxide
DSC	Differential scanning calorimeter
equiv	Equivalent
ESI-MS	Electro-Spray Ionization Mass-Spectroscopic
Et ₂ O	Diethylether
EtOH	Ethanol
EtOAc	Ethyl acetate
Et ₃ N	Triethyl amine
etc	et cetera
Fig.	Figure
FTIR	Fourier-transform infrared spectroscopy
g	Grams
GC	Gas chromatography
HCl	Hydrochloric acid
h	Hour/s
Hz	Hertz
K ₂ CO ₃	Potassium carbonate
LN ₂	Liquid nitrogen

ABREVIATIONS

m	Multiplet
M ⁺	Molecular ion
MeOH	Methanol
mg	Milligrams
MgSO ₄	Magnesium sulfate
MHz	Megahertz
min	Minutes
mL	Milliliter
mmol	Millimole
NaOAc	Sodium acetate
n-BuLi	<i>n</i> -Butyllithium
Na ₂ SO ₄	Sodium sulfate
NEt ₃	Triethyl amine
NMR	Nuclear Magnetic Resonance
PPh ₃	Triphenylphosphine
Py	Pyridine
q	Quartet
RT(rt)	Room temperature
Rt	Retention time
s	Singlet
t	Triplet
TMEDA	Tetramethylethylenediamine
THF	Tetrahydrofuran
TLC	Thin layer chromatography
TEMPO	(2,2,6,6-Tetramethylpiperidin-1-yl)oxyl
TOF	Turnover frequency
TON	Turnover number
[Fe ₂ (CO) ₉]	Diiron nonacarbonyl
[Fe(CO) ₅]	Iron Pentacarbonyl
[Rh(COD)BF ₄]	Bis(1,5-cyclooctadiene)rhodium(I) tetrafluoroborate

Synopsis Report

	Synopsis of the thesis to be submitted to the Academy of Scientific and Innovative Research for the award of the degree of Doctor of Philosophy in Chemical Science
Name of the Candidate	Mr. Sen Anirban
Enrollment No. and Date	Ph. D. in Chemical Sciences (10CC15A26026); 1 st August, 2015
Title of the Thesis	Chiral Ligand and Transition Metal (Rh, Fe) Complexes for Catalytic Alkoxylation, Polymerization, Hydrosilylation and Hydrogenation
Research Supervisor	Dr. Samir H. Chikkali

1. Introduction:

The thesis title is “**Chiral Ligand and Transition Metal (Rh, Fe) Complexes for Catalytic Alkoxylation, Polymerization, Hydrosilylation and Hydrogenation**”. This thesis is organized into five different chapters. The first chapter briefly describes the importance of homogeneous catalysis, specially to prepare different organo-silicon compounds due to their wide range of applications in silicon polymer chemistry, protecting group chemistry, organic-inorganic hybrid materials and surface coating chemistry as well as different chiral compounds used as drugs and pharmaceuticals. In chapter-2, an iron complex along with a phosphine ligand have been successfully implemented for the Z-selective hydrosilylation of internal alkynes. A preliminary mechanistic investigation has been performed, and a plausible reaction mechanism has been proposed. In chapter-3, an iron complex has been synthesized and successfully implemented for the alkoxylation of silanes along with a phosphine ligand. In an extension to this methodology, this catalytic system has been successfully implemented to prepare silicon polymers which have been successfully depolymerized under ambient condition. In addition, this catalyst has also been implemented to carry out tandem hydrosilylation-alkoxylation of internal alkynes. Chapter-4 deals with the synthesis of a hybrid phosphine-phosphite ligand in one pot and its application in rhodium catalysed asymmetric hydrogenation of several functionalised olefins. In chapter-5, the thesis work has been summarized and the future directions related to this field have been discussed.



Dr. Samir H. Chikkali (Supervisor)



Anirban Sen (Candidate)

2. Statement of the Problem:

i) Organo-silanes have found numerous application in drug discovery, bio-medical agents, electronics, photonics. Organosilane polymers are used as oil, rubbers, resins, adhesives, coatings. In addition to this, organosilicon compounds are also versatile synthetic intermediates in organic synthesis. Beside others, two approaches to prepare such organosilicon compounds are, i) catalytic hydrosilylation of alkynes and ii) catalytic alkoxylation of silanes. Over the past few decades, significant advancement has been achieved in both methods. However, these achievements were primarily based on noble transition metal (4d, 5d) catalysts. These metals have very low natural abundance on earth's crust, thus very costly. This poses a great threat to the economics of these metals, as well as their sustainability. To address these challenges, researchers have employed naturally abundant and cost-effective 3d transition metals for such transformation. Though it could resolve the issue of high cost and sustainability, the harsh reaction conditions and use of highly reactive reagents often limit their practical applicability. Thus, there is an enormous demand to design concise, practical, sustainable synthetic approaches using 3d transition metal catalysts through which one can perform these transformations under ambient conditions without using any highly reactive reagent.

ii) Asymmetric hydrogenation has remained an important and challenging research area in industry as well as academia since the products obtained are highly useful in pharmaceutical, agrochemical and perfumery industries. Noble metals such as Rh, Ru, Ir along with different chiral bidentate phosphine ligands are routinely used to carry out such transformation. As already discussed, these noble metals are highly scarce on the earth's crust. In addition to this, the bidentate chiral phosphine ligands used in such transformation involve multistep synthesis, thus often making these ligands even costlier than the noble metals. So, now the scientific community is paying good attention to replace these precious noble metals with earth abundant 3d transition metals. However, simplifying the ligand synthesis remains mostly ignored. Thus, there is a pressing need to develop ligands which could be synthesized much more easily.

3. Objectives:

As discussed in the above section, the field of homogeneous catalysis is facing a flux from both the metal as well as ligand synthesis frontier. Focused efforts are needed to streamline this flux. Thus, our objectives are i) design and synthesis of easy-to-use catalytic system based on earth



Dr. Samir H. Chikkali (Supervisor)



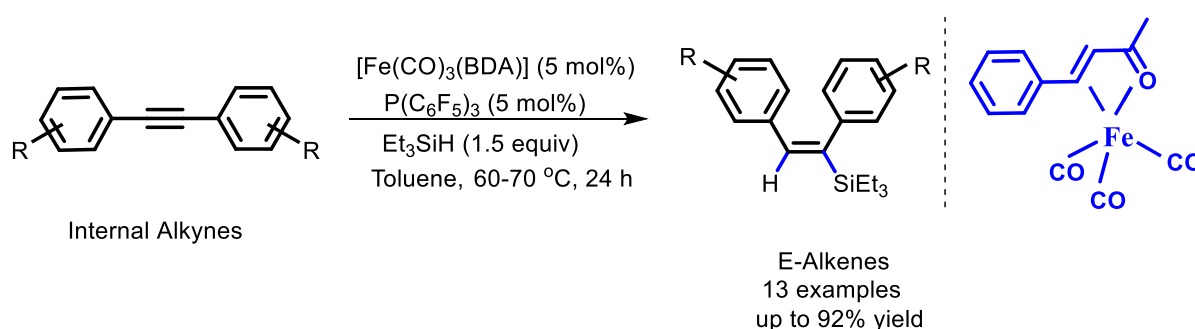
Anirban Sen (Candidate)

abundant 3d transition metals to prepare organo-silicon compounds under ambient condition without using any highly reactive additives, **ii**) design and synthesis of a chiral bidentate phosphorus ligand in a straightforward and concise manner and implement it in asymmetric hydrogenation to prepare chiral compounds.

4. Methodology and Result:

Chapter 2. Radical Iron Breaks the Myth: (Z)-Selective Hydrosilylation of Alkynes

Hydrosilylation of Alkynes represent one of the most straightforward, atom economical access to prepare organo-silicon compounds. In recent past, iron catalysis has attracted a lot of attention, since it is abundant, affordable, and biocompatible, thus fits for green and sustainable chemistry applications. In addition to this, iron's distinctive electronic structures allow it to mediate different types of chemical reactions. In literature, few reports are there where iron catalysts have been successfully implemented for the hydrosilylation of internal alkynes. However, in all these reports, either organometallic reagents or organic base have been used for the success of the reaction which often creates a problem for the functional group tolerance of the reaction. Thus, development of a highly reactive additive free methodology would be highly useful. Chapter 2 discusses the development of iron catalysed (Z)-selective hydrosilylation of internal alkynes along with a phosphine ligand without the use of any highly reactive additive. The hydrosilylation reaction exhibited broad substrate scope and tolerated functional groups, such as -Cl, -Br, -OMe, -COOMe, with different types of silanes at 60 to 70 °C (Scheme 1). The reaction can easily be scaled up to gram scale. A preliminary mechanistic investigation revealed a radical pathway for the reaction.



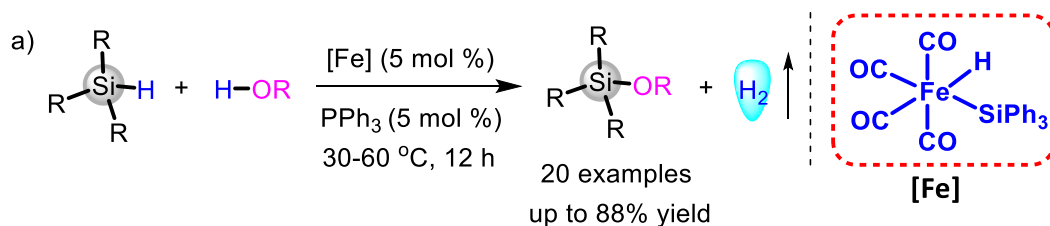
Scheme 1. (Z)-Selective hydrosilylation of internal Alkynes by iron complex along with a phosphine ligand.

Dr. Samir H. Chikkali (Supervisor)

Anirban Sen (Candidate)

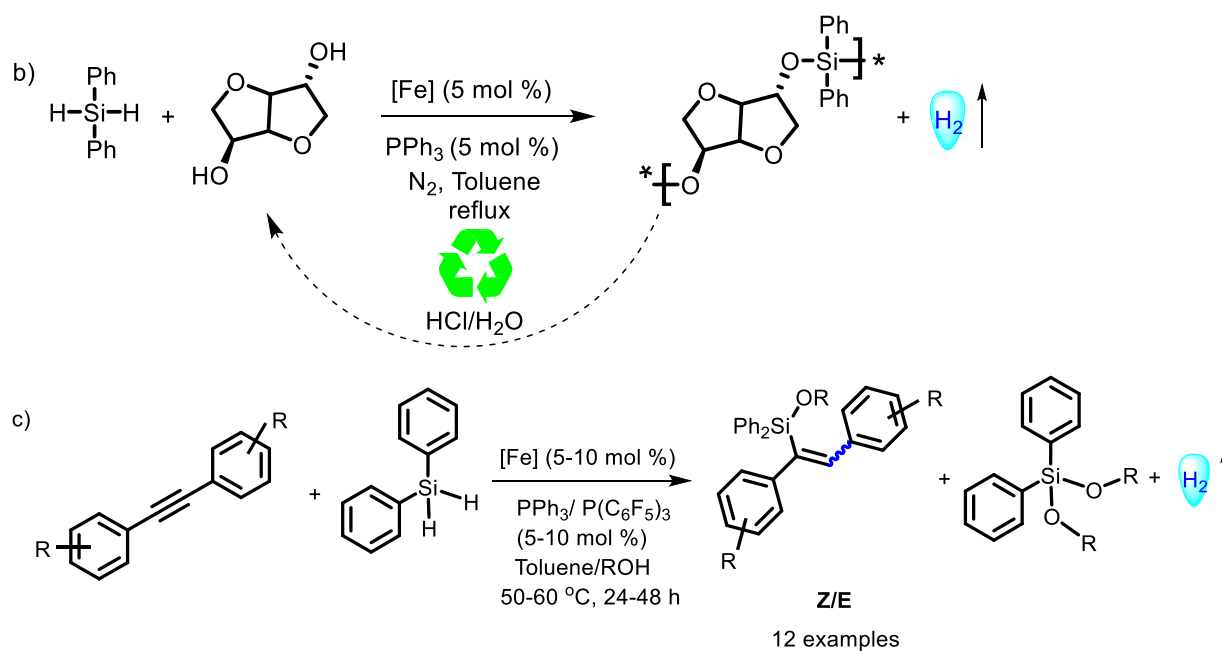
Chapter 3. Catalytic Alkoxylation, Polymerization of Silanes and Tandem Hydrosilylation-Alkoxylation of Alkynes: An Iron Blitzkrieg

For hydrosilane alcoholysis, a variety of transition metal complexes along with main group Lewis acid/base catalysts have been developed. Surprisingly, iron is not well explored for this reaction. For example, Riley and co-workers reported $\text{Fe}(\text{H})_2(\text{PMePh}_2)_4$ and $\text{Fe}(\text{H})_2(\text{N}_2)(\text{PEtPh}_2)_3$ in 1980 for silane alcoholysis which were only active for $(\text{EtO})_3\text{SiH}$ but inactive for Et_3SiH . Subsequently, in 1998, Brookhart and co-workers reported the $\text{Cp}(\text{CO})(\text{PPh}_3)\text{Fe}^+$ fragment to catalyse silane alcoholysis in presence of non-coordinating counter anion. However, this methodology only works with phenol, when ethanol is used, catalyst deactivation occurs rapidly. As a result, developing more efficient and selective iron catalyst for silane alcoholysis is highly desirable. To achieve this, we synthesized an iron catalyst by following a literature-reported procedure and successfully developed an iron-catalysed methodology for alkoxylation of silanes to produce hydrogen gas and silyl ethers. The reaction works efficiently with different silanes as well as different alcohols containing electron donating as well as electron withdrawing groups. To demonstrate the synthetic utility of this methodology, the iron catalyst was successfully implemented to synthesize degradable polysilylether from bio-based isosorbide and commercially available diphenylsilane by dehydrogenative cross-coupling. Finally, this iron catalyst was successfully utilised to develop a methodology of tandem alkoxylation-hydrosilylation of internal alkynes, which would pave the way for a novel approach to create structurally diverse organosilicon compounds. In literature, only one platinum-catalyst is known to achieve such transformation.



Dr. Samir H. Chikkali (Supervisor)

Anirban Sen (Candidate)



Scheme 2. a) Catalytic alkoxylation of silane by iron complex along with a phosphine ligand, b) catalytic dehydrogenative polymerization of diphenylsilane and isosorbide by iron complex along with a phosphine ligand and its hydrolytic degradation, c) tandem hydrosilylation-alkoxylation of internal alkyne by iron complex along with a phosphine ligand.

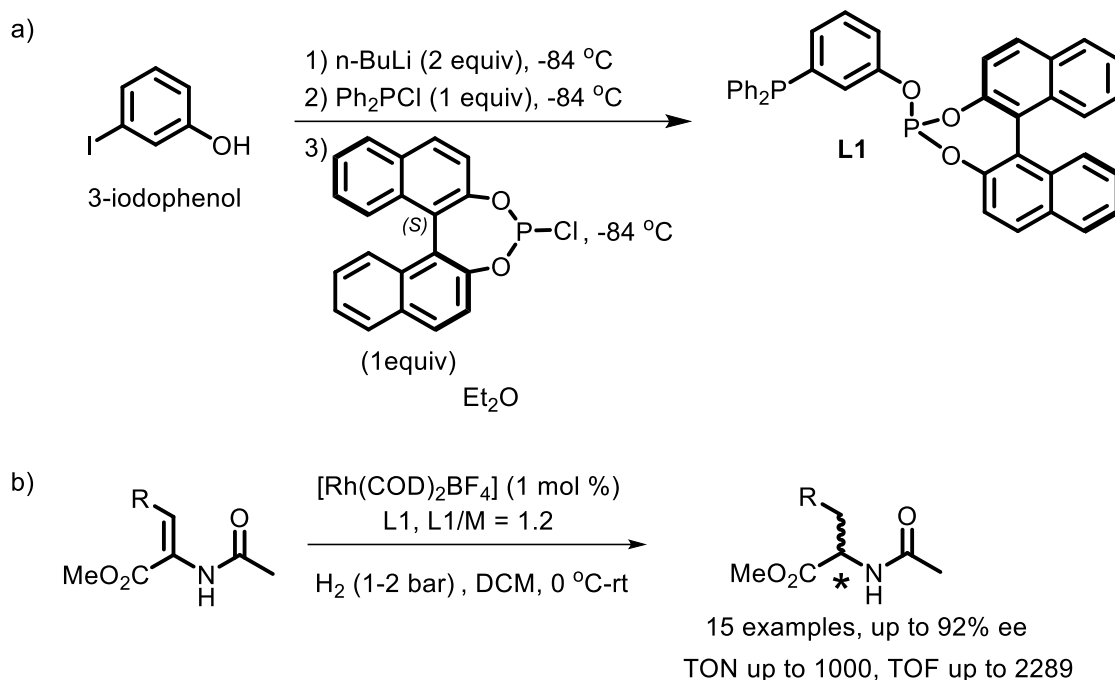
Chapter 4. One Pot Synthesis of Hybrid Phosphine-phosphite Ligand and Its Implication in Asymmetric Hydrogenation

The seemingly mature field of transition metal catalysed asymmetric hydrogenation continues to excel beyond the 2001 Noble Prize and offers access to enantiopure advanced pharmaceutical intermediates (API). Chiral bidentate phosphorus ligands play a defining role in asymmetric hydrogenation and continue to dominate the academic and industrial research. However, the synthesis of privileged bidentate phosphine ligands is a tedious task with multiple synthetic steps and many a time, such lengthy and lousy protocols are industrially unattractive. Although bidentate ligands deliver better selectivities and catalytic performance, their synthesis has always been an obstacle to their success. To crack this synthetic bottleneck, here we have prepared a binol-based phosphine-phosphite ligand in one pot. Its coordination property has been studied with $[\text{Rh}(\text{COD})_2\text{BF}_4]$. It has been utilized in asymmetric hydrogenation of several functionalized olefins where it showed excellent yield (up to 98%),

Dr. Samir H. Chikkali (Supervisor)

Anirban Sen (Candidate)

enantioselectivity (up to 92%), and reactivity (TOF 1200). Its reactivity has also been compared with its symmetrical counterparts bis-phosphine and bis-phosphite. The practical relevance of hybrid ligand is demonstrated by scaling up the reaction to 1 g and by synthesizing DOPA (90% ee), a drug widely employed for the treatment of Parkinson's disease. Computational investigations using density functional theory indicate that the R isomer is preferred by 3.8 kcal/mol over the S isomer, which corroborates well with experimental observation.



Scheme 3. a) One pot synthesis of phosphine-phosphite ligand, b) application of this ligand in Rh catalysed asymmetric hydrogenation of functionalized olefins.

5. Summary:

We have developed a methodology using iron-based catalyst system for the hydrosilylation of internal alkynes without the use of any highly reactive additive under mild condition. This reaction can easily be scaled up to gram scale and further functionalization of the product has also been performed. Elementary mechanistic studies revealed that the reaction follows a radical pathway (Chapter-2). In addition to this, we have successfully synthesized an iron complex and implemented it for the alkoxylation of silanes along with a phosphine ligand under ambient condition. We have extended this methodology to prepare silicon polymers which can be easily depolymerized to its starting monomer under hydrolytic condition. We have also

Dr. Samir H. Chikkali (Supervisor)

Anirban Sen (Candidate)

utilized the catalyst system to carry out tandem hydrosilylation-alkoxylation of alkynes with diphenylsilane in an alcoholic solvent (Chapter-3). Further, we have synthesized a hybrid phosphine-phosphite ligand in one pot and successfully implemented it for the rhodium catalysed asymmetric hydrogenation of functionalized olefins with good to excellent enantioselectivity under mild condition. The activity of this hybrid phosphine-phosphite ligand was also compared with its symmetrical counterparts bis-phosphine and bis-phosphite ligand (Chapter-4). High selectivity and excellent functional group tolerance have been observed in all these transformations. To sum up, it is neither the success story of the metal nor the triumph of the ligand alone, rather, it is the metal-ligand synergy that makes the journey of homogeneous catalysis so much fascinating, intriguing and remarkable.

6. Future Directions:

The field of homogeneous catalysis is mainly dominated by precious metals such as rhodium, ruthenium, iridium, palladium, platinum. These precious metal catalysts have several advantages, such as readily available and easy to handle synthetic precursors, broad substrate scope, high reactivity & predictable selectivity. Besides this, a well-studied mechanism, involving two-electron redox processes, has made precious metals, the undisputed champion of this field. However, these precious metals (Rh, Ru, Ir, Pd, and Pt) are the least abundant transition metals on earth's crust and are in the danger zone of being extinct within the next 50 years, which poses a serious threat from a sustainability perspective. It is due to their scarcity, extraction of these metals is highly tedious thus associated with higher cost, higher global warming potential as well as a higher risk for its continuous supply. To combat these difficulties, enough attention has been paid to the development of catalysts based on 3d transition metals such as Mn, Fe, Co, Ni & Cu, mainly because of their greater earth abundance, lower cost, lower toxicity & environmentally benign nature as compared to noble metals. However, base metals show unique reactivity as compared to noble metals. They exhibit variable coordination geometry, single-electron redox processes, facile ligand exchange & multiple spin states. In addition to this, facile change of oxidation state as well as the presence of radical intermediate, make it difficult for mechanistic study, thus impeding catalyst development. The above discussion clearly explains that base metals can't be used as a direct drop-in replacement for noble metals which in turn creates a new chemical space for "rational



Dr. Samir H. Chikkali (Supervisor)



Anirban Sen (Candidate)

ligand design” where the different arm of the ligands, taking care of different properties of the metal might be advantageous. Also, many existing ligands involve multiple synthetic steps and show poor scalability, thus associated with a higher price which makes it impractical for use in large-scale processes, thus enlarges the chemical space required for “rational ligand design”. Finally, the presence of a versatile ligand toolbox will find application in other catalytic transformations beyond any particular reaction.

7. Publications:

List of Publications:

- 1. Sen, A.;** Kumar, R. and Chikkali, S. “One Pot Synthesis of Hybrid Phosphine-phosphite Ligand and Its Implications in Highly Active and Selective Rhodium Catalyzed Asymmetric Hydrogenation”, *Eur. J. Org. Chem.*, **2022**, 2022, e202101447.
- 2. Sen, A.** and Chikkali, S. “C1-symmetric diphosphorus ligands in metal-catalyzed asymmetric hydrogenation to prepare chiral compounds”, *Org. Biomol. Chem.*, **2021**, 19, 9095-9137.
- 3. Sen, A;** Kumar, R; Tewari, T and Chikkali, S. “Radical iron breaks the myth: (Z)-selective alkylation of Alkynes”, manuscript under preparation.
- 4. Sen, A;** Kumar, R; Tewari, T and Chikkali, S. “Catalytic Alkoxylation, Polymerization of Silanes & tandem Alkoxylation-Hydrosilylation of Alkynes: An Fe blitzkrieg”, manuscript under preparation.
- 5. Khopade, K.;** **Sen, A.** and Chikkali, S. “Highly selective process for the preparation of sitagliptin via rhodium catalysed asymmetric hydrogenation”, *Asian J. Org. Chem.*, **2020**, 9, 189-191.
- 6. Koshti, V.;** **Sen, A** and Chikkali, S. “Self-assembly of P-chiral supramolecular phosphines on rhodium and direct evidence for Rh-catalyst-substrate interactions”, *Dalton Trans.*, **2017**, 46, 13966-13973.
- 7. Kumar, R;** **Sen, A;** Tewari, T and Chikkali, S. “Iron catalyzed isomerization of olefins: A green approach”, manuscript under preparation.



Dr. Samir H. Chikkali (Supervisor)



Anirban Sen (Candidate)

8. Kumar, R.; Sen, A. and Chikkali, S. "Rhodium catalysed asymmetric hydroformylation of olefin by using hybrid ligand", manuscript under preparation.

List of Patents:

1. Chikkali, S.; Pandey, S. and Sen, A. "A phosphine-phosphite ligand, process for preparation and application thereof", IN201811016872 A 2019-11-08.

2. Sen, A; Kumar, R; Chikkali, S. "Novel iron based catalyst system and application thereof", patent filed.

8. References:

1. Sen, A. and Chikkali, S. "C1-symmetric diphosphorus ligands in metal-catalyzed asymmetric hydrogenation to prepare chiral compounds", *Org. Biomol. Chem.*, **2021**, *19*, 9095-9137.

2. Sen, A.; Kumar, R. and Chikkali, S. "One Pot Synthesis of Hybrid Phosphine-phosphite Ligand and Its Implications in Highly Active and Selective Rhodium Catalyzed Asymmetric Hydrogenation", *Eur. J. Org. Chem.*, **2022**, *2022*, e202101447.

3. Hu, M. Y.; He, P.; Qiao, T. Z.; Sun, W.; Li, W. T.; Lian, J.; Li, J. H.; Zhu, S. F. "Iron Catalyzed Regiodivergent Alkyne Hydrosilylation", *J. Am. Chem. Soc.*, **2020**, *142*, 16894–16902.

4. Chang, S.; Scharrer, E.; Brookhart, M. "Catalytic Silane Alcoholysis Based on the $C_5H_5(CO)(PPh_3)Fe^+$ Moiety. NMR Spectroscopic Identification of Key Intermediates", *J. Mol. Catal. A*, **1998**, *130*, 107-119.



Dr. Samir H. Chikkali (Supervisor)



Anirban Sen (Candidate)

Chapter 1

Introduction

1.1 Introduction to Catalysis

For the last couple of decades, modern chemical industry has always been remained as a crucial and essential pillar for the global economy. Over 80% of all industrial processes created since 1980 rely on catalysts, making catalysis a key component of the chemical industry. The large financial incentive associated with global catalyst market clearly tells why it is necessary to comprehend existing catalytic processes and create new ones. The word "catalysis" was first coined by Berzelius in 1836 to describe a growing body of scientific evidence.¹ A half-century later, Wilhelm Ostwald defined catalysts as molecules that change the rate of chemical reactions without appearing in the final products.¹ This implies that a catalyst can also slow down a reaction, according to Ostwald! The current definition is as follows: A catalyst is something that speeds up a chemical reaction's progress toward equilibrium without being permanently engaged.¹ When the catalyst is used, the energy profile of the reaction is altered because new routes with lower activation energies become viable which increases the reaction rate (Figure 1.1). The activity and efficiency of catalysts can be quantified in terms of turnover number (TON) and turnover frequency (TOF).

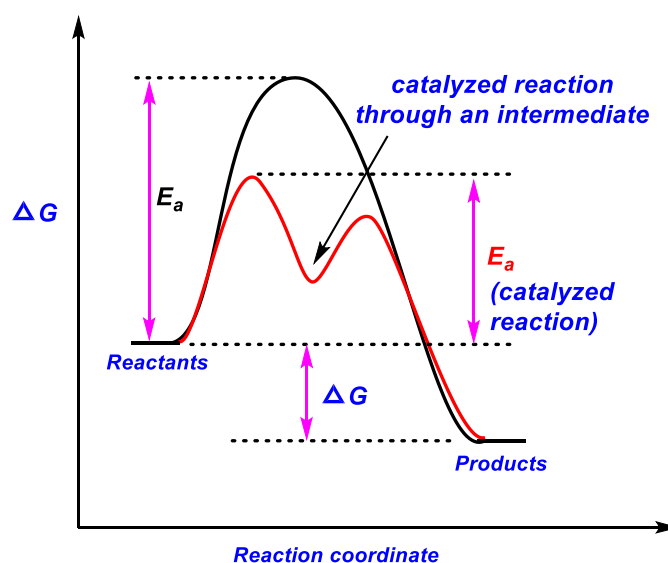


Figure 1.1: A simplified Gibbs free energy diagram showing the influence of the catalyst (ΔG , the Gibbs free energy change).

Catalysts are broadly divided into two classes: homogeneous, and heterogeneous.¹ A homogeneous catalyst is a chemical species that coexists with its products and reactants in the same phase, often a liquid solution. Heterogeneous catalysts, which are typically solids, are substances that exist in a different phase from the products or reactants of the reactions they catalyse. Both catalysts have their own advantages as well as drawbacks. Since, homogeneous

catalysts are present in the same phase with the reactants, they show generally higher reactivity and better selectivity under mild reaction condition as compared to their heterogeneous counterparts.^{2, 3} Also, in case of homogeneous system, the catalyst is well defined which enables kinetic studies as well as elucidation of structure-activity relationship much more easily. However, homogeneous catalysts are difficult to remove from the reaction mixture and are rarely recycled, thus the final product may have metal impurities. Maintaining the content of harmful metals below the permitted levels is crucial for the pharmaceutical industry, thus requires additional purification techniques. On the other hand, heterogeneous catalysts are easily recoverable through phase separation or straightforward filtration, allowing for little metal contamination in the final product. Additionally, they frequently show greater stability than homogeneous catalysts and are frequently recyclable, which lowers the cost and environmental effect of a process. It is mainly due to this reason, the contribution of homogeneous catalytic processes to the chemical industry is only about 17–20%, which is much less than the contribution of heterogeneous catalytic processes.⁴ However, the importance of homogeneous catalysis is significantly growing. Homogeneous catalysis is becoming increasingly important, especially in the pharmaceutical and polymer industries. In an organometallic catalyst, ligands surround the central metal. The properties of the catalyst are governed by both the metal as well as ligands. The relative simplicity of catalyst modification by altering the ligand environment is the key to the effectiveness of organometallic catalysts. In homogeneous catalysis, ligand effects are crucial. Ligands tune the sterics (cone angle, bite angle) and electronics (sigma donation, pi acceptance) around the metal centre to enhance the rate and selectivity of a particular reaction, which in turn improves raw material and energy usage and minimizes waste (Figure 1.2).

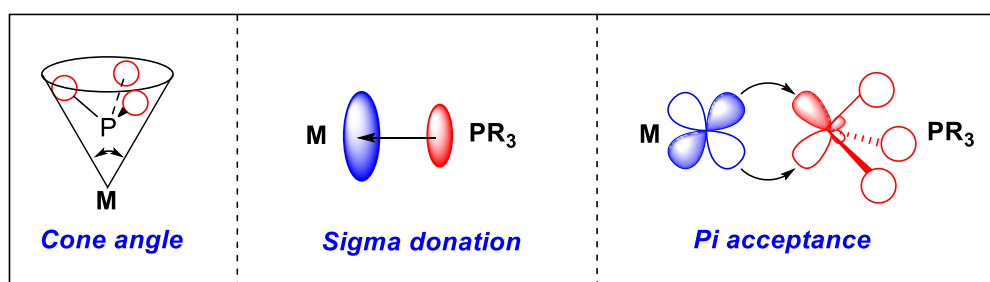


Figure 1.2: Steric and electronic effects exerted by ligands to metal centre.

By simply altering the ligands, a single metal can produce a range of products from a single substrate. Figure 1.3 shows the products that can be produced from butadiene using different nickel catalysts. When allylnickel(II) complexes are utilised as catalysts, polymers are

produced whereas when nickel(0) is the catalyst precursor, the resultant products are cyclic dimers and the all-trans trimer (Figure 1.3).⁵

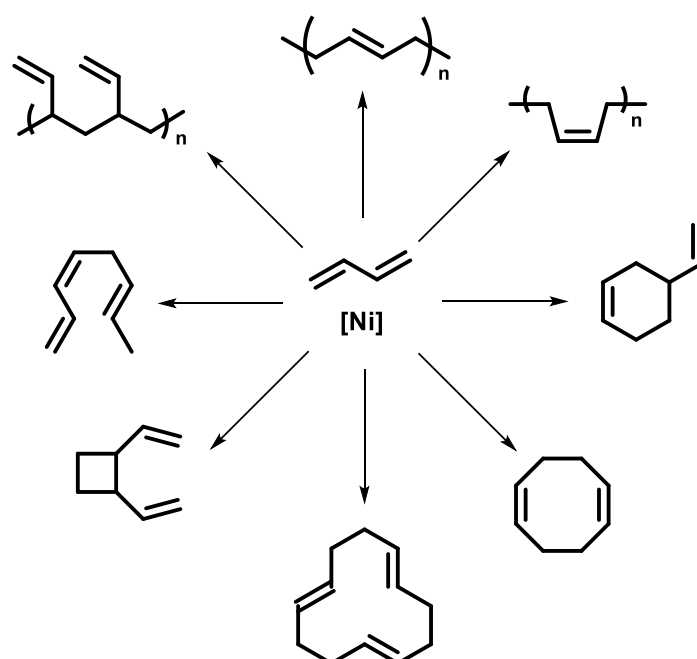


Figure 1.3: Effect of ligands and valence state of metal on the selectivity in nickel catalysed reaction of butadiene.

There are numerous instances of homogeneous catalytic reactions that are used in a wide range of organic transformations, both in the chemical industry and in research labs around the world. Some important chemical reactions that are catalysed by homogeneous systems, include hydroformylation, olefin metathesis, asymmetric hydrogenation, olefin oligomerization, C-C cross coupling, aryl amination, hydroamination, and hydrosilylation.⁶

1.2 Introduction to hydrosilylation

In the earth's crust, silicon is the second-most abundant element. In addition to this, silicon compounds are often regarded as non-toxic and environmentally benign. It is mainly due to this reason, significant quantity of organosilicon compounds are utilised on a daily basis. Organosilicon compounds are generally distinguished by their stable and inert carbon-silicon bonds.⁷ Organosilanes, organosilyl halides, and the related ethers are particularly accessible and provide simple options for diverse functionalizations. Organosilicon compounds have complimentary physical features to their common pure carbon analogues, which make them appealing for a range of commercial applications. As a result, organosilicon compounds are frequently utilised as oils, rubbers, and resins, as well as in adhesives and coatings.⁸ Silicones (siloxanes) are now

widely used in everyday commodities thanks to the discovery and development of organosilane polymers. Organosilanes are also employed in a wide range of industries, such as pharmaceuticals, the development of biomedical products, electronics, and photonics.⁹

From a synthetic perspective, organosilanes are also versatile intermediates. For example, Hiyama coupling, Hiyama-Denmark coupling¹⁰, Sakurai allylation¹¹, Tamao-Fleming oxidation¹², Peterson olefination¹³, Brook rearrangement¹⁴ involve the transformation of C-Si bond (Figure 1.4).

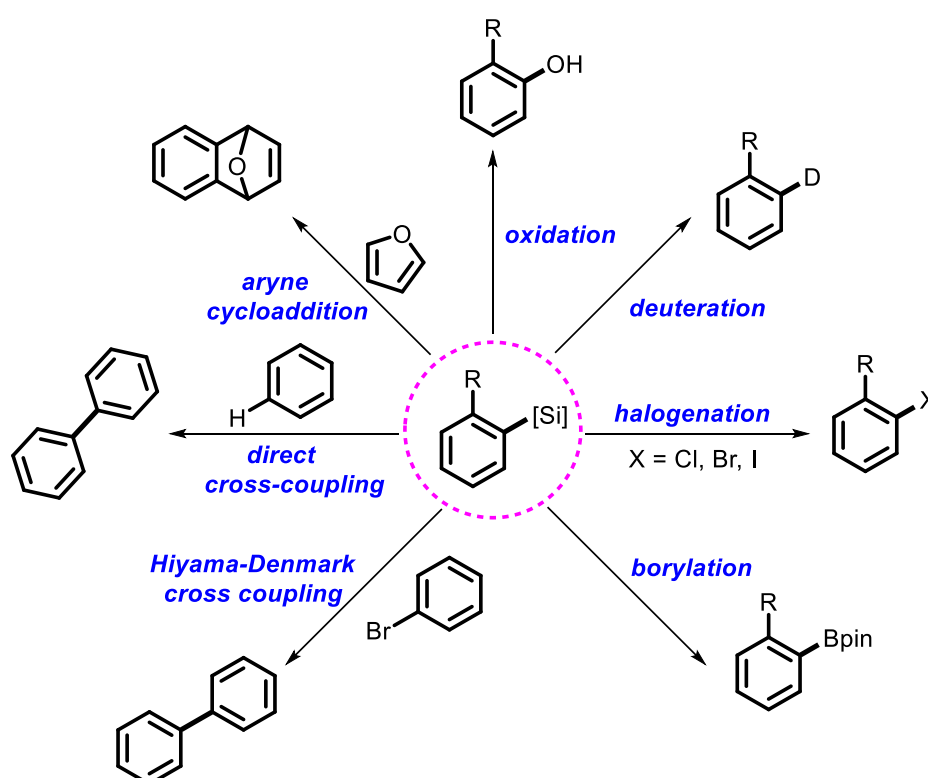


Figure 1.4: Different chemical transformation involving C-Si bond.

Catalytic hydrosilylations, one of the various processes for forming C-Si bonds, enable the straightforward addition of silanes (Si-H) to a variety of multiple bonds, such as olefins and alkynes. Theoretically, there are no by-products or wastes produced with hydrosilylation, making them completely atomic economic (Figure 1.5).^{15, 16}

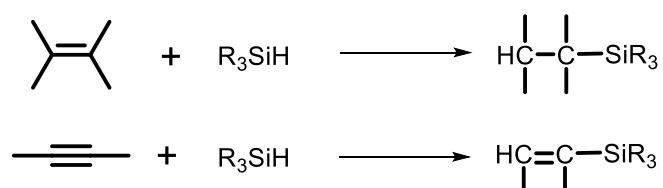


Figure 1.5: Hydrosilylation reactions.

In addition to being employed on a small scale in laboratories, these reactions have also been exploited in the chemical industry to create useful organosilicon compounds. They have really been shown to be among the silicone industry's most effective reactions. It is possible to directly alter the characteristics of polymers or inorganic materials by performing hydrosilylations with functionalized silanes. By crosslinking with a different vinyl silicon reagent, poly(dimethylsiloxane), a substantial variety of silicone rubber, can be functionalized. (Figure 1.6).¹⁷

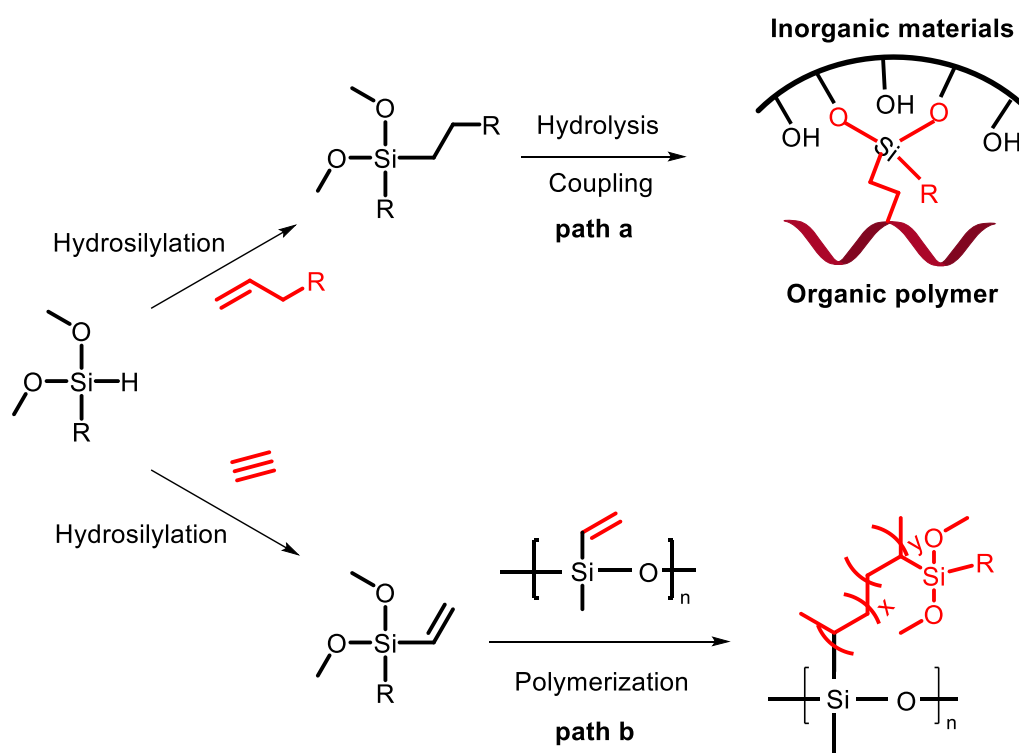


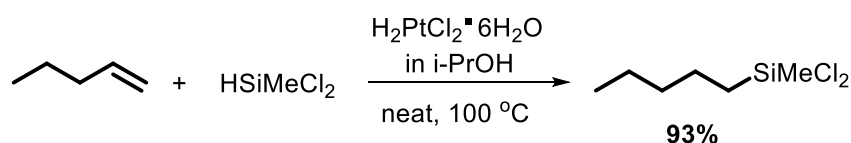
Figure 1.6: Utilization of silane reagent: path (a): interfacial bonding by a silane coupling agent; path (b): crosslinking reaction between vinyl-containing silane and silicone polymers.

1.2.1 Hydrosilylation by noble metals

Platinum-based catalysts have dominated this sector since the hydrosilylation process was first described in the literature in 1947.¹⁸ When Speier's catalyst (H_2PtCl_6) was first developed, it represented a significant advance. Later, Karstedt further advanced this field by creating a platinum(0) complex using vinyl-siloxane ligands.¹⁹

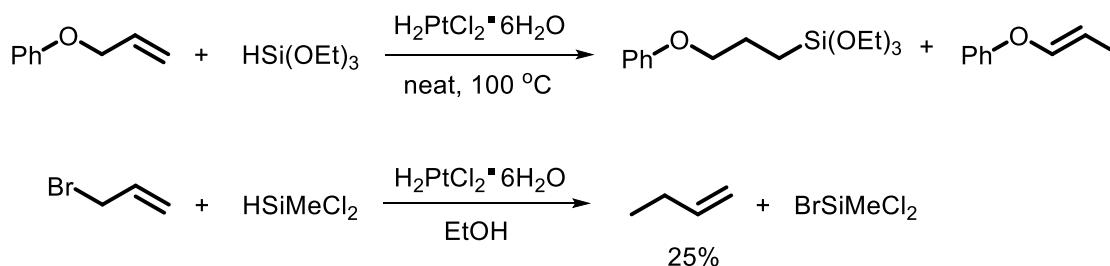
Hexachloroplatinic acid ($\text{H}_2\text{PtCl}_6 \cdot 6\text{H}_2\text{O}$) was identified by John L. Speier in 1957 as a highly effective catalyst for anti-Markovnikov alkene hydrosilylation.²⁰ Both the hydrated and the partially dehydrated form of the hexachloroplatinic acid can be employed. It is typically dissolved in an organic solvent. A solution of $\text{H}_2\text{PtCl}_6 \cdot 6\text{H}_2\text{O}$ in isopropyl alcohol is known as

"Speier's catalyst.". One distinguishing feature of this system is the induction period, which occurs when hexachloroplatinic acid is converted into the active Pt(0) catalyst which is followed by a rapid exothermic hydrosilylation reaction. Numerous functionalized alkenes can be hydrosilylated using Speier's catalyst. Different functional groups, such as amine, carbonyl, carboxylate, halide, alcohol, can be tolerated. As low as 10^{-8} moles of catalyst can be used for the hydrosilylation process of 1 mole of substrate, employing Speier's catalyst. Due to its exceptionally high turnover number (TON) and turnover frequency (TOF), Pt is employed on an industrial scale as a disposable catalyst despite its high cost (Scheme 1.1).²⁰



Scheme 1.1: 1-pentene hydrosilylation with dichloromethylsilane by Speier's catalyst.

However, some side reactions are catalysed by Speier's catalyst. For instance, isomerization and side reactions occur during the reaction of allyl phenyl ether with silanes.²⁰ Because of competing hydrodehalogenation, allyl halides are not appropriate substrates for Speier's catalyst (Scheme 1.2).²¹



Scheme 1.2: Hydrosilylation of allyl bromide and allyl phenyl ether using Speier's catalyst.

Karstedt's catalyst, which was first reported in 1973, is currently one of the most crucial platinum catalysts for industrial use.²² Karstedt's catalyst exhibits superior olefin hydrosilylation activity and is more soluble in organosilanes than Speier's catalyst. Although in-situ reduction is not required, induction period still persists mainly due to the ligand exchange process.²³ Unfortunately, there are several side products to hydrosilylation using the Karstedt catalyst, such as formation of isomeric olefins, reduced alkenes, and dehydrocondensation adducts. The finished materials' quality or characteristics are adversely

affected by these impurities. Additionally, Karstedt's catalyst, often decomposes as a result of dissociation of the weakly attached vinylsiloxane ligands, forming Pt(0) colloids and platinum black which causes colouration of the final product (Figure 1.7).

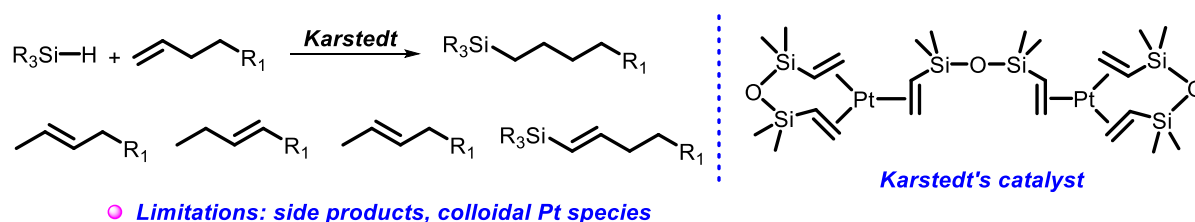
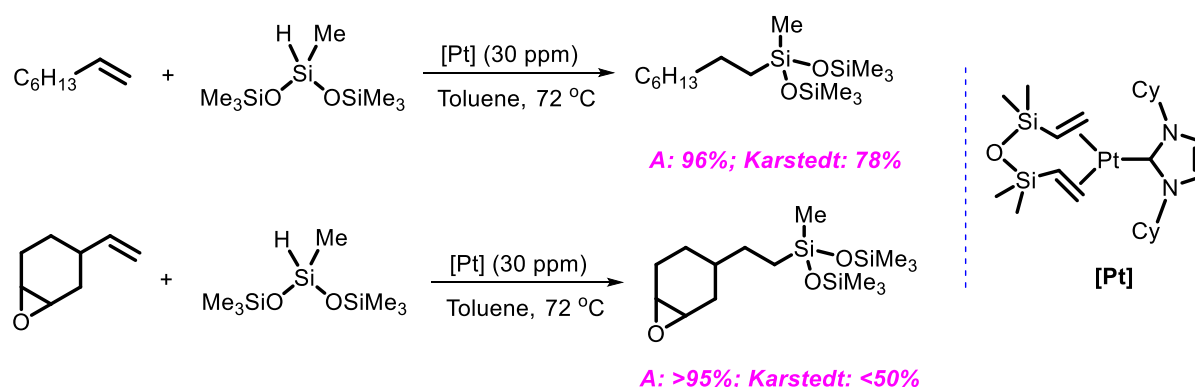


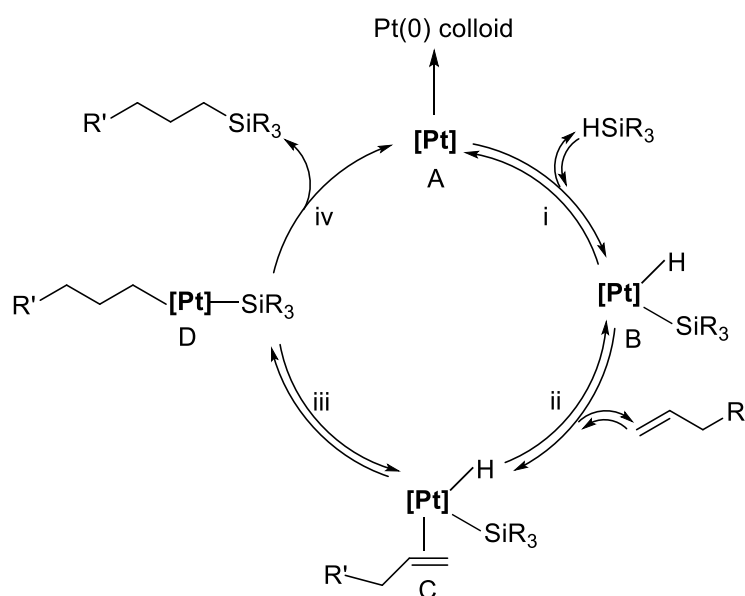
Figure 1.7: Hydro-silylation reaction by Karstedt's catalyst with different side products.

To address this issue, several changes that might increase the original catalyst's stability were proposed. Phosphine ligands help to prevent colloid formation and catalyst degradation, but they also lower TOF.^{24, 25} Recently, Pt(0) complexes assisted by N-heterocyclic carbene (NHC) were reported to be effective hydro-silylation catalysts. Good reaction rates could still be attained with a loading of 30 ppm or less, despite the fact that these complexes are a little less reactive than the Karstedt catalyst. More importantly, the reaction produced no colloidal Pt species, and the number of undesirable by-products was significantly reduced. The steric hindrance that the carbene substituents provided around the Pt metal seems to be another factor influencing the reactivity and selectivity of these catalysts; the cyclohexyl moiety was found to be the most effective. Additional applications of the Pt-carbene catalysts include their chemoselectivity and tolerance to reactive functionalities such as free alcohols, protected alcohols, silylether, ketones, esters, and epoxides (Scheme 1.3).^{26, 27}



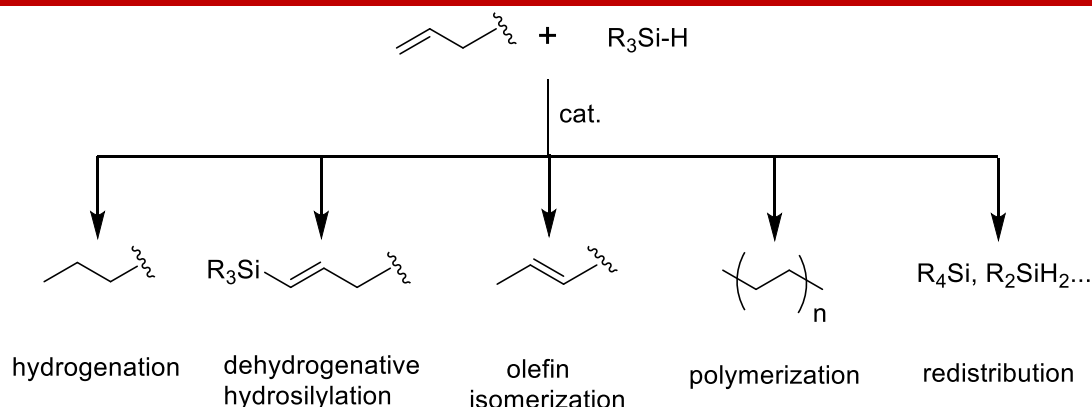
Scheme 1.3: Regio- and chemo-selectivity in hydro-silylation reaction catalysed by Pt-carbene complex.

For Pt catalysis, the first model put forth by Chalk and Harrod is still largely accepted (Scheme 1.4). There are four simple steps in this mechanism: i) H-Si is oxidatively added to low valent metal (A) to form a silyl hydride complex (B); ii) the olefin is coordinated to produce complex (C); iii) formation of the alkyl silyl complex (D) by the migratory insertion of the olefin into the Pt-H bond; iv) reductive elimination to produce hydrosilylation product and regenerate the catalyst. Step (iv) is regarded as the irreversible rate-determining step while steps (i) to (iii) are reversible. Pt(0) particle production is connected to catalyst deactivation.²⁸ Anti-Markovnikov addition products are mostly generated in hydrosilylation processes catalysed by Speier's and Karstedt's catalysts. The Chalk-Harrod mechanism can be used to explain how anti-Markovnikov products are formed. This mechanism involves insertion of an olefin into the Pt-H bond to form a terminal alkyl complex. On the other hand, inserting into the Pt-Si bond would have produced an intermediate in which Pt is connected to a carbon which is sterically more hindered. Additionally, the anti-Markovnikov addition product demonstrates how metal hydride species swiftly react with C=C via migratory insertion and β -hydride elimination to generate the most stable terminal alkyl complex (Scheme 1.4).



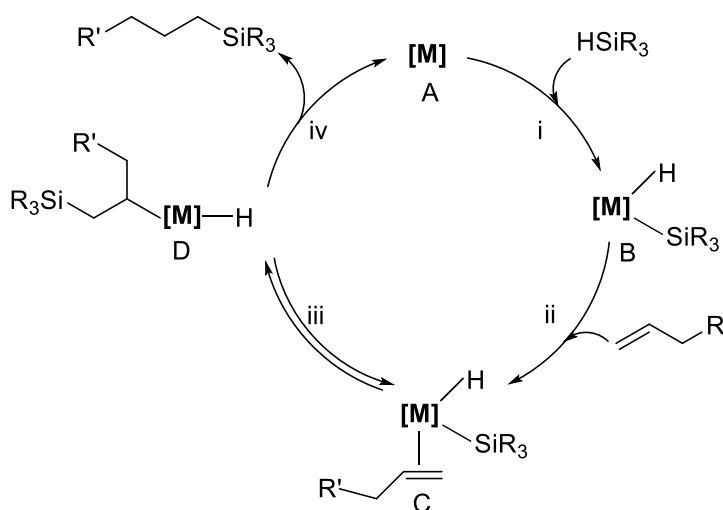
Scheme 1.4: Chalk-Harrod mechanism for Pt catalyzed hydrosilylation.

During alkene hydrosilylation by transition metal complexes, several side reactions are frequently seen. These include dehydrogenative silylation, oligomerization, polymerization, isomerization, reduction of alkenes and redistribution (Scheme 1.5).²⁹



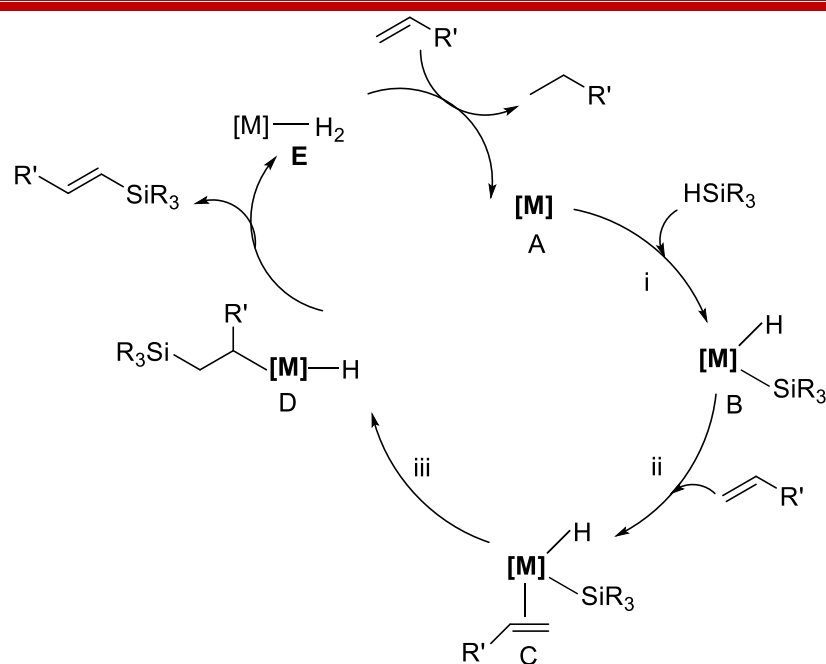
Scheme 1.5: Common side-products of transition metal-catalyzed hydrosilylation.

All of these byproducts cannot be attributed to the Chalk-Harrod catalytic cycle. The dehydrogenative silylation reaction, as opposed to the hydrosilylation, is frequently preferred by complexes of Fe, Co, Ni, and Pd. Wrighton and colleagues introduced the modified Chalk-Harrod mechanism in 1977 to explain the generation of dehydrogenative silylation products (vinylsilanes). According to the authors, migratory insertion of an alkene into an M-Si bond occurs more rapidly than into an M-H bond (Scheme 1.6).³⁰



Scheme 1.6: Modified Chalk-Harrod mechanism for hydrosilylation.

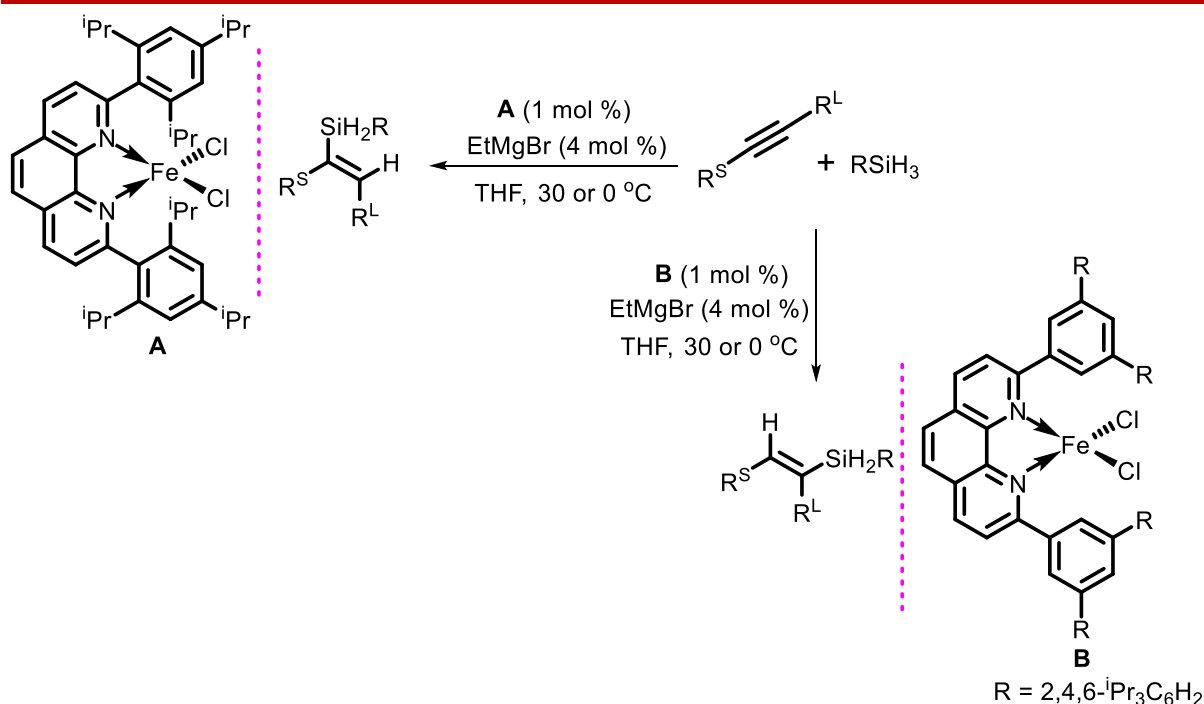
According to Scheme 1.7, the formation of the side-products of dehydrogenative silylation is explained by the modified Chalk-Harrod mechanism.



Scheme 1.7: The mechanism of dehydrogenative hydrosilylation.

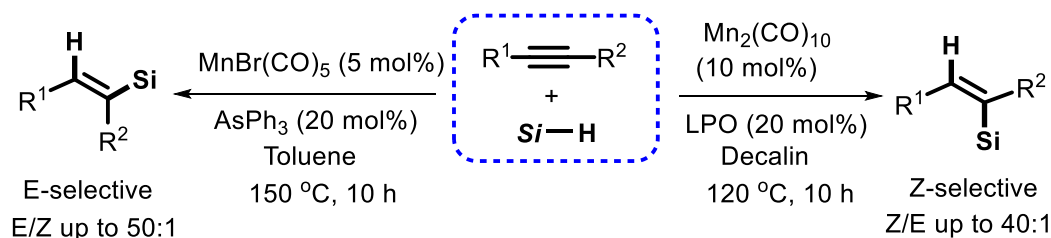
1.2.3 Hydrosilylation by base metals

Hydrosilylation reactions are typically performed with precious metals (Pt, Rh). However, these precious metals are the least abundant transition metals on earth's crust which poses a serious threat from a sustainability perspective for this field. To combat these difficulties, scientists are now paying attention for the developments of catalysts based on 3d transition metals mainly because of their greater earth abundance, lower cost, lower toxicity & environmentally benign nature as compared to noble metals. For instance, Zhu and colleagues reported in 2020 that iron complexes comprising 2,9-diaryl-1,10-phenanthroline ligands and catalytic amounts of EtMgBr as a reductant hydrosilylated terminal and internal alkynes with primary silanes. Most interestingly, by merely altering the ligand substitution pattern, the catalytic system presented here can totally reverse the regioselectivity of diverse alkynes. The reactions involving terminal alkynes specifically showed turnover numbers (TONs) up to 35 500 and turnover frequencies up to 35.5 s^{-1} , which are so far reported to be the highest values for such reactions. According to mechanistic studies, the iron catalysts may have promoted hydrosilylation through the $2e^-$ redox cycle, and the observed regioselectivity may have been brought about by maximising the overlap between the iron and alkyne orbitals. The hydrosilylation process outlined here offers a very effective way to make valuable di- and trisubstituted olefins under ambient condition.³¹



Scheme 1.8: Iron-catalyzed regiodivergent hydrosilylation of internal alkynes.

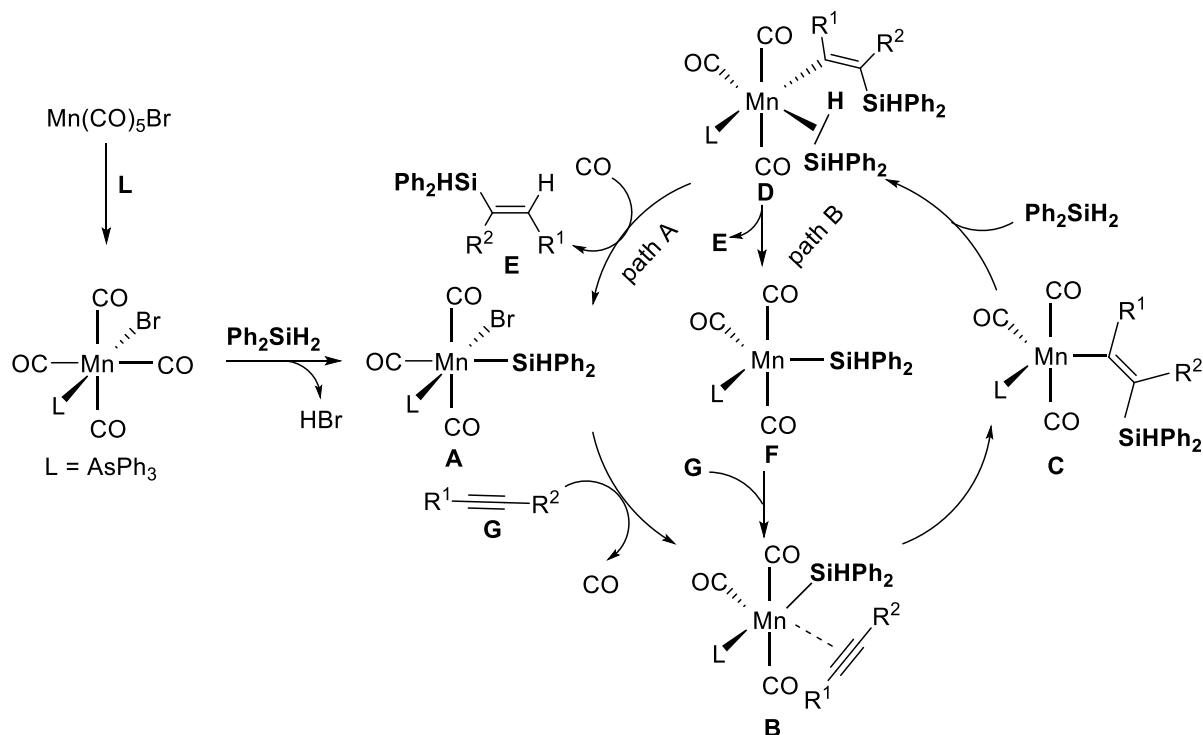
In 2018, Wang and co-workers reported manganese catalysed alkyne hydrosilylation, exhibiting diverse selectivities. Using mononuclear $\text{MnBr}(\text{CO})_5$ and the arsenic ligand AsPh_3 , E-products were formed in a very selective manner. While the dinuclear catalyst $\text{Mn}_2(\text{CO})_{10}$ and LPO (dilauroyl peroxide) enabled the reversed synthesis of Z compounds with good to excellent stereo- and regioselectivity. This kind of reaction stereoselectivity control is unique in the literature. Mechanistic investigation revealed the duality of manganese catalyst where organometallic pathway is involved for E-selective route whereas radical pathway is involved for Z-selective route.³²



Scheme 1.9: Mn-catalyzed regiodivergent hydrosilylation of internal alkynes.

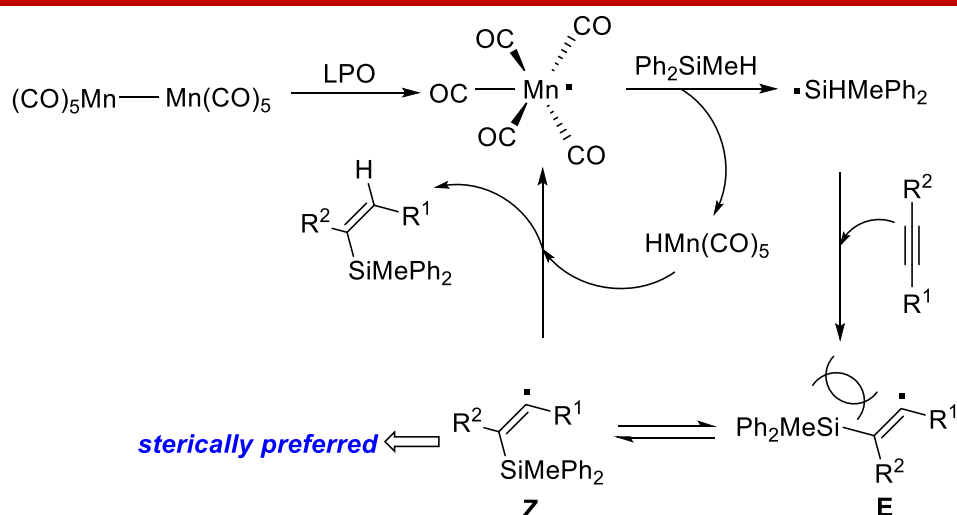
A ligand substitution and silylation initiate the process, producing Mn-Si species A (Scheme 1.10). It goes through a CO/alkyne exchange (B), followed by an alkyne (G) insertion into the Mn-Si bond, resulting in a (β -silyl)alkenyl-Mn intermediate (C). The co-ordination of silane gives species D, followed by σ -bond metathesis leads to the formation of E-selective product

(E) and regenerates Mn-Si species A, thus closing the catalytic cycle (path A) (Scheme 1.10). A different option would be for species D to directly release product E, resulting in intermediate F, which interacted with alkyne (G) to regenerate complex B (path B) (Scheme 1.10).



Scheme 1.10: Proposed mechanism for Mn-catalyzed *E*-selective hydrosilylation of internal alkynes.

In presence of radical initiator, LPO, a radical mechanism was proposed for *Z*-selective hydrosilylation reaction. Homolysis of $\text{Mn}_2(\text{CO})_{10}$ results in $(\text{CO})_5\text{Mn}^\cdot$, which reacts with silane to form $\text{HMn}(\text{CO})_5$ and a silyl radical. The silyl radical reacts with the alkyne to produce *E*- and *Z*-configured alkenyl radicals. These radicals subsequently undergo hydrogenolysis with $\text{HMn}(\text{CO})_5$ to produce the desired *Z*-selective product and regenerate the $(\text{CO})_5\text{Mn}^\cdot$ species. Most likely because the diphenylmethylsilyl group posed a less steric hindrance, hydrogenolysis of the *Z*-alkenyl radical was favoured (Scheme 1.11).



Scheme 1.11: Proposed mechanism for Mn-catalyzed Z-selective hydrosilylation.

1.3 Introduction to alkoxylation of silanes

Silyl ethers are one of the most important silicon compounds due to their wide range of application in silicon polymers³³, protecting group chemistry³⁴, organic-inorganic hybrid materials³⁵ and surface coating chemistry (Figure 1.8).³⁶

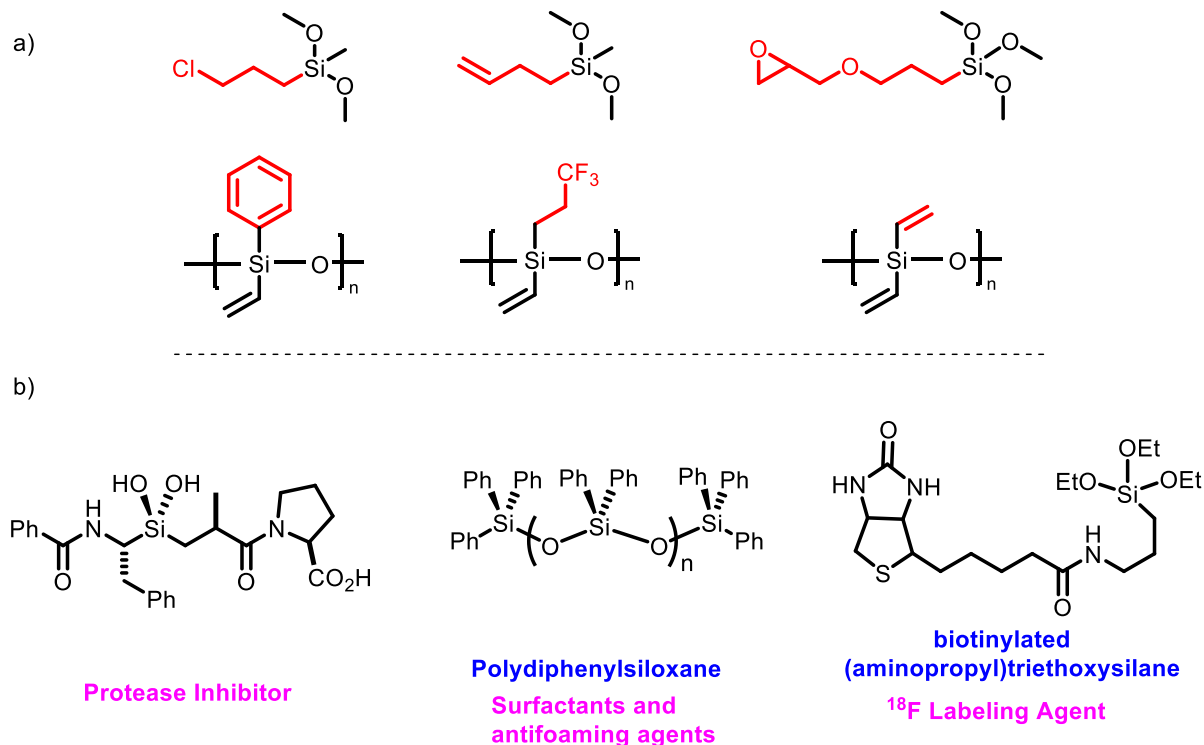
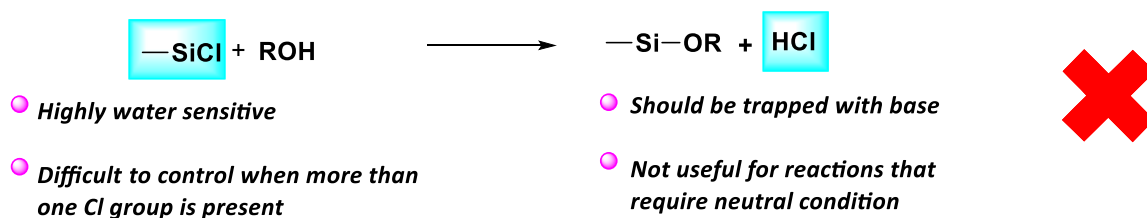


Figure 1.8: (a) Selected functionalized silanes and silicone polymers; (b) examples of organosilanes with industrial application.

Silyl ethers are generally prepared by reacting alcohols and halo silanes in presence of stoichiometric amount of base. However, these methods are not environmentally benign and suffer from several drawbacks, such as these methods can't be used when the reaction has to be performed under neutral condition. Furthermore, controlling the degree of condensation is also problematic when several Si-X bonds are present in the substrate. To circumvent these limitations, the most appealing and atom-economic route could be catalytic dehydrogenative silylation of alcohols with hydrosilanes, which produces the clean fuel hydrogen as the sole byproduct (Figure 1.9).³⁷

Traditional synthesis



Catalytic synthesis

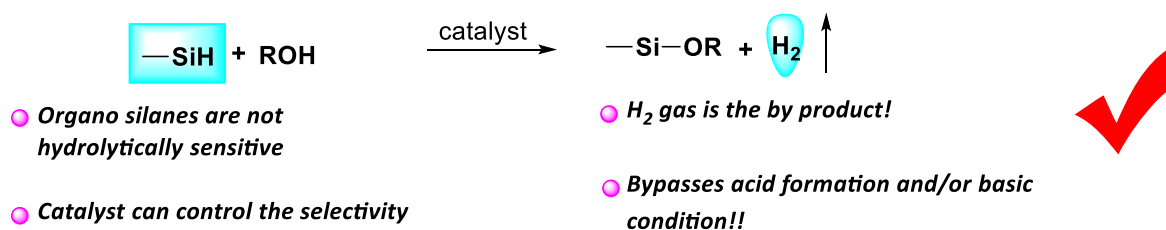
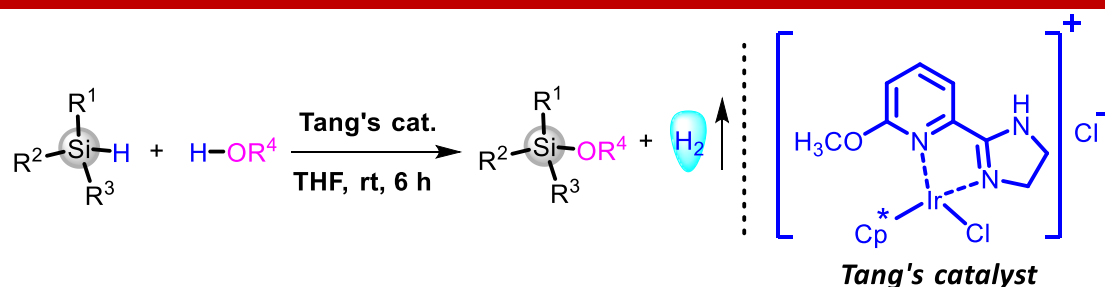


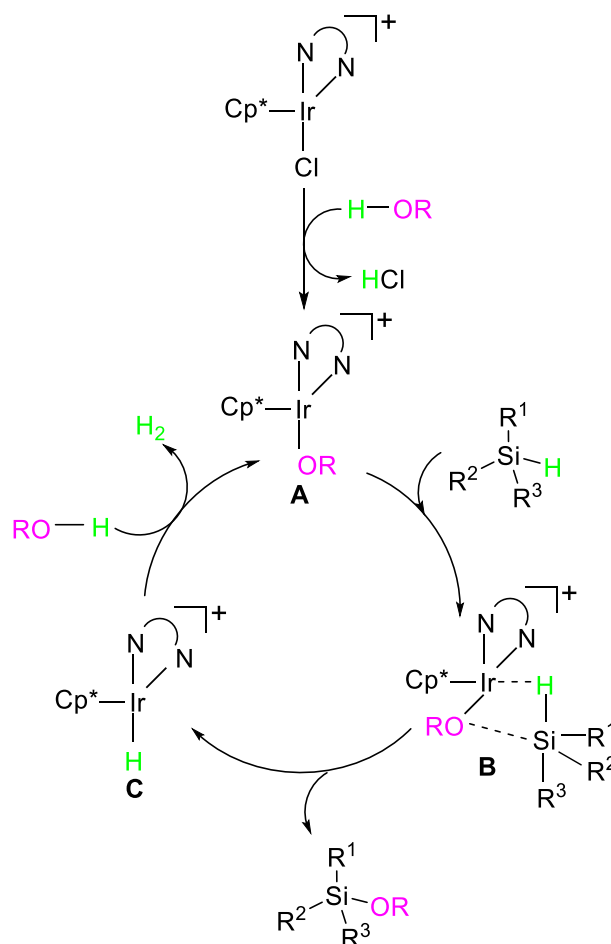
Figure 1.9: Traditional vs catalytic synthesis of alkoxy silanes.

1.3.1 Alkoxylation of silanes by noble metals

The hydroxylation and alkoxylation of organosilanes to yield hydrogen gas and silanols or silyl ethers were successfully carried out by Luo and co-workers using an Ir catalyst. This methodology tolerated a variety of sterically hindered silanes containing alkyl, aryl, and ether groups satisfactorily (Scheme 1.12).³⁸ A plausible mechanism was proposed on the basis of experimental findings and earlier publications (Scheme 1.13). Chloride would first be released from the 18-electron complex, and then alcohol would be coordinated to form the active catalyst A. Through transition state B, subsequent σ -metathesis with silane produced the product as well as the iridium hydride species C. The active catalyst A would be regenerated by further eliminating the molecular hydrogen through a similar kind of σ -metathesis.



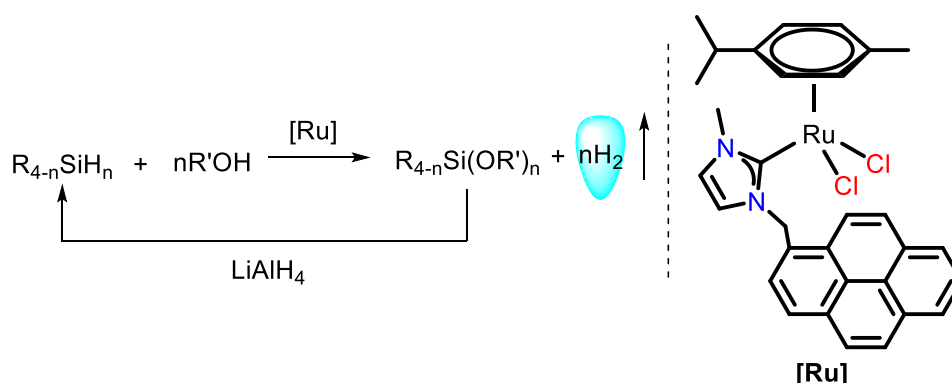
Scheme 1.12: Ir-catalyzed alkoxylation of silanes.



Scheme 1.13: Proposed mechanism for Ir-catalyzed alkoxylation of silanes.

Mata and co-workers reported an efficient Ru based catalyst, $[\text{Ru}(\text{p-cym})(\text{Cl})_2(\text{NHC})]$, for the simultaneous synthesis of molecular hydrogen and silyl ether during the room-temperature coupling of silanes and alcohols. Silyl ether could be used in the silicone industry or recycled into the appropriate hydrosilane by using lithium aluminium hydride (LiAlH_4) or other reducing agents. The ruthenium catalyst is robust enough to carry out the reactions without the need for any additional additives or particular safety measures like inert atmospheres or high temperatures. The hydrosilane/alcohol mixture is stable, non-toxic, versatile, and can be

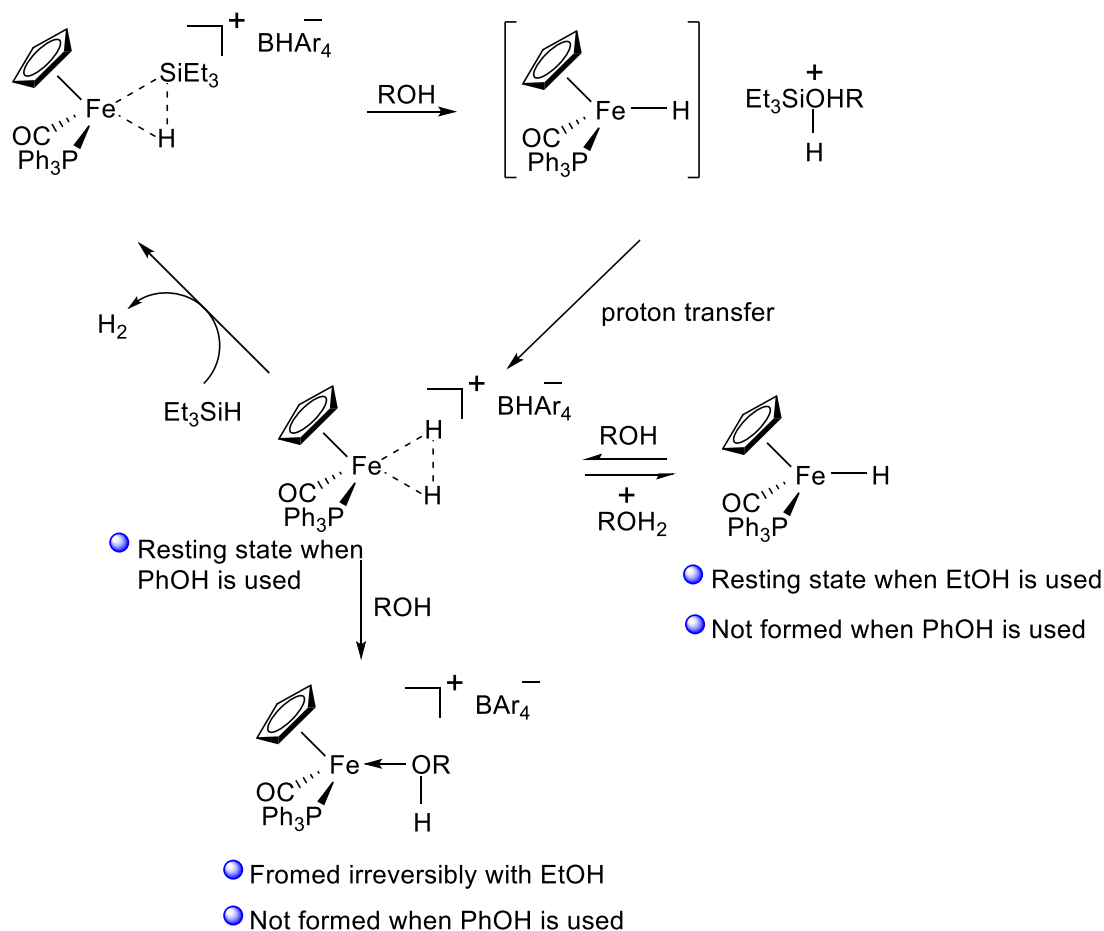
utilised with a wide range of silanes and alcohols. These characteristics expand the range of possible uses for the silane/alcohol pair as a reliable liquid hydrogen oxygen carrier (LOHC) in the automotive sector (Scheme 1.14).³⁹



Scheme 1.14: Ru-catalyzed alkoxylation of silanes.

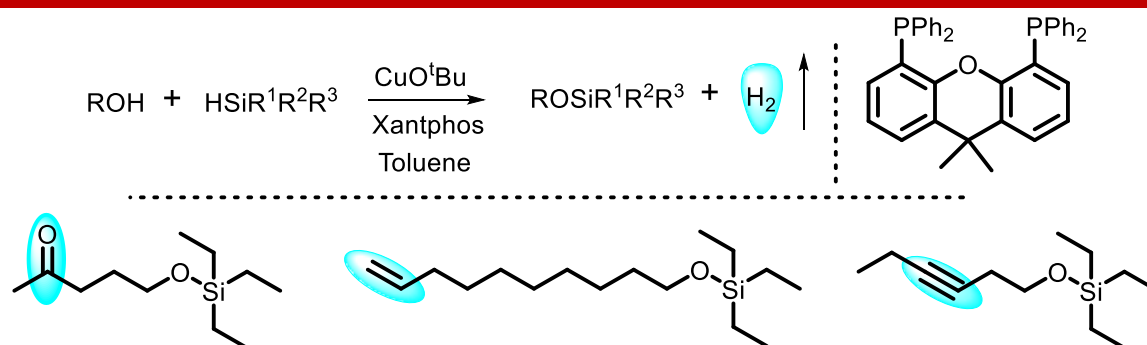
1.3.2 Alkoxylation of silanes by base metals

In 1998 Brookhart and co-workers reported silane alcoholysis, catalysed by $[Cp(CO)PPh_3Fe]^+$ fragment in presence of non-coordinating counter ion BAR_4^- ($Ar = 3,5-(CF_3)_2C_6H_3$). Catalyst deactivation happens rapidly when ethanol is used. But when phenol is used, the catalytic process keeps going until all of the phenol has been consumed. Low temperature NMR spectroscopy has shown that the formation of the silyl ether and the η^2-H_2 complex occurs when an alcohol is added to the iron silane complex. The next step of the reaction pathway, however, depends on the type of alcohol used. The neutral iron hydride complex, which is the catalyst's resting state, is easily formed when ethanol is present by deprotonating the dihydrogen complex. When this species is reprotonated to give the dihydrogen complex, ethanol replaces H_2 effectively to put an end to the catalytic cycle. But unlike ethanol, phenol doesn't interact with the dihydrogen complex in the same way. Phenol neither deprotonates the dihydrogen complex nor displaces H_2 from the metal centre. So, high turnover number can be achieved with phenol as neither of pathway is available for catalyst deactivation (Scheme 1.15).⁴⁰

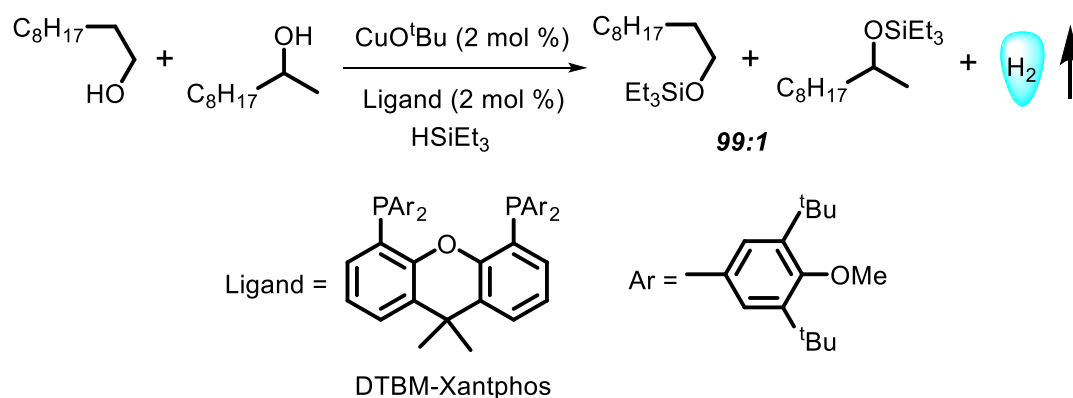


Scheme 1.15: Fe-catalyzed alkoxylation of silanes.

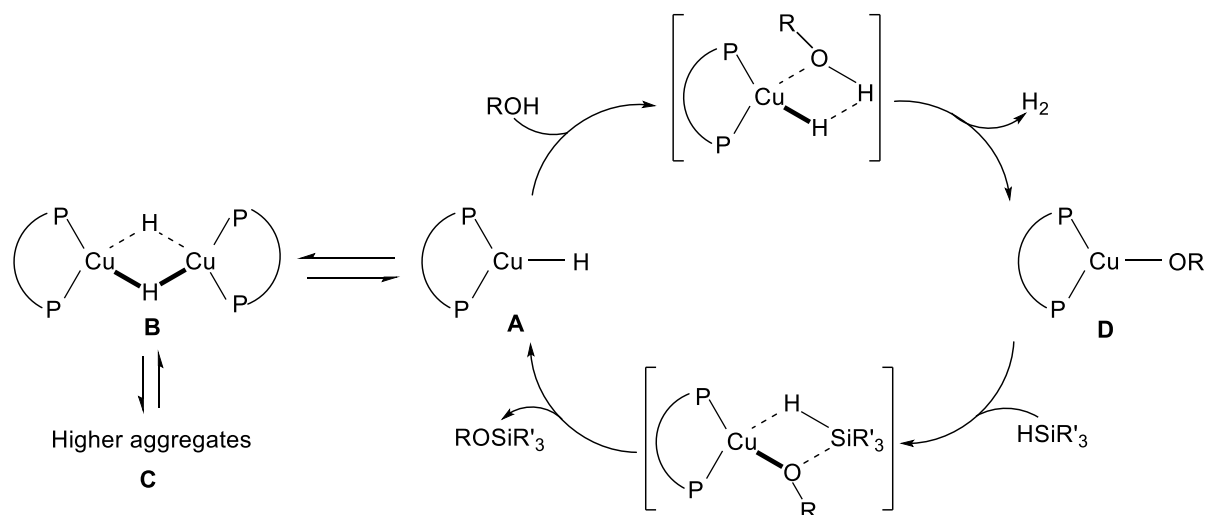
In 2005, Sawamura and co-workers reported xanthene ligated Cu(I) complexes as efficient catalysts for dehydrogenative alcohol silylation with very high activity and wide substrate scope. In fact, silyl ethers of 9-decen-1-ol, 3-hexyn-1-ol, 5-hydroxy-2-pentanone were obtained in good yields while the unsaturated bonds remained intact (Scheme 1.16). The selective silylation of a sterically less congested hydroxy group over a more congested one with relatively small silanes, such as PhMe_2SiH and Et_3SiH , was another benefit of this catalytic system (Scheme 1.17). Phosphine ligated Cu(I) hydride A species was proposed to be the active species, which remains in equilibrium with dimer B or higher aggregates C that are less active or inactive. Through σ -bond metathesis, hydride A and ROH react to form alkoxocopper(I) D and H_2 . In the next step, a metathesis occurred between silane and D, affording silyl ether and A (Scheme 1.18).⁴¹



Scheme 1.16: Cu(I)-catalyzed alkoxylation of silanes.



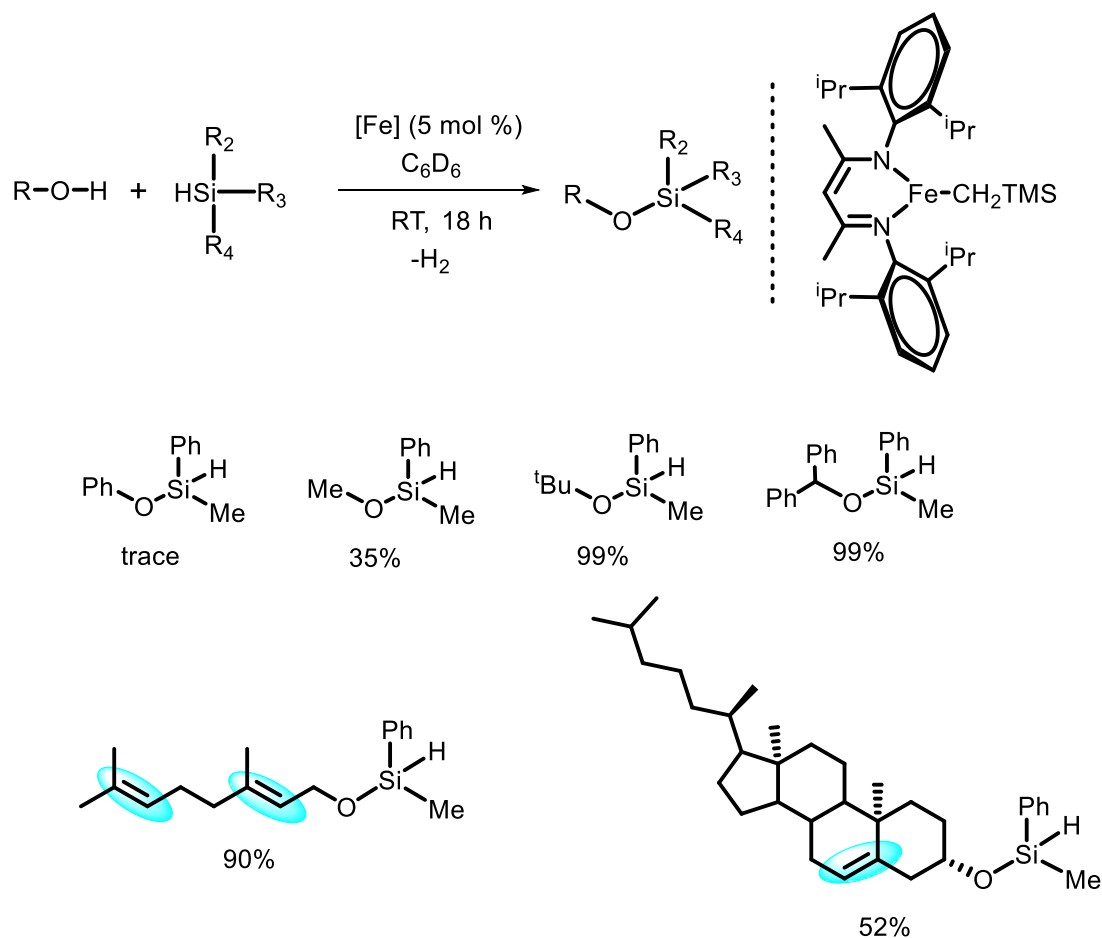
Scheme 1.17: Selective silylation of a primary alcohol in presence of a secondary alcohol.



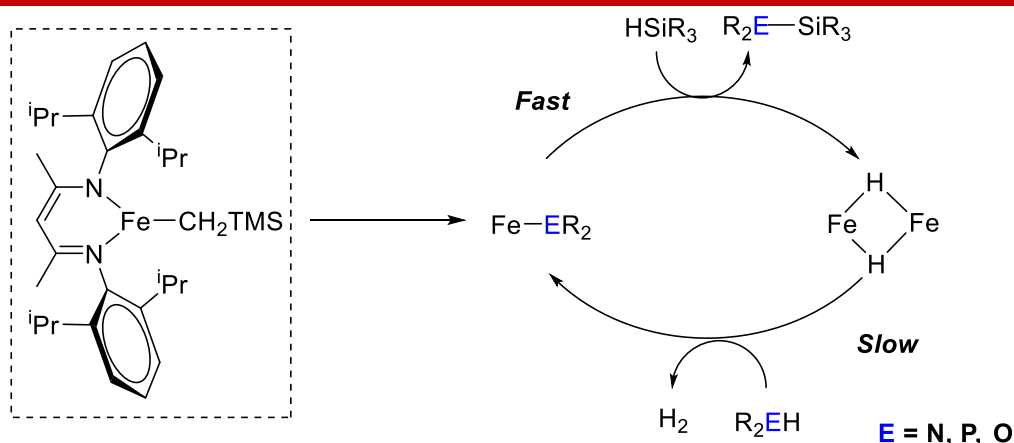
Scheme 1.18: Proposed mechanism of Cu(I) catalyzed silylation.

In 2020, Webster and co-workers reported an iron catalysed dehydrocoupling of silanes with amines, alcohols and phosphines. However, the type of alcohol used seems to matter, and there is an intriguing difference in reactivity between phenol and aliphatic alcohols. For e.g., phenol only yields a very small quantity of product while aliphatic alcohols generate siloxane practically quantitatively (except MeOH). Numerous complex organic motifs, such as (-)

menthol, cholesterol, linalool, and β -citronellol, can be heterodehydrocoupled to produce the silylated product without any sign of double bond functionalization or isomerization (Scheme 1.19). After a thorough mechanistic investigation, it was concluded that the rate-limiting step was most likely the protonolysis of an iron hydride dimer to generate an iron-amido and release hydrogen. Deuterium labelling experiments indicated a modest primary KIE, which is compatible with rate limiting protonolysis and suggests that the RLS occurs via a nonlinear transition state (Scheme 1.20).⁴²



Scheme 1.19: Fe-catalyzed alkoxylation of silanes.



Scheme 1.20: Proposed mechanism of Fe-catalysed silylation.

1.4 Introduction to asymmetric hydrogenation

Chirality now plays a significant part in the synthesis and creation of pharmaceuticals. The majority of newly discovered medicines are chiral. Drugs' interaction with biological targets such as proteins, nucleic acids, and cellular membranes determines a large portion of their pharmacological activity. A chiral medication may have one enantiomer that is a treatment for a certain ailment, while the other enantiomer of the same molecule may not only be harmful but also inactive. As a result, chirality is crucial in the world of pharmaceuticals. In the design and synthesis of pharmaceuticals, it is essential to synthesise a molecule as a single enantiomer. For e.g., patients with Parkinson's disease are treated with Dopa which is chiral. It has been found that only one enantiomer of this molecule is effective in restoring nerve function while the other enantiomer is not effective rather toxic (Figure 1.10).⁴³ So, only one enantiomer of the medicine must be marketed.

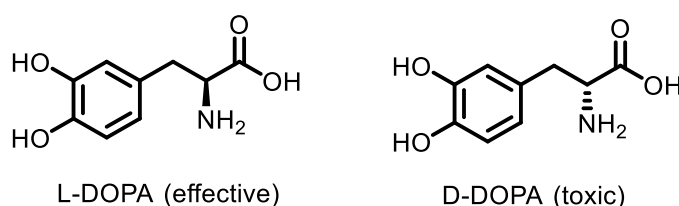


Figure 1.10: Structure of two enantiomers of Dopa.

In fact, it is not just pharmaceuticals which must be produced in enantiomerically pure form. In the USA, the Japanese beetle, *Popillia japonica*, is a well-known pest that harms a number of ornamental plants and agricultural crops. The pheromone of this species, japonilure, a γ -lactone isolated from virgin females, has been employed in traps to entice males. The structure of japonilure was determined to be (R, Z)-5-(1-decenyl) oxacyclopentan-2-one. Small

quantities of its (S, Z)-isomer substantially inhibit the male response. Given the industrial importance of japonilure, it is really very important to synthesize this molecule in high optical purity (Figure 1.11).⁴⁴

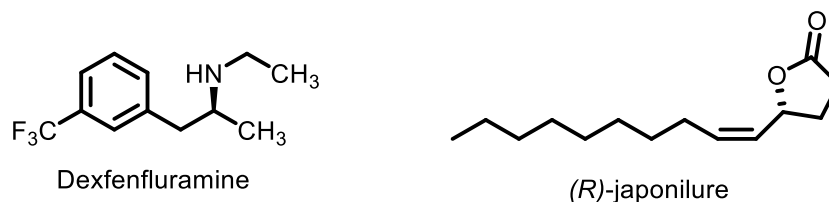


Figure 1.11: Structure of dexfenfluramine and (R)-japonilure.

Enantiomerically pure substances are prepared most efficiently by using asymmetric catalysis. Asymmetric catalysis achieves the objectives of green technique for the synthesis of chiral compounds by producing less waste and showing high atom economy and high efficiency. In asymmetric catalysis, transition metal catalysed asymmetric hydrogenation of unsaturated compounds (olefins, ketones, imines) is the most widely used method to prepare chiral compounds.

When an prochiral olefin binds with an achiral metal-ligand complex (achiral catalyst), two enantiomeric complexes are formed which react at equal rates to give achiral products. However, when a prochiral olefin binds with a chiral metal-ligand complex (chiral catalyst), diastereomeric complexes are formed. Since diastereomers have different chemical properties, they undergo reaction at different rate. This bias in the reaction rate can give one enantiomer preferentially over the other.

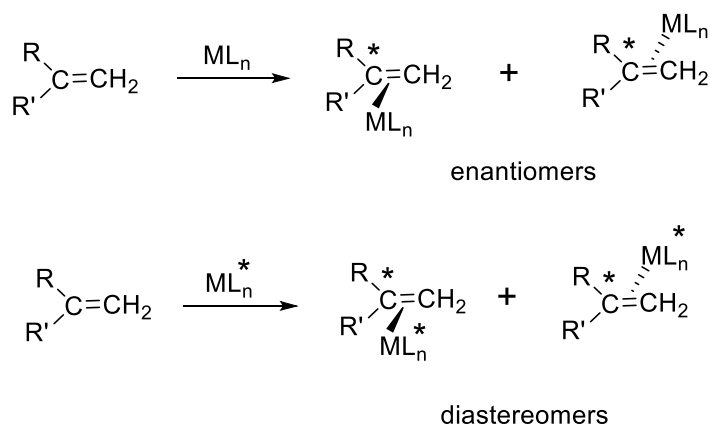
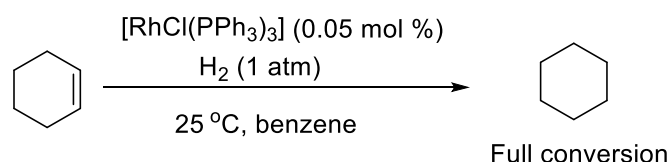
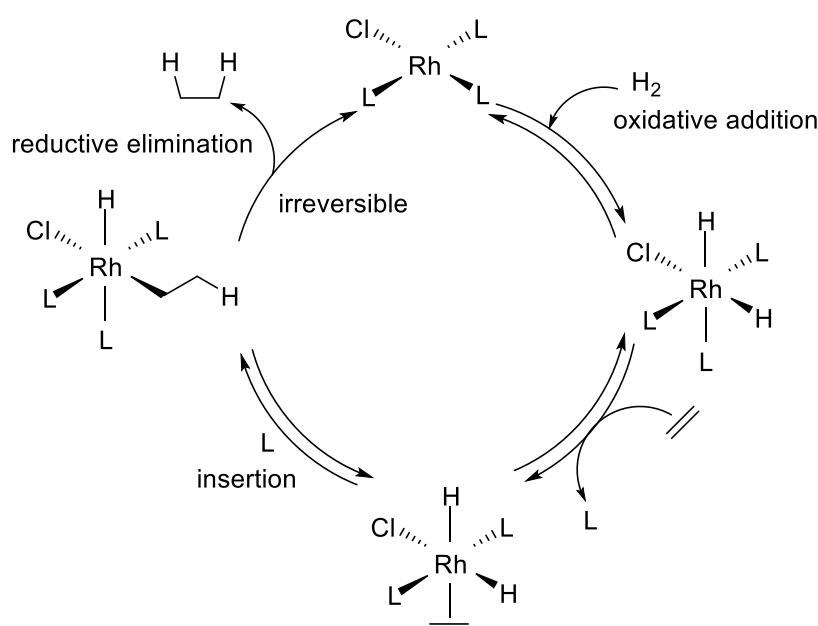


Figure 1.12: Diastereomeric and enantiomeric substrate-catalyst complex.

Wilkinson reported one of the first instances of a homogeneous transition metal catalyst for hydrogenation in 1966. Alkenes were hydrogenated using hydrogen gas and $[\text{RhCl}(\text{PPh}_3)_3]$ as the catalyst precursor under mild reaction condition (Scheme 1.21). Scheme 1.22 depicts the catalytic cycle for hydrogenation of alkenes.⁴⁵



Scheme 1.21: Hydrogenation of cyclohexane by Wilkinson's catalyst.



Scheme 1.22: Mechanism of hydrogenation of alkenes using Wilkinson's catalyst.

The catalytic cycle proceeds with the oxidative addition of hydrogen to the 16-electron Rh^+ species to produce the 18-electron dihydride Rh^{3+} complex. Then the olefin coordinates to rhodium by replacing triphenylphosphine. Migratory insertion of the olefin into the Rh-H bond, followed by reductive elimination gives the hydrogenated product. Triphenylphosphine coordinates again to form the 16-electron Rh^+ species to continue the catalytic cycle (Scheme 1.21). Different functional groups such as keto, nitro, esters, hydroxyl, cyano, chloro, carboxylic acids were well tolerated under the reaction condition.

Despite the initial success of Wilkinson's catalyst $[\text{RhCl}(\text{PPh}_3)_3]$ and the cationic RhL_2^+ catalyst (developed later by Schrock and Osborn) in hydrogenation of unsaturated organic compounds, enantioselectivity remained a challenge in the face of rising demands for chiral bioactive

molecules. By substituting triphenylphosphine with chiral monophosphines in the Wilkinson's catalyst in 1968, Knowles and Horner unlocked the possibility of asymmetric hydrogenation.

1.4.1 Asymmetric hydrogenation by noble metals

By substituting triphenylphosphine with chiral monophosphines in the Wilkinson's catalyst, Knowles and Horner first unlocked the potential of asymmetric hydrogenation. In 1968, they independently reported the first asymmetric hydrogenation of olefins by using chiral Rh complexes with low enantioselectivity (3-15%).^{46, 47} Kagan reported improvements to this system for the asymmetric hydrogenation of unsaturated prochiral acids in 1971 using an in situ generated catalyst made of rhodium and a chiral diphosphine ligand, obtained from (+)-ethyl tartrate, DIOP and reported 72% ee (Figure 1.13).⁴⁸

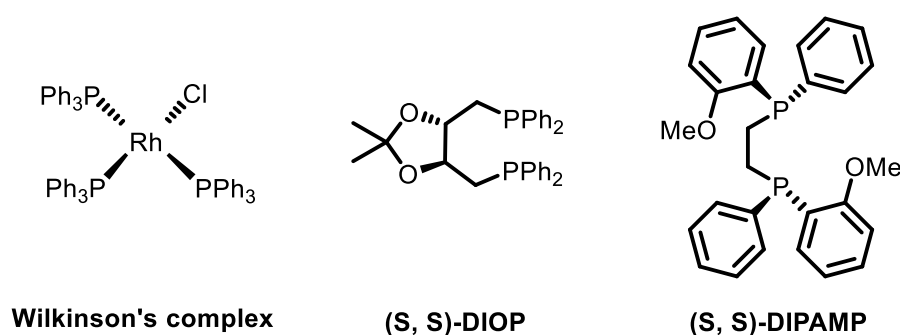
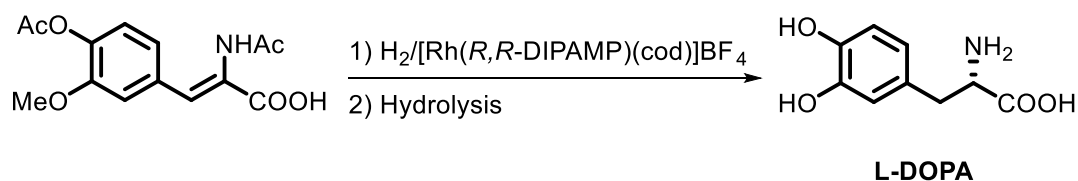


Figure 1.13: Early achievements in asymmetric hydrogenation.

Shortly after him, Knowles synthesized C₂-symmetric ligand DIPAMP and commercialized the L-DOPA synthesis which is used to treat Parkinson's disease with 95% ee. For this remarkable achievement Knowles received the Noble prize in 2001 (Scheme 1.23).⁴⁹



Scheme 1.23: Synthesis of L-DOPA via asymmetric hydrogenation.

The discovery of BINAP is another significant development in asymmetric hydrogenation. In the 1980s, Noyori developed the C₂-symmetric ligand BINAP and successfully implemented in Rh-catalyzed asymmetric hydrogenation of α-(acylamino)acrylic acids.^{50, 51} However, the real breakthrough came when Noyori and Takaya developed a BINAP-Ru dicarboxylic acid

complex and applied it successfully in the asymmetric hydrogenation of various functionalized olefins.⁵² In the 1990s, Noyori made another significant discovery about BINAP when he found that BINAP-Ru diamine complexes were effective catalysts for the asymmetric hydrogenation of unfunctionalized ketones.⁵³ After seeing the success story of BINAP, chemists modified the structure of BINAP in many different ways and several excellent ligands such as H₈-BINAP⁵⁴, SEGPHOS⁵⁵, Tunephos⁵⁶ were reported afterwards (Figure 1.14).

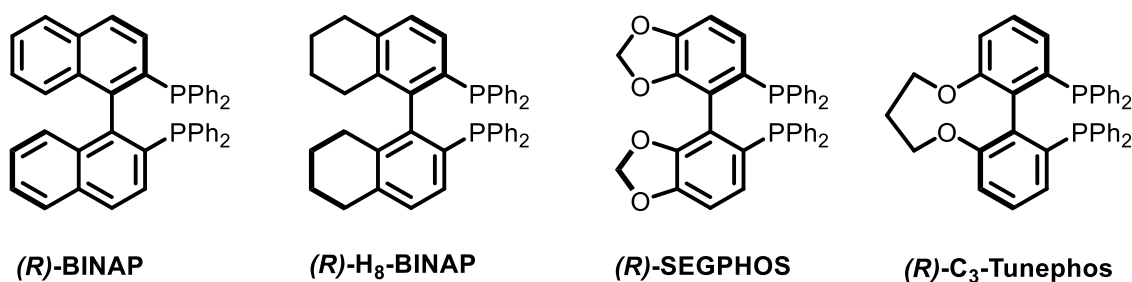
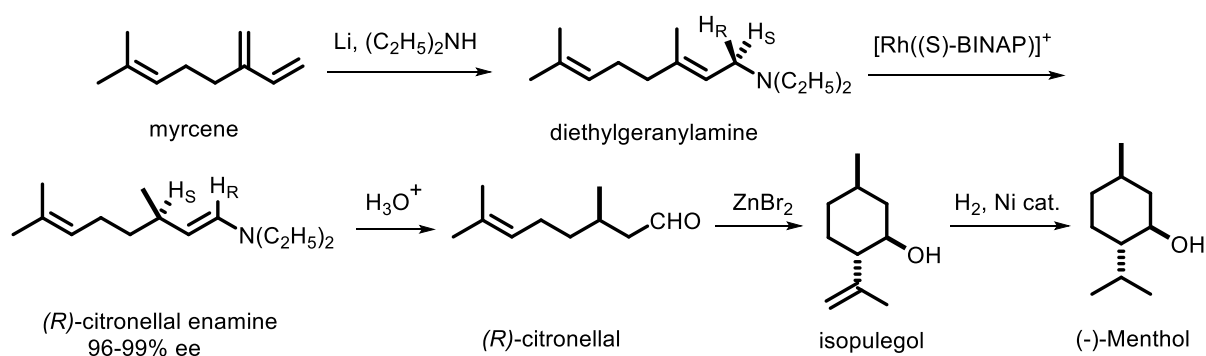


Figure 1.14: Atropisomeric biaryl bisphosphine ligands.

One of the most widely used fragrance compounds globally is (-)-Menthol. In the 1950s, the Japanese company Takasago began producing menthol. While their starting compounds and procedures changed over time, they made a significant advancement by developing the first asymmetric (-)-menthol synthesis in the 1980s, which is still utilised today by employing Rh-BINAP catalyst system (Scheme 1.24).⁵⁷



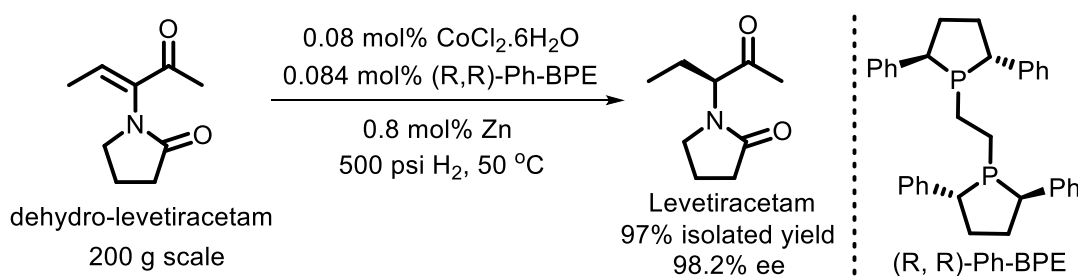
Scheme 1.24: Takasago (-)-Menthol process.

1.4.2 Asymmetric hydrogenation by base metals

Asymmetric hydrogenations are typically performed with precious metals such as rhodium, ruthenium & iridium. However, these precious metals are the least abundant transition metals

on earth's crust and in the danger zone of being depleted within the next 50 years which poses a serious threat from a sustainability perspective for this field. To combat these difficulties, enough attention has been paid in recent times for the developments of catalysts based on 3d transition metals such as Mn, Fe, Co, Ni & Cu, mainly because of their greater earth abundance, lower cost, lower toxicity & environmentally benign nature as compared to noble metals.

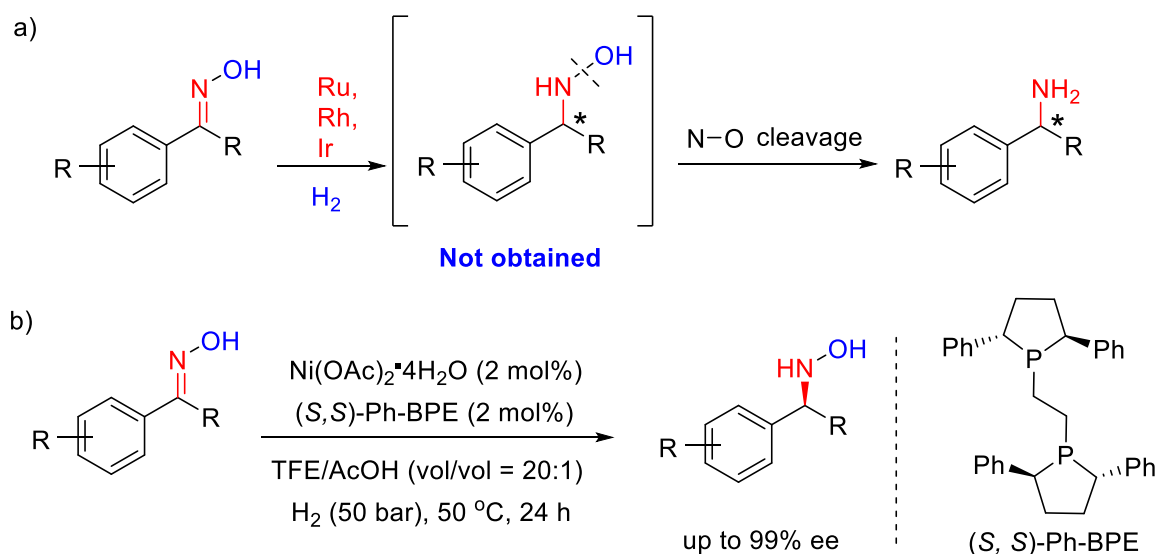
A breakthrough was achieved in the field of base metal catalysed asymmetric hydrogenation when Chirik and co-workers developed a zinc-activation technique suitable for high-throughput reaction discovery that helped to locate several cobalt-phosphine mixtures for the asymmetric hydrogenation of functionalized alkenes.⁵⁸ They successfully carried out the asymmetric synthesis of Levetiracetam, a drug to treat epilepsy at 200 g scale with only 0.08 mol% cobalt catalyst loading with excellent enantioselectivity which showed initial promise for the competence of base metals with noble metals (Scheme 1.25). Stoichiometric studies revealed that facile ligand dissociation takes place from cobalt catalyst (*R, R*)-Ph-BPE-CoCl₂ (II) in methanol. However, in presence of Zn, Co (II) is reduced to Co (I), which diminishes phosphine lability and increases inertness to MeOH substitution.⁵⁸



Scheme 1.25: Cobalt catalyzed AH of dehydro-levetiracetam.

As hydroxylamines frequently respond to biotransformations with both organic and inorganic molecules, they appear to play important roles in biological activities and/or physiological processes. It's still quite difficult to catalytically reduce oximes to hydroxylamines while maintaining the N-O group intact. Due to the repulsion between the lone pairs of the N and O atoms in the N-O group, the N-O bond has a tendency to quickly break under reduction conditions. Zhang and co-workers, solved this long-standing problem by developing Ni catalysed asymmetric hydrogenation of oximes to chiral hydroxylamines in presence of AcOH. A readily available bisphosphine nickel complex was used for this transformation which afforded a series of chiral hydroxylamines and ethers with excellent yield and enantioselectivity. Computational studies revealed that several noncovalent interactions

between the catalyst and the substrate favour to achieve such a high reactivity and selectivity (Scheme 1.26).⁵⁹



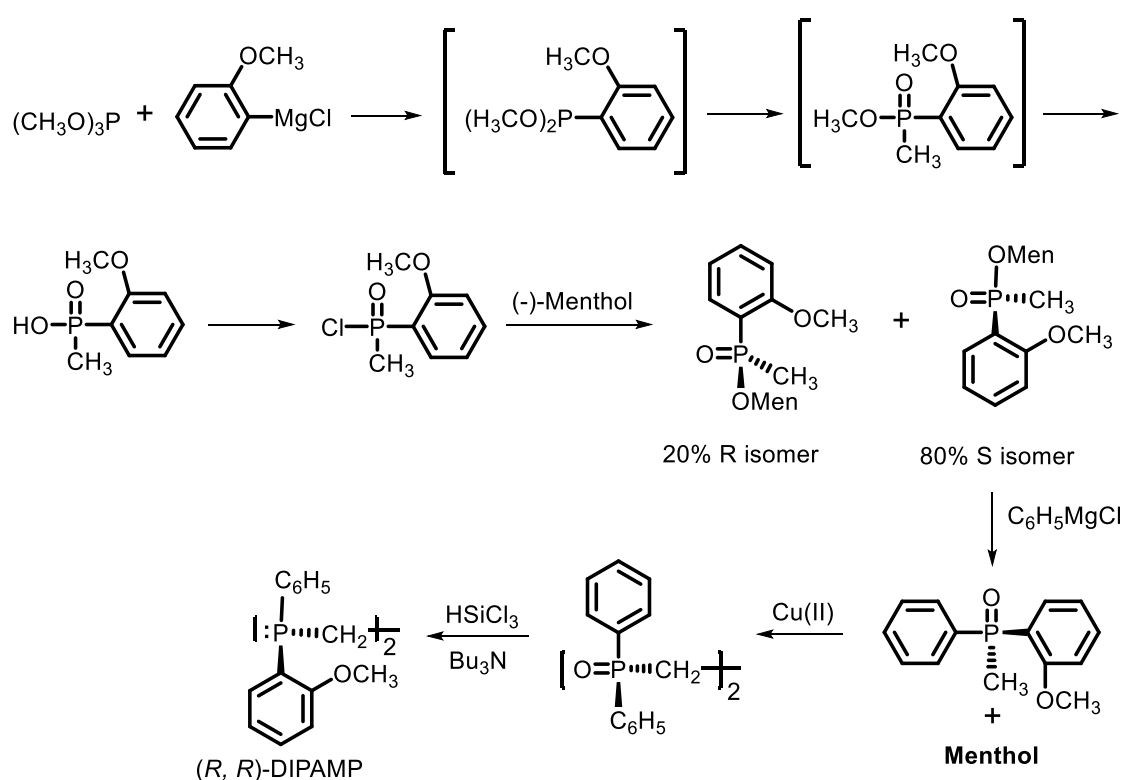
Scheme 1.26: a) Noble metal catalyzed asymmetric hydrogenation of oxime to amine, b) Ni-catalysed asymmetric hydrogenation of oximes to chiral hydroxylamines.

1.5 Setting the goals

1.5.1 Statement of the problem

i) Organo-silanes have found numerous application in drug discovery, bio-medical agents, electronics, photonics. Organosilane polymers are used as oil, rubbers, resins, adhesives, coatings. In addition to this, organosilicon compounds are also versatile synthetic intermediates in organic synthesis. Beside others, two approaches to prepare such organosilicon compounds are, i) catalytic hydrosilylation of alkynes and ii) catalytic alkoxylation of silanes. Over the past few decades, significant advancement has been achieved in both methods. However, these achievements were primarily based on noble transition metal (4d, 5d) catalysts. These metals have very low natural abundance on earth's crust, thus very costly. This poses a great threat to the field from economic as well as sustainability perspective. To address these challenges, researchers have employed naturally abundant and cost-effective 3d transition metals for such transformation. Though it could resolve the issue of high cost and sustainability, the harsh reaction conditions and use of highly reactive reagents often limit their practical applicability. Thus, there is an enormous demand to design concise, practical, sustainable synthetic approaches using 3d transition metal catalysts through which one can perform these transformations under ambient conditions without using any highly reactive reagent.

ii) Asymmetric hydrogenation has remained an important and challenging research area in industry as well as academia since the products obtained are highly useful in pharmaceutical, agrochemical and perfumery industries. Noble metals such as Rh, Ru, Ir along with different chiral bidentate phosphine ligands are routinely used to carry out such transformation. As already discussed, these noble metals are highly scarce on the earth's crust. In addition to this, the bidentate chiral phosphine ligands used in such transformation involve multistep synthesis, thus often making these ligands even costlier than the noble metals. For e.g., the bidentate ligand, DIPAMP, which was utilised for the industrial scale synthesis of drug L-DOPA by asymmetric hydrogenation, involves multiple step synthesis (Scheme 1.27).



Scheme 1.27: Synthetic procedure for DIPAMP.

So, now the scientific community is paying good attention to replace these precious noble metals with earth abundant 3d transition metals. However, simplifying the ligand synthesis remains mostly ignored. Thus, there is a pressing need to develop ligands which could be synthesized in fewer steps.

1.5.2 Objectives

As discussed in the above section, the field of homogeneous catalysis is facing a flux from both the metal as well as ligand synthesis frontier. Focused efforts are needed to streamline this flux.

Thus, our objectives are **i)** design and synthesis of easy-to-use catalytic system based on earth abundant 3d transition metals to prepare organo-silicon compounds under ambient condition without using any highly reactive additives, **ii)** design and synthesis of a chiral bidentate phosphine ligand in a straightforward and concise manner and implement it in asymmetric hydrogenation to prepare chiral compounds.

1.6 References

- 1) Rothenberg, G. *Catalysis: Concepts and Green Applications*, Wiley – VCH: Weinheim, 2008.
- 2) Garrett, C. E.; Prasad, K. *Adv. Synth. Catal.* **2004**, *346*, 889-900.
- 3) Li, C.; Liu, Y. *Bridging Heterogeneous and Homogeneous Catalysis: Concepts, Strategies, and Applications*, Wiley – VCH: Weinheim, 2014.
- 4) Astruc, D. *Organometallic chemistry and catalysis*, Springer: Berlin, New York, 2002.
- 5) van Leeuwen, P. W. N. M. *Homogeneous Catalysis-Understanding the Art*; Kluwer Academic Publishers: Dordrecht, 2004.
- 6) Cornils, B.; Herrmann, W. A.; Beller, M.; Paciello, R. *Applied Homogeneous Catalysis with Organometallic Compounds*; Wiley-VCH, Weinheim, 1996.
- 7) a) Rochow, E. G. *Silicon and Silicones: About Stone-age Tools, Antique Pottery, Modern Ceramics, Computers, Space Materials and How They All Got That Way*, Springer, Berlin, 1987. b) Murugavel, R.; Voigt, A.; Walawalkar, M. G.; Roesky, H. W. *Chem. Rev.* **1996**, *96*, 2205–2236. c) Fleming, I.; Barbero, A.; Walter, D. *Chem. Rev.* **1997**, *97*, 2063–2192.
- 8) Marciniec, B. *Coord. Chem. Rev.* **2005**, *249*, 2374–2390.
- 9) Miller, R. D.; Michl, J. *Chem. Rev.* **1989**, *89*, 1359-1410.
- 10) Denmark, S. E.; Regens, C. S. *Acc. Chem. Res.* **2008**, *41*, 1486-1499.
- 11) Fleming, I.; Dunoguès, J.; Smithers, R. In *Organic Reactions*; John Wiley & Sons, Inc.: 2004.

-
- 12) a) Tamao, K.; Ishida, N.; Tanaka, T.; Kumada, M. *Organometallics* **1983**, *2*, 1694-1696.
b) Fleming, I.; Henning, R.; Plaut, H. J. *Chem. Soc., Chem. Commun.* **1984**, 29-31.
- 13) Peterson, D. J. *J. Org. Chem.* **1968**, *33*, 780-784.
- 14) Brook, A. G. *Acc. Chem. Res.* **1974**, *7*, 77-84.
- 15) Marciniak, B. *Hydrosilylation: A Comprehensive Review on Recent Advances*, Springer, Poland, 2009.
- 16) Marciniak, B. *Coord. Chem. Rev.* **2005**, *249*, 2374-2390.
- 17) Roy, A. K. *Adv. Organomet. Chem.* **2008**, *55*, 1 – 59.
- 18) Sommer, L. H.; Pietrusza, E. W.; Whitmore, F. C. *J. Am. Chem. Soc.* **1947**, *69*, 188–188.
- 19) Karstedt, B. D. General Electric Company, US3775452A, 1973.
- 20) a) Speier, J. L.; Webster, J. A.; Barnes, G. H. *J. Am. Chem. Soc.* **1957**, *79*, 974-979. b) Belyakova, Z. V.; Pomerantseva, M. G.; Efimova, L. A.; Chernyshev, E. A.; Storozhenko, P. A. *Russ. J. Gen. Chem.* **2010**, *80*, 728-733. c) Rochow, E. G. *J. Am. Chem. Soc.* **1945**, *67*, 963-965.
- 21) Saam, J. C.; Speier, J. L. *J. Am. Chem. Soc.* **1958**, *80*, 4104-4106.
- 22) Karstedt, B. D. Patent DE 2307085 A1, 1973.
- 23) Stein, J.; Lewis, L. N.; Gao, Y.; Scott, R. A. *J. Am. Chem. Soc.* **1999**, *121*, 3693-3703.
- 24) Yamamoto, K.; Hayashi, T.; Kumada, M. *J. Am. Chem. Soc.* **1971**, *93*, 5301-5302.
- 25) Watanabe, H.; Asami, M.; Nagai, Y. *J. Organomet. Chem.* **1980**, *195*, 363-373.
- 26) Markó, I. E.; Stérin, S.; Buisine, O.; Mignani, G.; Branlard, P.; Tinant, B.; Declercq, J.-P. *Science* **2002**, *298*, 204-206.
- 27) Markó, I. E.; Stérin, S.; Buisine, O.; Berthon, G.; Michaud, G.; Tinant, B.; Declercq, J.-P. *Adv. Synth. Catal.* **2004**, *346*, 1429-1434.
- 28) Chalk, A. J.; Harrod, J. F. *J. Am. Chem. Soc.* **1965**, *87*, 16-21.

-
- 29) Marciniak, B.; Gulinski, J.; Urbaniak, W.; Kornetka, Z. W. *Comprehensive Handbook on Hydrosilylation*; Pergamon: Oxford, UK, 1992.
- 30) Schroeder, M. A.; Wrighton, M. S. *J. Organomet. Chem.* **1977**, *128*, 345-358.
- 31) Hu, M.-Y.; He, P.; Qiao, T.-Z.; Sun, W.; Li, W.-T.; Lian, J.; Li, J.-H.; Zhu, S.-F. *J. Am. Chem. Soc.* **2020**, *142*, 16894–16902.
- 32) Yang, X.; Wang, C. *Angew. Chem., Int. Ed.* **2018**, *57*, 923–928.
- 33) a) Pouget, E.; Tonnar, J.; Lucas, P.; Lacroix-Desmazes, P.; Ganachaud, F.; Boutevin, B. *Chem. Rev.* **2010**, *110*, 1233-1277. b) Cheng, C.; Watts, A.; Hillmyer, M. A.; Hartwig, J. F. *Angew. Chem., Int. Ed.* **2016**, *55*, 11872-11876.
- 34) Protection for the Hydroxyl Group. *Greene's Protective Groups in Organic Synthesis*, 5th ed.; Wuts, P. G. M., Ed. John Wiley & Sons, Inc.: 2014; pp 17–471.
- 35) a) Zou, H.; Wu, S. S.; Shen, J. *Chem. Rev.* **2008**, *108*, 3893-3957. b) Brook, M. A. *Silicon in Organic, Organometallic, and Polymer Chemistry*; Wiley: New York, 2000. c) Xu, L.-W.; Chen, Y.; Lu, Y. *Angew. Chem., Int. Ed.* **2015**, *54*, 9456-9466.
- 36) Lejars, M.; Margaillan, A.; Bressy, C. *Chem. Rev.* **2012**, *112*, 4347-4390.
- 37) Gao, D.; Cui, C. *Chem. - Eur. J.* **2013**, *19*, 11143-11147.
- 38) Luo, N.; Liao, J.; Ouyang, L.; Wen, H.; Zhong, Y.; Liu, J.; Tang, W.; Luo, R. S. *Organometallics* **2020**, *39*, 165–171.
- 39) Ventura-Espinosa, D.; Carretero-Cerdan, A.; Baya, M.; García, H.; Mata, J. A. *Chem.-Eur. J.* **2017**, *23*, 10815–10821.
- 40) Chang, S.; Scharrer, E.; Brookhart, M. *J. Mol. Catal. A* **1998**, *130*, 107–119.
- 41) Ito, H.; Watanabe, A.; Sawamura M. *Org. Lett.* **2005**, *7*, 1869–1871.
- 42) Gasperini, D.; King, A. K.; Coles, N. T.; Mahon, M. F.; Webster, R. L. *ACS Catal.* **2020**, *10*, 6102–6112.

-
- 43) Dollor, H. J. L-DOPA: Plasma pharmacokinetics and conversion to dopamine in the brain, Pennsylvania State University, USA, 1976.
- 44) Tumlinson, J. H.; Klein, M. G.; Doolittle, R. E.; Provcaux, A. T. *Science* **1977**, *197*, 789–792.
- 45) Osborn, J. A.; Jardine, F. H.; Young, J. F.; Wilkinson, G. J. *Chem. Soc.(A) Inorg. Phys. Theor.* **1966**, 1711-1732.
- 46) (a) Knowles, W. S.; Sabacky, M. J. *Chem. Commun.* **1968**, *22*, 1445-1446. b) Knowles, W. S. *Angew. Chem. Int. Ed.* **2002**, *41*, 1998-2007.
- 47) Greber, G.; Kricheldorf, H. R. *Angew. Chem. Int. Ed.* **1968**, *7*, 942-942.
- 48) Dang, T. P.; Kagan, H. B. *Chem. Commun.* **1971**, 481-481.
- 49) Knowles, W. S. *J. Chem. Educ.* **1986**, *63*, 222-225.
- 50) Miyashita, A.; Yasuda, A.; Takaya, H.; Toriumi, K.; Ito, T.; Souchi, T.; Noyori, R. *J. Am. Chem. Soc.* **1980**, *102*, 7932-7934.
- 51) Miyashita, A.; Takaya, H.; Souchi, T.; Noyori, R. *Tetrahedron* **1984**, *40*, 1245-1253.
- 52) Noyori, R.; Ohta, M.; Hsiao, Y.; Kitamura, M.; Ohta, T.; Takaya, H. *J. Am. Chem. Soc.* **1986**, *108*, 7117-7119.
- 53) Ohkuma, T.; Ooka, H.; Hashiguchi, S.; Ikariya, T.; Noyori, R. *J. Am. Chem. Soc.* **1995**, *117*, 2675-2676.
- 54) Zhang, X.; Mashima, K.; Koyano, K.; Sayo, N.; Kumobayashi, H.; Akutagawa, S.; Takaya, H. *Tetrahedron Lett.* **1991**, *32*, 7283-7286.
- 55) Saito, T.; Yokozawa, T.; Ishizaki, T.; Moroi, T.; Sayo, N.; Miura, T.; Kumobayashi, H. *Adv. Synth. Catal.* **2001**, *343*, 264-267.
- 56) Zhang, Z.; Qian, H.; Longmire, J.; Zhang, X. *J. Org. Chem.* **2000**, *65*, 6223-6226.
- 57) Noyori R. *Adv. Synth. Catal.* **2003**, *345*, 15-32.

58) Friedfeld, M. R.; Zhong, H. Y.; Ruck, R. T.; Shevlin, M.; Chirik, P. J. *Science* **2018**, *360*, 888–893.

59) Li, B.; Chen, J.; Liu, D.; Gridnev, I. D.; Zhang, W. *Nat Chem.* **2022**, *14*, 920-927.

Chapter 2

Radical Iron Breaks the Myth: (E)-selective Hydrosilylation of Alkynes

2.1 Abstract

Hydrosilylation of Alkynes represent one of the most straightforward, atom economical method to prepare organo-silicon compounds. In recent past, iron catalysis has attracted a lot of attention, as it is abundant, affordable, and biocompatible. In addition to this, iron's distinctive electronic structures allow it to mediate different types of chemical reactions. In literature, few reports are there where iron catalysts have been successfully implemented for the hydrosilylation of internal alkynes. However, in all these reports, either organometallic reagents or organic base have been used for the success of the reaction which often creates a problem for the functional group tolerance of the reaction. Thus, development of additive free methodology would be highly useful. To achieve this, we have developed a methodology of iron catalysed (E)-selective hydrosilylation of internal alkynes along with a phosphine ligand without the use of any highly reactive additive. The hydrosilylation reaction exhibited broad substrate scope and tolerated functional groups, such as -Cl, -Br, -OMe, with different types of silanes at 60 to 70 °C. The reaction can easily be scaled up to gram scale. A preliminary mechanistic investigation revealed a radical pathway for the reaction. (E)-selective hydrosilylation proceeding through one electron pathway, is quite uncommon in literature. To the best of our knowledge, this type of phenomenon has not been previously known with base metal catalysts.

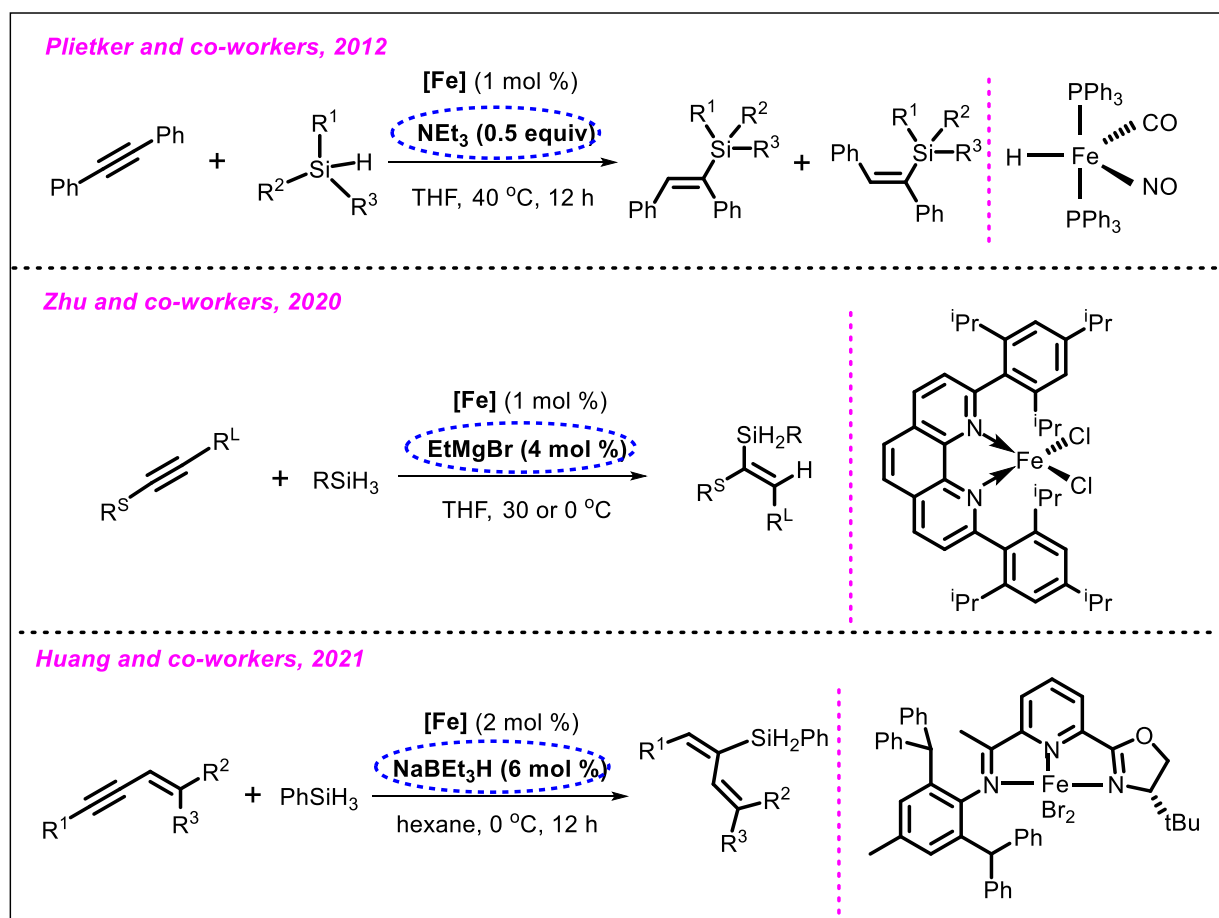
2.2 Introduction

Organosilanes are useful substances with low toxicity and reasonable stability. They have found a wide range of applications for the manufacture of silicone materials such as coatings, adhesives, lubricants¹, defence materials and life science products.² In addition to this, organosilanes are also versatile reagents which can be used in a variety of synthetic transformations.³ Catalytic hydrosilylation of multiple bonds, for example, olefins and alkynes, represent one of the most straightforward way to access organosilanes with perfect atom economy. It is mainly due to this reason; these reactions have attracted tremendous attention from industry as well as academia. In general, noble metals such as Pt (mainly), Pd, Rh, Ru based catalytic systems are used to perform these reactions.⁴ However, these noble metals have very low abundance on the earth crust. Therefore, these metals are highly costly and are going to be finished in near future. It is mainly due to this reason, tremendous

attention has been given to replace these precious metals with earth abundant transition metals such as Fe, Mn, Co, Ni etc. Among these transition metals, iron has the maximum abundance on earth crust, and is inexpensive. Also, it is non-toxic and has unique electronic structure which make iron even more attractive for developing new catalyst in this field.

Internal alkynes are quite challenging substrates for hydrosilylation, due to the following reasons: i) low polarity of C-C triple bond, ii) control of regio and stereo-selectivity, iii) formation of undesired hydrogenation by-products. It is mainly due to these reasons, there is only a handful of reports where iron metal has been successfully utilised to carry out hydrosilylation reaction of internal alkynes. For e.g., in 2012, Plietker and co-workers reported a well-defined iron hydride complex $[\text{FeH}(\text{CO})(\text{NO})(\text{PPh}_3)_2]$, for hydrosilylation of internal alkynes at 40-60 °C in THF solvent.⁵ However, 0.5 equivalent NEt_3 is needed for the success of the reaction. In 2020, Zhu and co-workers reported iron complexes bearing 2,9-diaryl-1,10-phenanthroline ligands for regio-selective alkyne hydrosilylation.⁶ Here, EtMgBr has to be used as a reductant to generate the active catalyst. In 2021, Huang and co-workers reported an iron catalysed regio and stereo-selective hydrosilylation of 1,3-enynes to access 1,3-dienylsilanes. Here, NaBEt_3H has to be used as an activator for the success of the reaction.⁷ These highly reactive reagents mainly help to generate low valent iron species which acts as an actual catalyst in the reaction. However, these highly reactive additives create a problem for functional group tolerance of the reaction.

In addition to this, the complexity of the ligand component is frequently underappreciated, and even completely ignored, in the development of novel potent homogeneous catalysts. Undoubtedly, a perfect catalytic system consists of affordable, stable, and modular ligands in addition to a readily available, less toxic metal center, like iron or manganese. When examining freshly revealed ligand scaffolds, it is apparent that a few of them can only be produced in small quantities under unique circumstances, such as in a glovebox. The development of useful & practical ligands is still a challenge, particularly for non-noble metal catalysts. To bridge this gap, development of an easy to use iron catalysed methodology without the use of a highly reactive reagent would be highly useful.

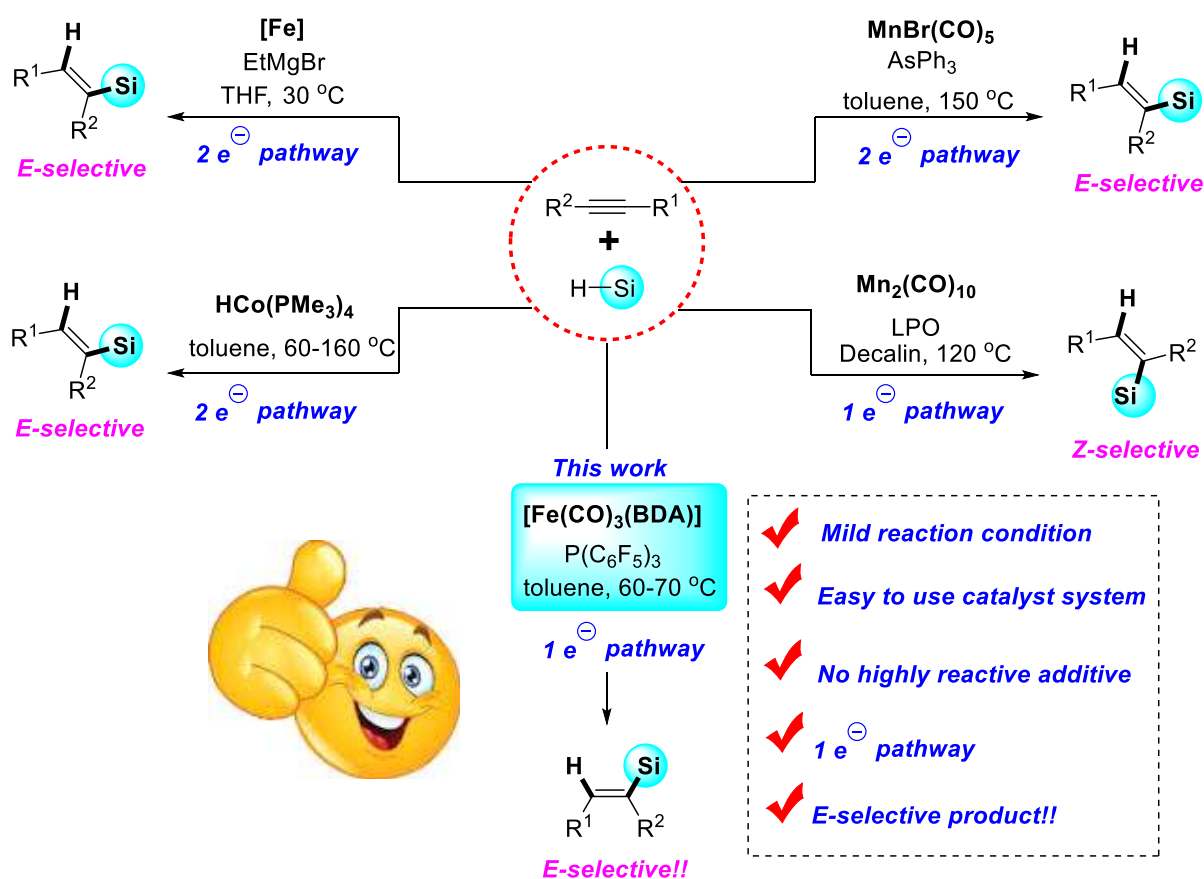


Scheme 2.1: Iron catalysed hydrosilylation of alkynes.

Another challenge in hydrosilylation reaction by base metals lies in lack of fundamental understanding of the reaction mechanism. Key mechanistic insights are much needed to come up with a better base metal catalyst. In case of olefin hydrosilylation by noble metals, the reaction is known to proceed through Chalk-Harrod mechanism, involving Si-H oxidative addition, alkene insertion into M-H bond, and reductive elimination of the corresponding alkylsilane.⁸ In order to explain the generation of unsaturated by-products, a modified Chalk-Harrod mechanism, involving alkene insertion into M-SiR₃ bond, has also been proposed.⁹ However, base metals tend to participate in one electron reaction pathway and often adopt high spin electronic configuration which make the study of the reaction mechanism much more difficult.¹⁰ It has also been observed that the thoroughly studied base metal catalysts often operate through widely varied mechanism. For example, in 2018, Wang and co-workers reported hydrosilylation of alkynes where E-products were achieved with mononuclear MnBr(CO)₅ in presence of arsenic ligand, AsPh₃ by following a two electron pathway.

Whereas Z-products were obtained when the reaction was performed with dinuclear catalyst $\text{Mn}_2(\text{CO})_{10}$ and dilauroyl peroxide. Mechanistic investigation revealed the involvement of a radical pathway here.¹¹ In 2020, Zhu and co-workers reported an iron catalysed hydrosilylation of alkynes where mechanistic studies suggested the involvement of two-electron redox cycle.⁶ In 2016, Petit and co-workers reported regio and stereoselective hydrosilylation of unsymmetrical alkynes by a well-defined cobalt complex and proposed standard two-electron mechanism for the reaction.¹² The above discussions clearly suggest why it is very important to do the mechanistic study for a newly developed base metal catalyst system.

Herein, we report an iron catalysed (E)-selective hydrosilylation of internal alkynes along with a phosphine ligand without the use of any highly reactive additive under mild condition. A preliminary mechanistic investigation revealed a radical pathway for the reaction. (E)-selective hydrosilylation proceeding through one electron pathway, is quite uncommon in literature. Rate law determination, Hammett analyses, control experiments were performed and a mechanism has been proposed on the basis of these experiments.

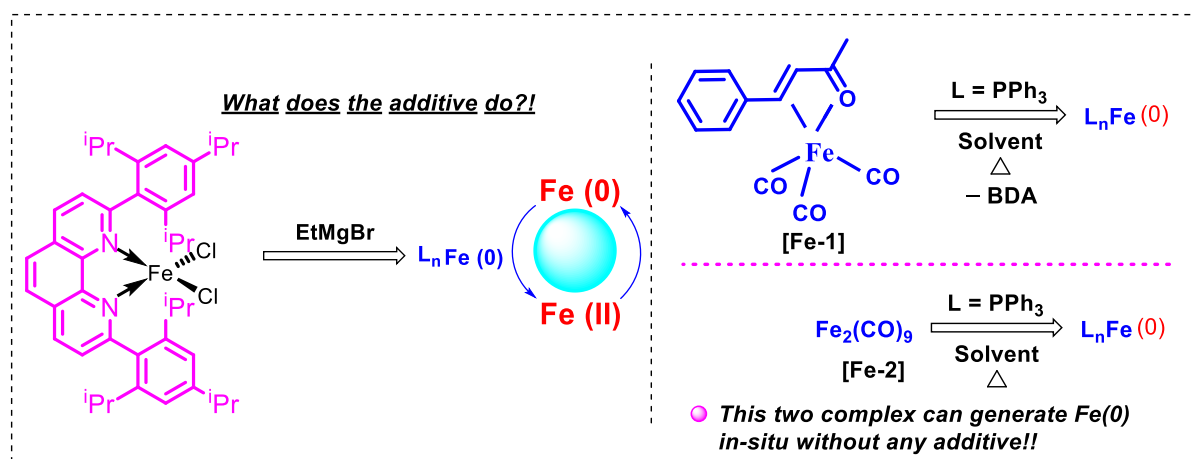


Scheme 2.2: One electron vs two electron pathway for base metal catalysed hydrosilylation of alkynes.

2.3 Results and discussion

2.3.1 Rationale for iron complex

To develop a highly reactive additive free iron catalysed methodology, we first went through the literature. It turned out that highly reactive additives are mainly added to generate a low valent iron species from the high valent iron precatalyst and these low valent iron species actually catalyses the reaction. To solve this challenge, we thought to use an iron complex where the iron metal is already in low oxidation state. In this regard, the two iron complex, [Fe(CO)₃BDA] (BDA = (E)-4-phenylbut-3-en-2-one) and [Fe₂(CO)₉] caught our attention.

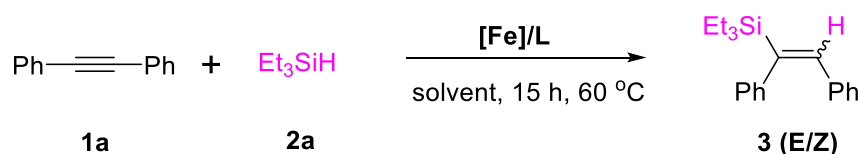


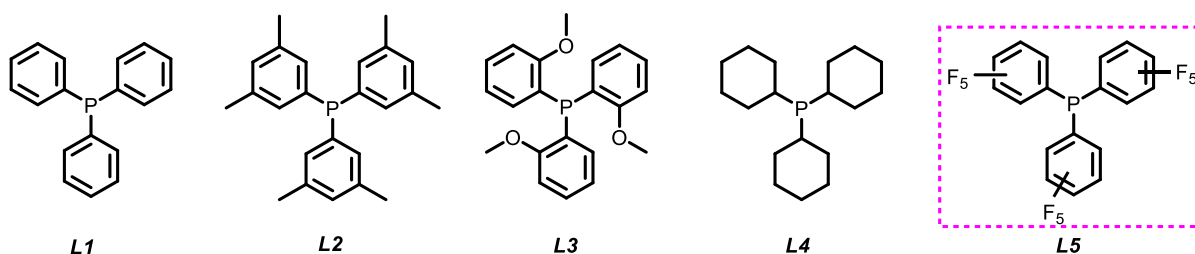
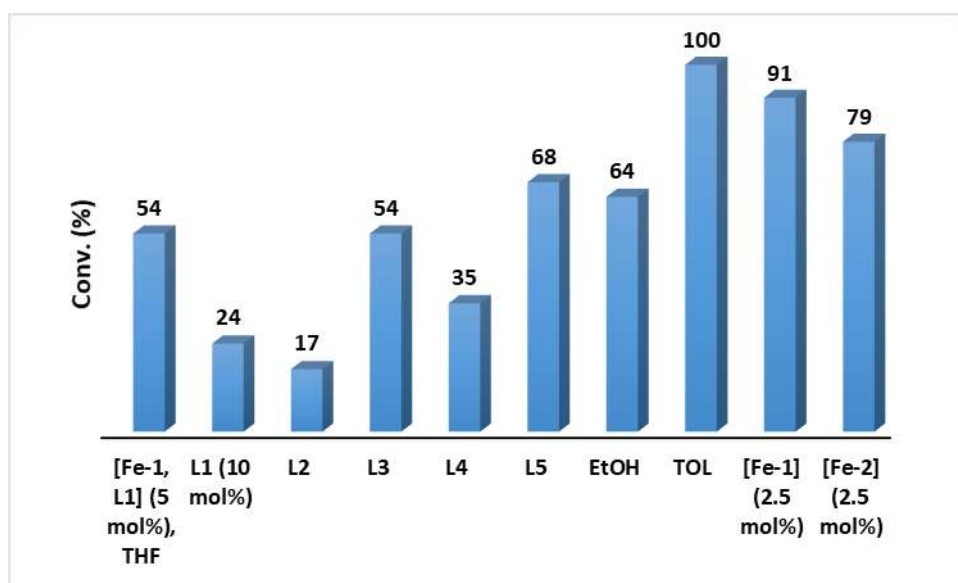
Scheme 2.3: Effect of additives in iron catalysed hydrosilylation reaction.

2.3.2 Reaction optimization

We started our investigation with the coupling reaction between diphenylacetylene (1a) and triethylsilane (2a) in presence of 5 mol % iron complex [Fe-1] and 5 mol % PPh₃ (L1) at 60 °C for 15 h in THF solvent. To our delight, it afforded 54% conversion. When the ligand loading was increased to 10 mol %, conversion decreased to 24%. These observations suggested that with increase in ligand loading, catalyst activity decreases. When the ligand was changed to L2, conversion reduced to 17%. When L3 ligand was used under identical condition, 54% conversion was obtained. When L4 ligand was implemented, conversion reduced to 35%. With L5 ligand, 68% conversion was obtained. Then we changed the solvent to EtOH, it afforded 64% conversion. Finally, changing the solvent to toluene, afforded full conversion. When the catalyst loading was reduced to 2.5 mol %, 91% conversion was obtained. With [Fe-2] complex, 79% conversion was obtained. Thus, iron complex [Fe-1], ligand L5, toluene solvent found to be optimal for this reaction. Under the optimized condition, hydrosilylated product was obtained with very high E/Z selectivity (98/2).

Table 2.1. Optimization for iron catalysed hydrosilylation of diphenylacetylene with triethylsilane^{a, b}



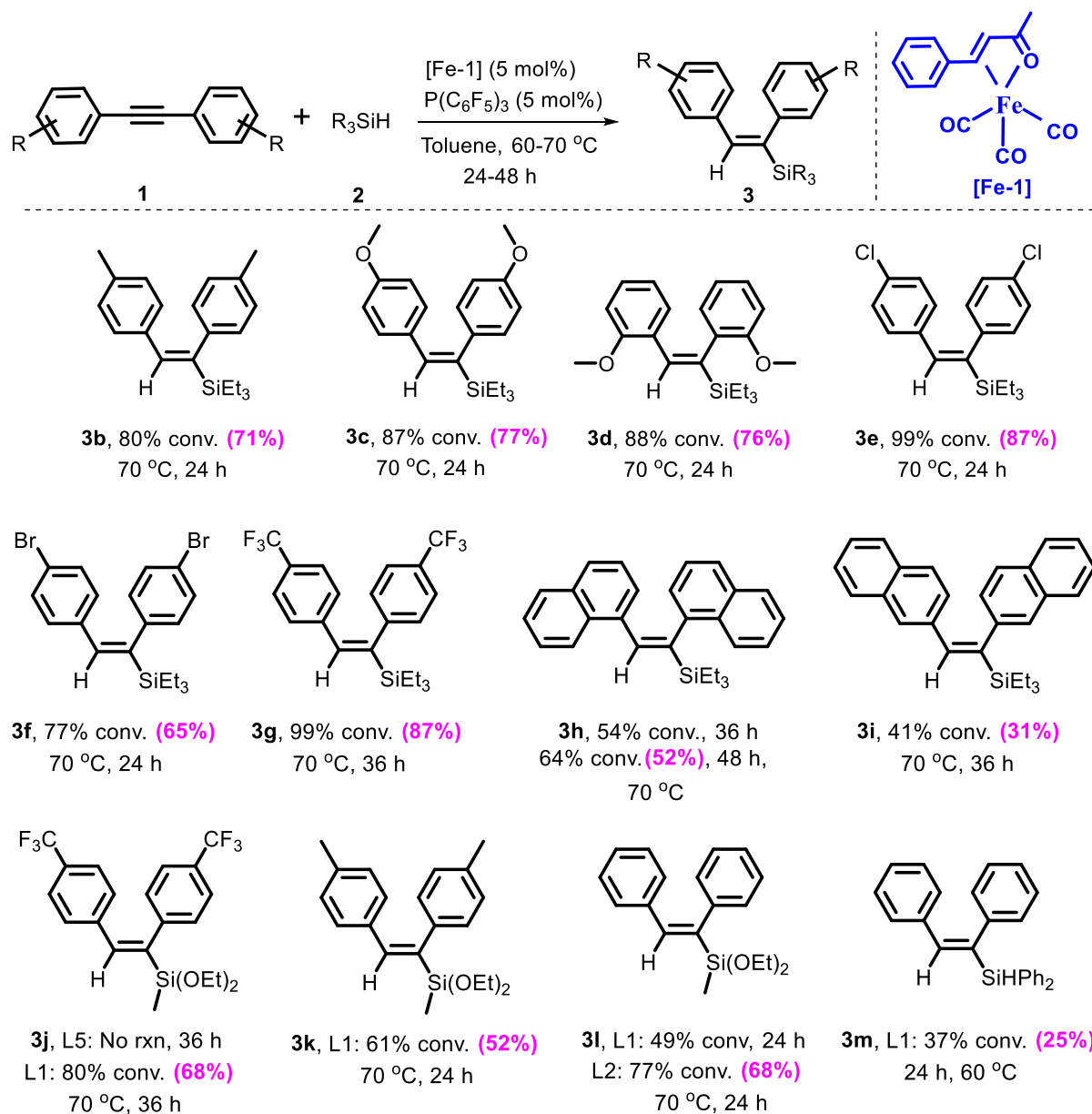


^aReaction conditions: diphenylacetylene (44.55 mg, 0.25 mmol), triethylsilane (40 mg, 0.375 mmol), iron complex (0.00625-0.0125 mmol). ^bConversions were determined with respect to starting alkyne by gas chromatography.

2.3.3 Substrate scope for hydrosilylation of alkynes

After optimizing the reaction condition, we further extended the scope of this iron catalysed hydrosilylation reaction with a range of alkynes and silanes. Alkynes containing electron donating groups such as $-\text{CH}_3$, $-\text{OMe}$ at para and ortho position were well tolerated under the reaction condition and afforded good to excellent conversion and yield (3b-d). The reaction works equally well with alkyne substrates containing different electron withdrawing substituents such as $-\text{Cl}$, $-\text{Br}$, $-\text{CF}_3$ and good to excellent conversion and yield were achieved (3e-g). However, conversion varied with different functional groups, indicating the subtle effects of these functional groups into the reaction. Alkyne substrates with naphthyl substituents also participated in the reaction, however the conversions were little lower may be due to steric reason (3h-i). When the silane was changed to $\text{HSiMe}(\text{OEt})_2$, L1 found to be the best ligand over L5. With L5, different alkynes containing electron withdrawing as well

as electron donating groups were successfully coupled with $\text{HSiMe}(\text{OEt})_2$, producing good to excellent conversion and yield (3j-k). When diphenylacetylene was coupled with $\text{HSiMe}(\text{OEt})_2$, L2 found to perform better than L1 (3l). With Ph_2SiH_2 , less conversion was obtained with L1, may be due to steric hindrance of the silane (3m).



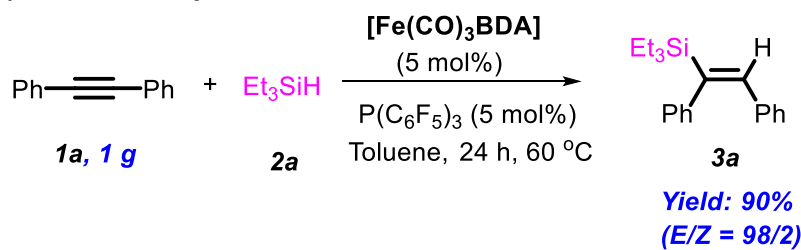
Scheme 2.4: Substrate scope for hydrosilylation of alkynes.^{a, b, c}

^aConditions: alkyne **1** (0.25 mmol), silane **2** (0.375 mmol), $[\text{Fe-1}]$ (3.575 mg, 0.0125 mmol, 5 mol %), L5 (6.8 mg, 0.0125 mmol, 5 mol %). ^bConversions were determined by gas chromatography with respect to starting alkyne. ^cYields of the isolated compounds are given in the parenthesis.

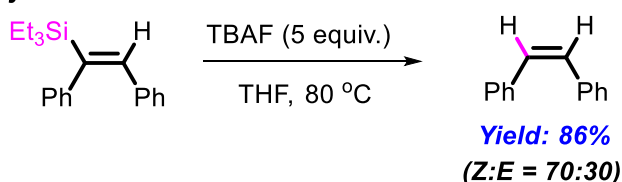
2.3.4 Application

To further assess the practicality of this methodology, hydrosilylation of diphenylacetylene was carried out on gram scale with triethylsilane in presence of 5 mol % [Fe-1]/L5 catalyst system in toluene at 60 °C for 24 h which afforded excellent yield (90%) with excellent stereoselectivity ($E/Z = 98/2$). The utility of the vinylsilanes (3a) was demonstrated by further derivatization. Protodesilylation can be carried out with vinylsilanes (3a), on treatment with TBAF, delivering the alkene in 86% yield. To check the chemoselectivity of this catalyst system, a 1:1 mixture of diphenylacetylene and styrene was used as substrate for coupling with Et_3SiH , where hydrosilylation proceeded selectively with alkyne, delivering the product 3a with a near quantitative recovery of styrene.

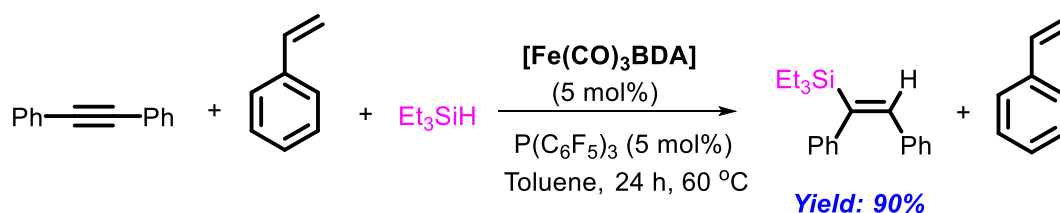
a) Gram-scale synthesis



b) Protodesilylation reaction



c) Chemoselective hydrosilylation



Scheme 2.5: Gram-scale synthesis, application of vinylsilanes and chemoselective hydrosilylation.

2.3.5 Mechanistic aspects

Olefin hydrosilylation generally proceeds through Chalk-Harrod mechanism. Later, Wrighton and co-workers established the modified Chalk-Harrod mechanism to explain the formation of dehydrogenative silylation products. Radical pathways must also be taken into account, as

is typical for base-metal catalysts. Since only a handful of iron catalysts are known for alkyne hydrosilylation, it becomes very important to pursue mechanistic investigation to understand the fundamentals of their reactivity and selectivity.

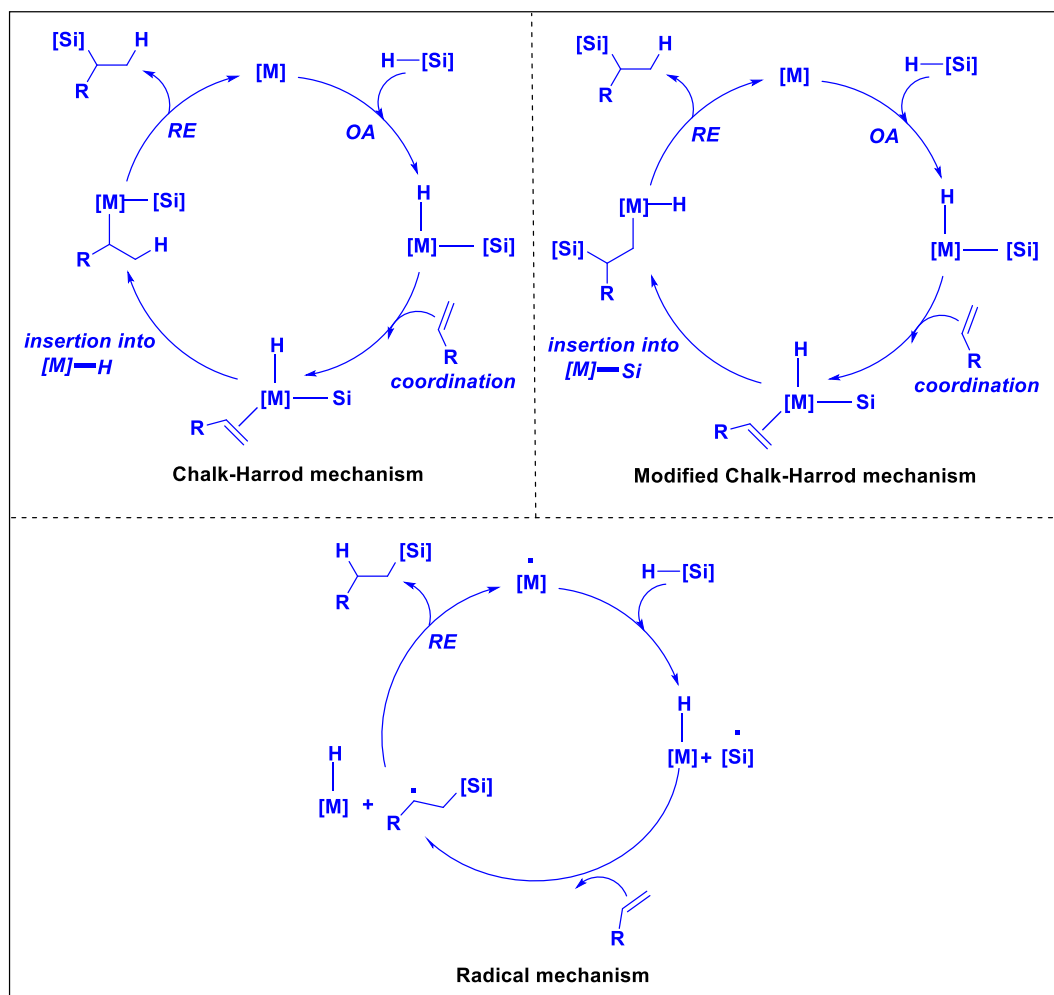


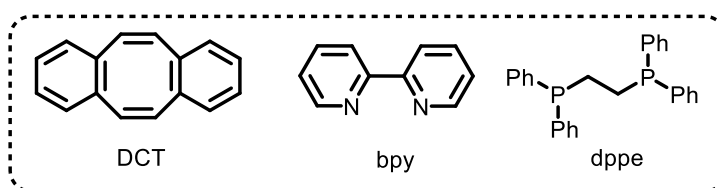
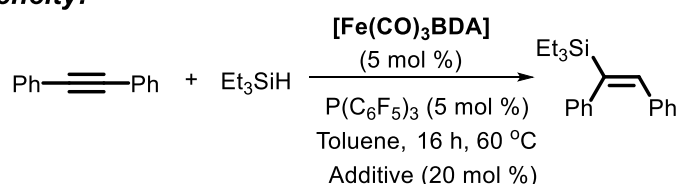
Figure 2.1: Possible transition metal catalysed hydrosilylation mechanisms.

2.3.5.1 Mechanistic experiments

In order to understand the mechanism, four different types of experiments were performed: a) homogeneity test, b) radical trap experiment, c) control experiment, d) reaction in presence of isolated mono-nuclear iron complex. The introduction of external additives (20 mol %) to the hydrosilylation reaction led to the lowering in yield of 3a. In presence of DCT, the yield reduced to 45%. Whereas in presence of strong Lewis bases, such as, bipyridine, 1,2-bis(diphenylphosphino)ethane, the reaction completely shuts down. These may arise due to the blocking of the vacant site for substrate co-ordination to the catalyst, suggesting that the

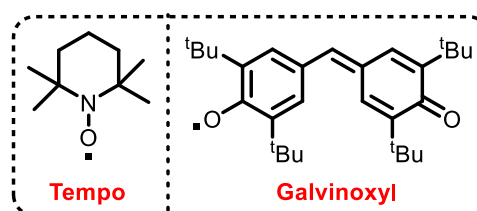
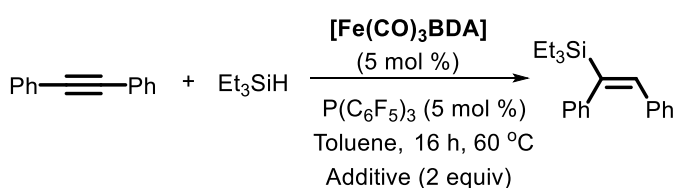
reaction most likely follows homogeneous pathway. The reaction in presence of 2.0 equivalent of TEMPO or Galvinoxyl as a radical scavenger, suppressed the catalysis completely, suggesting that a radical intermediate was involved in the hydrosilylation reaction. TEMPO adduct with the metal was detected in ESI-MS. As a control experiment, when the reaction was carried out in absence of alkyne, homocoupling of silane was detected in GC-MS which reveals the presence of silyl radical in the reaction medium. In addition to this, we have successfully prepared a well-defined iron complex, by following a literature reported procedure. This complex was equally active in hydrosilylation reaction in presence of phosphine ligand. However, the reaction completely shuts down in presence of TEMPO or Galvinoxyl.

a) Test for homogeneity:

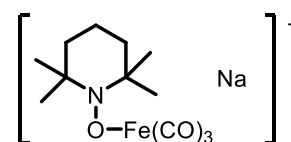


Additive	none	DCT	dppe	bpy
Yield	92%	45%	No rxn	No rxn

b) Radical trap experiment:

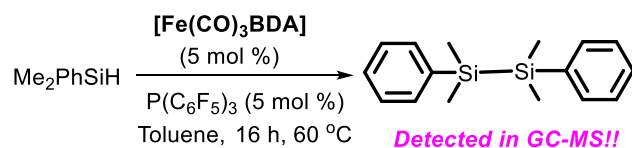


Additive	none	Tempo	Galvinoxyl
Yield	92%	No rxn	No rxn

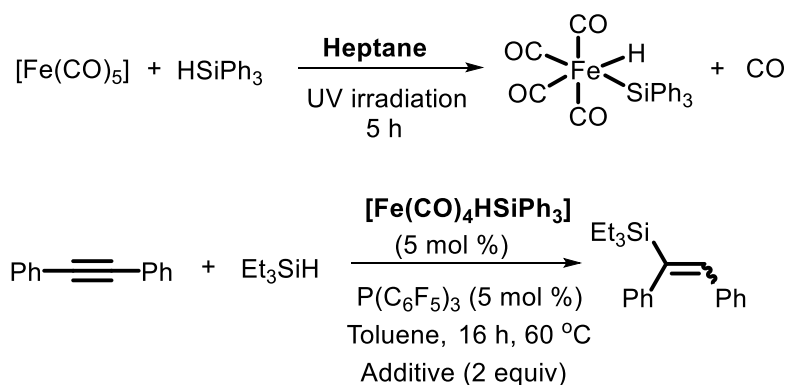


MW = 319.11
Detected in ESI-MS!!

c) Control experiment:



d) Synthesis of iron complex:



Additive	none	Tempo	Galvinoxyl
Yield	92%	No rxn	No rxn

Scheme 2.6: Mechanistic experiments.

2.3.6 Kinetic analysis

2.3.6.1 Rate law determination

Kinetic analysis of the [Fe-1] catalysed hydrosilylation of diphenylacetylene 1a with triethylsilane 2a was performed in toluene solution. A linear plot showing the production of the coupled product 3a, suggested a constant rate of reaction. Formation of coupled product was there even after the 6 min and 9 min of the reaction, suggesting the absence of an induction period for hydrosilylation reaction. For the reaction performed at $[\text{1a}] = 0.25 \text{ M}$, $[\text{2a}] = 0.375 \text{ M}$, with a varying initial concentration of [Fe-1] (0.00625-0.025 M); it was found that formation of coupled product 3a increased linearly with increasing concentration of [Fe-1] (Fig 2.34, a). This suggested that the reaction was first order with [Fe-1] (Fig 2.2, a). When the reaction was conducted with a varied initial concentration of alkyne [1a] (0.25-0.625 M), the rate of the reaction remained almost the same, suggesting zeroth order with [1a] (Fig 2.2, b). In a similar way, when the reaction was performed with a varied initial concentration of silane [2a] (0.25-1 M), the rate of the reaction increased linearly with higher

[2a], indicating first order with [2a] (Fig 2.2, c). Thus, the simple rate equation can be formulated as indicated in eq 1 based on these experimental results. The above results suggest that alkyne hydrosilylation may not be involved in the rate-determining step. Similar rate dependence was observed for iron catalysed hydrosilylation of ketones, as reported by Gade and co-workers.¹³

$$\text{rate} = k[\text{Fe-1}]^1[\text{1a}]^0[\text{2a}]^1 \quad (1)$$

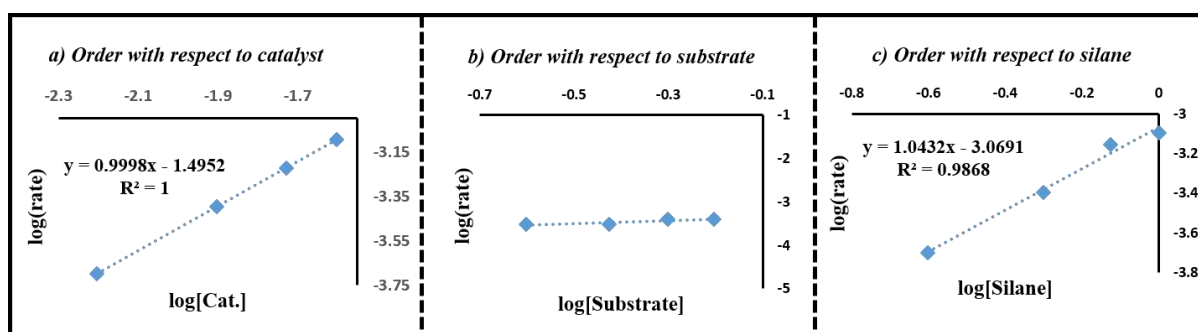


Fig 2.2. Kinetic analysis for the [Fe-1] catalysed hydrosilylation of 1a with 2a: a) plot of log(rate) vs log[Cat.], b) plot of log(rate) vs log[Substrate], c) log(rate) vs log[Silane].

2.3.6.2 Linear-free-energy relationships

The initial rates of the hydrosilylation process of alkynes with electrically distinct para substituents were then determined. The correlation between the initial rates and the σ_p values, which produced a nearly linear fit with a slope of 0.289, was used to draw the Hammett plot (Fig 2.3, a). Thus, the magnitude of ρ value is very small and it is positive. It suggested that strongly electron withdrawing groups on the alkyne favour the hydrosilylation reaction to a greater extent.

2.3.6.3 Eyring analysis

To gain insight into the overall kinetic barrier of the reaction, reaction rates were measured at different temperatures and Eyring plot was constructed (Fig 2.3, b). The activation parameters were found to be $\Delta H^\ddagger = 77.731 \text{ kJ mol}^{-1}$, $\Delta S^\ddagger = -76.72 \text{ J K}^{-1} \text{ mol}^{-1}$, $\Delta G^\ddagger_{(323 \text{ K})} = 102.51 \text{ kJ mol}^{-1}$. The rate-determining step likely involves an associative pathway, as suggested by the negative activation entropy.

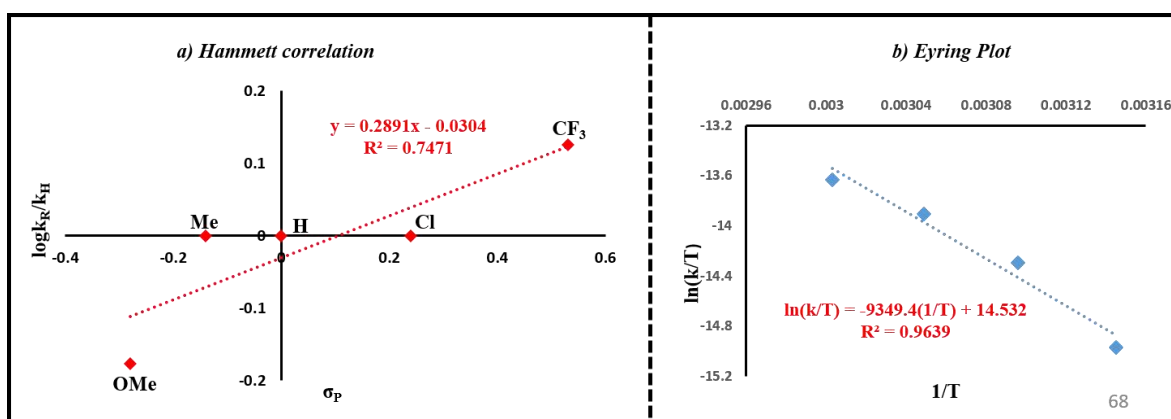


Figure 2.3: a) Hammett plot correlation using different alkynes, b) Eyring plot for [Fe-1] catalysed hydrosilylation of 1a with 2a.

2.3.7 Proposed catalytic cycle

Taking all these pieces of mechanistic findings and literature reports into account, a plausible mechanism for Fe-catalysed hydrosilylation of alkyne is presented below (Fig 2.4). First, Fe(0) abstracts a hydrogen atom from the Si-H bond to generate a silyl radical along with the formation of Fe(I)-H which is the rate determining step of the reaction. This is consistent with (i) the reaction rate is only dependent on [Fe] and [silane], (ii) the formation of an associative activated complex, (iii) the reaction is quenched in presence of radical scavenger, (iv) detection of Si-Si homo-coupled product in GC-MS and TEMPO-Fe adduct in ESI-MS. Now, the formed silyl radical could add to the alkyne to afford *E*- and *Z*- configured alkenyl radical which could further undergo another hydrogen atom transfer (HAT) process to yield the desired hydrosilylation product. This process regenerates Fe(0), thus constitutes an Fe(0)/Fe(1) catalytic cycle (Cycle 1). Due to the silyl group's steric hindrance, hydrogenolysis of the *Z*-alkenyl radical is often favoured, therefore if this pathway is followed, *Z*-vinylsilane should be formed as the major product. This is well documented in the literature.^{11, 14} However, we were getting *E*-vinylsilane as the major product which is, to the best of our knowledge, unprecedented in the literature where the reaction follows one electron pathway. To justify the product stereochemistry, we think, the alkyne probably coordinates with the metal after the first step (Fig 2.4). Here, it is worth mentioning that the alkyne did not appear in the rate law. Then, probably, the silyl radical attacks over the alkyne to form an Fe(II)-alkenyl species which on subsequent reductive elimination could afford *E*-vinylsilane along with the regeneration of Fe(0). Presence of electron withdrawing group

over the alkyne could favour the silyl radical attack on the alkyne as well as in the subsequent reductive elimination. This constitutes an Fe(0)/Fe(I)/Fe(II) catalytic cycle (Cycle 2). Additional experiments to support this catalytic cycle are currently underway in our lab.

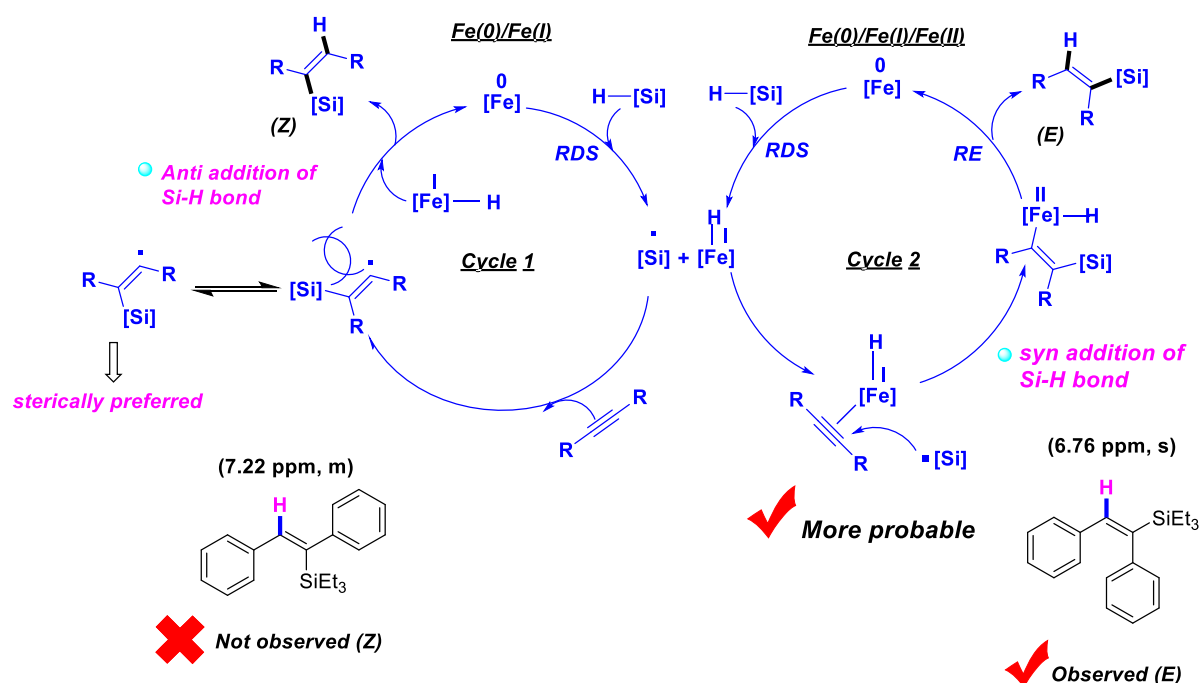


Figure 2.4: Proposed catalytic cycle for iron catalysed hydrosilylation of alkynes.

2.4 Experimental section:

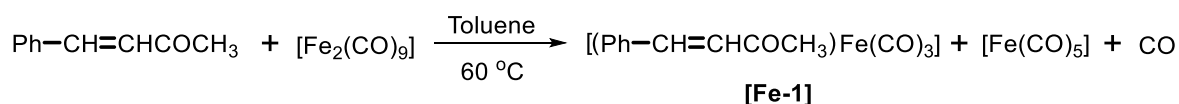
2.4.1 Methods and materials:

All manipulations were carried out under an inert atmosphere using standard Schlenk technique, cannula filtration or m-Braun glove box. Solvents were dried by standard procedures unless otherwise mentioned.¹ THF was dried on sodium/benzophenone. Di-iron nonacarbonyl, organosilanes, diphenyl acetylene were purchased from Sigma-Aldrich. All other reagents/chemicals, solvents were purchased from local suppliers (Spectrochem Pvt. Ltd.; Avra Synthesis Pvt. Ltd.; Thomas Baker Pvt. Ltd. etc). Solution NMR spectra were recorded on a Bruker Avance 200, 400 and 500 MHz instruments at 298K unless mentioned otherwise. Chemical shifts are referenced to external reference TMS (^1H and ^{13}C) or or 85% H_3PO_4 ($\Xi = 40.480747$ MHz, ^{31}P). Coupling constants are given as absolute values. Multiplicities are given as follows s: singlet, d: doublet, t: triplet, m: multiplet, quat: quaternary carbon. Mass spectra were recorded on Thermo Scientific Q-Exactive mass spectrometer with Hypersil gold C18 column 150 x 4.6 mm diameter 8 μm particle size

mobile phase used is 90% methanol + 10% water + 0.1% formic acid. The GC conversion of the products were determined by HP-5 column (30 m) on an Agilent 7890B GC system.

2.4.2 Synthesis of Tricarbonyl(benzylideneacetone)iron complex

We began with the synthesis of $[\text{Fe}(\text{CO})_3(\text{BDA})]$ complex by following a known literature procedure (scheme 2.7).¹⁵ 10.05 g (0.0685 mol) of benzylideneacetone, 25 g (0.0685 mol) of $[\text{Fe}_2(\text{CO})_9]$ were suspended in dry toluene (150 ml) in a Schlenk flask. The above suspension was heated at 60 °C for 5 hours, after which volatiles were evaporated under vacuum. Then the residue was purified by silica gel column chromatography, eluting with pet ether/ethyl acetate (99/1). The product was obtained as orange red crystals (6.05 g, 32%).



Scheme 2.7: Synthesis of $[(\text{Ph-CH=CHCOCH}_3)\text{Fe}(\text{CO})_3]$

$^1\text{H NMR}$ (500 MHz, CDCl_3): $\delta = 7.2$ (m, 4H), 7.13 (m, 1H), 5.98 (d, $J = 9.7$ Hz, 1H, Ph-CH), 3.05 (d, $J = 9.7$ Hz, 1H, =CHCO), 2.48 (s, 3H, $-\text{CH}_3$).

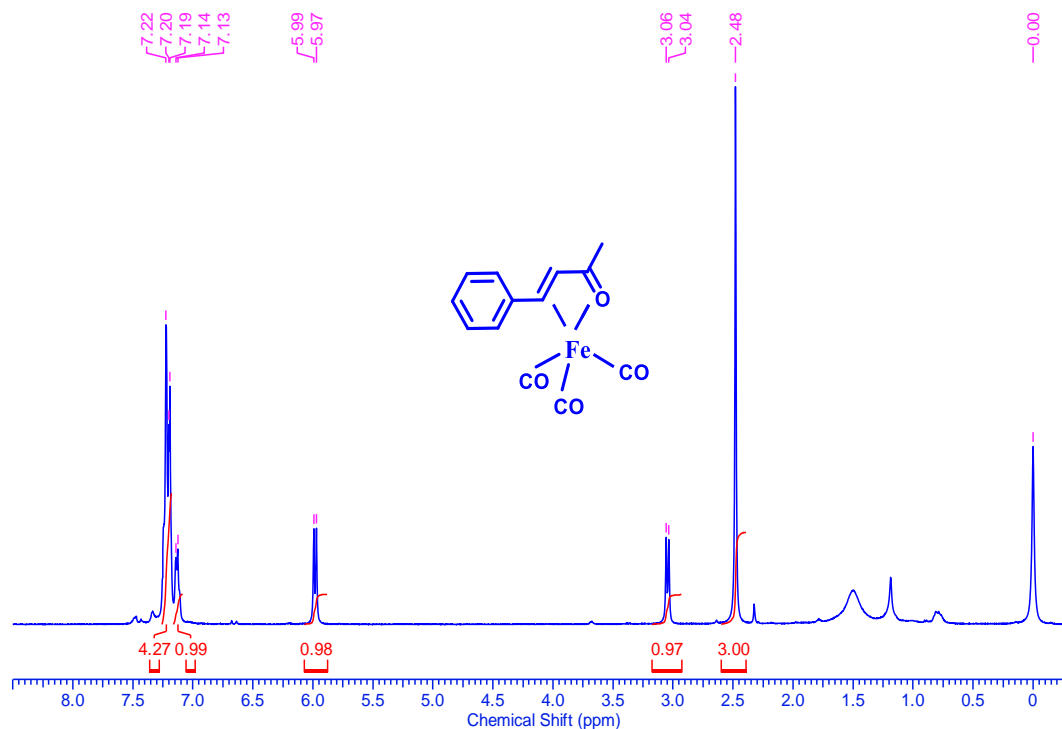


Figure 2.5: $^1\text{H NMR}$ spectrum of $[(\text{Ph-CH=CHCOCH}_3)\text{Fe}(\text{CO})_3]$.

2.4.3 General procedure for iron catalysed hydrosilylation of alkynes:

Alkyne **1** (0.25 mmol), silane **2** (0.375 mmol), [Fe-1] (3.575 mg, 0.0125 mmol, 5 mol %), L5 (6.8 mg, 0.0125 mmol, 5 mol %) were introduced in a 10 mL teflon-valved flask equipped with a magnetic stir bar under argon atmosphere. Toluene (1 mL) was added to the reaction mixture. The reaction mixture was stirred at 60-70 °C for 24-48 h. The mixture was extracted with diethyl ether (3 × 10 mL). After that, the layers of mixed diethyl ether were dried over sodium sulfate and concentrated under vacuum. After evaporation of the solvent, the crude reaction mixture was purified by silica gel column chromatography (petroleum ether/EtOAc 50/1), yielding the hydrosilylated product. The conversion was determined by gas chromatography with respect to starting alkyne.

GC method 1: GC analysis was carried out on an Agilent 7890B GC system using HP-05 column (30 m × 320 μm × 0.25 μm), split ratio 30:1, column pressure 10 psi, injector temperature of 260 °C, detector temperature of 330 °C, argon carrier gas. Temperature program: Initial temperature 70 °C, hold for 1 min.; ramp 1: 4 °C/min. to 120 °C; ramp 2: 10 °C/min. to 250 °C; ramp 3: 20 °C/min. to 320 °C, hold for 2 min. This method was applied for analysing substrates 1a, 1b, 1c, 1d, 1e, 1f, 1g, 1j, 1k, 1l, 1m.

GC method 2: GC analysis was carried out on an Agilent 7890B GC system using HP-05 column (30 m × 320 μm × 0.25 μm), split ratio 30:1, column pressure 10 psi, injector temperature of 260 °C, detector temperature of 330 °C, argon carrier gas. Temperature program: Initial temperature 70 °C, hold for 1 min.; ramp 1: 4 °C/min. to 120 °C; ramp 2: 10 °C/min. to 250 °C, hold for 3 min; ramp 3: 20 °C/min. to 320 °C, hold for 5 min.

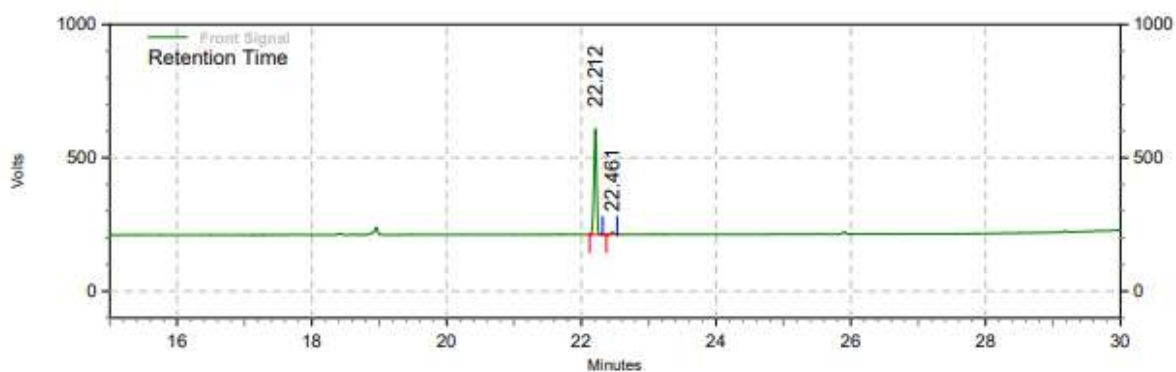
This method was applied for analysing substrates 1h, 1i.

Table 2.2. GC retention time for alkynes, hydrosilylated products and conversion

Substrate	Retention time (min)	Product	Retention time (min)	Conversion (%)
1a	17.7	3a	22.2, 22.5	>99
1b	20.7	3b	23.8	80
1c	23.9	3c	26.3	87

1d	22.8	3d	24.5	88
1e	22.5	3e	25.5	>99
1f	24.09	3f	27.14	77
1g	17.3	3g	21.5	>99
1h	29.2	3h	30.3	64
1i	30.2	3i	31.6	41
1j	17.3	3j	20.4, 20.8	84
1k	20.7	3k	22.8, 23.1	61
1l	17.7	3l	21.1, 21.3	77
1m	17.7	3m	27.7, 28.0	38

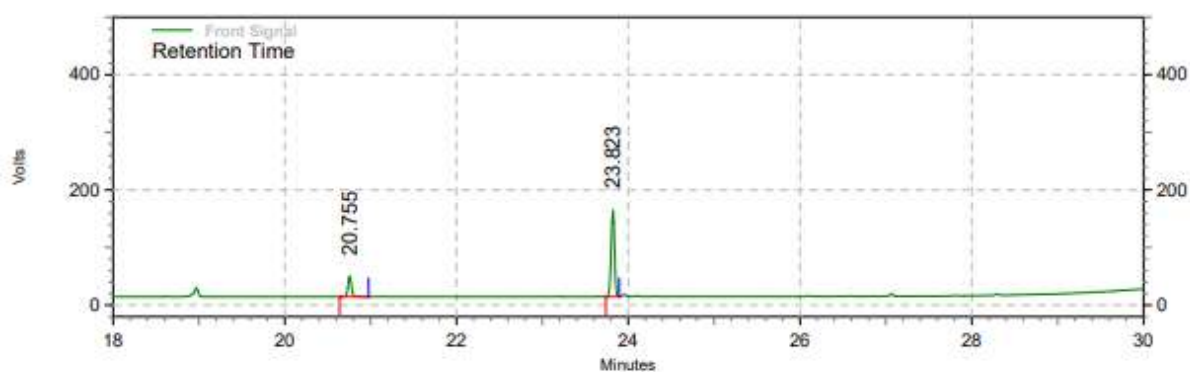
2.4.4 GC chromatogram of substrate scope



Front Signal Results

Retention Time	Area	Area %	Height	Height %
22.212	8344692	97.77	3055631	97.73
22.461	190173	2.23	70873	2.27
Totals	8534865	100.00	3126504	100.00

Figure 2.6: GC chromatogram of 3a (Table 2.1., under optimized condition).

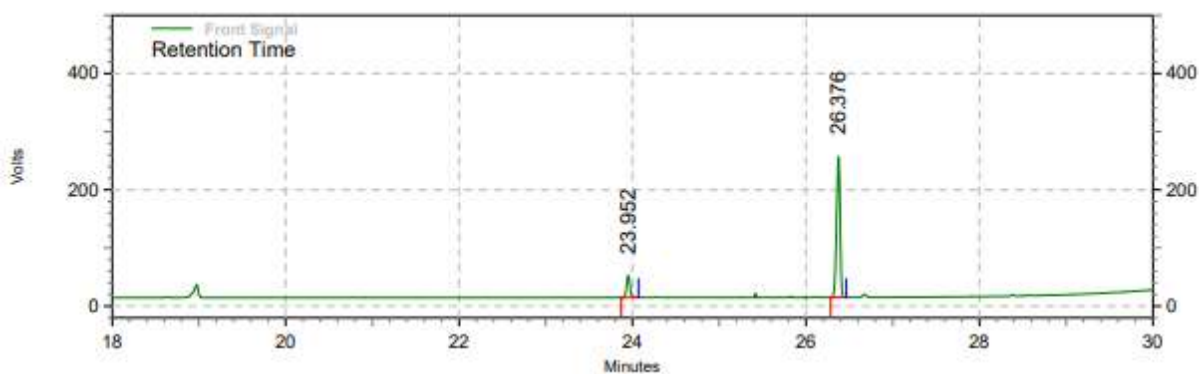


Front Signal Results

Retention Time	Area	Area %	Height	Height %
20.755	761648	19.56	273978	19.20
23.823	3132564	80.44	1152919	80.80

Totals	Area	Area %	Height	Height %
	3894212	100.00	1426897	100.00

Figure 2.7: GC chromatogram of 3b.

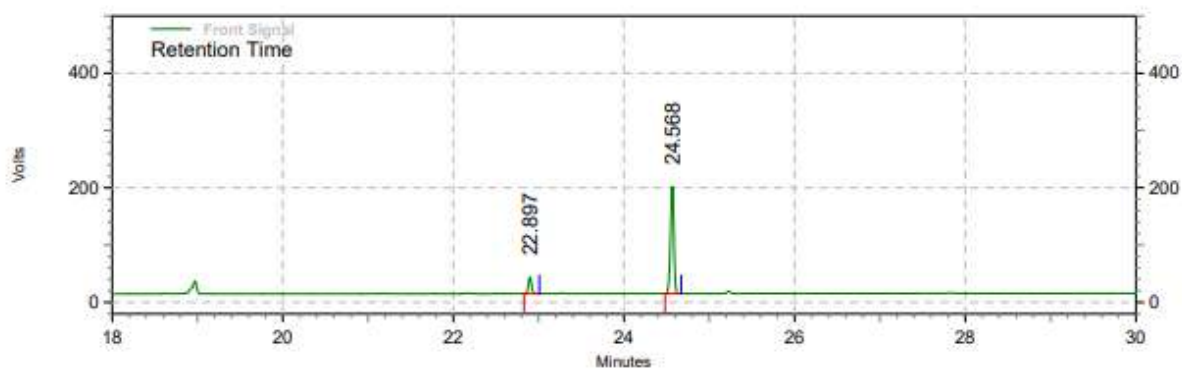


Front Signal Results

Retention Time	Area	Area %	Height	Height %
23.952	778761	12.86	290848	13.52
26.376	5277096	87.14	1860009	86.48

Totals	Area	Area %	Height	Height %
	6055857	100.00	2150857	100.00

Figure 2.8: GC chromatogram of 3c.

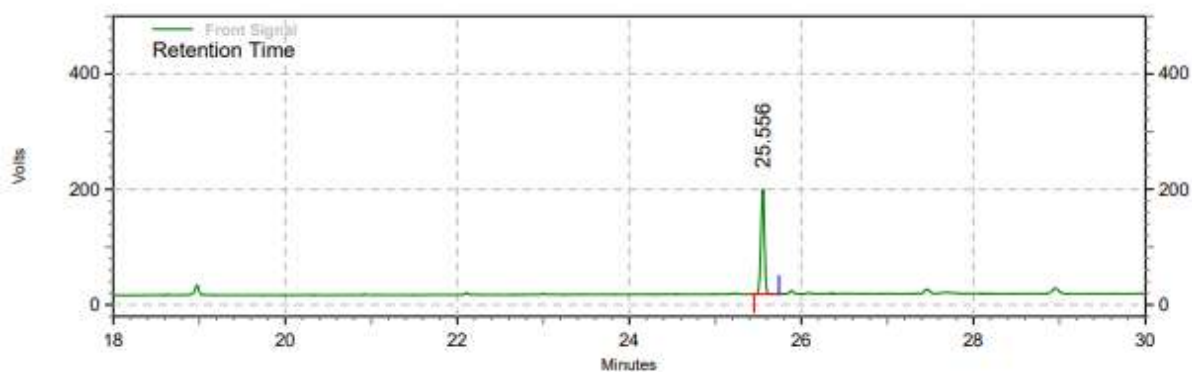


**Front Signal
Results**

Retention Time	Area	Area %	Height	Height %
22.897	566007	12.36	222525	13.41
24.568	4013290	87.64	1436860	86.59

Totals	4579297	100.00	1659385	100.00
--------	---------	--------	---------	--------

Figure 2.9: GC chromatogram of 3d.

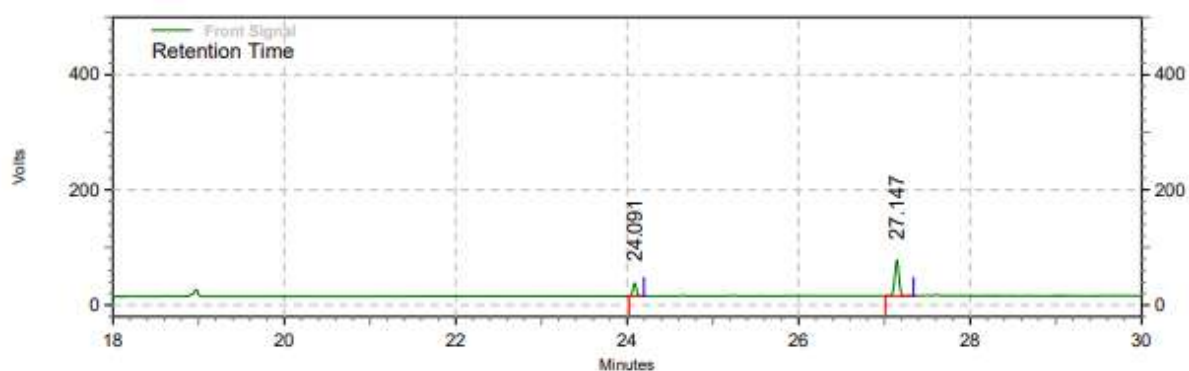


**Front Signal
Results**

Retention Time	Area	Area %	Height	Height %
25.556	3977981	100.00	1394675	100.00

Totals	3977981	100.00	1394675	100.00
--------	---------	--------	---------	--------

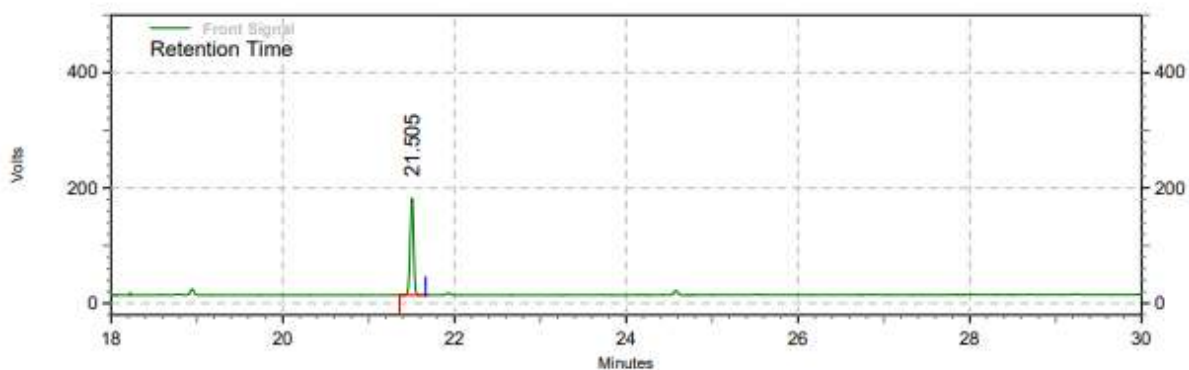
Figure 2.10: GC chromatogram of 3e.



Front Signal Results

Retention Time	Area	Area %	Height	Height %
24.091	483260	23.42	171179	26.54
27.147	1579950	76.58	473798	73.46
Totals	2063210	100.00	644977	100.00

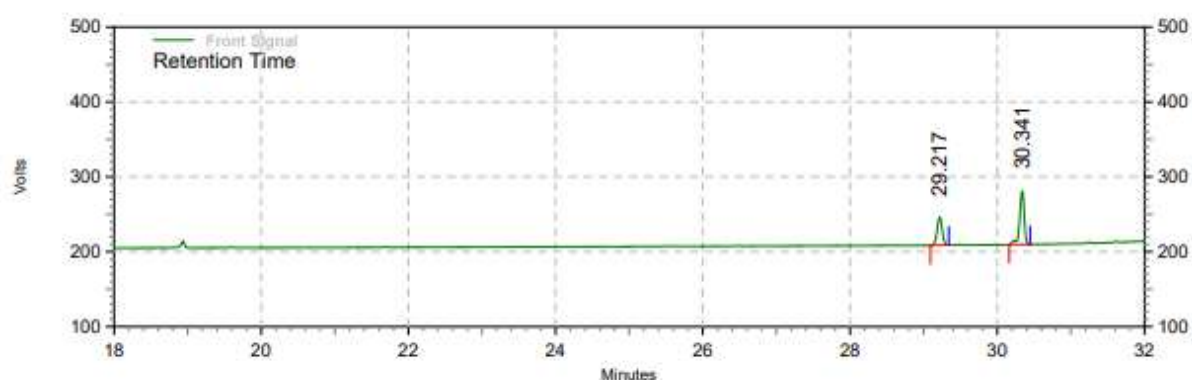
Figure 2.11: GC chromatogram of 3f.



Front Signal Results

Retention Time	Area	Area %	Height	Height %
21.505	3572061	100.00	1291141	100.00
Totals	3572061	100.00	1291141	100.00

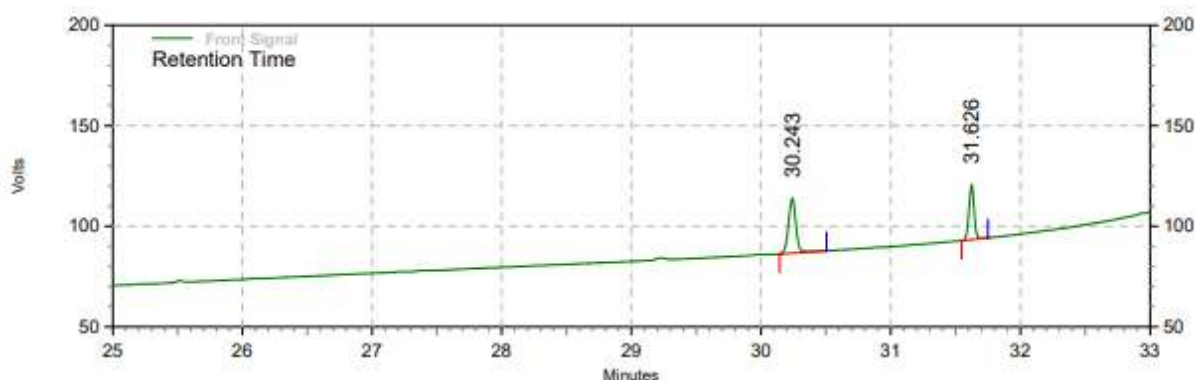
Figure 2.12: GC chromatogram of 3g.



Front Signal Results

Retention Time	Area	Area %	Height	Height %
29.217	1374250	36.55	286564	34.26
30.341	2385578	63.45	549843	65.74
Totals	3759828	100.00	836407	100.00

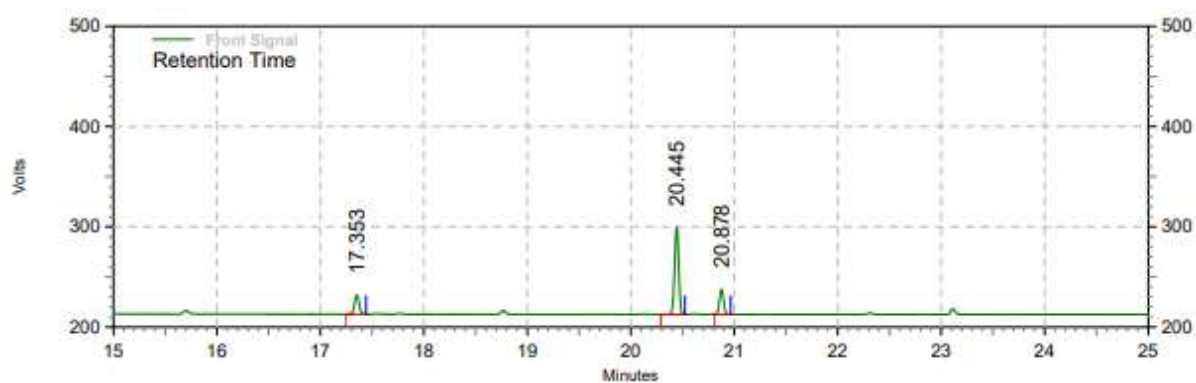
Figure 2.13: GC chromatogram of 3h.



Front Signal Results

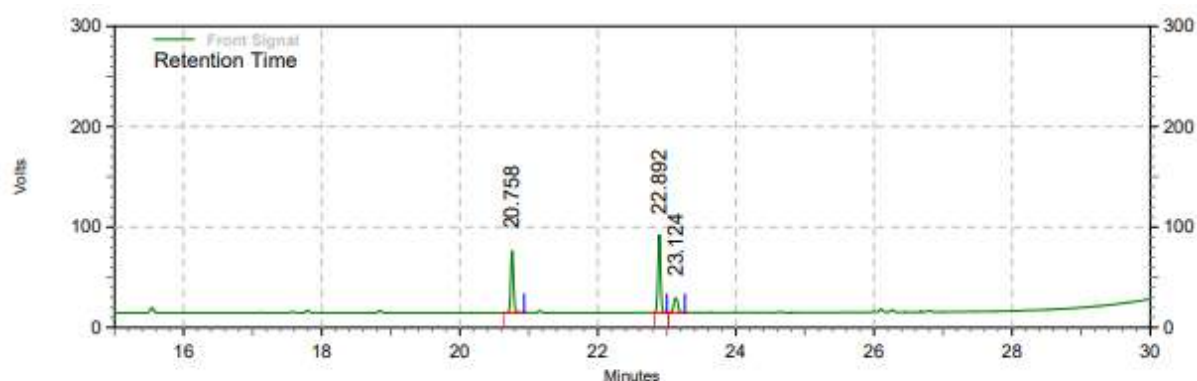
Retention Time	Area	Area %	Height	Height %
30.243	824164	58.88	209689	50.19
31.626	575464	41.12	208097	49.81
Totals	1399628	100.00	417786	100.00

Figure 2.14: GC chromatogram of 3i.

**Front Signal
Results**

Retention Time	Area	Area %	Height	Height %
17.353	452627	15.88	146983	14.58
20.445	1860525	65.29	669645	66.41
20.878	536430	18.82	191646	19.01
Totals	2849582	100.00	1008274	100.00

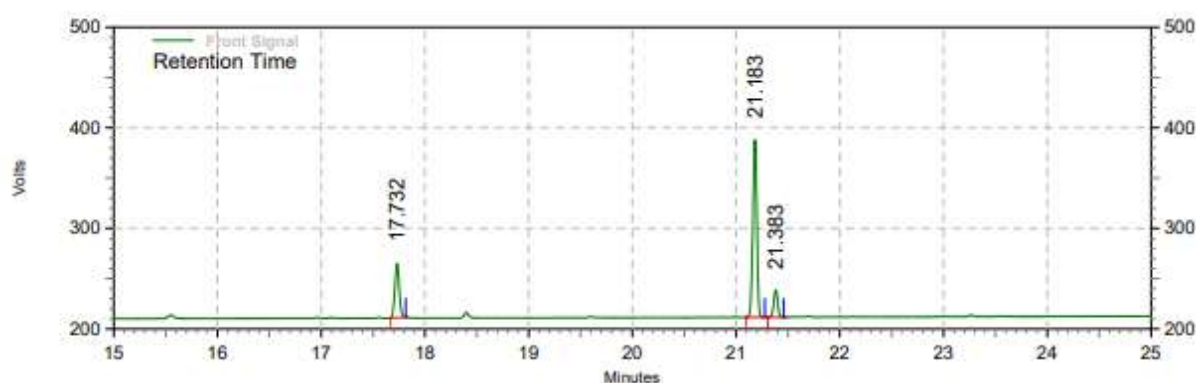
Figure 2.15: GC chromatogram of 3j.



Front Signal Results

Retention Time	Area	Area %	Height	Height %
20.758	1283624	38.61	475603	40.24
22.892	1584368	47.66	595043	50.35
23.124	456200	13.72	111175	9.41
Totals	3324192	100.00	1181821	100.00

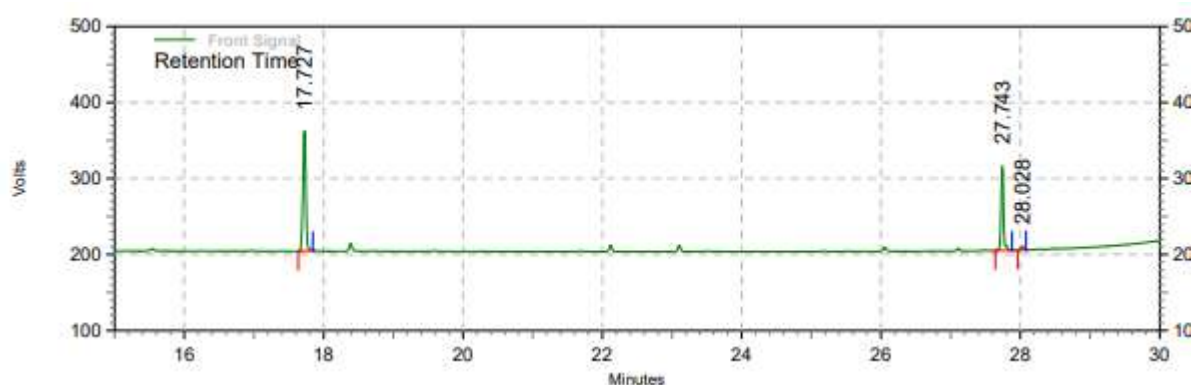
Figure 2.16: GC chromatogram of 3k.



Front Signal Results

Retention Time	Area	Area %	Height	Height %
17.732	1216614	22.52	414453	20.95
21.183	3629051	67.17	1354301	68.47
21.383	557011	10.31	209193	10.58
Totals	5402676	100.00	1977947	100.00

Figure 2.17: GC chromatogram of 3l.



Front Signal Results

Retention Time	Area	Area %	Height	Height %
17.727	3543930	62.29	1210354	57.55
27.743	2051336	36.05	850890	40.46
28.028	94341	1.66	41924	1.99
Totals	5689607	100.00	2103168	100.00

Figure 2.18: GC chromatogram of 3m.

2.4.5 ^1H NMR of isolated compounds

Triethyl-[(Z)-(1,2-diphenylvinyl)]silane (3a)

^1H NMR (200 MHz, CDCl_3): δ 7.32 (m, 2H), 7.22 (m, 1H), 7.11 (m, 3H), 7.03 (m, 2H), 6.98 (m, 2H), 6.8 (s, C=CH, 1H), 0.99 (t, $J = 7.9$ Hz, 9H), 0.68 (q, $J = 7.9$ Hz, 6H).

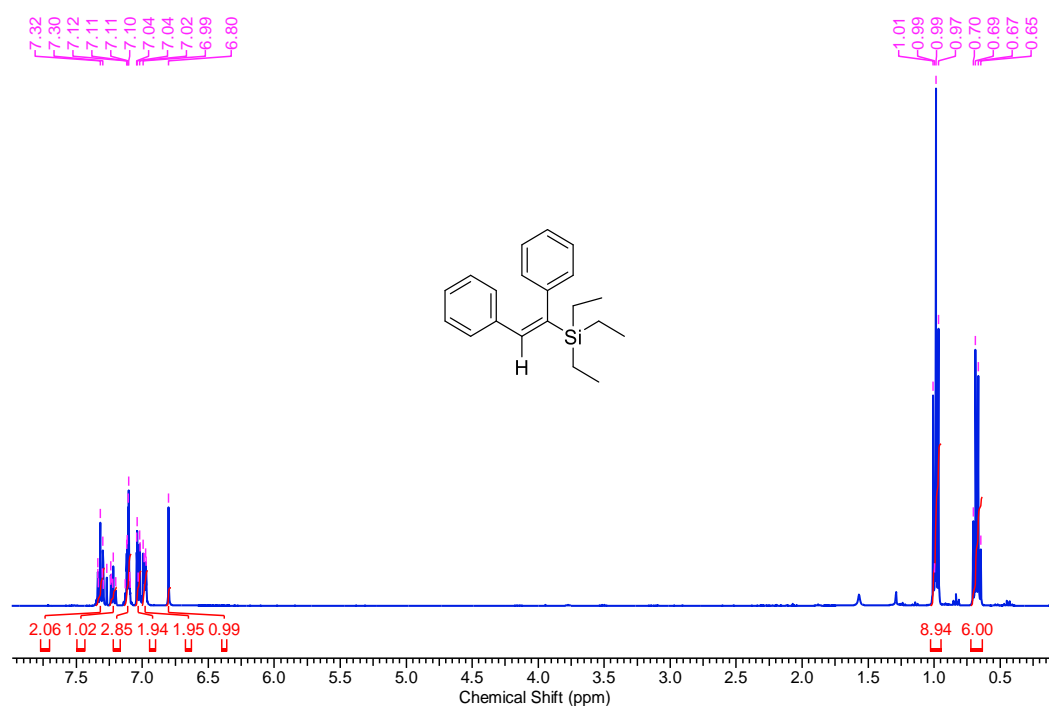


Figure 2.19: ¹H NMR spectrum of triethyl-[(Z)-(1,2-diphenylvinyl)]silane (3a).

(E)-(1,2-bis(4-methoxyphenyl)vinyl)triethylsilane (3c)

¹H NMR (200 MHz, CDCl₃): δ = 6.91 (m, 6H), 6.68 (d, J = 4.1 Hz, 2H), 6.63 (s, 1H), 3.83 (s, 3H, -OCH₃), 3.73 (s, 3H, -OCH₃), 0.95 (t, J = 7.8 Hz, 9H, -Si-C-(CH₃)₃), 0.63 (q, J = 7.8 Hz, 6H, -Si(CH₂)₃).

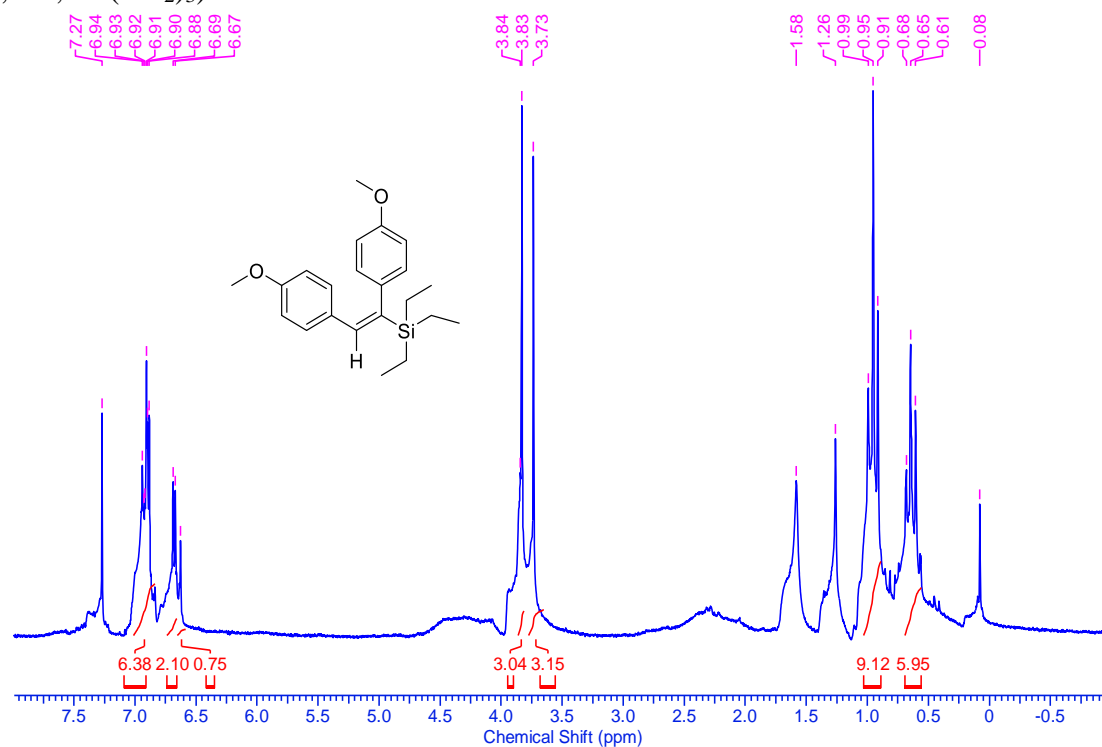


Figure 2.20: ^1H NMR spectrum of (E)-(1,2-bis(4-methoxyphenyl)vinyl)triethylsilane (3c).

(E)-(1,2-bis(2-methoxyphenyl)vinyl)triethylsilane (3d)

^1H NMR (400 MHz, CDCl_3): δ = 7.15 (m, 2H), 7.06 (m, 1H), 6.83 (m, 2H), 6.79 (m, 3H), 6.56 (t, J = 5.6 Hz, 1H), 3.85 (s, 3H, - OCH_3), 3.75 (s, 3H, - OCH_3), 0.97 (t, J = 7.8 Hz, 9H, - $\text{Si-C}(\text{CH}_3)_3$), 0.65 (q, J = 7.8 Hz, 6H, - $\text{Si}(\text{CH}_2)_3$).

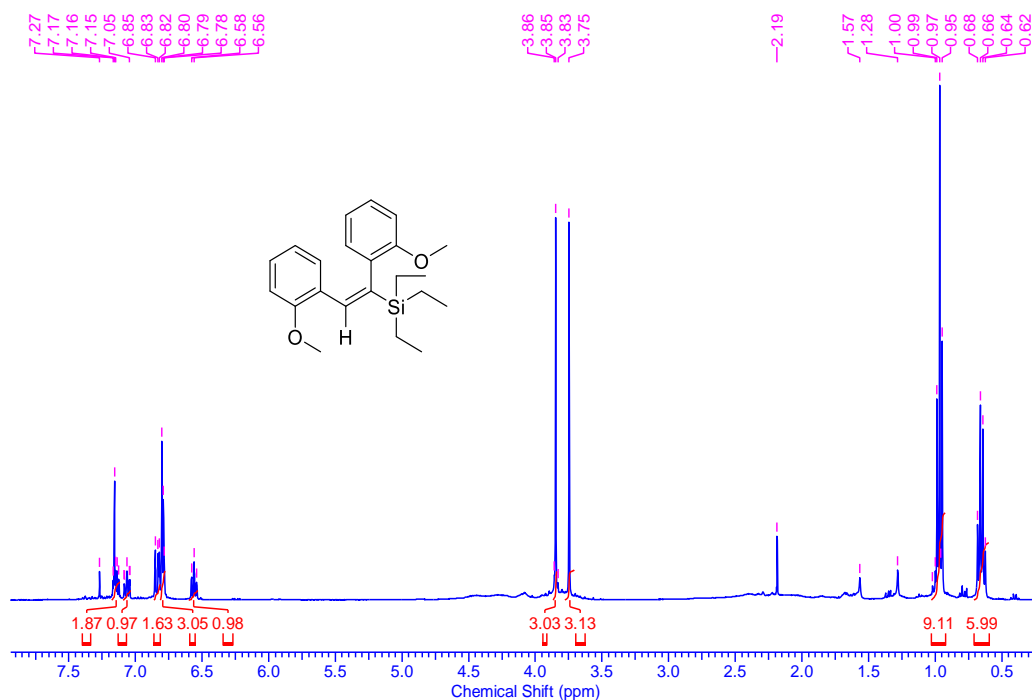


Figure 2.21: ^1H NMR spectrum of (E)-(1,2-bis(4-chlorophenyl)vinyl)triethylsilane (3d).

(E)-(1,2-bis(4-chlorophenyl)vinyl)triethylsilane (3e)

^1H NMR (400 MHz, CDCl_3): δ = 7.54 (d, J = 7 Hz, 2H), 7.35 (d, J = 8.1 Hz, 2H), 7.16 (m, 4H), 7.01 (s, 1H, - $\text{C}=\text{CH}$), 1.22 (t, J = 8.3 Hz, 9H, - $\text{Si-C}(\text{CH}_3)_3$), 0.91 (q, J = 9 Hz, 6H, - $\text{Si}(\text{CH}_2)_3$).

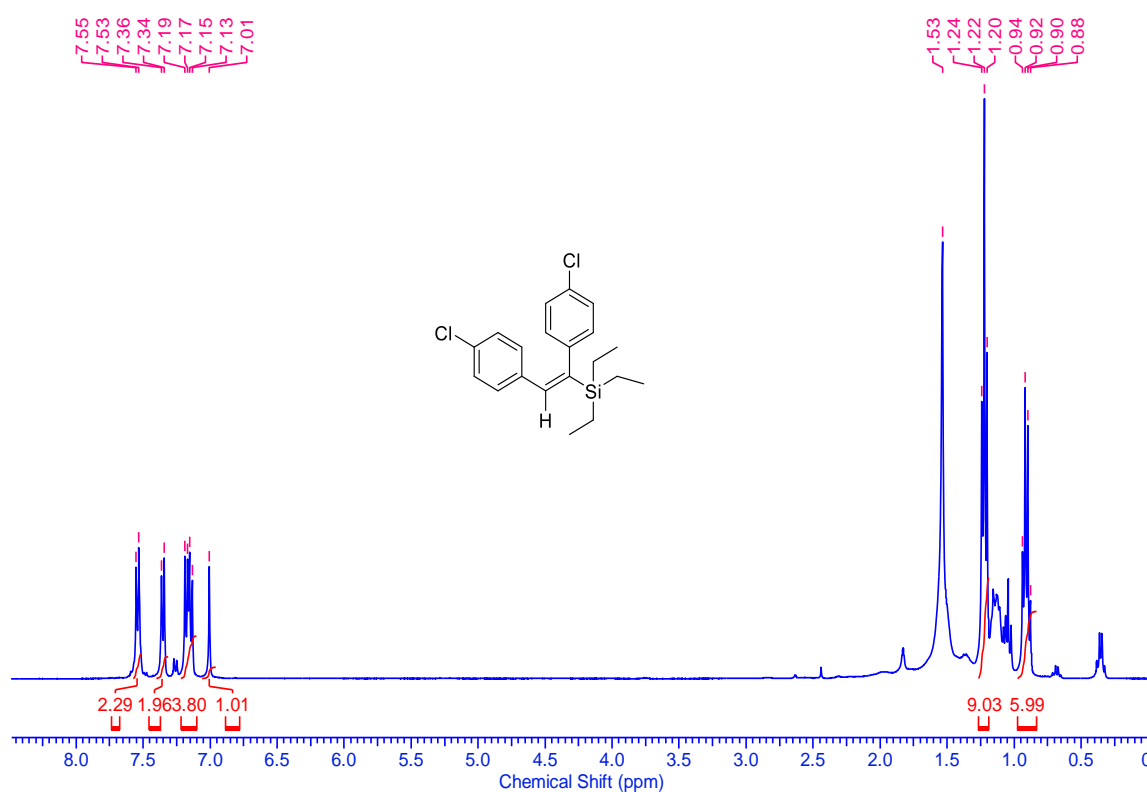


Figure 2.22: ^1H NMR spectrum of (E)-(1,2-bis(4-chlorophenyl)vinyl)triethylsilane (3e).

(E)-(1,2-bis(4-bromophenyl)vinyl)triethylsilane (3f)

^1H NMR (500 MHz, CDCl_3): δ = 7.45 (s, 1H), 7.43 (s, 1H), 7.27 (d, J = 3 Hz, 1H), 7.25 (s, 1H), 6.88 (s, 1H), 6.86 (s, 1H), 6.84 (s, 1H), 6.82 (s, 1H), 6.74 (s, 1H), 0.97 (t, J = 7.6 Hz, 9H, -Si-C-(CH_3)₃), 0.65 (q, J = 7.6 Hz, 6H, -Si(CH_2)₃).

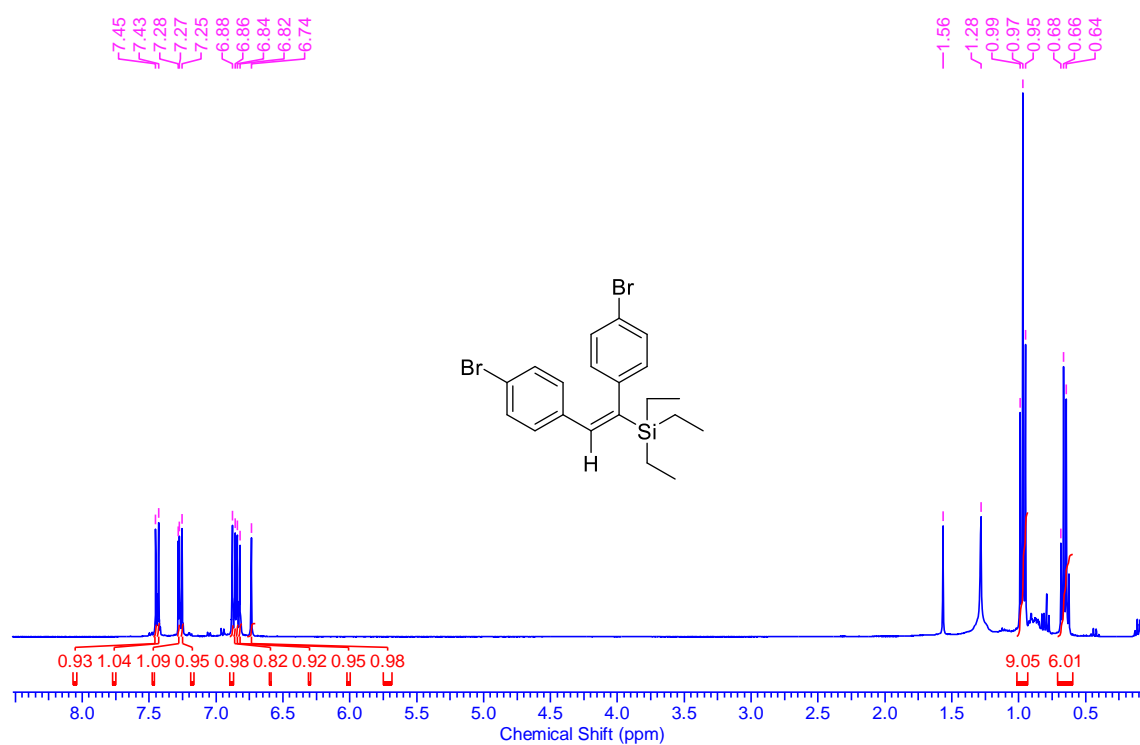


Figure 2.23: ¹H NMR spectrum of (E)-(1,2-bis(4-bromophenyl)vinyl)triethylsilane (3f).

(E)-(1,2-bis(4-(trifluoromethyl)phenyl)vinyl)triethylsilane (3g)

¹H NMR (500 MHz, CDCl₃): δ = 7.58 (d, J = 8.3 Hz, 2H), 7.37 (d, J = 8.3 Hz, 2H), 7.11 (d, J = 8.3 Hz, 2H), 7.03 (d, J = 8.3 Hz, 2H), 6.87 (s, 1H, C=C-H), 0.98 (t, J = 7.6 Hz, 9H, -Si-C-(CH₃)₃), 0.68 (q, J = 7.6 Hz, 6H, -Si(CH₂)₃).

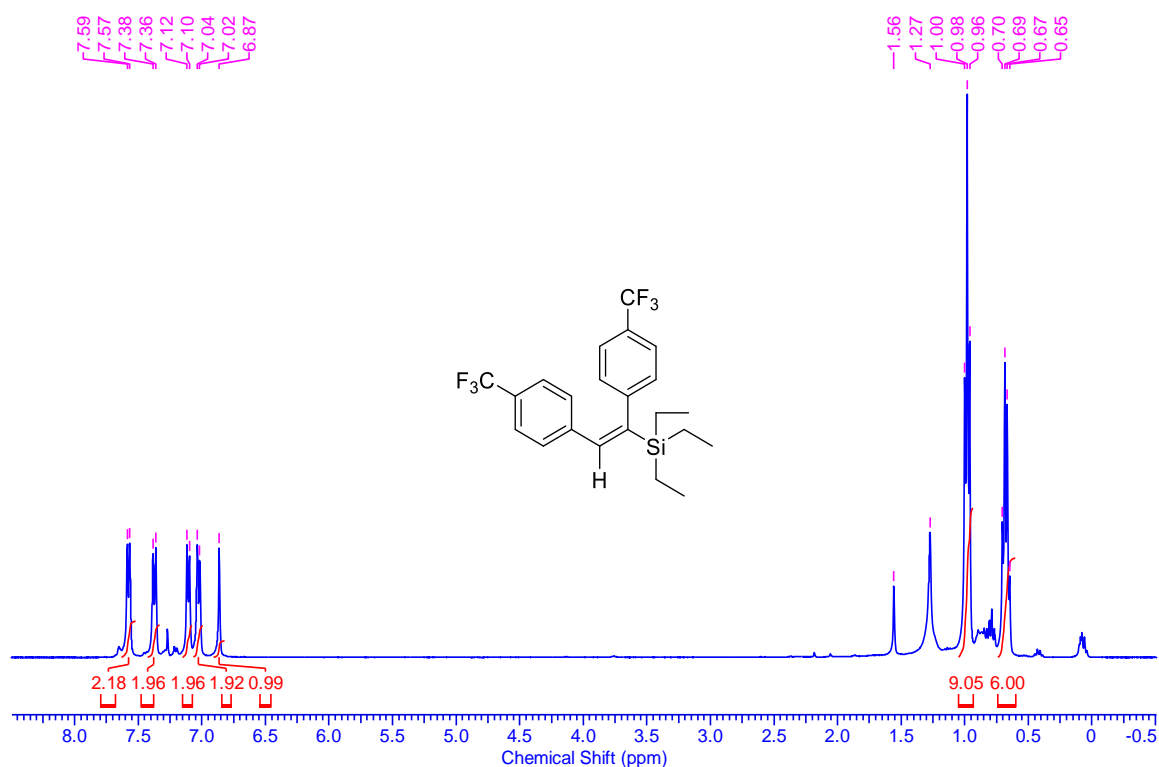


Figure 2.24: ^1H NMR spectrum of (E)-(1,2-bis(4-(trifluoromethyl)phenyl)vinyl)triethylsilane (3g).

(E)-(1,2-di(naphthalen-2-yl)vinyl)triethylsilane (3i)

^1H NMR (400 MHz, CDCl_3): δ = 7.8 (m, 8H), 7.65 (m, 1H), 7.55 (m, 3H), 7.47 (m, 2H), 7.41 (d, J = 9.46 Hz, 1H), 7.36 (m, 2H), 7.2 (d, J = 8.35 Hz, 1H), 7.06 (s, 1H), 7.0 (d, J = 8.35 Hz, 1H), 1.03 (t, J = 7.8 Hz, 9H, -Si-C-(CH_3)₃), 0.73 (q, J = 7.8 Hz, 6H, -Si(CH_2)₃).

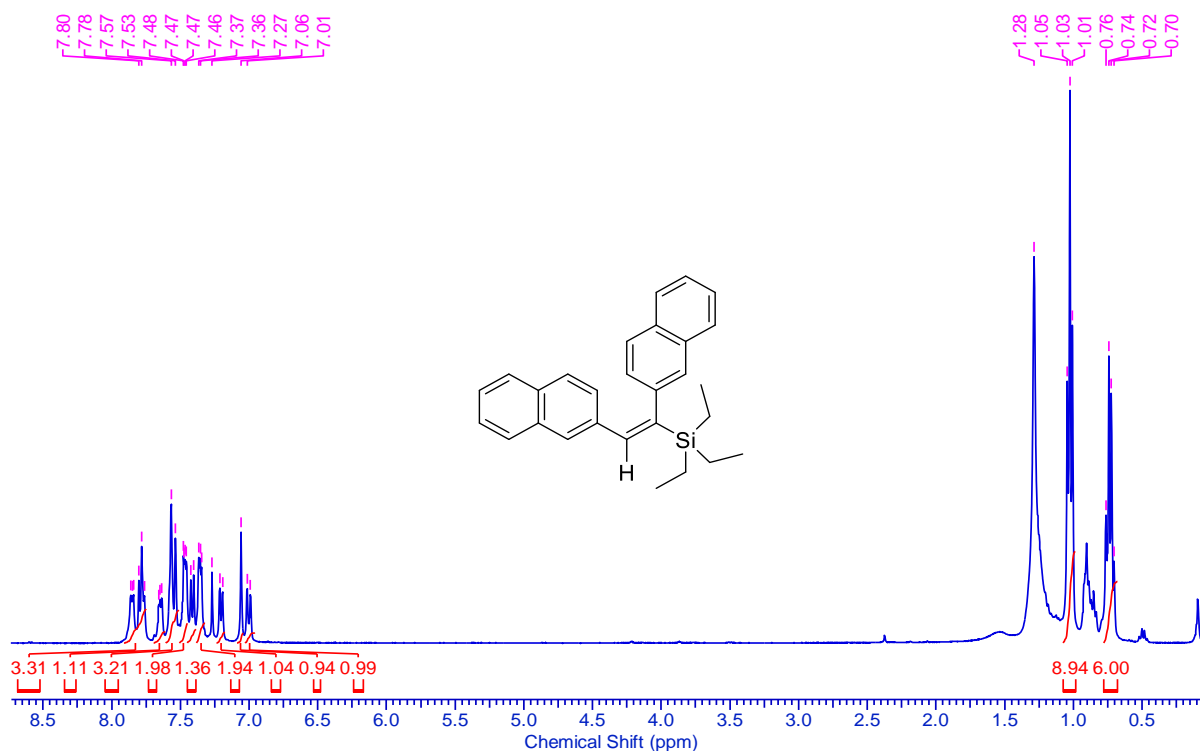


Figure 2.25: ^1H NMR spectrum of (E)-(1,2-di(naphthalen-2-yl)vinyl)triethylsilane (3i).

(E)-(1,2-diphenylvinyl)diphenylsilane (3m)

^1H NMR (500 MHz, CDCl_3): δ = 7.6 (m, 2H), 7.58 (d, 2H), 7.42 (m, 2H), 7.38 (m, 4H), 7.19 (m, 3H), 7.12 (m, 3H), 7.03 (m, 5H), 5.31 (s, 1H).

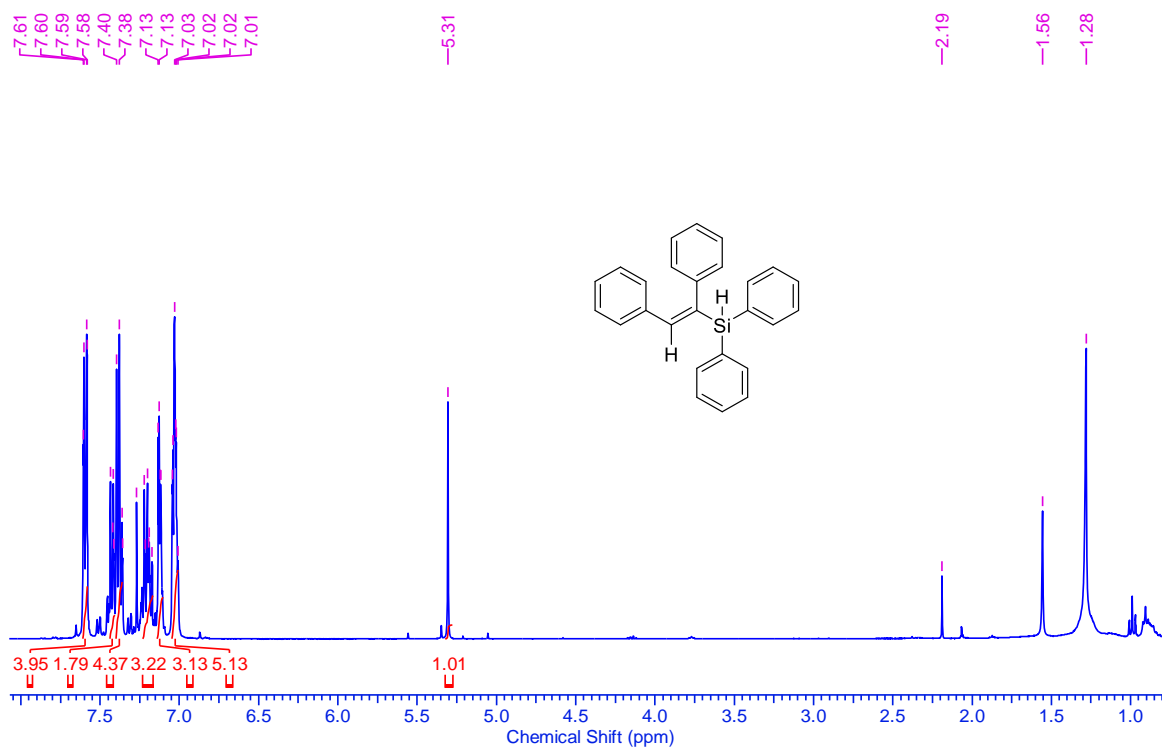
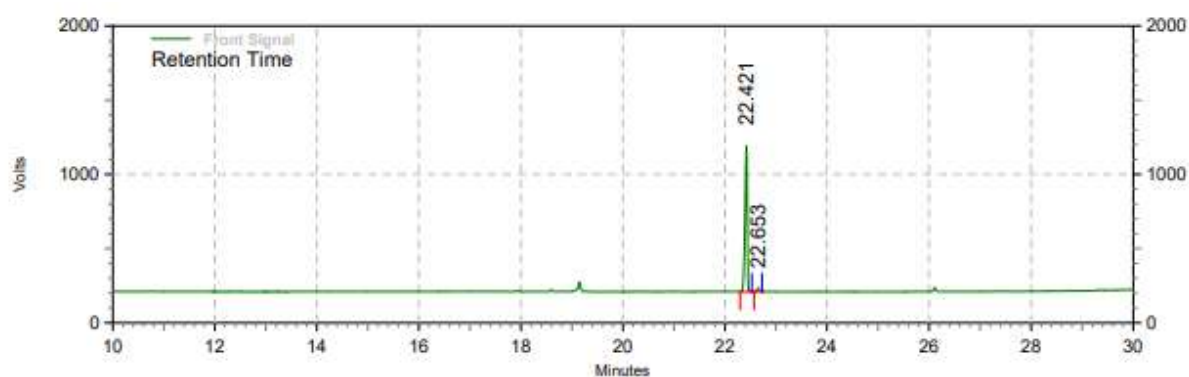


Figure 2.26: ¹H NMR spectrum of (E)-(1,2-diphenylvinyl)diphenylsilane (3m).

2.4.6 Gram scale synthesis

Diphenylacetylene **1a** (1 g, 5.62 mmol), triethylsilane **2a** (980 mg, 8.43 mmol), [Fe-1] (80 mg, 0.281 mmol, 5 mol %), L5 (150 mg, 0.281 mmol, 5 mol %) were introduced in a 100 mL Schlenk flask equipped with a magnetic stir bar under argon atmosphere. Toluene (20 mL) was added to the reaction mixture. The reaction mixture was stirred at 70 °C for 24 h. The mixture was extracted with diethyl ether (3 × 20 mL). After that, the layers of mixed diethyl ether were dried over sodium sulfate and concentrated under vacuum. After evaporation of the solvent, the crude reaction mixture was purified by silica gel column chromatography (petroleum ether/EtOAc 50/1), yielding the hydrosilylated product. GC analysis showed full conversion with no starting alkyne ($R_t = 17.7$ min) with excellent E/Z ratio (98/2). The product was isolated in 90% yield (1.48 g).



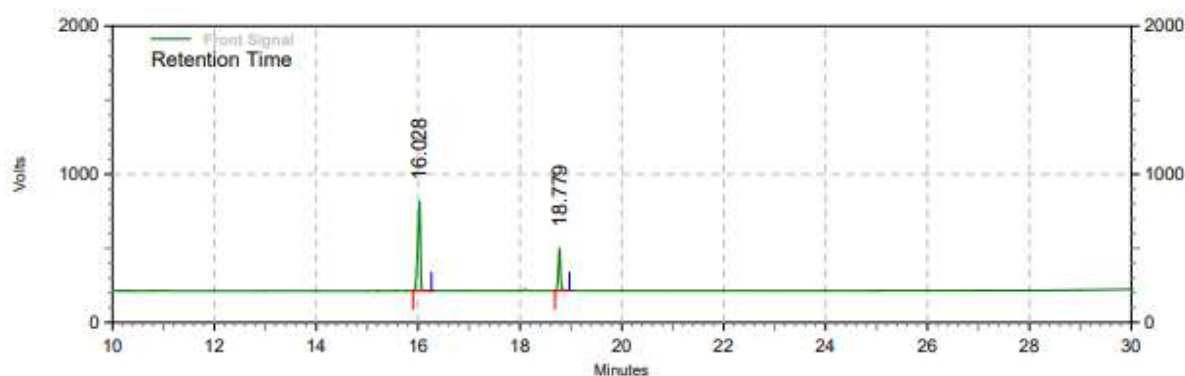
**Front Signal
Results**

Retention Time	Area	Area %	Height	Height %
22.421	22687095	97.93	7538810	97.65
22.653	480082	2.07	181419	2.35
Totals	23167177	100.00	7720229	100.00

Figure 2.27: GC chromatogram for gram scale reaction of 1a.

2.4.7 Protodesilylation reaction

3a (74 mg, 0.25 mmol), TBAF (1 M in THF, 1 mL, 1 mmol) were taken to a 10 mL teflon-valved flask equipped with a magnetic stir bar under argon atmosphere. THF (2 mL) was added to the reaction mixture. The reaction mixture was stirred at 80 °C for 24 h. The solvent was evaporated under vacuum. The residue was purified by silica gel column chromatography eluting with petroleum ether/EtOAc (v/v 50/1) to give a colourless viscous liquid (39 mg, 86%). GC analysis showed that it was Z/E mixture alkene in 71/29 ratio.



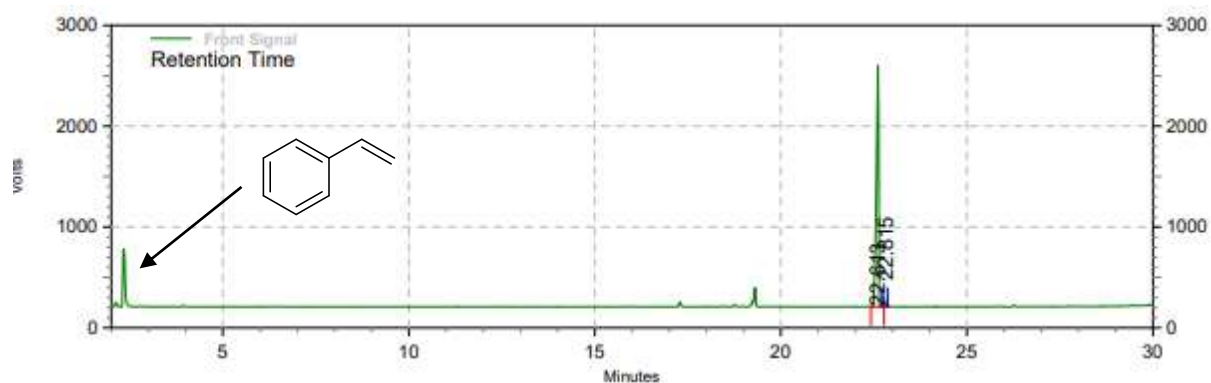
Front Signal Results

Retention Time	Area	Area %	Height	Height %
16.028	16563078	71.26	4637054	67.71
18.779	6680885	28.74	2211359	32.29
Totals	23243963	100.00	6848413	100.00

Figure 2.28: GC chromatogram for protodesilylation reaction.

2.4.8 Chemoselective hydrosilylation

Diphenylacetylene **1a** (44.55 mg, 0.25 mmol), triethylsilane **2a** (40 mg, 0.375 mmol), [Fe-1] (3.575 mg, 0.0125 mmol, 5 mol %), L5 (6.8 mg, 0.0125 mmol, 5 mol %) were introduced in a 10 mL teflon-valved flask equipped with a magnetic stir bar under argon atmosphere. Styrene (26 mg, 0.25 mmol) was also added to it under argon. Toluene (1 mL) was added to the reaction mixture. The reaction mixture was stirred at 60 °C for 24 h. The mixture was extracted with diethyl ether (10 mL) and passed through a short pad of silica and then injected in GC. GC analysis showed no presence of starting alkyne ($R_t = 17.7$ min). However, styrene and hydrosilylated product of alkyne ($R_t = 22.6, 22.8$) were present there.



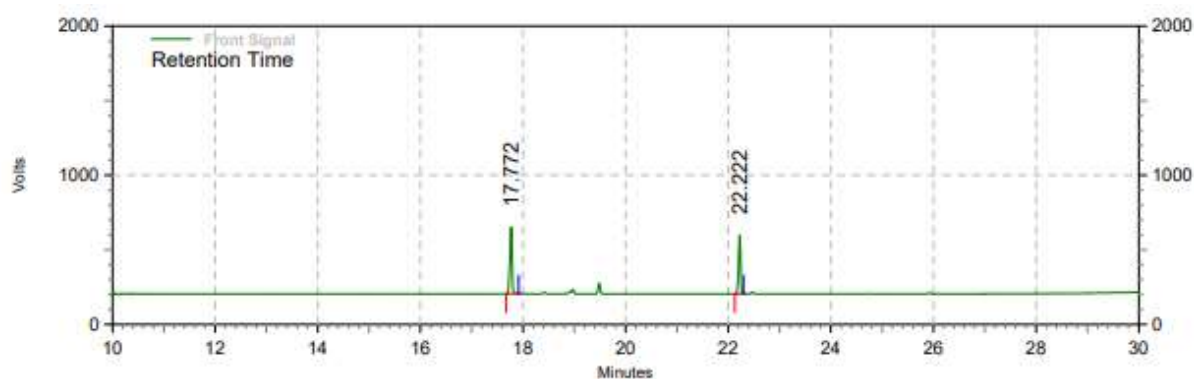
Front Signal Results

Retention Time	Area	Area %	Height	Height %
22.613	74742941	98.84	18335524	98.04
22.815	877403	1.16	365607	1.95
Totals	75620344	100.00	18701131	100.00

Figure 2.29: GC chromatogram for chemoselective hydrosilylation reaction.

2.4.9 Test for homogeneity

Diphenylacetylene **1a** (44.55 mg, 0.25 mmol), triethylsilane **2a** (40 mg, 0.375 mmol), [Fe-1] (3.575 mg, 0.0125 mmol, 5 mol %), L5 (6.8 mg, 0.0125 mmol, 5 mol %) were introduced in a 10 mL teflon-valved flask equipped with a magnetic stir bar under argon atmosphere. DCT (10.2 mg, 0.05 mmol) or [dppe (20 mg, 0.05 mmol) or bpy (7.8 mg, 0.05 mmol)] was also added to it under argon. Toluene (1 mL) was added to the reaction mixture. The reaction mixture was stirred at 60 °C for 16 h. The mixture was extracted with diethyl ether (10 mL) and passed through a short pad of silica and then injected in GC. GC analysis showed 45% conversion with respect to starting alkyne ($R_t = 17.7$ min) for DCT. However, in case of dppe or bpy, there was no conversion.



Front Signal Results

Retention Time	Area	Area %	Height	Height %
17.772	10310793	55.49	3422937	53.27
22.222	8270680	44.51	3002608	46.73
Totals	18581473	100.00	6425545	100.00

Figure 2.30: GC chromatogram for hydrosilylation reaction of **1a** in presence of DCT.

2.4.10 Radical trap experiment

Diphenylacetylene **1a** (44.55 mg, 0.25 mmol), triethylsilane **2a** (40 mg, 0.375 mmol), [Fe-1] (3.575 mg, 0.0125 mmol, 5 mol %), L5 (6.8 mg, 0.0125 mmol, 5 mol %) were introduced in a 10 mL teflon-valved flask equipped with a magnetic stir bar under argon atmosphere. TEMPO (78 mg, 0.5 mmol) or [galvinoxyl (211 mg, 0.5 mmol)] was also added to it under argon. Toluene (1 mL) was added to the reaction mixture. The reaction mixture was stirred at 60 °C for 16 h. The mixture was extracted with diethyl ether (10 mL) and passed through a short pad of silica and then injected in GC. GC analysis showed no conversion with respect to starting alkyne ($R_t = 17.7$ min) for both TEMPO and galvinoxyl. To our delight, TEMPO adduct with the metal was detected in ESI-MS (Fig 2.31).

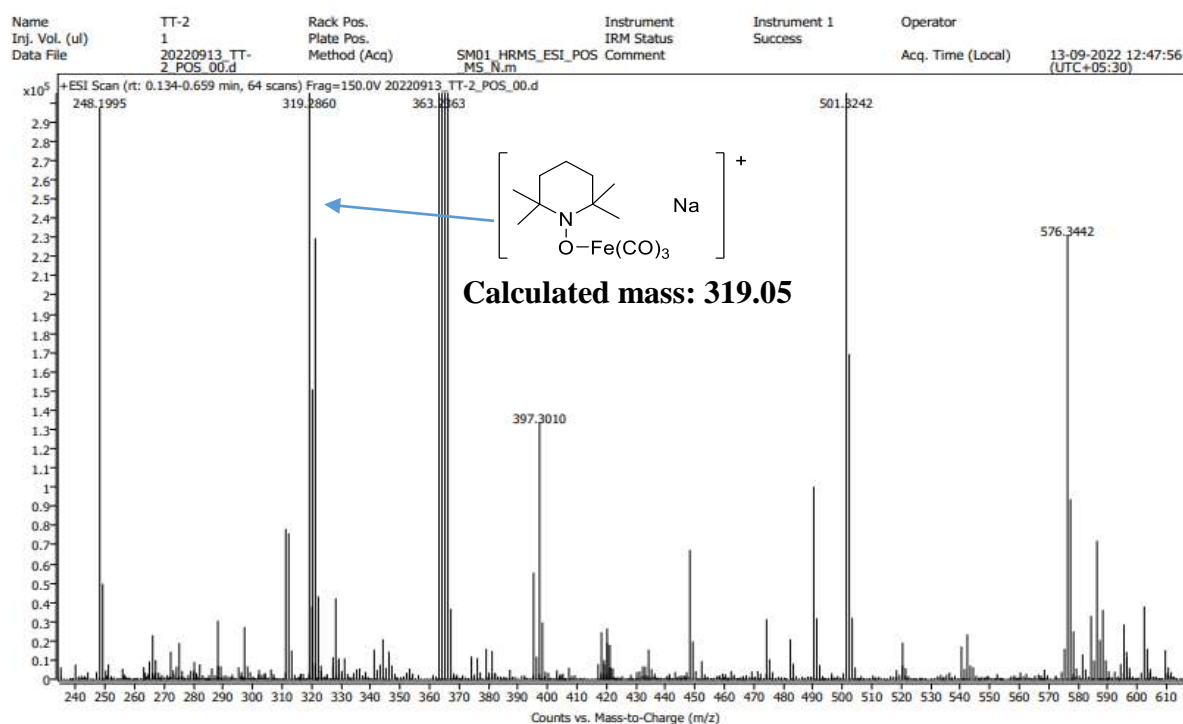


Figure 2.31: ESI-MS for hydrosilylation reaction of **1a** in presence of TEMPO.

2.4.11 Control experiment

Triethylsilane **2a** (29 mg, 0.25 mmol), [Fe-1] (3.575 mg, 0.0125 mmol, 5 mol %), L5 (6.8 mg, 0.0125 mmol, 5 mol %) were introduced in a 10 mL teflon-valved flask equipped with a magnetic stir bar under argon atmosphere. Toluene (1 mL) was added to the reaction mixture. The reaction mixture was stirred at 60 °C for 16 h. The mixture was extracted with diethyl ether (10 mL) and passed through a short pad of silica and then injected in GC-MS. GC-MS analysis showed the presence of silane coupled product (PhMe₂Si-SiMe₂Ph, calculated mass 270.13) with [M+H]⁺ (Fig 2.32).

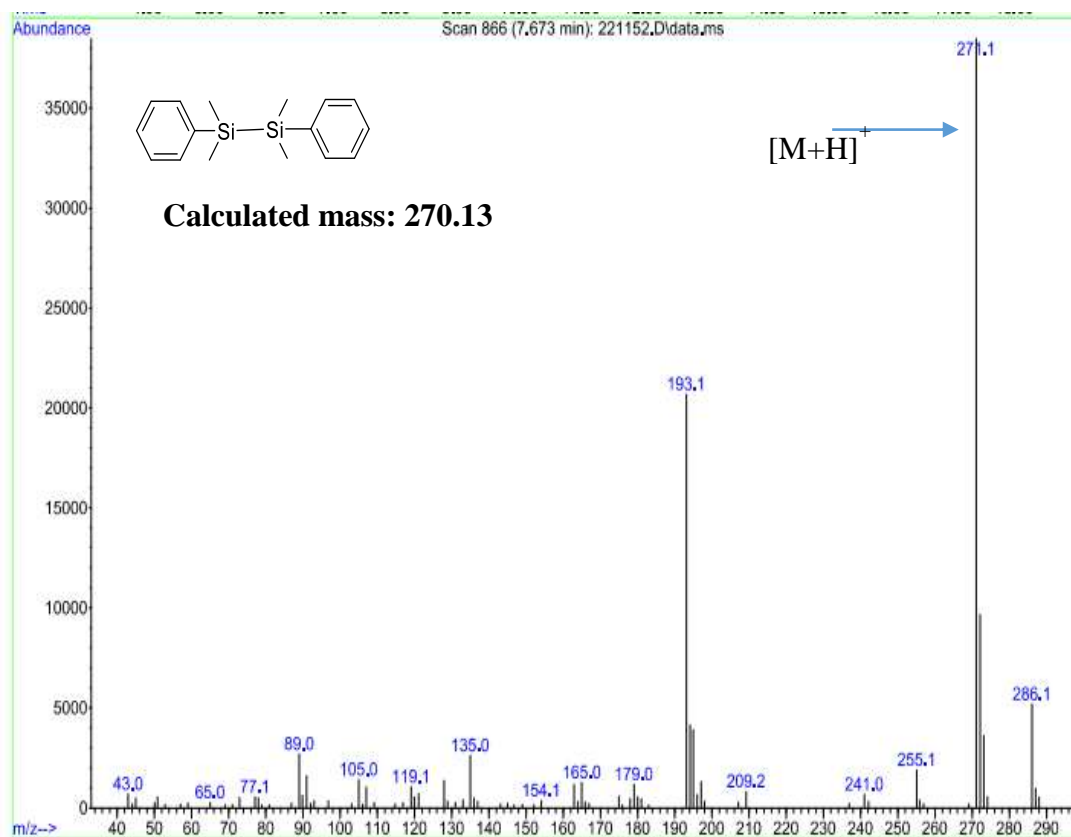


Figure 2.32: GC-MS for control experiment.

2.4.12 Synthesis of iron complex $[\text{Fe}(\text{CO})_4\text{HSiPh}_3]$:

The iron catalyst was made by following a literature reported procedure.¹⁶ A mixture of 15 ml of $\text{Fe}(\text{CO})_5$ (22 g, 0.11 mol) and 25.5 g of $(\text{C}_6\text{H}_5)_3\text{SiH}$ (0.098 mol) were taken in a Schlenk flask in 180 mL heptane and was irradiated for 22 h. The carbon monoxide evolution was fast at first (one bubble per second), but it had nearly ceased by the conclusion of the reaction time. There was little decomposition. The reaction mixture was filtered and the pale yellow, clear solution was cooled slowly in the refrigerator. White crystalline compound $[\text{Fe}(\text{CO})_4\text{HSiPh}_3]$ was formed in good yield (70%).

$[\text{Fe}(\text{CO})_4(\text{H})(\text{SiPh}_3)]$

$^1\text{H NMR}$ (500 MHz, C_6D_6): $\delta = 7.46$ (m, 6H), 6.93 (m, 9H), -9.18 (s, 1H).

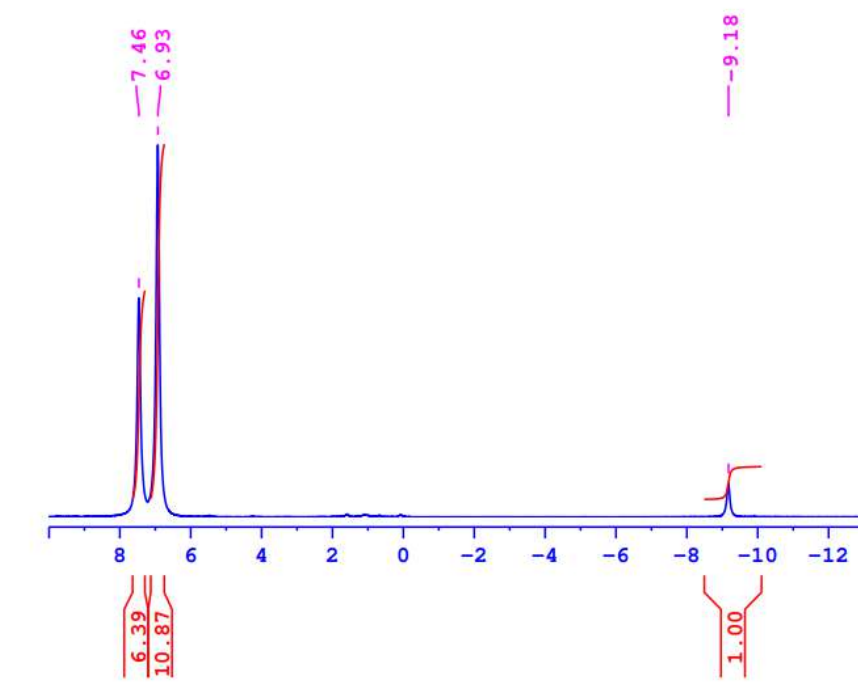


Figure 2.33: ^1H NMR spectrum of $[\text{Fe}(\text{CO})_4(\text{H})(\text{SiPh}_3)]$.

2.4.13 Hydrosilylation procedure:

Alkyne **1a** (44.55 mg, 0.25 mmol), silane **2a** (40 mg, 0.375 mmol), $[\text{Fe}(\text{CO})_4\text{HSiPh}_3]$ (5.35 mg, 0.0125 mmol, 5 mol %), L5 (6.8 mg, 0.0125 mmol, 5 mol %) were introduced in a 10 mL teflon-valved flask equipped with a magnetic stirrer under argon atmosphere. Toluene (1 mL) was added to the reaction mixture. The reaction mixture was stirred at 60 °C for 16 h. The mixture was extracted with diethyl ether (3×10 mL). After that, the layers of mixed diethyl ether were dried over sodium sulfate and concentrated under vacuum. After evaporation of the solvent, the crude reaction mixture was purified by silica gel column chromatography (petroleum ether/EtOAc 50/1), yielding (92%) the hydrosilylated product.

However, when the same reaction was carried out after adding TEMPO (78 mg, 0.5 mmol) or [galvinoxyl (211 mg, 0.5 mmol)], there was no conversion.

2.4.14 Rate order determination

The initial rate method was used to determine the rate of the hydrosilylation reaction with different reaction components. Using MS Excel, the product concentration vs. time (min) plot data was linearly fitted. The reaction rate is represented by the slope of the linear fitting. The

reaction rate is represented by the slope of the linear fitting. The $\log(\text{rate})$ vs. $\log(\text{conc})$ plot for each component was then used to determine the order of the reaction.

2.4.14.1 Rate order determination for [Fe-1]/L5:

To determine the order of the hydrosilylation reaction with respect to [Fe-1]/L5 catalyst system, the initial rates at different concentration of [Fe-1]/L5 were determined. In an oven dried teflon-screw capped tube, diphenylacetylene (0.25 mmol, 44.55 mg), triethylsilane (0.375 mmol, 40 mg) were taken under argon atmosphere. Specific amount of [Fe-1] and $\text{P}(\text{C}_6\text{F}_5)_3$ were added (as shown in table 2.3) to the tube. Dodecane (0.25 mmol, 42.6 mg, 57 μL) was added to the tube as an internal standard. Required amount of toluene was added to make the volume 1.0 mL. The tube was closed under argon and placed in a pre-heated oil bath at 60 °C. The aliquot was collected first after 6 min. Then it was collected at a constant interval of 3 min and the yield of the 3a (M) was determined with the help of GC. The data were collected till 18 min.

Table 2.3. Rate of hydrosilylation reaction at different initial concentration of catalyst

Entry	[Fe-1] (mg)	$\text{P}(\text{C}_6\text{F}_5)_3$ (mg)	Initial Conc. of [Fe-1]/L5 [M]	Initial rate (M/min)	R^2
1	1.8	3.4	0.00625	0.0002	0.9843
2	3.6	6.8	0.0125	0.0004	0.9988
3	5.4	10.2	0.01875	0.0006	0.9897
4	7.2	13.6	0.025	0.0008	0.9448

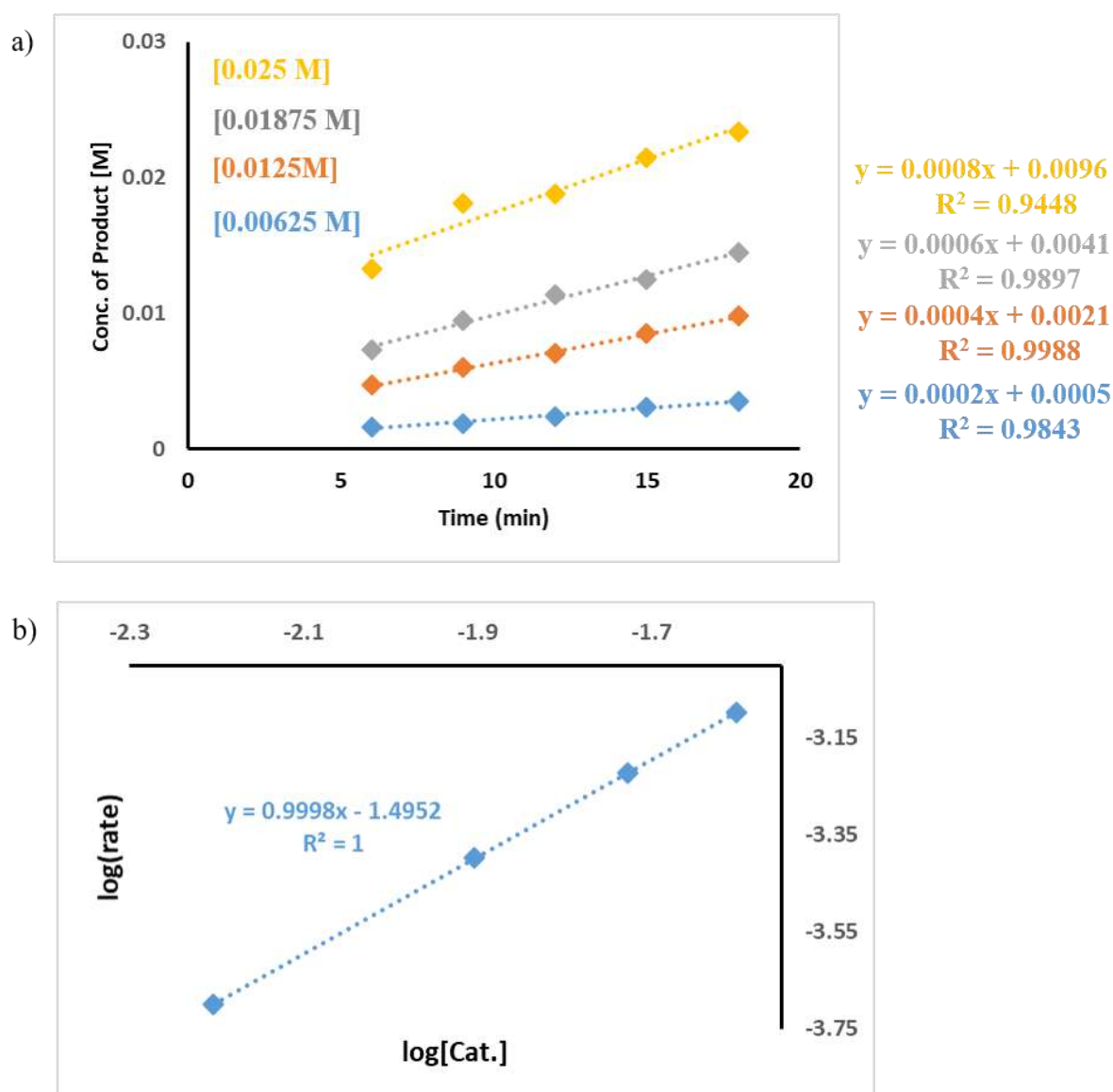


Figure 2.34: a) Time dependent formation of 3a at different concentration of catalyst. b) Plot of $\log(\text{rate})$ vs. $\log[\text{Cat.}]$.

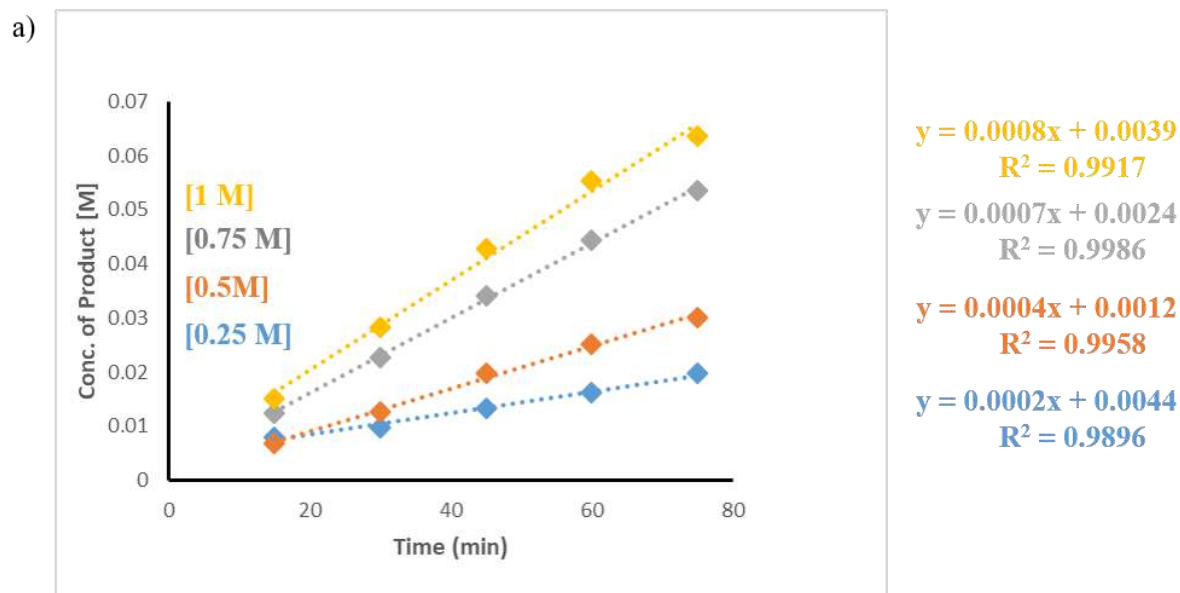
2.4.14.2 Rate order determination for triethylsilane:

To determine the order of the hydrosilylation reaction with respect to triethylsilane, the initial rates at different concentration of triethylsilane were determined. In an oven dried teflon-screw capped tube, diphenylacetylene (0.25 mmol, 44.55 mg), [Fe-1] (0.00625 mmol, 1.8 mg), $\text{P}(\text{C}_6\text{F}_5)_3$ (0.00625 mmol, 3.4 mg) were taken under argon atmosphere. Specific amount of triethylsilane was added (as shown in table 2.4) to the tube. Dodecane (0.25 mmol, 42.6 mg, 57 μL) was added to the tube as an internal standard. Required amount of toluene was added to make the volume 1.0 mL. The tube was closed under argon and placed in a pre-

heated oil bath at 60 °C. The aliquot was collected at constant 15 minutes interval and the yield of the 3a (M) was determined with the help of GC. The data were collected till 75 min.

Table 2.4. Rate of hydrosilylation reaction at different initial concentration of silane

Entry	Et ₃ SiH (mg)	Initial Conc. of [Et ₃ SiH] [M]	Initial rate (M/min)	R ²
1	29	0.25	0.0002	0.9896
2	58	0.5	0.0004	0.9958
3	87	0.75	0.0007	0.9986
4	116	1.0	0.0008	0.9917



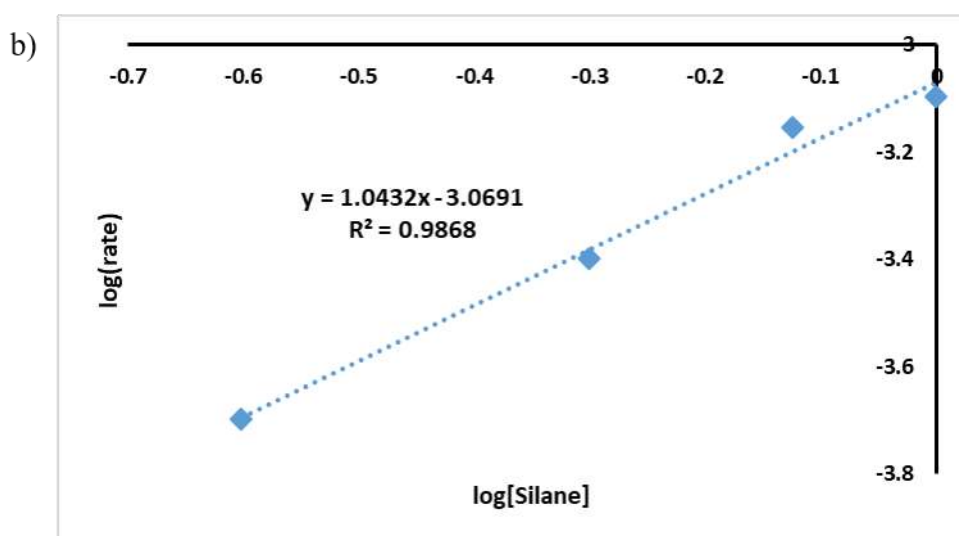


Figure 2.35: a) Time dependent formation of 3a at different concentration of Et_3SiH . b) Plot of $\log(\text{rate})$ vs. $\log[\text{Silane}]$.

2.4.14.3 Rate order determination for diphenylacetylene:

To determine the order of the hydrosilylation reaction with respect to diphenylacetylene, the initial rates at different concentration of diphenylacetylene were determined. In an oven dried teflon-screw capped tube, [Fe-1] (0.00625 mmol, 1.8 mg), $\text{P}(\text{C}_6\text{F}_5)_3$ (0.00625 mmol, 3.4 mg), triethylsilane (0.375 mmol, 40 mg) were taken under argon atmosphere. Specific amount of diphenylacetylene was added (as shown in table 2.5) to the tube. Dodecane (0.25 mmol, 42.6 mg, 57 μL) was added to the tube as an internal standard. Required amount of toluene was added to make the volume 1.0 mL. The tube was closed under argon and placed in a pre-heated oil bath at 60 $^\circ\text{C}$. The aliquot was collected at constant 15 min interval and the yield of the 3a (M) was determined with the help of GC. The data were collected till 75 minutes.

Table 2.5. Rate of hydrosilylation reaction at different initial concentration of alkyne

Entry	PhCCPh (mg)	Initial Conc. of [PhCCPh] [M]	Initial rate (M/min)	R^2
1	44.5	0.25	0.0003	0.9882
2	66.75	0.375	0.0003	0.9974
3	89	0.5	0.0004	0.999
4	111.25	0.625	0.0004	0.995

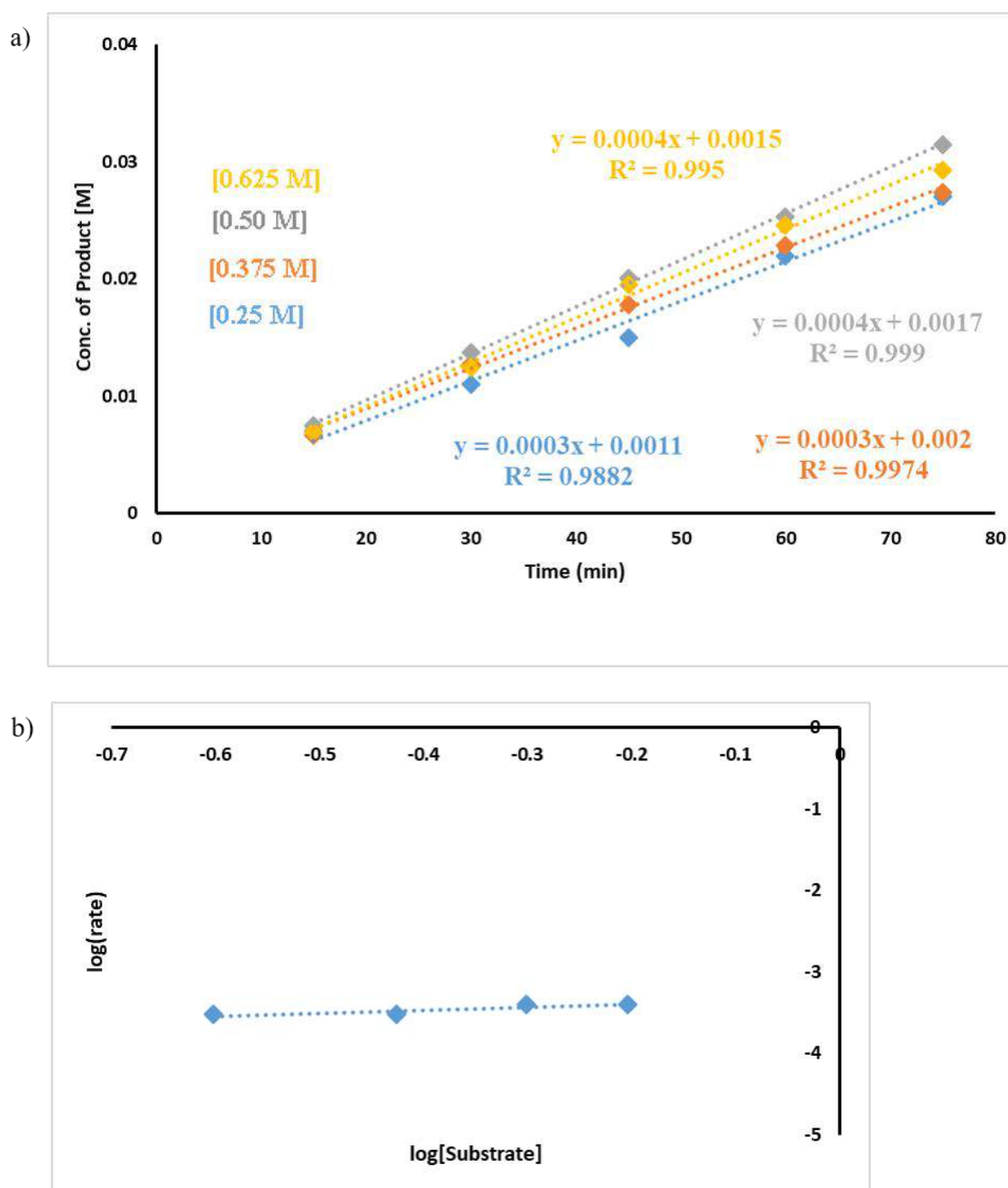


Figure 2.36: a) Time dependent formation of 3a at different concentration of diphenylacetylene. b) Plot of $\log(\text{rate})$ vs. $\log[\text{Substrate}]$.

2.4.15 Rate determination for hydrosilylation of substituted alkynes with triethylsilane

As mentioned in the earlier section, representative procedure of rate measurement was followed by taking [Fe-1] (0.00625 mmol, 1.8 mg), $\text{P}(\text{C}_6\text{F}_5)_3$ (0.00625 mmol, 3.4 mg),

triethylsilane (0.375 mmol, 40 mg) and 1,2-di-p-tolylethyne (0.25 mmol, 52 mg) or [1,2-bis(4-methoxyphenyl)ethyne (0.25 mmol, 59.57 mg); 1,2-diphenylethyne (0.25 mmol, 44.55 mg); 1,2-bis(4-chlorophenyl)ethyne (0.25 mmol; 61.8 mg); 1,2-bis(4-(trifluoromethyl)phenyl)ethyne (0.25 mmol, 78.55 mg)] under argon atmosphere. Dodecane (0.25 mmol, 42.6 mg, 57 μ L) was added to the tube as an internal standard. Required amount of toluene was added to make the volume 1.0 mL. The tube was closed under argon and placed in a pre-heated oil bath at 60 $^{\circ}$ C. The aliquot was collected at constant 15 minutes interval and the yield of the 3a (M) was determined with the help of GC. The data were collected till 75 minutes. The initial rate for the coupling reactions are shown below (Figure 2.37). The Hammett plot was drawn from the correlation between the initial rates and the σ_p values, i.e $\log(k_R/k_H)$ vs. σ_p and slope obtained was 0.289 (Figure 2.3, a).

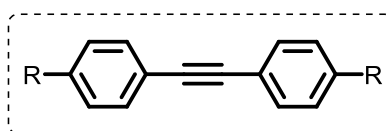
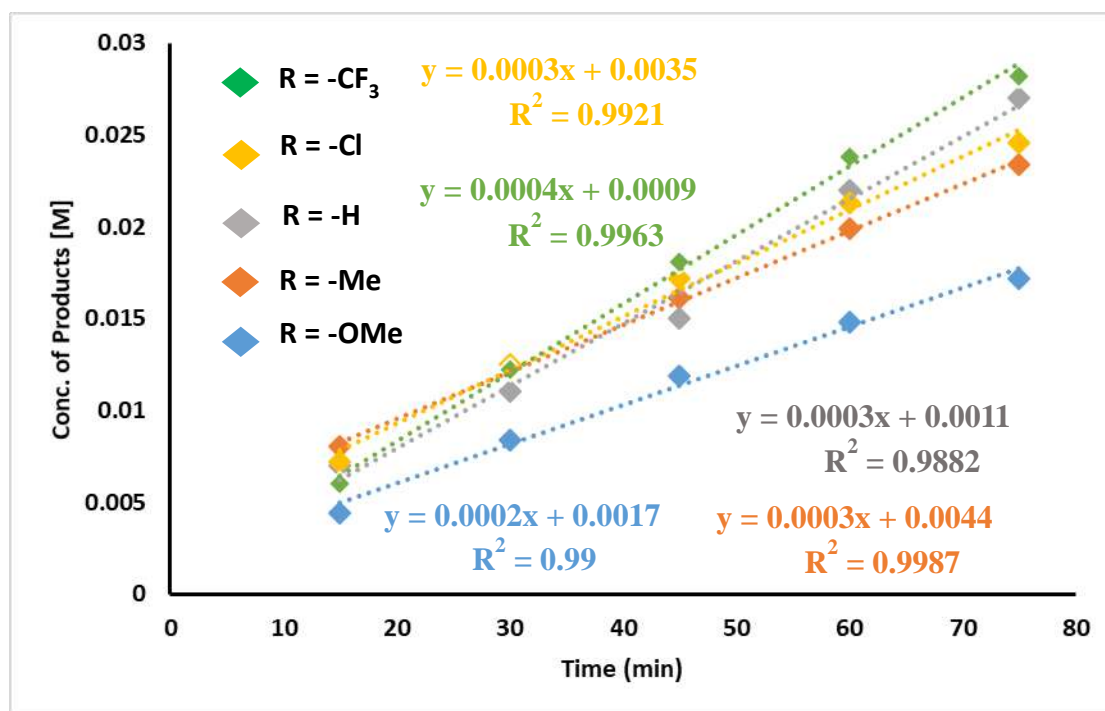


Figure 2.37: Time dependent formation of hydrosilylation products for the coupling of triethylsilane with different para-substituted alkynes.

2.4.16 Eyring analysis:

In an oven dried teflon-screw capped tube, diphenylacetylene (0.25 mmol, 44.55 mg), [Fe(BDA)(CO)₃] (2.5 mol %, 0.00625 mmol, 1.8 mg), P(C₆F₅)₃ (2.5 mol %, 0.00625 mmol, 3.4 mg), triethylsilane (0.375 mmol, 40 mg) were taken under argon atmosphere. Then internal standard dodecane (0.25 mmol, 42.6 mg, 57 μ L) and 1 mL toluene were added to it under argon and transferred to a preheated oil bath set at different temperatures 45 $^{\circ}$ C, 50 $^{\circ}$ C, 55 $^{\circ}$ C, 60 $^{\circ}$ C. The aliquot was taken at 15 minute intervals, and GC was used to track the yield. The reaction rate is represented by the slope of the linear fitting.

Table 2.6. Rate of hydrosilylation reaction at different temperature

k [M/min]	T (K)	1/T	ln (k/T)	ln (k)
1.00E-04	318	0.003145	-14.972	-9.21
2.00E-04	323	0.003096	-14.295	-8.517
3.00E-04	328	0.003049	-13.905	-8.112
4.00E-04	333	0.003003	-13.632	-7.824

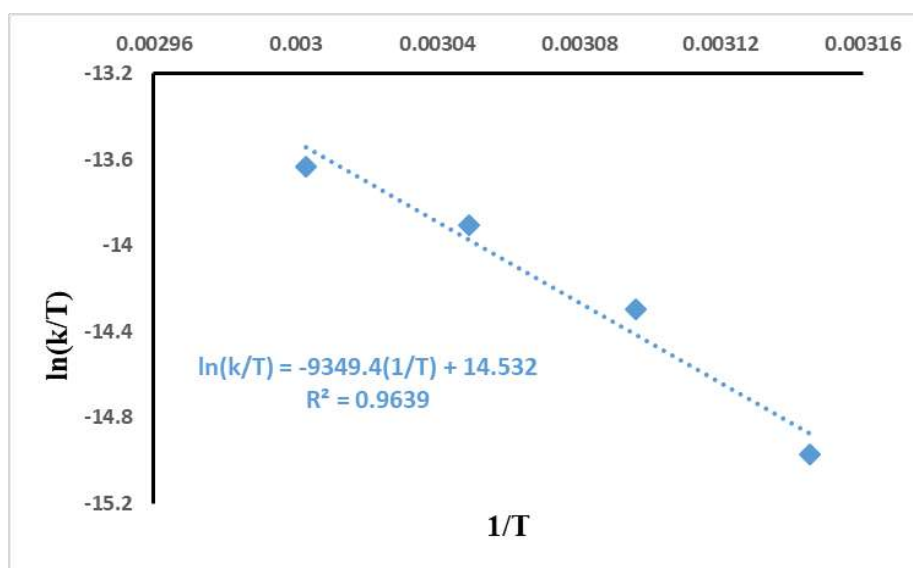


Figure 2.38: Eyring plot for [Fe-1] catalysed hydrosilylation of 1a with 2a in toluene.

Based on Eyring equation, activation thermodynamic parameters were calculated

Eyring equation

$$\ln(k/T) = -\Delta H^{\ddagger}/RT + \ln(k_B/h) + \Delta S^{\ddagger}/R$$

$$\Delta H^{\ddagger} = 77.731 \text{ kJ mol}^{-1}$$

$$\Delta S^\ddagger = -76.72 \text{ J K}^{-1} \text{ mol}^{-1}$$
$$\Delta G^\ddagger_{(323 \text{ K})} = 102.51 \text{ kJ mol}^{-1}$$

2.5 Conclusion

In summary, we have developed an iron catalysed (E)-selective hydrosilylation methodology for internal alkynes which work under mild condition without the use of any highly reactive additive. The reaction tolerates electron donating as well as electron withdrawing functional groups. This methodology can easily be scaled up to gram scale. Radical trap experiment revealed that the reaction proceeds through one electron pathway. The very low value of ρ (0.289) obtained from Hammett plot suggested that alkyne co-ordination is not involved in RDS. The negative activation entropy obtained from Eyring plot, indicated the involvement of an associative pathway in RDS. Kinetic analysis and mechanistic investigation suggest the possible involvement of a Fe(0)/Fe(I)/Fe(II) catalytic cycle. Further mechanistic studies are currently undergoing in our lab. (E)-selective hydrosilylation involving one electron pathway is quite unique in the literature.

2.6 References

- 1) Marciniak, B. *Coord. Chem. Rev.* **2005**, *249*, 2374-2390.
- 2) Franz, A. K.; Wilson, S. O. *J. Med. Chem.*, **2013**, *56*, 388-405.
- 3) Nakao, Y.; Hiyama, T. *Chem. Soc. Rev.* **2011**, *40*, 4893-4901.
- 4) (a) Meister, T. K.; Kuck, J. W.; Riener, K.; Pothig, A.; Herrmann, W. A.; Kuhn, F. E. *J. Catal.* **2016**, *337*, 157-166. (b) Tuttle, T.; Wang, D. Q.; Thiel, W.; Kohler, J.; Hofmann, M.; Weis, J. *Dalton Trans.* **2009**, 5894-5901. (c) Bokka, A.; Hua, Y. D.; Berlin, A. S.; Jeon, J. *ACS Catal.* **2015**, *5*, 3189-3195. (d) Komine, N.; Abe, M.; Suda, R.; Hirano, M. *Organometallics* **2015**, *34*, 432-437. (e) Bai, Y.; Zhang, F. X.; Li, J. Y.; Xu, Y. S.; Peng, J. J.; Xiao, W. J. *J. Organomet. Chem.* **2015**, *794*, 65-69.
- 5) Belger, C.; Plietker, B. *Chem. Commun.*, **2012**, *48*, 5419-5421.
- 6) Hu, M.-Y.; He, P.; Qiao, T.-Z.; Sun, W.; Li, W.-T.; Lian, J.; Li, J.-H.; Zhu, S.-F. *J. Am. Chem. Soc.* **2020**, *142*, 16894-16902.
- 7) Guo, Z.; Wen, H.; Liu, G.; Huang, Z. *Org. Lett.* **2021**, *23*, 2375-2379.

- 8) Chalk, A. J.; Harrod, J. F. *J. Am. Chem. Soc.* **1965**, *87*, 16-21.
- 9) Maruyama, Y.; Yamamura, K.; Nakayama, I.; Yoshiuchi, K.; Ozawa, F. *J. Am. Chem. Soc.* **1998**, *120*, 1421-1429.
- 10) Collman, J. P.; Hegedus, L. S.; Norton, J. R.; Finke, R. G. In *Principles and Applications of Organotransition Metal Chemistry*; University Science Books: Sausalito, CA, 1987; pp 306–333.
- 11) Yang, X.; Wang, C. *Angew. Chem., Int. Ed.* **2018**, *57*, 923-928.
- 12) RiveraHernandez, A.; Fallon, B. J.; Ventre, S.; Simon, C.; Tremblay, M. H.; Gontard, G.; Derat, E.; Amatore, M.; Aubert, C.; Petit, M. *Org. Lett.* **2016**, *18*, 4242-4245.
- 13) Bleith, T.; Gade, L. H. *J. Am. Chem. Soc.* **2016**, *138*, 4972-4983.
- 14) Liang, H.; Ji, Y.-X.; Wang, R.-H.; Zhang, Z.-H.; Zhang, B. *Org. Lett.* **2019**, *21*, 2750-2754.
- 15) Pandey, S.; Raj, K. V.; Shinde, D. R.; Vanka, K.; Kashyap, V.; Kurungot, S.; Vinod, C. P.; Chikkali, S. H. *J. Am. Chem. Soc.* **2018**, *140*, 4430–4439.
- 16) Graham, W. A. G.; Jetz, W. *Inorg. Chem.* **1971**, *10*, 4–9.

Chapter 3

Catalytic Alkoxylation, Polymerization of Silanes and Tandem Alkoxylation- Hydrosilylation of Alkynes: An Iron Blitzkrieg

3.1 Abstract

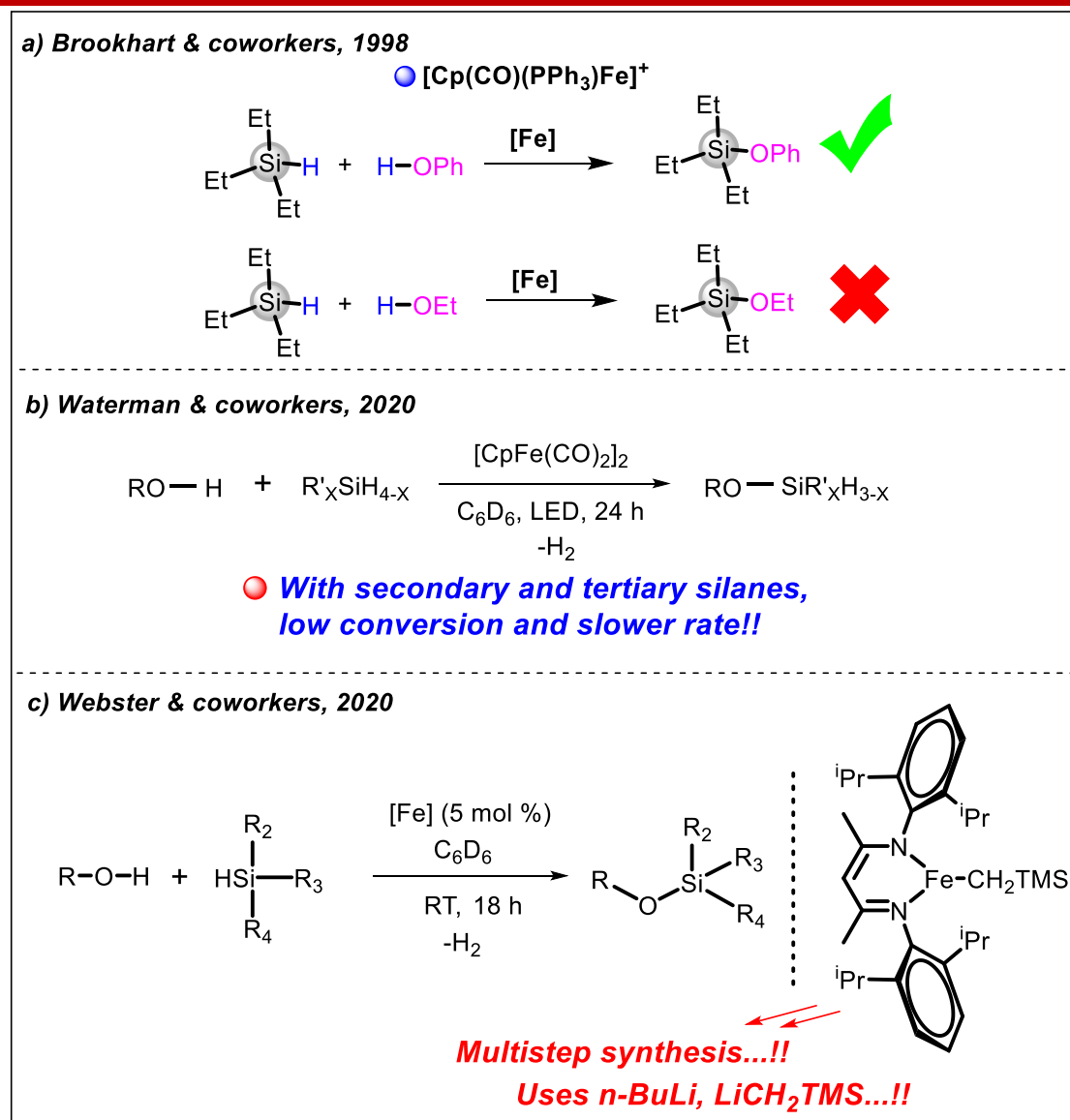
Silyl ethers are one of the most important silicon compounds due to their wide range of applications in silicon polymers, protecting group chemistry, organic-inorganic hybrid materials and surface coating chemistry. For hydrosilane alcoholysis, a variety of transition metal complexes along with main group Lewis acid/base catalysts have been developed. Surprisingly, iron is not well explored for this reaction. As a result, developing more efficient and selective iron catalyst for silane alcoholysis is highly desirable. To achieve this, we synthesized an iron catalyst by following a literature reported procedure and successfully developed an iron catalysed methodology for alkoxylation of silanes to produce hydrogen gas and silyl ethers. The reaction works efficiently with different silanes as well as different alcohols containing electron donating as well as electron withdrawing groups. To demonstrate the synthetic utility of this methodology, the iron catalyst was successfully implemented to synthesize degradable polysilylether from bio-based isosorbide and commercially available diphenylsilane by dehydrogenative cross coupling. Finally, this iron catalyst was successfully utilized to develop tandem alkoxylation-hydrosilylation of internal alkynes which would pave the way for a novel approach to creating structurally diverse organosilicon compounds. In literature, only one platinum-catalyst is known to achieve such transformation.

3.2 Introduction

Silyl ethers are one of the most important silicon compounds due to their wide range of application in silicon polymers¹, protecting group chemistry², organic-inorganic hybrid materials³ and surface coating chemistry⁴. Silyl ethers are generally prepared by reacting alcohols and halo silanes in presence of stoichiometric amount of base. However, these methods are not environmentally benign and suffer from several drawbacks, such as these methods can't be used when the reaction has to be performed under neutral condition. Furthermore, controlling the degree of condensation is also problematic when several Si-X bonds are present in the substrate. To circumvent these problems, the most appealing and atom-economic route could be catalytic dehydrogenative silylation of alcohols with hydrosilanes, which produces the clean fuel hydrogen as the sole byproduct.⁵

For hydrosilane alcoholysis, a variety of transition metal complexes⁶ along with main group Lewis acid/base catalysts⁷ have been developed. However, with transition metal complexes,

mostly late transition metals are involved in such transformation (perhaps because early transition metals tend to be more oxophilic). Yamada investigated a variety of acetylacetonate (acac) salts, with $\text{Cu}(\text{acac})_2$ producing the highest yields⁸, whereas Ito and Sawamura implemented Cu^9 and Au^{10} for such transformation. In recent past iron catalysis has received a lot of interest, since it is abundant, affordable, and biocompatible, thus fits for green and sustainable chemistry applications. In addition to this, iron's distinctive electronic structures allow it to mediate different types of chemical reactions.¹¹ As a result, developing more efficient and selective iron catalyst for silane alcoholysis is highly desirable. Surprisingly, iron is not well explored for this reaction. For example, Riley and co-workers reported in 1980, $[\text{Fe}(\text{H})_2(\text{PMePh}_2)_4]$ and $[\text{Fe}(\text{H})_2(\text{N}_2)(\text{PEtPh}_2)_3]$ for silane alcoholysis which were only active for $(\text{EtO})_3\text{SiH}$ but inactive for Et_3SiH . Subsequently, in 1998, Brookhart and co-workers reported the $[\text{Cp}(\text{CO})(\text{PPh}_3)\text{Fe}]^+$ fragment to catalyse silane alcoholysis in presence of non-coordinating counter anion.¹² However, the cationic iron complex was active only when phenol was used as alkoxyating agent but was inactive when ethanol was used as alkoxyating agent (Scheme 3.1, a). In 2020, Waterman and co-workers reported an iron catalysed silicon-oxygen heterodehydrocoupling reaction by commercially available cyclopentadienyl dicarbonyl iron dimer $[\text{CpFe}(\text{CO})_2]_2$, under photochemical condition.¹³ Alcohols and secondary or tertiary silanes can also react to form silyl ethers, although these reactions are distinguished by their slower reaction rates and lower conversions (Scheme 3.1, b). In the same year, Webster and co-workers reported an iron catalysed dehydrocoupling of silanes with alcohols at room temperature. However, the type of alcohol used seems to matter, and there is an intriguing difference in reactivity where phenol only produces a little quantity of product while aliphatic alcohols produce silyl ethers in almost quantitative yields (except methanol).¹⁴ In addition to this, the iron catalyst utilised here involves multiple step synthesis where $n\text{-BuLi}$, LiCH_2TMS are used in different steps (Scheme 3.1, c). These highly reactive organometallic reagents are pyrophoric in nature which makes the synthesis of the catalyst even more unattractive. Thus, iron is still in its infancy and a paradigm shift could be achieved by developing an easy to use iron based catalyst system for this field.



Scheme 3.1: Iron catalysed alkoxylation of silanes.

Herein, we report an iron-catalyzed methodology for alkoxylation of silanes to produce hydrogen gas and silyl ethers. Different types of silanes as well as different types of alcohols containing different functional groups can be easily used under this methodology. In addition to this, we successfully implemented this iron catalyst for hydrosilylation of internal alkynes. In this regard, it is worth mentioning that the already literature reported iron catalyzed hydrosilylation of internal alkynes involves the use of either organometallic reagents or organic base whereas in our case we do not need any such additives to perform the reaction successfully.¹⁵ Inspired by the success in alkoxylation of silanes and hydrosilylation of internal alkynes with the same iron catalyst, we anticipated that it might be possible to develop a tandem alkoxylation-hydrosilylation of internal alkynes in presence of

dihydrosilane and alcohol. Indeed, we developed an efficient iron catalyzed method of tandem alkoxylation-hydrosilylation of internal alkynes which would pave the way to create structurally diverse organosilicon compounds. In literature, only one platinum-catalyst is known to achieve such transformation.¹⁶ Finally, to demonstrate the synthetic utility of this methodology, the iron catalyst was successfully implemented to synthesize degradable polysilylether from bio-based isosorbide and commercially available diphenylsilane by dehydrogenative cross coupling. Synthesis of polysilylethers by dehydrogenative cross coupling with an earth abundant iron catalyst is much less explored in the literature.¹⁷

3.3 Results and discussion

3.3.1 Synthesis of iron complex (1)

To get an idea about the iron complex which would work for the alkoxylation of silanes, we went through the literature. We found that in 1989, Crabtree and co-workers reported an Ir catalyst which was highly active and selective for silane alcoholysis.¹⁸ We envisioned that an iron analog of this Ir catalyst could result an active catalyst for this reaction. With this idea we searched the literature and found an iron complex (1) which could produce a dihydride in the presence of an alcohol (Figure 3.1).¹⁹

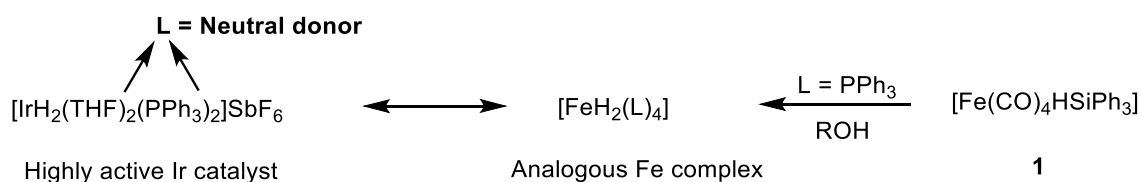
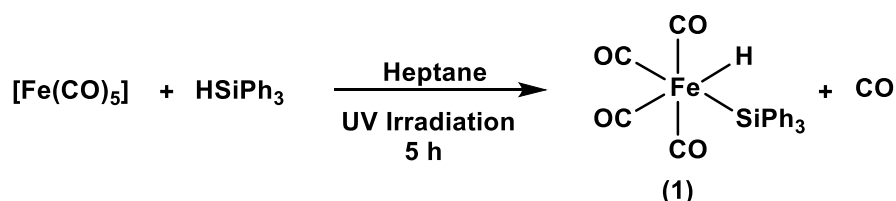


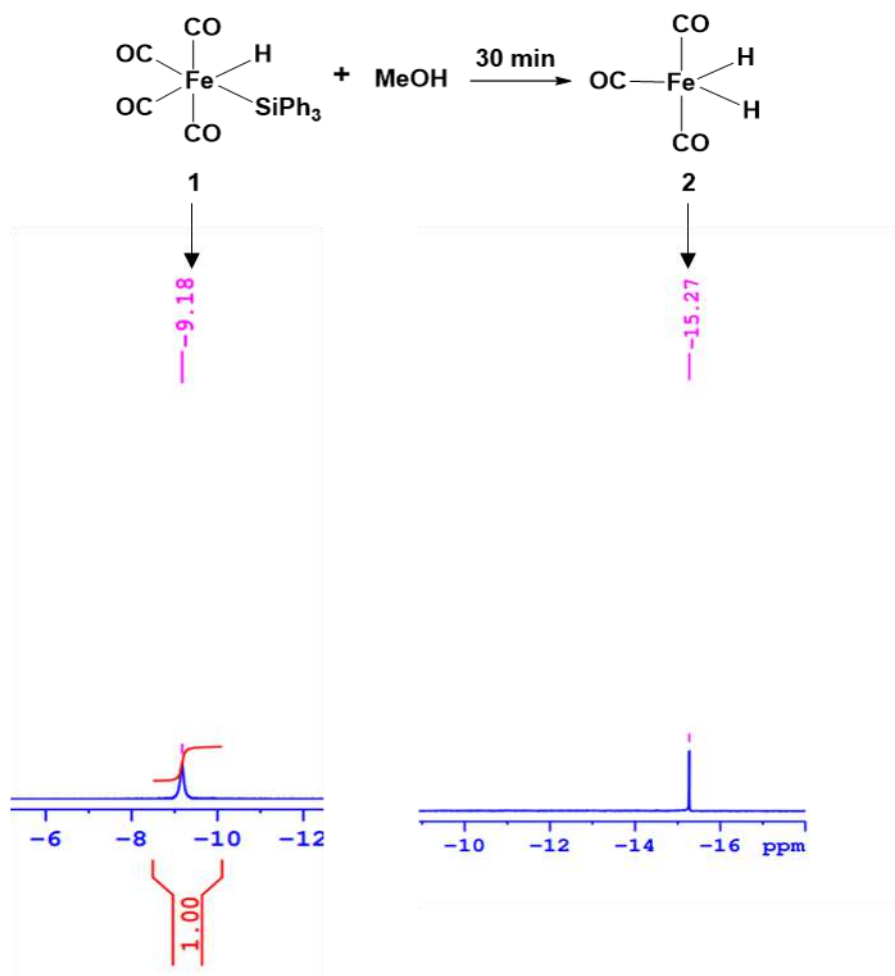
Figure 3.1: Analogous iron complex of highly active Ir catalyst.

With this idea in mind, we synthesized the iron complex (1) by following literature reported procedure (Scheme 3.2).^{19a}



Scheme 3.2: Synthesis of iron complex (1).

The synthesis of the iron complex (1) was confirmed by different spectroscopic tools. It showed a characteristic peak of monohydride at -8.94 ppm in ^1H NMR spectrum. When this complex was treated with MeOH and stirred for 30 minutes, the peak for monohydride at -9.18 ppm completely disappeared. Simultaneously, a new peak appeared at -15.27 ppm in ^1H NMR spectroscopy. This peak was found to be for iron dihydride complex (2). Thus, this simple NMR experiment showed that indeed iron complex (1) could produce a dihydride, in presence of an alcohol (Scheme 3.3).



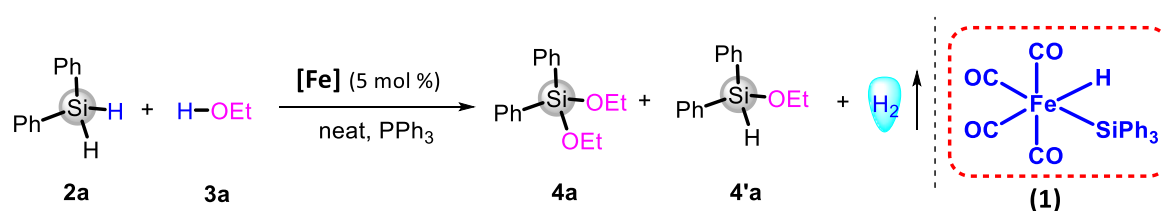
Scheme 3.3: Iron complex (1) affords a dihydride (2) on MeOH treatment.

3.3.2 Alkoxylation of silanes

With the desired iron complex (1) in hand, we started our investigation with the coupling reaction between simple primary alcohol ethanol (3a) and diphenylsilane (2a) in presence of 5 mol % iron complex (1) and 5 mol % PPh_3 at 60 °C for 12 h. To our delight, it afforded full conversion to the dialkoxylated product (4a) (Table 3.1, entry 1). When the temperature was decreased to 30 °C, no starting was there, with 93% dialkoxylated product (4a) and 7%

monoalkoxylated product (4'a) (Table 3.1, entry 2). Then the ligand loading was increased to 10 mol %, 24% dialkoxylated product (4a) was observed along with 75% monoalkoxylated product (4'a) (Table 3.1, entry 3). When the ligand loading was further increased to 15%, monoalkoxylated product increased to 81% (Table 3.1, entry 4). These observations clearly indicate that as the ligand loading is increased from 5 mol %, the selectivity of the catalyst towards dialkoxylated product decreases. After this, we carried out the reaction in absence of ligand which afforded only 26% conversion (Table 3.1, entry 5). This clearly indicates that 5 mol % PPh₃ is needed for high catalyst activity. When the reaction time was reduced to 5 h in presence of 5 mol% PPh₃, full conversion was observed with 93% dialkoxylated product and 7% monoalkoxylated product (Table 3.1, entry 6). When the time was further reduced to 1.5 h, 44% dialkoxylated product was obtained with 56% monoalkoxylated product (Table 3.1, entry 7).

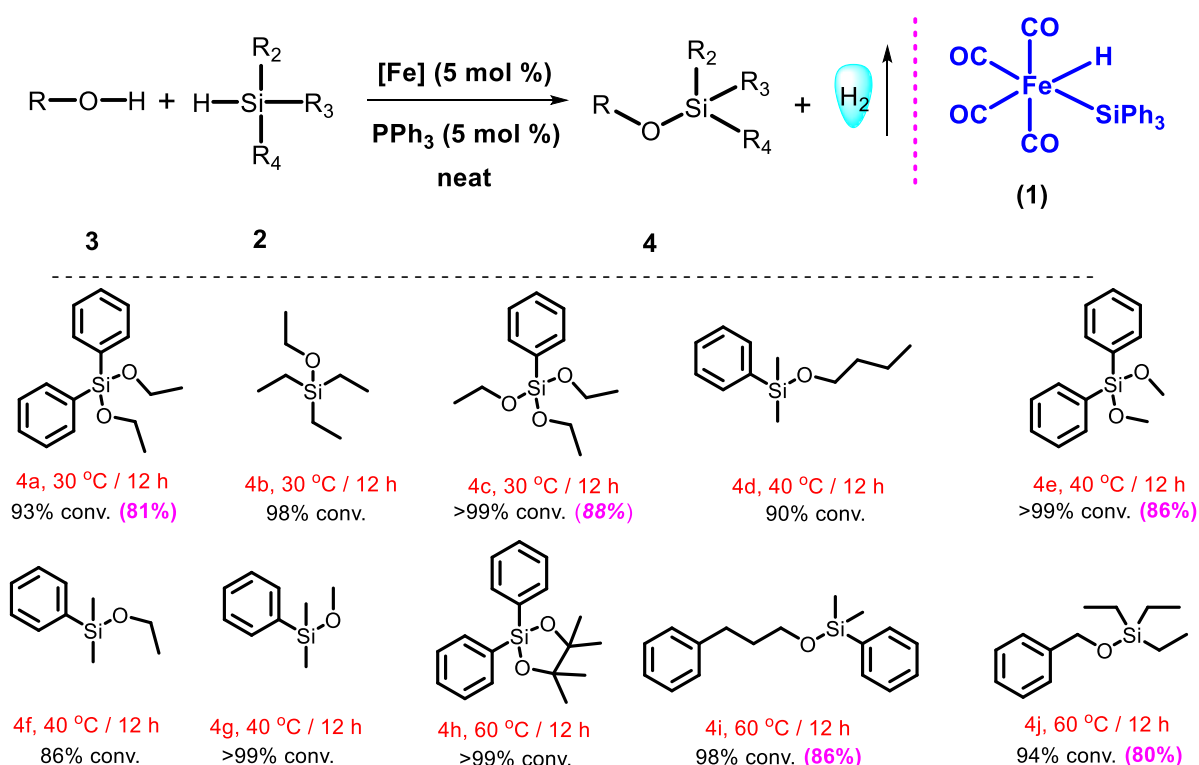
Table 3.1. Iron catalysed alkoxylation of silanes^{a,b}

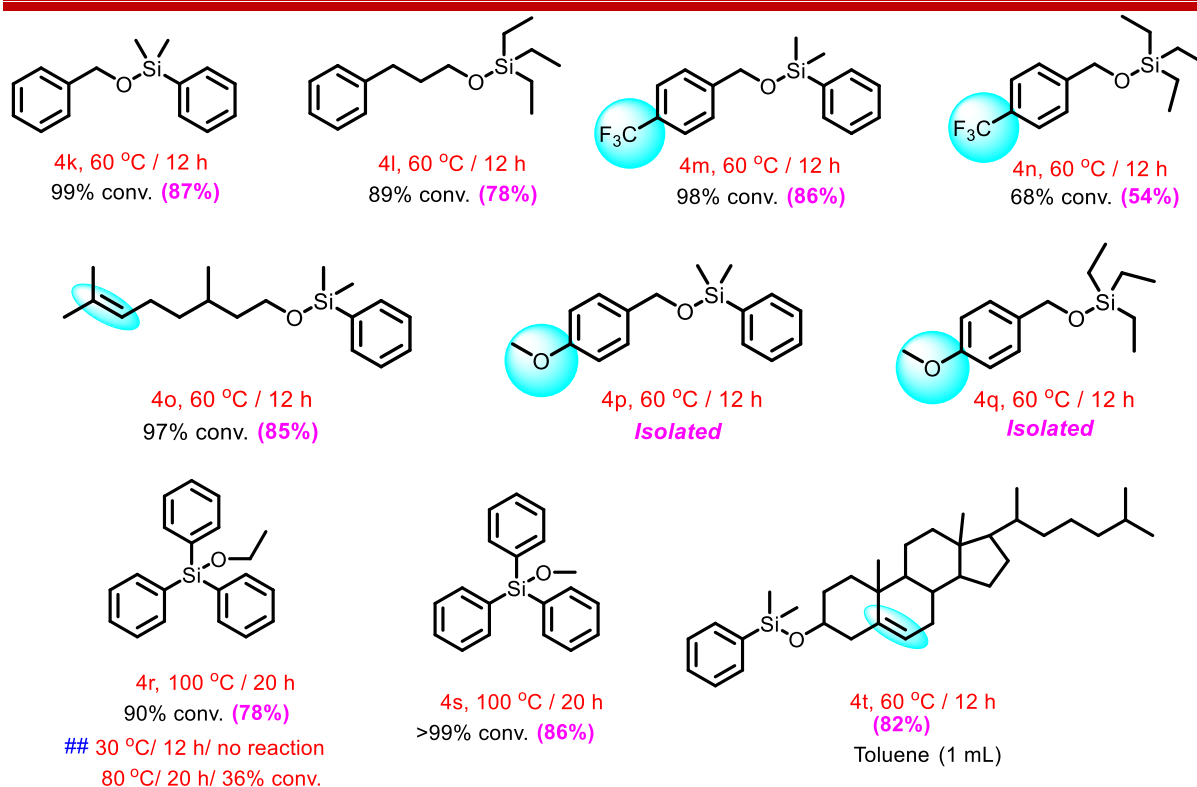


entry	PPh ₃ (mol%)	temp (°C)	time (h)	conv (%) (selectivity)
1.	5	60	12	>99 (4a)
2.	5	30	12	>99 (93:7) (4a:4'a)
3.	10	30	12	99 (24:75) (4a:4'a)
4.	15	30	12	98 (17:81) (4a:4'a)
5.	-	30	12	26 (8:92) (4a:4'a)
6.	5	30	5	>99 (93:7) (4a:4'a)
7.	5	30	1.5	>99 (44:56) (4a:4'a)

^aReaction conditions: Silane (92 mg, 0.5 mmol), ethanol (1.0 mL, 17 mmol), iron complex (1) (10.7 mg, 0.025 mmol). ^bConversions were determined with respect to starting silane by gas chromatography.

After optimizing the reaction condition, we further extended the scope of this iron catalysed Si-O coupling reaction to a range of alcohols and silanes. The smooth reaction of a number of primary benzylic or nonactivated alcohols 4a-4g and 4i-4l produced products in good to exceptional conversions and yields. Electron donating functional groups (4p-q) as well as electron withdrawing functional groups (4m-n) are well tolerated under the reaction condition. Complex organic motifs such as β -citronellol (4o) and cholesterol (4t) undergo heterodehydrocoupling to produce silylated product without any evidence of double bond isomerization. However, in case of triphenylsilane higher temperature is needed (100 °C) to achieve good to excellent yield (4r-s), may be due to the steric reason of triphenylsilane. In some cases (4h-4q, 4t), the reaction has been performed at 60 °C to achieve higher/full conversion within 12 h (Scheme 3.4). In case of substrate 3t, toluene was used as a solvent (1 mL).





Scheme 3.4: Substrate scope of alkoxylation.^{a,b}

^aReaction conditions: Silane (1 mmol), alcohol (0.5 mmol), iron complex (1) (10.7 mg, 0.025 mmol), PPh₃ (6.6 mg, 0.025 mmol). Here GC conversions were determined with respect to starting alcohol. This condition was adopted for reactions where other alcohols (except methanol/ethanol/butanol) were used.

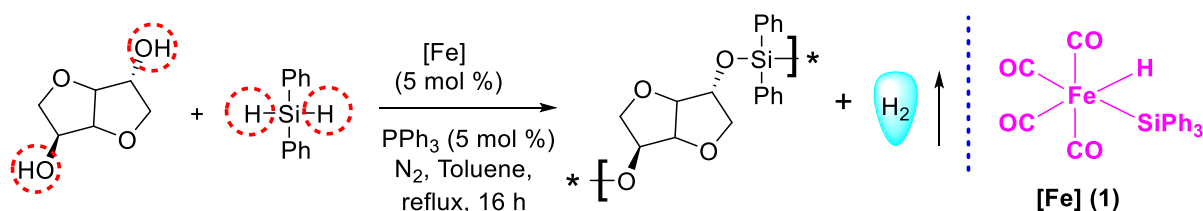
^bReaction conditions: Silane (0.5 mmol), alcohol (1.0 mL), iron complex (1) (10.7 mg, 0.025 mmol), PPh₃ (6.6 mg, 0.025 mmol). Here GC conversions were determined with respect to starting silane. This condition was adopted for reactions where methanol/ethanol/butanol was used as alcohol.

3.3.3 Dehydrogenative polymerization of silanes

Poly(silylether)s (PSE) are fascinating class of polymer, mainly due to the presence of Si-O-C linkage in their backbone. Because Si-O-C bonds are susceptible to alcoholysis and basic or acidic hydrolysis, these materials have a specific degradability due to their unusual connection. Bulky substituents surrounding the silylether link, on the other hand, can provide robust materials. As a result, poly(silylether)s have found variety of applications in industry.²⁰ The production of silyl ethers from various available resources has been reported using a number of synthetic approaches. Transition-metal-catalysed condensation

polymerisation of alcohols with silanes is one of the most often utilised techniques. Although Pd, Pt, Rh, Mn metals have been explored to synthesize PSEs, surprisingly iron remained less explored (only two reports) in this field.¹⁷ Iron has a lot of potential as a good replacement for these metal catalysts because it is affordable, earth abundant, and biocompatible. With this idea, isosorbide and diphenyl silane were chosen for polycondensation reaction in presence of 5 mol % iron catalyst (1) along with 5 mol % PPh₃ in toluene solvent for 16 h. In this regard, it is worth mentioning that these chiral and nontoxic bifunctional isohexides have a unique aliphatic bicyclic structure with two fused tetrahydrofuran rings that gives the molecule a lot of strength and rigidity. Because of this, adding isohexides to the polymer backbone can enhance the polymer's thermal and mechanical properties, making it desirable for high-temperature applications like flame retardants. Ph₂SiH₂ and isosorbide (IS) had an efficient reaction. The absence of the silane hydrogen (SiH) peak at $\delta = 4.92$ ppm and the hydroxy peak of IS at $\delta = 2.96$ ppm in the ¹H NMR spectrum indicates that the starting compounds were consumed. The number average molecular weight (M_n) was found to be 2800 gmol⁻¹ using gel permeation chromatography (GPC) (Table 3.2).

Table 3.2. Polymerization of isosorbide with diphenyl silane^a

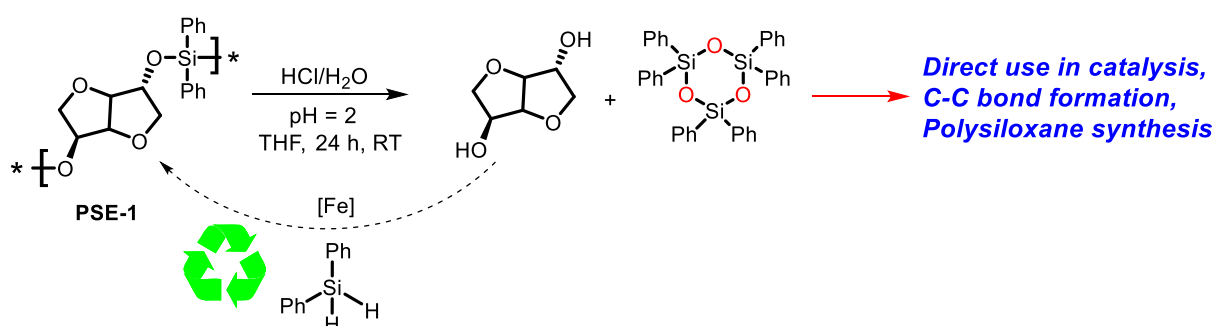


Entry	Monomer	Silane	Polymer	Time (h)	M_n (gmol ⁻¹)	\bar{D}	Yield (%)
1.	Isosorbide (IS)	Ph ₂ SiH ₂	PSE-1	16	2800	1.3	74

^aReaction condition: Isosorbide (263 mg, 1.8 mmol), silane (331 mg, 1.8 mmol), iron complex (1) (38.5 mg, 0.09 mmol), PPh₃ (24 mg, 0.09 mmol), Toluene (2.0-2.5 mL).

In the sustainable production and use of polymers, degradability of the polymer is a crucial factor.²¹ Hydrolytically degradable polymers are of special interest because of their potential use in medical fields such the administration of protein-based vaccines and nucleic acids as well as the treatment of inflammatory diseases.²² In fact, we degraded the PSE-1 by following

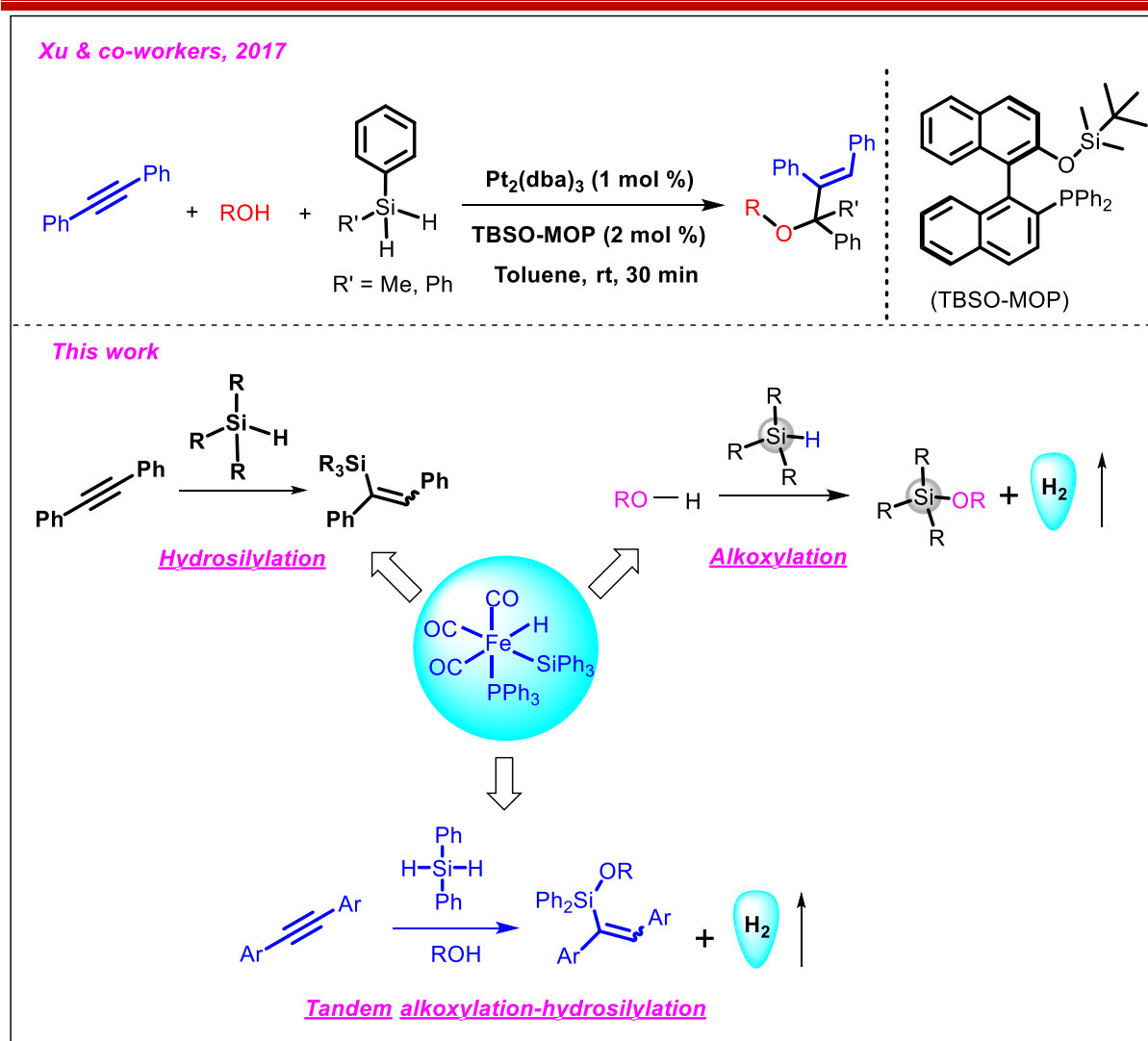
a known literature procedure.^{17a} The PSE-1 was treated with 10 vol % HCl/H₂O (pH 2) in THF at room temperature for 24 h. Full degradation of PSE-1 was observed with the generation of starting monomer isosorbide (m/z 146.1 g mol⁻¹) as confirmed by GC-MS (Scheme 3.5). The diol monomer isosorbide was recovered nearly quantitatively and in NMR spectroscopy no degradation products could be detected. In this regard, it is worth mentioning that the degraded products of PSE-1 are primarily alcohols and silanol derivatives which are neutral and non-toxic, therefore prevents any drastic changes in the pH of the surrounding environment.



Scheme 3.5: Hydrolytic degradation of PSE-1.

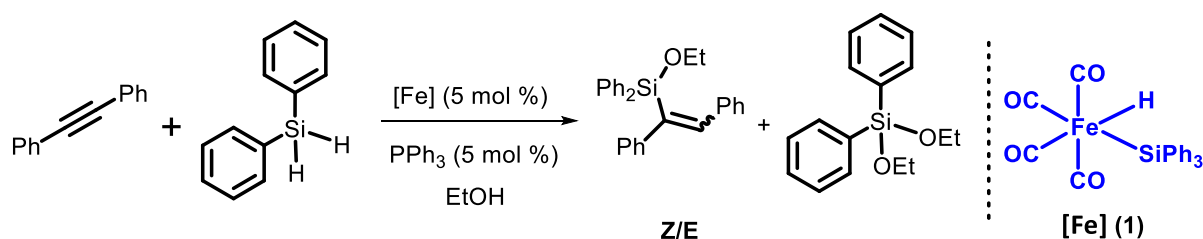
3.3.4 Tandem alkoxylation-hydrosilylation of alkynes

Now, from our earlier chapter-2, we already know that this iron complex (1) is active for the hydrosilylation of diphenylacetylene. After getting success in alkoxylation of silane with this iron complex (1), we anticipated that it could be possible to develop a tandem hydrosilylation-alkoxylation of internal alkyne with the same iron catalyst if we use a silane having two hydrogens. In this regard, it is worth mentioning that in 2017, Xu and co-workers reported such type of transformation in literature using Pt catalyst (Scheme 3.6).¹⁶



Scheme 3.6: Tandem alkoxylation-hydrosilylation reaction.

We started investigation with the coupling reaction among diphenylsilane (2 equivalent), diphenylacetylene and ethanol in presence of 5 mol % iron catalyst (1) and 5 mol % PPh₃ for 20 h at 50 °C. It afforded 95% conversion arising from tandem alkoxylation-hydrosilylation reaction. When the silane equivalent was reduced to 1.2 equivalent, conversion was reduced to 80%. When the reaction was performed at 40 °C, in presence of 2 equivalent silane for 20 h, 85% conversion was obtained (Table 3.3).

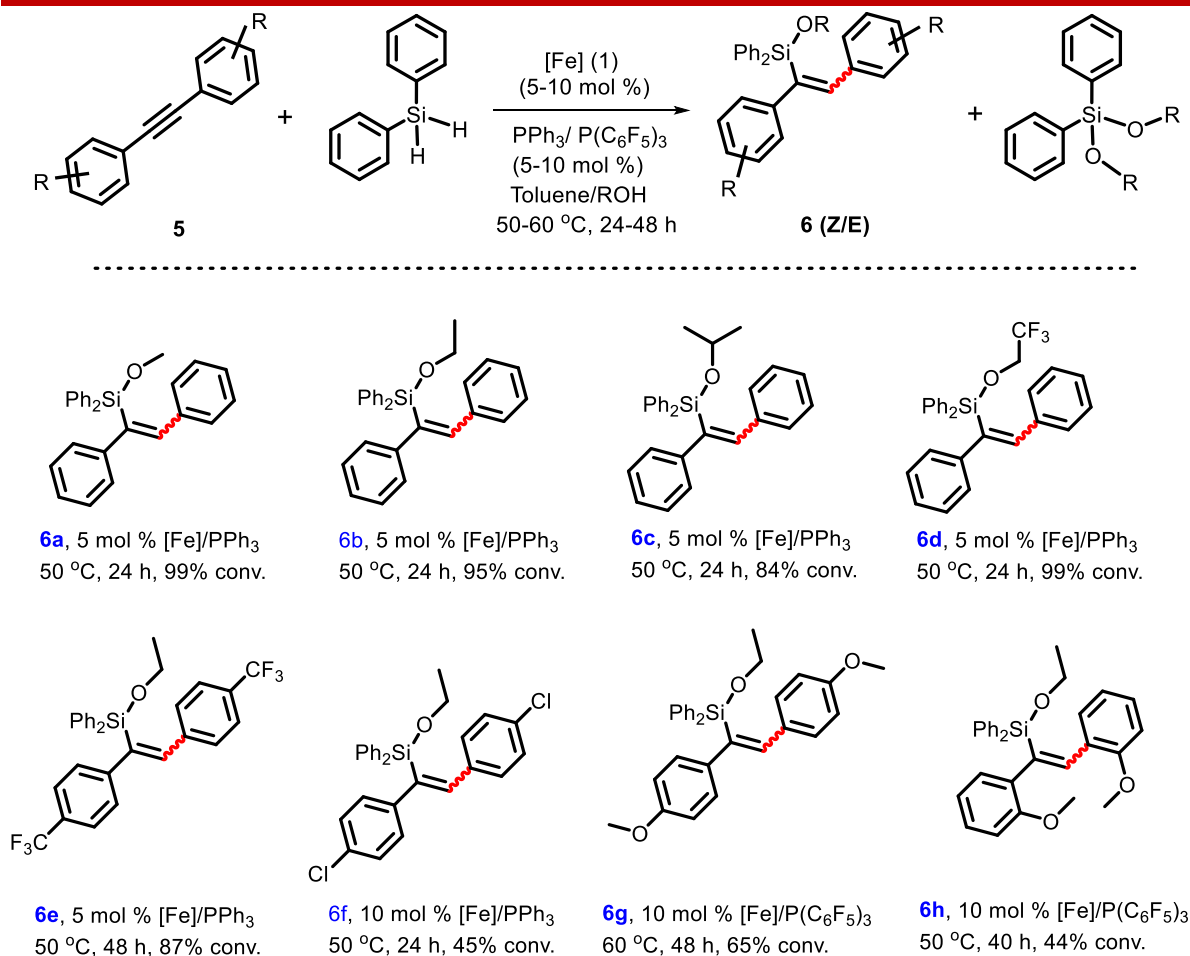
Table 3.3. Optimization for the iron-catalysed hydrosilylation of diphenylacetylene with diphenylsilane in the presence of alcohol: alcoholysis/hydrosilylation cascade^{a,b}

entry	Time (h)	Temp (°C)	Silane (equiv)	Conv (%) (Z/E)
1.	20	50	2	95
2.	20	50	1.2	84
3.	20	40	2	87

^aReaction conditions: Diphenylacetylene (45 mg, 0.25 mmol), silane (0.3-0.5 mmol), iron complex (1) (5.4 mg, 0.0125 mmol), PPh₃ (3.3 mg, 0.0125 mmol) and 1 mL EtOH.

^bConversions were determined with respect to starting alkyne.

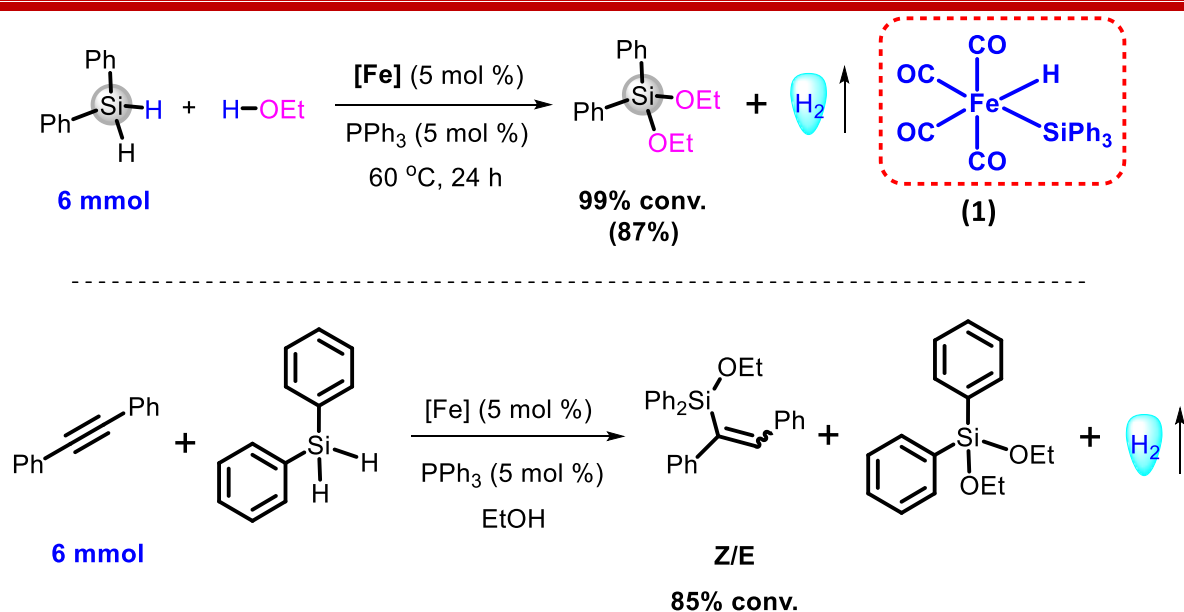
With the optimized reaction condition, we further extended the scope of this tandem alkoxylation-hydrosilylation reaction to a range of different alcohols. In case of primary alcohols such as MeOH, CF₃CH₂OH, full conversions were obtained (Scheme 3.7; 6a, 6d). In case of secondary alcohol such as IPA, little less conversion (84%) was obtained, may be due to steric reason (Scheme 3.7; 6c). Electron withdrawing substituents such as -CF₃, -Cl at para position of diphenylacetylene were well tolerated. However, the conversion of these substrates varied with different substituents, suggesting the important role of substituents in such reaction (Scheme 3.7; 6e-6f). Longer time was required to achieve good conversion for 6e, (48 h). Strong electron donating substituent such as -OMe at ortho and para position of diphenyl acetylene was also well tolerated in the reaction. However, here P(C₆F₅)₃ performed better than PPh₃, suggesting the importance of the electronic effect of the ligand in such reaction (Scheme 3.7; 6g-6h). For substrates 5e-h, toluene/alcohol solvent mixture was used to solubilize the substrate.



Scheme 3.7: Substrate scope for iron catalyzed tandem alkoxylation-hydrosilylation reaction.^a

^aReaction conditions: Alkyne (0.25 mmol), silane (0.5 mmol), iron complex (0.0125-0.0250 mmol), PPh₃ (0.0125-0.0250 mmol), P(C₆F₅)₃ (0.0250 mmol) and 1 mL EtOH (for 5a-d)/0.5 mL EtOH+ 0.5 mL toluene (for 5e-h).

To further assess the applicability of these transformations, we performed gram scale synthesis for alkoxylation of silanes and tandem alkoxylation-hydrosilylation of alkynes. In case of alkoxylation reaction, we performed the reaction with 6 mmol diphenylsilane in presence of 5 mol % iron complex and 5 mol % PPh₃ at 60 °C for 24 h in EtOH solvent which afforded 99% dialkoxyated product with 87% isolated yield. In case of tandem alkoxylation-hydrosilylation reaction, we carried out the reaction with 6 mmol diphenylacetylene and 12 mmol diphenylsilane in presence of 5 mol % iron complex and 5 mol % PPh₃ at 50 °C for 24 h which afforded 85% conversion.



Scheme 3.8: Gram scale iron catalysed alkoxylation and tandem alkoxylation-hydrosilylation reaction.

3.4 Experimental section:

3.4.1 Methods and materials:

All manipulations were carried out under an inert atmosphere using standard Schlenk technique, cannula filtration or m-Braun glove box. Solvents were dried by standard procedures unless otherwise mentioned.¹ THF was dried on sodium/benzophenone. Di-iron nonacarbonyl, organosilanes, diphenyl acetylene were purchased from Sigma-Aldrich. All other reagents/chemicals, solvents were purchased from local suppliers (Spectrochem Pvt. Ltd.; Avra Synthesis Pvt. Ltd.; Thomas Baker Pvt. Ltd. etc). Solution NMR spectra were recorded on a Bruker Avance 200, 400 and 500 MHz instruments at 298K unless mentioned otherwise. Chemical shifts are referenced to external reference TMS (¹H and ¹³C) or or 85% H₃PO₄ ($\delta = 40.480747$ MHz, ³¹P). Coupling constants are given as absolute values. Multiplicities are given as follows s: singlet, d: doublet, t: triplet, m: multiplet, quat: quaternary carbon. Mass spectra were recorded on Thermo Scientific Q-Exactive mass spectrometer with Hypersil gold C18 column 150 x 4.6 mm diameter 8 μ m particle size mobile phase used is 90% methanol + 10% water + 0.1% formic acid. The GC conversion of the products were determined by HP-5 column (30 m) on an Agilent 7890B GC system.

3.4.2 Synthesis of iron pre-catalyst $[\text{Fe}(\text{CO})_4\text{HSiPh}_3]$ (1):

The iron catalyst was prepared by following a modified literature procedure.²

A mixture of 15 ml of $[\text{Fe}(\text{CO})_5]$ (22 g, 0.11 mol) and 25.5 g of $(\text{C}_6\text{H}_5)_3\text{SiH}$ (0.098 mol) were taken in a Schlenk flask in 180 mL heptane and was irradiated for 22 h. The carbon monoxide evolution was fast at the beginning (one bubble per second), but it had nearly ceased by the conclusion of the reaction time. There was little decomposition. The reaction mixture was filtered and the pale yellow, clear solution was cooled in the refrigerator slowly. White crystalline compound (1) was formed in good yield (70%). We wanted to check the role of methanol. We took complex-1 (10 mg) in a NMR tube and added methanol (0.5 mL) to it. After 30 min, we recorded the ^1H NMR which showed a new peak at -15.3 ppm. Literature reports suggested that an iron dihydride was formed (complex-2).³



^1H NMR (500 MHz, C_6D_6): $\delta = 7.46$ (m, 6H), 6.93 (m, 9H), -9.18 (s, 1H).

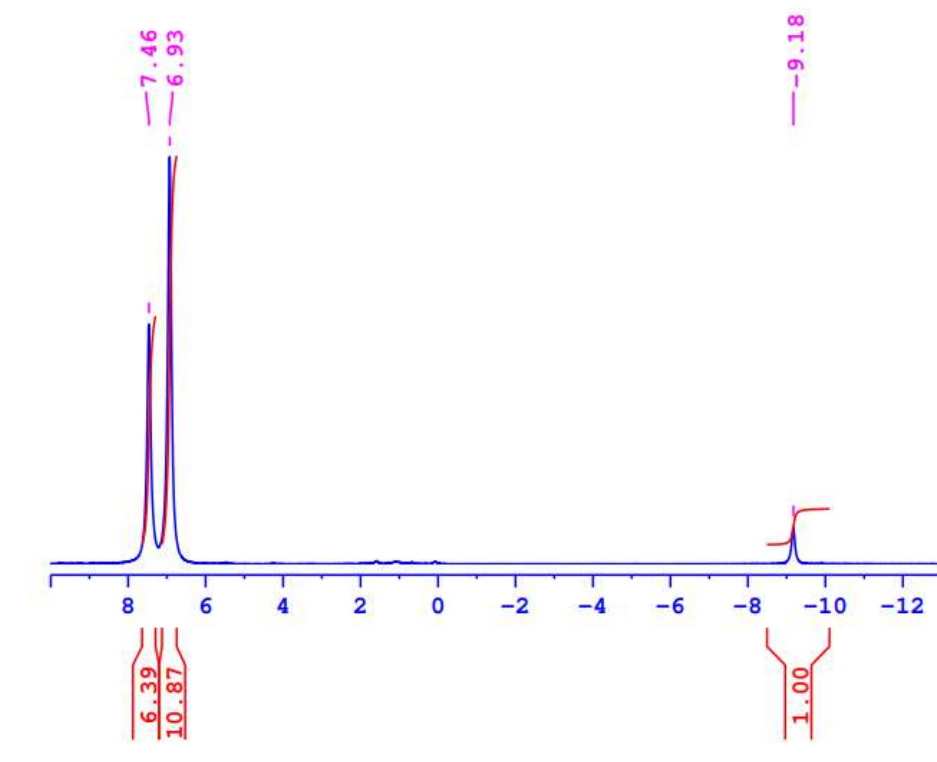


Figure 3.2: ^1H NMR spectrum of $[\text{Fe}(\text{CO})_4\text{HSiPh}_3]$ (1).

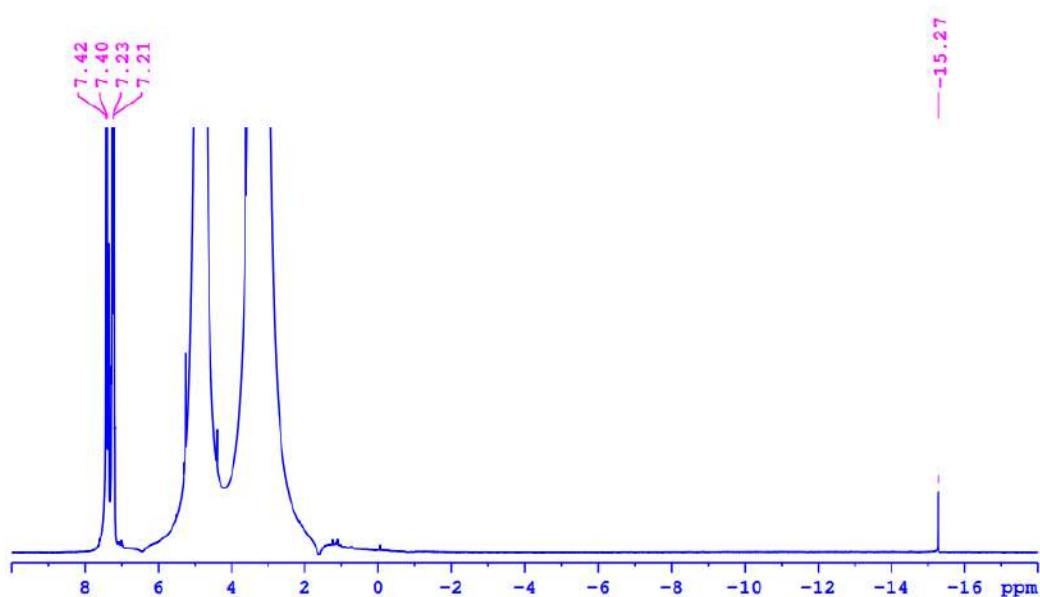


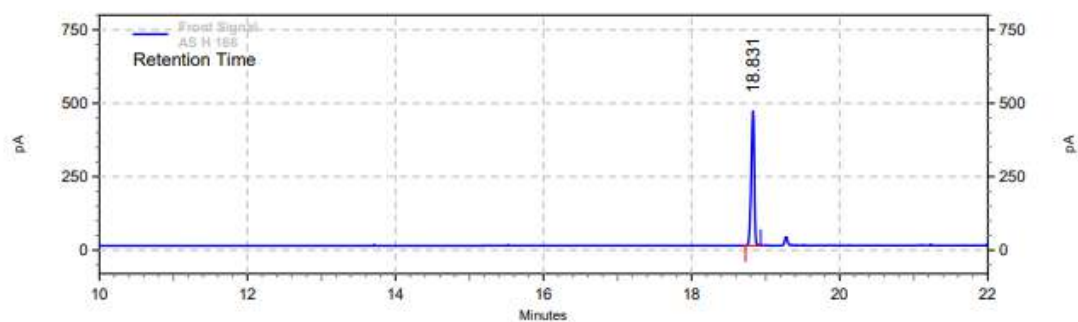
Figure 3.3: ^1H NMR spectrum of **2** (in D_2O capillary).

3.4.3 GC analysis for table 3.1:

Conversion was determined with respect to starting Ph_2SiH_2 (**2a**), appearing at $t = 13.5$ min by applying the following GC condition. $\text{Ph}_2\text{SiH}(\text{OEt})$ (**4'a**) appeared at $t = 17.1$ min and $\text{Ph}_2\text{Si}(\text{OEt})_2$ (**4a**) appeared at $t = 18.8$ min in this method.

GC condition: HP-5 column, isothermal at $70\text{ }^\circ\text{C}$ for 1.0 min, $4\text{ }^\circ\text{C min}^{-1}$ to $120\text{ }^\circ\text{C}$, $10\text{ }^\circ\text{C min}^{-1}$ to $250\text{ }^\circ\text{C}$, $20\text{ }^\circ\text{C min}^{-1}$ to $320\text{ }^\circ\text{C}$ for 2 min, with 10 psi pressure.

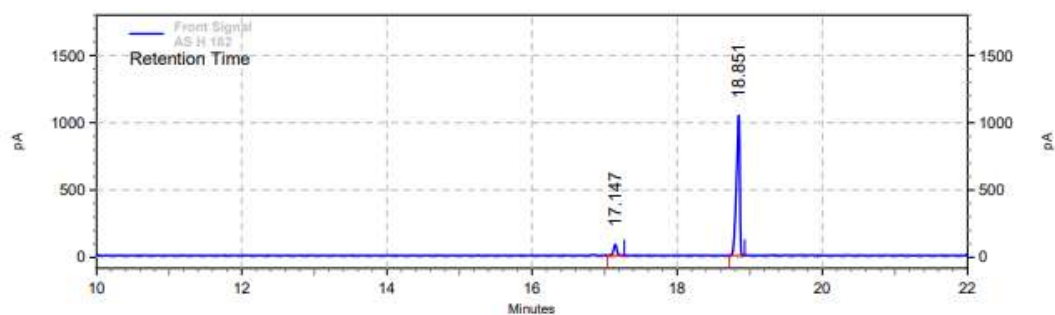
3.4.4 GC chromatogram for each entry of table3.1:

Front Signal
Results

Retention Time	Area	Area %	Height	Height %
18.831	10189045	100.00	3512161	100.00

Totals	10189045	100.00	3512161	100.00
--------	----------	--------	---------	--------

Figure 3.4: GC chromatogram of entry 1, table 3.1.

Front Signal
Results

Retention Time	Area	Area %	Height	Height %
17.147	1867567	6.76	624630	7.26
18.851	25753512	93.24	7980834	92.74

Totals	27621079	100.00	8605464	100.00
--------	----------	--------	---------	--------

Figure 3.5: GC chromatogram of entry 2, table 3.1.

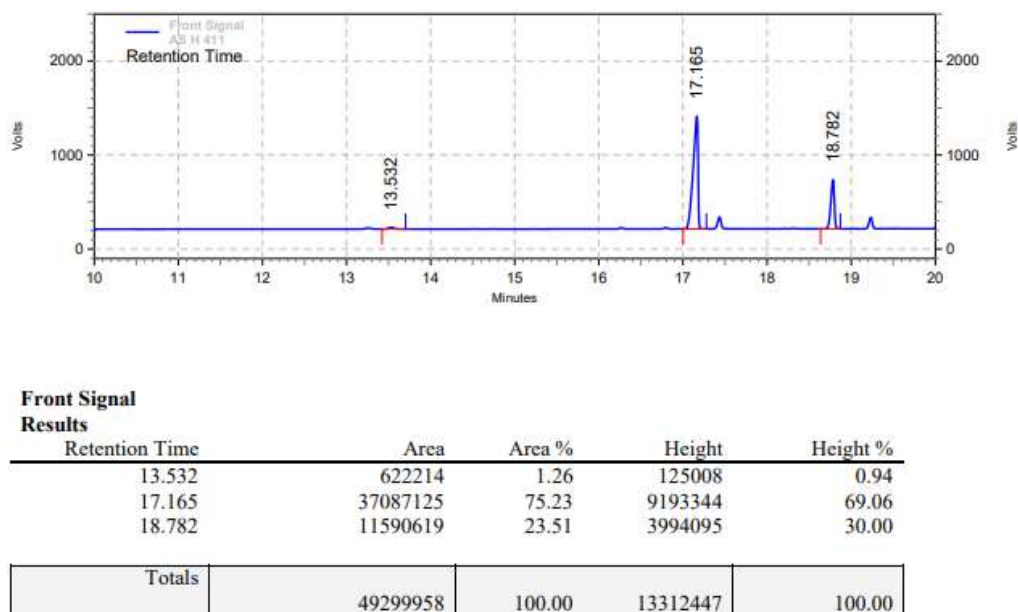


Figure 3.6: GC chromatogram of entry 3, table 3.1.

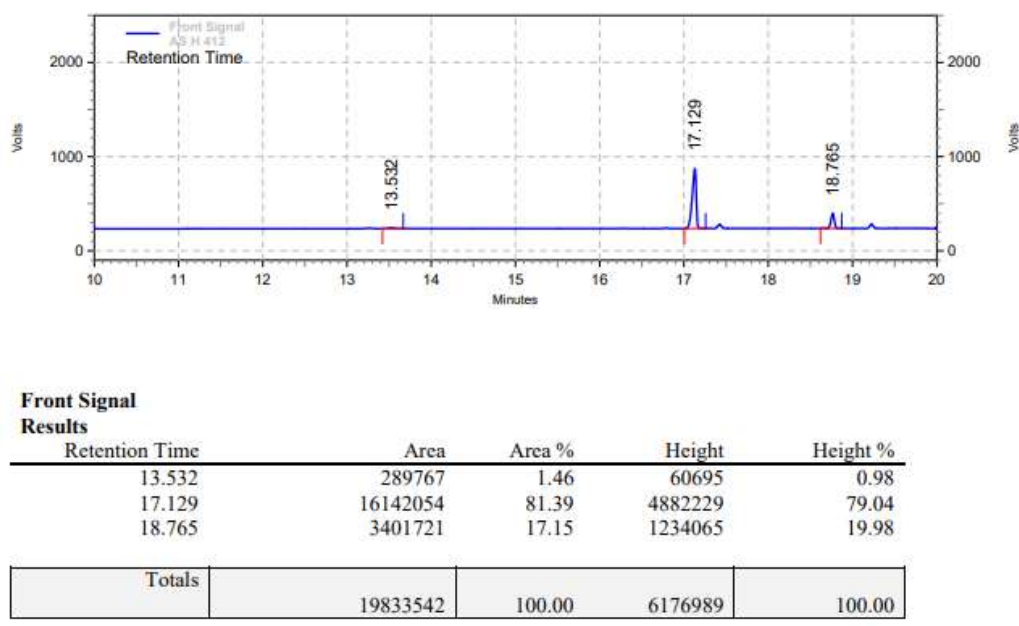


Figure 3.7: GC chromatogram of entry 4, table 3.1.

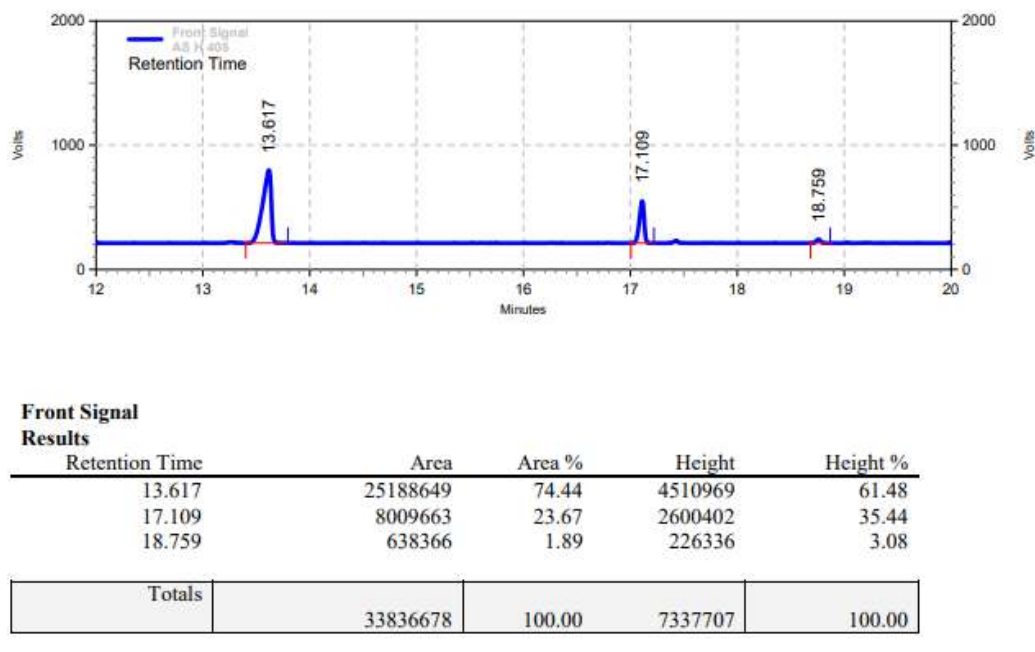


Figure 3.8: GC chromatogram of entry 5, table 3.1.

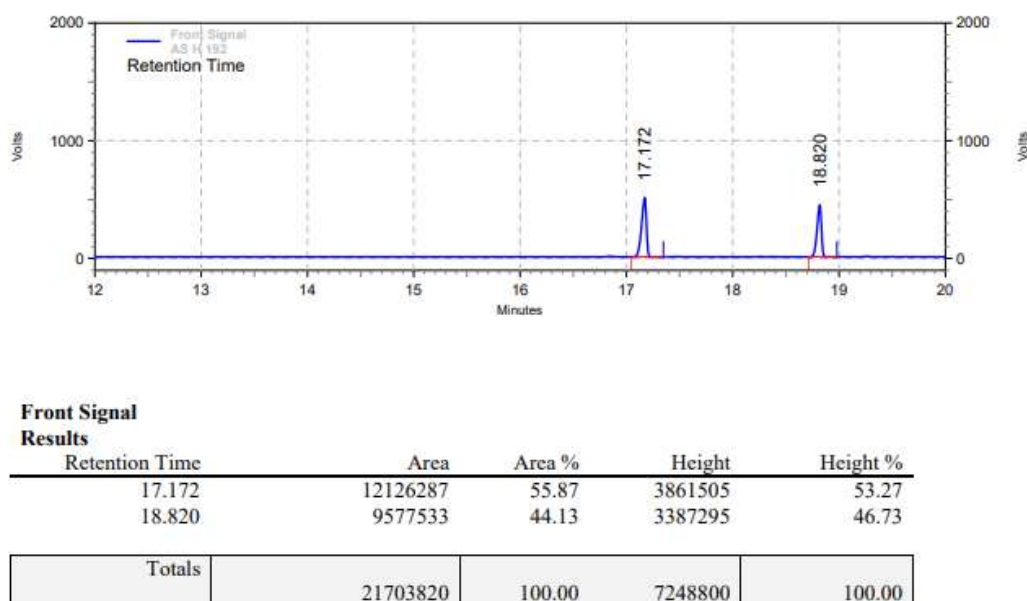


Figure 3.9: GC chromatogram of entry 7, table 3.1.

3.4.5.1 General procedure for iron catalysed Alkoxylation of silanes (GP-I):

Organosilane (1 mmol), $[\text{Fe}(\text{CO})_4\text{HSiPh}_3]$ (10.7 mg, 0.025 mmol, 5 mol %), PPh_3 (6.6 mg, 0.025 mmol, 5 mol %) and alcohol (0.5 mmol) were introduced in a 10 mL Teflon-valved flask equipped with a magnetic stir bar under argon atmosphere. This condition was adopted for reactions where other alcohols (except methanol/ethanol/butanol) were used. The reaction mixture was stirred at 30–60 °C for 12–20 h. Here conversions were determined with respect

to starting alcohol by gas chromatography. The mixture was extracted with diethyl ether (3×10 mL). After that, the layers of mixed diethyl ether were dried over sodium sulfate and concentrated under vacuum. After evaporation of the solvent, the crude reaction mixture was purified by silica gel column chromatography (petroleum ether/EtOAc 50/1), yielding the silyl ether product.

GC condition: HP-5 column, isothermal at 70 °C for 1.0 min, 4 °C min⁻¹ to 120 °C, 10 °C min⁻¹ to 250 °C, 20 °C min⁻¹ to 320 °C for 2 min, with 10 psi pressure.

3.4.5.2 General procedure for iron catalysed Alkoxylation of silanes (GP-II):

Organosilane (0.5 mmol), [Fe(CO)₄HSiPh₃] (10.7 mg, 0.025 mmol, 5 mol %), ligand (6.6 mg, 0.025 mmol, 5 mol %) and alcohol (1.0 mL) were introduced in a 10 mL Teflon-valved flask equipped with a magnetic stir bar under argon atmosphere. The reaction mixture was stirred at 30-60 °C for 5-24 h. This condition was adopted for reactions where methanol/ethanol/butanol was used as alcohol. Here conversions were determined with respect to starting silane by gas chromatography. The mixture was extracted with diethyl ether (3×10 mL). After that, the layers of mixed diethyl ether were dried over sodium sulfate and concentrated under vacuum. After evaporation of the solvent, the crude reaction mixture was purified by silica gel column chromatography (petroleum ether/EtOAc 50/1), yielding the silyl ether product.

GC condition: Same GC condition was used as mentioned above.

Table 3.4. GC retention time for starting alcohols, silylether products and conversion (GP-I)

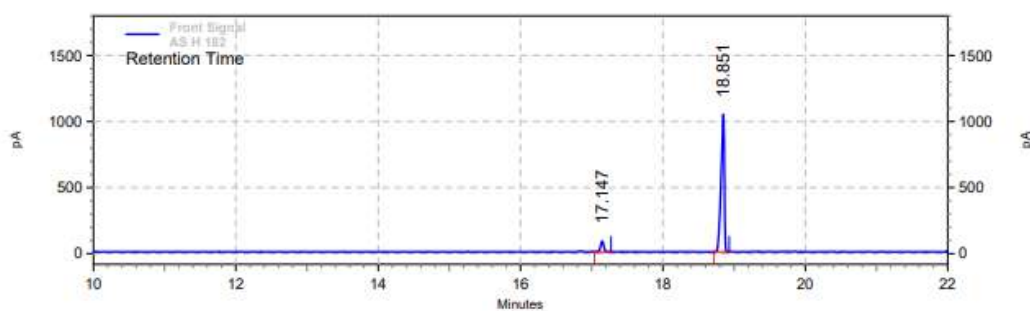
Alcohol	Retention time (min)	Product	Retention time (min)	Conversion (%)
3h		4h	21.0	>99
3i	8.0	4i	20.6	98
3j	3.8	4j	14.9	94
3k	3.8	4k	18.4	99
3l	8.0	4l	18.0	89

3m	5.2	4m	18.7	98
3n	5.2	4n	15.6	68
3o	8.4	4o	20.4	97

Table 3.5. GC retention time for starting silane, silylether products and conversion (GP-II)

Silane	Retention time (min)	Product	Retention time (min)	Conversion (%)
2b	1.54	4b	2.7	98
2c		4c	11.9	>99
2d	2.7	4d	10.5	90
2e	13.5	4e	17.8	>99
2f	2.5	4f	5.9	86
2g	2.5	4g	4.9	>99
2r	22.2	4r	23.3	89.5
2s	22.2	4s	23.0	>99

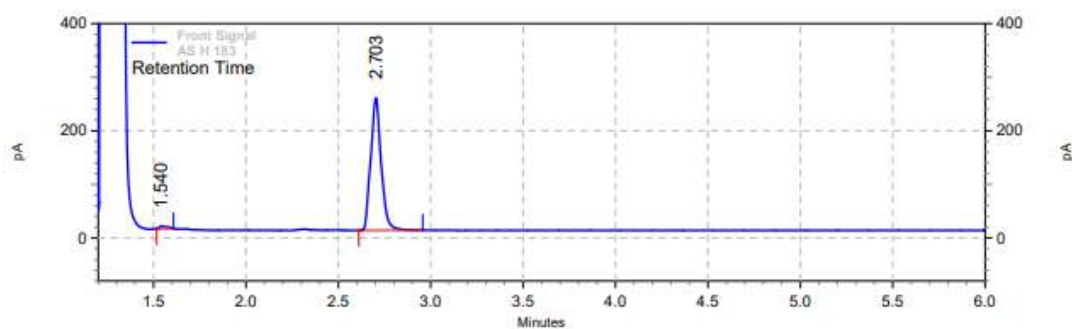
3.4.6 GC chromatogram for substrate scope of Alkoxylation of Silane:

Front Signal
Results

Retention Time	Area	Area %	Height	Height %
17.147	1867567	6.76	624630	7.26
18.851	25753512	93.24	7980834	92.74

Totals	27621079	100.00	8605464	100.00
--------	----------	--------	---------	--------

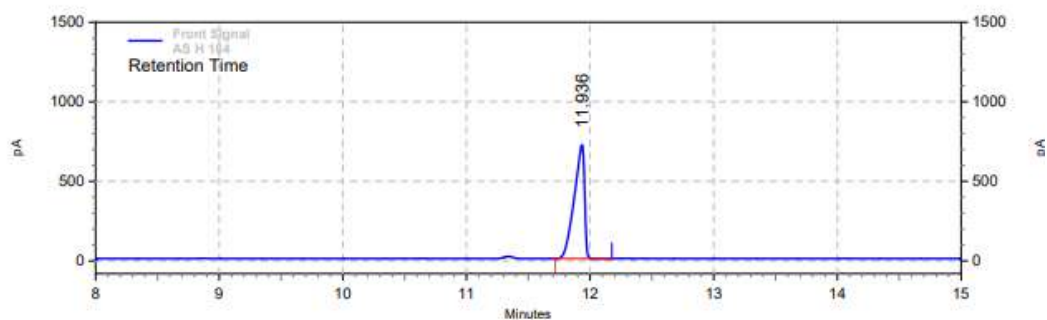
Figure 3.10: GC chromatogram of 4a.

Front Signal
Results

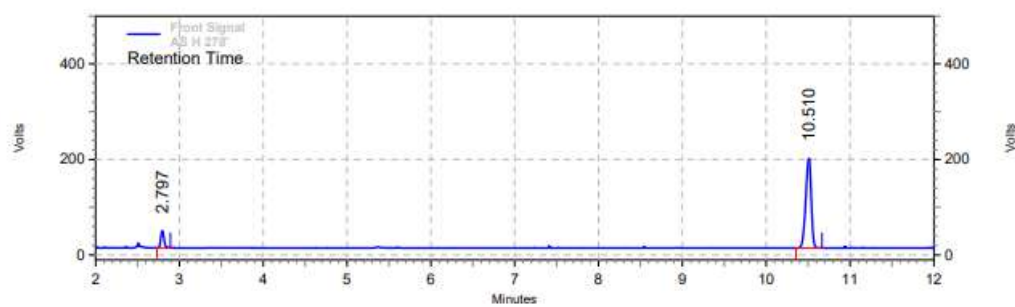
Retention Time	Area	Area %	Height	Height %
1.540	116282	1.54	39887	2.06
2.703	7440106	98.46	1896431	97.94

Totals	7556388	100.00	1936318	100.00
--------	---------	--------	---------	--------

Figure 3.11: GC chromatogram of 4b.

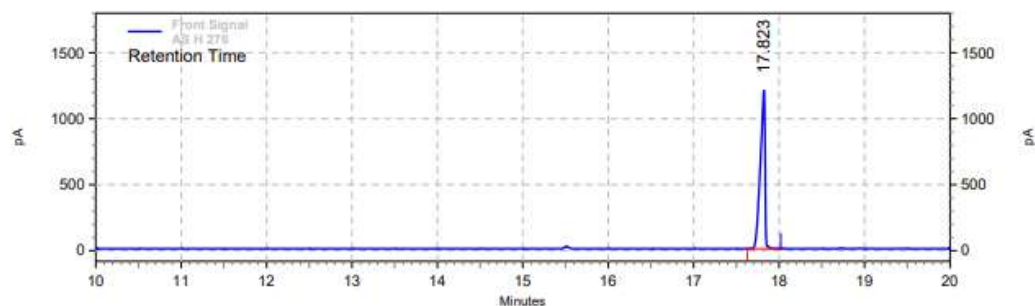

**Front Signal
Results**

Retention Time	Area	Area %	Height	Height %
11.936	31817344	100.00	5494852	100.00
Totals	31817344	100.00	5494852	100.00

Figure 3.12: GC chromatogram of 4c.

**Front Signal
Results**

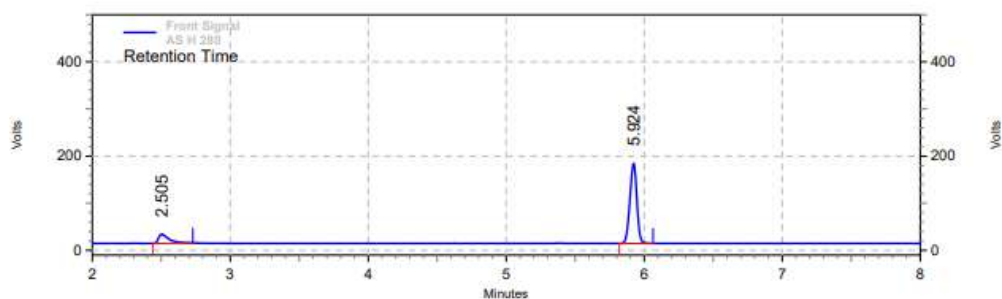
Retention Time	Area	Area %	Height	Height %
2.797	740744	10.16	273909	15.98
10.510	6551874	89.84	1440286	84.02
Totals	7292618	100.00	1714195	100.00

Figure 3.13: GC chromatogram of 4d.


**Front Signal
Results**

Retention Time	Area	Area %	Height	Height %
17.823	35359532	100.00	9212271	100.00

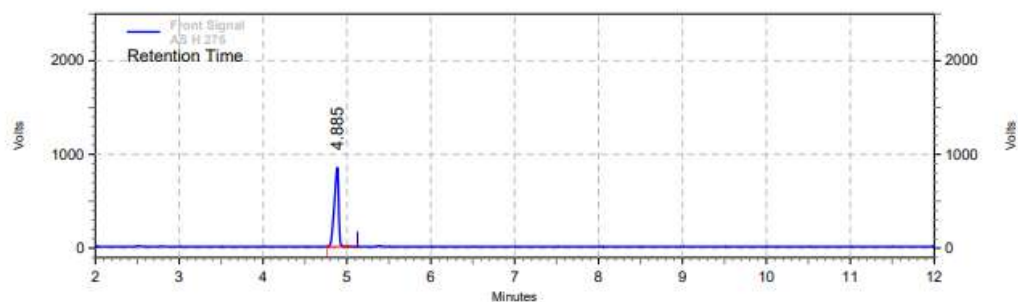
Totals	35359532	100.00	9212271	100.00
--------	----------	--------	---------	--------

Figure 3.14: GC chromatogram of 4e.

**Front Signal
Results**

Retention Time	Area	Area %	Height	Height %
2.505	764852	14.35	146621	10.11
5.924	4563347	85.65	1303342	89.89

Totals	5328199	100.00	1449963	100.00
--------	---------	--------	---------	--------

Figure 3.15: GC chromatogram of 4f.

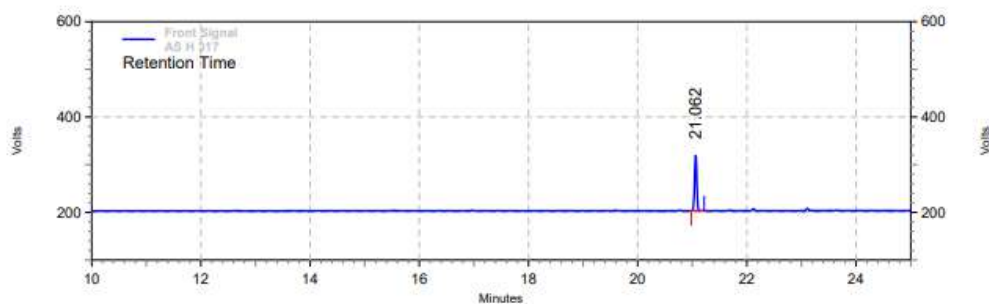


**Front Signal
Results**

Retention Time	Area	Area %	Height	Height %
4.885	23409071	90.68	6494186	91.18
23.033	2405250	9.32	628422	8.82

Totals	Area	Area %	Height	Height %
	25814321	100.00	7122608	100.00

Figure 3.16: GC chromatogram of 4g.

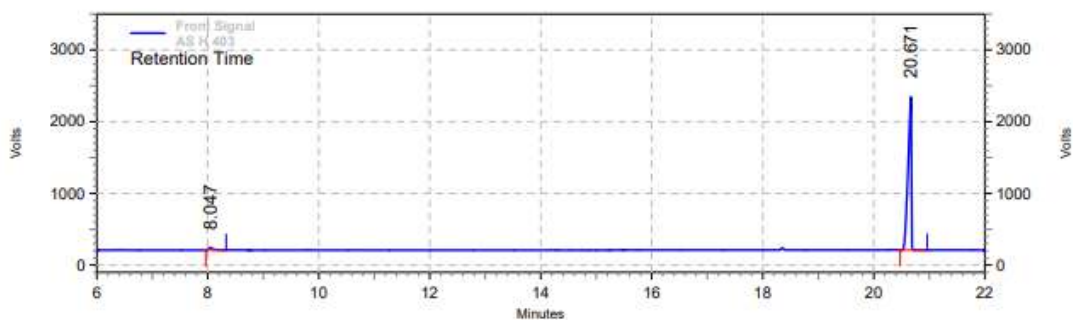


**Front Signal
Results**

Retention Time	Area	Area %	Height	Height %
21.062	2485290	100.00	889666	100.00

Totals	Area	Area %	Height	Height %
	2485290	100.00	889666	100.00

Figure 3.17: GC chromatogram of 4h.

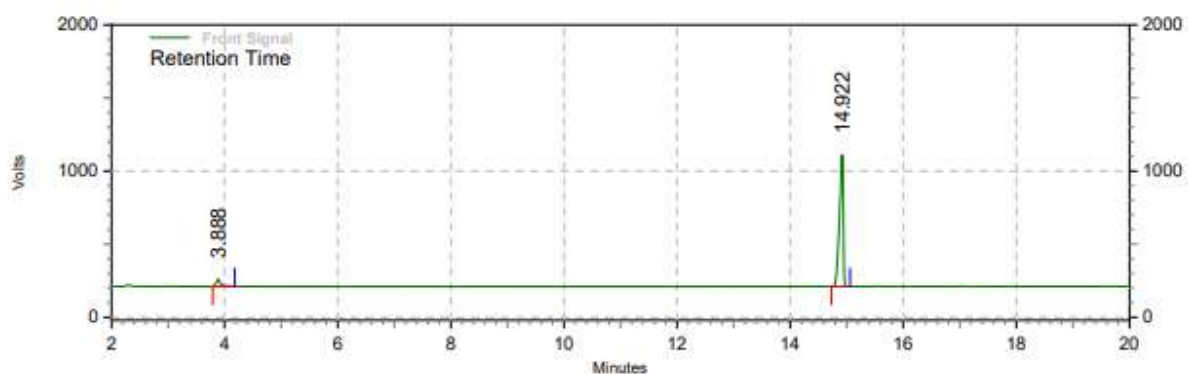


Front Signal Results

Retention Time	Area	Area %	Height	Height %
8.047	1477865	2.09	265533	1.59
20.671	69281902	97.91	16400617	98.41

Totals	Area	Area %	Height	Height %
	70759767	100.00	16666150	100.00

Figure 3.18: GC chromatogram of 4i.

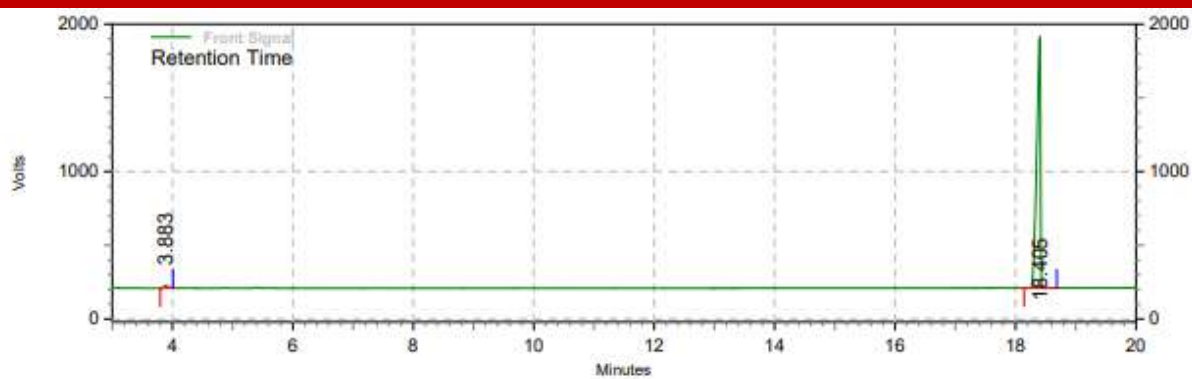


Front Signal Results

Retention Time	Area	Area %	Height	Height %
3.888	2050678	5.97	371728	5.10
14.922	32311642	94.03	6912276	94.90

Totals	Area	Area %	Height	Height %
	34362320	100.00	7284004	100.00

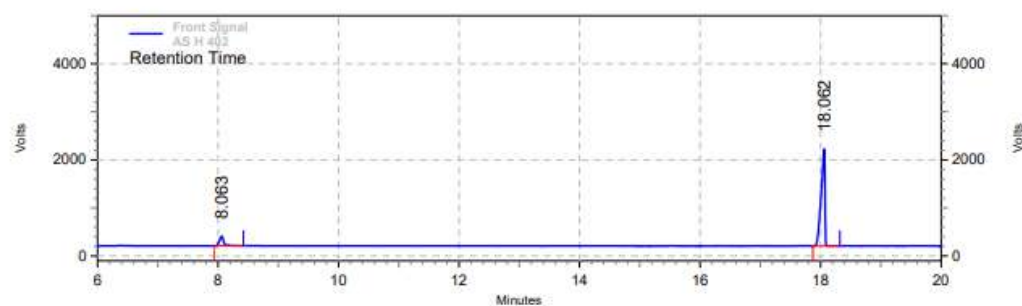
Figure 3.19: GC chromatogram of 4j



Front Signal Results

Retention Time	Area	Area %	Height	Height %
3.883	595429	1.05	136479	1.03
18.405	55906923	98.95	13085095	98.97
Totals	56502352	100.00	13221574	100.00

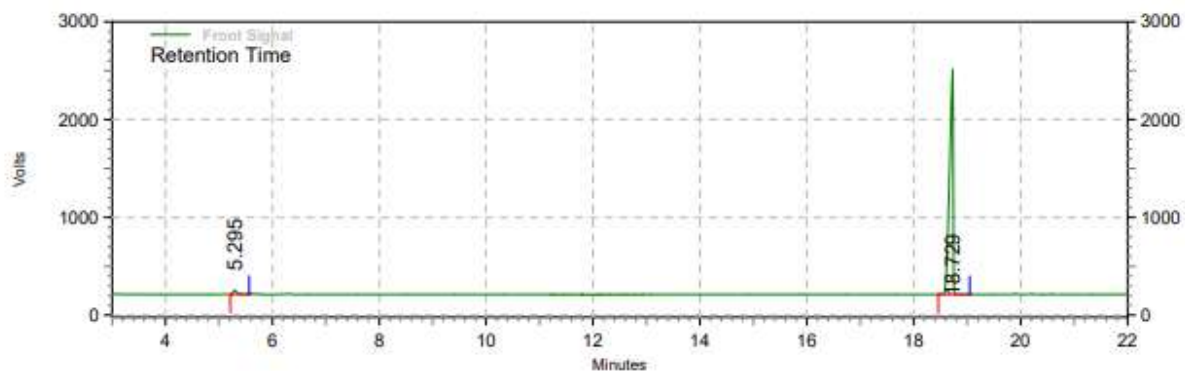
Figure 3.20: GC chromatogram of 4k.



Front Signal Results

Retention Time	Area	Area %	Height	Height %
8.063	7989463	10.59	1529466	9.00
18.062	67428257	89.41	15463873	91.00
Totals	75417720	100.00	16993339	100.00

Figure 3.21: GC chromatogram of 4l.

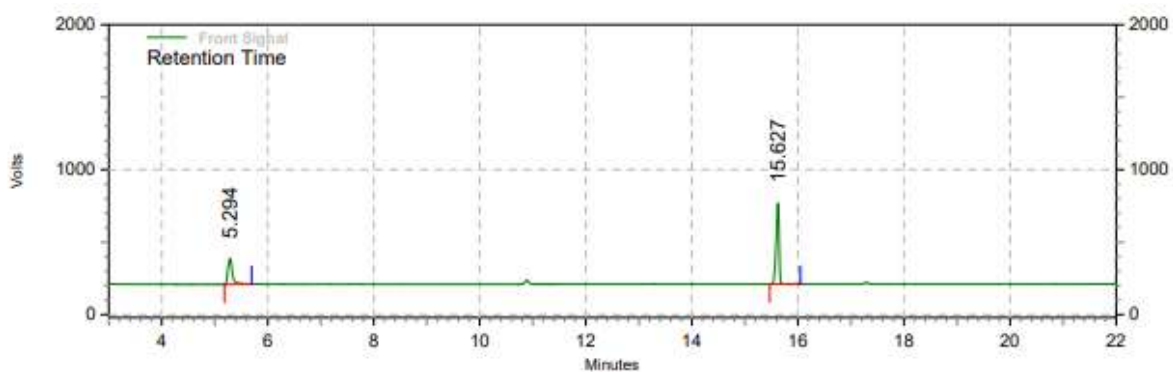


Front Signal Results

Retention Time	Area	Area %	Height	Height %
5.295	1571933	1.84	307239	1.71
18.729	83651164	98.16	17647358	98.29

Totals	85223097	100.00	17954597	100.00
--------	----------	--------	----------	--------

Figure 3.22: GC chromatogram of 4m.

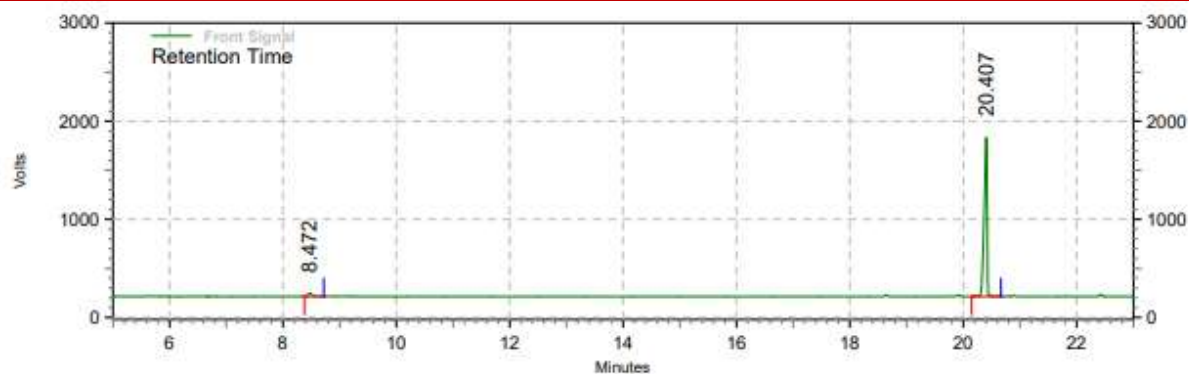


Front Signal Results

Retention Time	Area	Area %	Height	Height %
5.294	8006248	32.44	1368482	24.21
15.627	16676840	67.56	4282953	75.79

Totals	24683088	100.00	5651435	100.00
--------	----------	--------	---------	--------

Figure 3.23: GC chromatogram of 4n.

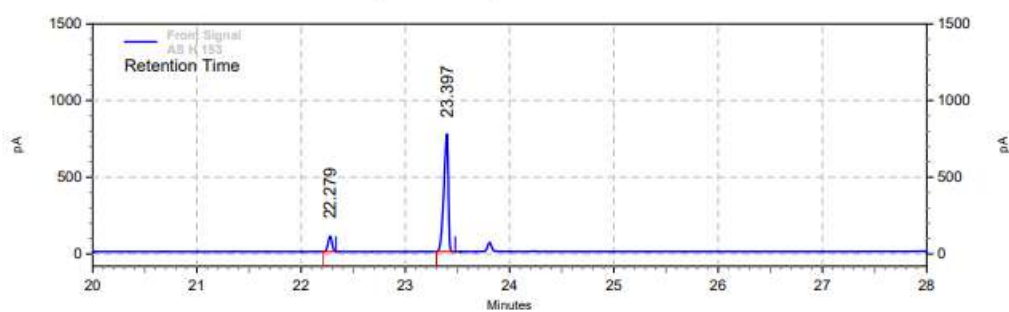


Front Signal Results

Retention Time	Area	Area %	Height	Height %
8.472	1234337	2.64	279959	2.20
20.407	45458360	97.36	12445419	97.80

Totals	Area	Area %	Height	Height %
	46692697	100.00	12725378	100.00

Figure 3.24: GC chromatogram of 4o.

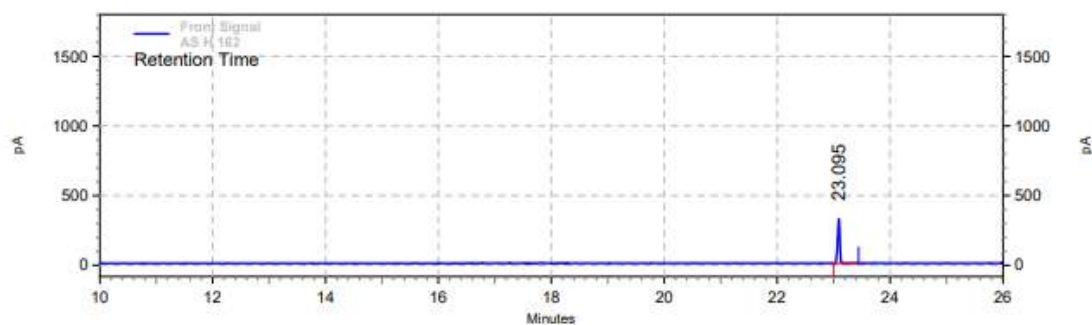


Front Signal Results

Retention Time	Area	Area %	Height	Height %
22.279	2025875	10.52	766670	11.54
23.397	17230954	89.48	5877453	88.46

Totals	Area	Area %	Height	Height %
	19256829	100.00	6644123	100.00

Figure 3.25: GC chromatogram of 4r.


**Front Signal
Results**

Retention Time	Area	Area %	Height	Height %
23.095	6635952	100.00	2424668	100.00
Totals	6635952	100.00	2424668	100.00

Figure 3.26: GC chromatogram of 4s.

3.4.7 ^1H NMR for isolated compounds of alkoxylation of silanes:

Diethoxydiphenylsilane (4a)

^1H NMR (200 MHz, CDCl_3): δ = 7.7 (m, 4H), 7.42 (m, 6H), 3.9 (q, J = 7.3 Hz, 4H), 1.29 (t, J = 6.7 Hz, 6H).

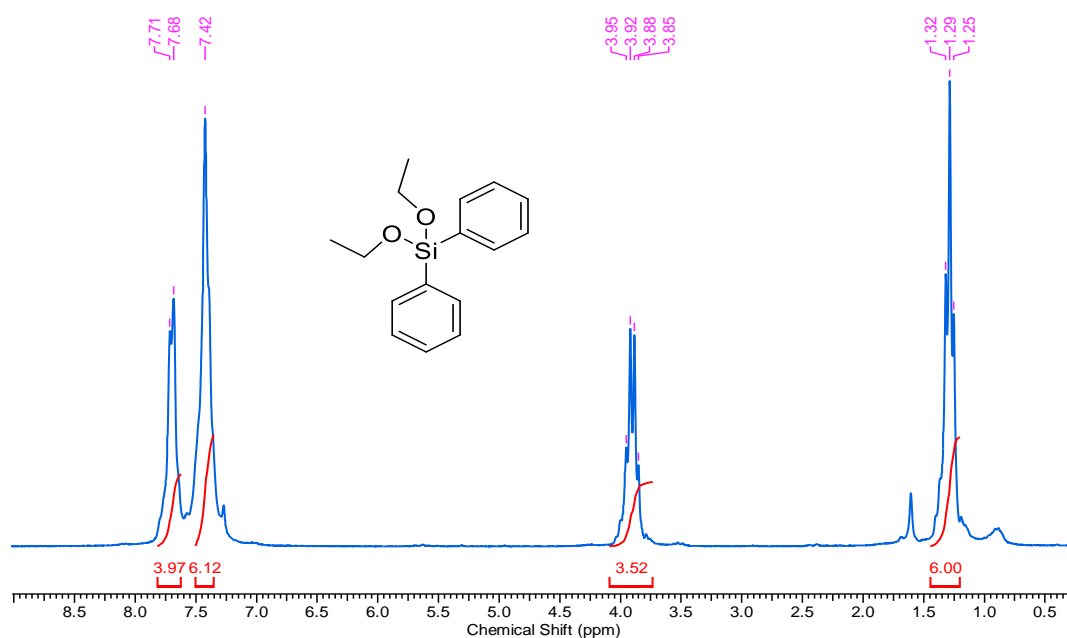


Figure 3.27: ^1H NMR spectrum of 4a.

triethoxy(phenyl)silane (4c)

$^1\text{H NMR}$ (500 MHz, CDCl_3): $\delta = 7.60$ (m, 2H, -Ph), 7.31 (m, 3H, -Ph), 3.79 (q, $J = 7.06$ Hz, 6H, $-\text{CH}_2$), 1.17 (t, $J = 6.97$ Hz, 9H, $-\text{CH}_3$).

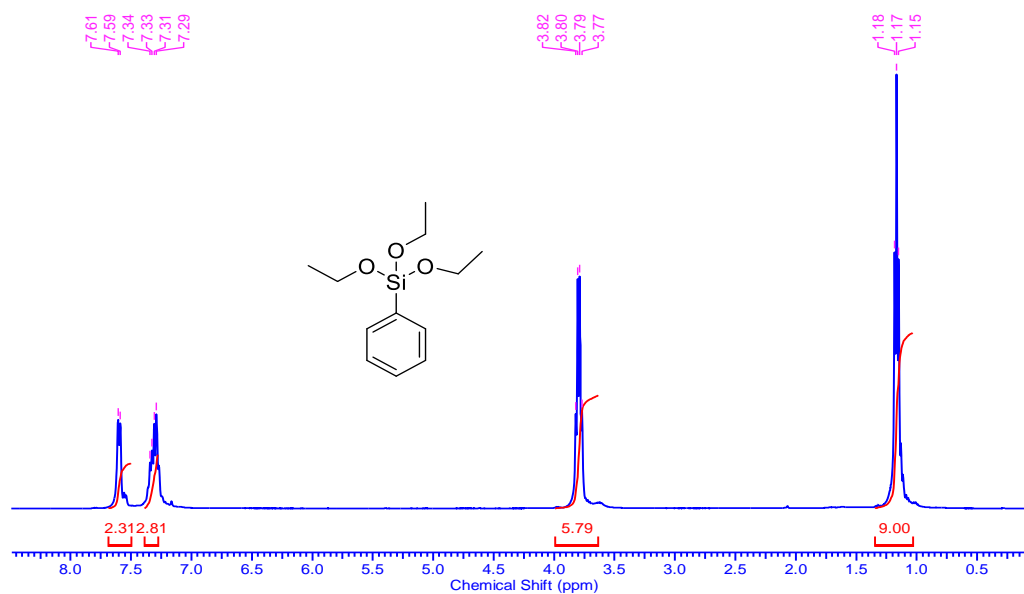


Figure 3.28: $^1\text{H NMR}$ spectrum of 4c.

Dimethoxydiphenylsilane (4e)

$^1\text{H NMR}$ (500 MHz, CDCl_3): $\delta = 7.56$ (m, 4H, -Ph), 7.27 (m, 6H, -Ph), 3.52 (s, 6H, $-\text{CH}_3$).

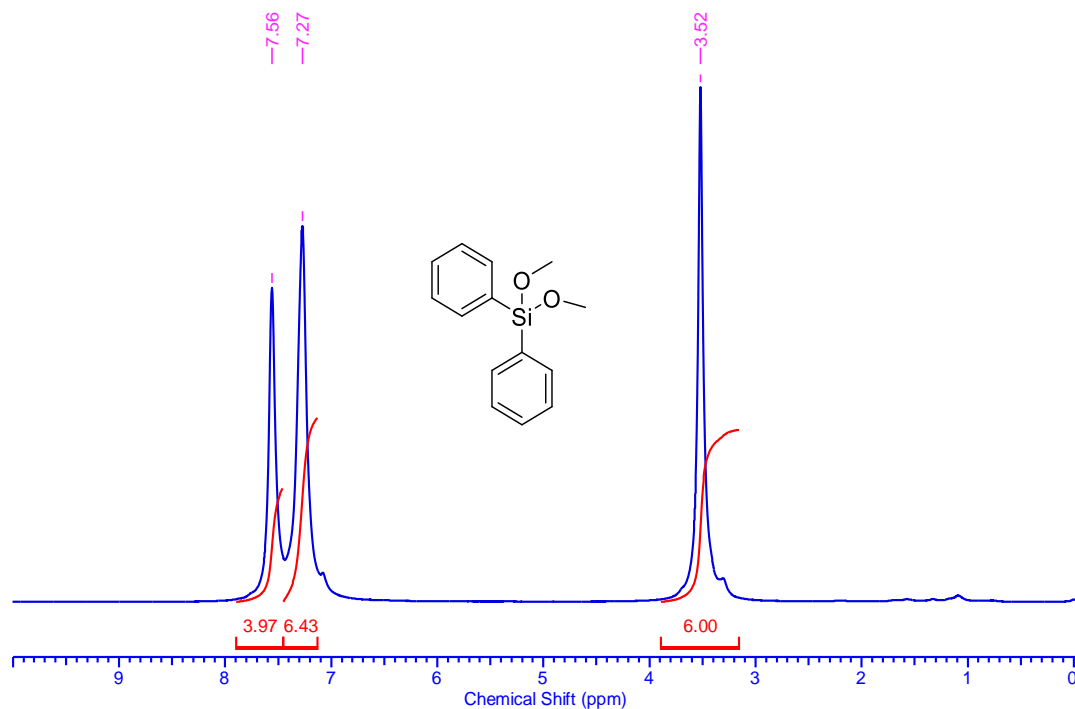


Figure 3.29: $^1\text{H NMR}$ spectrum of 4e.

dimethyl(phenyl)(3-phenylpropoxy)silane (4i)

$^1\text{H NMR}$ (400 MHz, CDCl_3): $\delta = 7.54$ (m, 1H, -Ph), 7.49 (m, 2H, -Ph), 7.30 (m, 3H, -Ph), 7.15 (q, $J = 7.6$ Hz, 2H, -Ph), 7.06 (m, 2H, Ph), 3.54 (t, $J = 7.1$ Hz, 2H, O- CH_2), 2.57 (t, $J = 8$ Hz, 2H, - CH_2Ph), 1.76 (m, 2H, C- CH_2 -C), 0.29 (s, 6H, - $\text{Si}(\text{CH}_3)_2$).

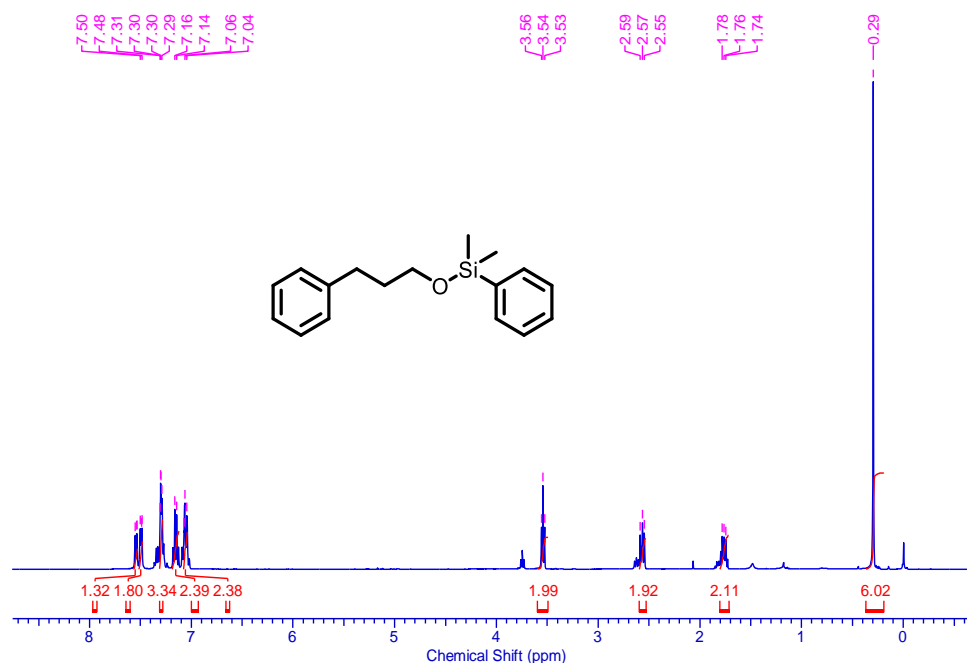


Figure 3.30: $^1\text{H NMR}$ spectrum of 4i.

(benzyloxy)triethylsilane (4j)

$^1\text{H NMR}$ (500 MHz, CDCl_3): $\delta = 7.61$ (d, 1H, -Ph), 7.33 (m, 3H, -Ph), 7.18 (m, 1H, -Ph), 4.69 (s, 2H, O- CH_2), 0.93 (t, $J = 7.3$ Hz, 9H, CH_3), 0.61 (q, $J = 8.3$ Hz, 6H, - SiCH_2).

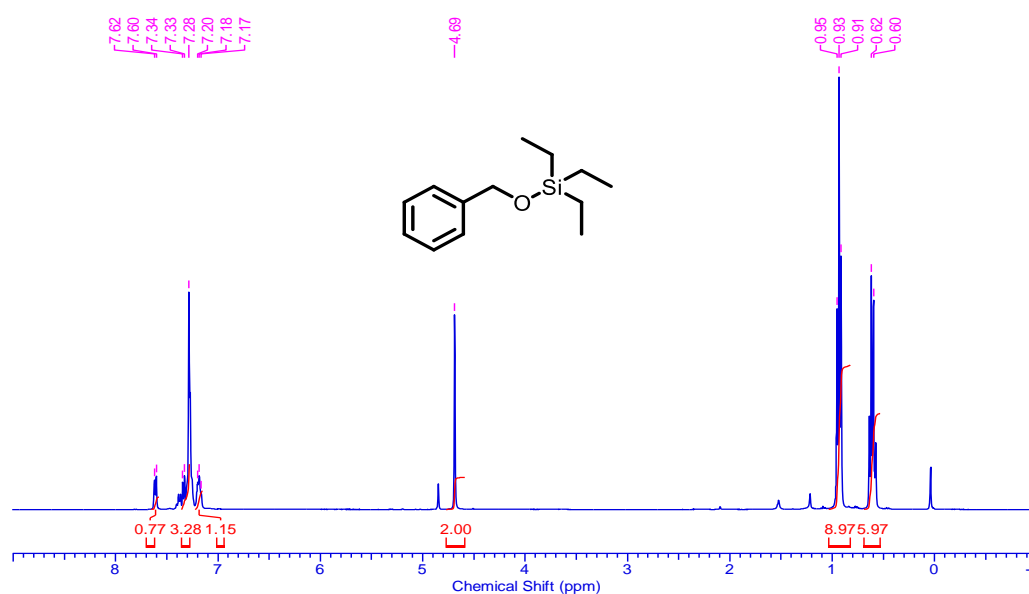


Figure 3.31: $^1\text{H NMR}$ spectrum of 4j.

(benzyloxy)dimethyl(phenyl)silane (4k)

$^1\text{H NMR}$ (400 MHz, CDCl_3): $\delta = 7.51$ (m, 2H, -Ph), 7.29 (m, 3H, -Ph), 7.21 (m, 4H, -Ph), 7.14 (m, 1H, -Ph), 4.60 (s, 2H, $-\text{CH}_2\text{Ph}$), 0.32 (s, 6H, $-\text{Si}(\text{CH}_3)_2$).

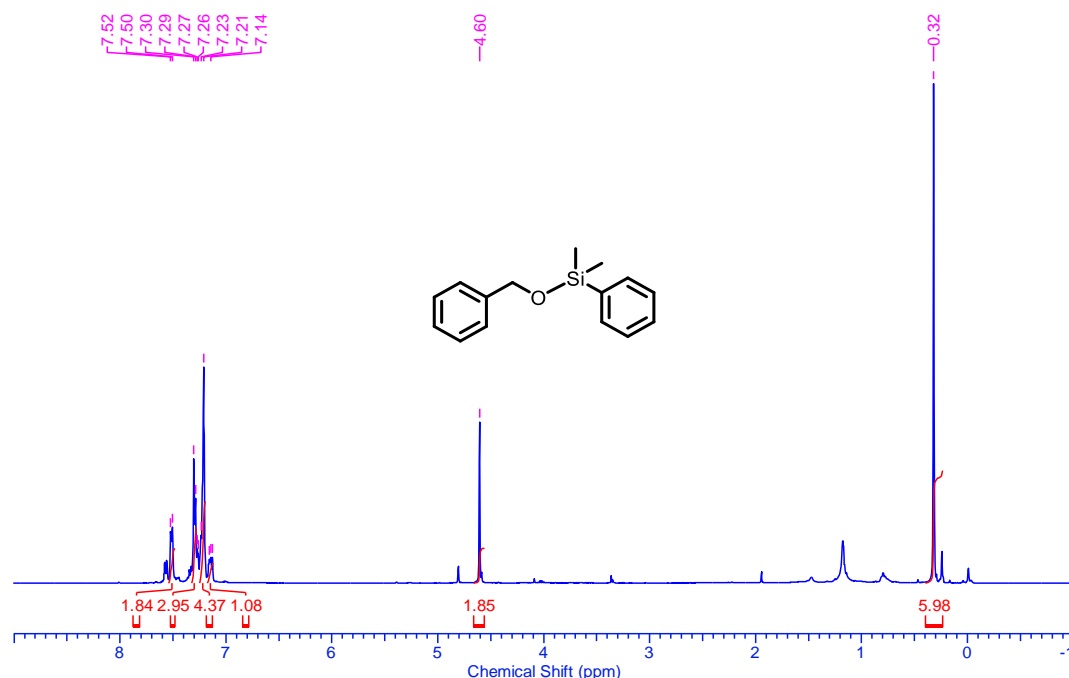


Figure 3.32: $^1\text{H NMR}$ spectrum of 4k.

triethyl(3-phenylpropoxy)silane (4l)

$^1\text{H NMR}$ (200 MHz, CDCl_3): $\delta = 7.57$ (m, 1H, -Ph), 7.35 (m, 1H, -Ph), 7.20 (m, 3H, -Ph), 3.60 (t, $J = 6.4$ Hz, 2H, CH_2), 2.84 (t, $J = 7.9$ Hz, 2H, CH_2), 1.82 (m, 2H, CH_2), 0.92 (t, $J = 7.9$ Hz, 9H, CH_3), 0.56 (q, $J = 8.7$ Hz, 6H, $-\text{SiCH}_2$).

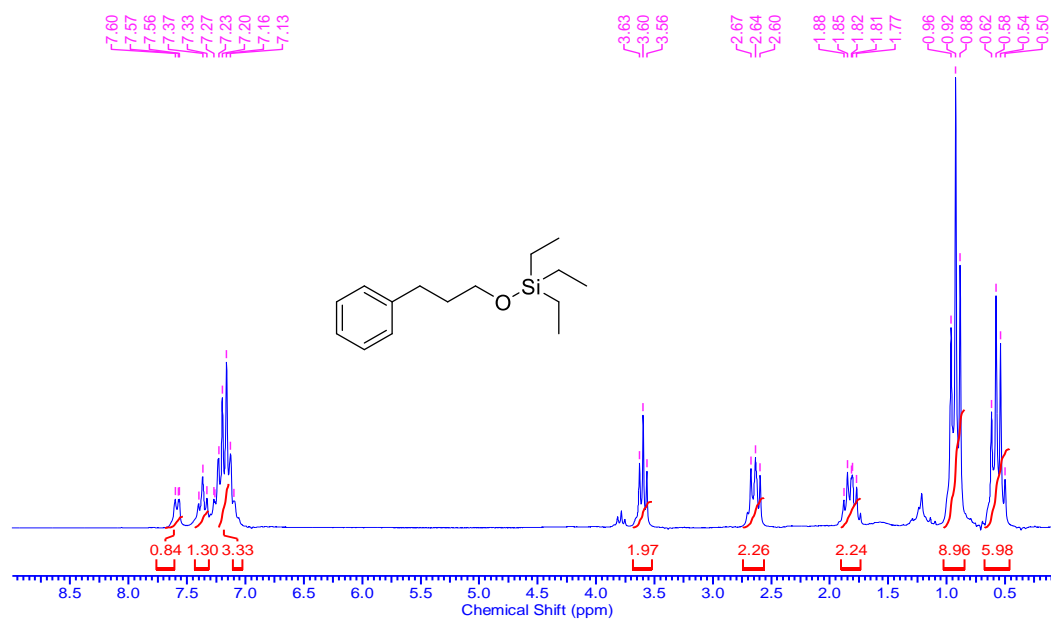


Figure 3.33: ¹H NMR spectrum of 4l.

dimethyl(phenyl)((4-(trifluoromethyl)benzyl)oxy)silane (4m)

¹H NMR (500 MHz, CDCl₃): δ = 7.49 (m, 1H, -Ph), 7.40 (m, 3H, -Ph), 7.24 (m, 5H, -Ph), 4.57 (s, 2H, -CH₂Ph), 0.27 (s, 6H, -Si(CH₃)₂).

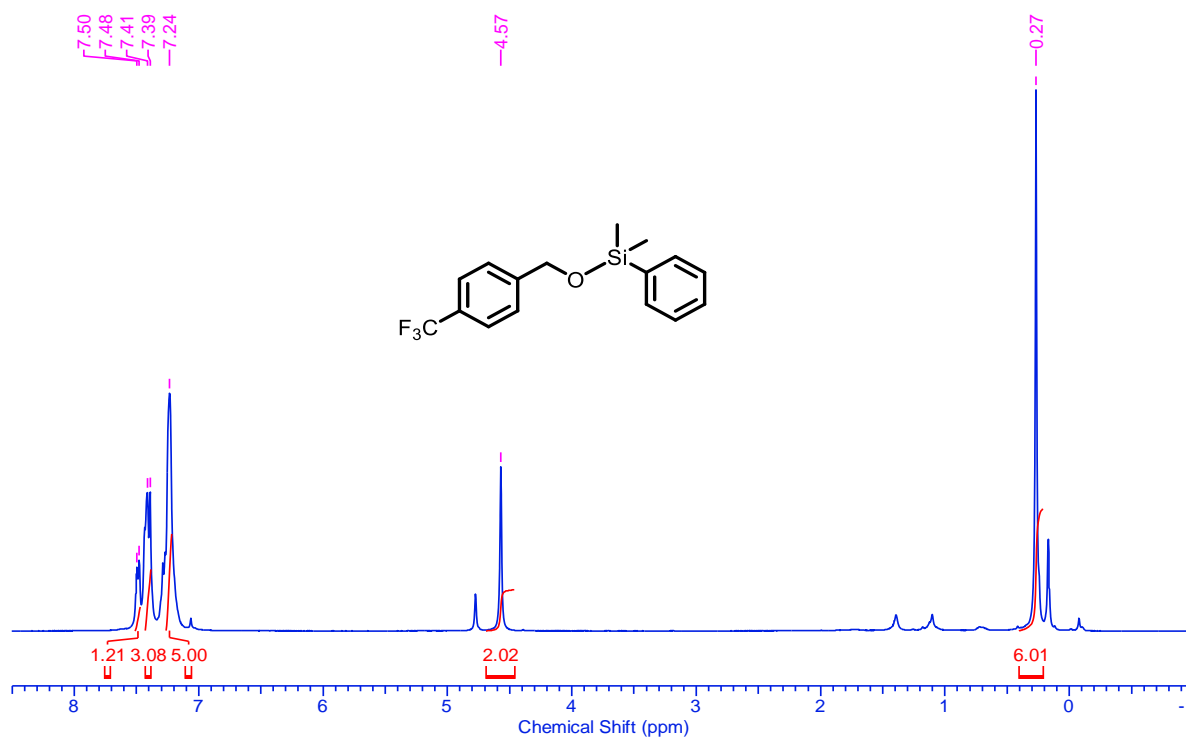


Figure 3.34: ¹H NMR spectrum of 4m.

triethyl((4-(trifluoromethyl)benzyl)oxy)silane (4n)

$^1\text{H NMR}$ (400 MHz, CDCl_3): $\delta = 7.61$ (d, $J = 8.1$ Hz, 2H, -Ph), 7.47 (d, $J = 8.1$ Hz, 2H, -Ph), 4.81 (s, 2H, $-\text{CH}_2\text{Ph}$), 1.01 (t, $J = 8$ Hz, 9H, $-\text{CH}_3$), 0.69 (q, $J = 9.5$ Hz, 6H, $-\text{CH}_2$).

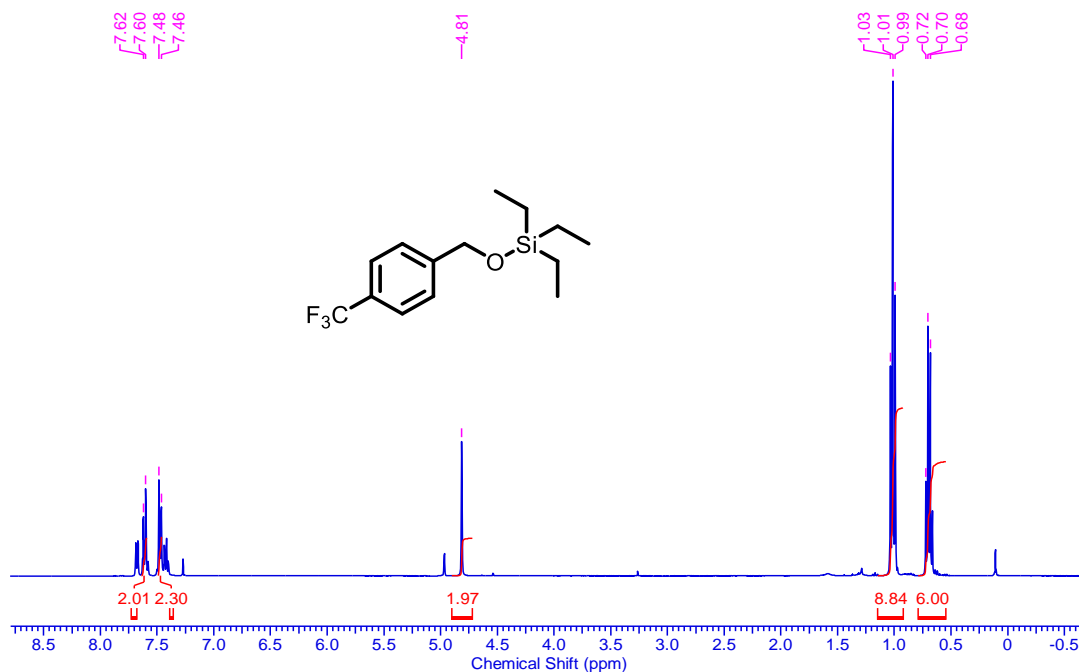


Figure 3.35: $^1\text{H NMR}$ spectrum of 4n.

((3,7-dimethyloct-6-en-1-yl)oxy)dimethyl(phenyl)silane (4o)

$^1\text{H NMR}$ (400 MHz, CDCl_3): $\delta = 7.49$ (m, 2H, -Ph), 7.29 (m, 3H, -Ph), 5.0 (t, $J = 8$ Hz, 1H, $\text{HC}=\text{C}$), 3.55 (m, 2H, $\text{CH}_2\text{-O}$), 1.86 (m, 2H, $\text{CH}_2\text{-C}=\text{C}$), 1.59 (s, 3H, $\text{CH}_3\text{-C}=\text{C}$), 1.51 (s, 3H, $\text{CH}_3\text{-C}=\text{C}$), 1.44 (m, 1H), 1.25 (m, 3H), 1.04 (m, 1H), 0.75 (d, $J = 7$ Hz, 3H, $\text{OCH}_2\text{CH}_2\text{CH}(\text{CH}_3)\text{CH}_2$), 0.29 (s, 6H, $-\text{Si}(\text{CH}_3)_2$).

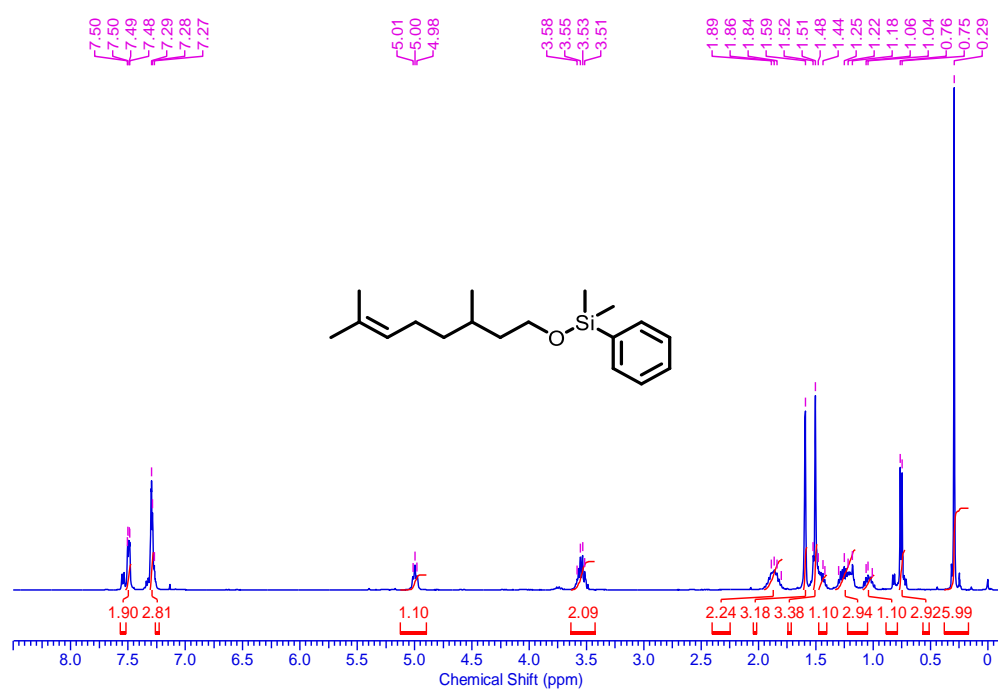


Figure 3.36: ¹H NMR spectrum of 4o.

((4-methoxybenzyl)oxy)dimethyl(phenyl)silane (4p)

¹H NMR (500 MHz, CDCl₃): δ = 7.51 (m, 2H, -Ph), 7.30 (m, 3H, -Ph), 7.12 (d, *J* = 8.4 Hz, 2H, -Ph), 6.76 (d, *J* = 8.6 Hz, 2H, -Ph), 4.54 (s, 2H, -CH₂Ph), 3.69 (s, 3H, OCH₃), 0.31 (s, 6H, -Si(CH₃)₂).

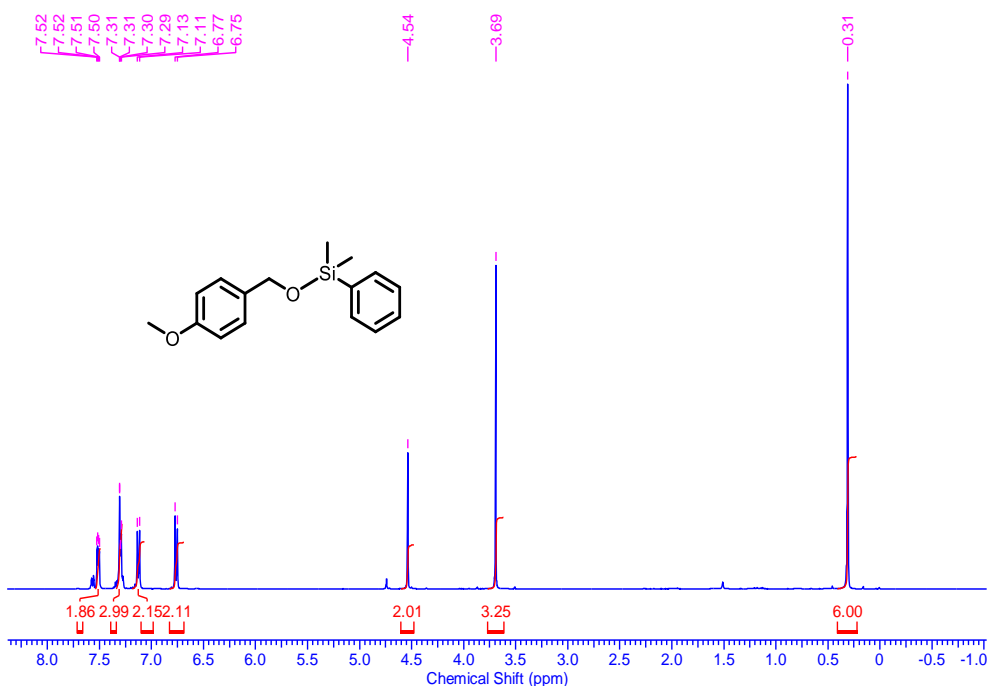


Figure 3.37: ¹H NMR spectrum of 4p.

triethyl((4-methoxybenzyl)oxy)silane (4q)

$^1\text{H NMR}$ (400 MHz, CDCl_3): $\delta = 7.14$ (m, 2H, -Ph), 6.76 (m, 2H, -Ph), 4.56 (s, 2H, O-CH₂), 3.68 (s, 3H, OCH₃), 0.87 (m, 9H, C-CH₃), 0.54 (m, 6H, -SiCH₂).

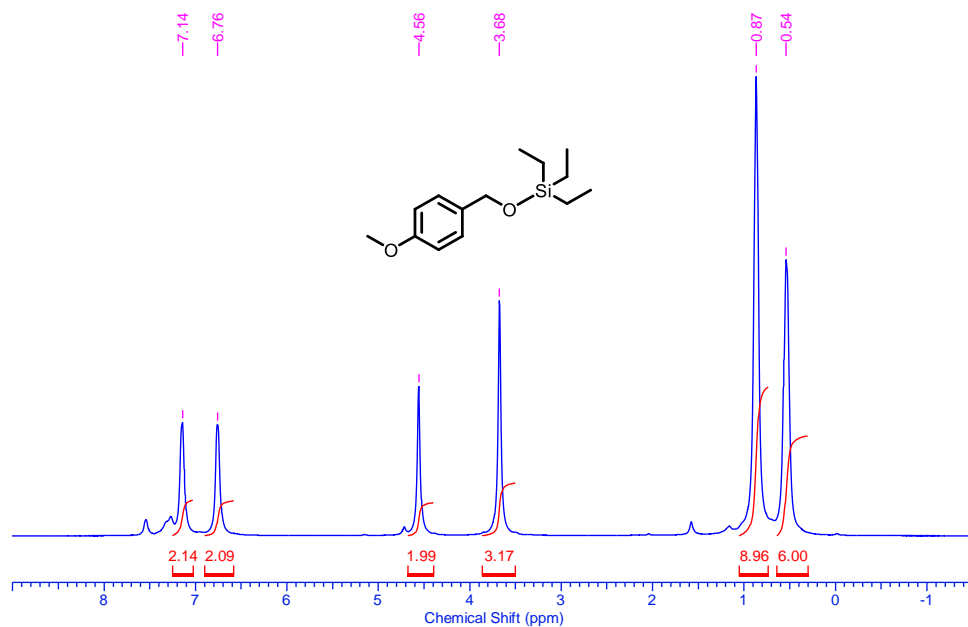


Figure 3.38: $^1\text{H NMR}$ spectrum of 4q.

ethoxytriphenylsilane (4r)

$^1\text{H NMR}$ (400 MHz, CDCl_3): $\delta = 7.67$ (m, 6H, -Ph), 7.44 (m, 9H, -Ph), 3.93 (q, $J = 7.18$, 2H, -OCH₂), 1.29 (t, $J = 7.18$, 3H, CH₃).

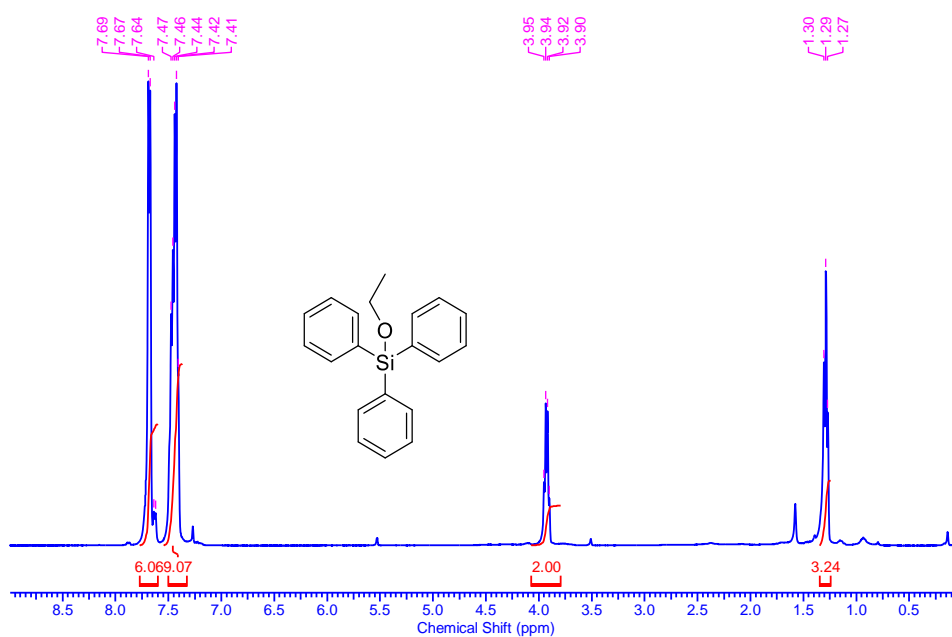


Figure 3.39: $^1\text{H NMR}$ spectrum of 4r.

methoxytriphenylsilane (4s)

$^1\text{H NMR}$ (500 MHz, CDCl_3): $\delta = 7.54$ (m, 6H, -Ph), 7.32 (m, 9H, -Ph), 3.55 (s, 3H, $-\text{OCH}_3$).

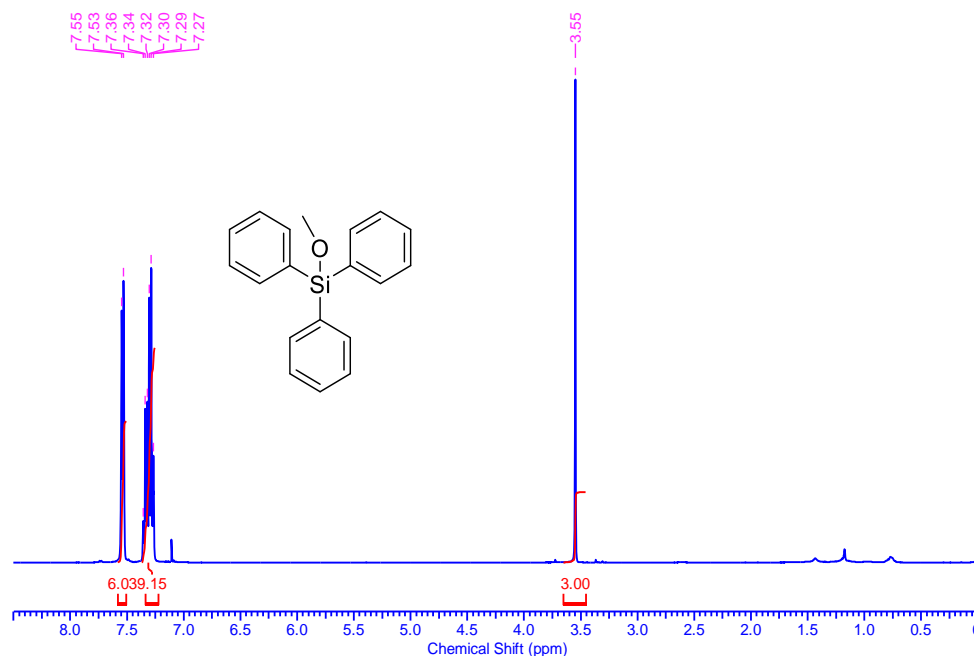


Figure 3.40: $^1\text{H NMR}$ spectrum of 4s.

((10,13-dimethyl-17-(6-methylheptan-2-yl)-2,3,4,7,8,9,10,11,12,13,14,15,16,17-tetradecahydro-1H-cyclopenta[a]phenanthren-3-yl)oxy)dimethyl(phenyl)silane (4t)

$^1\text{H NMR}$ (400 MHz, CDCl_3): $\delta = 7.63$ (m, 2H, -Ph), 7.39 (m, 3H, -Ph), 5.27 (m, 1H, $-\text{CH}=\text{C}$), 3.52 (m, 1H, O-CH), 2.32 (m, 1H), 2.18 (m, 1H), 1.98 (m, 2H), 1.80 (m, 2H), 1.72 (m, 1H), 1.52 (m, 9H), 1.33 (m, 2H), 1.27 (m, 2H), 1.12 (m, 5H), 0.99 (s, 5H), 0.91 (d, $J = 7.19$ Hz, 4H), 0.87 (d, $J = 6.29$ Hz, 6H, CH_3 -26, 27), 0.67 (s, 3H, CH_3 -16), 0.40 (s, 6H, $-\text{Si}(\text{CH}_3)_2$).

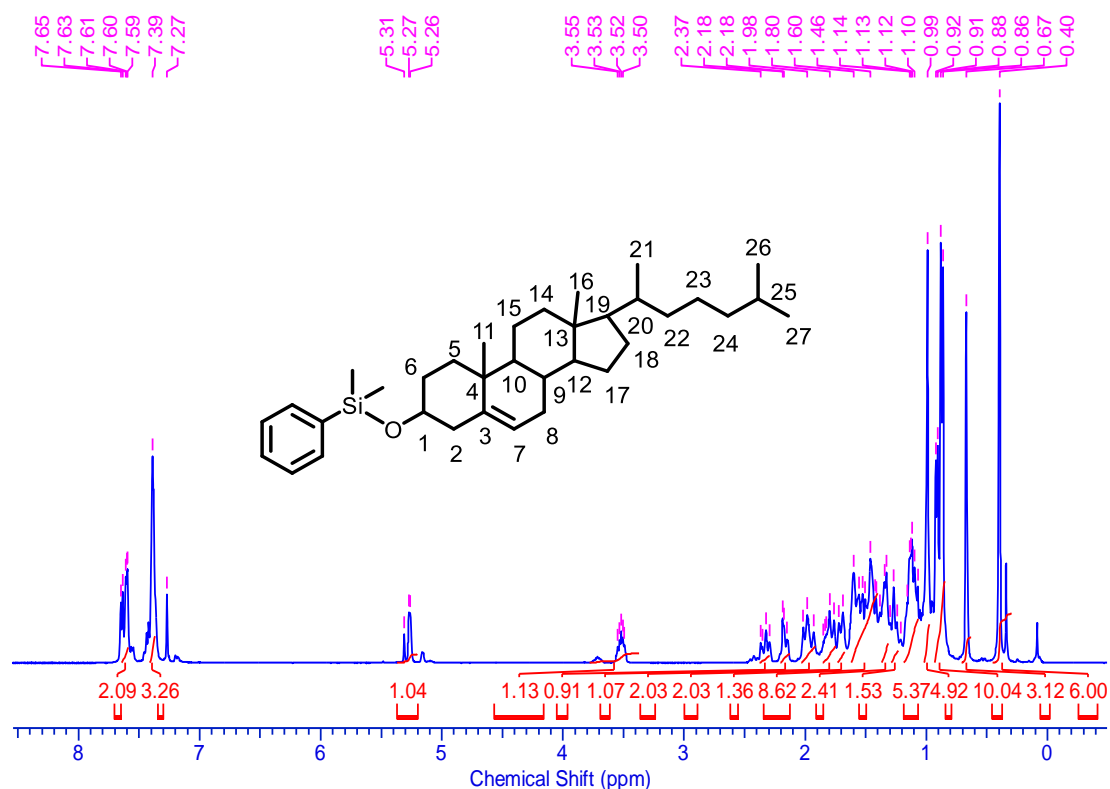


Figure 3.41: ¹H NMR spectrum of 4t.

3.4.8 General procedure for iron catalysed synthesis of PSE:

Monomer (1.8 mmol), hydrosilane (1.8 mmol), Fe(CO)₄HSiPh₃ (0.09 mmol, 39 mg, 5 mol%), ligand (0.09 mmol, 24 mg, 5 mol%) and Toluene (2.0-2.5 mL) were introduced in a 50 mL Schlenk flask equipped with a magnetic stir bar under argon atmosphere. The Schlenk flask was then fitted with a condenser with Argon inlet and outlet. The reaction mixture was then heated for a set amount of time at reflux temperature. The reaction progress was monitored on a regular basis by extracting a tiny amount of sample for NMR spectroscopic analysis. After the reaction, a little amount of CH₂Cl₂ (1–2 mL) was added to the crude reaction mixture, followed by the addition of MeOH (10–12 mL) in a portioned manner to generate a biphasic mixture. The unreacted material was removed from the top layer, and the bottom pale/off-white-coloured solid/viscous component was washed multiple times with MeOH. Finally, the resultant polymers were vacuum-dried to a consistent weight for characterization (Yield = 74%).

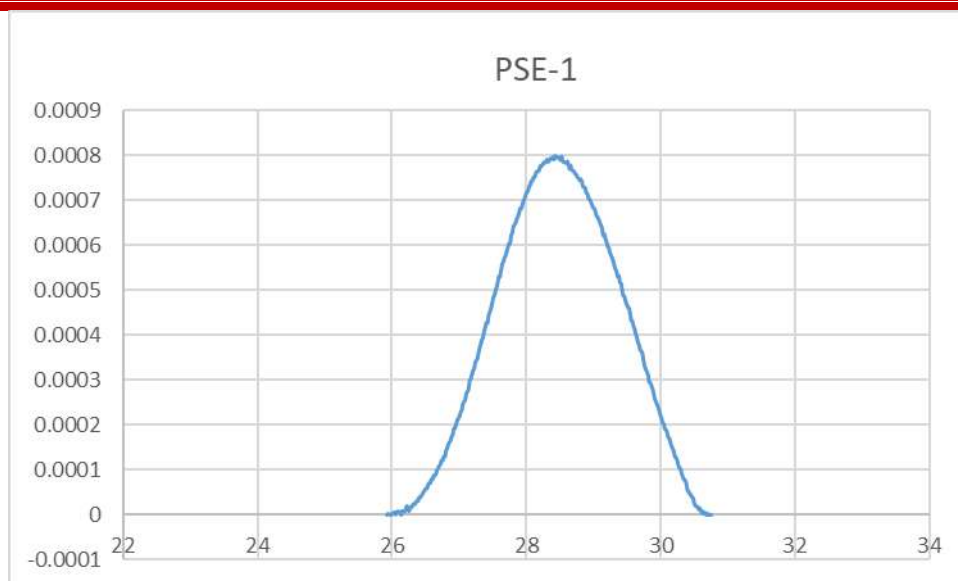


Figure 3.42: GPC of PSE-1.

3.4.9 NMR spectrum for PSE-1:

Isosorbide + Ph₂SiH₂ (16 h), PSE-1

¹H NMR (400 MHz, CDCl₃): δ = 7.42 (m, 10H, -Ph), 4.36 (m, 4H, -OCH & -CH bridged), 3.83 (m, 2H, -CH₂), 3.49 (m, 2H, -CH₂).

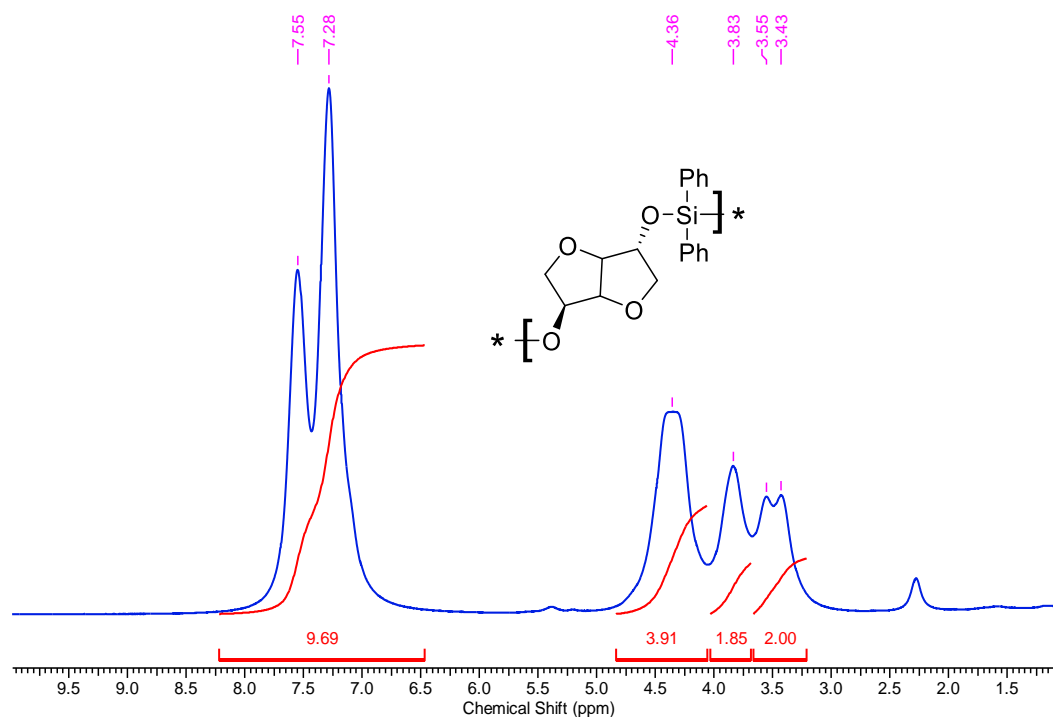


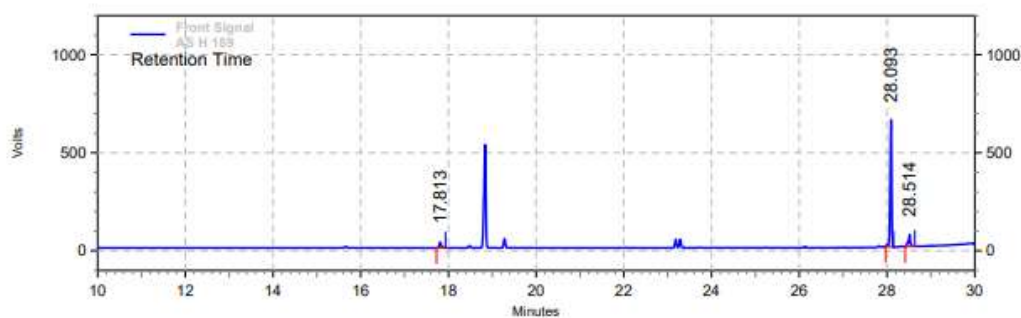
Figure 3.43: ¹H NMR spectrum of Isosorbide + Ph₂SiH₂ (16 h), PSE-1.

3.4.10 GC analysis for table 3.3:

Conversion was determined with respect to starting diphenylacetylene (5a), appearing at $t = 17.8$ min by applying the following GC condition. The product after tandem alkoxylation-hydrosilylation of alkyne appeared at $t = 28.0$ and $t = 28.5$ min in this method.

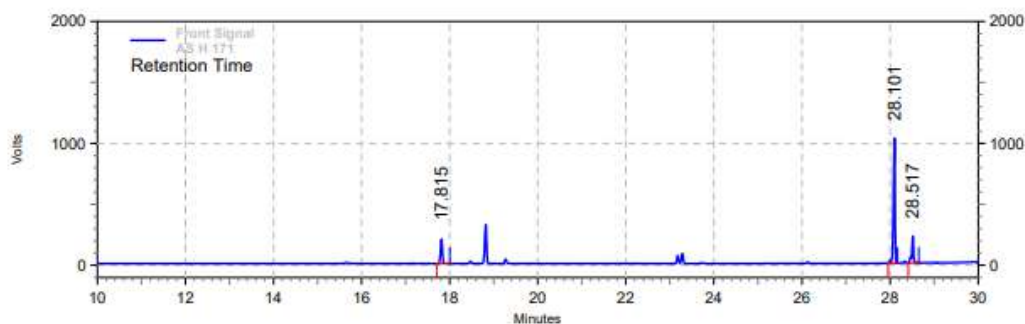
GC condition: HP-5 column, isothermal at $70\text{ }^{\circ}\text{C}$ for 1.0 min, $4\text{ }^{\circ}\text{C min}^{-1}$ to $120\text{ }^{\circ}\text{C}$, $10\text{ }^{\circ}\text{C min}^{-1}$ to $250\text{ }^{\circ}\text{C}$, $20\text{ }^{\circ}\text{C min}^{-1}$ to $320\text{ }^{\circ}\text{C}$ for 2 min, with 10 psi pressure.

3.4.11 GC chromatogram for each entry of table3.3:



Front Signal Results				
Retention Time	Area	Area %	Height	Height %
17.813	669930	4.94	226029	3.99
28.093	11459177	84.52	4982137	87.85
28.514	1429426	10.54	463333	8.17
Totals	13558533	100.00	5671499	100.00

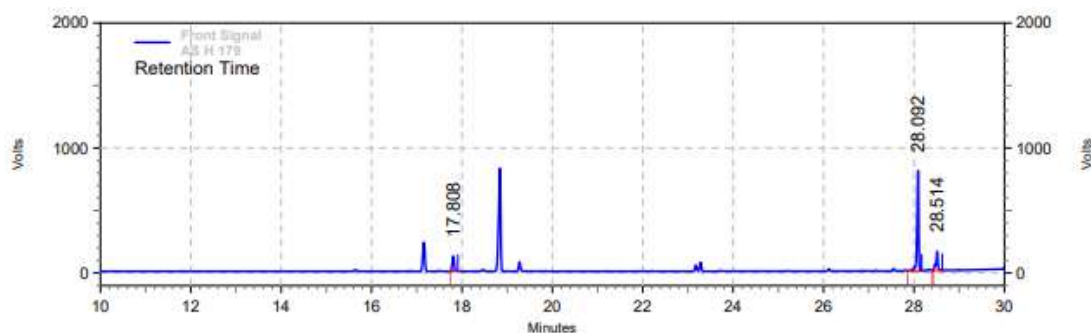
Figure 3.44: GC chromatogram of entry 1, table 3.3.


**Front Signal
Results**

Retention Time	Area	Area %	Height	Height %
17.815	4445389	15.77	1534806	13.85
28.101	19282536	68.40	7868223	71.00
28.517	4464231	15.84	1679680	15.16

Totals	28192156	100.00	11082709	100.00
--------	----------	--------	----------	--------

Figure 3.45: GC chromatogram of entry 2, table 3.3.


**Front Signal
Results**

Retention Time	Area	Area %	Height	Height %
17.808	2685270	12.83	931548	11.30
28.092	14899225	71.19	6144356	74.56
28.514	3343199	15.97	1164557	14.13

Totals	20927694	100.00	8240461	100.00
--------	----------	--------	---------	--------

Figure 3.46: GC chromatogram of entry 3, table 3.3.

3.4.12 General procedure for iron catalysed tandem Alkoxylation-hydrosilylation of alkynes:

Alkyne (0.25 mmol), silane (0.5 mmol), $\text{Fe}(\text{CO})_4\text{HSiPh}_3$ (0.0125-0.025 mmol, 5-10 mol %), ligand (0.0125-0.025 mmol, 5-10 mol %), alcohol (0.5 mL) and toluene (0.5 mL) were introduced in a 10 mL Teflon-valved flask equipped with a magnetic stir bar under argon atmosphere. The reaction mixture was stirred at 50-60 °C for 24-48 h. The mixture was

extracted with diethyl ether (3×10 mL). After that, the layers of mixed diethyl ether were dried over sodium sulfate and concentrated under vacuum. After evaporation of the solvent, the crude reaction mixture was purified by silica gel column chromatography (petroleum ether/EtOAc 50/1), yielding the product. The conversion was determined by gas chromatography with respect to starting alkyne.

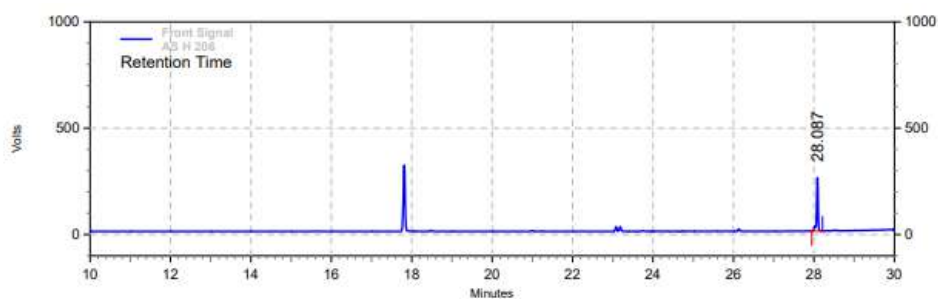
GC method 1: GC analysis was carried out on an Agilent 7890B GC system using HP-05 column ($30 \text{ m} \times 320 \text{ } \mu\text{m} \times 0.25 \text{ } \mu\text{m}$), split ratio 30:1, column pressure 10 psi, injector temperature of $260 \text{ }^\circ\text{C}$, detector temperature of $330 \text{ }^\circ\text{C}$, argon carrier gas. Temperature program: Initial temperature $70 \text{ }^\circ\text{C}$, hold for 1 min.; ramp 1: $4 \text{ }^\circ\text{C}/\text{min.}$ to $120 \text{ }^\circ\text{C}$; ramp 2: $10 \text{ }^\circ\text{C}/\text{min.}$ to $250 \text{ }^\circ\text{C}$; ramp 3: $20 \text{ }^\circ\text{C}/\text{min.}$ to $320 \text{ }^\circ\text{C}$, hold for 2 min. This method was applied for analysing substrates 5a, 5b, 5c, 5d, 5e.

GC method 2: GC analysis was carried out on an Agilent 7890B GC system using HP-05 column ($30 \text{ m} \times 320 \text{ } \mu\text{m} \times 0.25 \text{ } \mu\text{m}$), split ratio 30:1, column pressure 10 psi, injector temperature of $260 \text{ }^\circ\text{C}$, detector temperature of $330 \text{ }^\circ\text{C}$, argon carrier gas. Temperature program: Initial temperature $70 \text{ }^\circ\text{C}$, hold for 1 min.; ramp 1: $4 \text{ }^\circ\text{C}/\text{min.}$ to $120 \text{ }^\circ\text{C}$; ramp 2: $10 \text{ }^\circ\text{C}/\text{min.}$ to $250 \text{ }^\circ\text{C}$, hold for 3 min; ramp 3: $20 \text{ }^\circ\text{C}/\text{min.}$ to $320 \text{ }^\circ\text{C}$, hold for 5 min. This method was applied for analysing substrates 5f, 5g, 5h.

Table 3.6. GC retention time for substrates, products and conversion

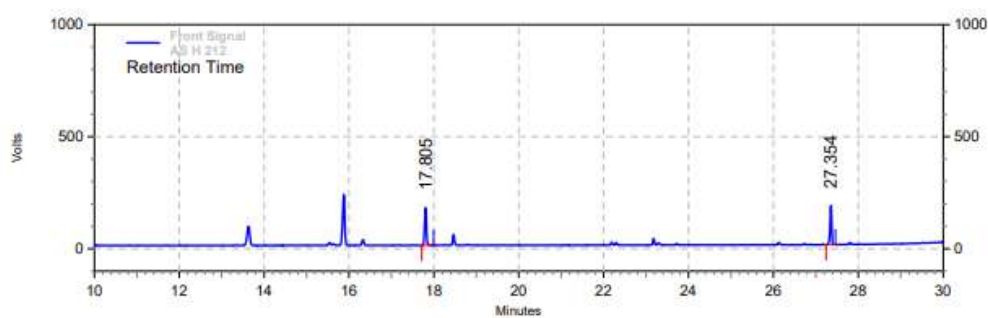
Substrate	Retention time (min)	Product	Retention time (min)	Conversion (%)
5a	17.8	6a	28.0	>99
5c	17.8	6c	27.3	48
5d	17.8	6d	28.0, 28.5	84
5e	17.3	6e	27.1	87
5f	22.0	6f	32.0	45
5g	23.9	6g	32.6	65
5h	22.8	6h	31.1	44

3.4.13 GC chromatogram for substrate scope of tandem Alkoxylation-hydrosilylation:


**Front Signal
Results**

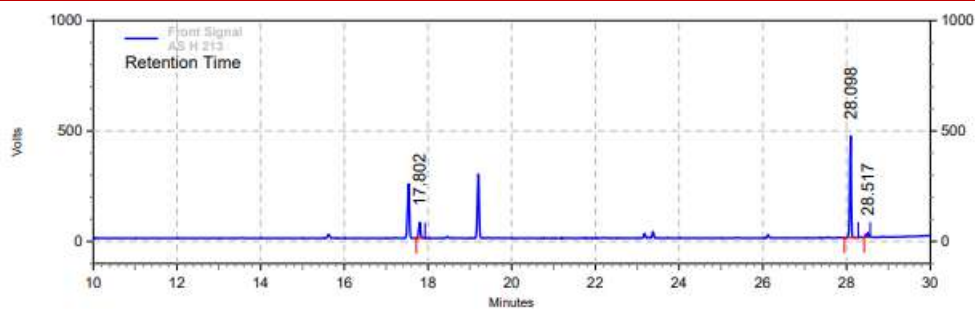
Retention Time	Area	Area %	Height	Height %
28.087	4749684	100.00	1928936	100.00
Totals	4749684	100.00	1928936	100.00

Figure 3.47: GC chromatogram of 6a.


**Front Signal
Results**

Retention Time	Area	Area %	Height	Height %
17.805	3724886	51.96	1287513	49.18
27.354	3444299	48.04	1330287	50.82
Totals	7169185	100.00	2617800	100.00

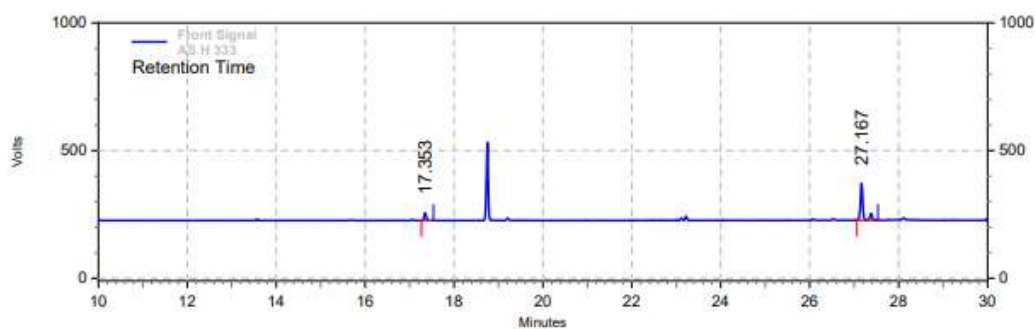
Figure 3.48: GC chromatogram of 6c.



Front Signal Results

Retention Time	Area	Area %	Height	Height %
17.802	1578700	15.21	547595	12.91
28.098	8223809	79.21	3537862	83.39
28.517	580234	5.59	156881	3.70
Totals	10382743	100.00	4242338	100.00

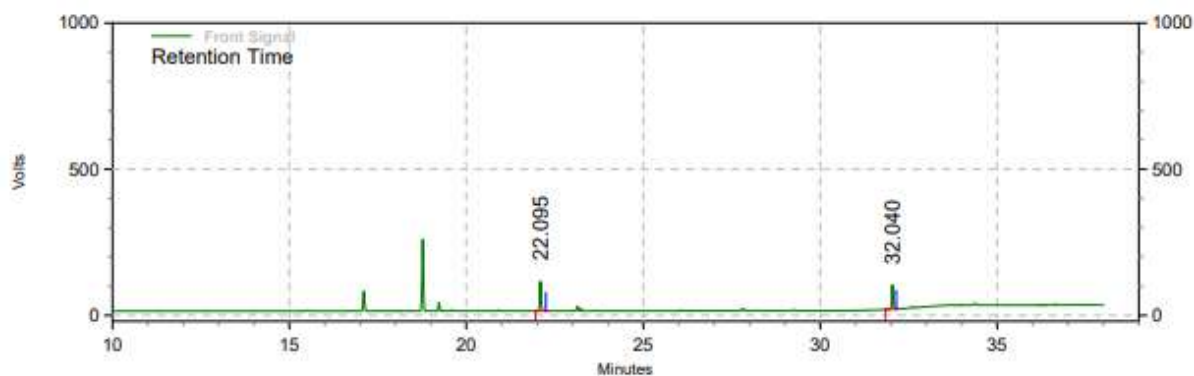
Figure 3.49: GC chromatogram of 6d.



Front Signal Results

Retention Time	Area	Area %	Height	Height %
17.353	718442	13.43	227918	17.08
27.167	4630794	86.57	1106147	82.92
Totals	5349236	100.00	1334065	100.00

Figure 3.50: GC chromatogram of 6e.

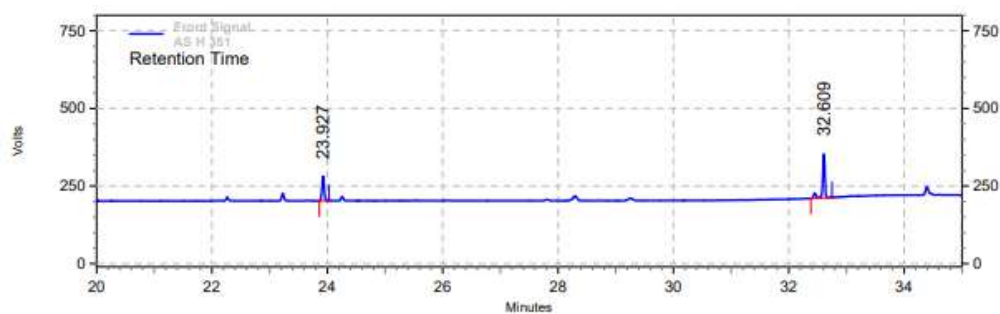


Front Signal Results

Retention Time	Area	Area %	Height	Height %
22.095	2176402	55.00	779813	55.02
32.040	1780611	45.00	637409	44.98

Totals	3957013	100.00	1417222	100.00
--------	---------	--------	---------	--------

Figure 3.51: GC chromatogram of 6f.

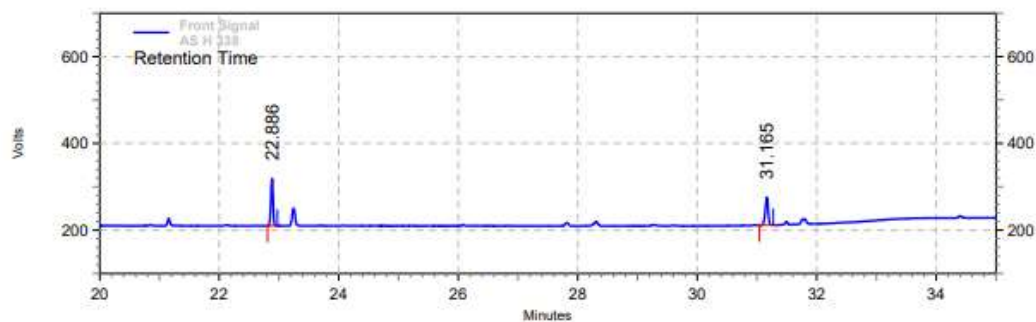


Front Signal Results

Retention Time	Area	Area %	Height	Height %
23.927	1591681	34.61	608330	35.93
32.609	3006616	65.39	1084925	64.07

Totals	4598297	100.00	1693255	100.00
--------	---------	--------	---------	--------

Figure 3.52: GC chromatogram of 6g.



Front Signal Results

Retention Time	Area	Area %	Height	Height %
22.886	2134424	56.08	832847	62.90
31.165	1671816	43.92	491143	37.10
Totals	3806240	100.00	1323990	100.00

Figure 3.53: GC chromatogram of 6h.

3.4.14 ^1H NMR of isolated compounds for substrate scope of tandem Alkoxylation-hydrosilylation:

(E)-(1,2-diphenylvinyl)(methoxy)diphenylsilane (6a)

^1H NMR (200 MHz, CDCl_3): δ = 7.58 (m, 5H), 7.34 (m, 8H), 7.12 (m, 2H), 7.0 (m, 6H), 3.57 (s, 3H).

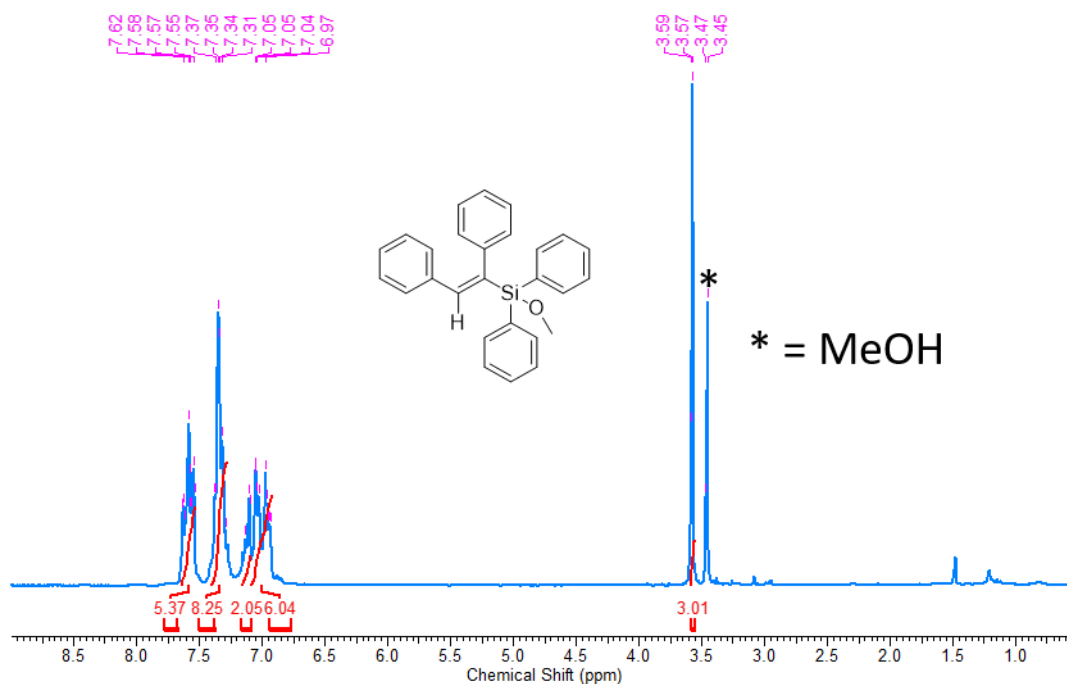


Figure 3.54: ^1H NMR spectrum of 6a.

(E)-(1,2-diphenylvinyl)(ethoxy)diphenylsilane (6b)

$^1\text{H NMR}$ (200 MHz, CDCl_3): $\delta = 7.65$ (m, 4H), 7.42 (m, 7H), 7.17 (m, 6H), 7.03 (m, 4H), 3.77 (q, $J = 7$ Hz, 2H), 1.17 (t, $J = 7$ Hz, 3H).

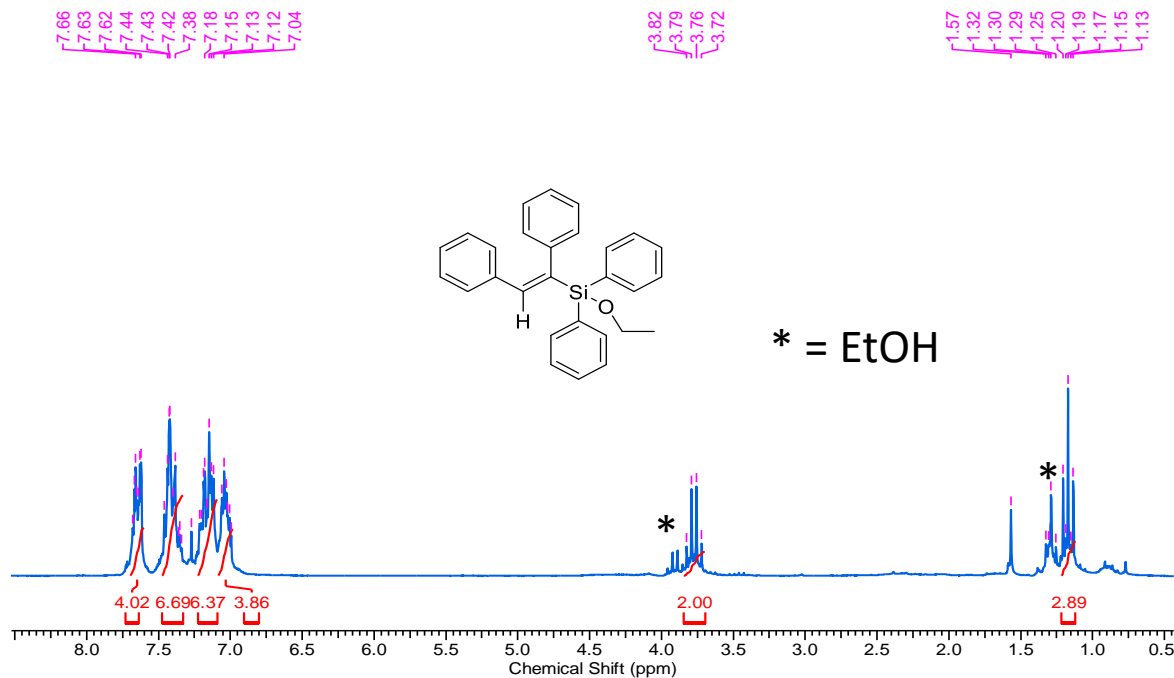


Figure 3.55: $^1\text{H NMR}$ spectrum of 6b.

(E)-(1,2-diphenylvinyl)(isopropoxy)diphenylsilane (6c)

$^1\text{H NMR}$ (200 MHz, CDCl_3): $\delta = 7.66$ (dd, $J = 7.7$ Hz, $J = 1.9$ Hz, 4H), 7.4 (m, 7H), 7.16 (m, 6H), 7.02 (m, 4H), 4.1 (m, 1H), 1.13 (d, $J = 6.1$ Hz, 6H).

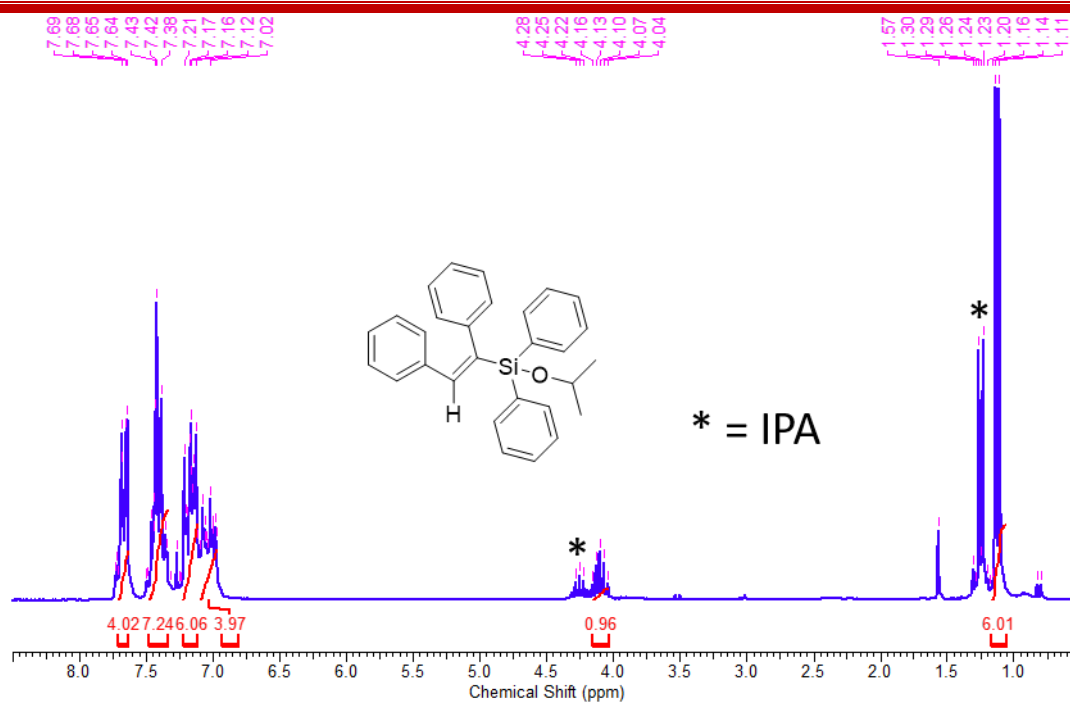


Figure 3.56: ^1H NMR spectrum of **6c**.

(E)-(1,2-diphenylvinyl)diphenyl(2,2,2-trifluoroethoxy)silane (6d**)**

^1H NMR (200 MHz, CDCl_3): δ = 7.53 (dd, J = 7.6 Hz, J = 2 Hz, 4H), 7.34 (m, 6H), 7.1 (m, 7H), 6.93 (m, 4H), 3.78 (q, J = 8.4, 2H).

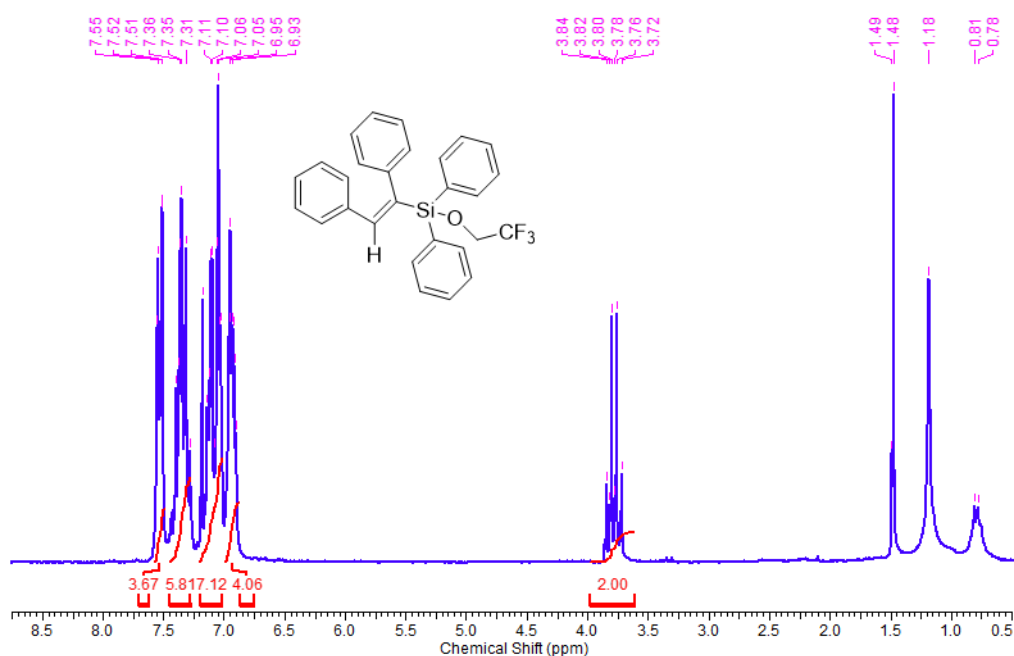


Figure 3.57: ^1H NMR spectrum of **6d**.

(E)-(1,2-bis(4-(trifluoromethyl)phenyl)vinyl)(ethoxy)diphenylsilane (6e)

$^1\text{H NMR}$ (500 MHz, CDCl_3): δ = 7.58 (d, J = 6.7 Hz, 3H), 7.51 (d, J = 6.2 Hz, 2H), 7.30 (m, 11H), 7.05 (s, 1H), 7.1 (s, 1H), 6.97 (d, J = 7.6 Hz, 2H), 3.79 (q, J = 7.6 Hz, 2H), 1.17 (t, J = 6.7 Hz, 3H).

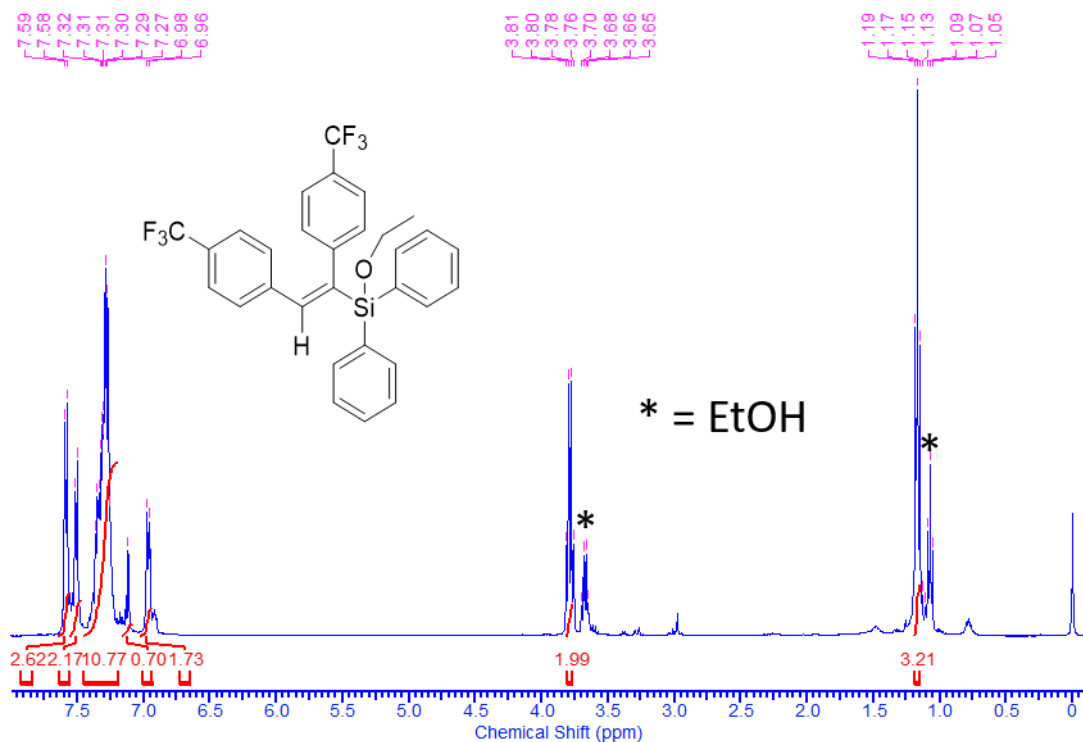


Figure 3.58: $^1\text{H NMR}$ spectrum of 6e.

(E)-(1,2-bis(4-chlorophenyl)vinyl)(ethoxy)diphenylsilane (6f)

$^1\text{H NMR}$ (400 MHz, CDCl_3): δ = 7.60 (q, J = 8.1 Hz, 3H), 7.53 (d, J = 7.4 Hz, 3H), 7.36 (m, 2H), 7.31 (d, J = 8.1 Hz, 5H), 7.08 (d, J = 8.77 Hz, 1H), 7.02 (m, 2H), 6.84 (m, 3H), 3.69 (q, J = 6.7 Hz, 2H), 1.09 (t, J = 7.4 Hz, 3H).

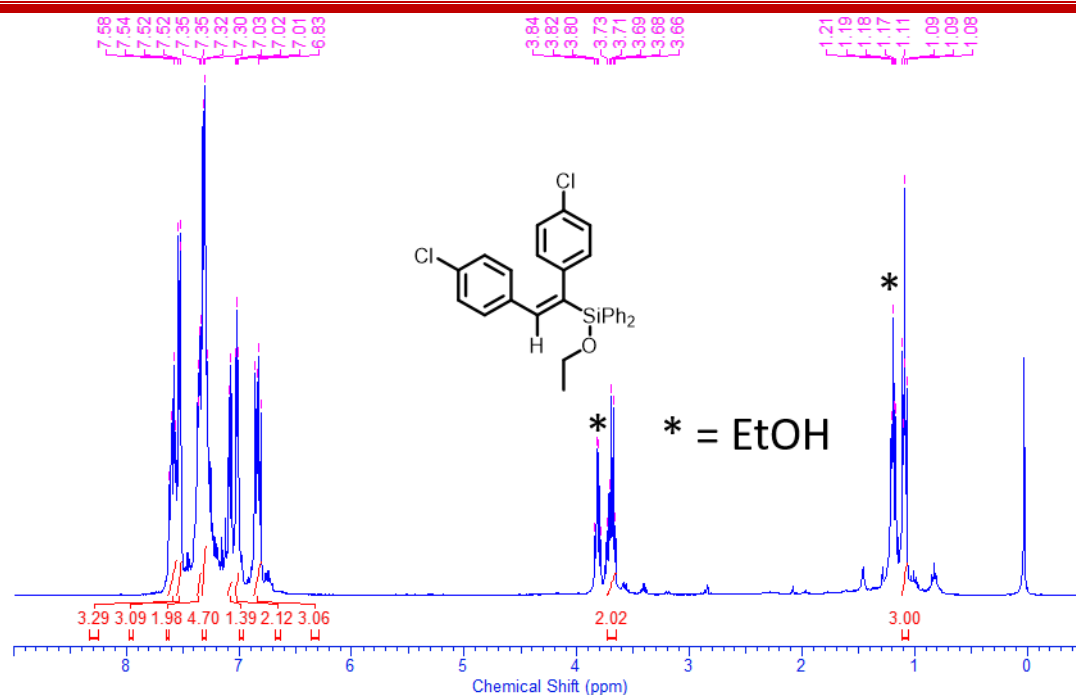


Figure 3.59: $^1\text{H NMR}$ spectrum of 6f.

(E)-(1,2-bis(4-methoxyphenyl)vinyl)(ethoxy)diphenylsilane (6g)

$^1\text{H NMR}$ (500 MHz, CDCl_3): δ = 7.63 (d, J = 6.8 Hz, 4H), 7.43 (m, 2H), 7.37 (m, 4H), 7.04 (s, 1H), 6.99 (d, J = 8.8, 2H), 6.93 (d, J = 8.8 Hz, 2H), 6.76 (d, J = 8.4 Hz, 2H), 6.67 (d, J = 8.8 Hz, 2H), 3.79 (s, 3H), 3.76 (m, 2H), 3.75 (s, 3H), 1.17 (t, J = 7.2 Hz, 3H).

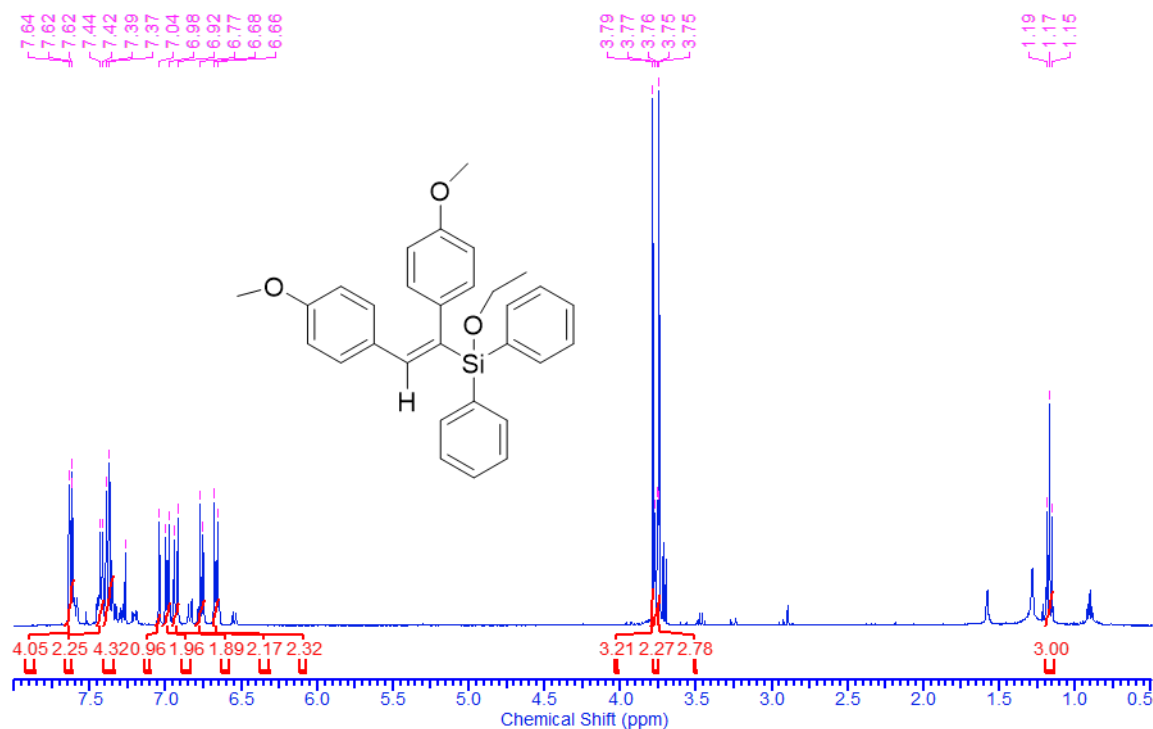


Figure 3.60: $^1\text{H NMR}$ spectrum of 6g.

(E)-(1,2-bis(2-methoxyphenyl)vinyl)(ethoxy)diphenylsilane (6h)

$^1\text{H NMR}$ (400 MHz, CDCl_3): δ = 7.61 (d, J = 7.2 Hz, 4H), 7.47 (t, J = 7.8 Hz, 2H), 7.40 (t, J = 7.2 Hz, 4H), 7.05 (s, 1H), 6.97 (dd, J = 18.6 Hz, J = 7.8 Hz, 4H), 6.78 (d, J = 8.4 Hz, 2H), 6.67 (d, J = 8.4 Hz, 2H), 3.89 (q, J = 7.8 Hz, 2H), 3.79 (s, 3H), 3.75 (s, 3H), 1.28 (m, 3H).

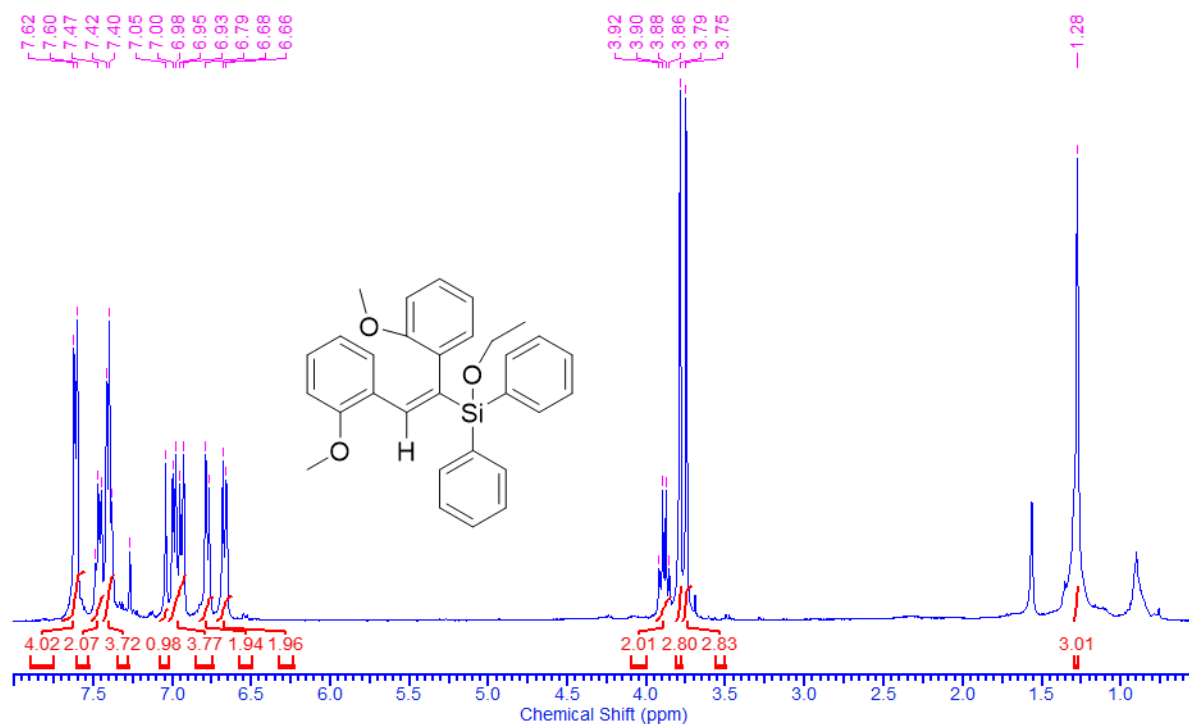


Figure 3.61: $^1\text{H NMR}$ spectrum of 6h.

3.5 Conclusion

In summary, we have rationally synthesized an iron complex by following literature reported procedure and successfully implemented it along with phosphine ligand in alkoxylation of silane for different array of alcohols and silanes under ambient condition. This methodology was successfully extended to make poly(silylether) from bio-based isosorbide and diphenylsilane which can be depolymerized to starting isosorbide under mildly acidic condition. Remarkably, we have realized a tandem alkoxylation-hydrosilylation reaction by using this iron catalyst system which involves diphenylacetylene, diphenylsilane in alcoholic solvent. It could pave the way for more potential application.

3.6 References

1. (a) Pouget, E.; Tonnar, J.; Lucas, P.; Lacroix-Desmazes, P.; Ganachaud, F.; Boutevin, B. *Chem. Rev.* **2010**, *110*, 1233-1277. (b) Cheng, C.; Watts, A.; Hillmyer, M. A.; Hartwig, J. F. *Angew. Chem., Int. Ed.* **2016**, *55*, 11872-11876.
2. (a) Protection for the Hydroxyl Group. Greene's Protective Groups in Organic Synthesis, 5th ed.; Wuts, P. G. M., Ed. John Wiley & Sons, Inc.: 2014; pp 17-471. (b) Kocienski, P. J. Hydroxyl Protecting Groups, Protecting Groups, 3rd ed.; Georg Thieme Verlag: 2003; pp 187-350.
3. (a) Zou, H.; Wu, S. S.; Shen, J. *Chem. Rev.* **2008**, *108*, 3893-3957. (b) Brook, M. A. Silicon in Organic, Organometallic, and Polymer Chemistry; Wiley: New York, 2000. (c) Xu, L.-W.; Chen, Y.; Lu, Y. *Angew. Chem., Int. Ed.* **2015**, *54*, 9456-9466.
4. Lejars, M.; Margailan, A.; Bressy, C. *Chem. Rev.* **2012**, *112*, 4347-4390.
5. Gao, D.; Cui, C. *Chem. - Eur. J.* **2013**, *19*, 11143-11147.
6. Selected examples: (a) Miller, R. L.; Maifeld, S. V.; Lee, D. *Org. Lett.* **2004**, *6*, 2773-2776. (b) Mirza-Aghayan, M.; Boukherroub, R.; Bolourtchian, M. *J. Organomet. Chem.* **2005**, *690*, 2372-2375. (c) Rendler, S.; Auer, G.; Oestreich, M. *Angew. Chem., Int. Ed.* **2005**, *44*, 7620-7624. (d) Mukherjee, D.; Thompson, R. R.; Ellern, A.; Sadow, A. D. *ACS Catal.* **2011**, *1*, 698-702. (e) Weickgenannt, A.; Mohr, J.; Oestreich, M. *Tetrahedron* **2012**, *68*, 3468-3479. (f) Fukumoto, K.; Kasa, M.; Nakazawa, H. *Inorg. Chim. Acta* **2015**, *431*, 219-221.
7. Selected examples: (a) Tanino, K.; Yoshitani, N.; Moriyama, F.; Kuwajima, I. *J. Org. Chem.* **1997**, *62*, 4206-4207. (b) Le Bideau, F.; Coradin, T.; Henique, J.; Samuel, E. *Chem. Commun.* **2001**, 1408-1409. (c) Grajewska, A.; Oestreich, M. *Synlett* **2010**, *2010*, 2482-2484. (d) Weickgenannt, A.; Mewald, M.; Muesmann, T. W. T.; Oestreich, M. *Angew. Chem., Int. Ed.* **2010**, *49*, 2223-2226. (e) Weickgenannt, A.; Mewald, M.; Oestreich, M. *Org. Biomol. Chem.* **2010**, *8*, 1497-1504. (f) Krüger, A.; Albrecht, M. *Chem. - Eur. J.* **2012**, *18*, 652-658. (g) Blandez, J. F.; Primo, A.; Asiri, A. M.; Alvaro, M.; Garcia, H. *Angew. Chem., Int. Ed.* **2014**, *53*, 12581-12586. (h) Cardoso, J. M. S.; Lopes, R.; Royo, B. *J. Organomet. Chem.* **2015**, *775*, 173-177. (i) Dhakshinamoorthy, A.; Concepcion, P.; Garcia, H. *Chem. Commun.* **2016**, *52*, 2725-2728. (j) Vijjamarri, S.; Chidara, V. K.; Rousova, J.; Du, G. *Catal. Sci. Technol.* **2016**, *6*, 3886-3892.
8. Gunji, Y.; Yamashita, Y.; Ikeno, T.; Yamada, T. *Chem. Lett.* **2006**, *35*, 714-715.
9. Ito, H.; Watanabe, A.; Sawamura, M. *Org. Lett.* **2005**, *7*, 1869-1871.

-
10. (a) Ito, H.; Takagi, K.; Miyahara, T.; Sawamura, M. *Org. Lett.* **2005**, *7*, 3001–3004. (b) Ito, H.; Saito, T.; Miyahara, T.; Zhong, C.; Sawamura, M. *Organometallics* **2009**, *28*, 4829–4840.
11. (a) Monica, F. D.; Buonerba, A.; Capacchione, C. *Adv. Synth. Catal.*, **2019**, *361*, 265–282. (b) Fürstner, A. *ACS Cent. Sci.*, **2016**, *2*, 778–789.
12. (a) Chang, S.; Scharrer, E.; Brookhart, M. *J. Mol. Catal. A* **1998**, *130*, 107–119. (b) Hasazeldine, R. N.; Parish, R. V.; Riley, B. F. *J. Chem. Soc., Dalton Trans.* **1980**, 705–708.
13. Reuter, M. B.; Cibuzar, M. P.; Hammerton, J.; Waterman, R. Y. *Dalton Trans.* **2020**, *49*, 2972–2978.
14. Gasperini, D.; King, A. K.; Coles, N. T.; Mahon, M. F.; Webster, R. L. *ACS Catal.* **2020**, *10*, 6102–6112.
15. (a) Guo, Z.; Wen, H.; Liu, G.; Huang, Z. *Org. Lett.* **2021**, *23*, 2375–2379. (b) Hu, M.-Y.; He, P.; Qiao, T.-Z.; Sun, W.; Li, W.-T.; Lian, J.; Li, J.-H.; Zhu, S.-F. *J. Am. Chem. Soc.* **2020**, *142*, 16894–16902. (c) Belger, C.; Plietker, B. *Chem. Commun.* **2012**, *48*, 5419–5421.
16. Xu, J.-X.; Chen, M.-Y.; Zheng, Z.-J.; Cao, J.; Xu, Z.; Cui, Y.-M.; Xu, L.-W. *ChemCatChem* **2017**, *9*, 3111–3116.
17. (a) Vijjamari, S.; Hull, M.; Kolodka, E.; Du, G. *ChemSusChem* **2018**, *11*, 2881–2888. (b) Fouilloux, H.; Rager, M.-N.; Ríos, P.; Conejero, S.; Thomas, C. M. *Angew. Chem., Int. Ed.* **2022**, *61*, e202113443. (c) Vijjamari, S.; Streed, S.; Serum, E. M.; Sibi, M. P.; Du, G. *ACS Sustain. Chem. Eng.* **2018**, *6*, 2491–2497. (d) Lazaro, G.; Fernández-Alvarez, F. J.; Iglesias, M.; Horna, C.; Vispe, E.; Sancho, R.; Lahoz, F. J.; Iglesias, M.; Perez-Torrente, J. J.; Oro, L. A. *Catal. Sci. Technol.* **2014**, *4*, 62–70. (e) J. M. Mabry, M. K. Runyon, W. P. Weber, *Macromolecules* **2002**, *35*, 2207–2211; (f) Y. Li, Y. Kawakami, *Macromolecules* **1999**, *32*, 6871–6873. (g) Farcaş-Johnson, M. A.; Kyne, S. H.; Webster, R.L. *Chem. Eur. J.* **2022**, *28*, e202201642. (h) Lichtenberg, C., Viciu, L., Adelhardt, M., Sutter, J., Meyer, K., de Bruin, B. and Grützmacher, H. *Angew. Chem., Int. Ed.*, **2015**, *54*, 5766–5771.
18. Luo, X.-L.; Crabtree, R. H. *J. Am. Chem. Soc.* **1989**, *111*, 2527–2535.
19. (a) Graham, W. A. G.; Jetz, W. *Inorg. Chem.* **1971**, *10*, 4–9. (b) Bellachioma, G.; Cardaci, G. *Inorg. Chem.* **1982**, *21*, 3232–3234.

-
20. (a) Curry, J. E.; Byrd, J. D. *J. Appl. Polym. Sci.* **1965**, *9*, 295–311. (b) Zhang, Y.; Zhu, Z.; Bai, Z.; Jiang, W.; Liu, F.; Tang, J. *RSC Adv.* **2017**, *7*, 16616–16622. (c) Li, Y.; Seino, M.; Kawakami, Y. *Macromolecules* **2000**, *33*, 5311–5314. (d) Wang, X.-Q.; Zhai, X.-Y.; Wu, B.; Bai, Y.-Q.; Zhou, Y.-G. *ACS Macro Lett.* **2020**, *9*, 969–973. (e) Chen, X.; Fang, L.; Chen, X.; Zhou, J.; Wang, J.; Sun, J.; Fang, Q. *ACS Sustainable Chem. Eng.* **2018**, *6*, 13518–13523. (f) Mabry, J. M.; Paulasaari, J. K.; Weber, W. P. *Polymer* **2000**, *41*, 4423–4428. (g) Yun, S. B.; Park, Y. T. *Bull. Korean Chem. Soc.* **2008**, *29*, 2373–2378. (h) Jung, I. K.; Park, Y. T. *Bull. Korean Chem. Soc.* **2011**, *32*, 1303–1309. (i) Jung, E. A.; Park, Y. T. *Bull. Korean Chem. Soc.* **2012**, *33*, 2031–2036. (j) Gao, S.; Liu, Y.; Feng, S.; Lu, Z. *J. Mater. Chem. A* **2019**, *7*, 17498–17504. (k) Wang, M.; Zhang, Q.; Wooley, K. L. *Biomacromolecules* **2001**, *2*, 1206–1213; (l) Parrott, M. C.; Luft, J. C.; Byrne, J. D.; Fain, J. H.; Napier, M. E.; DeSimone, J. M. *J. Am. Chem. Soc.* **2010**, *132*, 17928–17932. (m) Ware, T.; Jennings, A. R.; Bassampour, Z. S.; Simon, D.; Son, D. Y.; Voit, W. *RSC Adv.* **2014**, *4*, 39991–40002. (n) Bunton, C. M.; Bassampour, Z. M.; Boothby, J. M.; Smith, A. N.; Rose, J. V.; Nguyen, D. M.; Ware, T. H.; Csaky, K. G.; Lippert, A. R.; Tsarevsky, N. V.; Son, D. Y. *Macromolecules* **2020**, *53*, 9890–9900.
21. Wu, W.-X.; Qu, L.; Liu, B.-Y.; Zhang, W.-W.; Wang, N.; Yu, X.-Q. *Polymer* **2015**, *59*, 187–193.
22. (a) Ortmann, P.; Heckler, I.; Mecking, S. *Green Chem.* **2014**, *16*, 1816–1827. (b) Pemba, A. G.; Flores, J. A.; Miller, S. A. *Green Chem.* **2013**, *15*, 325–329. (c) Liu, J.; Huang, Y.; Kumar, A.; Tan, A.; Jin, S.; Mozhi, A.; Liang, X. J. *Biotechnol. Adv.* **2014**, *32*, 693–710. (d) Paramonov, S. E.; Bachelder, E. M.; Beaudette, T. T.; Standley, S. M.; Lee, C. C.; Dashe, J.; Frechet, J. M. J. *Bioconjugate Chem.* **2008**, *19*, 911–919.

Chapter 4

One Pot Synthesis of Hybrid Phosphine-phosphite Ligand and Its Implication in Asymmetric Hydrogenation

This chapter has been adapted from following publication

Sen, A.; Kumar, R.; Pandey, S.; Vipin Raj, K.; Kumar, P.; Vanka, K.; Chikkali, S. H. *Eur. J. Org. Chem.* **2022**, e202101447.

4.1 Abstract

Although hybrid bidentate ligands are known to yield highly enantioselective products in asymmetric hydrogenation (AH), synthesis of these ligands is a tedious and time consuming process. Herein, one pot, atom economic synthesis of a hybrid phosphine-phosphite ligand 4-(3-(diphenylphosphinanyl)phenoxy)dinaphtho[2,1-*d*:1',2'-*f*][1,3,2]dioxaphosphine (**L1**) has been reported. After understanding the reactivity difference between an oxygen derived nucleophilic centre versus a carbon based nucleophile using ^{31}P NMR spectroscopy, one pot synthesis of a hybrid ligand, Senphos (**L1**), has been achieved in very good yields (72%). When Senphos was treated with $[\text{Rh}(\text{COD})_2\text{BF}_4]$, ^{31}P NMR revealed a doublet-of-doublet, suggesting bidentate coordination of **L1** to the rhodium center. Senphos, in the presence of rhodium catalyzes the AH of Methyl-2-acetamido-3-phenylacrylate and discloses an unprecedented turn over frequency (TOF) of 2289, the highest known for any phosphine-phosphite ligand, along with excellent enantio-selectivity (up to 92%). The generality of our approach is demonstrated by hydrogenating an array of substituted alkenes using Senphos and high activity and enantio-selectivity of up to 92% is achieved. The AH operates under mild conditions of 1-2 bar hydrogen pressure, at room temperature, within 5-25 minutes. The practical relevance of Senphos is demonstrated by scaling up the reaction to 1 g and by synthesizing DOPA (90% ee), a drug widely employed for the treatment of Parkinson's disease.

4.2 Introduction

The seemingly mature field of transition metal catalyzed asymmetric hydrogenation continues to excel beyond the 2001 Noble Prize¹⁻³ and offers access to enantiopure advanced pharmaceutical intermediates (API).⁴⁻⁸ Chiral phosphorus ligands play a defining role in asymmetric hydrogenation and continue to dominate the academic and industrial research. Traditionally, ligand designing has been arbitrary and involves a hit and trial method, hard labour, experience, intuition and above all, serendipity (Figure 4.1., left). On the other hand, “on purpose” ligand design has been more of an industrial exercise with limited success. Thus, the quest to discover new chiral phosphorus ligands continues to intensify, as there is no universal ligand that can meet the increasing demand of the pharmaceutical industry.^{9,10} In the process, BINAP, DIPAMP, TangPhos, DuanPhos, DuPhos, ZhangPhos, among other ligands, have been discovered and a large ligand library of diphosphorus ligands has been

developed.¹¹⁻¹³ In addition to diphosphines, hybrid di-phosphorous ligands have attracted significant attention in the recent past.^{14-25,26} However, the synthesis of privileged bidentate ligands is a tedious task with multiple synthetic steps and, many a times, such lengthy and lousy protocols are industrially unattractive. Although bidentate ligands deliver better selectivities and catalytic performance, their synthesis has always been an obstacle to their success. In fact, in many cases, the steps are non-trivial synthetic operations, which poses a great challenge for automation. However, the notion that bidentate ligands require multiple synthetic steps is being challenged and innovative synthetic strategies are being devised to minimize the preparative steps.^{27,28} Three strategies are being mainly explored that include i) the use of supramolecular ligands, ii) accelerated synthesis *via* high throughput screening and, iii) one pot ligand synthesis. The straightforward 1-2 step synthesis of supramolecular ligands has been developed in the last decade and these ligands have been successfully applied in asymmetric hydrogenation.²⁹⁻³¹ To accelerate the overall discovery process, high throughput screening (HTS) is being utilized in asymmetric hydrogenation.³² The HTS does not necessarily rely on easy to synthesize ligands, but uses modular ligands, commercially available ligands, a mixture of ligands and even enzymes. Thus, the overall discovery process is expedited using HTS and not necessarily the ligand synthesis. Although hybrid bidentate ligands such as BINAPHOS have found applications in several mechanistically unrelated reactions such as asymmetric hydrogenation, hydroformylation and allylic substitution, there are hardly any reports on the “one pot” synthesis of hybrid-bidentate ligands for asymmetric transformations.

Herein, we disclose the first one pot synthesis of the hybrid phosphine-phosphite ligand **L1** (Senphos) (Figure 4.1., right). Furthermore, Senphos coordinates to Rh to yield a catalyst with excellent activity and selectivity in the asymmetric hydrogenation of alkenes. The generality of the approach is demonstrated by subjecting di- and tri-substituted alkenes to asymmetric hydrogenation. The practical utilization of our approach is demonstrated by the asymmetric synthesis of DOPA, a commercial drug for treating Parkinson’s disease.

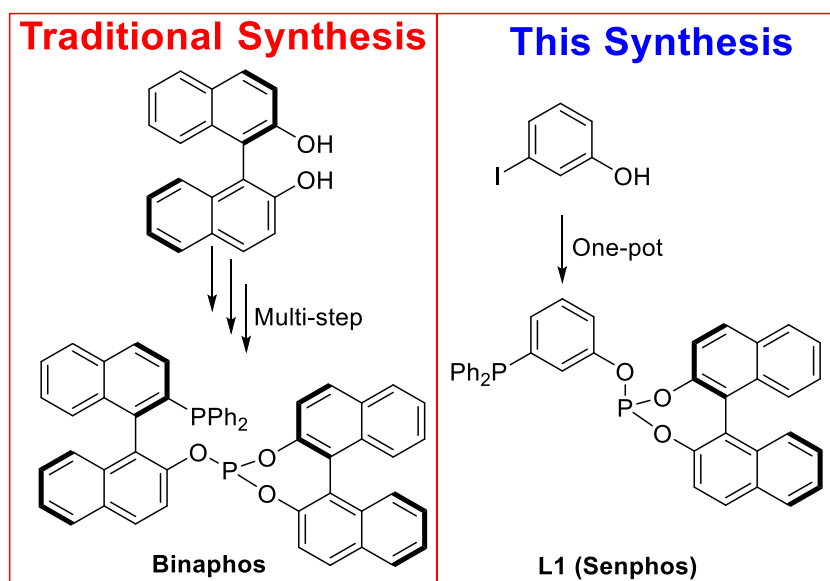


Figure 4.1: Representative traditional hybrid ligand synthesis (left) and this work (right).

4.3 Results and discussion

4.3.1 Ligand design, mechanistic understanding, synthesis and coordination

Traditionally, bidentate hybrid phosphine-phosphite ligands were being prepared using a step-by-step protocol and typically, 2-5 steps were required. The most closely related ligand **1** has been prepared in four steps (Figure 4.2.),³³ ligand **2** in three steps,^{34,35} **3** in three-four steps³⁶ and ligand **4** was prepared in two steps.^{37,38}

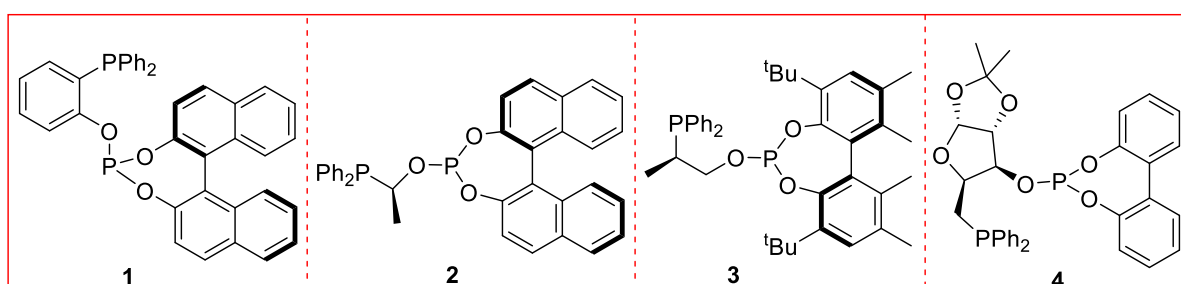
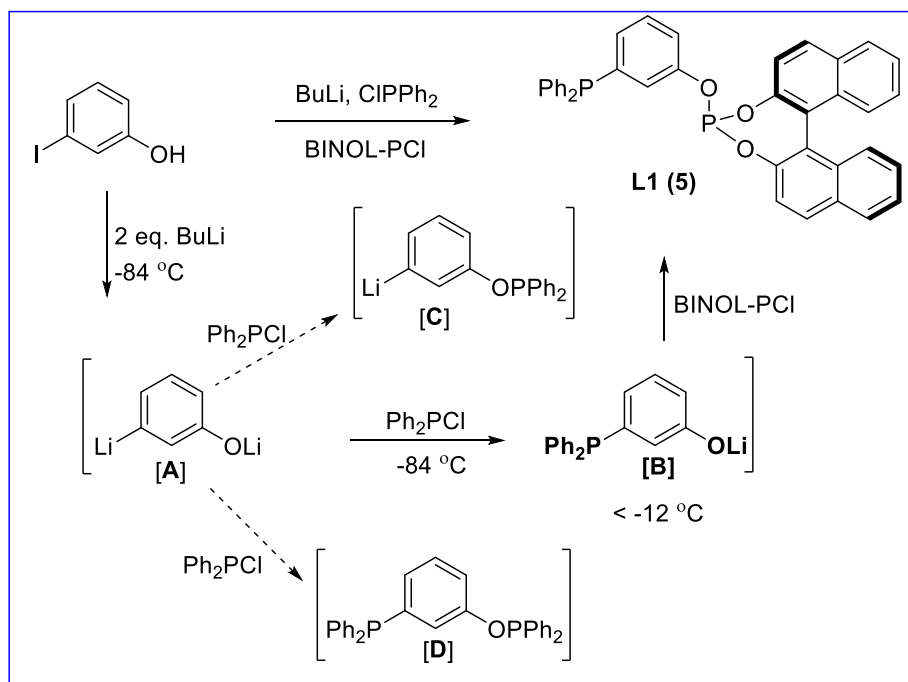


Figure 4.2: Representative chiral phosphine-phosphite ligands.

A paradigm shift could be achieved if a hybrid phosphine-phosphite ligand can be prepared in one pot. Although highly desirable, one pot, modular synthesis of phosphine-phosphite ligand is still a distant goal. In addition to the synthetic challenge, a rational ligand design should also ensure that the resultant ligand will generate active catalytic species for the desired reaction. Given the above reports and understanding, we pondered if one pot synthesis of phosphine-phosphite could be a reality. We anticipated that simple and readily available

halophenols could yield chiral ligands with inequivalent P-donors. Ligand parameters such as donating ability, flexibility of the two donor arms, ligand bite angle, and the rigidity of the backbone were considered and one pot synthesis of phosphine-phosphite ligand 4-(3-(diphenylphosphinane)phenoxy)dinaphtho[2,1-*d*:1',2'-*f*][1,3,2]dioxaphosphine (**L1**) was undertaken.

3-iodophenol (3.772 mmol) was lithiated using *n*-BuLi (7.544 mmol) at -84 °C for 3 hours and stoichiometric amount of diphenylchlorophosphine (3.772 mmol) was added (Scheme 4.1.). In our attempts to understand the reactivity between a C-nucleophile versus a O-nucleophile, we followed the reaction with ³¹P NMR as a function of time. Theoretically, such reactions display a statistical mixture (Scheme 4.1.). In our endeavor to arrest the intermediate **[B]**, the reaction was performed at low temperature (-50 to 0 °C). A ³¹P NMR spectrum recorded after 30 minutes of addition of ClPPh₂ revealed a resonance at -1.30 ppm which can be assigned to P-C coupled product **[B]** (Scheme 4.1.).³⁹ In addition to this, another peak was observed at 114 ppm (Figure 4.5.). The second peak is assigned to O-P coupled product **[C]**.⁴⁰ However, we argued that the temperature of the NMR tube might be much higher than the bath (-50 °C) temperature and, by the time a spectrum is recorded, the unreacted ClPPh₂ might react with O-nucleophile (at this higher temperature of about 25 °C) to yield compound **[C]**. To probe this hypothesis, same experiment was repeated and the NMR was recorded at -30 °C after 50 mins. of addition of ClPPh₂. Interestingly, under these conditions, we could observe a resonance at -1.30 ppm for **[B]**, along with unreacted ClPPh₂ at 81.17 ppm and **[C]** at 109.73 ppm (Figure 4.9.). The formation of **[C]** at this low temperature may be due to the temperature rise during NMR sample preparation (syringing out the reaction content to NMR tube, and mounting it in an NMR machine) and instrument cooling procedures. Although these investigations did not present a conclusive picture, low temperature ³¹P NMR experiments (Figure 4.9., 4.10.) gave the impression that the C-P bond could be selectively formed, if the reaction is performed at lower temperature. Above reaction was repeated, after 2 hours of addition of ClPPh₂ (bath temp. -12 °C), volatiles were stripped off and the reaction mixture was dried to obtain solid residue. To our delight, a ³¹P NMR spectrum (Figure 4.11.) of this residue in dry DMSO revealed selective formation of intermediate **[B]** (-2.33 ppm) and O-P coupled product **[C]** or **[D]** could not be observed.



Scheme 4.1: Proposed mechanism and one pot synthesis of **L1**.

The mechanistic understanding enabled us to design one pot protocol for the preparation of hybrid ligand **L1**. After 2 hours of ClPPh_2 addition, the reaction mixture was cooled to -84°C and phosphorochloridite was added. Filtration, washing and purification produced a white powder in 72% isolated yield, which was identified as **L1** after complete characterization.⁴¹ Based on above *in-situ* NMR findings, it is proposed that the reaction proceeds *via* intermediates **[A]** and **[B]**. Literature reports indicate that $-\text{CLi}$ is more likely to be attacked by electrophiles than $-\text{OLi}$.^{42, 43} Thus, intermediate **[B]** is anticipated to be generated *in situ*, which upon addition of phosphorochloridite produces **L1**. A ^{31}P NMR spectrum of this powder revealed two singlets at -5.14 and 144.24 ppm (Figure 4.13.). The former resonance can be assigned to phosphine, while the latter can be designated to phosphite phosphorus.⁴⁴ Identity of **L1** was further established using a combination of 1-2D NMR measurements (Figure 4.14.-4.18.). These NMR findings were further corroborated by Electrospray Ionization Mass Spectrometry, which revealed a molecular ion peak at $m/z = 593.14$ Da $[\text{M}+\text{H}]^+$ (Figure 4.19.).

It is well established in the literature that the coordination mode of a ligand strongly influences the outcome of an asymmetric reaction. Therefore, after having established the synthesis of Senphos, we examined the coordination behavior of **L1** with rhodium. Senphos (59.26 mg) was treated with 40.6 mg of $[(\text{COD})_2\text{Rh}(\text{BF}_4)]$ in dichloromethane. The resultant

mixture revealed two doublet-of-doublet centered at 121.15 (dd, $^1J_{\text{Rh-P}} = 278$, $^2J_{\text{P-P}} = 35$ Hz) and 29.17 (dd, $^1J_{\text{Rh-P}} = 147$, $^2J_{\text{P-P}} = 35$ Hz) ppm (Figure 4.3.). The former can be assigned to up-field shifted phosphite phosphorus and the latter originates from phosphine phosphorus. The phosphite phosphorus revealed a $^2J_{\text{P-P}}$ coupling of 35 Hz and $^1J_{\text{P-Rh}}$ coupling of 278 Hz, while the phosphine displayed 35 Hz P-P coupling and 143 Hz $^1J_{\text{Rh-P}}$ coupling. These chemical shifts and coupling constants are similar to those reported in the literature and establish coordination of **L1** to rhodium.⁴⁵⁻⁴⁸

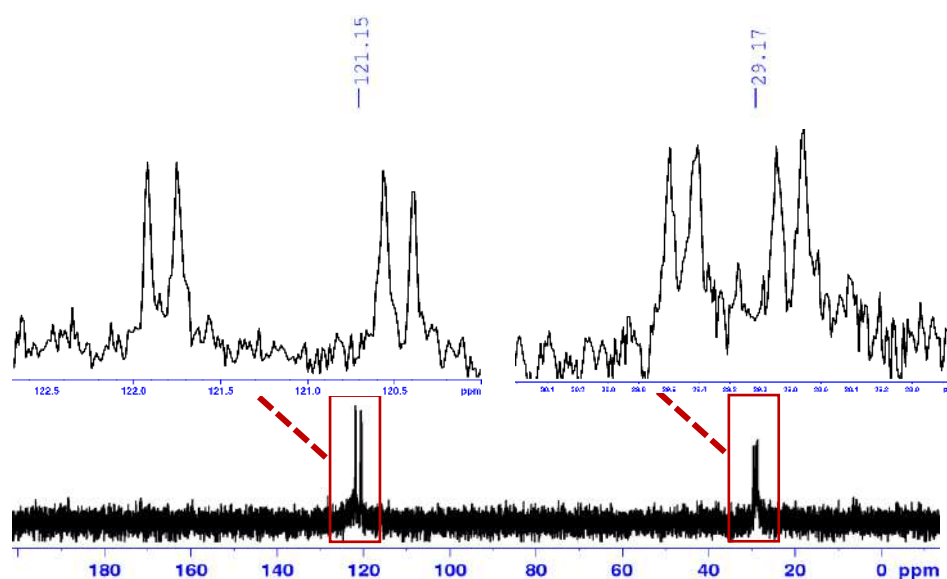


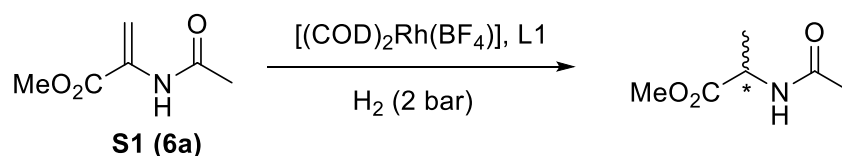
Figure 4.3: ^{31}P NMR spectrum of $[(\text{L1})(\text{COD})\text{Rh}(\text{BF}_4)]$ in CDCl_3 .

4.3.2 Rhodium catalyzed asymmetric hydrogenation

After having established the coordination behavior of Senphos (**L1**), the performance of this hybrid ligand was evaluated in the asymmetric hydrogenation of challenging 1,1-disubstituted and 1,1,2-trisubstituted alkenes. The anticipated catalytically active species was generated *in situ* by mixing **L1** with $[(\text{COD})_2\text{Rh}(\text{BF}_4)]$ and Table 4.1. summarizes the most important results. Methyl-acetamidoacrylate (**S1**) was chosen as a benchmark substrate for preliminary screening. The initial screening at 2 bar hydrogen pressure and room temperature (~ 31 °C) revealed full conversion and a moderate enantiomeric excess of 46% (Table 4.1., entry 1) in THF. Under similar conditions, a better enantiomeric excess of 83% and 76% was observed in TCE and DCM respectively (Table 4.1., entry 2-3). As full conversion was observed in 60 minutes, the reaction time was reduced to 45 and then to 35 minutes. DCM outperformed

TCE and displayed full conversion with 83% ee in 35 minutes (Table 4.1., entry 7). Thus, DCM appears to perform better and therefore, the remaining reactions were carried out in DCM. Screening the reaction time revealed that 5 minutes are sufficient for full conversion (TOF = 1200) and an excellent ee of 87% was observed (Table 4.1., entry 10). Thus, preliminary optimization of reaction conditions suggested 2 bar hydrogen pressure, room temperature, 5 minutes, DCM and a ligand to metal ratio of 1:1.2 as the optimal reaction conditions.

Table 4.1. Rhodium-phosphine-phosphite catalyzed asymmetric hydrogenation of methyl acetamidoacrylate (S1).^a



Entry	Solvent	Time (mins.)	% Conv.	Ee%	TOF
1	THF	60	>99	46	100
2	TCE	60	>99	83	100
3	DCM	60	>99	76	100
4	TCE	45	>99	78	133
5	DCM	45	>99	80	133
6	TCE	35	84	68	144
7	DCM	35	>99	83	172
8	DCM	20	>99	85	300
9	DCM	15	>99	86	400
10	DCM	5	>99	87	1200

^aConditions: Methyl acetamidoacrylate (36 mg, 0.25 mmol); [(COD)₂Rh(BF₄)] (1 mg, 0.0025 mmol); **L1** (1.8 mg, 0.0030 mmol); Solvent-1 mL, THF-Tetrahydrofuran; TCE-Tetrachloroethane; Dichloromethane; H₂ pressure-2 bar; Temperature- 31 °C; TOF-Turnover frequency, no by-product observed.

With the optimal conditions in hand, the scope of asymmetric hydrogenation was examined. 1,1-disubstituted and 1,1,2-trisubstituted alkenes such as methyl 2-acetamidoacrylate (S1), dimethyl 2-methylenesuccinate (S2), methyl-2-acetamido-3-phenylacrylate (S3), methyl 2-acetamido-3-(2-methoxyphenyl)propanoate (S4), methyl 2-acetamido-3-(4-methoxyphenyl)propanoate (S5), methyl 2-acetamido-3-(*p*-tolyl) propanoate (S6), methyl 2-acetamido-3-(2-fluorophenyl)propanoate (S7), methyl 2-acetamido-3-(3-bromophenyl)propanoate (S8), methyl 2-acetamido-3-(3-nitrophenyl)propanoate (S9), methyl 2-acetamido-3-(4-chlorophenyl)propanoate (S10), methyl 2-acetamido-3-(4-nitrophenyl)propanoate (S11), methyl 2-acetamido-3-(2,3-dimethoxyphenyl)propanoate (S12), methyl 2-acetamido-3-(2,4-dimethoxyphenyl)propanoate (S13), methyl 2-acetamido-3-(4-acetoxy-3-methoxyphenyl)propanoate (S14), methyl 2-acetamido-3-(3,4-dichlorophenyl)propanoate (S15) were hydrogenated using L1. The resultant chiral products 7a-7o obtained from substrates S1-S15, respectively, have been presented below (Figure 4.4.). Asymmetric hydrogenation of dimethyl 2-methylenesuccinate (S2) revealed reduced ee of just 28% (Figure 4.4., 7b). While, asymmetric hydrogenation of 1,1,2-trisubstituted alkene S3 displayed an excellent ee of 92% and a TOF of 1200 (Figure 4.4., 7c).

Next, we attempted the asymmetric hydrogenation of substituted methyl-2-acetamido-3-phenylacrylate and the effect of electron donating and electron withdrawing substituents on the ee and the TOF was examined. Electron donating substituents such as methoxy (S4, S5) displayed reduced selectivity of 68-71%, while methyl (S6) substituted substrates revealed lower selectivity (72%) and TOF (400). These observations indicate that, although methoxy and methyl groups can be tolerated, the activity and selectivity is reduced. The catalyst also tolerates electron withdrawing groups such as nitro, fluoro, chloro, bromo, but at the cost of reduced ee and TOF (Figure 4.4., 7h-7k) as compared to the parent substrate S3. Further increasing the substitution either with donating substituents (7m) or with withdrawing substituents (7o) diminishes the enantiomeric excess to 50-79% and the TOF to 200. These observations clearly signify that the substituents do play an important role and can indeed interfere with the catalytic transformation. When the asymmetric hydrogenation was performed at 0 °C, high enantiomeric excess of up to 92% (Figure 4.4., 7d) was observed (Table 4.4.). Thus, the Senphos (L1) ligand appears to catalyze the asymmetric hydrogenation of a small library of substrates S1-S15 to the corresponding chiral products 7a-o with excellent enantiomeric excess and TOF.

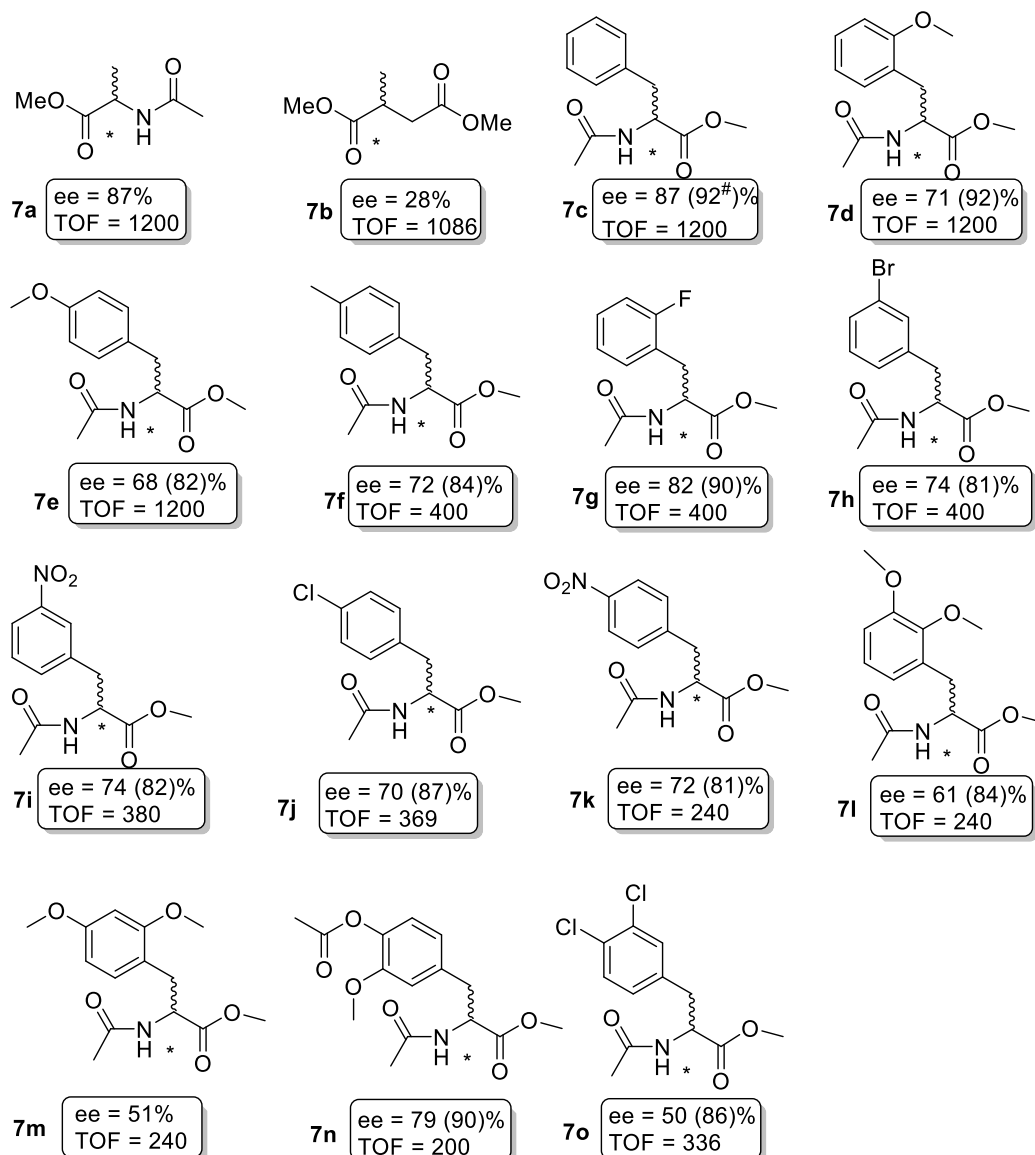


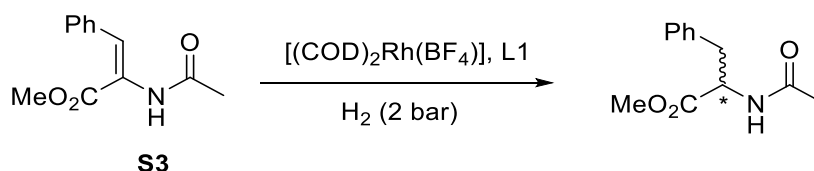
Figure 4.4: Rh-L1 catalyzed asymmetric hydrogenation of alkenes. Numbers in the bracket indicate % enantiomeric excess at 0 °C, #AH at -2 °C.³⁷

4.3.3 High TOF, TON and scale up experiments

After demonstrating the wide reaction scope, we set out to validate the synthetic utility of Senphos (**L1**). Methyl-2-acetamido-3-phenylacrylate (**S3**) was chosen as the model substrate for the high turnover frequency, turn-over number and scale up experiments and Table 4.2. summarizes the results. At 2 bar hydrogenation pressure and 38 °C temperature, **S3** displayed an enhanced TOF of 2289 (Table 2, entry 2). To the best of our knowledge, this is the highest TOF ever reported for **S3** using a hybrid ligand. The TON experiments (Table 2, entry 3-4) indicate that 0.1 mol% catalyst loading (TON = 1000) is sufficient to obtain full conversion

with little lower ee (78%). The practical usage of **L1** in asymmetric hydrogenation has been demonstrated by scaling up the reaction to 1 g scale. 1 g of Methyl-2-acetamido-3-phenylacrylate was exposed to 2 bar hydrogen pressure at 31 °C for 20 minutes leading to >99% conversion along with 80% ee.

Table 4.2. Rhodium-phosphine-phosphite catalyzed asymmetric hydrogenation of methyl-2-acetamido-3-phenylacrylate (S3).



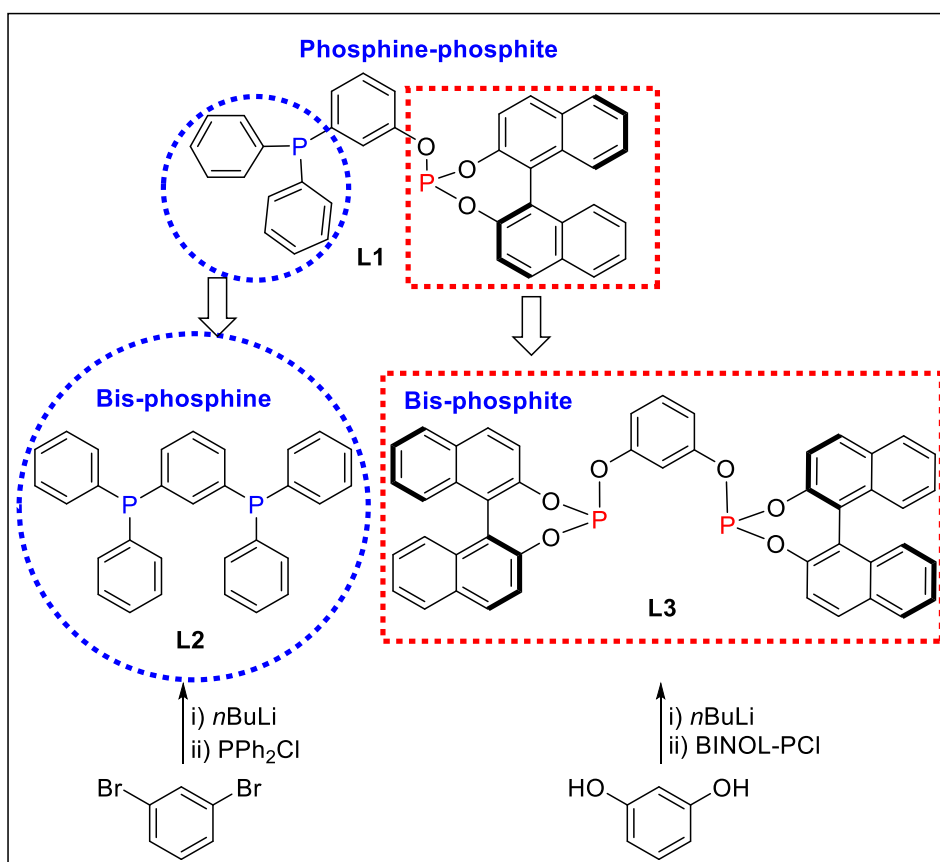
Entry	DCM (mL)	Sub:Cat	Time (min)	Conv. (%)	Ee (%)	TOF	TON
1 ^a	1.5	150	5.5	98	82	1598	147
2 ^b	2	200	5	95	71	2289	190
3 ^c	2	400	2 h	92	87	184	368
4 ^d	5	1000	12 h	99	78	83	1000
5 ^e	22	100	20	>99	80	300	100

Conditions: H₂ pressure-2 bar; Temperature- 25-38 °C; TOF-Turn-over frequency; TON-Turn-over number. ^aMethyl-2-acetamido-3-phenylacrylate- 82.22 mg, [(COD)₂Rh(BF₄)]- 1 mg, **L1**- 1.8 mg; ^bMethyl-2-acetamido-3-phenylacrylate- 110 mg, [(COD)₂Rh(BF₄)]- 1 mg, **L1**- 1.8 mg; ^cMethyl-2-acetamido-3-phenylacrylate- 110 mg, [(COD)₂Rh(BF₄)]- 0.5 mg, **L1**- 0.9 mg; ^dMethyl-2-acetamido-3-phenylacrylate- 275 mg, [(COD)₂Rh(BF₄)]- 0.5 mg, **L1**- 0.9 mg; ^eMethyl-2-acetamido-3-phenylacrylate- 1g, [(COD)₂Rh(BF₄)]- 19 mg, **L1**- 32.5 mg.

4.3.4 Synthesis of DOPA

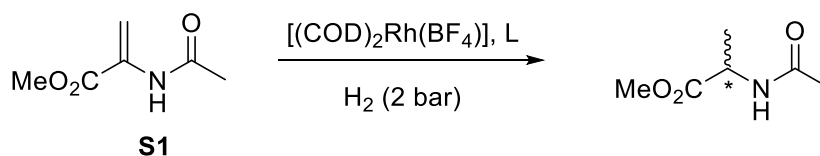
L-DOPA is the most commonly used drug for treating Parkinson's disease and is commercially produced using asymmetric hydrogenation.^{49,50} To demonstrate the practical significance of our methodology, we evaluated the performance of Senphos (**L1**) in asymmetric hydrogenation to produce the final DOPA compound. To our delight, asymmetric hydrogenation of the precursor **6n** (Scheme 4.2.) under mild conditions (1 bar hydrogen pressure, 0 °C, 1 mol % catalyst loading) and the hydrolysis of the resultant intermediate

hybrid ligand **L1** out performed **L2** and **L3**, and demonstrated its superiority over the parent ligands.



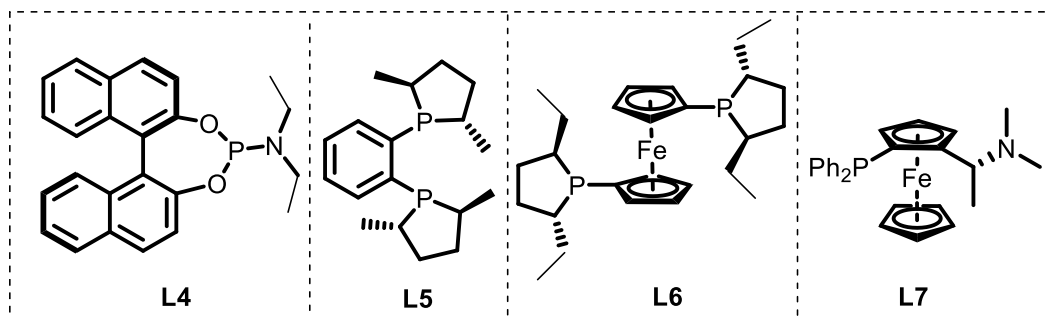
Scheme 4.3: Synthesis of parent bis-phosphine (**L2**) and bis-phosphite (**L3**) ligands.

Table 4.3. Rhodium-catalyzed asymmetric hydrogenation of methyl-2-acetamidoacrylate (S1**)^a**



Entry	L	Time (min)	% Conv.	Ee%	TOF
1	L2	5	>99	00	1200
2	L3	15	82	79	246
3	L1	5	>99	87	1200

4*	L4	5	<1	ND	ND
5*	L5	5	<1	ND	ND
6*	L6	5	<1	ND	ND
7*	L7	5	<1	ND	ND



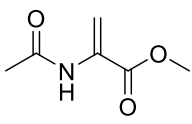
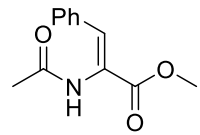
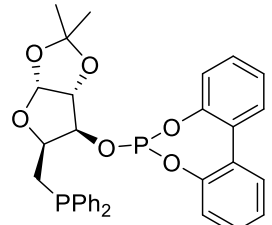
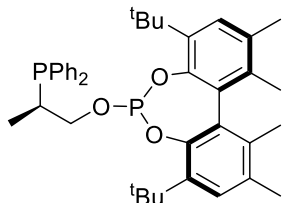
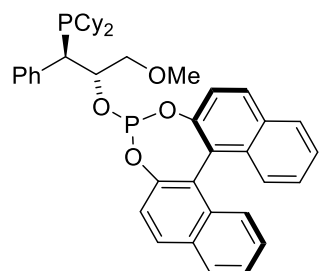
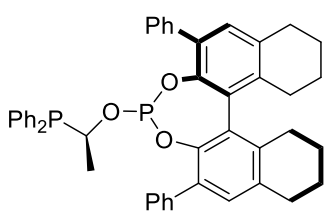
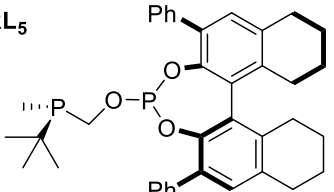
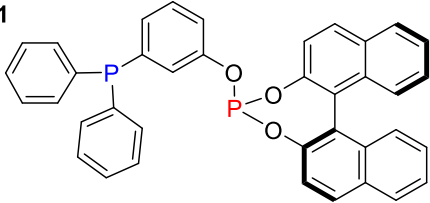
^aConditions: Methyl-2-acetamidoacrylate- 0.25 mmol; [(COD)₂Rh(BF₄)]- 0.0025 mmol; L- 0.0030 mmol; L/M: 1.2 equivalent; Solvent (DCM)-1 mL, H₂ pressure-2 bar; Temperature- 31 °C; TOF-Turnover frequency. * Substrate = Methyl-2-acetamido-3-phenylacrylate. L4 = (*R*)-*N,N*-diethyldinaphtho-[2,1-*d*:1',2'-*f*][1,3,2-dioxaphosphine-4-amine or Monophos (L/M: 2.2); L5 = (*S,S*)-Me-DUPHOS; L6 = (*R,R*)-Et-Ferrocene; L7 = (*R*)-(-)-*N,N*-Dimethyl-1-[(*S*)-2-(diphenylphosphino)-ferrocenyl]ethylamine; ND = Not determined due to low conversion.

4.3.6 Comparison with literature reported hybrid phosphine-phosphite ligands and privileged ligands

To know where Senphos (**L1**) stands in terms of its activity in asymmetric hydrogenation, we compared the performance of **L1** with the literature reported phosphine-phosphite ligands. Chart 4.1. provides an overview of the activity of various hybrid ligands in the asymmetric hydrogenation of two benchmark substrates, methyl-2-acetamidoacrylate (**S1**) and Methyl-2-acetamido-3-phenylacrylate (**S3**). The literature reported ligand **RL1** displayed a TOF of 1200 for **7a**, while AH of **S3** led to a TOF of 653.³⁷ The remaining reported ligands **RL2-RL5** displayed a TOF of 4-6 in the asymmetric hydrogenation of **S1** and **S3** even at an elevated pressure of 20 bar of hydrogen^{35-37,52-56} while Senphos (**L1**) revealed a TOF of 1200 in the asymmetric hydrogenation of **S1** and 2289 for **S3**. Thus, **L1** outperformed **RL1-RL5** and displayed the highest TOF in the asymmetric hydrogenation of the tri-substituted alkene **S3**. **RL1-RL5** disclosed enantiomeric excess in the range of 84-99%, while **L1** delivered 87-92% ee, which is on the lower side. The performance of privileged ligands (L4-L7) such as

Monophos, Duphos, etc. versus **L1** was examined and table 4.3. (entry 4-7) summarizes the results. As evident, the privileged ligands displayed only 1% conversion, while **L1** displayed full conversion, under identical conditions.

Chart 4.1. Overview of activity of various phosphine-phosphite ligands in the AH of S1 and S3.

 <p style="text-align: center;">S1</p>	 <p style="text-align: center;">S3</p>
<p>RL₁</p>  <p>H₂ = 1 bar, 7a, TOF = 1200, ee = 88%; 7c, TOF = 653, ee = 84%; Chem Comm. 2000, 2383</p>	<p>RL₂</p>  <p>H₂ = 4 bar, 7c, TOF = 4.1, ee = 99% Organometallics 2010, 29, 5791</p>
<p>RL₃</p>  <p>H₂ = 20 bar, TOF for 7a/c = 5.5, ee = 99% (7a), 98% (7c) Organometallics 2011, 30, 6718</p>	<p>RL₄</p>  <p>H₂ = 20 bar, 7c, TOF = 5.5, ee = 99% Organic Letters 2013, 15, 3634</p>
<p>RL₅</p>  <p>H₂ = 20 bar, 7a, TOF = 4.1, ee = 98% Organometallics 2014, 33, 2960</p>	<p>L1</p>  <p>H₂ = 2 bar, 7a, TOF = 1200, ee = 87%, 7c, TOF = 2289, ee = 92%</p>

4.4 Experimental section

4.4.1 Methods and materials

Unless noted otherwise, all manipulations were carried out under an inert atmosphere using standard Schlenk technique, cannula filtration or m-Braun glove box. Solvents were dried by standard procedures unless otherwise mentioned. Tetrahydrofuran was dried from sodium/benzophenone and dichloromethane from calcium hydride under argon atmosphere. Methyl 2-acetamidoacrylate, dimethyl itaconate, alpha-acetamidocinnamic acid, 3-iodophenol, n-butyllithium solution, S/R-BINOL were purchased from Sigma-Aldrich. Bis (1,5-cyclooctadiene)rhodium(I) tetrafluoroborate, chlorodiphenylphosphine were purchased from Alfa-Aesar. Methyl ester of alpha-Acetamidocinnamic acid derivatives were prepared employing known procedures.⁴¹ All other reagents/chemicals, solvents were purchased from local suppliers (Spectrochem Pvt. Ltd.; Avra Synthesis Pvt. Ltd.; Thomas Baker Pvt. Ltd. etc). Solution NMR spectra were recorded on a Bruker Avance 200, 400 and 500 MHz instruments at 298K unless mentioned otherwise. Chemical shifts are referenced to external reference TMS (¹H and ¹³C) or H₃PO₄ (³¹P). Coupling constants are given as absolute values. Multiplicities are given as follows s: singlet, d: doublet, t: triplet, m: multiplet, quat: quaternary carbon. Mass spectra were recorded on Thermo Scientific Q-Exactive mass spectrometer with Hypersil gold C18 column 150 × 4.6 mm diameter 8 μm particle size mobile phase used is 90% methanol + 10% water + 0.1% formic acid.

The enantiomeric excess of the products was determined by chiral HPLC on an Agilent Technologies 1260 Infinity instrument with Chiralpak IB column (20 cm), Chiralpak AD-H column (20 cm) and an Agilent 7890B GC system with supelco beta dex 225 column (30 m). Optical rotation was measured at 589 nm on JASCO (P-2000) polarimeter using 10 mm cell.

4.4.2 One pot synthesis of hybrid ligand L1

4.4.2.1 Investigating the reactivity of P-C versus P-O bond formation

Hybrid ligands are usually designed to obtain an optimum balance of reactivity and selectivity. Hybrid ligand feature two donor atoms with different donating ability and thus create asymmetric electronic environment around the catalytic metal center. Since two differently abled donor atoms have to be introduced in the same molecule, synthesis of hybrid ligands is a multistep and tedious affair. A familiar example would be BINAPHOS, which

outperforms many non-hybrid counter parts in asymmetric hydrogenation and hydroformylation, but synthesis of this ligand is multistep and tedious.

In our attempt to address this, we envisioned synthesis of a hybrid phosphine-phosphite ligand **L1** (Scheme 4.1.). We wanted to probe the reactivity of C-nucleophile versus O-nucleophile and see if we can selectively trap only one of them under defined reaction conditions. 3-iodophenol (220 mg, 1 mmol), dissolved in 20 ml Et₂O, was treated with 2 equivalents of n-BuLi (1.0 mL, 2.0 mmol, 2.0 molar solution in hexane) at -84 °C and the content was stirred for 3 hours. Subsequently, 1 equivalent of chlorodiphenylphosphine (0.18 mL, 1.0 mmol) was added to the reaction mixture at -84 °C and progress of the reaction was monitored by ³¹P NMR spectroscopy. A ³¹P NMR spectrum recorded after 30 minutes of addition revealed a resonance at -1.3 ppm which can be assigned to P-C coupled product [**B**]. In addition to this, another peak was observed at +114 ppm (Figure 4.6.). The second peak is assigned to O-P coupled product [**C**].

³¹P NMR data was collected after 60 minutes and 100 minutes and a stacked NMR spectrum is presented in Figure 4.9. Based on these observations, one may conclude that C- and O-nucleophile both react with chlorodiphenylphosphine and it is difficult to distinguish the reactivity. However, we argued that the temperature of the NMR tube might be much higher than the bath (-27 °C) temperature and, by the time a spectrum is recorded, the unreacted ClPPh₂ might react with O-nucleophile (at this higher temperature of about 25 °C) to yield compound [**C**] (Scheme 4.1.). When the two resonance were integrated, it was observed that the intensity of O-P coupled product [**C**] decreases with time (see Chart 4.2.). This finding suggests that species [**C**] is a transient species, which is probably forming due to increased temperature during NMR sample preparation and measurements.

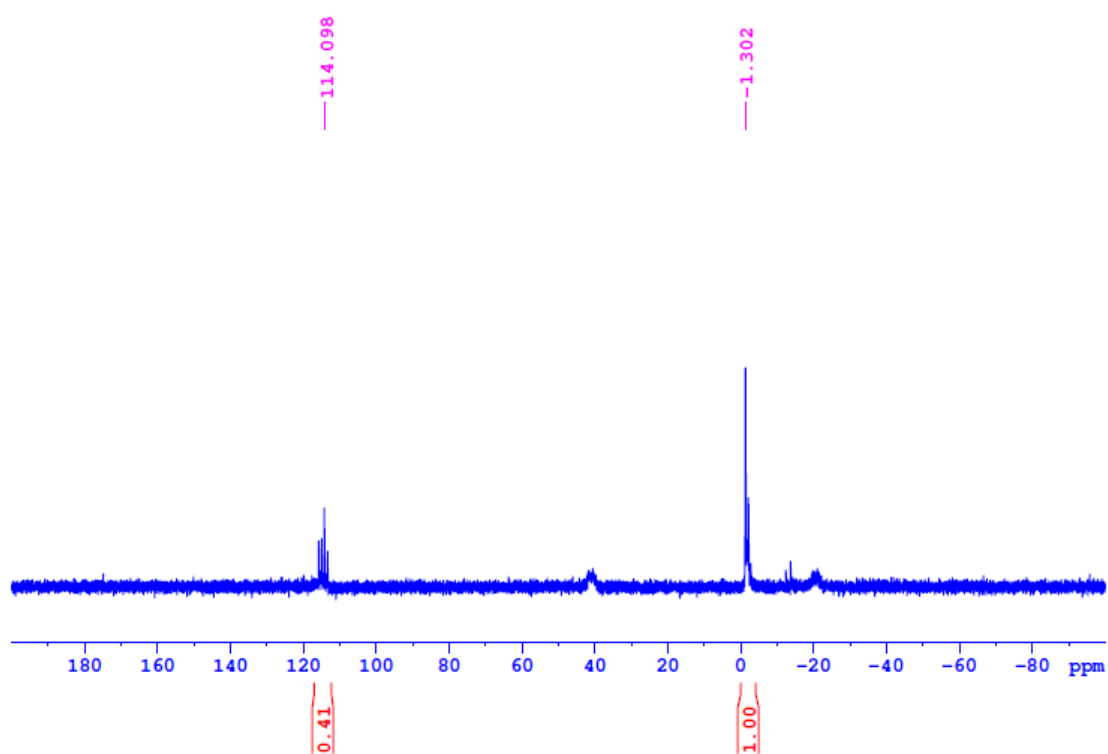


Figure 4.5: ^{31}P NMR spectrum after 30 minutes of addition of Ph_2PCl .

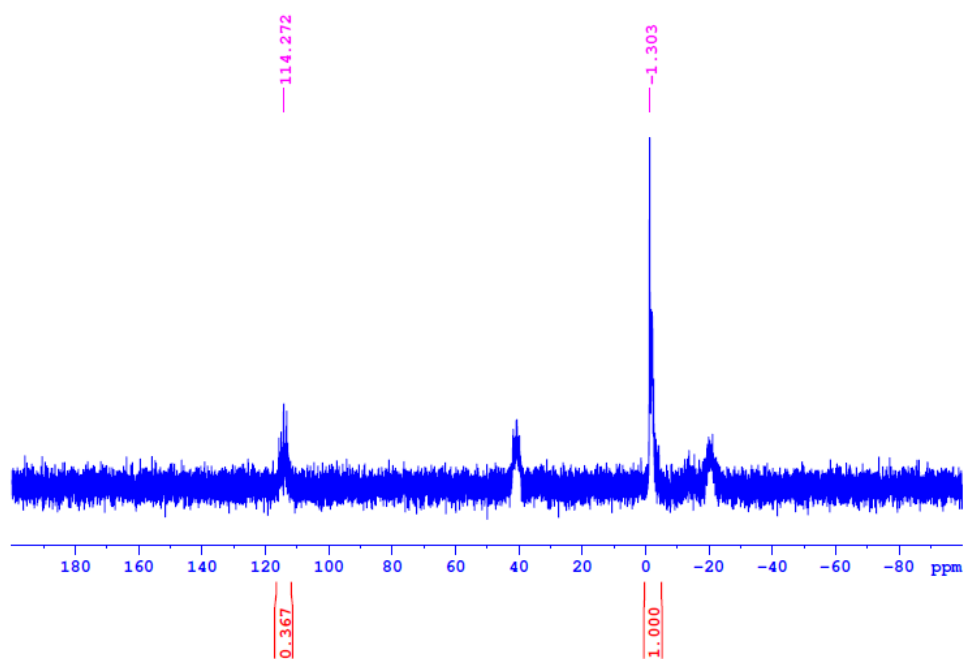


Figure 4.6: ^{31}P NMR spectrum after 60 minutes of addition of Ph_2PCl .

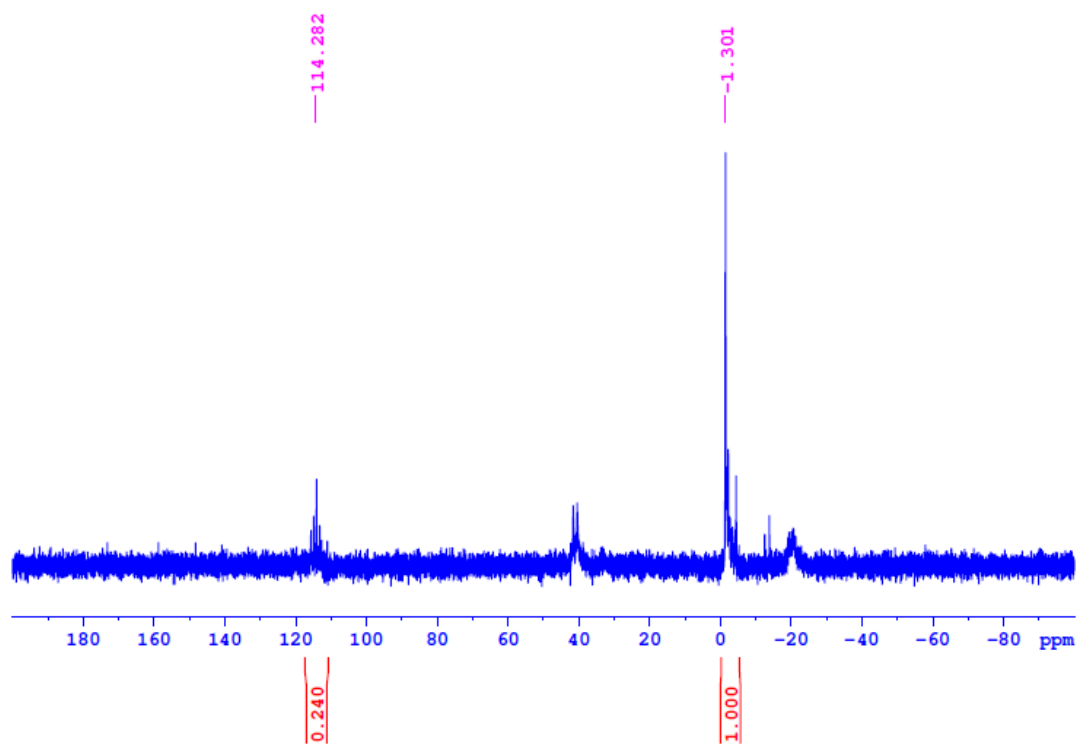


Figure 4.7: ^{31}P NMR spectrum after 100 minutes of addition of Ph_2PCl .

Chart 4.2. ^{31}P NMR data for *in-situ* detected intermediates.

^{31}P NMR	Species [B]	Species [C]
^{31}P NMR chemical shift (ppm)	-1.3	114
Integration after 30 min.	1.0	0.41
Integration after 60 min.	1.0	0.37
Integration after 100 min.	1.0	0.24

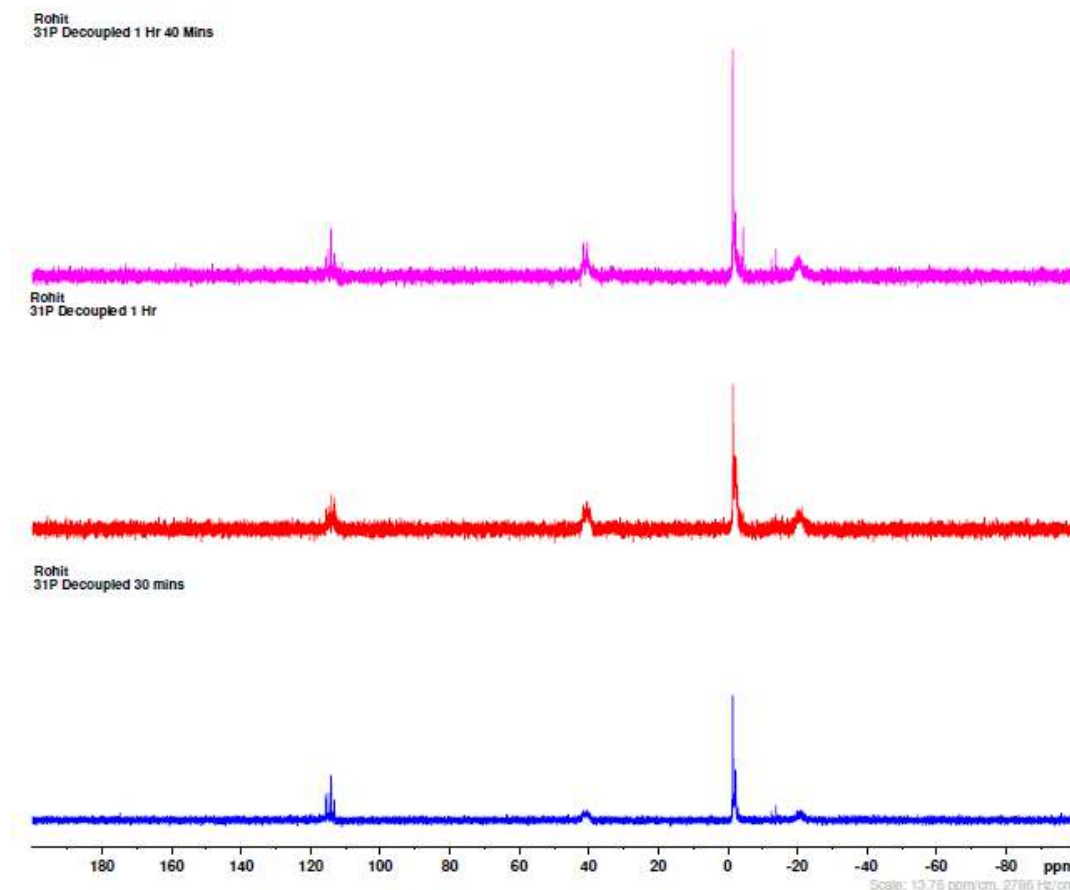


Figure 4.8: Stacked, time resolved, ^{31}P NMR spectra after addition of Ph_2PCl .

To probe this hypothesis, same experiment was repeated and the NMR was recorded at -30 $^\circ\text{C}$ after 50 min of addition of Ph_2PCl . Interestingly, under these conditions, we could observe a resonance at 81.17 ppm for unreacted ClPPh_2 along with peaks at -5.32 (for P-C product [B]) and 109.73 ppm (for P-C product [D]) (Figure 4.9.). Another ^{31}P NMR spectrum was recorded at -40 $^\circ\text{C}$ from the same reaction mixture after 80 mins (Figure 4.10.). We found similar observation as at -30 $^\circ\text{C}$ but with reduced integration for Ph_2PCl peak. The formation of O-P coupled product at this low temperature may be due to the temperature rise during NMR sample preparation (syringing out the reaction content to NMR tube, and mounting it in an NMR machine) and instrument cooling procedures. Thus, the low temperature ^{31}P NMR experiments suggested that the P-C bond could be selectively formed, if the reaction (addition of Ph_2PCl) is performed at lower (between -20 to -10 $^\circ\text{C}$) temperature.

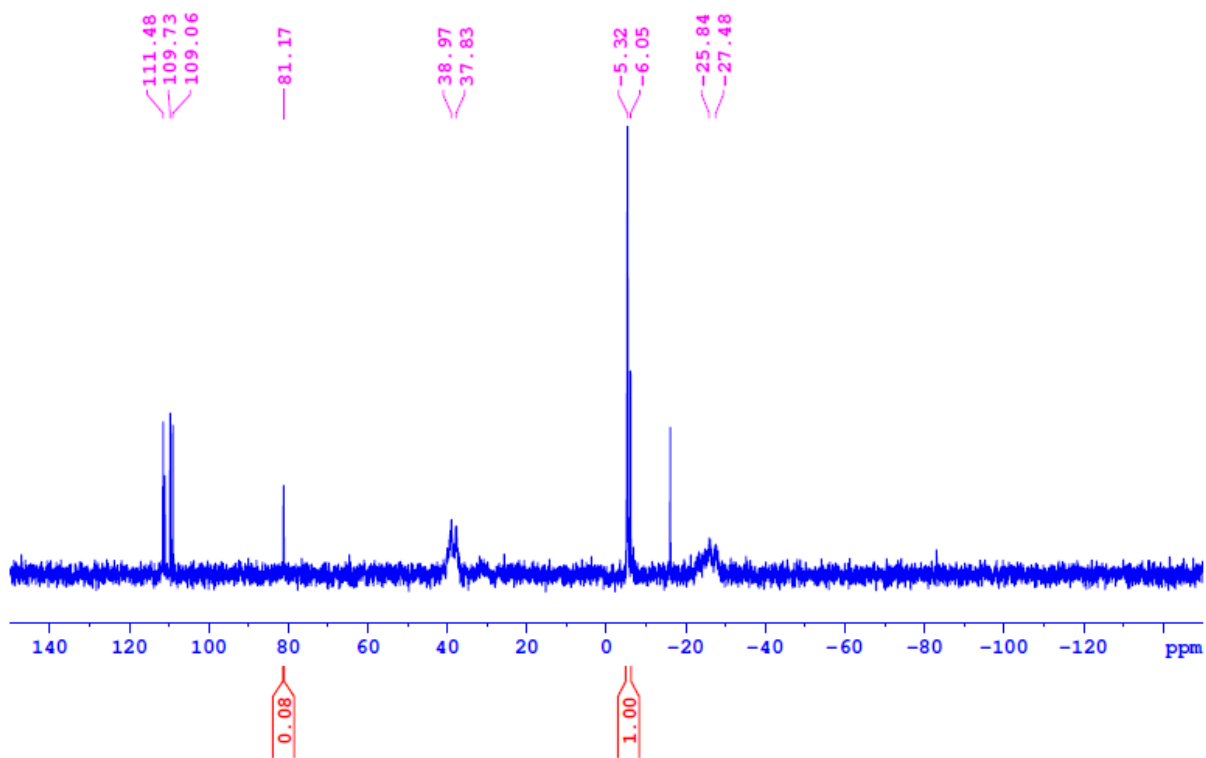


Figure 4.9: ^{31}P NMR spectrum after 50 min of addition of Ph_2PCl at $-30\text{ }^\circ\text{C}$.

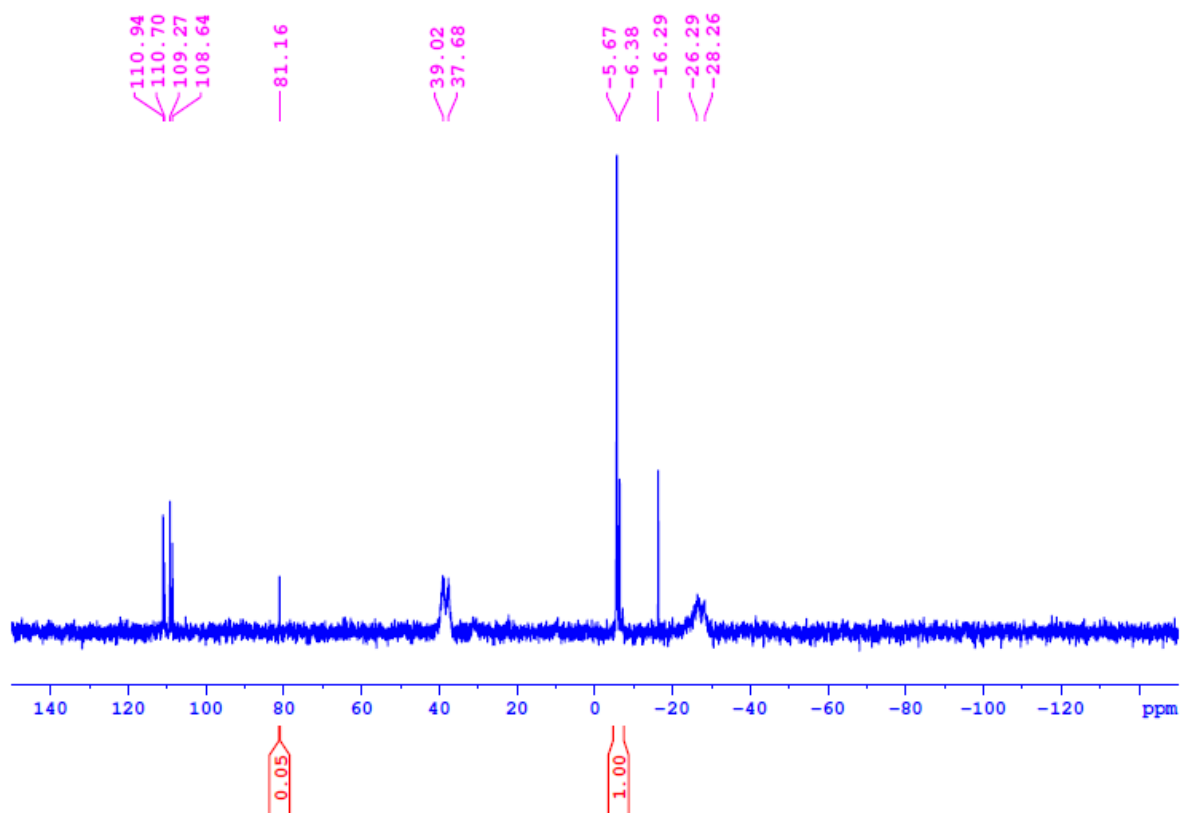


Figure 4.10: ^{31}P NMR spectrum after 80 mins. of addition of Ph_2PCl at $-40\text{ }^\circ\text{C}$.

After understanding the reactivity using *in-situ* ^{31}P NMR experiments, other reaction conditions were optimized. 3-iodophenol (220 mg, 1.0 mmol) was dissolved in 20 ml diethyl ether in a Schlenk flask and was treated with 2 equivalents of *n*-BuLi (1.0 mL, 2.0 mmol, 2.0 molar solution in hexane) at $-84\text{ }^{\circ}\text{C}$, for 3 hours. Subsequently, 1 equivalent of chlorodiphenylphosphine (0.18 mL, 1.0 mmol) was added to the reaction mixture at $-84\text{ }^{\circ}\text{C}$ and the Schlenk was left for 2 hours. The temperature of the bath rose to almost $-12\text{ }^{\circ}\text{C}$ in these 2 hours. After this, volatiles were stripped off and the reaction mixture was dried to obtain solid residue.

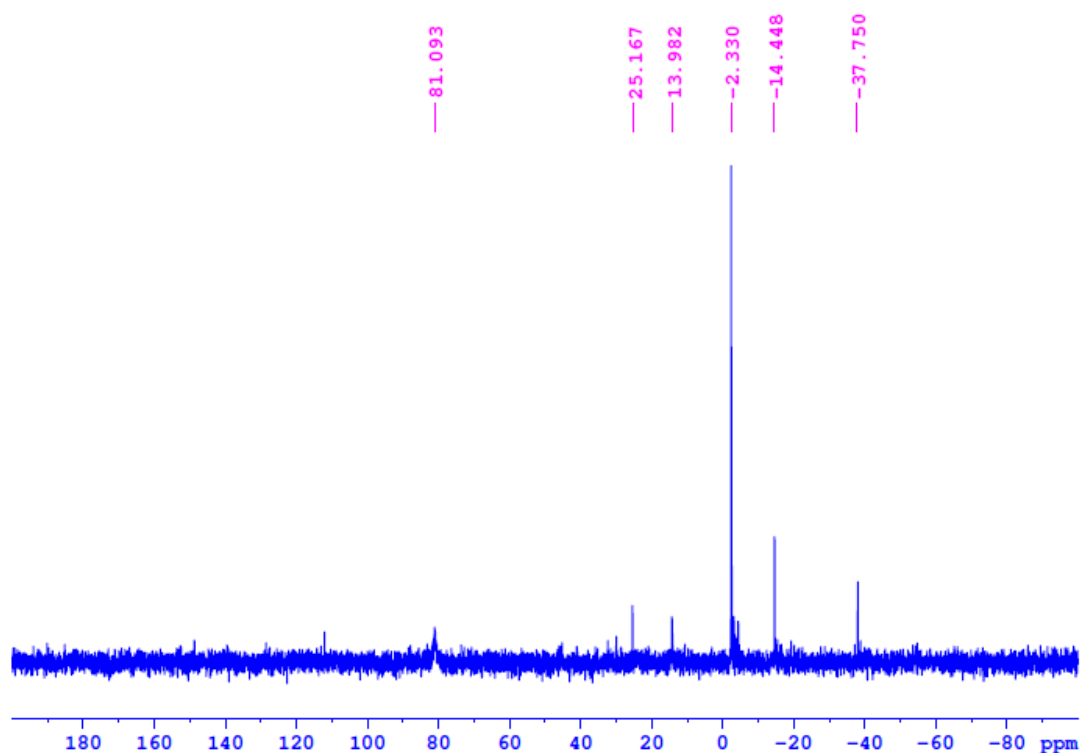


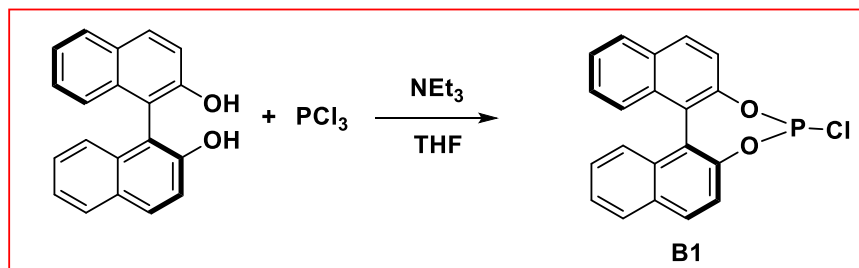
Figure 4.11: ^{31}P NMR spectrum after 120 minutes of addition of Ph_2PCl at room temperature (in dry DMSO). Probable impurities: \$ = ClPPh_2 , * = HPPh_2 , # = LiPPh_2 .

To our delight, a ^{31}P NMR spectrum (Figure 4.11.) of this residue in dry DMSO revealed selective formation of intermediate **[B]** (-2.33 ppm) and O-P coupled product **[D]** could not be observed. The reaction was almost quantitative with minor Ph_2PCl peak at 81.09 ppm.

After having understood the reactivity of the two nucleophiles, we then tailored reaction conditions to suit selective formation of **[B]** *in-situ* and attempted one pot synthesis of **L1** and the procedure is as under.

4.4.2.2 Synthesis of phosphorchloridite

Synthesis of phosphorchloridite (**B1**) was accomplished according to the literature reported procedure.^{57a} ^{31}P NMR (CDCl_3 , 298K) $\delta = 178.5$.



Scheme 4.4: Synthesis of phosphorchloridite **B1**.

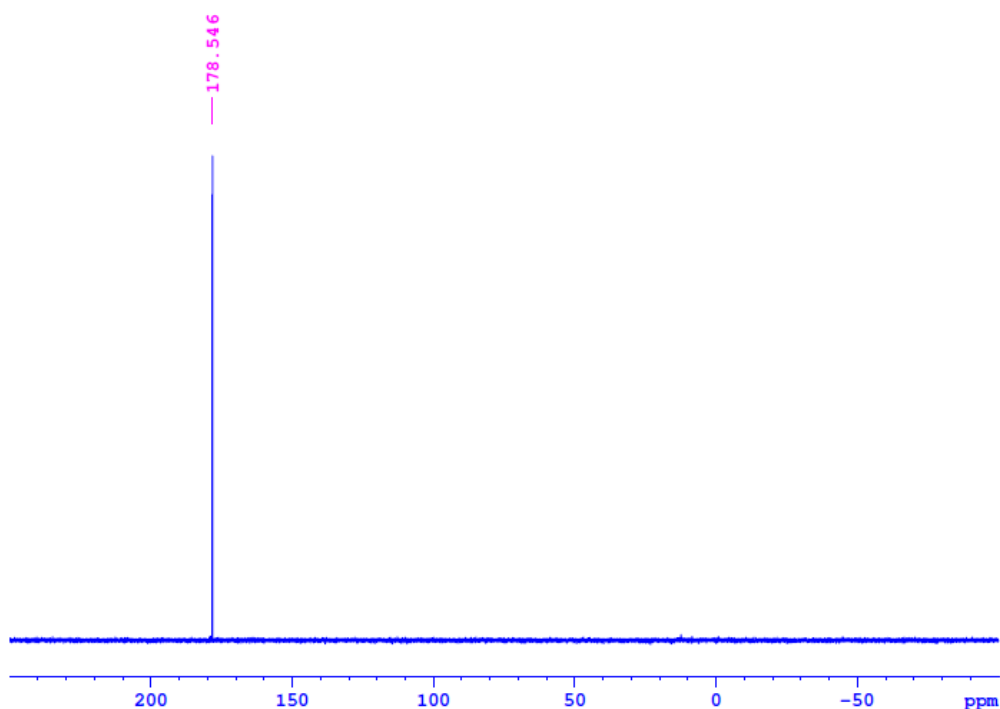


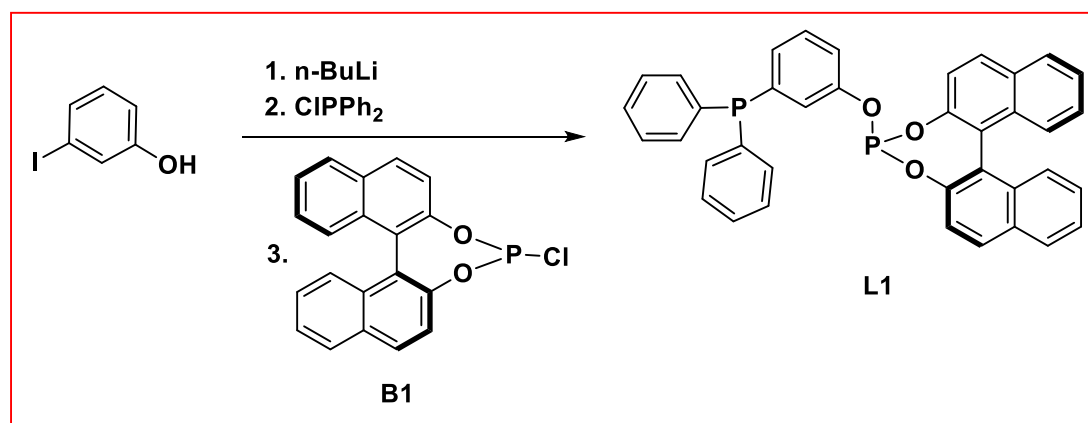
Figure 4.12: ^{31}P NMR spectrum of phosphorchloridite (**B1**).

4.4.2.3 Synthesis of phosphine-phosphite ligand (**L1**)

Hybrid phosphine-phosphite ligand **L1** (Senphos) was synthesized using one pot approach. In an oven dried Schlenk flask 3-iodo phenol (830 mg, 3.77 mmol, 1 equiv) was taken and 100 mL of dry diethyl ether was added. The resultant solution was cooled to $-84\text{ }^\circ\text{C}$ and *n*-BuLi (2.0 M in hexane, 3.77 mL, 7.54 mmol, 2 equiv) was added drop wise. Subsequently, the reaction mixture was stirred for the next 3 hours within which the bath temperature rises to $0\text{ }^\circ\text{C}$. Subsequently, the reaction mixture was cooled to $-84\text{ }^\circ\text{C}$ and chlorodiphenylphosphine

(0.68 mL, 3.77 mmol, 1 equiv) was drop wise added to it. The reaction mixture was stirred for next two hours, during which the reaction temperature rises to $-12\text{ }^{\circ}\text{C}$. In another round bottom flask, phosphorochloridite (1.32 g, 3.77 mmol, 1 equiv) was dissolved in dry diethyl ether (40 mL) and was added to the above reaction mixture at $-84\text{ }^{\circ}\text{C}$. After complete addition, the reaction mixture was stirred for 1 hour in the same bath. Subsequently, the flask was taken out of the bath and stirred for 1 hour at room temperature. The content was passed through celite bed, filtered with the help of cannula filtration and volatiles were evaporated to get white coloured residue. The white residue was washed twice with dry hexane (20 mL) to obtain 4-(3-(diphenylphosphinanyl)phenoxy)dinaphtho[2,1-*d*:1',2'-*f*][1,3,2]dioxaphosphepine (**L1** or **Senphos**) as white coloured solid in 72 % yield (1.6 g).

^{31}P NMR (125 MHz, CDCl_3 , 298K) $\delta = 144.24$ (s, phosphite), -5.14 (s, phosphine). ^1H NMR (400 MHz, CD_3COCD_3 , 298K) $\delta = 5.27$ (s, CH_2Br_2 , Internal standard), 7.04 (d, 1H), 7.15-7.18 (m, 1H), 7.23-7.26 (m, 2H), 7.30-7.33 (m, 8H), 7.43-7.51 (m, 9H), 7.61 (d, 1H), 7.98-8.07 (m, 3H), 8.16 (d, 1H). ^{13}C NMR (100 MHz, CD_3COCD_3 , 298K) $\delta = 152.6$, 148.0 (d, $J = 65$ Hz), 141.0 (d, $J = 15.5$ Hz), 137.6 (d, $J = 16$ Hz), 134.7, 134.5, 133.6, 133.3, 132.8, 132.2, 131.8, 131.2, 131.1, 130.7, 130.1, 129.7, 129.6, 127.4, 126.4 (d, $J = 24$ Hz), 122.4, 121.8 (d, $J = 10$ Hz). **HRMS**: m/z calculated for $\text{C}_{38}\text{H}_{26}\text{O}_3\text{P}_2 = 592.13$, found = 593.14 ($\text{M}+\text{H}$) $^+$. Elemental analysis [for $\text{C}_{38}\text{H}_{26}\text{O}_3\text{P}_2+\text{C}_7\text{H}_8$ (Toluene)], Calculated: C = 78.94, H = 5.01; Found: C = 78.98, H = 4.43.



Scheme 4.5: Synthesis of hybrid phosphine-phosphite ligand **L1** or **Senphos**.

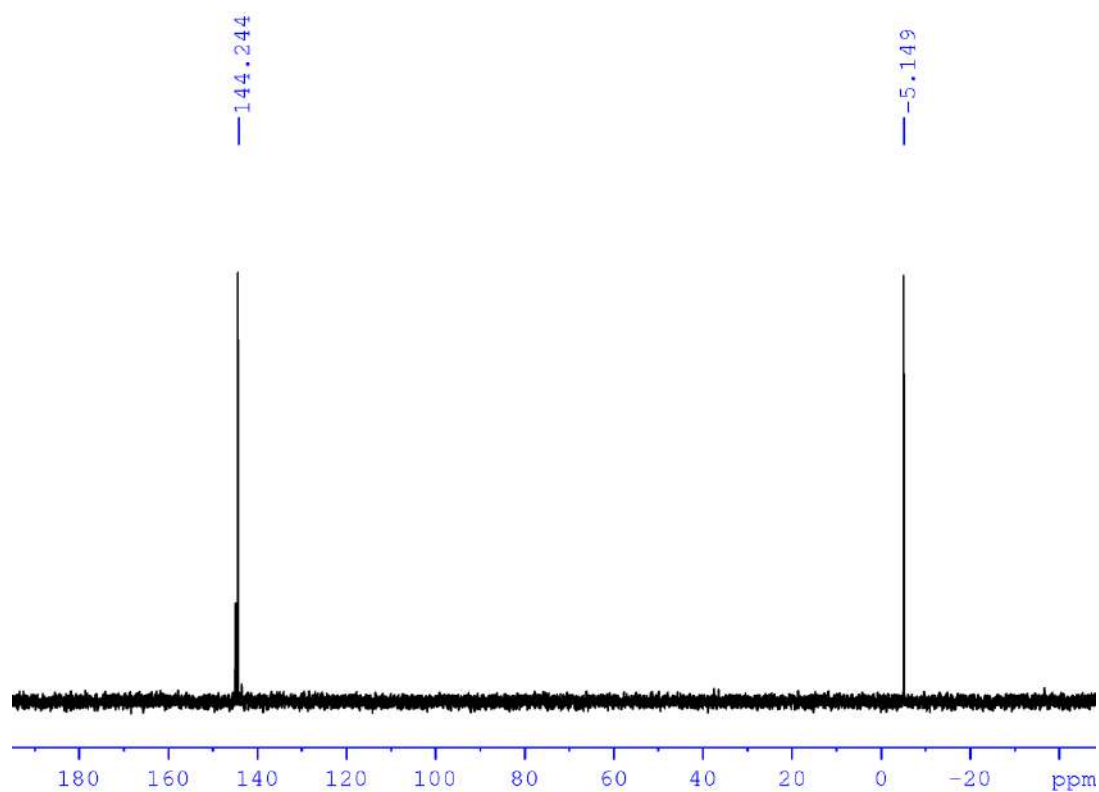


Figure 4.13: ^{31}P NMR spectrum of hybrid phosphine-phosphite ligand (**L1**).

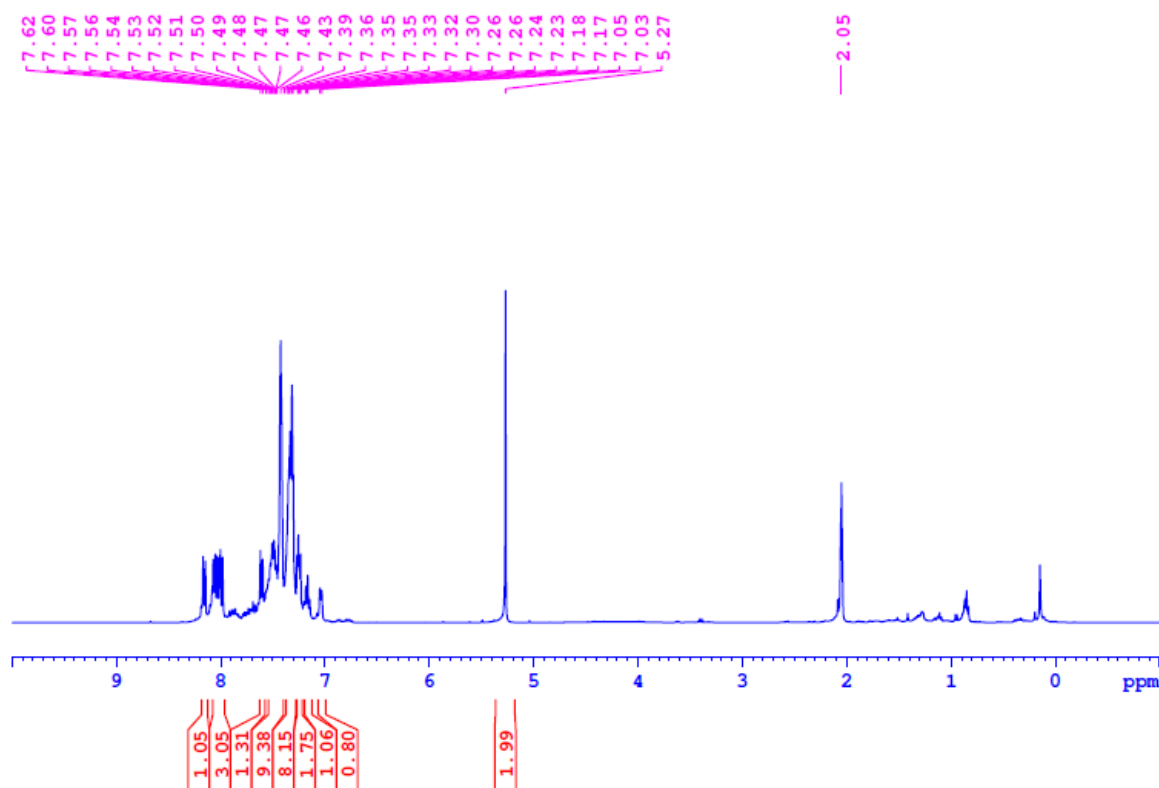


Figure 4.14: ^1H NMR spectrum of hybrid phosphine-phosphite ligand (**L1**).

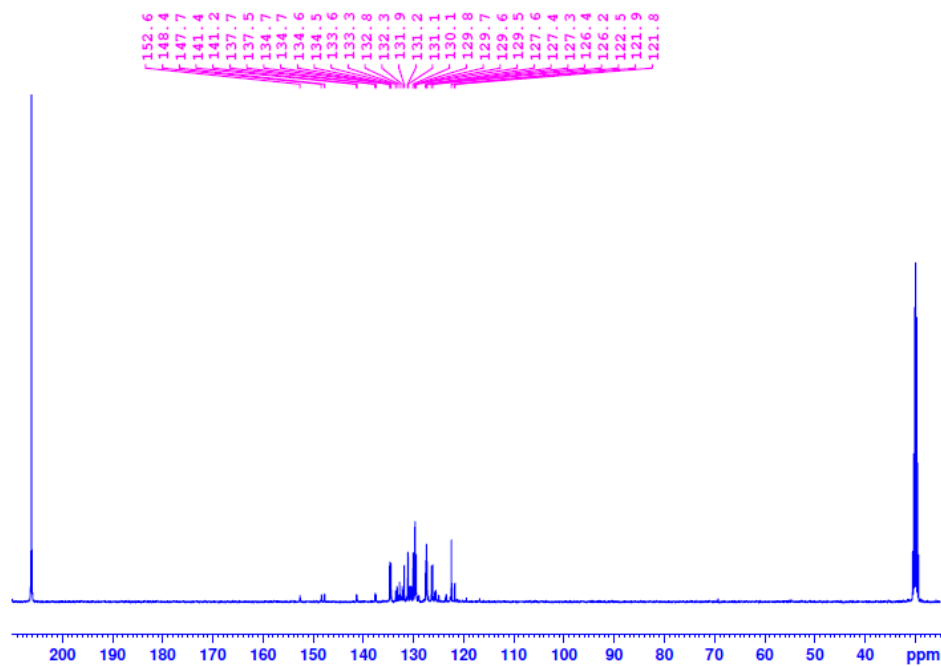


Figure 4.15: ^{13}C NMR spectrum of hybrid phosphine-phosphite ligand (**L1**).

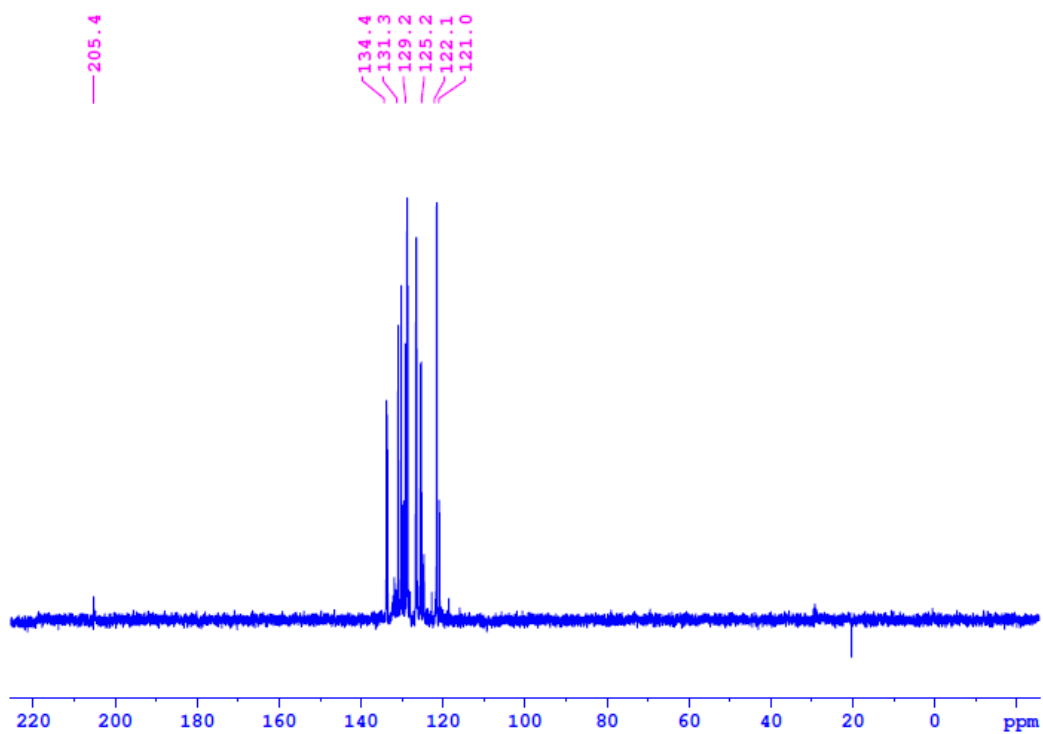


Figure 4.16: DEPT NMR spectrum of hybrid phosphine-phosphite ligand (**L1**).

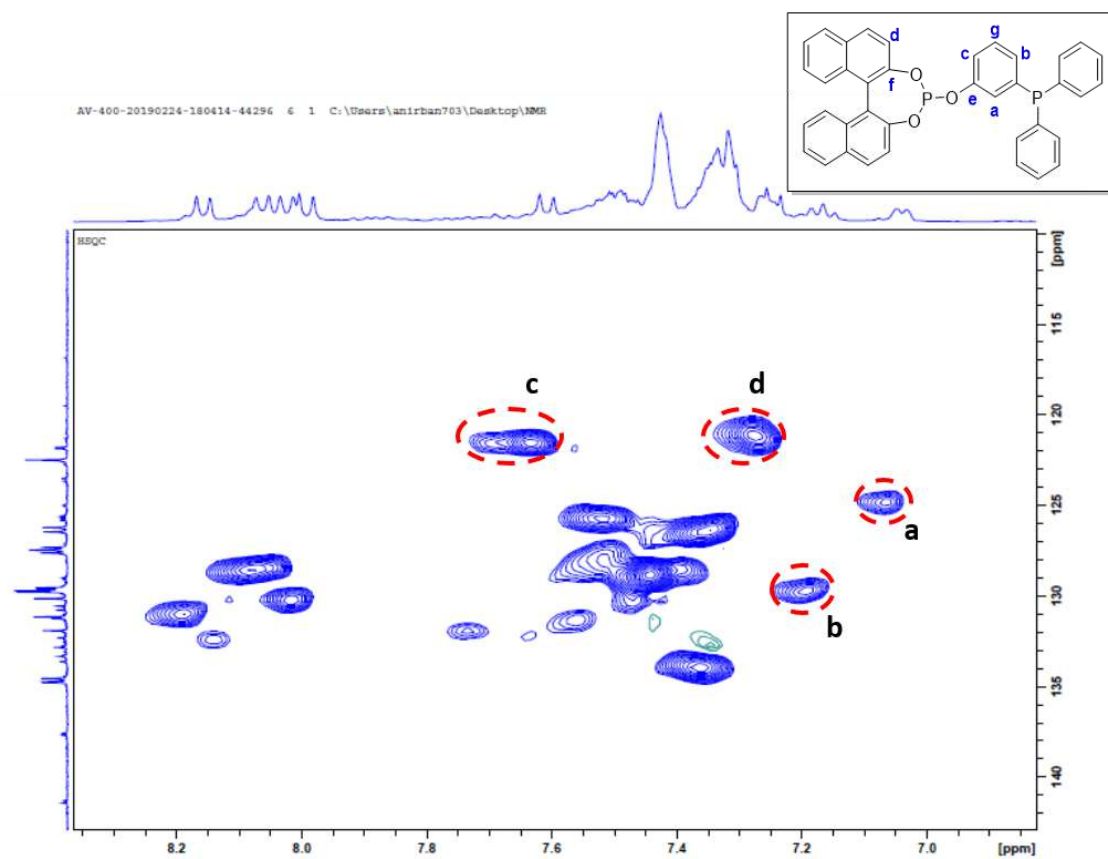


Figure 4.17: Direct C-H correlation (HSQC) NMR spectrum of hybrid phosphine-phosphite ligand (**L1**).

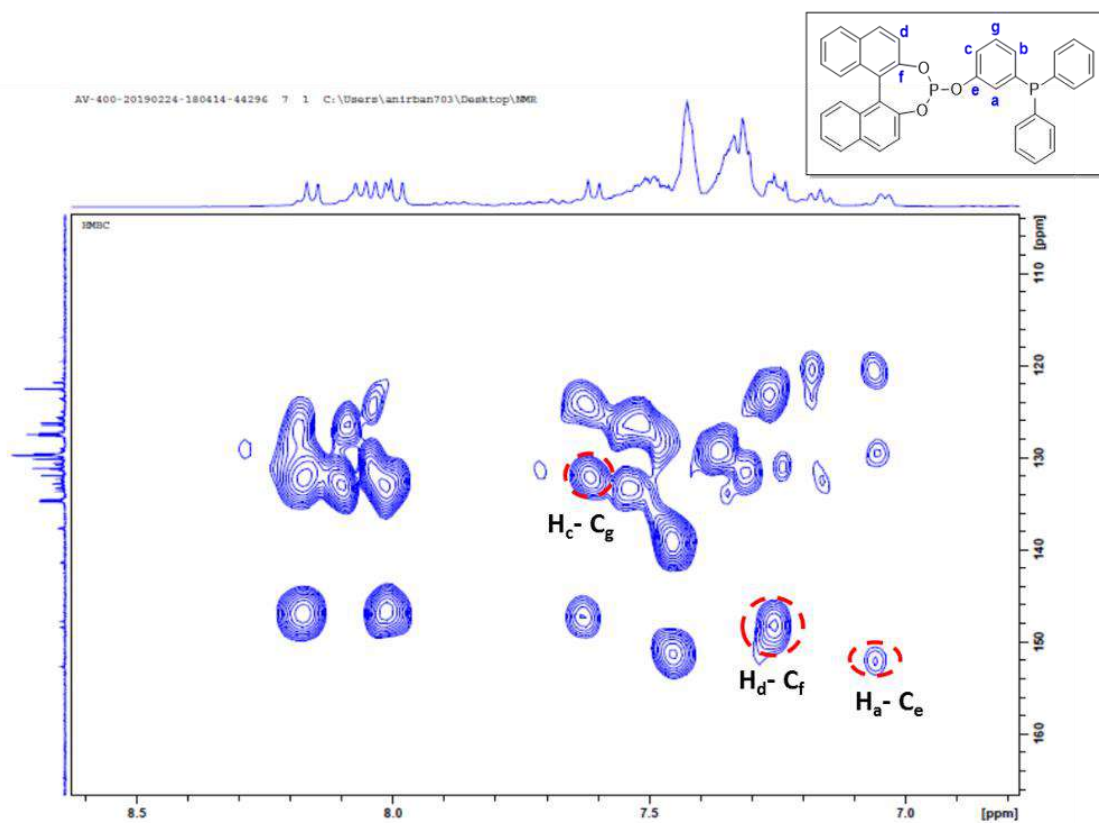


Figure 4.18: Long range C-H correlation (HMBC) NMR spectrum of hybrid phosphine-phosphite ligand (**L1**).

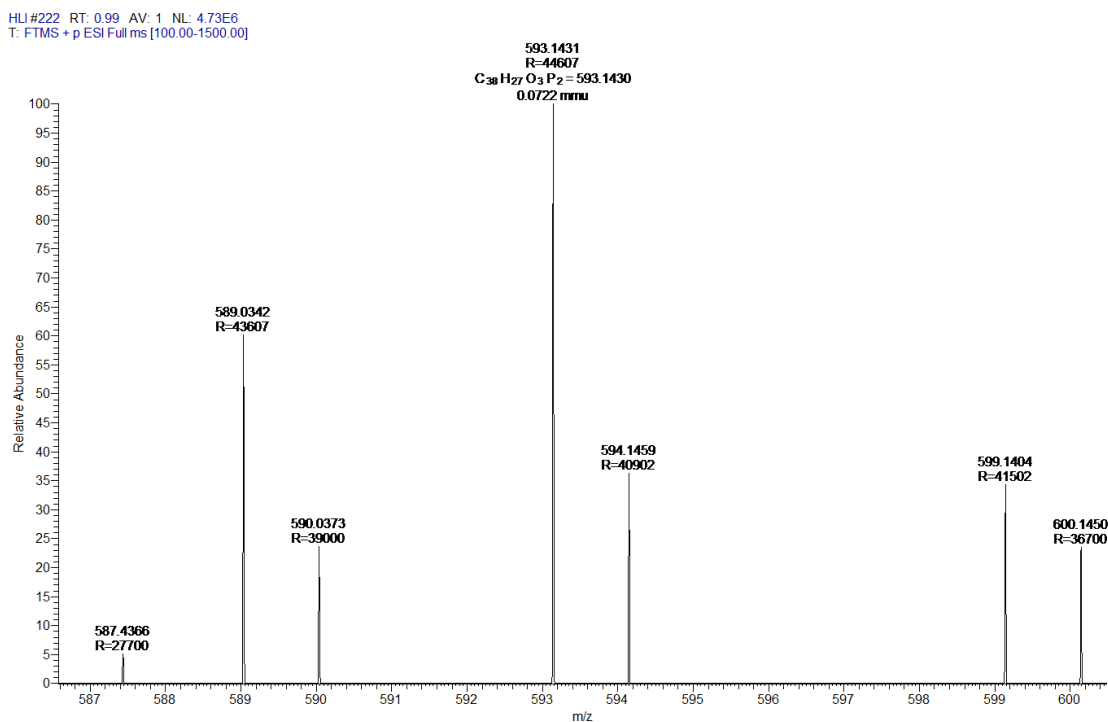
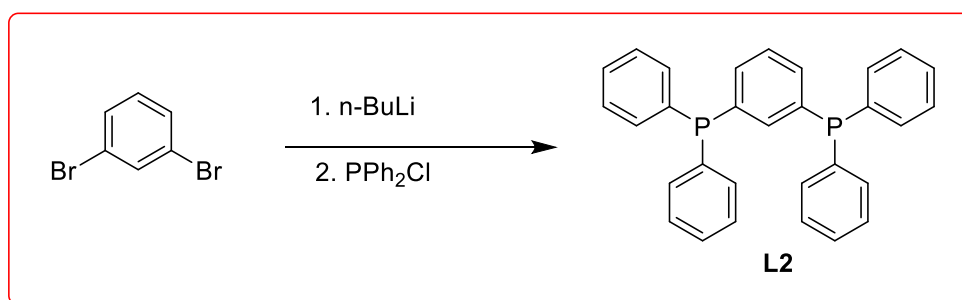


Figure 4.19: ESI-MS spectrum of phosphine-phosphite ligand (**L1**) showing $[M+H]^+$ peak.

4.4.3 Synthesis of bis-phosphine ligand (L2)

1, 3-dibromobenzene (310 mg, 1.31 mmol, 1 equiv) was taken in a Schlenk flask and was dissolved in dry diethyl ether (20 mL). The resultant solution was cooled to $-84\text{ }^{\circ}\text{C}$ and 1.45 mL *n*-BuLi was (2.89 mmol, 2 M solution in hexane) added to it. The solution was stirred for 2 hours before adding 0.58 mL of PPh_2Cl (3.3 mmol, 2.5 equiv) at $-84\text{ }^{\circ}\text{C}$. The resultant mixture was stirred overnight at room temperature and volatiles were evaporated to obtain a residue. Dichloromethane was added to above residue and the solution was filtered. Volatiles were evaporated and residue was purified by silica gel chromatography (using petroleum ether) to produce anticipated ligand **L2** in 74% (432 mg) isolated yield.

^{31}P NMR (CDCl_3 , 298K): $\delta = -4.68$ (s). ^1H NMR (400 MHz, CDCl_3 , 298K): $\delta = 7.51$ (d, $J = 7.3$ Hz, 2H), 7.47 (d, $J = 6.8$ Hz, 2H), 7.38 (m, 17H), 7.25 (m, 3H). ^{13}C NMR (100 MHz, CDCl_3 , 298K): $\delta = 140.7$ (d, $J = 18.57$ Hz), 136.5 (d, $J = 12.38$ Hz), 136.1 (d, $J = 18.57$ Hz), 133.9 (d, $J = 19.58$ Hz), 132.4, 132.2, 131.9, 130.2 (d, $J = 7.4$ Hz), 129.2, 128.9 (d, $J = 7.42$ Hz), 123.3 (d, $J = 7.94$ Hz).



Scheme 4.6: Synthesis of bis-phosphine ligand **L2**.

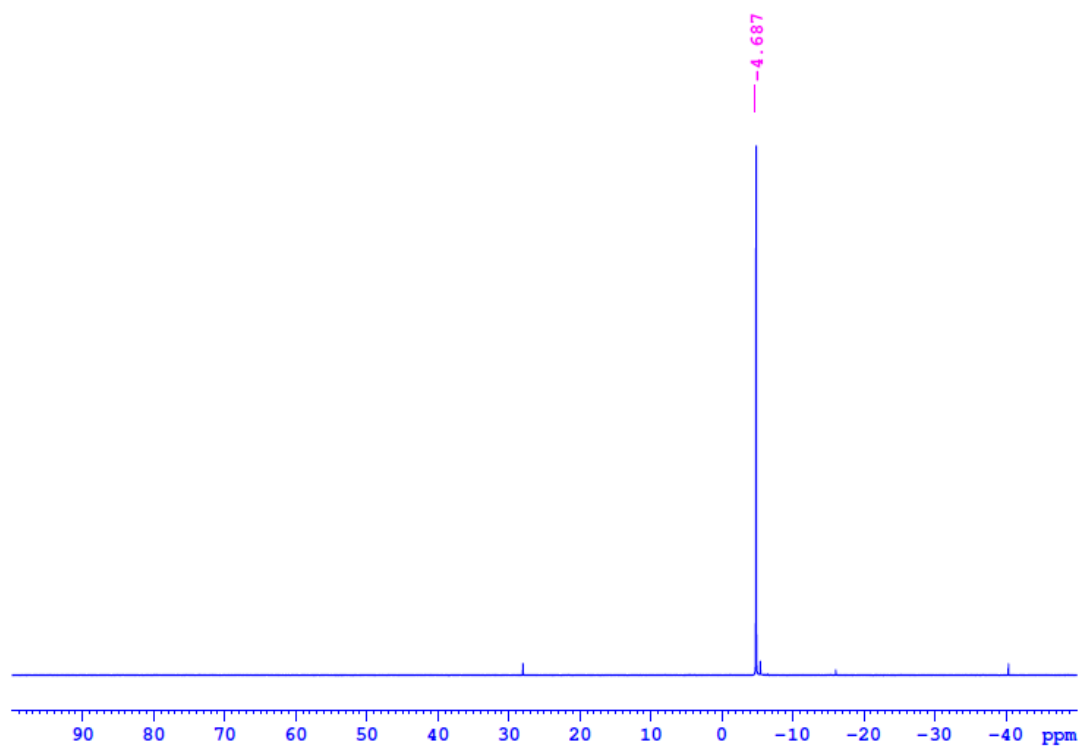


Figure 4.20: ^{31}P NMR spectrum of bis-phosphine ligand (**L2**).

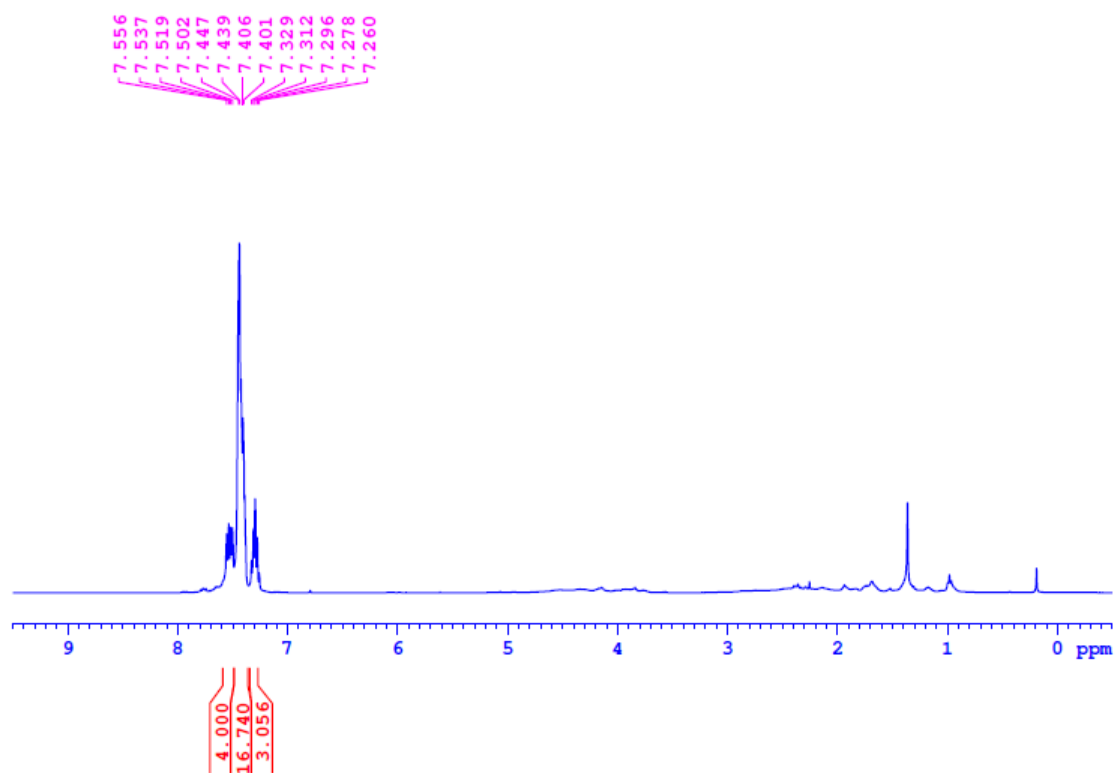


Figure 4.21: ^1H NMR spectrum of bis-phosphine ligand (**L2**).

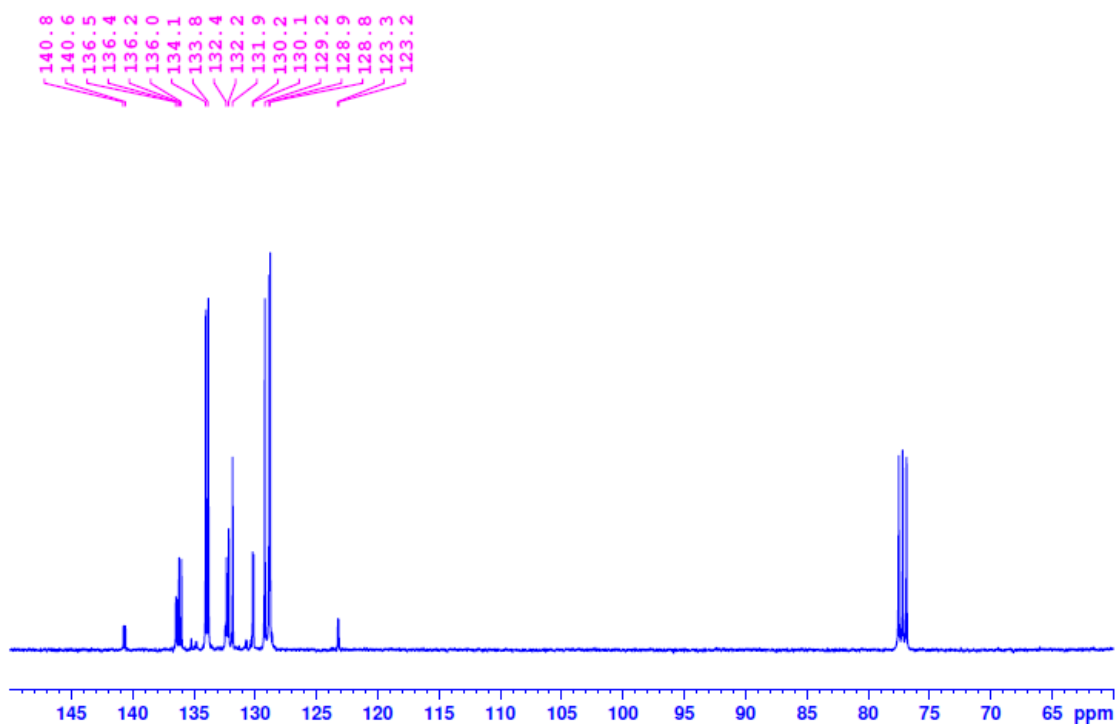


Figure 4.22: ^{13}C NMR spectrum of bis-phosphine ligand (**L2**).

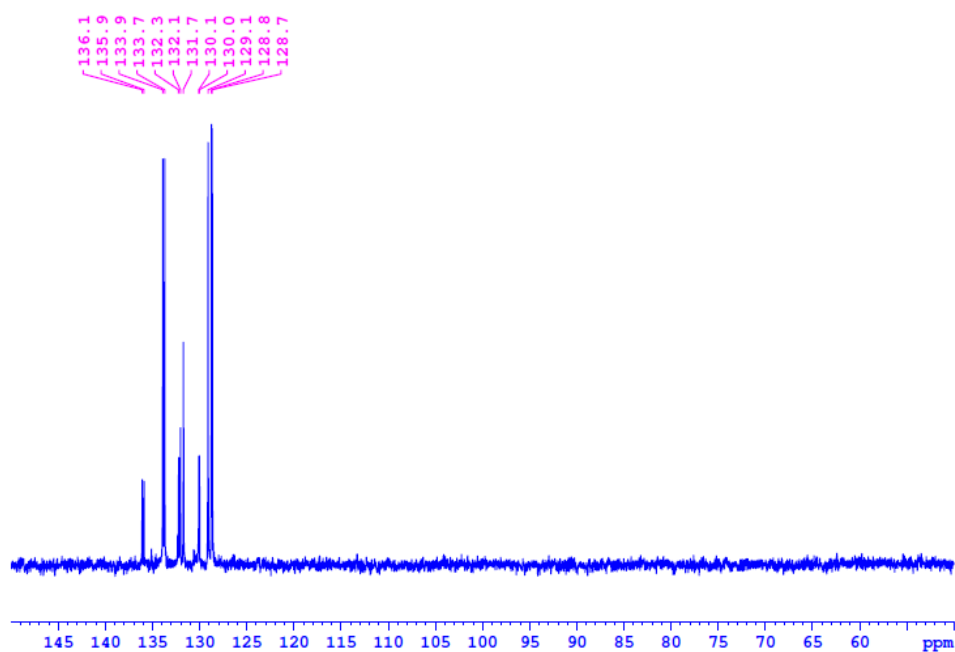


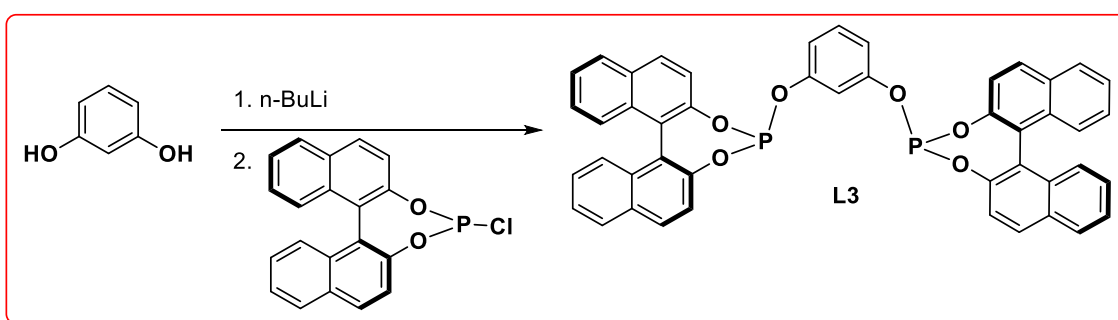
Figure 4.23: DEPT NMR spectrum of bis-phosphine ligand (**L2**).

4.4.4 Synthesis of bis phosphite ligand (**L3**)

Synthesis of bis-phosphite ligand was performed by following a modified literature procedure.^{57b} In an oven dried Schlenk flask resorcinol (186 mg, 1.689 mmol, 1 equiv) was taken and was dissolved in dry tetrahydrofuran (10 mL). The Schlenk was cooled to $-84\text{ }^{\circ}\text{C}$

and 1.78 mL of *n*BuLi (3.56 mmol, 2.0 molar solution in hexane, 2.1 equiv) was dropwise added to it. The reaction mixture was allowed to warm to room temperature and was stirred for 2 hours. Subsequently, the Schlenk was again cooled to -84 °C and phosphorchloridite (1.244 g, 3.547 mmol, 2.1 equiv) was added to above mixture and the content was stirred for 4 hours. After completion of reaction, the solution was passed through a celite bed and solvent was stripped off under vacuum to yield **L3** in 68% (840 mg) yield.

^{31}P NMR (CDCl_3 , 298K): $\delta = 143.92$ (s). ^1H NMR (400 MHz, CDCl_3 , 298K): $\delta = 8.06$ (d, $J = 9$ Hz, 2H), 8 (m, 6H), 7.63 (d, $J = 8.6$ Hz, 2H), 7.48 (m, 10H), 7.33 (m, 6H), 7.11 (s, 1H), 7.07 (d, $J = 8.44$ Hz, 1H).



Scheme 4.7: Synthesis of bis-phosphite ligand (**L3**).

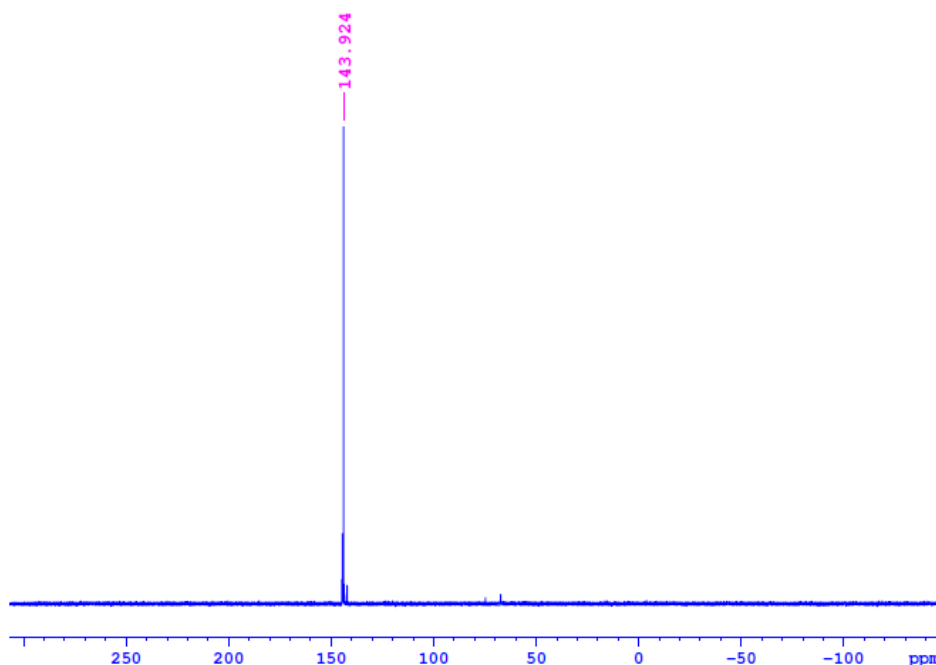


Figure 4.24: ^{31}P NMR spectrum of bis-phosphite (**L3**).

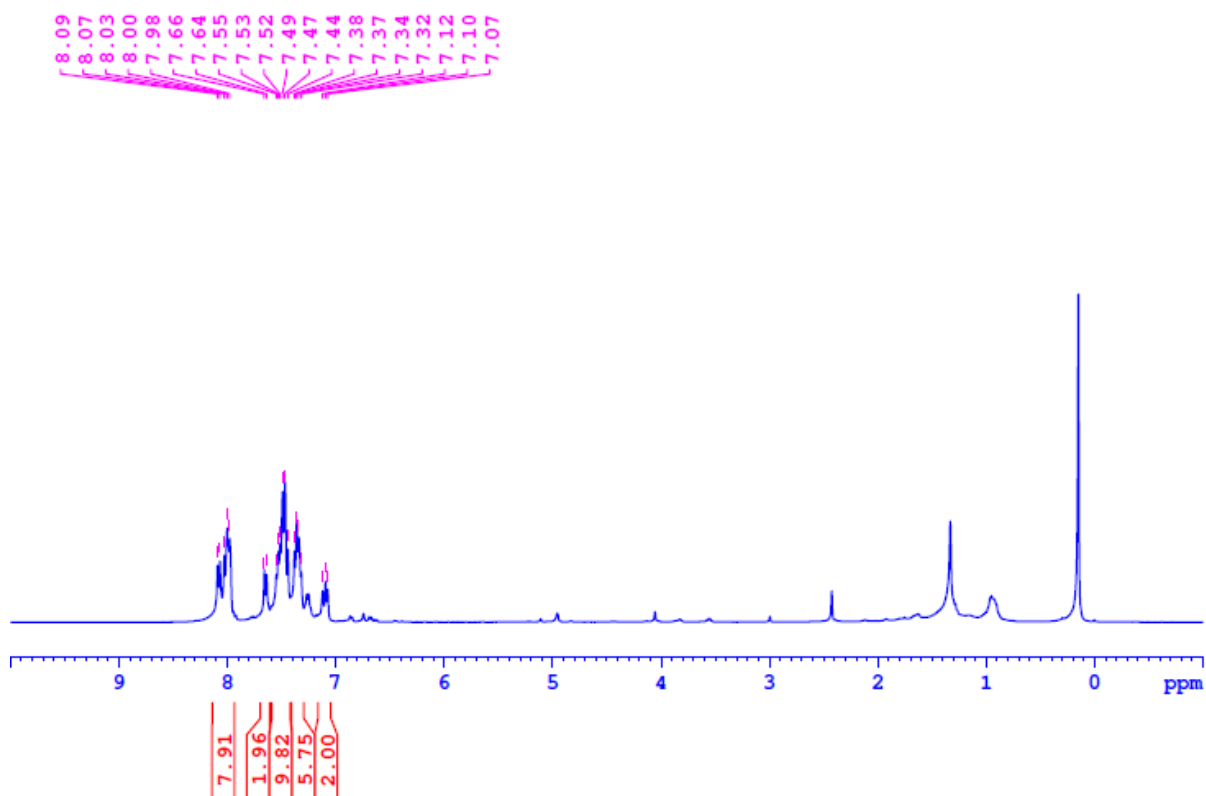
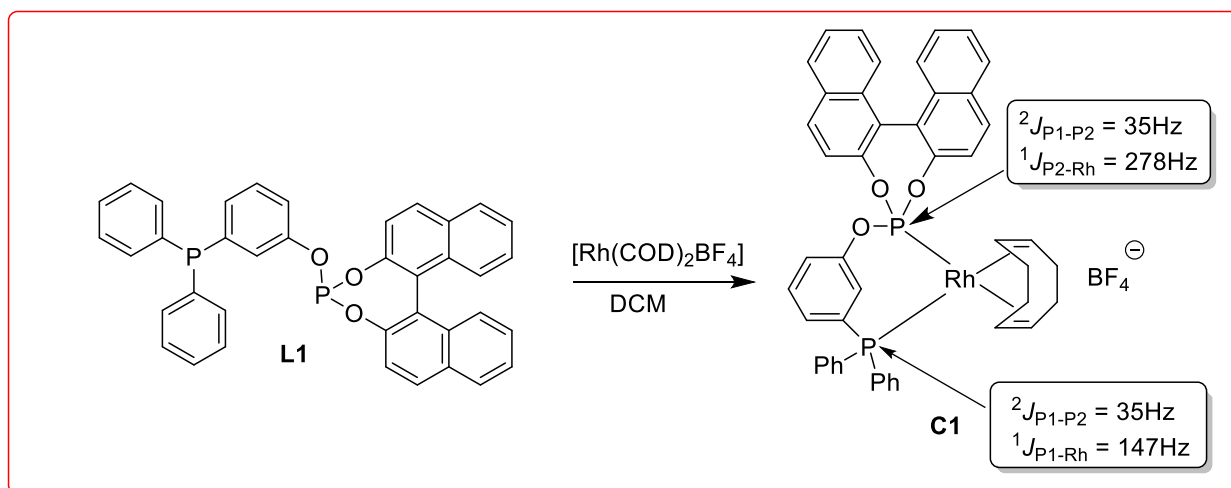


Figure 4.25: ^1H NMR spectrum of hybrid bis-phosphite ligand (**L3**).

4.4.5 Investigating the coordination behavior of ligand **L1**

In a Schlenk flask $[\text{Rh}(\text{COD})_2\text{BF}_4]$ (40.6 mg, 0.0614 mmol) and ligand (**L1**) (59.26 mg, 0.0614 mmol) was taken and it was dissolved in dry dichloromethane (10 mL). The resultant reaction mixture was allowed to stir at room temperature for 5 hours. Solvent was evaporated in vacuum to get solid in quantitative yield.

^{31}P NMR (CDCl_3 , 298K): $\delta = 121.15$ (dd, $^1J_{\text{Rh-P}} = 278$ Hz, $^2J_{\text{P-P}} = 35$ Hz) and 29.17 (dd, $^1J_{\text{Rh-P}} = 147$ Hz, $^2J_{\text{P-P}} = 35$ Hz). ^1H NMR (500 MHz, CDCl_3 , 298K): $\delta = 8.39$ (d, $J = 9.7$ Hz, 1H), 8.07–8.1 (m, 2H), 7.93 (d, $J = 10.47$ Hz, 1H), 7.65–7.72 (m, 2H), 7.06–7.57 (m, 19H), 6.88 (s, 1H), 6.66–6.74 (m, 1H), 5.33–5.74 (m, 4H), 2.64–2.66 (m, 2H), 2.49 (d, $J = 9.7$ Hz, 3H), 2.4 (s, 3H).



Scheme 4.8: Synthesis of **L1**-Rh complex **C1**.

^{31}P NMR displayed a doublet of doublet (dd, $^1J_{\text{Rh-P}} = 147$, $^2J_{\text{P-P}} = 35$ Hz) at 29.17 ppm for phosphine arm (down field shift compared to free ligand) and another doublet of doublet (dd, $^1J_{\text{Rh-P}} = 278$, $^2J_{\text{P-P}} = 35$ Hz) at 121.15 ppm for phosphite arm (up field shift compared to free ligand) (Figure 4.3.). Above ^{31}P NMR observation suggested that ligand is coordinating to Rh metal center preferably in square planar geometry along with one cyclooctadiene molecule.

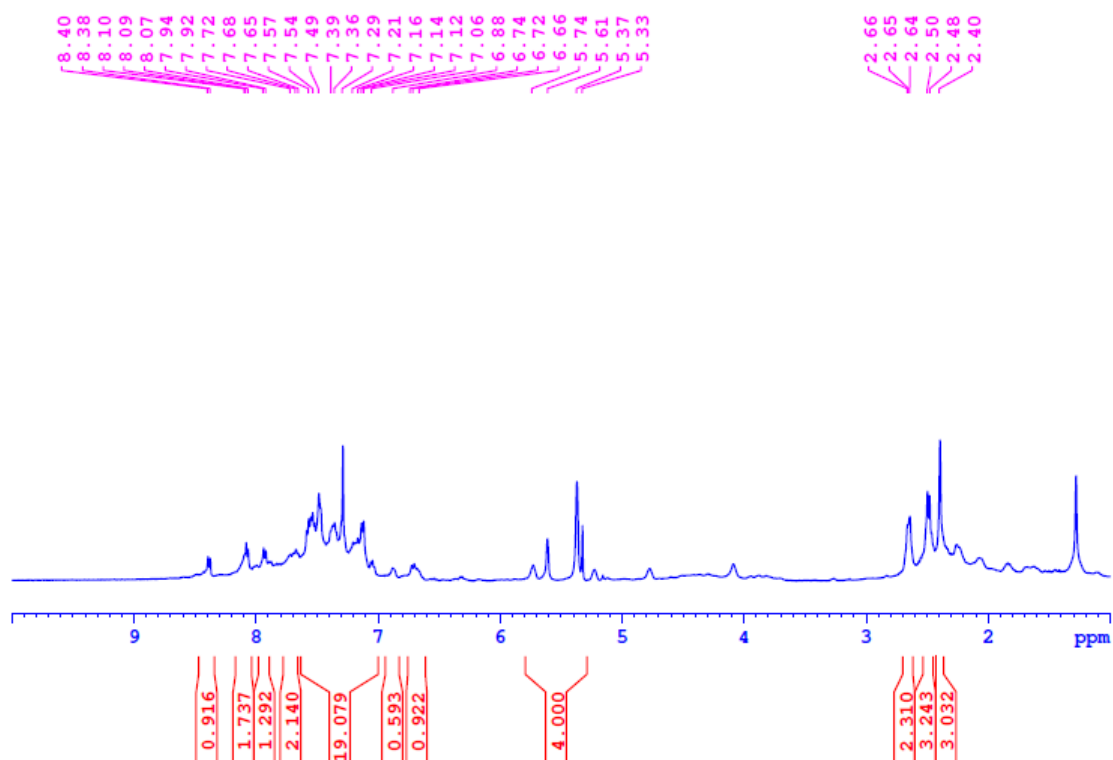


Figure 4.26: ^1H NMR spectrum of Rh complex with ligand **L1**.

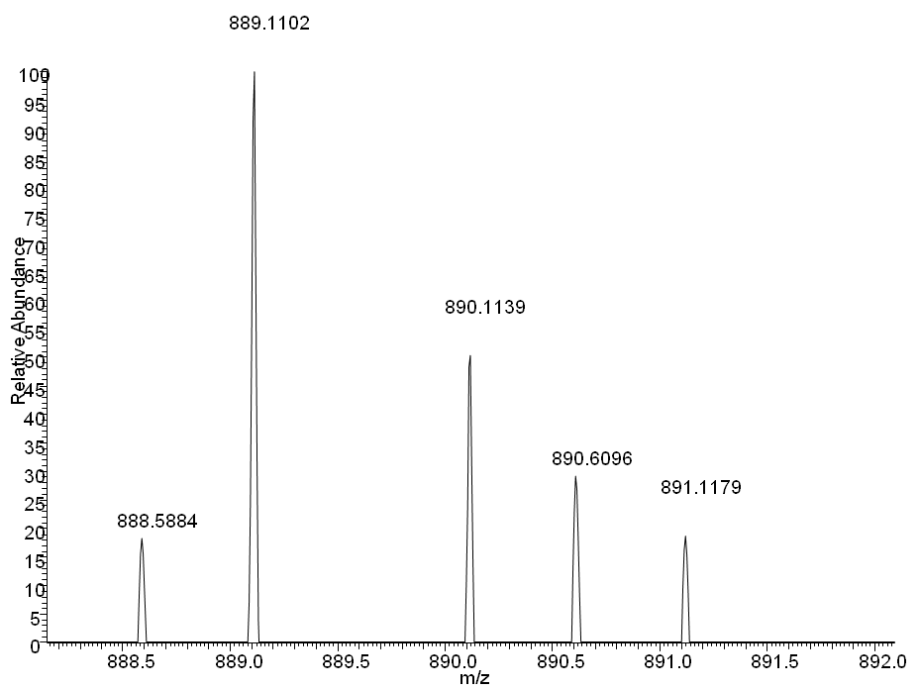


Figure 4.27: ESI-MS spectrum of Rh complex with ligand **L1** ($m/z = 889.11$ $[M-H]^+$).

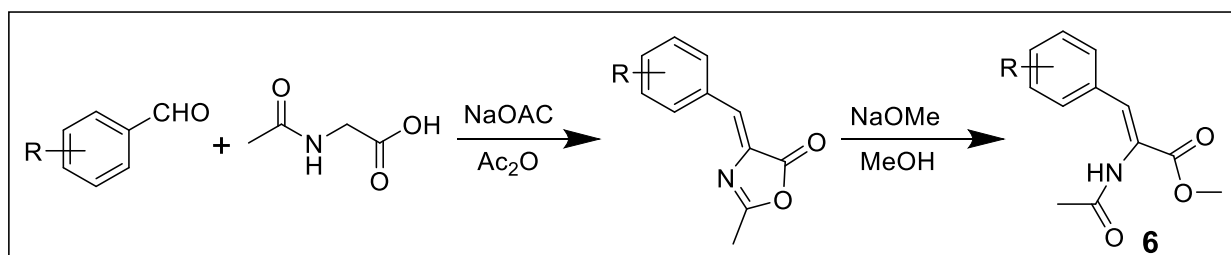
4.4.6 Synthesis of substrates

Substrates (**6d**, **6e**, **6f**, **6g**, **6h**, **6i**, **6j**, **6k**, **6n** and **6o**) were prepared by following literature procedures.⁵⁸⁻⁶¹ While, **6l** and **6m** were prepared by modifying literature procedure.⁶² The synthetic details are as under.

In a round bottom flask, aromatic aldehyde (1.14 g, 6.86 mmol, 1 equiv), N-acylglycine (964 mg, 8.23 mmol, 1.2 equiv), anhydrous sodium acetate (732 mg, 8.92 mmol, 1.3 equiv) and acetic anhydride (3.2 ml, 34.3 mmol, 5 equiv) were mixed and heated at 120 °C for 8 hours. The reaction content was allowed to cool to room temperature and 30% aqueous ethanol (40 mL) was added. The mixture was stirred for 30 min and the resultant precipitate was filtered and dried. Sodium methoxide (371 mg, 6.86 mmol) in 20 mL MeOH was added and the reaction content was stirred overnight. Volatiles were evaporated and solvent extraction of the reaction mixture was done by using dichloromethane (150 mL) and aqueous ammonium chloride (100 mL) solution. Finally, the organic layer was washed with brine solution twice and dried over sodium sulphate. The organic layer was concentrated and purified by silica gel column chromatography by using pet ether and ethyl acetate as eluent (80:20 to 50:50). Yield for **6l** = 35%, for **6m** = 38%.

6l: ¹H NMR (500 MHz, DMSO-d₆, 298K): δ = 9.39 (s, 1H_e), 7.62 (d, 1H), 7.42 (s, 1H), 6.60 (m, 2H), 3.83 (s, 3H_d), 3.80 (s, 3H_c), 3.68 (s, 3H_b), 1.95 (s, 3H_a).

6m: ¹H NMR (500 MHz, DMSO-d₆, 298K): δ = 9.52 (s, 1H_b), 7.28 (s, 1H), 7.21-7.19 (m, 1H), 7.10-7.07 (m, 2H), 3.81 (s, 3H), 3.72 (s, 3H), 3.70 (s, 3H), 1.93 (s, 3H_a).



Scheme 4.9: Synthesis of substrates **6c-6o**.

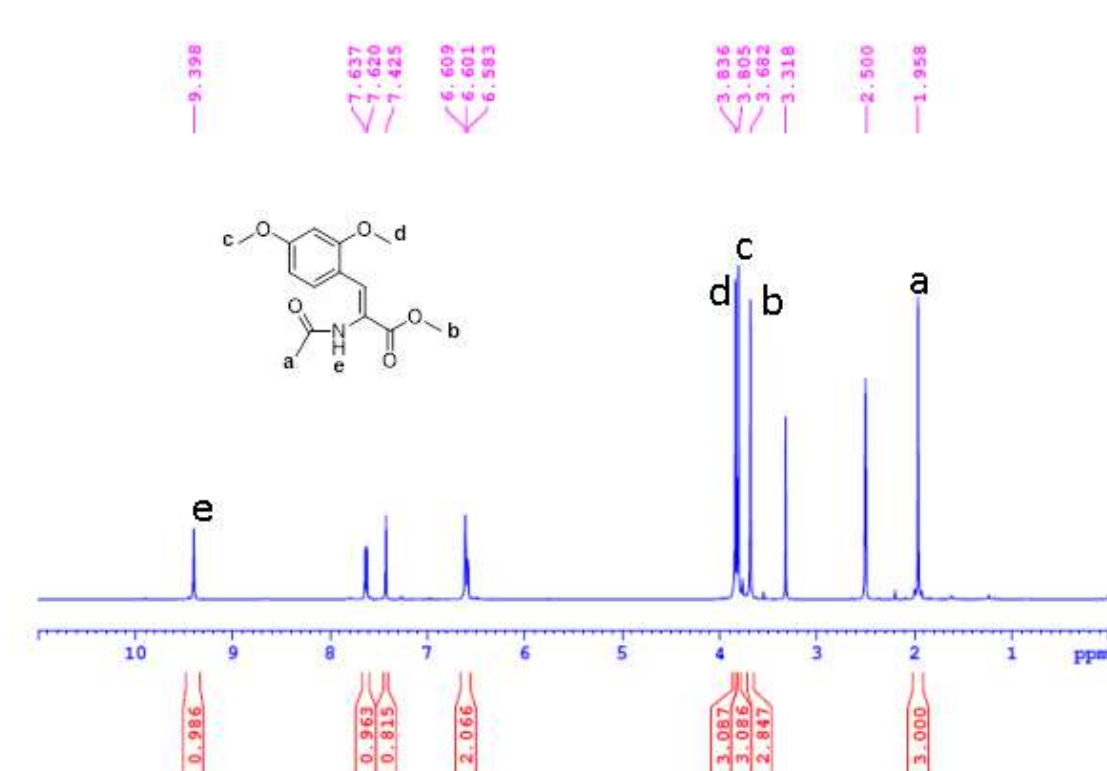


Figure 4.28: ¹H NMR spectrum of methyl (Z)-2-acetamido-3-(2,4-dimethoxyphenyl)acrylate (6l).

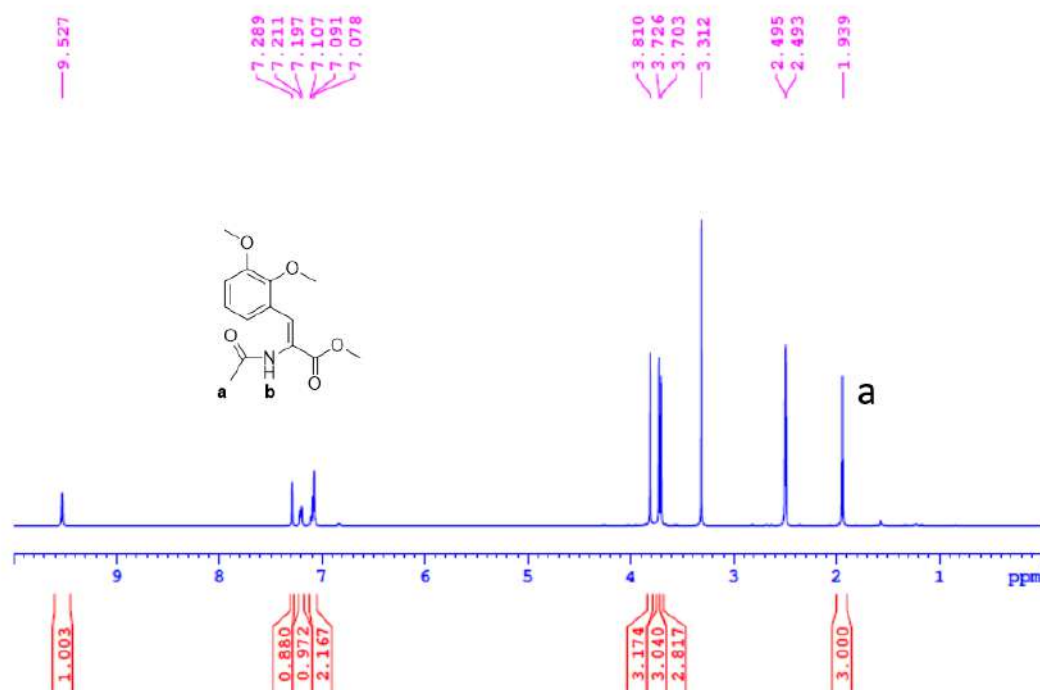
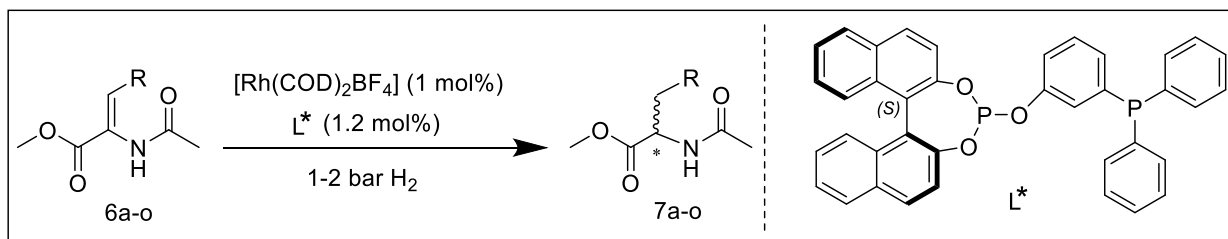


Figure 4.29: ¹H NMR spectrum of methyl (Z)-2-acetamido-3-(2,3-dimethoxyphenyl)acrylate (6m).

4.4.7 General procedure for Asymmetric hydrogenation



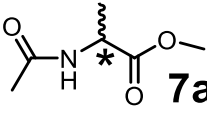
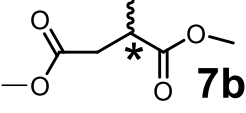
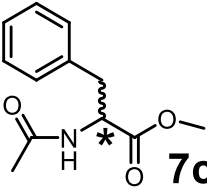
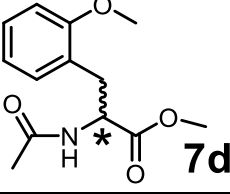
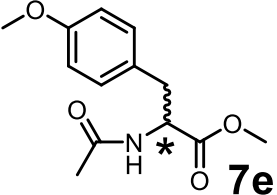
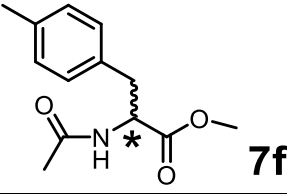
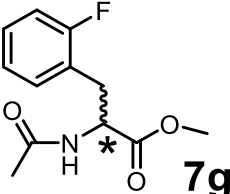
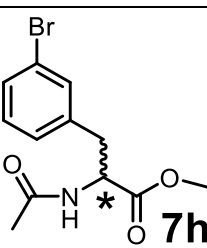
Scheme 4.10: Asymmetric hydrogenation of alkenes.

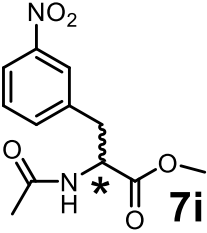
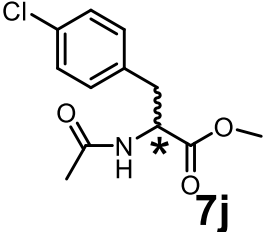
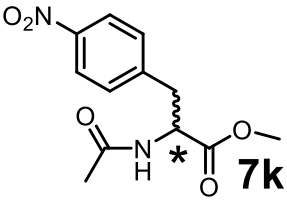
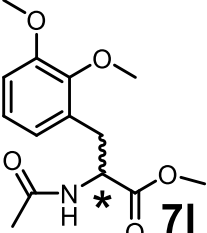
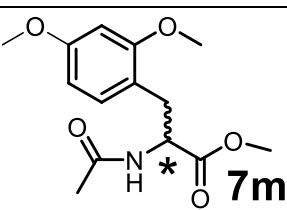
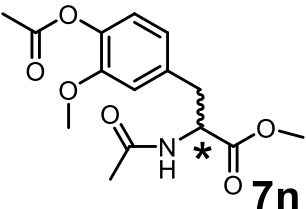
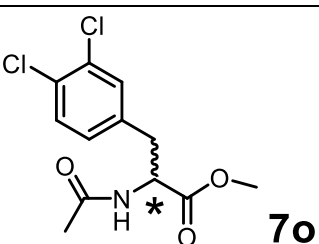
Procedure A: Asymmetric hydrogenation experiments were carried out in a stainless steel autoclave (450 mL) equipped with pressure inlet-outlet, safety rupture valve and pressure gauge. In a glove box, 4 mL glass vials with screw-cap and septa were charged with Rh precursor of $[\text{Rh}(\text{COD})_2\text{BF}_4]$ (1 mg, 0.0025 mmol), ligand (1.8 mg, 0.003 mmol), solvent (1 mL), substrate (0.25 mmol) along with Teflon stirring bars. The charged vials were transferred to autoclave. Before starting the catalytic reactions, the charged autoclave was purged three times with 5 bars of hydrogen and then pressurized to 2 bars. The reaction mixture was stirred at room temperature ($\sim 30^\circ\text{C}$) for 5 to 25 minutes. After asymmetric hydrogenation, the excess gas was vented. The reaction mixture was passed through a short column of silica using dichloromethane as the eluent to remove the ligand and rhodium. The solvent was evaporated under reduced pressure and the product was dried. The conversion and enantioselectivity were determined by GC and/or HPLC using chiral columns. Enantiomeric excess was determined by chiral HPLC on a Chiralpak-IB, ADH column or GC using Supelco- β -dex 225 column.

Procedure B (at low temperature): The asymmetric hydrogenation experiments were carried out in a stainless steel autoclave (450 mL) equipped with pressure inlet-outlet, safety rupture valve and pressure gauge. In a glove box, 4 mL glass vials with screw-cap and septa were charged with $[\text{Rh}(\text{COD})_2\text{BF}_4]$ (1 mg, 0.0025 mmol), ligand (1.8 mg, 0.003 mmol), solvent (1 mL), substrate (0.25 mmol) along with Teflon stirring bars. The charged vials were transferred to a precooled autoclave kept in an ice bath. Before starting the catalytic reactions, the charged autoclave was purged three times with 4 bars of hydrogen and then pressurized to 1 bar. The reaction mixture was stirred at 0°C (or -2°C) for desired time as indicated in table S1. After asymmetric hydrogenation, the excess gas was vented. The reaction mixture was passed through a short silica plug using dichloromethane. The solvent was evaporated under reduced pressure and the product was dried. The conversion and enantioselectivity were

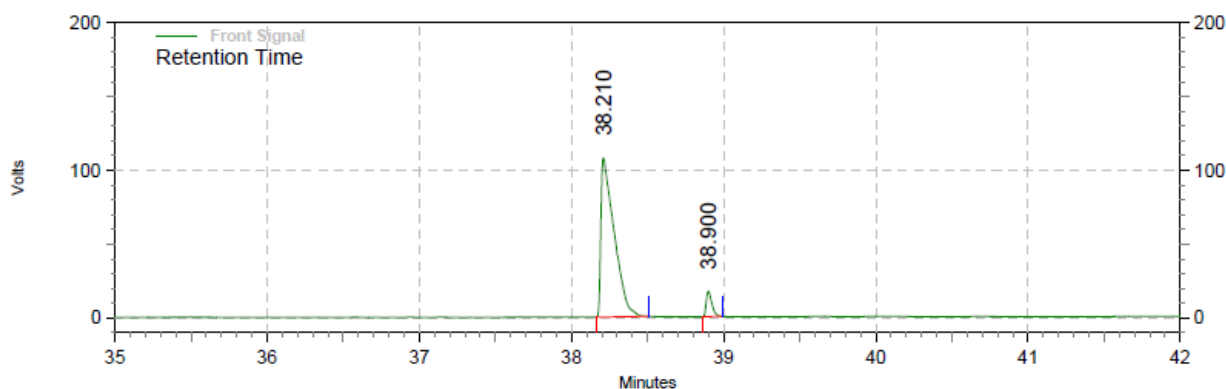
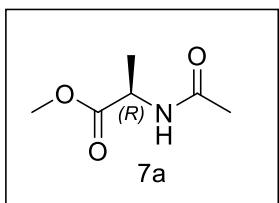
determined by GC and/or HPLC using chiral columns. Enantiomeric excess was determined by chiral HPLC on a Chiralpak-IB, ADH column or GC using Supelco- β -dex 225 column.

Table 4.4. Asymmetric hydrogenation of alkenes using phosphine-phosphite ligand **L1**.

Substrate	Temp. °C	Time. min	H ₂ atm	Conversion %	Ee %
 7a	RT (31)	5	2	>99	87
 7b	RT (30)	5.5	2	>99	28
 7c	-2	300	1	>99	92
	RT (35)	5	2	>99	87
 7d	0	60	1	>99	92
	RT (34)	5	2	>98	71
 7e	0	60	1	>99	82
	RT (34)	5	2	>99	68
 7f	0	60	1	>99	84
	RT (30)	15	2	>99	72
 7g	0	60	1	>99	90
	RT (30)	15	2	>99	82
 7h	0	60	1	>99	81
	RT (30)	15	2	>99	74

 7i	0	60	1	>99	82
	RT (31)	15	2	>95	74
 7j	0	60	1	>99	87
	RT (30)	15	2	>91	70
 7k	0	120	1	>99	81
	RT (31)	25	2	>99	72
 7l	0	120	1	>99	84
	RT (31)	25	2	>99	61
 7m	RT (31)	25	2	>99	51
 7n	0	120	1	>99	90
	RT (29)	30	2	>99	79
 7o	0	60	1	>99	86
	RT (31)	15	2	>84	50

Methyl acetyl-*D*-alaninate (7a): White solid. GC condition: Supelco beta dex 225 isothermal at 70 °C for 10.0 min, 2 °C min⁻¹ to 110 °C, 7 °C min⁻¹ to 210 °C, flow 1ml/min with 14.831 psi pressure; $t_{(R)} = 38.29$ min, $t_{(S)} = 38.90$ min. Methyl acetyl-*D*-alaninate shows $[\alpha]^{25} = -26$ (c 1.0, CHCl₃), comparing this value with literature, this compound has been assigned to be (*R*) isomer.⁶³ Procedure A: 87% ee.

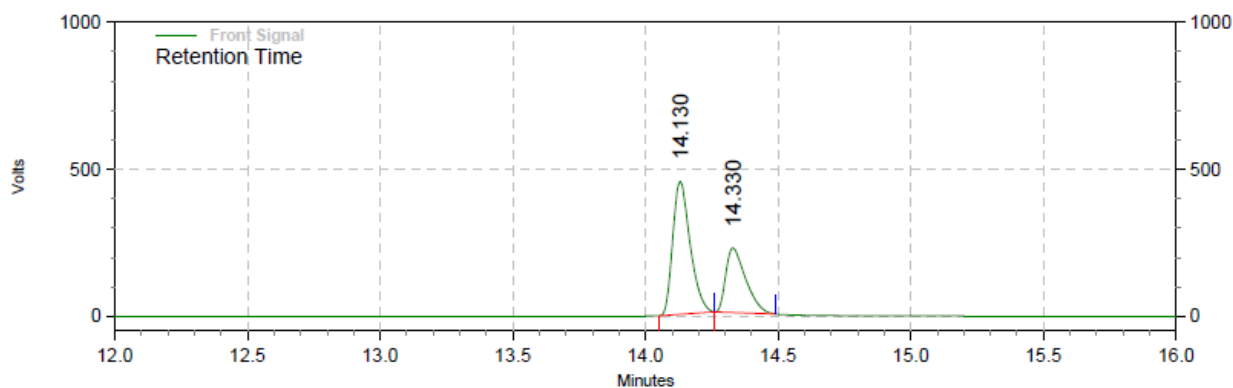
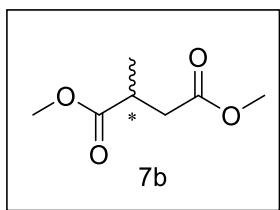


**Front Signal
Results**

Retention Time	Area	Area %	Height	Height %
38.210	5013646	93.65	827890	86.12
38.900	339927	6.35	133478	13.88
Totals	5353573	100.00	961368	100.00

Figure 4.30: HPLC chromatogram of **7a**.

Dimethyl 2-methylsuccinate (7b): Colour less liquid. GC condition: Supelco beta dex 225 isothermal at 75 °C for 2.0 min, 4 °C min⁻¹ to 120 °C, 50 °C min⁻¹ to 220 °C, flow 1ml/min with 14.831 psi pressure; $t_{(R)}$ (major) = 14.13 min, $t_{(R)}$ (minor) = 14.33 min. Procedure A: 28% ee.

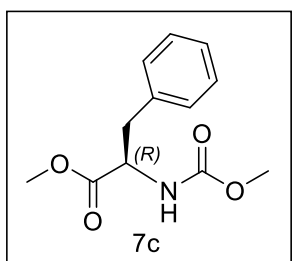


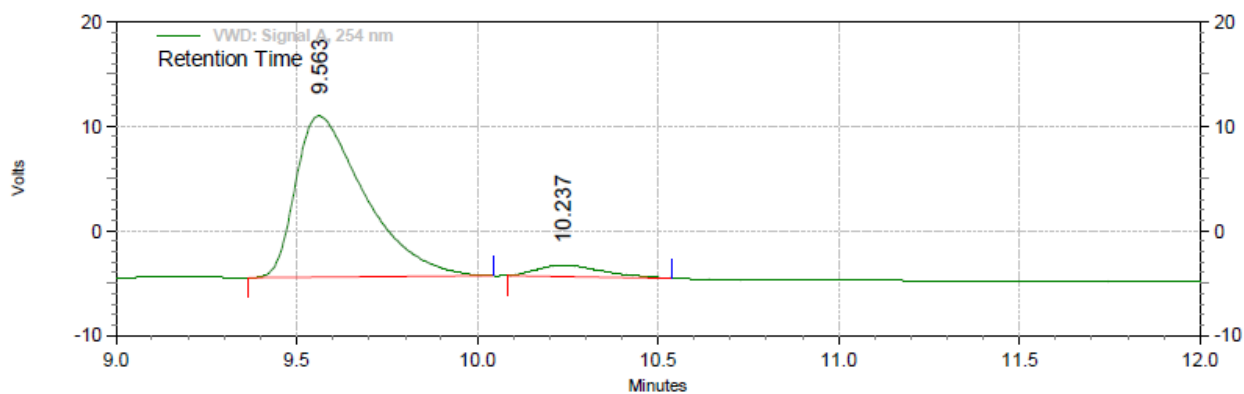
Front Signal Results

Retention Time	Area	Area %	Height	Height %
14.130	15812715	64.27	3470777	67.25
14.330	8791162	35.73	1690285	32.75
Totals	24603877	100.00	5161062	100.00

Figure 4.31: HPLC chromatogram of **7b**.

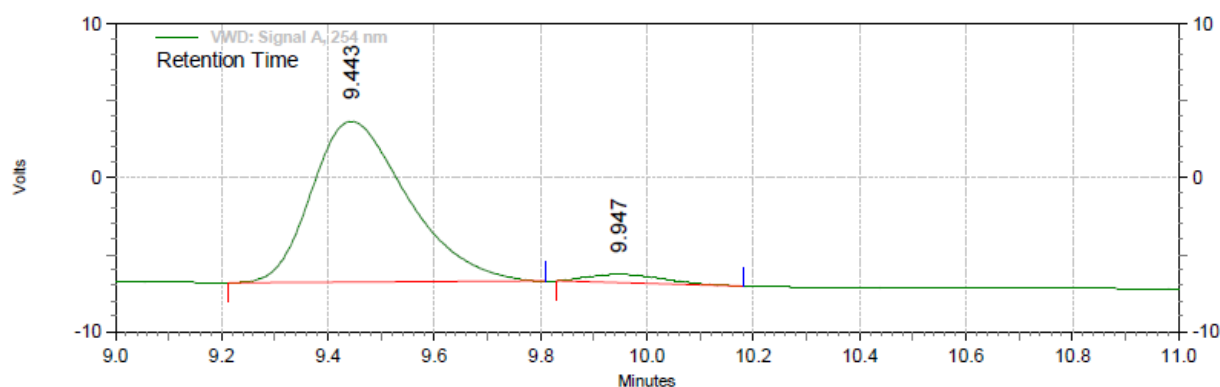
Methyl (methoxycarbonyl)-D-phenylalaninate (7c): White solid. HPLC condition: Daicel chiralpak IB, 1.0 ml/min, UV (λ 254 nm), 10% 2-PrOH/Hexane, t_R (major) = 9.5 min; t_R (minor) = 10.2 min. Methyl (methoxycarbonyl)-D-phenylalaninate shows $[\alpha]^{25} = -98$ (c 1.0, CHCl_3), by comparing the above specific rotation, **7c** has been assigned to be (R) isomer.⁶³ Procedure A: 88% ee; Procedure B at -2 °C: 92% ee.





**VWD: Signal A,
254 nm Results**

Retention Time	Area	Area %	Height	Height %
9.563	3453966	93.95	258630	93.58
10.237	222232	6.05	17734	6.42
Totals				
	3676198	100.00	276364	100.00

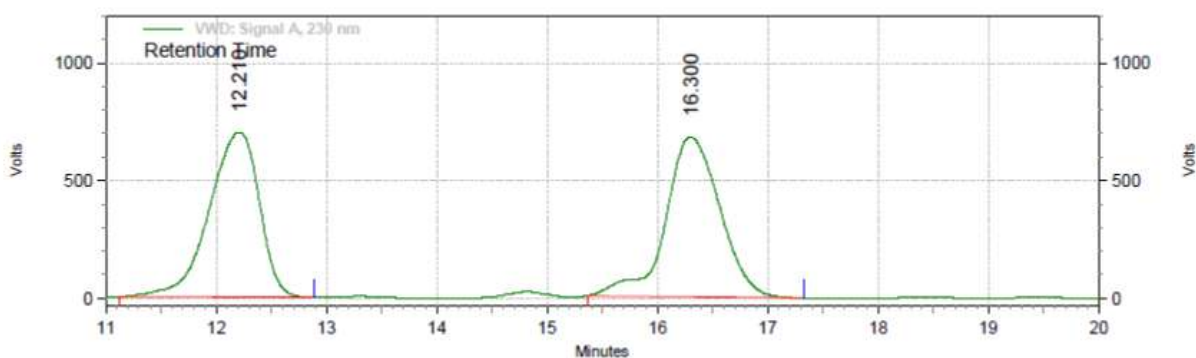
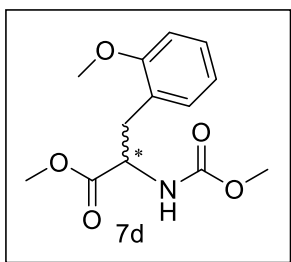


**VWD: Signal A,
254 nm Results**

Retention Time	Area	Area %	Height	Height %
9.443	2193360	96.13	175311	95.21
9.947	88348	3.87	8815	4.79
Totals				
	2281708	100.00	184126	100.00

Figure 4.32: HPLC chromatogram of **7c**, ee = 88% (top), 92% (bottom).

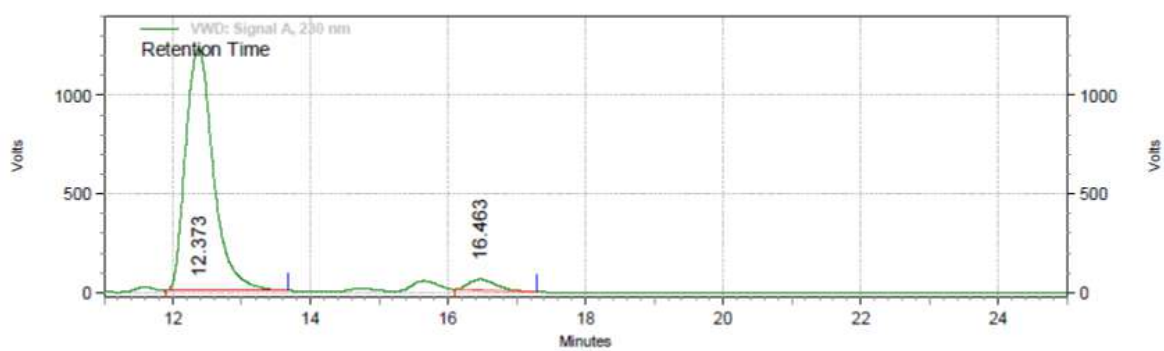
Methyl 2-((methoxycarbonyl)amino)-3-(2-methoxyphenyl)propanoate (7d): White solid. HPLC condition: Daicel chiralpak ADH, 1.0 ml/min, UV (λ 230 nm), 10% 2-PrOH/Hexane, t_R (major) = 12.3 min; t_R (minor) = 16.4 min. Procedure A: 71% ee; Procedure B: 92% ee.



VWD: Signal A, 230 nm Results

Retention Time	Area	Area %
12.210	371353610	48.65
16.300	392025496	51.35
Totals	763379106	100.00

Figure 4.33: HPLC chromatogram of racemic 7d.

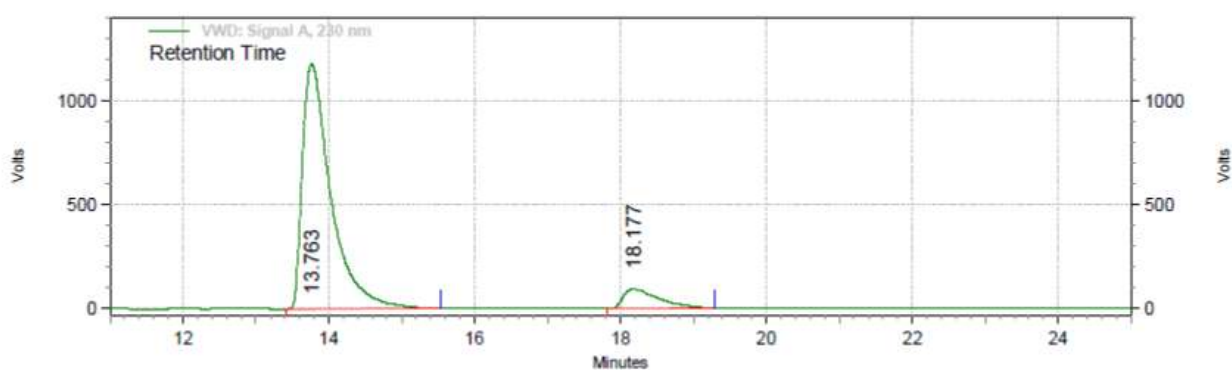
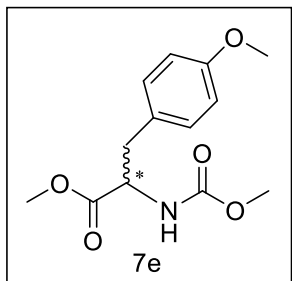


VWD: Signal A, 230 nm Results

Retention Time	Area	Area %
12.373	580107128	95.93
16.463	24607605	4.07
Totals	604714733	100.00

Figure 4.34: HPLC chromatogram of 7d.

Methyl 2-((methoxycarbonyl)amino)-3-(4-methoxyphenyl)propanoate (7e): White solid. HPLC condition: Daicel chiralpak ADH, 1.0 ml/min, UV (λ 230 nm), 10% 2-PrOH/Hexane, t_R (major) = 13.7 min; t_R (minor) = 18.1 min. Procedure A: 68% ee; Procedure B: 82% ee.

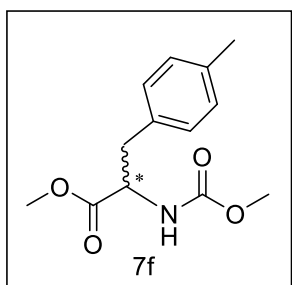


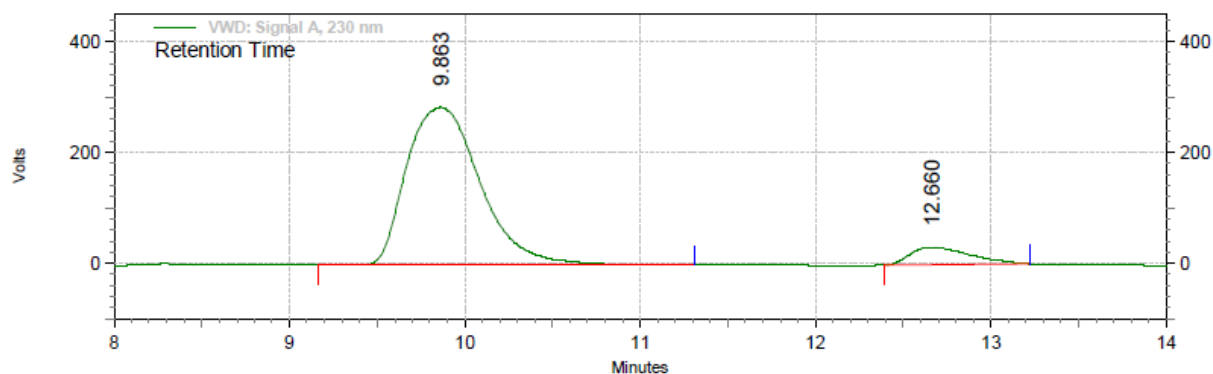
VWD: Signal A, 230 nm Results

Retention Time	Area	Area %
13.763	535140421	91.03
18.177	52753608	8.97
Totals	587894029	100.00

Figure 4.35: HPLC chromatogram of **7e**.

Methyl 2-((methoxycarbonyl)amino)-3-(*p*-tolyl)propanoate (7f): White solid. HPLC condition: Daicel chiralpak ADH, 1.0 ml/min, UV (λ 230 nm), 10% 2-PrOH/Hexane, t_R (major) = 9.8 min; t_R (minor) = 12.6 min. Procedure A: 72% ee; Procedure B: 84% ee.





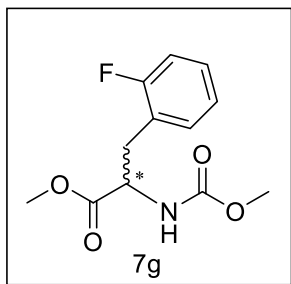
**VWD: Signal A,
230 nm Results**

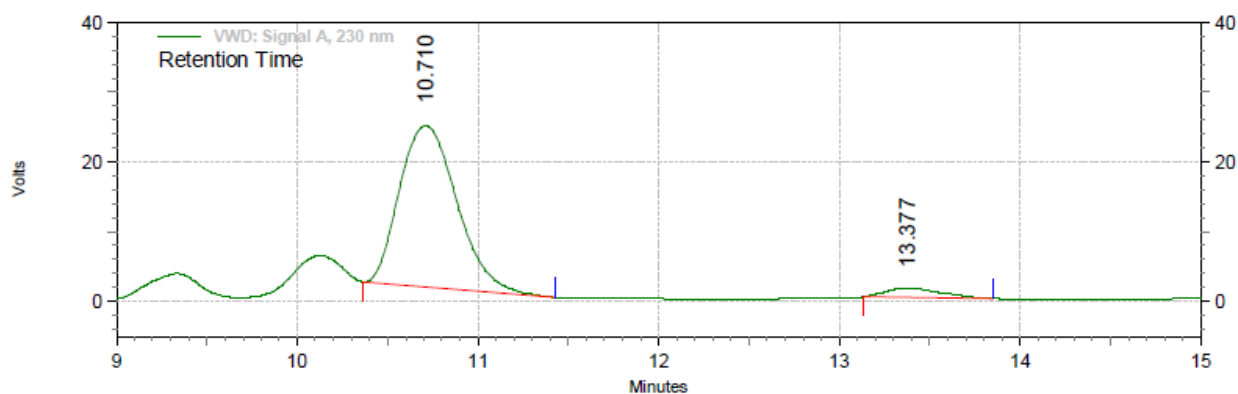
Retention Time	Area	Area %	Height	Height %
9.863	140294007	91.94	4773826	90.10
12.660	12299652	8.06	524338	9.90
Totals				
	152593659	100.00	5298164	100.00

Figure 4.36: HPLC chromatogram of **7f**.

Methyl 3-(2-fluorophenyl)-2-((methoxycarbonyl)amino)propanoate (7g): White solid.

HPLC condition: Daicel chiralpak ADH, 1.0 ml/min, UV (λ 230 nm), 10% 2-PrOH/Hexane, t_R (major) = 10.7 min; t_R (minor) = 13.3 min. Procedure A: 82% ee; Procedure B: 90% ee.



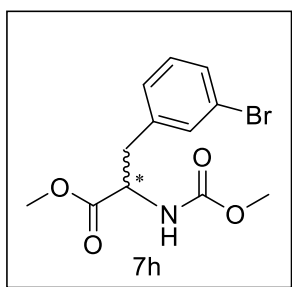


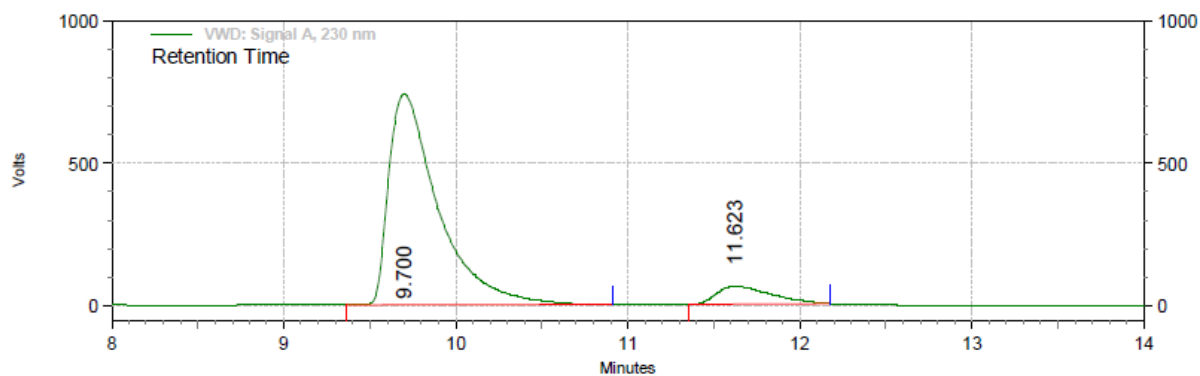
**VWD: Signal A,
230 nm Results**

Retention Time	Area	Area %	Height	Height %	
10.710	8568189	94.76	388156	94.80	
13.377	474269	5.24	21301	5.20	
Totals		9042458	100.00	409457	100.00

Figure 4.37: HPLC chromatogram of **7g**.

Methyl 3-(3-bromophenyl)-2-((methoxycarbonyl)amino)propanoate (7h): White solid.
 HPLC condition: Daicel chiralpak AD-H, 1.0 ml/min, UV (λ 230 nm), 10% 2-PrOH/Hexane,
 t_R (major) = 9.7 min; t_R (minor) = 11.6 min. Procedure A: 74% ee; Procedure B: 81% ee.



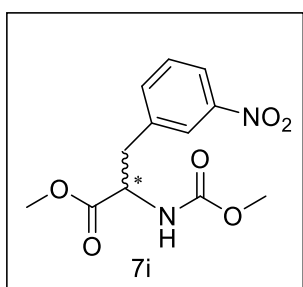


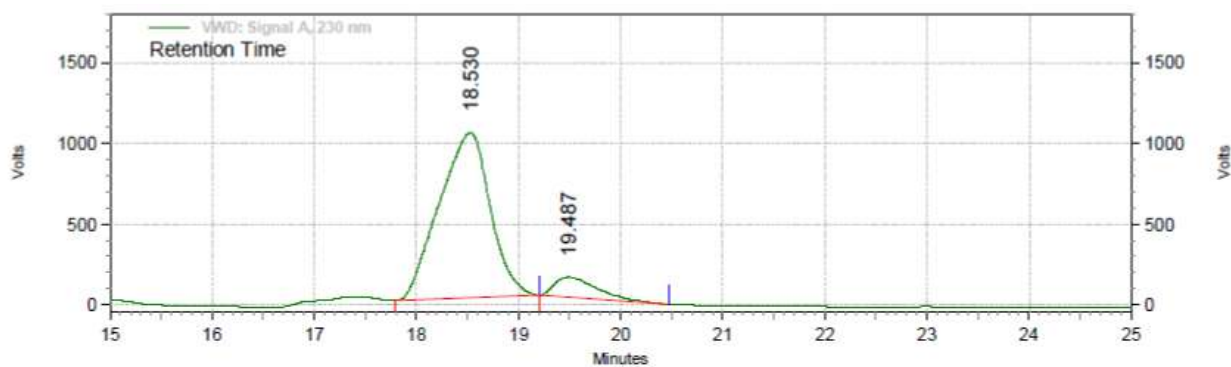
**VWD: Signal A,
230 nm Results**

Retention Time	Area	Area %	Height	Height %	
9.700	248117281	91.50	12412609	92.05	
11.623	23058018	8.50	1071780	7.95	
Totals		271175299	100.00	13484389	100.00

Figure 4.38: HPLC chromatogram of **7h**.

Methyl 2-((methoxycarbonyl)amino)-3-(3-nitrophenyl)propanoate (7i): White solid.
HPLC condition: Daicel chiralpak AD-H, 1.0 ml/min, UV (λ 230 nm), 10% 2-PrOH/Hexane, t_R (major) = 18.5 min; t_R (minor) = 19.4 min. Procedure A: 74% ee; Procedure B: 82% ee.





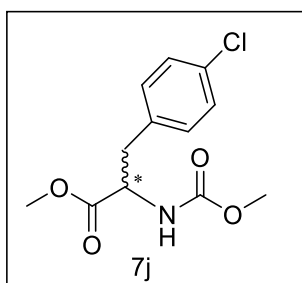
VWD: Signal A, 230 nm Results		
Retention Time	Area	Area %
18.530	595705170	90.75
19.487	60694318	9.25
Totals	656399488	100.00

Figure 4.39: HPLC chromatogram of **7i**.

Methyl 3-(4-chlorophenyl)-2-((methoxycarbonyl)amino)propanoate (7j): White solid.

HPLC condition: Daicel chiralpak AD-H, 1.0 ml/min, UV (λ 230 nm), 10% 2-PrOH/Hexane,

t_R (major) = 11.8 min; t_R (minor) = 14.5 min. Procedure A: 70% ee; Procedure B: 87% ee.



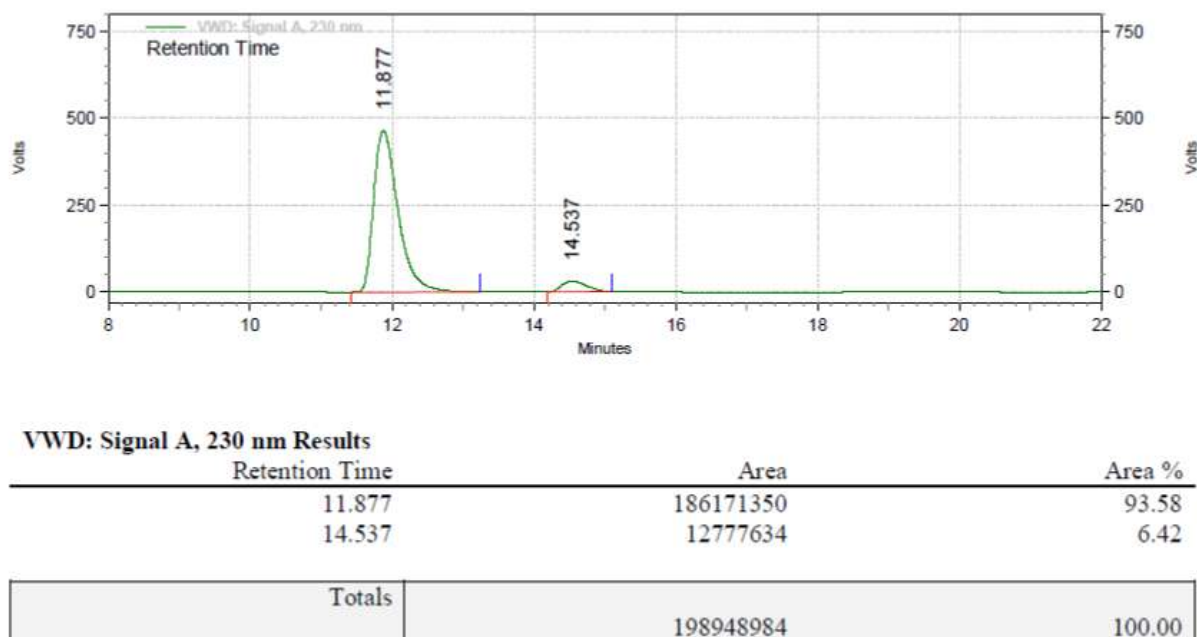
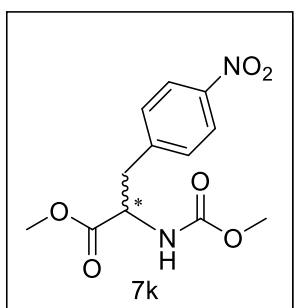
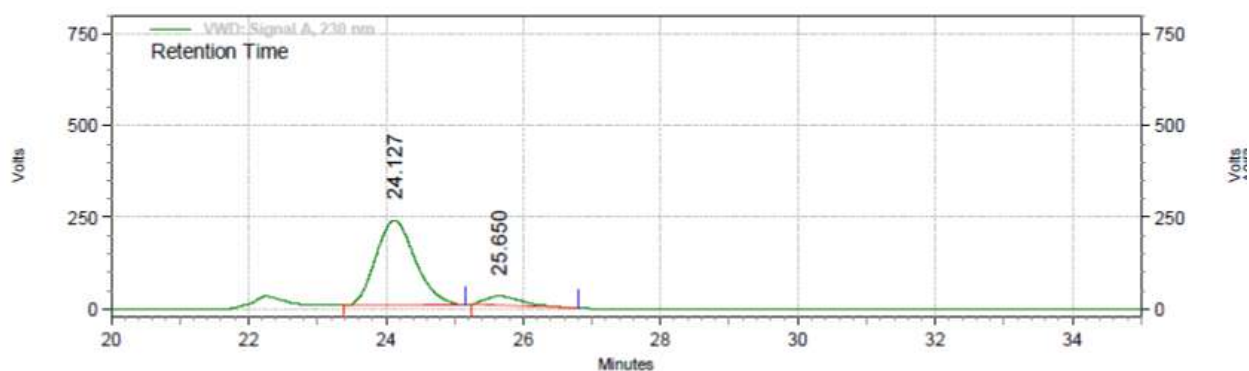


Figure 4.40: HPLC chromatogram of **7j**.

Methyl 2-((methoxycarbonyl)amino)-3-(4-nitrophenyl)propanoate (7k): White solid.
HPLC condition: Daicel chiralpak AD-H, 1.0 ml/min, UV (λ 230 nm), 10% 2-PrOH/Hexane,
 t_R (major) = 24.1 min; t_R (minor) = 25.6 min. Procedure A: 72% ee; Procedure B: 81% ee.

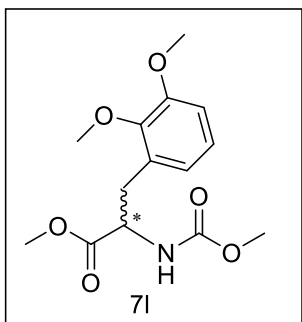


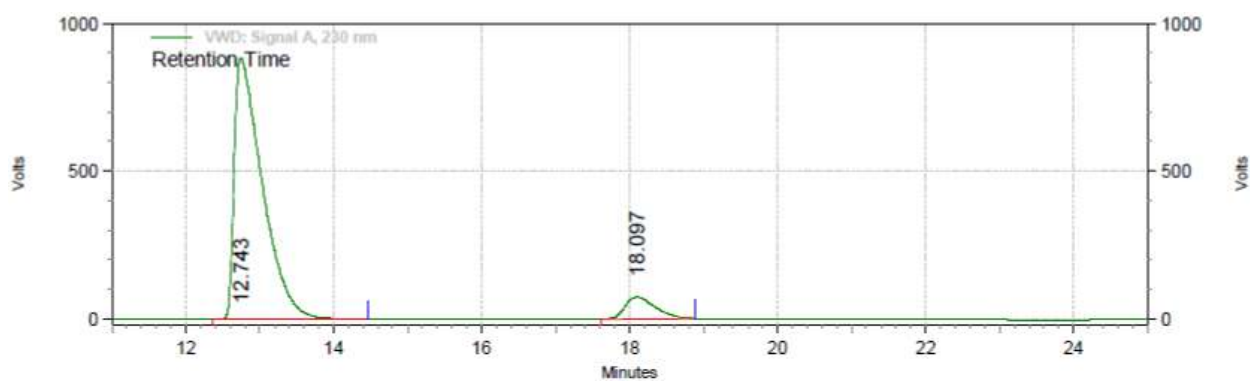


VWD: Signal A, 230 nm Results		
Retention Time	Area	Area %
24.127	155097372	91.19
25.650	14984932	8.81
Totals	170082304	100.00

Figure 4.41: HPLC chromatogram of **7k**.

Methyl 3-(2,3-dimethoxyphenyl)-2-((methoxycarbonyl)amino)propanoate (7l): White solid. HPLC condition: Daicel chiralpak AD-H, 1.0 ml/min, UV (λ 230 nm), 10% 2-PrOH/Hexane, t_R (major) = 12.7 min; t_R (minor) = 18.1 min. Procedure A: 61% ee; Procedure B: 84% ee.

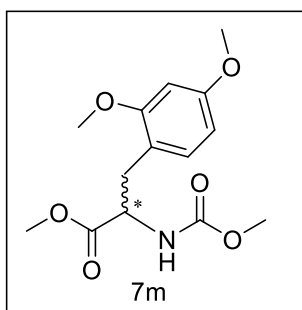


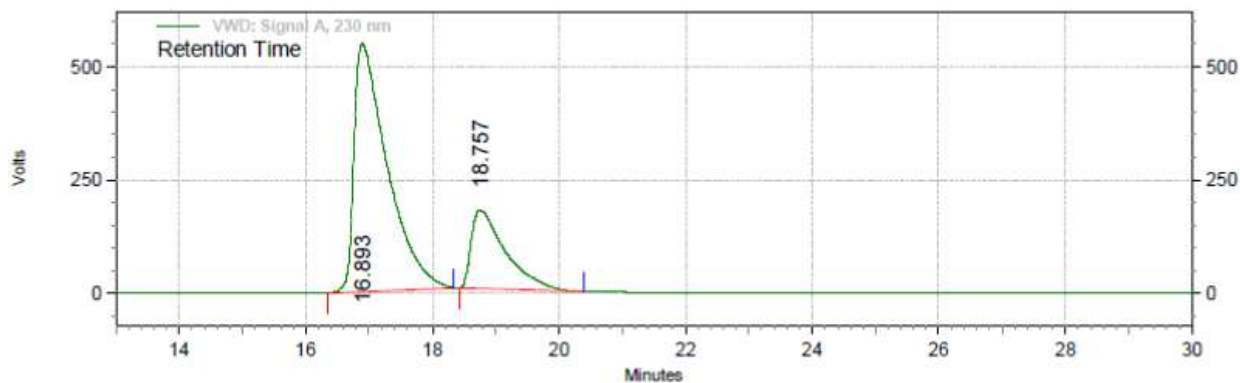
**VWD: Signal A, 230 nm Results**

Retention Time	Area	Area %
12.743	394435111	91.74
18.097	35498735	8.26
Totals	429933846	100.00

Figure 4.42: HPLC chromatogram of **7l**.

Methyl 3-(2,4-dimethoxyphenyl)-2-((methoxycarbonyl)amino)propanoate (7m): White solid. HPLC condition: Daicel chiralpak IB, 1.0 ml/min, UV (λ 230 nm), 10% 2-PrOH/Hexane, t_R (major) = 16.8 min; t_R (minor) = 18.7 min. Procedure A: 51% ee.





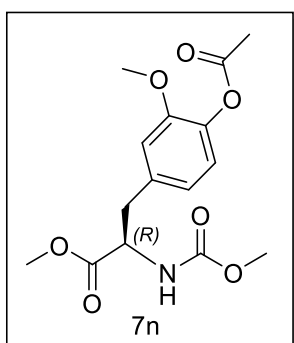
**VWD: Signal A,
230 nm Results**

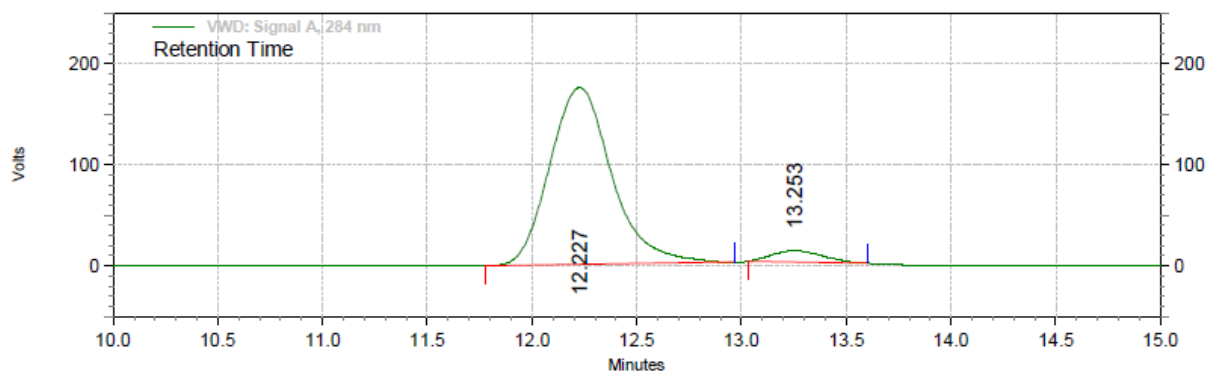
Retention Time	Area	Area %	Height	Height %
16.893	335398642	75.37	9186961	75.90
18.757	109584919	24.63	2917144	24.10
Totals		444983561	12104105	100.00

Figure 4.43: HPLC chromatogram of **7m**.

Methyl (S)-3-(4-acetoxy-3-methoxyphenyl-2-((methoxycarbonyl)amino)propanoate (7n):

White solid. HPLC condition: Daicel chiralpak AD-H, 1.0 ml/min, UV (λ 284 nm), 15% 2-PrOH/Hexane, t_R (major) = 12.2 min; t_R (minor) = 13.2 min. Methyl (S)-3-(4-acetoxy-3-methoxyphenyl-2-((methoxycarbonyl)amino)propanoate shows $[\alpha]^{25} = -61^\circ$ (c 2.0, CHCl_3) rotation. By comparing the above specific rotation with literature, it has been assigned to be (*R*) isomer of **7n**.⁶⁴ Procedure A: 79% ee; Procedure B: 90% ee.



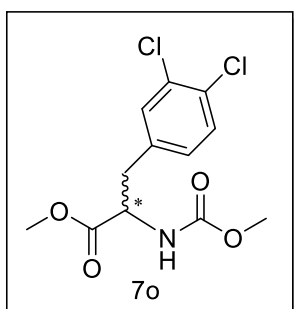


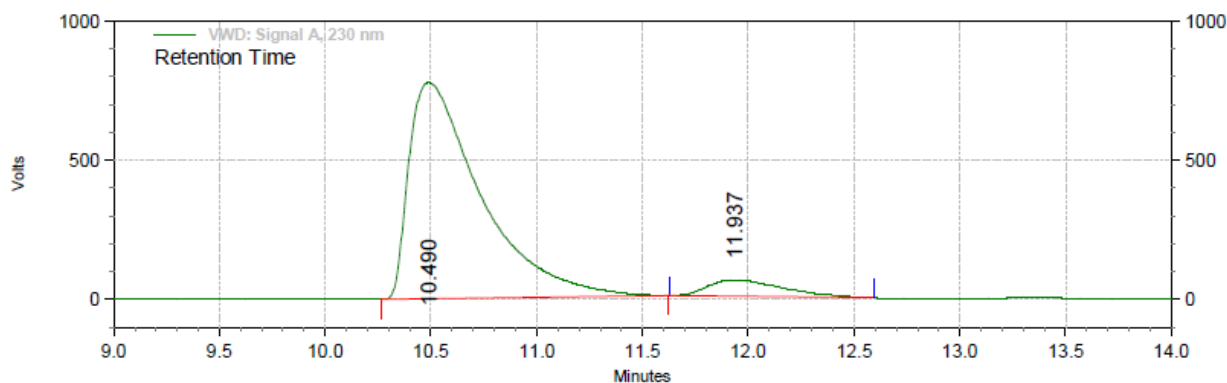
**VWD: Signal A,
284 nm Results**

Retention Time	Area	Area %	Height	Height %
12.227	60640926	95.04	2939032	94.07
13.253	3164687	4.96	185365	5.93
Totals				
	63805613	100.00	3124397	100.00

Figure 4.44: HPLC chromatogram of **7n**.

Methyl 3-(3,4-dichlorophenyl)-2-((methoxycarbonyl)amino)propanoate (7o): White solid. HPLC condition: Daicel chiralpak AD-H, 1.0 ml/min, UV (λ 284 nm), 15% 2-PrOH/Hexane, t_R (major) = 10.5 min; t_R (minor) = 11.9 min. Procedure A: 50% ee; Procedure B: 86% ee.





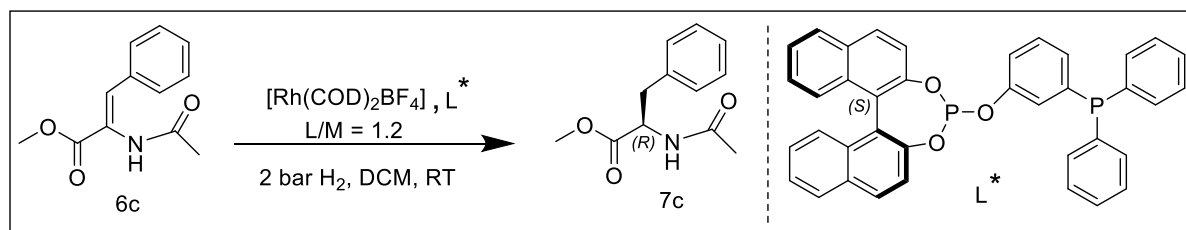
**VWD: Signal A,
230 nm Results**

Retention Time	Area	Area %	Height	Height %
10.490	308543842	92.69	13045142	93.03
11.937	24334422	7.31	976745	6.97
Totals	332878264	100.00	14021887	100.00

Figure 4.45: HPLC chromatogram of **7o**.

4.4.8 High turn-over number experiment:

General procedure: The asymmetric hydrogenation experiments were carried out in a stainless steel autoclave (450 mL) equipped with pressure inlet-outlet, safety rupture valve and pressure gauge. Required quantity of substrate was taken in a glass vial inside a glove box. A stock solution of $[\text{Rh}(\text{COD})_2\text{BF}_4]$ and **L1** was prepared. From this stock solution, required (as reported in Table 4.5.) amount of **L1** and Rh-precursor solution was added to the glass vials. Subsequently, required quantity of solvent was added along with Teflon stirring bars. The charged vials were transferred to autoclave under the positive flow of argon and septa was removed. Before starting the catalytic reactions, the charged autoclave was purged three times with 5 bars of dihydrogen and then pressurized to 2 bars. The reaction mixture was stirred at room temperature for stipulated time as shown below (Table 4.5.). After asymmetric hydrogenation, excess gas was vented. The reaction mixture was passed through a short column of silica gel using dichloromethane as the eluent to remove the rhodium catalyst. The solvent was removed under reduced pressure and the product was dried under vacuum. The conversion and enantioselectivity were determined by HPLC using Chiralpak-IB column.



Scheme 4.11: Asymmetric hydrogenation of methyl-2-acetamido-3-phenylacrylate (**6c**).

Table 4.5. Rhodium-phosphine-phosphite catalyzed asymmetric hydrogenation of **6c** to **7c**.

Entry	Subst. (mmol)	DCM (ml)	Cat. (mol %)	Conv. %	Time (hr)	Temp. (°C)	ee%	TON
1	0.25	1	0.125	94	1	30	86	188
2	0.5	2	0.125	92	2	28	87	368
3	1.0	4	0.125	>99	5	28	78	800
4	1.25	5	0.125	>99	12	25	78	1000

Conditions: H₂ pressure: 2 bar.

4.4.9 DOPA synthesis

The asymmetric hydrogenation product **7n** is the penultimate DOPA precursor. 95 mg (0.307 mmol) of **7n** was taken in a round bottom flask. 1 mL HBr and 1 mL AcOH was added to it and the content was heated to 100 °C for 6 hours. Subsequently, volatiles were evaporated under vacuum and were collected in a liquid nitrogen trap. The residue was washed properly by diethyl ether, hexane and dichloromethane twice (2 × 5 mL). The liquid solvent was decanted and the compound was dried under vacuum to obtain 54 mg (88% yield) of solid. ¹H NMR suggests the formation of DOPA.

¹H NMR (200 MHz, D₂O, 298K) δ = 2.96-3.07 (m, 2H), 4.16 (t, 1H), 6.57-6.77 (m, 3H).

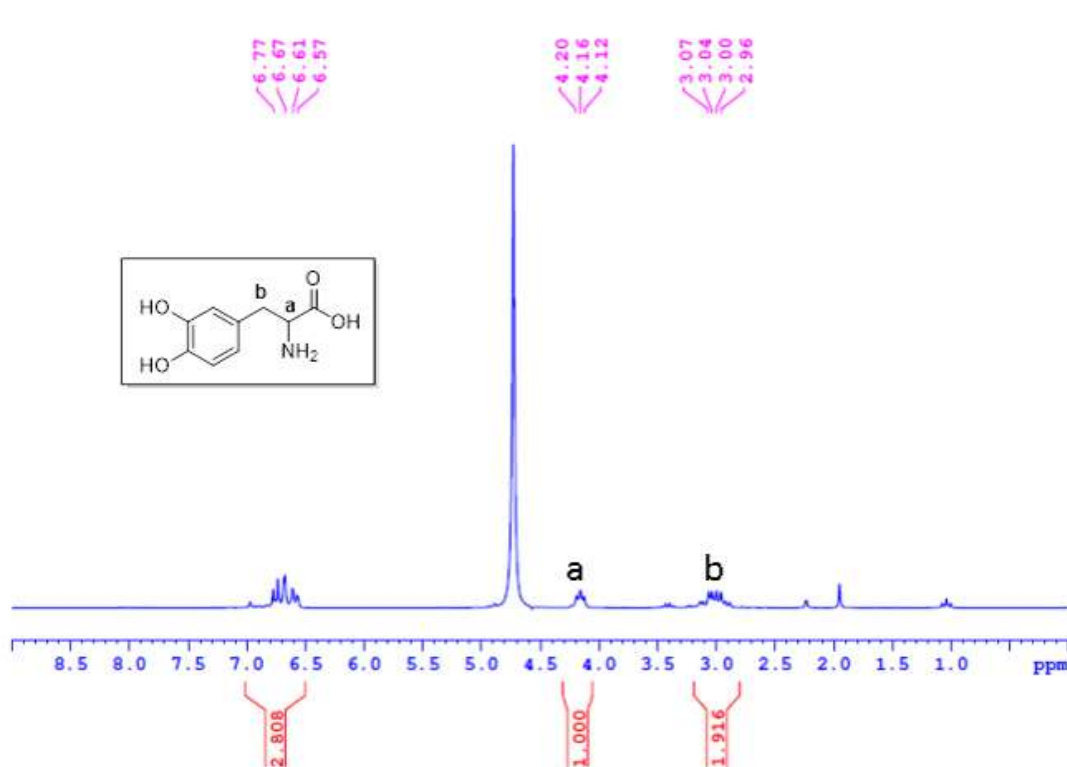
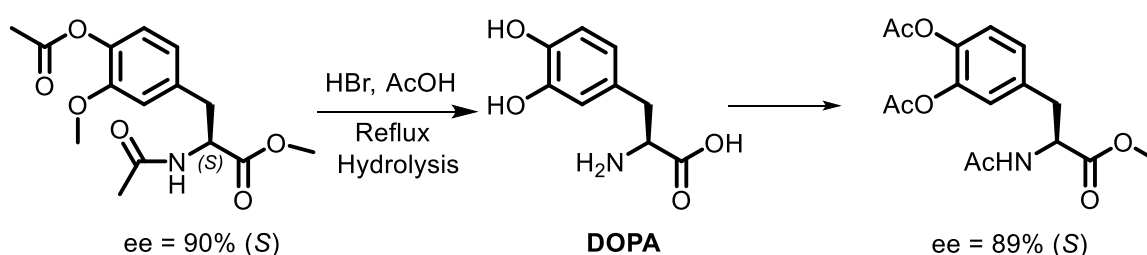


Figure 4.46: ^1H NMR spectrum of D-DOPA.

4.4.10 Establishing the enantiomeric excess after hydrolysis of 7n

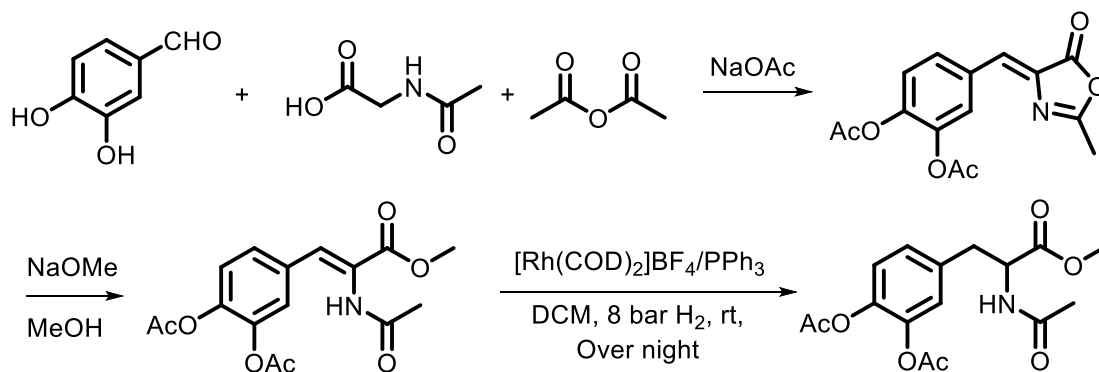
The DOPA was not soluble in organic solvents. Therefore, the hydroxyl groups were protected and DOPA was transformed to 4-(2-acetamido-3-methoxy-3-oxopropyl)-1,2-phenylene diacetate using a literature reported procedure.⁶⁵ The resultant compound was subjected to HPLC analysis after establishing a method using racemic 4-(2-acetamido-3-methoxy-3-oxopropyl)-1,2-phenylene diacetate.



Scheme 4.12: Determination of enantiomeric excess of DOPA after hydrolysis.

The racemic compound (Z)-4-((2-methyl-5-oxooxazol-4(5H)-ylidene)methyl)-1,2-phenylene diacetate was prepared by following a literature reported procedure.⁶⁶ The azalactone (1 g, 3.3 mmol, 1 equiv) was suspended in anhydrous MeOH (15 ml) and MeONa was added to it (216 mg, 4 mmol, 1.2 equiv). The content was stirred for 6 hours at room temperature. The

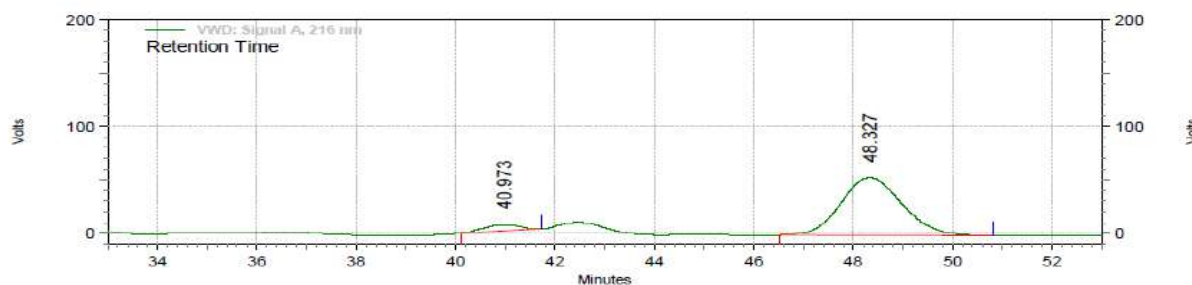
reaction progress was monitored by TLC and after completion of the reaction volatiles were evaporated. The resultant residue was partitioned between DCM (50 ml) and saturated NH_4Cl solution (50 ml). The organic phase was separated, washed with brine and dried over Na_2SO_4 . It was concentrated and finally purified by silica gel column chromatography.



Scheme 4.13: Synthesis of (Z)-4-(2-acetamido-3-methoxy-3-oxoprop-1-en-1-yl)-1,2-phenylene diacetate and its hydrogenation.

The acetoxy protected compound was hydrogenated by using $[\text{Rh}(\text{COD})_2\text{BF}_4]/\text{PPh}_3$ (1 mol%, L/M = 2.2) in DCM under 8 bar hydrogen pressure at room temperature. The hydrogenation reaction was confirmed by $^1\text{H-NMR}$ spectroscopy. Finally, HPLC method was developed for this racemic compound. HPLC Method: Daicel chiralpak IC, 1.0 ml/min, UV (λ 216 nm), 20% 2-PrOH/Hexane, t_{R} (minor) = 40.9 min; t_{R} (major) = 48.3 min.

After establishing a HPLC method for above racemic sample, the ee for chiral 4-(2-acetamido-3-methoxy-3-oxopropyl)-1,2-phenylene diacetate was determined. The ee was found to be 89% after protecting the DOPA. These observations suggest that the enantiomeric excess remains almost unaffected after hydrolysis which is also in accordance with the literature reports.⁶⁷



**VWD: Signal A,
216 nm Results**

Retention Time	Area	Area %	Height	Height %
40.973	4554764	5.61	89370	9.00
48.327	76664874	94.39	903544	91.00
Totals	81219638	100.00	992914	100.00

Figure 4.47: HPLC chromatogram of protected (after hydrolysis) DOPA.

4.5 Conclusions

In summary, understanding the reactivity difference between two nucleophiles through ^{31}P NMR and, sequential addition of chlorodiphenylphosphine and phosphochloridite to 3-iodophenol revealed the selective formation of the hybrid phosphine-phosphite ligand 4-(3-(diphenylphosphinanyl)phenoxy)dinaphtho[2,1-*d*:1',2'-*f*][1,3,2]dioxaphosphepine (L1 or Senphos) in one pot. ^{31}P NMR spectrum unraveled two singlets at -5.14 and 144.24 ppm, confirming the existence of Senphos, which was isolated as a white solid in 72% yield. The reaction of Senphos with $[\text{Rh}(\text{COD})_2\text{BF}_4]$ disclosed doublet-of-doublet in a ^{31}P NMR spectrum, suggesting bidentate coordination of L1 to the rhodium center. Senphos was found to catalyze asymmetric hydrogenation of Methyl 3-acetamidoacrylate within 5 minutes at 2 bar hydrogen pressure. An unprecedented turn over frequency (TOF) of 2289 was observed in the Senphos-Rh catalyzed AH of Methyl-2-acetamido-3-phenylacrylate under mild conditions. Following the initial success, the performance of L1 was evaluated in the AH of an array of substituted alkenes and the corresponding products 7a-7o were obtained with excellent enantiomeric excess (up to 92%), high TOF and TON. The synthetic utility of Senphos was demonstrated by scaling up the reaction to 1 g scale and by preparing DOPA, a drug used in the treatment of Parkinson. Comparison with bidentate bis-phosphine (L2) and bis-phosphite (L3) ligand authenticated the dominance of L1, as it outperformed the parent symmetrical counterparts. Remarkably, a comparison with literature reported hybrid phosphine-phosphite ligands further proved the outstanding reactivity of L1.

4.6 References

- (1) Noyori, R. *Adv. Synth. Catal.* **2003**, *345*, 15–32.
- (2) Knowles, W. S. *Angew. Chem., Int. Ed.* **2002**, *41*, 1998–2007.
- (3) Noyori, R.; Ohkuma, T. *Angew. Chem., Int. Ed.* **2001**, *40*, 40–73.
- (4) Ager, D. J.; de Vries, A. H. M.; de Vries, J. G. *Chem. Soc. Rev.* **2012**, *41*, 3340–3380.
- (5) Etayo, P.; Vidal-Ferran, A. *Chem. Soc. Rev.* **2013**, *42*, 728–754.
- (6) Meemken, F.; Baiker, A. *Chem. Rev.* **2017**, *117*, 11522–11569.
- (7) Xie, X.; Lu, B.; Li, W.; Zhang, Z. *Coord. Chem. Rev.* **2018**, *355*, 39–53.
- (8) Seo, C. S. G.; Morris, R. H. *Organometallics* **2019**, *38*, 47–65.
- (9) Kraft, S.; Ryan, K.; Kargbo, R. G. *J. Am. Chem. Soc.* **2017**, *139*, 11630–11641.
- (10) Margarita, C.; Andersson, P. G. *J. Am. Chem. Soc.* **2017**, *139*, 1346–1356.
- (11) Tang, W.; Zhang, X. *Chem. Rev.* **2003**, *103*, 3029–3069.
- (12) Verendel, J. J.; Pamies, O.; Dieguez, M.; Anderson, P. G. *Chem. Rev.* **2014**, *114*, 2130–2169.
- (13) Chirik, P. *Acc. Chem. Res.* **2015**, *48*, 1687–1695.
- (14) Fernández-Pérez, H.; Etayo, P.; Panossian, A.; Vidal-Ferran, A. *Chem. Rev.* **2011**, *111*, 2119–2176.
- (15) Pereira, M. M.; Calvete, M. J. F.; Carrilho, R. M. B.; Abreu, A. R. *Chem. Soc. Rev.* **2013**, *42*, 6990–7027.
- (16) van Leeuwen, P. W. N. M.; Kamer, P. C. J.; Claver, C.; Pámies, O.; Diéguez, M. *Chem. Rev.* **2011**, *111*, 2077–2118.
- (17) Lühr, S.; Holz, J.; Börner, A. *ChemCatChem* **2011**, *3*, 1708–1730.
- (18) Xie, J. H.; Zhou, Q. L. *Acc. Chem. Res.* **2008**, *41*, 581–593.
- (19) Hetterscheid, D. G. H.; Chikkali, S. H.; de Bruin, B.; Reek, J. N. H. *ChemCatChem* **2013**, *5*, 2785–2793.
- (20) Chikkali, S. H.; van der Vlugt, J. I.; Reek, J. N. H. *Coord. Chem. Rev.* **2014**, *262*, 1–15.
- (21) de Vries, J. G. *Top. Catal.* **2014**, *57*, 1306–1317.
- (22) Beliaev, A. *Org. Process Res. Dev.* **2016**, *20*, 724–732.
- (23) Knowles, W. S.; Noyori, R. *Acc. Chem. Res.* **2007**, *40*, 1238–1239.
- (24) Shultz, S. C.; Krska, S. W. *Acc. Chem. Res.* **2007**, *40*, 1320–1326.
- (25) Johnson, N. B.; Lennon, I. C.; Moran, P. H.; Ramsden, J. A. *Acc. Chem. Res.* **2007**, *40*, 1291–1299.

-
- (26) Hazeland, E. L.; Chapman, A. M.; Pringle, P. G.; Sparkes, H. A. *Chem. Commun.* **2015**, *51*, 10206–10209.
- (27) Pámies, O.; Magre, M.; Diéguez, M. *Chem. Rec.* **2016**, *16*, 1578–1590.
- (28) Lindner, R.; van den Bosch, B.; Lutz, M.; Reek, J. N. H.; van der Vlugt, J. I. *Organometallics* **2011**, *30*, 499–510.
- (29) Meeuwissen, J.; Reek, J. N. H. *Nat. Chem.* **2010**, *2*, 615–621.
- (30) Wieland, J.; Breit, B. *Nat. Chem.* **2010**, *2*, 832–837.
- (31) Mote, N. R.; Chikkali, S. H. *Chem. Asian J.* **2018**, *13*, 3623–3646.
- (32) Renom-Carrasco, M.; Lefort, L. *Chem. Soc. Rev.* **2018**, *47*, 5038–5060.
- (33) Velder, J.; Robert, T.; Weidner, I.; Neudörfl, J. M.; Lex, J.; Schmalz, H.-G. *Adv. Synth. Catal.* **2008**, *350*, 1309–1315.
- (34) Baber, R. A.; Clarke, M. L.; Orpen, A. G.; Ratcliffe, D. A. *J. Organomet. Chem.* **2003**, *667*, 112–119.
- (35) Fernández-Pérez, H.; Benet-Buchholz, J.; Vidal-Ferran, A. *Org. Lett.* **2013**, *15*, 3634–3637.
- (36) Arribas, I.; Vargas, S.; Rubio, M.; Suárez, A.; Domene, C.; Alvarez, E.; Pizzano, A. *Organometallics* **2010**, *29*, 5791–5804.
- (37) Pámies, O.; Diéguez, M.; Net, G.; Ruiz, A.; Claver, C. *Chem. Commun.* **2000**, 2383–2384.
- (38) Baker, M. J.; Pringle, P. G. *Chem. Commun.* **1993**, 314–316.
- (39) For commonly observed chemical shifts of such phosphines, see: Chikkali, S.; Gudat, D. *Eur. J. Inorg. Chem.* **2006**, *2006*, 3005–3009.
- (40) The ^{31}P NMR chemical shift assignment is based on literature, see: Bedford, R. B.; Draper, S. M.; Scully, P. N.; Welch, S. L. *New J. Chem.* **2000**, *24*, 745–747.
- (41) See experimental section for details.
- (42) Almena, J.; Foubelo, F.; Yus, M. *Tetrahedron* **1995**, *51*, 3365–3374.
- (43) Pastor, I. M.; Yus, M. *Tetrahedron* **2001**, *57*, 2365–2370 and the reference therein.
- (44) The observed ^{31}P NMR chemical shifts are in line with reported phosphine-phosphite shifts, see: Dindaroğlu, M.; Falk, A.; Schmalz, H.-G. *Synthesis* **2013**, *45*, 527–535.
- (45) Nozaki, K.; Sakai, N.; Nanno, T.; Higashijima, T.; Mano, S.; Horiuchi, T.; Takaya, H. *J. Am. Chem. Soc.* **1997**, *119*, 4413–4423.
- (46) Deerenberg, S.; Kamer, P. C. J.; van Leeuwen, P. W. N. M. *Organometallics* **2000**, *19*, 2065–2072.
-

- (47) Molina, D. A. C.; Casey, C. P.; Müller, I.; Nozaki, K.; Jäkel, C. *Organometallics* **2010**, *29*, 3362–3367.
- (48) Chikkali, S. H.; Bellini, R.; de Bruin, B.; van der Vlugt, J. I.; Reek, J. N. H. *J. Am. Chem. Soc.* **2012**, *134*, 6607–6616.
- (49) Knowles, W. S.; Sabacky, M. J.; Vineyard, B. D.; Weinkauff, D. J. *J. Am. Chem. Soc.* **1975**, *97*, 2567–2568.
- (50) Vineyard, B. D.; Knowles, W. S.; Sabacky, M. J.; Bachman, G. L.; Weinkauff, D. J. *J. Am. Chem. Soc.* **1977**, *99*, 5946–5952.
- (51) McFarlane, H. C. E.; McFarlane, W. *Polyhedron* **1988**, *7*, 1875–1879.
- (52) Etayo, P.; Núñez-Rico, J. L.; Vidal-Ferran, A. *Organometallics* **2011**, *30*, 6718–6725.
- (53) Lao, J. R.; Benet-Buchholz, J.; Vidal-Ferran, A. *Organometallics* **2014**, *33*, 2960–2963.
- (54) Fernández-Pérez, H.; Donald, S. M. A.; Munslow, I. J.; Benet-Buchholz, J.; Maseras, F.; Vidal-Ferran, A. *Chem. Eur. J.* **2010**, *16*, 6495–6508.
- (55) Huang, J.; Hong, M.; Wang, C.-C.; Kramer, S.; Lin, G.-Q.; Sin, X.-W. *J. Org. Chem.* **2018**, *83*, 12838–12846.
- (56) Selke, R.; Pracejus, H. *J. Mol. Catal.* **1986**, *37*, 213–225.
- (57) (a) Didyo, P.; Detz, R.; de Bruin, B.; Reek, J. N. H. *J. Am. Chem. Soc.* **2014**, *136*, 23, 8418–8429. (b) Ini, S.; Oliver, A. G.; Tilley, T. D.; Bergman, R. G. *Organometallics* **2001**, *20*, 18, 3839–3841.
- (58) Jia, J.; Ling, Z.; Zhang, Z.; Tamura, K.; Gridnev, I. D.; Imamoto, T.; Zhang, W. *Adv. Synth. Catal.* **2018**, *360*, 738–743.
- (59) Xu, K.; Yang, R.; Yang, S.; Jiang, C.; Ding, Z. *Org. Biomol. Chem.* **2019**, *17*, 8977–8981.
- (60) Khair, N.; Navas, R.; Suárez, B.; Álvarez, E.; Farnández, I. *Org. Lett.* **2008**, *10*, 3697–3700.
- (61) Willans, C. E.; Mulders, J. M. C. A.; de Vries, J. G.; de Vries, A. H. M. *J. Organomet. Chem.* **2003**, *687*, 494–497.
- (62) Wong, H. N. C.; Xu, Z. L.; Chang, H. M.; Lee, C. M. *Synthesis* **1992**, *1992*, 793–797.

- (63) Huang, J.; Hong, M.; Wang, C.-C.; Kramer, S.; Lin, G.-Q.; Sin, X.-W. *J. Org. Chem.* **2018**, *83*, 12838–2846.
- (64) Selke, R.; Pracejus, H. *J. Mol. Catal.* **1986**, *37*, 213–225.
- (65) Lyu, Q.; Zhang, J.; Neoh, K. G.; Li, C.; Chai, C. L. L. *Nanoscale* **2017**, *9*, 12409-12415.
- (66) Rosini, E.; Melis, R.; Molla, G.; Tessaro, D.; Pollegioni, L. *Adv. Synth. Catal.* **2017**, *359*, 3773-3781.
- (67) Oh, J.-S.; Lee, J.-W.; Ryu, T. H.; Lee, J. H.; Song, C. E. *Org. Biomol. Chem.* **2012**, *10*, 1052-1055.

Chapter 5

Summary and Outlook

This chapter has been partly adapted from following publication

Sen, A.; Chikkali, S. *Org. Biomol. Chem.*, **2021**, *19*, 9095-9137.

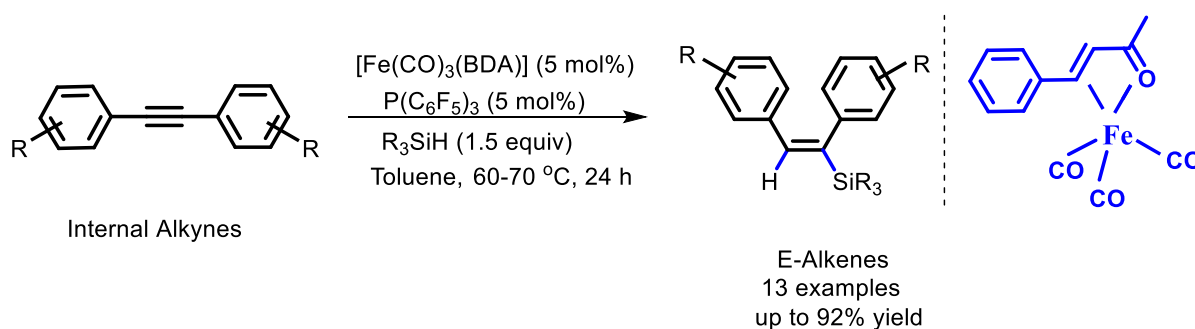
5.1 Summary

The journey of homogeneous catalysis revolves around the design and synthesis of metal-ligand complexes for different catalytic transformations. Most of these transformations in homogeneous catalysis involve the use of noble metals such as Pt, Pd, Rh, Ru, Ir etc. These metals, however, have very low abundance on the earth crust and will be finished within the coming few decades which poses a serious threat to the field from sustainability point of view. At the same time, most of the ligands used in catalysis (especially chiral ligands used in asymmetric catalysis) involve multiple step synthesis which often make these ligands even costlier than the precious metals. Thus, the field of homogeneous catalysis is facing a flux from both the metal as well as ligand synthesis frontier. In this context, the present thesis, entitled as **“Chiral Ligand and Transition Metal (Fe, Rh) Complexes for Catalytic Alkoxylation, Polymerization, Hydrosilylation and Hydrogenation”** describes the development of new synthetic methodologies to prepare organosilanes using earth abundant transition metal iron as well as one pot synthesis of a bidentate chiral phosphine ligand for asymmetric hydrogenation to prepare chiral compounds.

The chapter 1 briefly describes the importance of homogeneous catalysis, specially to prepare different organo-silicon compounds due to their wide range of applications in silicon polymer chemistry, protecting group chemistry, organic-inorganic hybrid materials and surface coating chemistry as well as different chiral compounds used as drugs and pharmaceuticals. However, most of the organo-silicon compounds are prepared by using noble transition metals (4d, 5d) which have very low natural abundance on earth's crust, thus very costly. To address these challenges, researchers have employed naturally abundant and cost-effective 3d transition metals for such transformation. Though it could resolve the issue of high cost and sustainability, the harsh reaction conditions and use of highly reactive reagents often limit their practical applicability. Thus, there is an enormous demand to design concise, practical, sustainable synthetic approaches using 3d transition metal catalysts through which one can perform these transformations under ambient conditions without using any highly reactive reagent. In addition to this, the bidentate chiral phosphine ligands used in asymmetric hydrogenation along with noble metals, to prepare chiral compounds, involve multistep synthesis, thus often making these ligands even costlier than the noble metals. Although, good attention has already been paid to replace these precious noble metals with earth abundant 3d transition metals, simplifying the ligand synthesis remains mostly ignored. So, there is a

pressing need to develop ligands which could be synthesized much more easily. Thus, the first chapter sets the objective for the thesis.

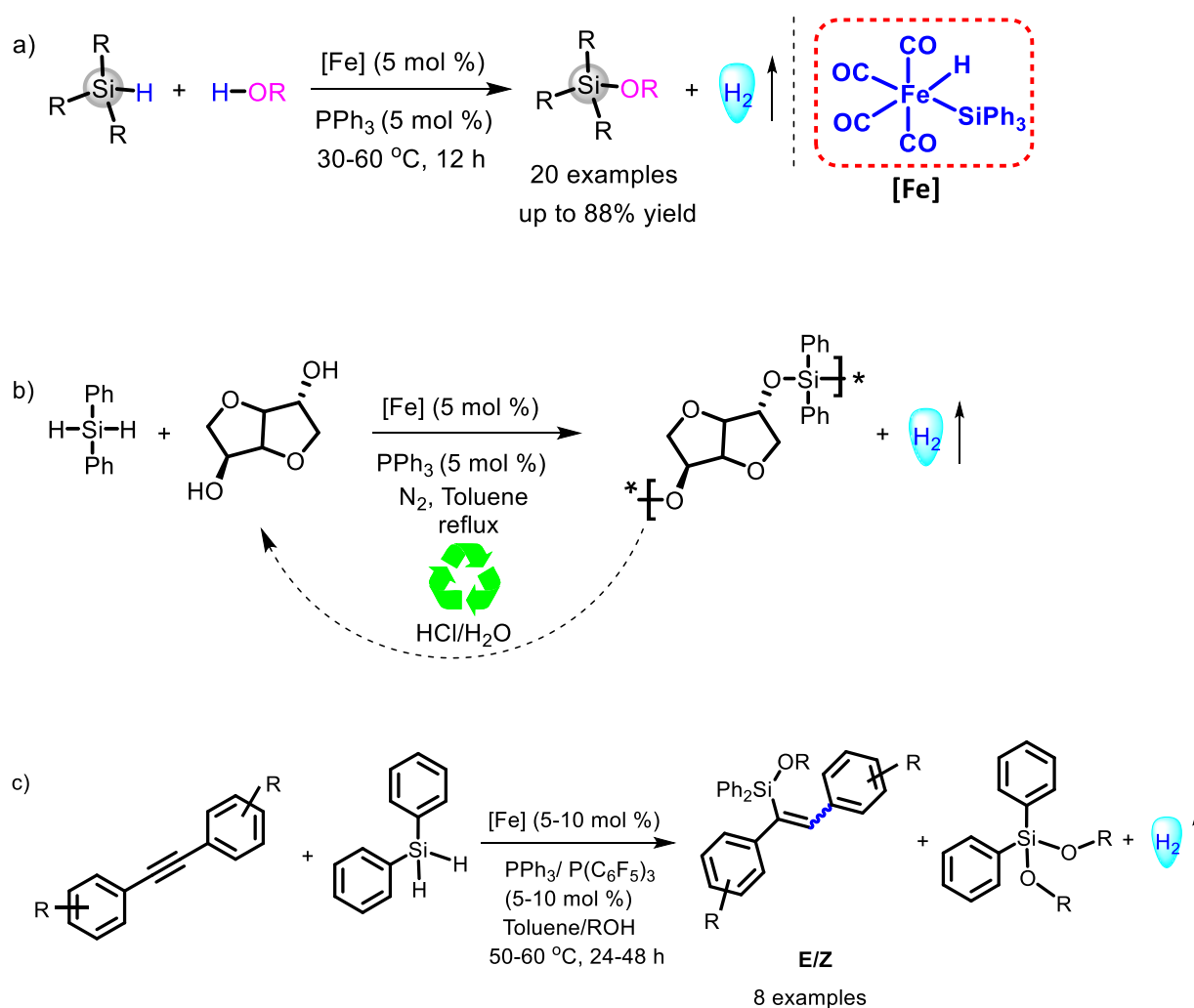
Hydrosilylation of alkynes represent one of the most straightforward, atom economical method to prepare organo-silicon compounds. In literature, few reports are there where iron catalysts have been successfully implemented for the hydrosilylation of internal alkynes. However, in all these reports, either organometallic reagents or organic bases have been used for the success of the reaction which often creates a problem for the functional group tolerance of the reaction. Thus, development of an additive free methodology would be highly useful. Chapter 2 discusses the development of iron catalysed (E)-selective hydrosilylation of internal alkynes along with a phosphine ligand without the use of any highly reactive additive. The hydrosilylation reaction exhibited broad substrate scope and tolerated functional groups, such as -Cl, -Br, -OMe, with different types of silanes at 60 to 70 °C (Scheme 1). The reaction can easily be scaled up to gram scale. A preliminary mechanistic investigation revealed a radical pathway for the reaction. (E)-selective hydrosilylation proceeding through one electron pathway, is quite uncommon in literature. To the best of our knowledge, this type of phenomenon has not been previously known with base metal catalysts.



Scheme 5.1: (E)-Selective hydrosilylation of internal Alkynes by iron complex along with a phosphine ligand.

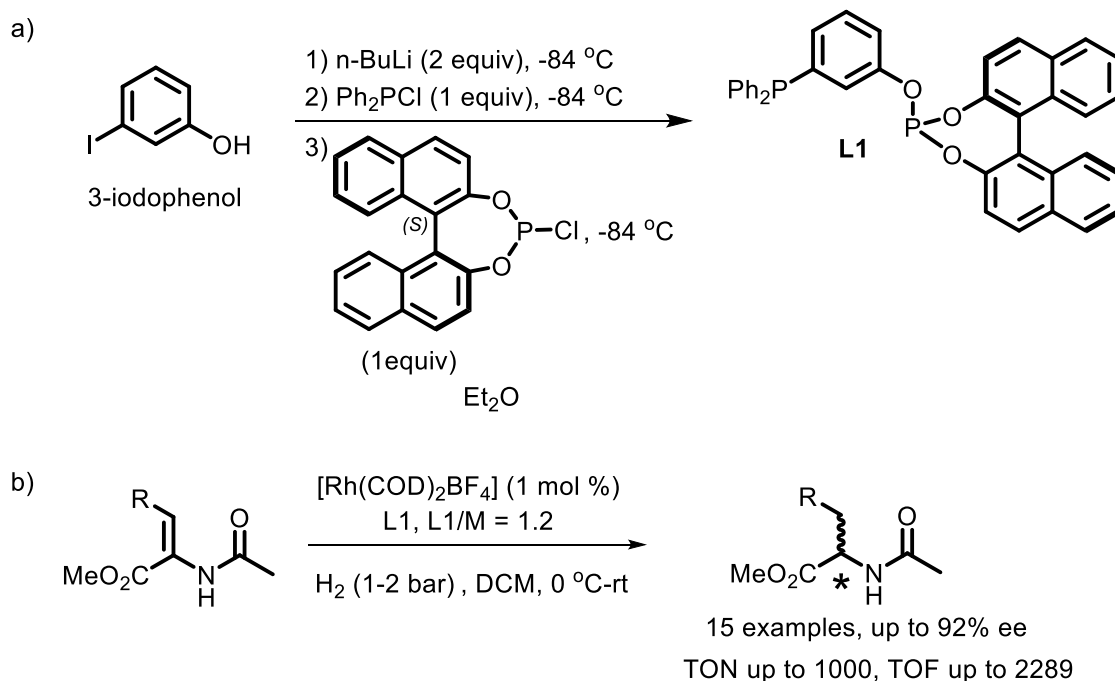
Silyl ethers are an important class of organosilanes which have found profound application in silicon polymers, protecting group chemistry, organic-inorganic hybrid materials and surface coating chemistry. For hydrosilane alcoholysis, a variety of transition metal complexes along with main group Lewis acid/base catalysts have been developed. Surprisingly, iron is not well explored for this reaction. As a result, developing more efficient and selective iron catalyst for silane alcoholysis is highly desirable. To achieve this, we synthesized an iron catalyst by following a literature-reported procedure and successfully developed an iron-catalysed methodology for alkoxylation of silanes to produce silyl ethers and hydrogen gas as the only by-product (Chapter 3). The reaction works efficiently with different silanes as well as different

alcohols containing electron donating as well as electron withdrawing groups. To demonstrate the synthetic utility of this methodology, the iron catalyst was successfully implemented to synthesize degradable polysilylether from bio-based isosorbide and commercially available diphenylsilane by dehydrogenative cross-coupling. Finally, this iron catalyst was successfully utilised to develop a methodology of tandem alkoxylation-hydrosilylation of internal alkynes, which would pave the way for a novel approach to create structurally diverse organosilicon compounds (Scheme 5.2). In literature, only one platinum-catalyst is known to achieve such transformation.



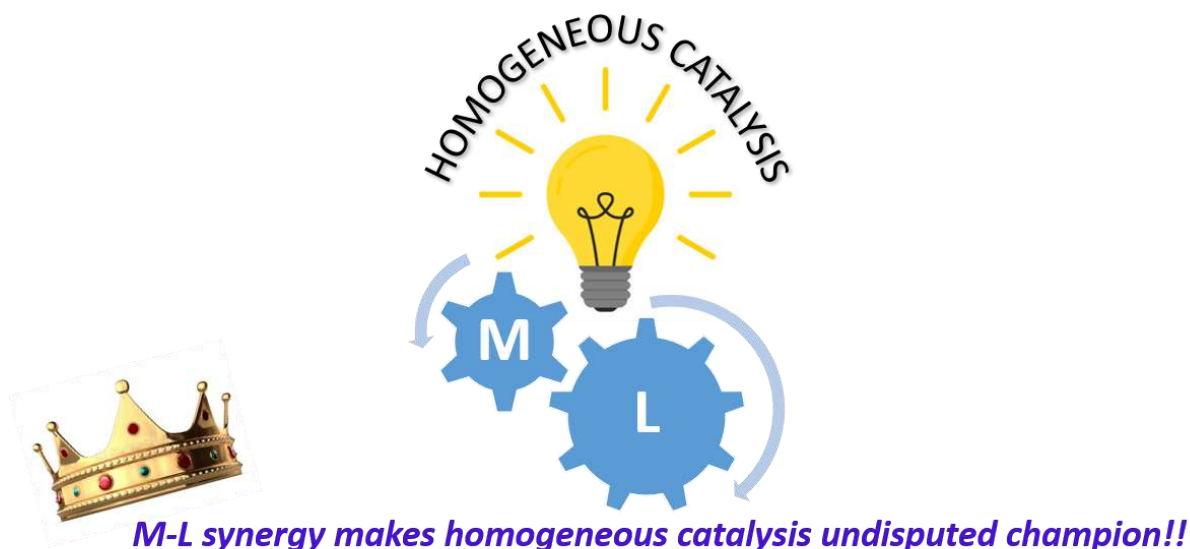
Scheme 5.2: a) Catalytic alkoxylation of silane by iron complex along with a phosphine ligand, b) catalytic dehydrogenative polymerization of diphenylsilane and isosorbide by iron complex along with a phosphine ligand and its hydrolytic degradation, c) tandem hydrosilylation-alkoxylation of internal alkyne by iron complex along with a phosphine ligand.

The seemingly mature field of transition metal catalysed asymmetric hydrogenation continues to excel beyond the 2001 Noble Prize and offers access to enantiopure advanced pharmaceutical intermediates (API). Chiral bidentate phosphorus ligands play a defining role in asymmetric hydrogenation and continue to dominate the academic and industrial research. However, the synthesis of privileged bidentate phosphine ligands is a tedious task with multiple synthetic steps and many a time, such lengthy and lousy protocols are industrially unattractive. Although bidentate ligands deliver better selectivities and catalytic performance, their synthesis has always been an obstacle to their success. To crack this synthetic bottleneck, we have prepared a binol-based phosphine-phosphite ligand in one pot. Its coordination property has been studied with $[\text{Rh}(\text{COD})_2\text{BF}_4]$. It has been utilized in asymmetric hydrogenation of several functionalized olefins where it showed excellent yield (up to 98%), enantioselectivity (up to 92%), and reactivity (TOF 1200) (Scheme 5.3). Its reactivity has also been compared with its symmetrical counterparts bis-phosphine and bis-phosphite. The practical relevance of hybrid ligand is demonstrated by scaling up the reaction to 1 g and by synthesizing DOPA (90% ee), a drug widely employed for the treatment of Parkinson's disease.



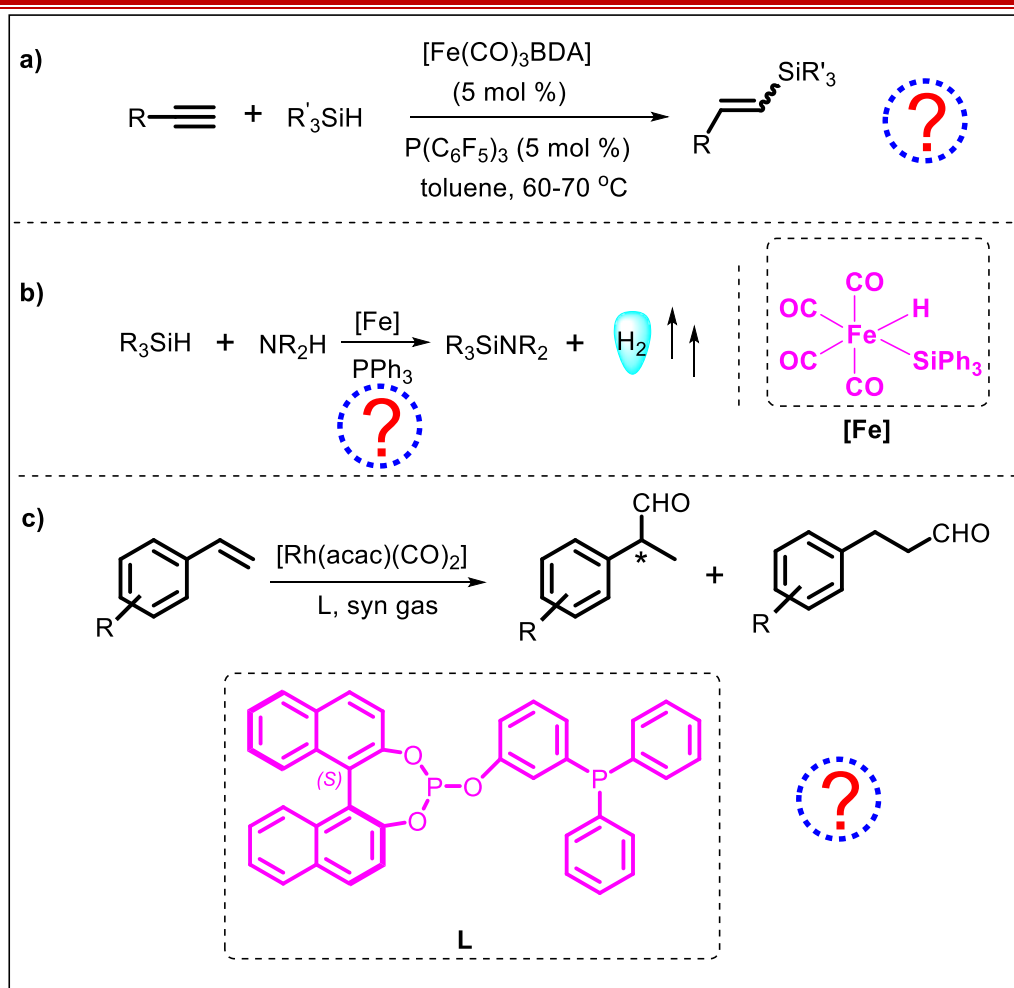
Scheme 5.3: a) One pot synthesis of phosphine-phosphite ligand, b) application of this ligand in Rh catalysed asymmetric hydrogenation of functionalized olefins.

To sum up, it is neither the success story of the metal nor the triumph of the ligand alone, rather, it is the metal-ligand synergy that makes the journey of homogeneous catalysis so much fascinating, intriguing and remarkable.



5.2 Outlook

We can think of extending the methodology of iron catalysed hydrosilylation to terminal alkynes from internal alkynes. It would be interesting to see the effect of different phosphine ligands in determining the regio and stereo-selectivity in such reactions (Scheme 5.4, a). In case of alkoxylation of silanes, we can think of extending the methodology from alcohols to amines to prepare amino-silanes as these are useful for the synthesis of ceramics, polymers and silicon based bases (Scheme 5.4, b). Hybrid phosphine-phosphite ligands are well known to give excellent enantiomeric excess in Rh metal catalysed asymmetric hydroformylation reaction. It would be very fascinating to examine how the hybrid ligand, synthesized in our lab, will perform in asymmetric hydroformylation reaction given that it showed high reactivity and good to excellent enantio-selectivity in the asymmetric hydrogenation of numerous functionalized olefins. (Scheme 5.4, c).



Scheme 5.4: a) Iron catalysed hydrosilylation of terminal alkynes, b) iron catalysed synthesis of amino-silanes, c) application of phosphine-phosphite ligand in asymmetric hydroformylation reaction.

The field of homogeneous catalysis is mainly dominated by precious metals such as rhodium, ruthenium, iridium, palladium, platinum. These precious metal catalysts have several advantages, such as readily available and easy to handle synthetic precursors, broad substrate scope, high reactivity & predictable selectivity. Besides this, a well-studied mechanism, involving two-electron redox processes, has made precious metals, the undisputed champion of this field. However, these precious metals (Rh, Ru, Ir, Pd, and Pt) are the least abundant transition metals on earth's crust and are in the danger zone of being extinct within the next 50 years, which poses a serious threat from a sustainability perspective. It is due to their scarcity, extraction of these metals is highly tedious thus associated with higher cost, higher global warming potential as well as a higher risk for its continuous supply. To combat these difficulties, enough attention has been paid to the development of catalysts based on 3d

transition metals such as Mn, Fe, Co, Ni & Cu, mainly because of their greater earth abundance, lower cost, lower toxicity & environmentally benign nature as compared to noble metals. However, base metals show unique reactivity as compared to noble metals. They exhibit variable coordination geometry, single-electron redox processes, facile ligand exchange & multiple spin states. In addition to this, facile change of oxidation state as well as the presence of radical intermediate, make it difficult for mechanistic study, thus impeding catalyst development. The above discussion clearly explains that base metals can't be used as a direct drop-in replacement for noble metals which in turn creates a new chemical space for "rational ligand design" where the different arm of the ligands, taking care of different properties of the metal might be advantageous. Also, many existing ligands involve multiple synthetic steps and show poor scalability, thus associated with a higher price which makes it impractical for use in large-scale processes, this enlarges the chemical space required for "rational ligand design". Finally, the presence of a versatile ligand toolbox will find application in other catalytic transformations beyond any particular reaction.

ABSTRACT

Name of the Student: Anirban Sen**Registration No.:** 10CC15A26026**Faculty of Study:** Chemical Sciences**Year of Submission:** 2023**AcSIR Academic Centre/CSIR Lab:**
CSIR-National Chemical Laboratory**Name of the Supervisor:**
Dr. Samir H. Chikkali**Title of the thesis:** Chiral Ligand and Transition Metal (Fe, Rh) Complexes for Catalytic Alkoxylation, Polymerization, Hydrosilylation and Hydrogenation

The journey of homogeneous catalysis revolves around the design and synthesis of metal-ligand complexes for different catalytic transformations. Most of these transformations involve the use of noble metals which have very low abundance on the earth crust. At the same time, most of the chiral ligands used in catalysis involve multiple step synthesis. Thus, the field is facing a flux from both the metal as well as ligand synthesis frontier. In this context, the present thesis, entitled as “**Chiral Ligand and Transition Metal (Fe, Rh) Complexes for Catalytic Alkoxylation, Polymerization, Hydrosilylation and Hydrogenation**” describes the strategies to address these challenges. This thesis is organized into five different chapters. **Chapter-1** briefly describes the importance of homogeneous catalysis, specially to prepare different organo-silicon compounds as well as different chiral compounds. In **chapter-2**, an iron complex along with a phosphine ligand have been successfully implemented for the E-selective hydrosilylation of internal alkynes with broad substrate scope and functional group tolerance under mild condition. A preliminary mechanistic investigation revealed a radical pathway for (E)-selective hydrosilylation which is quite uncommon in literature. In **chapter-3**, an iron complex has been synthesized and successfully implemented for the alkoxylation of silanes along with a phosphine ligand. In an extension to this methodology, this catalytic system has been successfully implemented to prepare silicon polymers which have been successfully depolymerized under ambient condition. In addition, this catalyst has also been implemented to carry out tandem hydrosilylation-alkoxylation of internal alkynes. **Chapter-4** deals with the synthesis of a hybrid phosphine-phosphite ligand in one pot and its application in rhodium catalysed asymmetric hydrogenation of several functionalised olefins. In **chapter-5**, the thesis work has been summarized and the future directions related to this field have been discussed. To sum up, it is neither the success story of the metal nor the triumph of the ligand alone, rather, it is the metal-ligand synergy that makes the journey of homogeneous catalysis so much fascinating, intriguing and remarkable.

List of Publications and Patents Emanating from the Thesis Work

1. **Sen, A.**; Kumar, R. and Chikkali, S. “One Pot Synthesis of Hybrid Phosphine-phosphite Ligand and Its Implications in Highly Active and Selective Rhodium Catalyzed Asymmetric Hydrogenation”, *Eur. J. Org. Chem.*, **2022**, 2022, e202101447.
2. **Sen, A.** and Chikkali, S. “C1-symmetric Diphosphorus Ligands in Metal-catalyzed Asymmetric Hydrogenation to Prepare Chiral Compounds”, *Org. Biomol. Chem.*, **2021**, 19, 9095-9137.
3. **Sen, A.**; Kumar, R.; Tewari, T. and Chikkali, S. “Radical Iron Breaks the Myth: (E)-selective Hydrosilylation of Alkynes”, Manuscript Under Preparation.
4. **Sen, A.**; Kumar, R.; Tewari, T. and Chikkali, S. “Catalytic Alkoxylation, Polymerization of Silanes and Tandem Alkoxylation-Hydrosilylation of Alkynes: An Iron Blitzkrieg”, Manuscript Under Preparation.
5. **Sen, A.**; Pandey, S. and Chikkali, S. “Highly Active and Enantioselective Asymmetric Hydrogenation of Alkenes Catalyzed by Rhodium Complexes of Phosphine-phosphite Ligands”, IN201811016872.
6. **Sen, A.**; Kumar, R. and Chikkali, S. “Iron Catalyzed Alkoxylation, Hydrosilylation, Tandem Hydrosilylation-alkoxylation and Dehydrogenative Polymerization: An Iron Blitzkrieg”, IN202211072434.

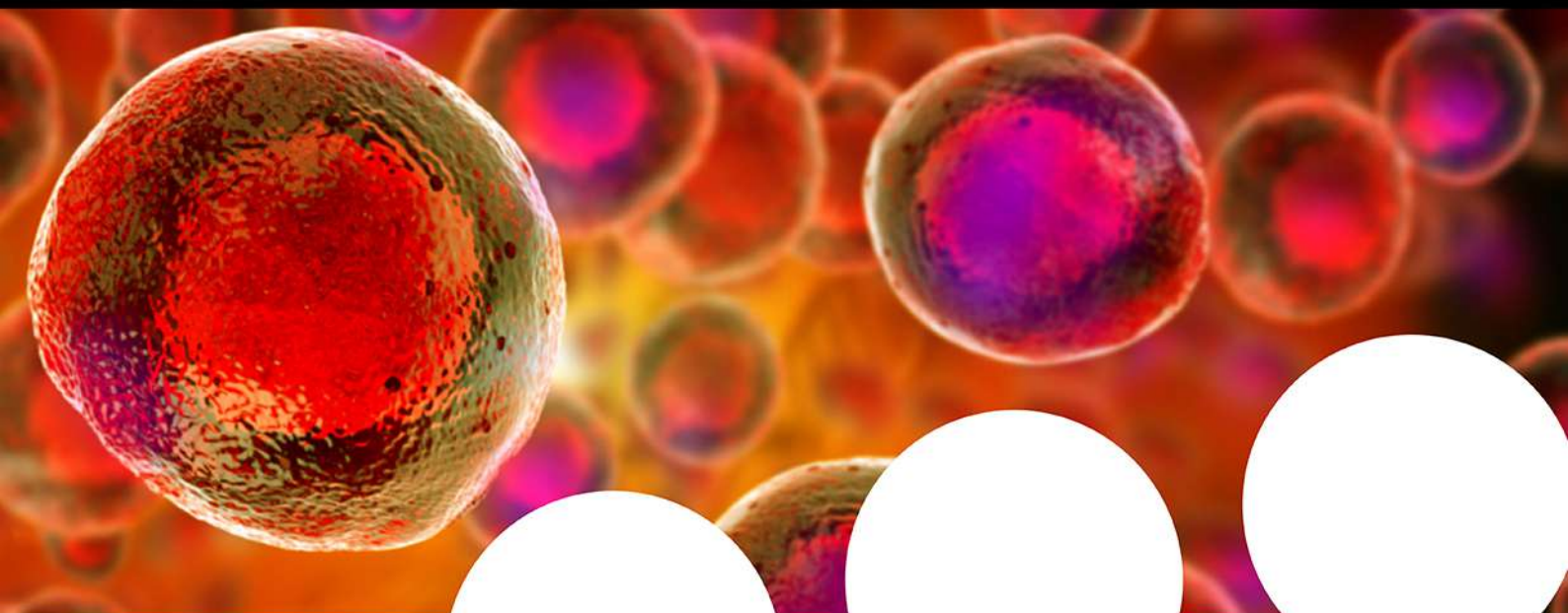
List of Publications Non-Emanating from the Thesis Work

1. Koshti, V.; **Sen, A.** and Chikkali, S. “Self-assembly of P-chiral Supramolecular Phosphines on Rhodium and Direct Evidence for Rh-catalyst-substrate Interactions”, *Dalton Trans.*, **2017**, 46, 13966-13973.
2. Khopade, K.; **Sen, A.** and Chikkali, S. “Highly Selective Process for the Preparation of Sitagliptin via Rhodium Catalysed Asymmetric Hydrogenation”, *Asian J. Org. Chem.*, **2020**, 9, 189-191.
3. Kumar, R.; **Sen, A.**; Tewari, T. and Chikkali, S. “Iron Catalyzed Isomerization of Olefins: A Green Approach”, Manuscript Under Preparation.
4. Kumar, R.; **Sen, A.** and Chikkali, S. “Rhodium Catalysed Asymmetric Hydroformylation of Olefin by Using Phosphine-phosphite Ligand”, Manuscript Under Preparation.

List of Oral/Poster Presented with Details

1. Poster presentation on **“Tracking the Role of Secondary Interaction in Asymmetric Hydrogenation Catalyzed by Rh-complexes”**, in **“21st International Conference on Organic Synthesis”** held on 11-16th December 2016 at IIT Bombay, India.
2. **Best poster award** on **“Modular Synthesis of P-OP Hybrid Ligand and Implication in Asymmetric Hydrogenation”**, in **National Science Day, NCL Research Foundation**, held on 26-27th Feb 2019 at CSIR-NCL, Pune, India.
3. Poster presentation on **“Modular Synthesis of P-OP Hybrid Ligand and Implication in Asymmetric Hydrogenation”**, in **“International Conference on Structural and Inorganic Chemistry-II (ICSIC-II)”** held on March 2019 at IISER, Pune.
4. Oral presentation at **‘Macro Meet’** on **“One Pot Synthesis of Hybrid Phosphine-phosphite Ligand and Its Implication in Asymmetric Hydrogenation”** in CSIR-National Chemical Laboratory held on December 2021 at Pune.
5. **Best oral presentation award** on **“Catalytic Alkoxylation, Polymerization of Silanes and Tandem Alkoxylation-hydrosilylation of Alkynes: An Iron Blitzkrieg”** in **NCL-Research Foundation Annual Students’ Conference** at CSIR-NCL Pune held on 29-30th Nov 2022.

Your research is important and needs to be shared with the world



Benefit from the Chemistry Europe Open Access Advantage

- Articles published open access have higher readership
- Articles are cited more often than comparable subscription-based articles
- All articles freely available to read, download and share.

Submit your paper today.



www.chemistry-europe.org

Mechanistically Guided One Pot Synthesis of Phosphine-Phosphite and Its Implication in Asymmetric Hydrogenation

Anirban Sen,^[a, b] Rohit Kumar,^[a, b] Swechcha Pandey,^[a] K. Vipin Raj,^[c] Pawan Kumar,^[a] Kumar Vanka,^[c] and Samir H. Chikkali*^[a, b]

Although hybrid bidentate ligands are known to yield highly enantioselective products in asymmetric hydrogenation (AH), synthesis of these ligands is an arduous process. Herein, a one pot, atom-economic synthesis of a hybrid phosphine-phosphite (L1) is reported. After understanding the reactivity difference between an O-nucleophile versus C-nucleophile, one pot synthesis of Senphos (L1) was achieved (72%). When L1 was treated with [Rh], ³¹P NMR revealed bidentate coordination to Rh. Senphos, in the presence of rhodium, catalyzes the AH of Methyl-2-acetamido-3-phenylacrylate and discloses an unprece-

dent turn over frequency of 2289, along with excellent enantio-selectivity (92%). The generality is demonstrated by hydrogenating an array of alkenes. The AH operates under mild conditions of 1–2 bar H₂ pressure, at room temperature. The practical relevance of L1 is demonstrated by scaling-up the reaction to 1 g and by synthesizing DOPA, a drug widely employed for the treatment of Parkinson's disease. Computational insights indicate that the *R* isomer is preferred by 3.8 kcal/mol over the *S* isomer.

Introduction

The seemingly mature field of transition metal-catalyzed asymmetric hydrogenation continues to excel beyond the 2001 Noble Prize^[1–3] and offers access to enantiopure advanced pharmaceutical intermediates (API).^[4–8] Chiral phosphorus ligands play a defining role in asymmetric hydrogenation and continue to dominate the academic and industrial research. Traditionally, ligand designing has been arbitrary and involves a hit and trial method, hard labor, experience, intuition and above all, serendipity (Figure 1, left). On the other hand, “on purpose” ligand design has been more of an industrial exercise with limited success. Thus, the quest to discover new chiral phosphorus ligands continues to intensify, as there is no universal ligand that can meet the increasing demand of the pharmaceutical industry.^[9,10] In the process, BINAP, DIPAMP, TangPhos, DuanPhos, DuPhos, ZhangPhos, among other ligands, have been discovered and a large ligand library of

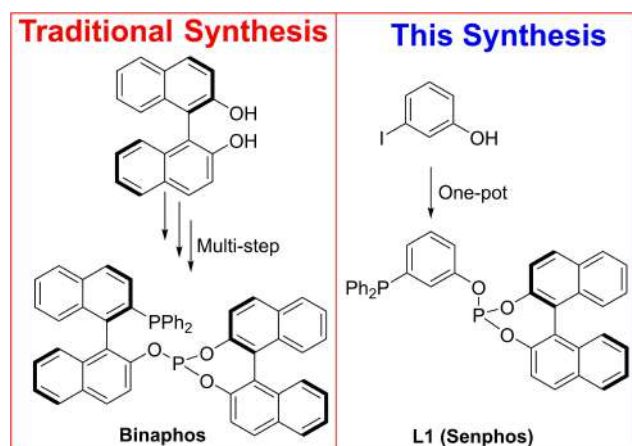


Figure 1. Representative traditional hybrid ligand synthesis (left) and this work (right).

diphosphorus ligands has been developed.^[11–13] In addition to diphosphines, hybrid di-phosphorous ligands have attracted significant attention in the recent past.^[14–25,26] However, the synthesis of privileged bidentate ligands is a tedious task with multiple synthetic steps and, many a times, such lengthy and lousy protocols are industrially unattractive. Although bidentate ligands deliver better selectivities and catalytic performance, their synthesis has always been an obstacle to their success. In fact, in many cases, the steps are non-trivial synthetic operations, which poses a great challenge for automation.

However, the notion that bidentate ligands require multiple synthetic steps is being challenged and innovative synthetic strategies are being devised to minimize the preparative steps.^[27,28] Three strategies are being mainly explored that

[a] A. Sen, R. Kumar, S. Pandey, P. Kumar, Dr. S. H. Chikkali
Polymer Science and Engineering Division
CSIR-National Chemical Laboratory
Dr. Homi Bhabha Road, Pune-411008,
India
E-mail: s.chikkali@ncl.res.in
http://academic.ncl.res.in/s.chikkali

[b] A. Sen, R. Kumar, Dr. S. H. Chikkali
Academy of Scientific and Innovative Research (AcSIR)
Sector 19, Kamla Nehru Nagar, Ghaziabad
201002, U. P., India

[c] K. Vipin Raj, Dr. K. Vanka
Physical and Materials Chemistry Division
CSIR-National Chemical Laboratory
Dr. Homi Bhabha Road, Pune-411008, India

Supporting information for this article is available on the WWW under
https://doi.org/10.1002/ejoc.202101447

include i) the use of supramolecular ligands, ii) accelerated synthesis *via* high throughput screening and, iii) one pot ligand synthesis. The straightforward 1–2 step synthesis of supramolecular ligands has been developed in the last decade and these ligands have been successfully applied in asymmetric hydrogenation.^[29–31] To accelerate the overall discovery process, high throughput screening (HTS) is being utilized in asymmetric hydrogenation.^[32] The HTS does not necessarily rely on easy to synthesize ligands, but uses modular ligands, commercially available ligands, a mixture of ligands and even enzymes. Thus, the overall discovery process is expedited using HTS and not necessarily the ligand synthesis. Although hybrid bidentate ligands such as BINAPHOS have found applications in several mechanistically unrelated reactions such as asymmetric hydrogenation, hydroformylation and allylic substitution, there are hardly any reports on the “one pot” synthesis of hybrid-bidentate ligands for asymmetric transformations.

Herein, we disclose the first one pot synthesis of the hybrid phosphine-phosphite ligand L1 (Senphos) (Figure 1, right). Furthermore, Senphos coordinates to Rh to yield a catalyst with excellent activity and selectivity in the asymmetric hydrogenation of alkenes. The generality of the approach is demonstrated by subjecting di- and tri-substituted alkenes to asymmetric hydrogenation. The practical utilization of our approach is demonstrated by the asymmetric synthesis of DOPA, a commercial drug for treating Parkinson’s disease. A ligand-substrate interaction is proposed to be responsible for the higher enantioselectivity, as predicted by density functional theory (DFT).

Results and Discussion

Ligand design, mechanistic understanding, synthesis, and coordination.

Traditionally, bidentate hybrid phosphine-phosphite ligands were being prepared using a step-by-step protocol and typically, 2–5 steps were required.^[33,34] The most closely related ligand **1** has been prepared in four steps,^[33] or in one step starting from a pre-formed C–P bond (Figure 2),^[35] ligand **2** in three steps,^[36] **3** in three-four steps^[37] and ligand **4** was prepared in two steps.^[38] A paradigm shift could be achieved if a hybrid phosphine-phosphite ligand can be prepared in one pot. Although highly desirable, one pot, modular synthesis of phosphine-phosphite ligand is still a distant goal. In addition to the synthetic challenge, a rational ligand design should also

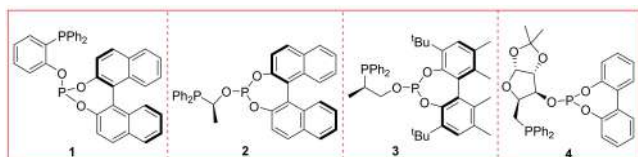


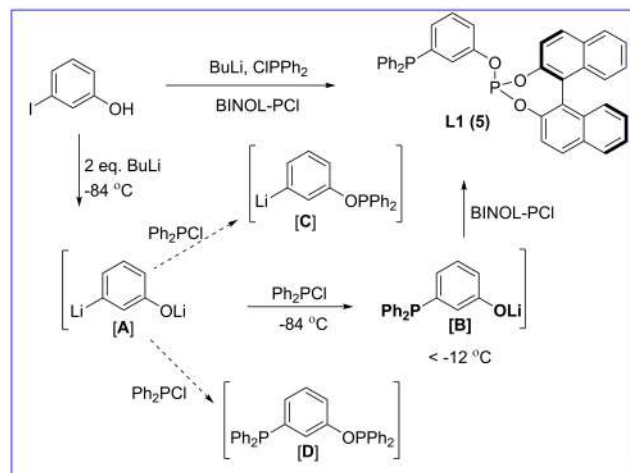
Figure 2. Representative chiral phosphine-phosphite ligands.

ensure that the resultant ligand will generate active catalytic species for the desired reaction.

Given the above reports and understanding, we pondered if one pot synthesis of phosphine-phosphite could be a reality. We anticipated that simple and readily available halophenols could yield chiral ligands with inequivalent P-donors. Ligand parameters such as donating ability, flexibility of the two donor arms, ligand bite angle, and the rigidity of the backbone were considered and one pot synthesis of phosphine-phosphite ligand 4-(3-(diphenylphosphinanyl)phenoxy)dinaphtho[2,1-d:1',2'-f][1,3,2]dioxaphosphepine (**L1**) was undertaken.

3-iodophenol (3.772 mmol) was lithiated using *n*-BuLi (7.544 mmol) at -84°C for 3 hours and stoichiometric amount of diphenylchlorophosphine (3.772 mmol) was added (Scheme 1). In our attempts to understand the reactivity between a C-nucleophile versus a O-nucleophile, we followed the reaction with ^{31}P NMR as a function of time and the details can be found in the supporting information. Although these investigations did not present a conclusive picture, low temperature ^{31}P NMR experiments (Figure S5, Figure S6) gave the impression that the C–P bond could be selectively formed, if the reaction is performed at lower temperature. Above reaction was repeated, after 2 hours of addition of ClPPh₂ (bath temp. -12°C), volatiles were stripped off and the reaction mixture was dried to obtain solid residue. To our delight, a ^{31}P NMR spectrum (Figure S7) of this residue in dry DMSO revealed selective formation of intermediate [B] (-2.33 ppm) and O–P coupled product [C] or [D] could not be observed.

The mechanistic understanding enabled us to design one pot protocol for the preparation of hybrid ligand **L1**. After 2 hours of ClPPh₂ addition, the reaction mixture was cooled to -84°C and phosphorochloridite was added. Filtration, washing, and purification produced a white powder in 72% isolated yield, which was identified at **L1** after complete characterization.^[41] Based on *in-situ* NMR findings, it is proposed that the reaction proceeds *via* intermediates [A] and [B]. Literature reports indicate that $-\text{Cl}$ is more likely to be attacked by electrophiles than $-\text{OLi}$.^[42,43] Thus, intermediate [B]



Scheme 1. Proposed mechanism and one pot synthesis of L1.

is anticipated to be generated *in situ*, which upon addition of phosphorchloridite produces **L1**. A ^{31}P NMR spectrum of this powder revealed two singlets at -5.14 and 144.24 ppm (Figure 3). The former resonance can be assigned to phosphine, while the latter can be designated to phosphite phosphorus.^[44] Identity of **L1** was further established using a combination of 1–2D NMR measurements (Figure S9–S14). These NMR findings were further corroborated by Electrospray Ionization Mass Spectrometry, which revealed a molecular ion peak at $m/z = 593.14$ Da $[\text{M} + \text{H}]^+$ (Figure S15).

It is well established in the literature that the coordination mode of a ligand strongly influences the outcome of an asymmetric reaction. Therefore, after having established the synthesis of Senphos, we examined the coordination behavior of **L1** with rhodium. Senphos (59.26 mg) was treated with 40.6 mg of $[(\text{COD})_2\text{Rh}(\text{BF}_4)]$ in dichloromethane. The resultant mixture revealed two doublet-of-doublet centered at 121.15 (dd, $^1J_{\text{Rh-P}} = 278$, $^2J_{\text{P-P}} = 35$ Hz) and 29.17 (dd, $^1J_{\text{Rh-P}} = 147$, $^2J_{\text{P-P}} = 35$ Hz) ppm (Figure 4). The former can be assigned to phosphite phosphorus and the latter originates from phosphine phosphorus. The phosphite phosphorus revealed a $^2J_{\text{P-P}}$ coupling of 35 Hz and $^1J_{\text{P-Rh}}$ coupling of 278 Hz, while the phosphine displayed 35 Hz P–P coupling and 143 Hz $^1J_{\text{Rh-P}}$

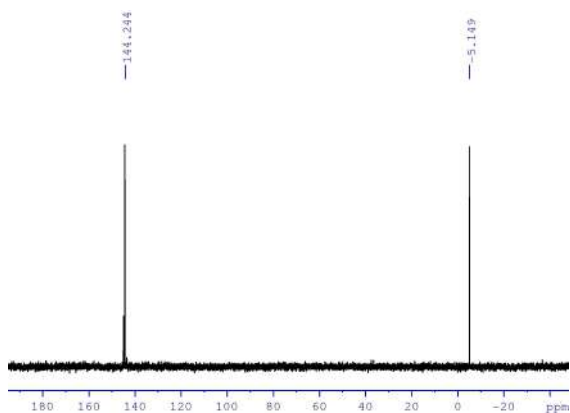


Figure 3. ^{31}P NMR spectrum of **L1** in CDCl_3 .

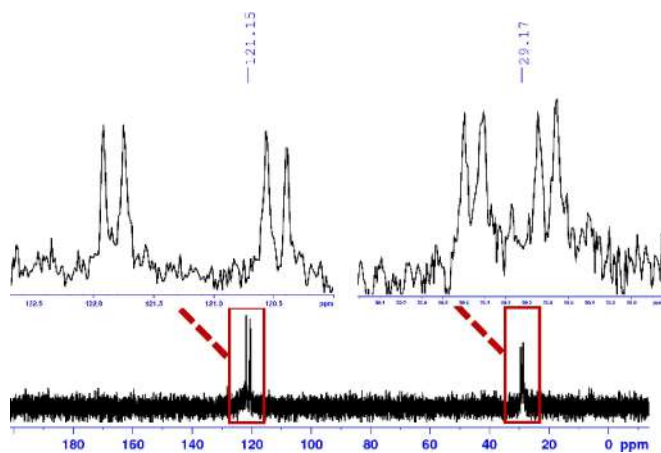


Figure 4. ^{31}P NMR spectrum of $[(\text{L1})(\text{COD})\text{Rh}(\text{BF}_4)]$ in CDCl_3 .

coupling. These chemical shifts and coupling constants are similar to those reported in the literature and establish coordination of **L1** to rhodium.^[45–48] The DFT optimized structure of the rhodium complex suggested a P–Rh–PO bite angle of 101.5° (see SI for details).

Rhodium-catalyzed asymmetric hydrogenation. After having established the coordination behavior of Senphos (**L1**), the performance of this hybrid ligand was evaluated in the asymmetric hydrogenation of 1,1-disubstituted and 1,1, 2-trisubstituted alkenes. The anticipated catalytically active species was generated *in situ* by mixing **L1** with $[(\text{COD})_2\text{Rh}(\text{BF}_4)]$ and Table 1 summarizes the most important results. Methyl-acetamidoacrylate (**6a**) was chosen as a benchmark substrate for preliminary screening. The initial screening at 2 bar hydrogen pressure and room temperature ($\sim 31^\circ\text{C}$) revealed full conversion and a moderate enantiomeric excess of 46% (Table 1, entry 1) in THF. Under similar conditions, a better enantiomeric excess of 83% and 76% was observed in TCE and DCM respectively (entry 2–3). As full conversion was observed in 60 minutes, the reaction time was reduced to 45 and then to 35 minutes. DCM outperformed TCE and displayed full conversion with 83% ee in 35 minutes (entry 5). Thus, DCM appears to perform better and therefore, the remaining reactions were carried out in DCM. Screening the reaction time revealed that 5 minutes are sufficient for full conversion (TOF = 1200) and an excellent ee of 87% was observed (Table 1, entry 6). Thus, preliminary optimization of reaction conditions suggested 2 bar hydrogen pressure, room temperature, 5 minutes, DCM and a ligand to metal ratio of 1:1.2 as the optimal reaction conditions.

With the optimal conditions in hand, the scope of asymmetric hydrogenation was examined. 1,1-disubstituted and 1,1,2-trisubstituted alkenes such as **6a**, **6b**, **6c**, **6d**, **6e**, **6f**, **6g**, **6h**, **6i**, **6j**, **6k**, **6l**, **6m**, **6n**, **6o** were hydrogenated using **L1**. The resultant chiral products **7a–7o** obtained from substrates **6a–6o**, respectively, have been presented in Figure 5. Asymmetric hydrogenation of dimethyl 2-methylsuccinate (**6b**) revealed reduced ee of just 28% (Figure 5, **7b**). While asymmetric hydrogenation of 1,1,2-trisubstituted alkene **6c** under identical reaction conditions displayed an excellent ee of 88% and a TOF

Table 1. Rhodium-phosphine-phosphite-catalyzed asymmetric hydrogenation of methyl acetamidoacrylate (**6a**).^[a]

Entry	Solvent	Time [mins.]	[%] Conv.	ee [%]	TOF
1	THF	60	> 99	46	100
2	TCE	60	> 99	83	100
3	DCM	60	> 99	76	100
4	TCE	35	84	68	144
5	DCM	35	> 99	83	172
6	DCM	5	> 99	87	1200

[a] Conditions: Methyl acetamidoacrylate – 0.25 mmol; $[(\text{COD})_2\text{Rh}(\text{BF}_4)]$ – 0.0025 mmol; **L1** – 0.0030 mmol; Solvent – 1 mL, THF-Tetrahydrofuran; TCE-Tetrachloroethane; Dichloromethane; H_2 pressure – 2 bar; Temperature – 31°C ; TOF-Turnover frequency, no by-product observed.

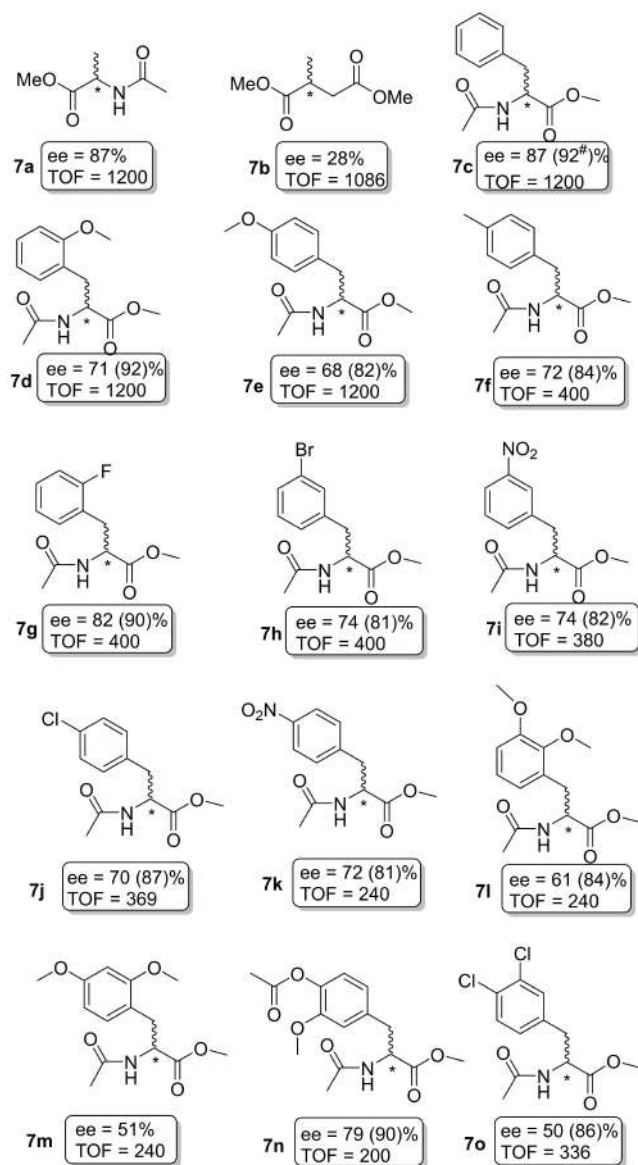


Figure 5. Rh-L1-catalyzed asymmetric hydrogenation of alkenes. Numbers in the bracket indicate % enantiomeric excess at 0 °C, ^aAH at –2 °C.

of 1200 (Figure 5, 7c). Next, we attempted the asymmetric hydrogenation of substituted methyl-2-acetamido-3-phenylacrylate and the effect of electron donating and electron withdrawing substituents on the ee and the TOF was examined. Electron donating substituents such as methoxy (6d, 6e) displayed reduced selectivity of 68–71%, while methyl (6f) substituted substrates revealed lower selectivity (72%) and TOF (400). These observations indicate that, although methoxy and methyl groups can be tolerated, the activity and selectivity is reduced. The catalyst also tolerates electron withdrawing groups such as nitro, fluoro, chloro, bromo, but at the cost of reduced ee and TOF (Figure 5, 7h–7k) as compared to the parent substrate 6c. Further increasing the substitution either with donating substituents (7m) or with withdrawing substituents (7o) diminishes the enantiomeric excess to 50–79% and

the TOF to 200. These observations clearly signify that the substituents do play an important role and can indeed interfere with the catalytic transformation.

When the asymmetric hydrogenation was performed at 0 °C, high enantiomeric excess of up to 92% (Figure 5, 7d) was observed (SI Table S1). Thus, the Senphos (L1) ligand appears to catalyze the asymmetric hydrogenation of a small library of substrates 6a–6o to the corresponding chiral products 7a–o with excellent enantiomeric excess and TOF.

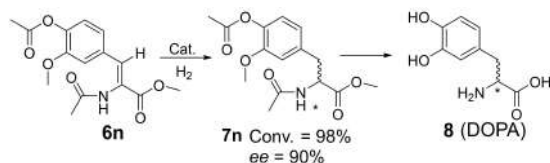
High TOF, TON and scale-up experiments. After demonstrating the wide reaction scope, we set out to validate the synthetic utility of Senphos (L1). Methyl-2-acetamido-3-phenylacrylate was chosen as the model substrate for the high turnover frequency, turn-over number and scale up experiments and Table 2 summarizes the results. At 2 bar hydrogenation pressure and 38 °C temperature, 6c displayed an enhanced TOF of 2289 (Table 2, entry 2). To the best of our knowledge, this is the highest TOF ever reported for 6c using a hybrid ligand. The TON experiments (Table 2, entry 3–4) indicate that 0.1 mol% catalyst loading (TON = 1000) is sufficient to obtain full conversion with little lower ee (78%). The practical usage of L1 in asymmetric hydrogenation has been demonstrated by scaling up the reaction to 1 g scale. 1 g of Methyl-2-acetamido-3-phenylacrylate was exposed to 2 bar hydrogen pressure at 31 °C for 20 minutes leading to > 99% conversion along with 80% ee.

Synthesis of DOPA. L-DOPA is the most commonly used drug for treating Parkinson's disease and is commercially produced using asymmetric hydrogenation.^[49,50] To demonstrate the practical significance of our methodology, we evaluated the performance of Senphos (L1) in asymmetric hydrogenation to produce the final DOPA compound. To our delight, asymmetric hydrogenation of the precursor 6n (Scheme 2) under mild conditions (1 bar hydrogen pressure) and the hydrolysis of the resultant intermediate produced 8 (DOPA) with an excellent isolated yield of 88% without affecting enantiomeric excess (SI

Table 2. Rhodium-phosphine-phosphite-catalyzed asymmetric hydrogenation of methyl-2-acetamido-3-phenylacrylate (6c).^[a]

Entry	Reaction		Time [mins.]	[%] Conv.	ee [%]	TOF	TON
	DCM [mL]	Sub: Cat					
1 ^[b]	1.5	150	5.5	98	82	1598	147
2 ^[c]	2	200	5	95	71	2289	190
3 ^[d]	2	400	2 hr	92	87	184	368
4 ^[e]	5	1000	12 hr	99	78	83	1000
5 ^[f]	22	100	20	> 99	80	300	100

[a] Conditions: H₂ pressure – 2 bar; Temperature – 25–38 °C; TOF-Turn-over frequency; TON-Turn-over number. [b] Methyl-2-acetamido-3-phenylacrylate – 82.22 mg, [(COD)₂Rh(BF₄)] – 1 mg, L1 – 1.8 mg, TOF; [c] Methyl-2-acetamido-3-phenylacrylate- 110 mg, [(COD)₂Rh(BF₄)] – 1 mg, L1 – 1.8 mg, TOF; [d] Methyl-2-acetamido-3-phenylacrylate – 110 mg, [(COD)₂Rh(BF₄)] – 0.5 mg, L1 – 0.9 mg, TON; [e] Methyl-2-acetamido-3-phenylacrylate – 275 mg, [(COD)₂Rh(BF₄)] – 0.5 mg, L1 – 0.9 mg, TON; [f] Methyl-2-acetamido-3-phenylacrylate – 1 g, [(COD)₂Rh(BF₄)] – 19 mg, L1 – 32.5 mg, TOF.



Scheme 2. Synthesis of DOPA.

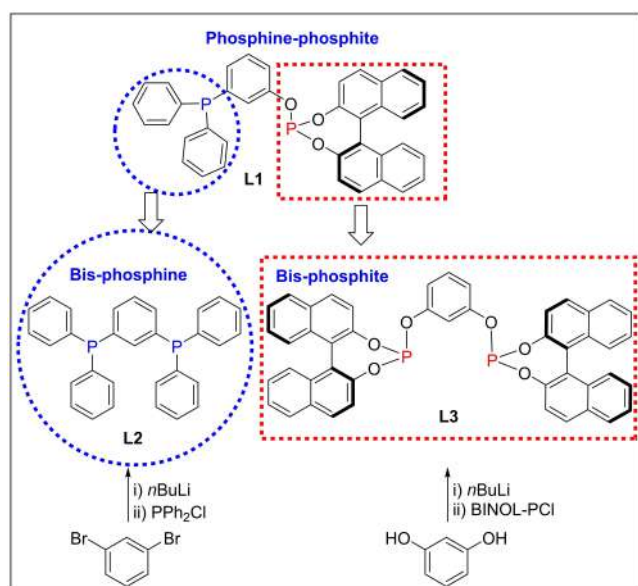
section 6). Thus, these results open up new avenues and the commercial potential of Senphos (L1) can be explored.

Synthesis of bis-phosphine (L2) and bis-phosphite (L3) ligand and comparison with L1. Given the excellent performance of the hybrid phosphine-phosphite ligand L1, we pondered how the symmetrical parent bis-phosphorus ligands would perform in the hydrogenation reaction. The bis-phosphine (L2) ligand was prepared using similar procedure as L1, although a slightly different synthetic protocol is reported previously (Scheme 3).^[51] 1,3-dibromo benzene (1.31 mmol) was treated with *n*-BuLi (2.88 mmol, 2.2 equivalent) at -84°C , followed by addition of diphenylchlorophosphine (3.3 mmol, 2.5 equivalent) at -84°C . Work-up followed by column chromatography produced L2. The ^{31}P NMR of this compound revealed a single resonance at -4.68 ppm (Figure S16) confirming the formation of the bis-phosphine. The identity of L2 was established using ^1H , ^{31}P and ^{13}C NMR spectroscopy. Along the same lines, the bis-phosphite ligand L3 (Scheme 3) was prepared by treating resorcinol (1.689 mmol) with *n*-BuLi (3.56 mmol; 2.1 equivalent) and *in situ* addition of BINOL-PCl (3.547 mmol; 2.1 equivalent).^[41] Observation of a single peak at 143.92 ppm in a ^{31}P NMR spectrum suggested the formation of the bis-phosphite ligand L3. Purification of the reaction mixture produced pure L3 in 68% yield. Performance of L2 and L3 in

the asymmetric hydrogenation of benchmark substrate **6a** (methyl-2-acetamidoacrylate) is compared in Table 3. As evident, the bis-phosphine ligand L2 is equally active and displays the same TOF as L1. However, L2 being a non-chiral ligand, produces only a racemic product after hydrogenation and therefore L2 is not relevant for this asymmetric hydrogenation reaction. On the other hand, bis-phosphite ligand L3 under identical hydrogenation conditions revealed, even after extended time period of 15 mins., an enantiomeric excess of 79% with a TOF of 246. Thus, the hybrid ligand L1 out-performed L2 and L3, and demonstrated its superiority over the parent ligands.

Comparison with literature reported hybrid phosphine-phosphite ligands and privileged ligands. To know where Senphos (L1) stands in terms of its activity in asymmetric hydrogenation, we compared the performance of L1 with the literature reported phosphine-phosphite ligands (see SI for details). Senphos (L1) revealed a TOF of 1200 in the asymmetric hydrogenation of **6a** and 2289 for **6c**. The performance of privileged ligands (L4–L7) such as Monophos, Duphos, etc. versus L1 is examined and Table 3 (runs 4–7) summarizes the results. As evident, the privileged ligands displayed only 1% conversion, while L1 displayed full conversion, under identical conditions.^[35–37,52,53]

Mechanistic insights of AH from DFT. In order to understand the mechanism of enantioselective asymmetric hydrogenation, we have carried out full quantum mechanical calculations using density functional theory (DFT) (see SI for details). Oxidative addition is expected to be the rate-determining transition state (Figure 6) for asymmetric hydrogenation when P-OP type hybrid ligands are employed.^[54] There are four different possibilities for the oxidative addition transition states, which arise due to the C_1 symmetry of the ligand and the prochiral nature of the substrate (Figure 6). The DFT results indicate that the transition states (TS-*re-3* and TS-*re-4*) that lead to the *R* enantiomer are more stable than the corresponding



Scheme 3. Synthesis of parent bis-phosphine (L2) and bis-phosphite (L3) ligands.

Table 3. Rhodium-catalyzed asymmetric hydrogenation of methyl-2-acetamidoacrylate (**6a**).^[a]

Entry	L	Time (mins)	[%] Conv.	ee [%]	TOF
1	L2	5	> 99	00	1200
2	L3	15	82	79	246
3	L1	5	> 99	87	1200
4*	L4	5	< 1	ND	ND
5*	L5	5	< 1	ND	ND
6*	L6	5	< 1	ND	ND
7*	L7	5	< 1	ND	ND

[a] Conditions: Methyl-2-acetamidoacrylate – 0.25 mmol; $[(\text{COD})_2\text{Rh}(\text{BF}_4)]$ – 0.0025 mmol; L – 0.0030 mmol; L/M: 1.2 equivalent; Solvent (DCM) – 1 mL, H_2 pressure – 2 bar; Temperature – 31°C ; TOF-Turnover frequency. * Substrate = Methyl-2-acetamido-3-phenylacrylate. L4 = (*R,R*)-N,N-diethyldinaphtho-[2,1-d:1',2'-f][1,3,2-dioxaphosphin-4-amine or Monophos (L/M: 2.2); L5 = (*S,S*)-Me-DUPHOS; L6 = (*R,R*)-Et-Ferrocene; L7 = (*R*)-(-)-N,N-Dimethyl-1-[(*S,S*)-2-(diphenylphosphino)-ferrocenyl]ethylamine; ND = Not determined due to low conversion.

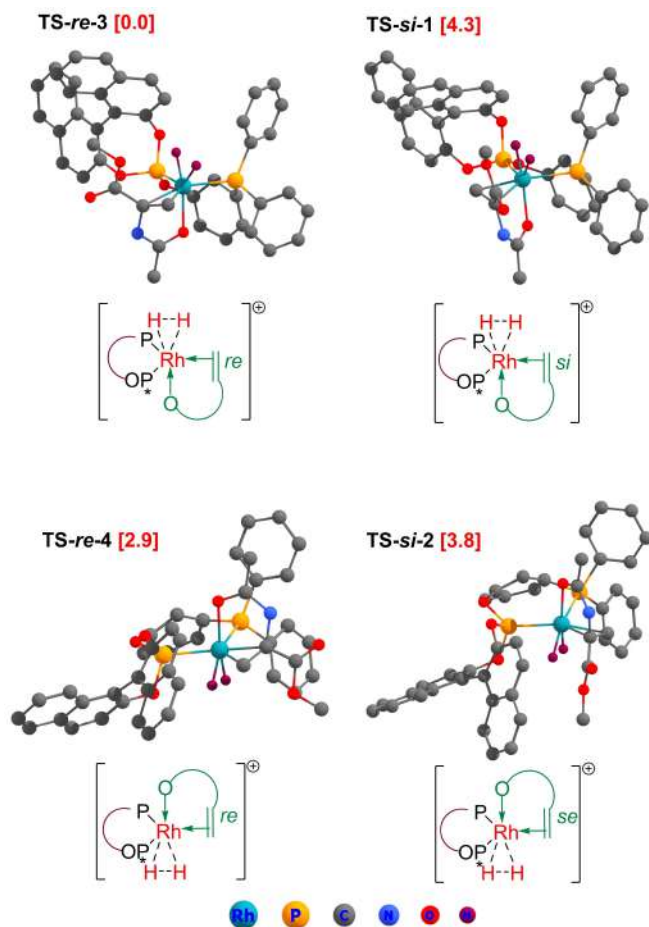


Figure 6. The relative free energies of the four transition state possibilities at the PBE/def-TZVP level of theory. Except for the relevant atoms on the rhodium, the rest of the hydrogen atoms have been removed for the purpose of clarity. All values are in kcal/mol.

transition states (**TS-si-1** and **TS-si-2**) that lead to the *S* enantiomer (Figure 6). The difference between the most stable *si* (**TS-si-2**) transition state and the *re* (**TS-re-3**) transition state is +3.8 kcal/mol, which shows the same trend as the experimental observations. To shed light into this difference in the energies of the four transition states, we have performed the Activation Strain analysis (see the SI for details).^[55] In this analysis, the TS is divided into three fragments f1, f2, and f3 (see SI Figure S43). The deformation energies of each fragment and the total interaction energy between them have been provided in Table 4. **TS-si-1** and **TS-re-3** show comparable deformation energies and interaction energies because of the same covalent bonding pattern, while **TS-si-2** and **TS-re-4** belong to another class where the covalent bonding pattern is different (Figure 6). **TS-si-1** and **TS-re-3** show lower deformation energies and interaction energies compared to **TS-si-2** and **TS-re-4**. Among **TS-si-1** and **TS-re-3**, the deformation energy of **TS-si-1** is lower by 7.6 kcal/mol. However, **TS-re-3** enjoys a more stable interaction energy of 12.6 kcal/mol *w.r.t.* **TS-si-1**.

Among **TS-si-2** and **TS-re-4**, the deformation energy is lower for **TS-re-4** by 3.2 kcal/mol, while **TS-si-2** has greater interaction

Table 4. The computed distortion energies of each fragment, total distortion energies (ΔE_d^+), and the total interaction energies (ΔE_i^+) of the four transition states at the PBE/def-TZVP level of theory.

TS	TS-si-1	TS-si-2	TS-re-3	TS-re-4
ΔE_d^+ (f1)	38.2	63.7	47.6	61.9
ΔE_d^+ (f2)	18.7	21.0	15.6	22.5
ΔE_d^+ (f3)	18.8	22.6	20.1	19.7
ΔE_d^+ (total) ^[a]	75.7	107.3	83.3	104.1
ΔE_i^+	-134.5	-167.7	-147.1	-165.9
$\Delta E^+ = \Delta E_d^+ + \Delta E_i^+$	-58.8	-60.4	-63.8	-61.8

[a] ΔE_d^+ (total) = ΔE_d^+ (f1) + ΔE_d^+ (f2) + ΔE_d^+ (f3).

energy of 1.8 kcal/mol compared to **TS-re-4**. Overall, **TS-re-3** becomes the most favorable transition state because of the perfect balance between the relatively lower deformation energy and the higher interaction energy.

We have also calculated the thermodynamic free energy (ΔG) values for the entire catalytic cycle for the case leading to the most stable transition state (**TS-re-3**) (Figure 7), and for an alternative pathway that would lead to the **TS-si-1** case (see Figure S45 in the ESI). As depicted in Figure 7, the first step is the displacement of two solvent molecules and the coordination of the substrate, which is highly exergonic (-30.2 kcal/mol) in nature. The next step is the formation of a trigonal bipyramidal Rh-H₂ complex with a favorable free energy change of 2.8 kcal/mol, which is followed by the oxidative addition (-1.2 kcal/mol), migratory insertion (-6.0 kcal/mol), and finally, reductive elimination steps (+10.1 kcal/mol). This results in the formation of the final *R* enantiomer. Two solvent molecules

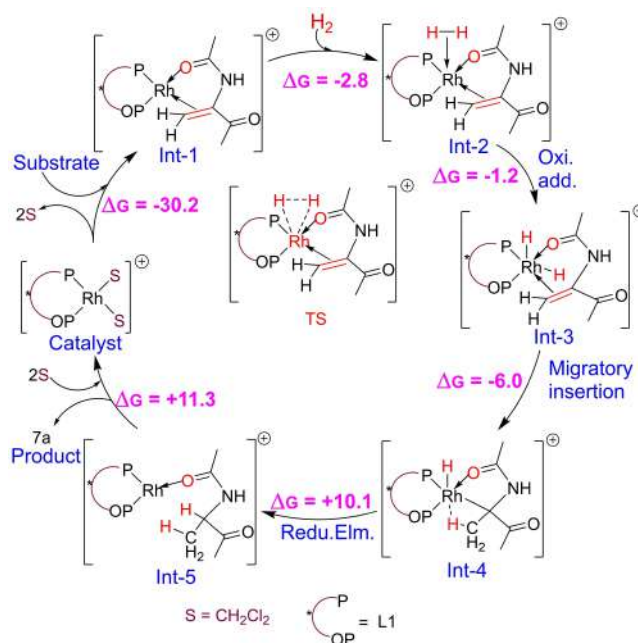


Figure 7. The computed free energy values for the catalytic cycle of asymmetric hydrogenation using the rhodium catalyst at the PBE/def-TZVP level of theory.

replace the product from rhodium and regenerate the catalytic species, with an energy cost of +11.3 kcal/mol.

Conclusion

In summary, understanding the reactivity difference between two nucleophiles through ^{31}P NMR and sequential addition of chlorodiphenylphosphine and phosphochloridite to 3-iodophenol revealed the selective formation of the hybrid phosphine-phosphite ligand 4-(3-(diphenylphosphinanyl)phenoxy)dinaphtho[2,1-*d*:1',2'-*f*][1,3,2]dioxaphosphine (L1 or Senphos) in one pot. ^{31}P NMR spectrum unraveled two singlets at -5.14 and 144.24 ppm, confirming the existence of Senphos, which was isolated as a white solid in 72% yield. The reaction of Senphos with $[\text{Rh}(\text{COD})_2\text{BF}_4]$ disclosed doublet-of-doublet in a ^{31}P NMR spectrum, suggesting bidentate coordination of L1 to the rhodium center. Senphos-Rh-catalyzed asymmetric hydrogenation of Methyl 3-acetamidoacrylate within 5 minutes at 2 bar hydrogen pressure. An unprecedented turn over frequency (TOF) of 2289 was observed in the Senphos-Rh-catalyzed AH of Methyl-2-acetamido-3-phenylacrylate under mild conditions. Following the initial success, the performance of L1 was evaluated in the AH of an array of substituted alkenes and the corresponding products **7a–7o** were obtained with excellent enantiomeric excess (up to 92%), high TOF and TON. The synthetic utility of Senphos was demonstrated by scaling up the reaction to 1 g scale and by preparing DOPA, a drug used in the treatment of Parkinson. Comparison with bidentate bis-phosphine (L2) and bis-phosphite (L3) ligand authenticated the dominance of L1, as it outperformed the parent symmetrical counterparts. Remarkably, a comparison with literature reported hybrid phosphine-phosphite ligands further proved the outstanding reactivity of L1. The asymmetric hydrogenation mechanism was evaluated using density functional theory (DFT). The computational investigations indicated that the formation of the "R" isomer was favoured by 3.8 kcal/mol over the "S" isomer. These results are in line with experimental findings, wherein "R" isomer was found to be the major isomer.

Experimental Section

Methods and materials. Unless noted otherwise, all manipulations were carried out under an inert atmosphere using standard Schlenk technique, cannula filtration or m-Braun glove box. Solvents were dried by standard procedures unless otherwise mentioned. Tetrahydrofuran was dried from sodium/benzophenone and dichloromethane from calcium hydride under argon atmosphere. Methyl 2-acetamidoacrylate, dimethyl itaconate, alpha-acetamidocinnamic acid, 3-iodophenol, *n*-butyllithium solution, S/R-BINOL were purchased from Sigma-Aldrich. Bis (1,5-cyclooctadiene)rhodium(I) tetrafluoroborate, chlorodiphenylphosphine were purchased from Alfa-Aesar. Methyl ester of alpha-Acetamidocinnamic acid derivatives were prepared employing known procedures. All other reagents/chemicals, solvents were purchased from local suppliers (Spectrochem Pvt. Ltd.; Avra Synthesis Pvt. Ltd.; Thomas Baker Pvt. Ltd. etc). Solution NMR spectra were recorded on a Bruker Avance 200, 400 and 500 MHz instruments at 298 K unless mentioned otherwise. Chemical shifts are referenced to external reference TMS (^1H and

^{13}C) or H_3PO_4 (^{31}P). Coupling constants are given as absolute values. Multiplicities are given as follows: s: singlet, d: doublet, t: triplet, m: multiplet, quat: quaternary carbon. Mass spectra were recorded on Thermo Scientific Q-Exactive mass spectrometer with Hypersil gold C18 column 150×4.6 mm diameter $8 \mu\text{m}$ particle size mobile phase used is 90% methanol+10% water+0.1% formic acid. The enantiomeric excess of the products was determined by chiral HPLC on an Agilent Technologies 1260 Infinity instrument with Chiralpak IB column (20 cm), Chiralpak AD-H column (20 cm) and an Agilent 7890B GC system with supelco beta dex 225 column (30 m). Optical rotation was measured at 589 nm on JASCO (P-2000) polarimeter using 10 mm cell.

Synthesis of 4-(3-(diphenylphosphinanyl)phenoxy)dinaphtho[2,1-*d*:1',2'-*f*][1,3,2]dioxaphosphine (L1): In an oven dried Schlenk flask 3-iodo phenol (830 mg, 3.77 mmol, 1 eqv.) was taken and 100 mL of dry diethyl ether was added. The resultant solution was cooled to -84°C and *n*-BuLi (2.0 M in hexane, 3.77 mL, 7.54 mmol, 2 eqv.) was added drop wise. Subsequently, the reaction mixture was stirred for the next 3 hours within which the bath temperature rises to 0°C . Subsequently, the reaction mixture was cooled to -84°C and chlorodiphenylphosphine (0.68 mL, 3.77 mmol, 1 eqv.) was drop wise added to it. The reaction mixture was stirred for next two hours, during which the reaction temperature rises to -12°C . In another round bottom flask, phosphochloridite (1.32 g, 3.77 mmol, 1 eqv.) was dissolved in dry diethyl ether (40 mL) and was added to the above reaction mixture at -84°C . After complete addition, the reaction mixture was stirred for 1 hour in the same bath. Subsequently, the flask was taken out of the bath and stirred for 1 hour at room temperature. The content was passed through celite bed, filtered with the help of cannula filtration and volatiles were evaporated to get white coloured residue. The white residue was washed twice with dry hexane (20 mL) to obtain 4-(3-(diphenylphosphinanyl)phenoxy)dinaphtho[2,1-*d*:1',2'-*f*][1,3,2]dioxaphosphine (L1) as white coloured solid in 72% yield (1.6 g).

^{31}P NMR (125 MHz, CDCl_3 , 298 K) $\delta = 144.24$ (s, phosphite), -5.14 (s, phosphine). ^1H NMR (400 MHz, CD_3COCD_3 , 298 K) $\delta = 5.27$ (s, CH_2Br_2 , Internal standard), 7.04 (d, 1H), 7.15–7.18 (m, 1H), 7.23–7.26 (m, 2H), 7.30–7.33 (m, 8H), 7.43–7.51 (m, 9H), 7.61 (d, 1H), 7.98–8.07 (m, 3H), 8.16 (d, 1H). ^{13}C NMR (100 MHz, CD_3COCD_3 , 298 K) $\delta = 152.6$, 148.0 (d, $J = 65$ Hz), 141.0 (d, $J = 15.5$ Hz), 137.6 (d, $J = 16$ Hz), 134.7, 134.5, 133.6, 133.3, 132.8, 132.2, 131.8, 131.2, 131.1, 130.7, 130.1, 129.7, 129.6, 127.4, 126.4 (d, $J = 24$ Hz), 122.4, 121.8 (d, $J = 10$ Hz). HRMS: m/z calculated for $\text{C}_{38}\text{H}_{26}\text{O}_3\text{P}_2 = 592.13$, found = 593.14 (M+H) $^+$. Elemental analysis [for $\text{C}_{38}\text{H}_{26}\text{O}_3\text{P}_2 + \text{C}_7\text{H}_8$ (Toluene)], Calculated: C = 78.94, H = 5.01; Found: C = 78.98, H = 4.43.

Synthesis of 1,3-bis (diphenylphosphanyl) benzene (L2): 1, 3-dibromobenzene (310 mg, 1.31 mmol, 1 eqv.) was taken in a Schlenk flask and was dissolved in dry diethyl ether (20 mL). The resultant solution was cooled to -84°C and 1.45 mL *n*-BuLi was (2.89 mmol, 2 M solution in hexane) added to it. The solution was stirred for 2 hours before adding 0.58 mL of PPh_2Cl (3.3 mmol, 2.5 eqv) at -84°C . The resultant mixture was stirred overnight at room temperature and volatiles were evaporated to give a residue. Dichloromethane was added to above residue and the solution was filtered. Volatiles were evaporated and residue was purified by silica gel chromatography (using petroleum ether) to yield anticipated ligand L2 in 74% isolated yield.

^{31}P NMR (400 MHz, CDCl_3 , 298 K): $\delta = -4.68$ (s). ^1H NMR (400 MHz, CDCl_3 , 298 K): $\delta = 7.51$ (d, $J = 7.3$ Hz, 2H), 7.47 (d, $J = 6.8$ Hz, 2H), 7.38 (m, 17H), 7.25 (m, 3H). ^{13}C NMR (100 MHz, CDCl_3 , 298 K): $\delta = 140.7$ (d, $J = 18.57$ Hz), 136.5 (d, $J = 12.38$ Hz), 136.1 (d, $J = 18.57$ Hz), 133.9 (d, $J = 19.58$ Hz), 132.4, 132.2, 131.9, 130.2 (d, $J = 7.4$ Hz), 129.2, 128.9 (d, $J = 7.42$ Hz), 123.3 (d, $J = 7.94$ Hz).

Synthesis of 1,3-bis(((4S,11b S)-dinaphtho[2,1-d:1',2'-f][1,3,2]dioxaphosphin-4-yl)oxy)benzene (L3): In an oven dried Schlenk flask resorcinol (186 mg, 1.689 mmol, 1 eqv.) was taken and was dissolved in dry tetrahydrofuran (10 mL). The Schlenk was cooled to -84°C and 1.78 mL of *n*-BuLi (3.56 mmol, 2.0 molar solution in hexane, 2.1 eqv.) was dropwise added to it. The reaction mixture was allowed to warm to room temperature and was stirred for 2 hours. Subsequently, the Schlenk was again cooled to -84°C and phosphorchloridite (1.244 g, 3.547 mmol, 2.1 eqv.) was added to above mixture and the content was stirred for 4 hours. After completion of reaction, the solution was passed through a celite bed and solvent was evaporated by applying vacuum to yield L3 in 68%.

^{31}P NMR (400 MHz, CDCl_3 , 298 K): $\delta = 143.92$ (s). ^1H NMR (400 MHz, CDCl_3 , 298 K): $\delta = 8.06$ (d, $J = 9$ Hz, 2H), 8 (m, 6H), 7.63 (d, $J = 8.6$ Hz, 2H), 7.48 (m, 10H), 7.33 (m, 6H), 7.11 (s, 1H), 7.07 (d, $J = 8.44$ Hz, 1H).

Asymmetric hydrogenation: Asymmetric hydrogenation experiments were carried out in a stainless steel autoclave (450 mL) equipped with pressure inlet-outlet, safety rupture valve and pressure gauge. In a glove box, 4 mL glass vials with screw-cap and septa were charged with $[\text{Rh}(\text{COD})_2\text{BF}_4]$ (1 mg, 0.0025 mmol), ligand (1.8 mg, 0.003 mmol), solvent (1 mL), substrate (0.25 mmol) along with Teflon stirring bars. The charged vials were transferred to autoclave. Before starting the catalytic reactions, the charged autoclave was purged three times with 5 bars of hydrogen and then pressurized to 2 bars. The reaction mixture was stirred at suitable temperature for desired time. After asymmetric hydrogenation, the excess gas was vented. The reaction mixture was passed through a short silica plug using dichloromethane. The solvent was stripped off under reduced pressure and the product was dried. Conversion and enantioselectivity was determined by GC and/or HPLC using chiral columns. The enantiomeric excess was determined by chiral HPLC on a Chiralpak-IB, ADH column or GC using Supelco- β -dex 225 column.

Methyl acetyl-D-alaninate (7a): White solid. GC condition: Supelco beta dex 225 isothermal at 70°C for 10.0 min, $2^{\circ}\text{C min}^{-1}$ to 110°C , $7^{\circ}\text{C min}^{-1}$ to 210°C , flow 1 ml/min with 14.831 psi pressure; t_{R} (major) = 38.29 min, t_{R} (minor) = 38.90 min. Procedure A: 87% ee.

Dimethyl 2-methylsuccinate (7b): Colour less liquid. GC condition: Supelco beta dex 225 isothermal at 75°C for 2.0 min, $4^{\circ}\text{C min}^{-1}$ to 120°C , $50^{\circ}\text{C min}^{-1}$ to 220°C , flow 1 ml/min with 14.831 psi pressure; t_{R} (major) = 14.10 min, t_{R} (minor) = 14.31 min. Procedure A: 28% ee.

Methyl (methoxycarbonyl)-D-phenylalaninate (7c): White solid. HPLC condition: Daicel chiralpak IB, 1.0 ml/min, UV (λ 254 nm), 10% 2-PrOH/Hexane, t_{R} (major) = 12.5 min; t_{R} (minor) = 13.6 min. Procedure A: 87% ee; Procedure B: 88% ee.

Methyl 2-((methoxycarbonyl)amino)-3-(2-methoxyphenyl)propanoate (7d): White solid. HPLC condition: Daicel chiralpak ADH, 1.0 ml/min, UV (λ 230 nm), 10% 2-PrOH/Hexane, t_{R} (major) = 12.3 min; t_{R} (minor) = 16.4 min. Procedure A: 71% ee; Procedure B: 92% ee.

Methyl 2-((methoxycarbonyl)amino)-3-(4-methoxyphenyl)propanoate (7e): White solid. HPLC condition: Daicel chiralpak ADH, 1.0 ml/min, UV (λ 230 nm), 10% 2-PrOH/Hexane, t_{R} (major) = 13.7 min; t_{R} (minor) = 18.1 min. Procedure A: 68% ee; Procedure B: 82% ee.

Methyl 2-((methoxycarbonyl)amino)-3-(*p*-tolyl)propanoate (7f): White solid. HPLC condition: Daicel chiralpak ADH, 1.0 ml/min, UV (λ 230 nm), 10% 2-PrOH/Hexane, t_{R} (major) = 9.8 min; t_{R} (minor) = 12.6 min. Procedure A: 72% ee; Procedure B: 84% ee.

Methyl 3-(2-fluorophenyl)-2-((methoxycarbonyl)amino)propanoate (7g): White solid. HPLC condition: Daicel chiralpak ADH, 1.0 ml/min, UV (λ 230 nm), 10% 2-PrOH/Hexane, t_{R} (major) = 10.7 min; t_{R} (minor) = 13.3 min. Procedure A: 82% ee; Procedure B: 90% ee.

Methyl 3-(3-bromophenyl)-2-((methoxycarbonyl)amino)propanoate (7h): White solid. HPLC condition: Daicel chiralpak ADH, 1.0 ml/min, UV (λ 230 nm), 10% 2-PrOH/Hexane, t_{R} (major) = 9.7 min; t_{R} (minor) = 11.6 min. Procedure A: 74% ee; Procedure B: 81% ee.

Methyl 2-((methoxycarbonyl)amino)-3-(3-nitrophenyl)propanoate (7i): White solid. HPLC condition: Daicel chiralpak ADH, 1.0 ml/min, UV (λ 230 nm), 10% 2-PrOH/Hexane, t_{R} (major) = 18.5 min; t_{R} (minor) = 19.4 min. Procedure A: 74% ee; Procedure B: 82% ee.

Methyl 3-(4-chlorophenyl)-2-((methoxycarbonyl)amino)propanoate (7j): White solid. HPLC condition: Daicel chiralpak ADH, 1.0 ml/min, UV (λ 230 nm), 10% 2-PrOH/Hexane, t_{R} (major) = 11.8 min; t_{R} (minor) = 14.5 min. Procedure A: 70% ee; Procedure B: 87% ee.

Methyl 2-((methoxycarbonyl)amino)-3-(4-nitrophenyl)propanoate (7k): White solid. HPLC condition: Daicel chiralpak ADH, 1.0 ml/min, UV (λ 230 nm), 10% 2-PrOH/Hexane, t_{R} (major) = 24.1 min; t_{R} (minor) = 25.6 min. Procedure A: 72% ee; Procedure B: 81% ee.

Methyl 3-(2,3-dimethoxyphenyl)-2-((methoxycarbonyl)amino)propanoate (7l): White solid. HPLC condition: Daicel chiralpak ADH, 1.0 ml/min, UV (λ 230 nm), 10% 2-PrOH/Hexane, t_{R} (major) = 12.7 min; t_{R} (minor) = 18.1 min. Procedure A: 61% ee; Procedure B: 84% ee.

Methyl 3-(2,4-dimethoxyphenyl)-2-((methoxycarbonyl)amino)propanoate (7m): White solid. HPLC condition: Daicel chiralpak IB, 1.0 ml/min, UV (λ 230 nm), 10% 2-PrOH/Hexane, t_{R} (major) = 16.8 min; t_{R} (minor) = 18.7 min. Procedure A: 51% ee.

Methyl (S)-3-(4-acetoxy-3-methoxyphenyl)-2-((methoxycarbonyl)amino)propanoate (7n): White solid. HPLC condition: Daicel chiralpak ADH, 1.0 ml/min, UV (λ 284 nm), 15% 2-PrOH/Hexane, t_{R} (major) = 12.2 min; t_{R} (minor) = 13.2 min. Procedure A: 79% ee; Procedure B: 90% ee.

Methyl 3-(3,4-dichlorophenyl)-2-((methoxycarbonyl)amino)propanoate (7o): White solid. HPLC condition: Daicel chiralpak ADH, 1.0 ml/min, UV (λ 284 nm), 15% 2-PrOH/Hexane, t_{R} (major) = 10.5 min; t_{R} (minor) = 11.9 min. Procedure A: 50% ee; Procedure B: 86% ee.

Acknowledgements

SHC is grateful to DST-SERB (CRG/2021/005385), CSIR-NCL (HCP-0011), India and AvH Bonn, Germany for the financial support. AS thanks CSIR and RK is grateful to UGC for senior research fellowship.

Conflict of Interest

The authors declare no conflict of interest.

Data Availability Statement

The data that support the findings of this study are available in the supplementary material of this article.

Keywords: Asymmetric hydrogenation · Catalysis · DOPA synthesis · One pot synthesis · Phosphine-phosphite ligand

- [1] R. Noyori, *Adv. Synth. Catal.* **2003**, *345*, 15–32.
 [2] W. S. Knowles, *Angew. Chem. Int. Ed.* **2002**, *41*, 1998–2007; *Angew. Chem.* **2002**, *114*, 2096–2107.
 [3] R. Noyori, T. Ohkuma, *Angew. Chem. Int. Ed.* **2001**, *40*, 40–73; *Angew. Chem.* **2001**, *113*, 40–75.
 [4] D. J. Ager, A. H. M. de Vries, J. G. de Vries, *Chem. Soc. Rev.* **2012**, *41*, 3340–3380.
 [5] P. Etayo, A. Vidal-Ferran, *Chem. Soc. Rev.* **2013**, *42*, 728–754.
 [6] F. Meemken, A. Baiker, *Chem. Rev.* **2017**, *117*, 11522–11569.
 [7] X. Xie, B. Lu, W. Li, Z. Zhang, *Coord. Chem. Rev.* **2018**, *355*, 39–53.
 [8] C. S. G. Seo, R. H. Morris, *Organometallics* **2019**, *38*, 47–65.
 [9] S. Kraft, K. Ryan, R. G. Kargbo, *J. Am. Chem. Soc.* **2017**, *139*, 11630–11641.
 [10] C. Margarita, P. G. Andersson, *J. Am. Chem. Soc.* **2017**, *139*, 1346–1356.
 [11] W. Tang, X. Zhang, *Chem. Rev.* **2003**, *103*, 3029–3069.
 [12] J. J. Verendel, O. Pamies, M. Dieguez, P. G. Anderson, *Chem. Rev.* **2014**, *114*, 2130–2169.
 [13] P. Chirik, *Acc. Chem. Res.* **2015**, *48*, 1687–1695.
 [14] H. Fernández-Pérez, P. Etayo, A. Panossian, A. Vidal-Ferran, *Chem. Rev.* **2011**, *111*, 2119–2176.
 [15] M. M. Pereira, M. J. F. Calvete, R. M. B. Carrilho, A. R. Abreu, *Chem. Soc. Rev.* **2013**, *42*, 6990–7027.
 [16] P. W. N. M. van Leeuwen, P. C. J. Kamer, C. Claver, O. Pámies, M. Diéguez, *Chem. Rev.* **2011**, *111*, 2077–2118.
 [17] S. Lühr, J. Holz, A. Börner, *ChemCatChem* **2011**, *3*, 1708–1730.
 [18] J. H. Xie, Q. L. Zhou, *Acc. Chem. Res.* **2008**, *41*, 581–593.
 [19] D. G. H. Hetterscheid, S. H. Chikkali, B. de Bruin, J. N. H. Reek, *ChemCatChem* **2013**, *5*, 2785–2793.
 [20] S. H. Chikkali, J. I. van der Vlugt, J. N. H. Reek, *Coord. Chem. Rev.* **2014**, *262*, 1–15.
 [21] J. G. de Vries, *Top. Catal.* **2014**, *57*, 1306–1317.
 [22] A. Beliaev, *Org. Process Res. Dev.* **2016**, *20*, 724–732.
 [23] W. S. Knowles, R. Noyori, *Acc. Chem. Res.* **2007**, *40*, 1238–1239.
 [24] S. C. Shultz, S. W. Kraska, *Acc. Chem. Res.* **2007**, *40*, 1320–1326.
 [25] N. B. Johnson, I. C. Lennon, P. H. Moran, J. A. Ramsden, *Acc. Chem. Res.* **2007**, *40*, 1291–1299.
 [26] E. L. Hazeland, A. M. Chapman, P. G. Pringle, H. A. Sparkes, *Chem. Commun.* **2015**, *51*, 10206–10209.
 [27] O. Pámies, M. Magre, M. Diéguez, *Chem. Rec.* **2016**, *16*, 1578–1590.
 [28] R. Lindner, B. van den Bosch, M. Lutz, J. N. H. Reek, J. I. van der Vlugt, *Organometallics* **2011**, *30*, 499–510.
 [29] J. Meeuwissen, J. N. H. Reek, *Nat. Chem.* **2010**, *2*, 615–621.
 [30] J. Wieland, B. Breit, *Nat. Chem.* **2010**, *2*, 832–837.
 [31] N. R. Mote, S. H. Chikkali, *Chem. Asian J.* **2018**, *13*, 3623–3646.
 [32] M. Renom-Carrasco, L. Lefort, *Chem. Soc. Rev.* **2018**, *47*, 5038–5060.
 [33] J. Velder, T. Robert, I. Weidner, J. M. Neudörfel, J. Lex, H.-G. Schmalz, *Adv. Synth. Catal.* **2008**, *350*, 1309–1315.
 [34] a) J. Wassenaar, J. N. H. Reek, *Org. Biomol. Chem.* **2011**, *9*, 1704–1713; b) G. M. Adams, A. S. Weller, *Coord. Chem. Rev.* **2018**, *355*, 150–172; c) A. Suarez, A. Pizzano, *Tetrahedron: Asymmetry.* **2001**, *12*, 2501–2504; d) R. Kranich, K. Eis, O. Geis, S. Muhle, J. W. Bats, H.-G. Schmalz, *Chem. Eur. J.* **2000**, *6*, 2874–2894.
 [35] M. J. Baker, P. G. Pringle, *J. Chem. Soc. Chem. Commun.* **1993**, 314–316.
 [36] a) H. Fernández-Pérez, J. Benet-Buchholz, A. Vidal-Ferran, *Org. Lett.* **2013**, *15*, 3634–3637; b) J. L. Nunez-Rico, P. Etayo, H. Fernandez-Perez, A. Vidal-Ferran, *Adv. Synth. Catal.* **2012**, *354*, 3025–3035.
 [37] I. Arribas, S. Vargas, M. Rubio, A. Suárez, C. Domene, E. Alvarez, A. Pizzano, *Organometallics* **2010**, *29*, 5791–5804.
 [38] O. Pámies, M. Diéguez, G. Net, A. Ruiz, C. Claver, *Chem. Commun.* **2000**, 2383–2384.
 [39] For commonly observed chemical shifts of such phosphines, see: S. Chikkali, D. Gudat, *Eur. J. Inorg. Chem.* **2006**, *2006*, 3005–3009.
 [40] The ³¹P NMR chemical shift assignment is based on literature, see: R. B. Bedford, S. M. Draper, P. N. Scully, S. L. Welch, *New J. Chem.* **2000**, *24*, 745–747.
 [41] See supporting information for details.
 [42] J. Almena, F. Foubelo, M. Yus, *Tetrahedron* **1995**, *51*, 3365–3374.
 [43] I. M. Pastor, M. Yus, *Tetrahedron* **2001**, *57*, 2365–2370. and the reference therein
 [44] The observed ³¹P NMR chemical shifts are in line with reported phosphine-phosphite shifts, see: M. Dindaroğlu, A. Falk, H.-G. Schmalz, *Synthesis* **2013**, *45*, 527–535.
 [45] K. Nozaki, N. Sakai, T. Nanno, T. Higashijima, S. Mano, T. Horiuchi, H. Takaya, *J. Am. Chem. Soc.* **1997**, *119*, 4413–4423.
 [46] S. Deerenberg, P. C. J. Kamer, P. W. N. M. van Leeuwen, *Organometallics* **2000**, *19*, 2065–2072.
 [47] D. A. C. Molina, C. P. Casey, I. Müller, K. Nozaki, C. Jäkel, *Organometallics* **2010**, *29*, 3362–3367.
 [48] S. H. Chikkali, R. Bellini, B. de Bruin, J. I. van der Vlugt, J. N. H. Reek, *J. Am. Chem. Soc.* **2012**, *134*, 6607–6616.
 [49] W. S. Knowles, M. J. Sabacky, B. D. Vineyard, D. J. Weinkauff, *J. Am. Chem. Soc.* **1975**, *97*, 2567–2568.
 [50] B. D. Vineyard, W. S. Knowles, M. J. Sabacky, G. L. Bachman, D. J. Weinkauff, *J. Am. Chem. Soc.* **1977**, *99*, 5946–5952.
 [51] H. C. E. McFarlane, W. McFarlane, *Polyhedron* **1988**, *7*, 1875–1879.
 [52] P. Etayo, J. L. Núñez-Rico, A. Vidal-Ferran, *Organometallics* **2011**, *30*, 6718–6725.
 [53] J. R. Lao, J. Benet-Buchholz, A. Vidal-Ferran, *Organometallics* **2014**, *33*, 2960–2963.
 [54] H. Fernández-Pérez, S. M. A. Donald, I. J. Munslow, J. Benet-Buchholz, F. Maseras, A. Vidal-Ferran, *Chem. Eur. J.* **2010**, *16*, 6495–6508.
 [55] I. Fernández, F. M. Bickelhaupt, *Chem. Soc. Rev.* **2014**, *43*, 4953–4967.

Manuscript received: November 30, 2021
 Revised manuscript received: December 10, 2021
 Accepted manuscript online: December 13, 2021



Cite this: *Org. Biomol. Chem.*, 2021, **19**, 9095

C₁-Symmetric diphosphorus ligands in metal-catalyzed asymmetric hydrogenation to prepare chiral compounds

Anirban Sen^{*a,b} and Samir H. Chikkali  ^{*a,b}

Asymmetric hydrogenation has remained an important and challenging research area in industry as well as academia due to its high atom economy and ability to induce chirality. Among several types of ligands, chiral bidentate phosphine ligands have played a pivotal role in developing asymmetric hydrogenation. Although C₂-symmetric chiral bidentate phosphine ligands have dominated the field, it has been found that several C₁-symmetric ligands are equally effective and, in many cases, have outperformed their C₂-symmetric counterparts. This review evaluates the possibility of the use of C₁-symmetric diphosphorus ligands in asymmetric hydrogenation to produce chiral compounds. The recent strategies and advances in the application of C₁-symmetric diphosphorus ligands in the metal-catalyzed asymmetric hydrogenation of a variety of C=C bonds have been summarized. The potential of diphosphorus ligands in asymmetric hydrogenation to produce pharmaceutical intermediates, bioactive molecules, drug molecules, agrochemicals, and fragrances is discussed. Although asymmetric hydrogenation appears to be a problem that has been resolved, a deep dive into the recent literature reveals that there are several challenges that are yet to be addressed. The current asymmetric hydrogenation methods mostly employ precious metals, which are depleting at a fast pace. Therefore, scientific interventions to perform asymmetric hydrogenation using base metals or earth-abundant metals that can compete with established precious metals hold significant potential.

Received 23rd June 2021,
Accepted 21st September 2021
DOI: 10.1039/d1ob01207j

rsc.li/obc

^aPolyolefin Lab, Polymer Science and Engineering Division, CSIR-National Chemical Laboratory, Dr Homi Bhabha Road, Pune 411008, India.

E-mail: s.chikkali@ncl.res.in; Tel: +91 2025903145

^bAcademy of Scientific and Innovative Research (AcSIR), Sector 19, Kamla Nehru Nagar, Ghaziabad 201002, U. P., India

1. Introduction

In the recent past, asymmetric catalysis has seen exponential growth since the products obtained are highly useful in the



Anirban Sen

Anirban Sen was born in West Bengal, India. He completed his B.Sc. at Maulana Azad College, University of Calcutta, in 2013. After completing his M.Sc. at Jadavpur University, he joined the research group of Dr Samir H. Chikkali at CSIR-National Chemical Laboratory, Pune, India, as a Junior Research Fellow (JRF) in July 2015. Currently, he is working on the design and synthesis of chiral phosphine ligands for asymmetric hydrogenation.



Samir H. Chikkali

Samir Chikkali earned his Ph.D. under the supervision of Prof. Dietrich Gudat from the University of Stuttgart, Germany. Subsequently, he did postdoctoral research with Prof. Joost Reek at the University of Amsterdam, the Netherlands and with Prof. Stefan Mecking at the University of Konstanz, Germany. In 2012 he returned to India and joined CSIR-National Chemical Laboratory (CSIR-NCL), Pune, to start his independent research career. Currently, he leads a team of highly motivated researchers studying ligand design, organometallic chemistry and catalysis, polyolefins, and sustainable polymers.

pharmaceutical, agrochemical, and perfumery industries. Ligands play a crucial role in this context. Ligands have to be optimized and tailored to carve out the microenvironment around the metal center depending upon the chemical reaction. Bidentate ligands form a chelate with the catalytically active metal center, thus creating a rigid environment around the metal center. This, in turn, helps to discriminate between the two faces of the incoming substrate and leads to enhanced selectivity. In the early 1970s, Prof. Kagan used the C_2 -symmetric ligand DIOP in the asymmetric hydrogenation (AH) of acylaminocinnamic acids and reported 72% enantioselectivity (ee).¹ Shortly after him, Knowles synthesized the C_2 -symmetric DIPAMP ligand and commercialized the L-DOPA (**2**) synthesis with 95% ee, which is used to treat Parkinson's disease (Scheme 1).² For this remarkable achievement, Knowles received the Nobel Prize in 2001. These early precedents garnered a lot of attention for the synthesis of other C_2 symmetric bidentate ligands. For instance, Noyori (jointly shared the Nobel Prize in 2001) and Takaya developed the C_2 -symmetric ligand BINAP and used it successfully in the Ru-catalyzed hydrogenation of olefins and ketones,^{3,4} while Burk and co-workers at DuPont developed DuPHOS which showed outstanding results in Rh catalyzed asymmetric hydrogenation of olefins.³⁻⁶ The C_2 -symmetric ligand reduces the number of possible competing diastereomeric transition states and thus helps in asymmetric induction.

In a seminal paper published in 1991, Achiwa and co-workers demonstrated that C_1 -symmetric ligands could be used successfully in asymmetric hydrogenation (Scheme 2).⁷ The authors argued that the intermediates are non-symmetrical in a catalytic cycle, so, two phosphine groups exert different steric and electronic effects on the metal-bound substrate. Thus, two chelating atoms fulfilling different roles might be crucial for effective enantiocontrol in an appropriate case.

Independent steric and electronic tuning of two different donor atoms to obtain a perfect ligand also makes the C_1 -symmetric ligand an attractive alternative for further development in asymmetric catalysis.^{8,9} In 1983 Knowles mentioned: "since achieving 95% ee only involves energy differences of about 2 kcal, which is no more than the barrier encountered in a simple rotation of ethane, it is unlikely that before the fact one can predict what kind of ligand structures will be effective".¹⁰ It is due to this physicochemical origin that ligand design remains a high-risk endeavor involving extensive trial and error, hard labor, intuition, experience, and above all serendip-

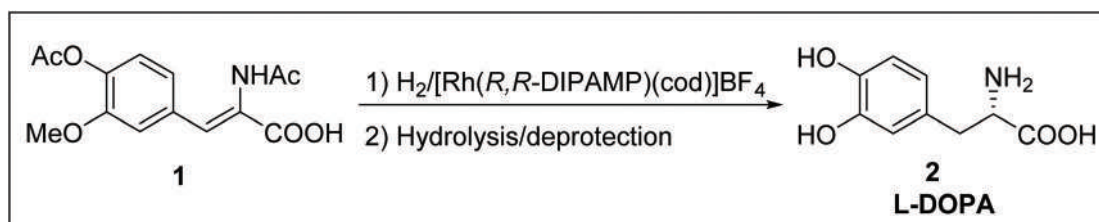
ity. As there is no universal chiral ligand, the quest to discover a structurally diverse ligand library continues to intensify as it will help to find an optimal ligand for a specific catalytic reaction from this ligand toolbox.

2. Classification, scope and objective

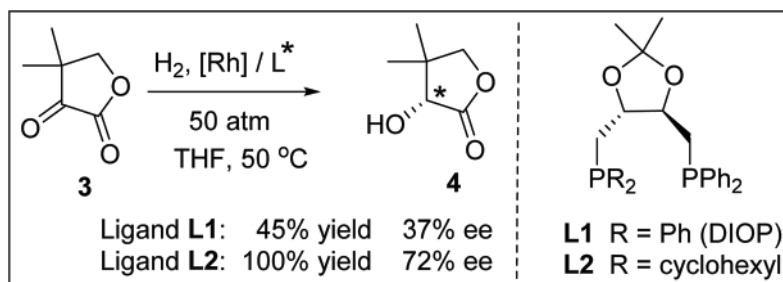
The last five decades have witnessed the development of thousands of structurally diverse chiral phosphorus ligands in asymmetric catalysis.^{11,12} Initial breakthroughs made by Kagan (DIOP, **L1**) and Knowles (DIPAMP, **L3**), followed by a notable contribution from Noyori (BINAP, **L5**) and Burk (DuPhos, **L6**) have inspired chemists to realize the full potential of asymmetric catalysis to synthesize chiral compounds. The chiral bidentate phosphorus ligands can be broadly classified (Fig. 1) into: (1) C_2 -symmetric ligands and (2) C_1 -symmetric ligands. The C_1 -symmetric ligands can be sub-divided into two categories: (a) non-symmetric diphosphorus ligands and (b) mixed donor ligands. The C_2 -symmetric ligands can be sub-divided (Fig. 2) into two categories: (a) P-chiral ligands and (b) ligands with backbone chirality. The ligands with backbone chirality can be sub-divided into two categories: (a) C-chiral ligands and (b) axially chiral ligands.

Among the thousands of chiral ligands developed so far, some C_2 -symmetric ligands are effective in several mechanistically unrelated reactions. For such ligands, Jacobsen coined the term "privileged ligands".¹³ In the case of the C_2 -symmetric ligands, the presence of two equivalent donor atoms reduces the number of possible transition states and diastereomeric intermediates which has a beneficial effect in increasing selectivity.¹⁴ In the case of the C_1 -symmetric ligands (Fig. 3), the reduction in the diastereomeric transition states is achieved mainly in two ways: (1) different steric and electronic effects (*trans* effect) of the two donor atoms favor the binding of the substrate to the catalyst in a particular way compared to the otherwise possible arrangements, and (2) the presence of a covalent linker in the ligand acts as a molecular recognition unit by showing attractive non-covalent interaction with the substrate, thus reducing the possible substrate-catalyst arrangements (Fig. 4).

The role of C_2 -symmetric ligands in asymmetric hydrogenation has been intensively reviewed.¹⁵⁻¹⁹ Therefore, this review aims to examine the C_1 -symmetric diphosphorus ligands and evaluate their performance in asymmetric hydrogenation. To



Scheme 1 Synthesis of L-DOPA via asymmetric hydrogenation (AH).



Scheme 2 Achiwa's hydrogenation studies with desymmetrized DIOP.

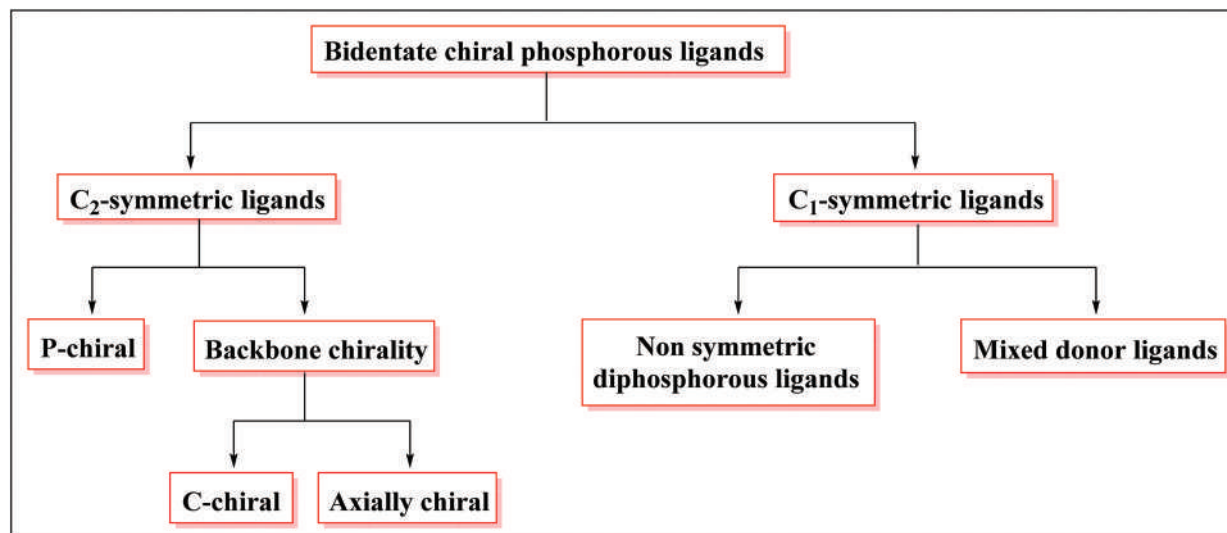
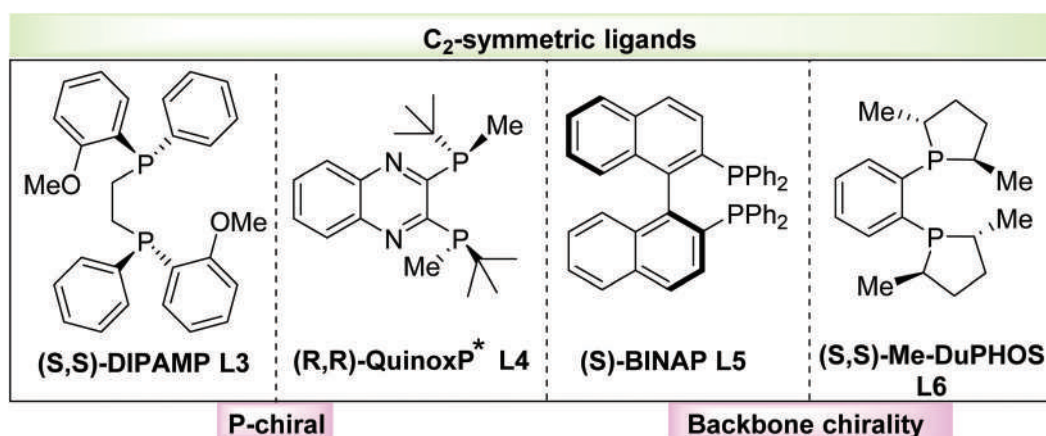


Fig. 1 General classification of chiral bidentate phosphorus ligands.

Fig. 2 Different types of C₂-symmetric ligands.

keep the volume of this review concise, we have omitted the synthetic aspects of different C₁-symmetric diphosphorus ligands. The C₁-symmetric diphosphorus ligands have been grouped into five categories, namely, C₁-symmetric P-chiral, C₁-symmetric ferrocene based diphosphorus, phosphine-phos-

phite and phosphine-phosphonite, phosphine-phosphoramidite and ferrocene-based diphosphorus ligands with a covalent linker. The utilization of these ligand classes in asymmetric hydrogenation to produce pharmaceutically relevant chiral compounds is examined.

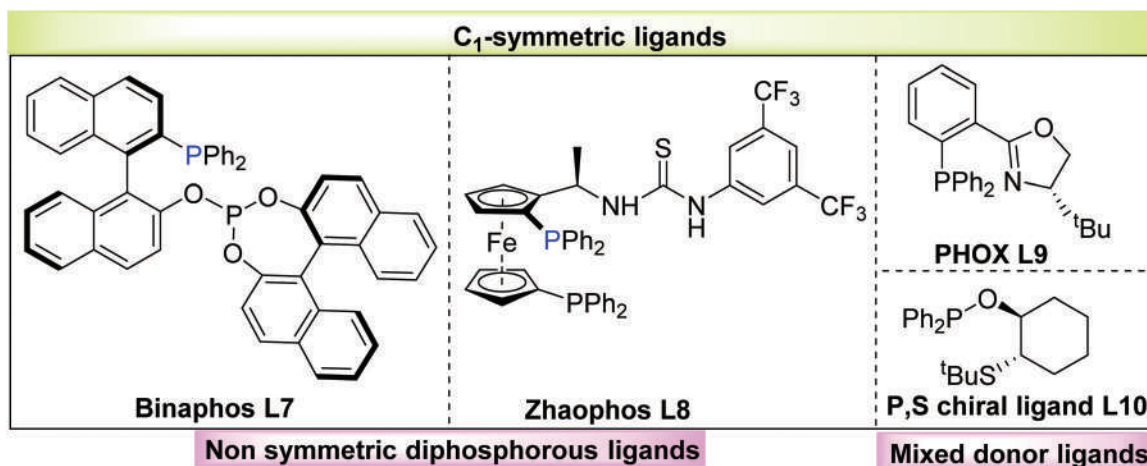


Fig. 3 Different types of C_1 -symmetric ligands.

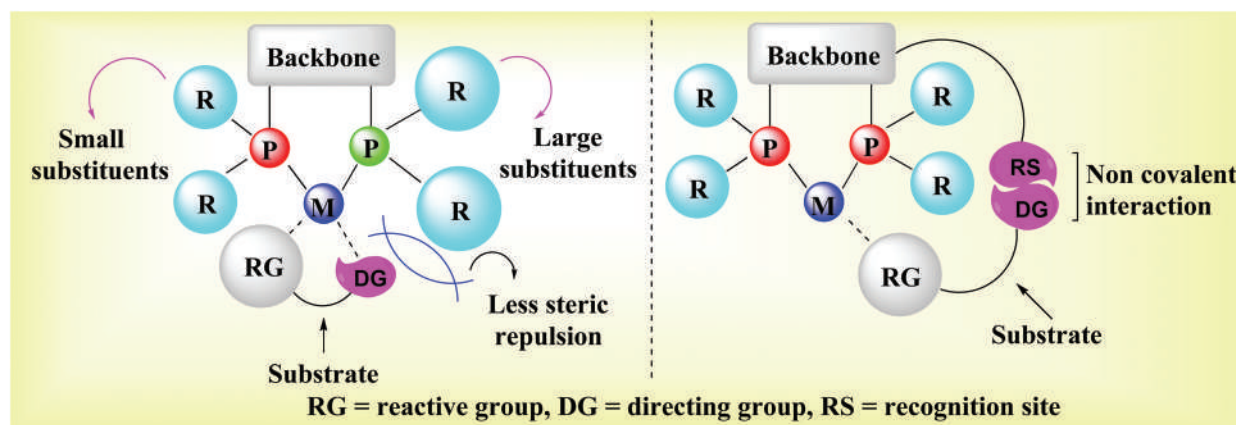


Fig. 4 Steric effect and non-covalent interaction helps in regio-facial and enantio-facial discrimination.

3. C_1 -Symmetric diphosphorus P-chiral ligands

One of the early examples of the P-chiral ligand is DIPAMP (L3) which exhibited high enantioselectivity in the industrial synthesis of *L*-DOPA (Scheme 1). There are reviews on P-chiral ligands; however, here we will discuss only the bidentate P-chiral ligands where the two donor atoms are different.^{20–22} Historically, the C_2 -symmetric ligands have been more successful in this context where the metal–ligand complex contains two non-adjacent hindered quadrants in the quadrant diagram which is accepted as a good design to achieve high enantioselectivity (Fig. 5). This has supplanted the development of the C_1 symmetric bidentate phosphine ligands in asymmetric hydrogenation. In 2004, Hoge and co-workers synthesized the three-hindered quadrant ligand tri-chickenfootphos (L11) and used it successfully in the asymmetric hydrogenation of several functionalized enamides (Fig. 6).²³

In 2008, Zhang and coworkers synthesized a new family of C_1 -symmetric bisphosphine ligands through the simple synthesis of the chiral binol derivatives (L15) and explored the asymmetric hydrogenation of several α and β -dehydroamino acid derivatives with good to excellent enantioselectivities.²⁴ In 2010, Senanayake and coworkers reported the synthesis of MeO-POP (L14) and successfully used it in the Rh-catalyzed asymmetric hydrogenation of α and β -(acylamino)acrylates with excellent enantioselectivity (Table 1).²⁵ In 2010, Zhang and coworkers synthesized the three-hindered quadrant bidentate phosphine ligand based on the phospholane ring (L16) and successfully used it in the asymmetric hydrogenation of several functionalized olefins with excellent reactivity (up to 10 000 TON) and selectivity.²⁶

Optically active α -amino ketones are very important building blocks found in many bioactive molecules. Zhang and co-workers first reported the asymmetric hydrogenation of cyclic α -dehydroamino ketones using 1 mol% TCFP-Rh complex with 97–99% enantioselectivity (Scheme 3). It is worth mentioning that (*S*)-TCFP (L11) outperformed many symmetric bidentate

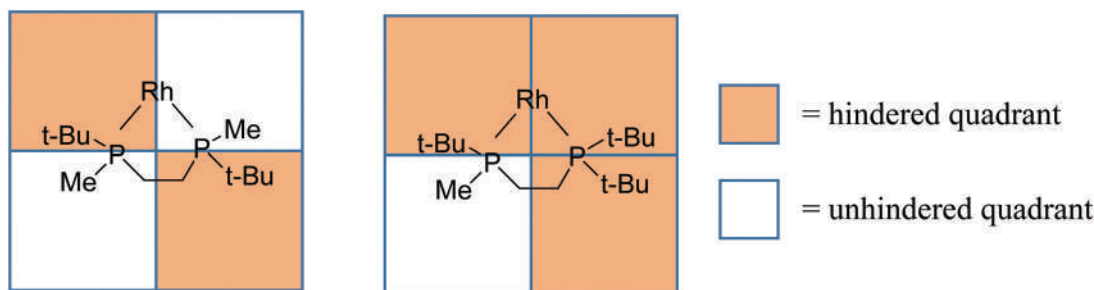


Fig. 5 Quadrant diagram of the traditional C_2 -symmetric and the three-hindered quadrant ligand.

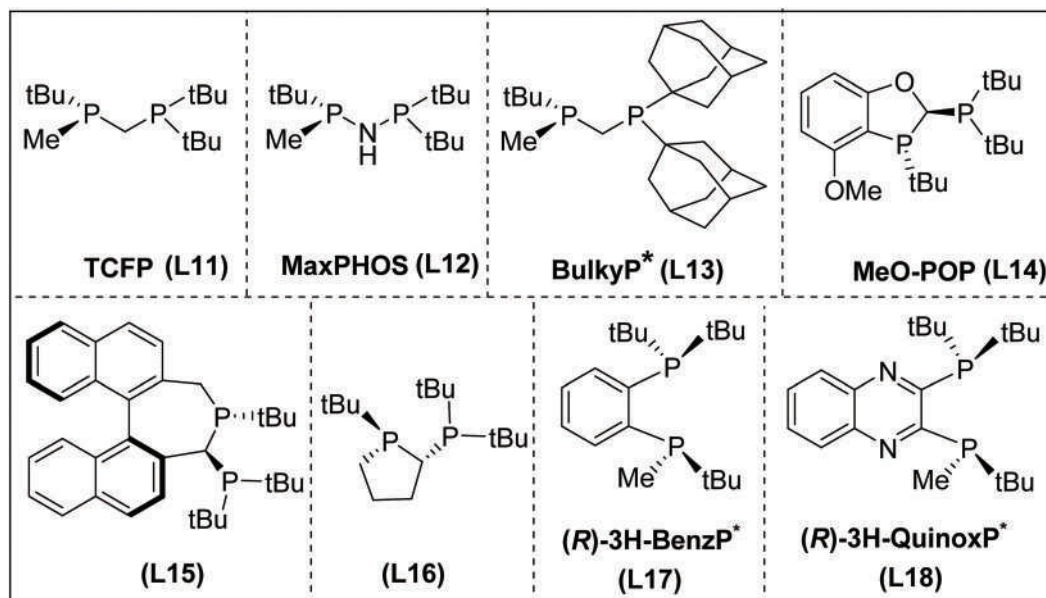


Fig. 6 C_1 -Symmetric diphenylphosphorus P-chiral ligands.

Table 1 AH of β -(acylamino)acrylic acid derivatives

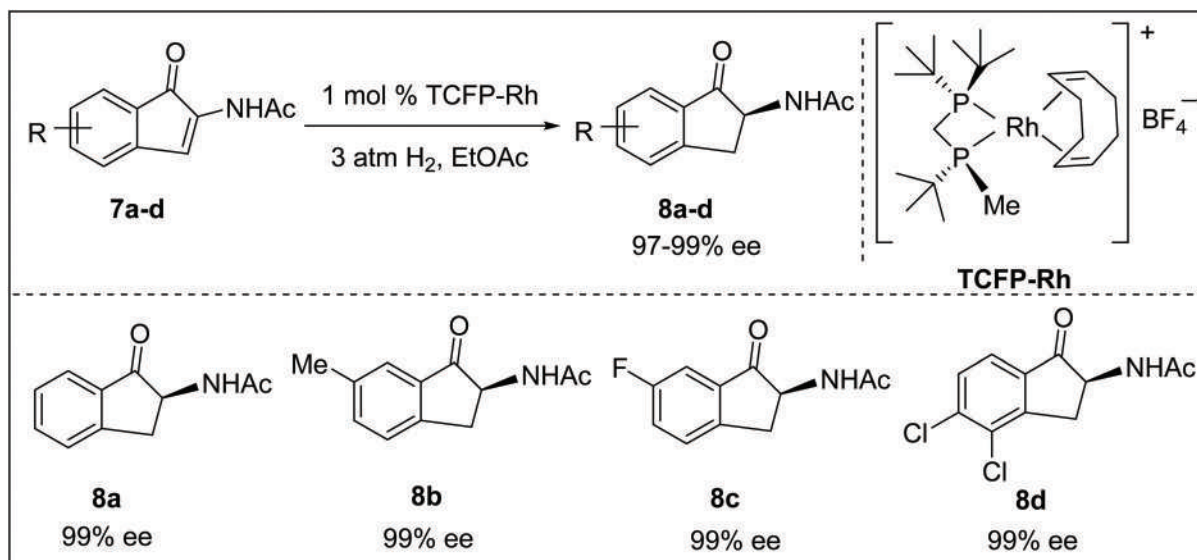
Entry	L	R, R' (geometry)	H ₂ (psi)	ee (%)
1	L14	Me, Me ((Z)-5a)	100	99
2	L14	Me, iPr ((Z)-5b)	100	99
3	L14	Ph, Me ((Z)-5c)	100	97
4	L16	Me, Me ((E)-5d)	50	98
5	L16	4-F-Ph, Me ((E/Z)-5e)	50	94

phosphine ligands like BINAP (L3), DuPHOS (L6), QuinoxP* (L4), etc. Less steric hindrance between the methyl group of the ligand and the Rh-chelate ring containing the NHAc group of the substrate determines the enantioselectivity.²⁷

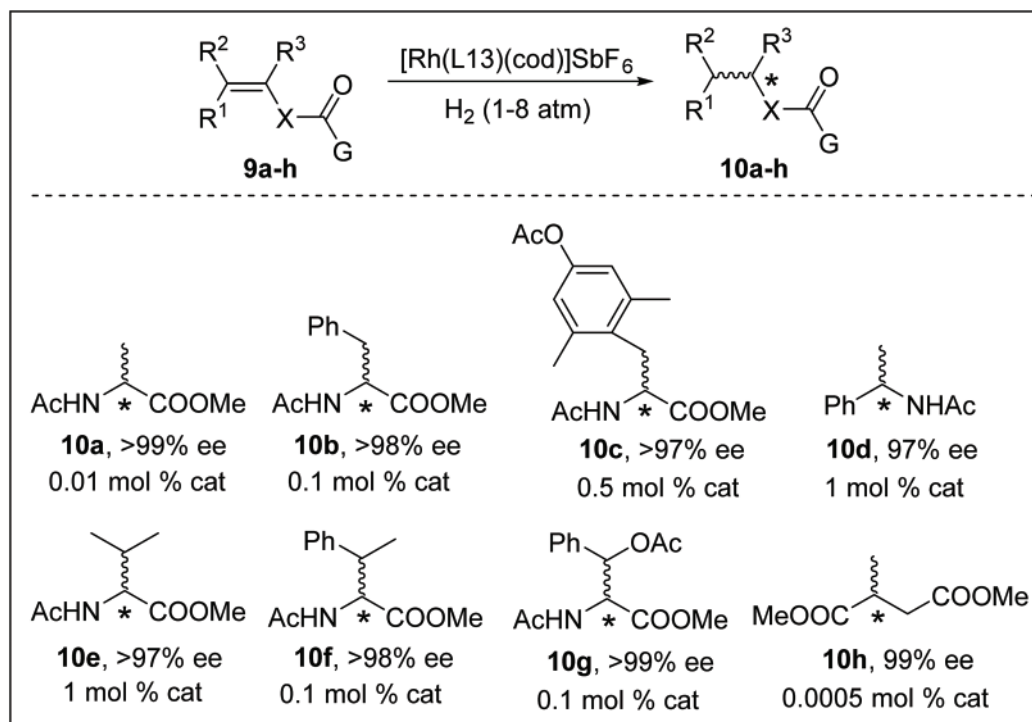
TCFP (L11) is a three-hindered quadrant ligand and it showed excellent activity and selectivity in Rh-catalyzed asym-

metric hydrogenation. However, it is an air-sensitive oil and is thus difficult to handle. To resolve this issue, Imamoto and co-workers replaced the di-*tert*-butylphosphino group in TCFP with the bulkier di-1-adamantylphosphino group. They synthesized the new ligand BulkyP* (L13) (Fig. 6) which is an air-stable crystalline solid. The Rh-complex of this ligand was successfully utilized in the asymmetric hydrogenation of several functionalized olefins. The reaction can be performed with 0.0005 mol% catalyst loading in some cases without any decrease in enantioselectivity. It also showed excellent reactivity and selectivity for some tetra substituted enamides (Scheme 4).²⁸ In this regard it is worth mentioning that these diphenylphosphine ligands (L11–L16) have a single atom linker and form small bite angles (4 membered chelate ring) with the metal, thus they are sterically less bulky and impose less steric repulsion on the other ligands at the metal center. It is for this reason that these ligands are more suitable for the asymmetric hydrogenation of hindered substrates such as tetra-substituted C=C bonds.

Optically active chiral cyclic β -amino alcohols are structurally important building blocks found in many bioactive mole-



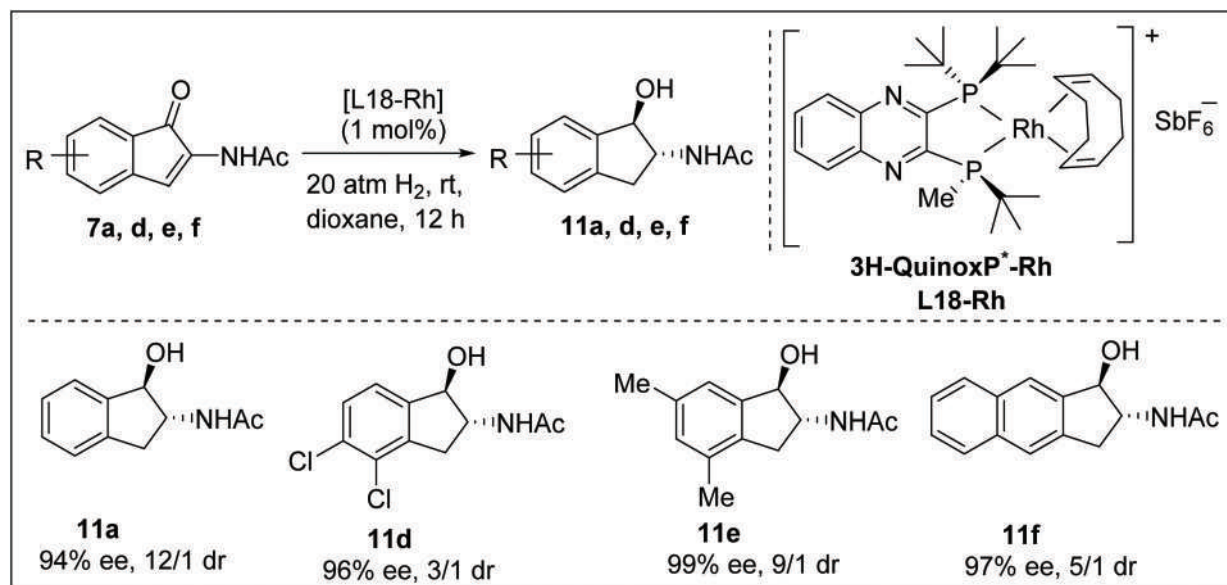
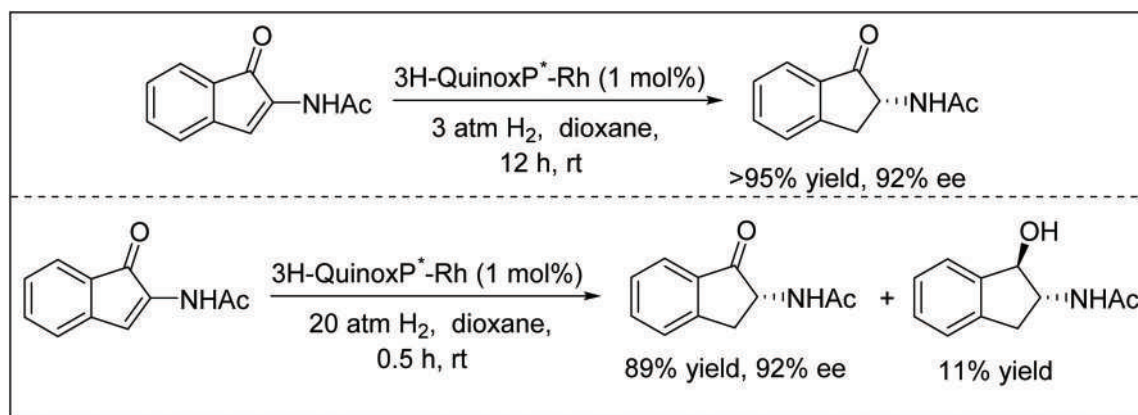
Scheme 3 AH of cyclic carbonyl compounds with an endocyclic vinyl group.

Scheme 4 AH of functionalized alkenes by $[\text{Rh}(\text{L13})(\text{COD})]\text{SbF}_6$.

cules. Zhang and coworkers realized a practical and efficient rhodium-catalyzed asymmetric hydrogenation to prepare this class of compounds *via* one-pot sequential reduction of C=C followed by C=O bonds. Using 1 mol% 3-H-QuinoxP*-Rh (**L18**-Rh) catalyst, a series of α -dehydroamino ketones were hydrogenated with excellent enantioselectivity and satisfactory diastereoselectivity in dioxane solvent. However, substrates containing an electron-withdrawing group (EWG) provided

lower diastereoselectivity compared to the electron-donating group (EDG) containing substrates (Scheme 5).²⁹

To shed light on the reaction mechanism, several control experiments were carried out. When the reaction was performed under lower (3 atm) hydrogen pressure in dioxane, only the C=C bond was reduced with 92% ee in quantitative yield (Scheme 6). After this, another reaction was carried out at 20 atm hydrogen pressure for 30 minutes. This afforded 89%

Scheme 5 AH of cyclic α -dehydro amino ketones by the L18-Rh complex.

Scheme 6 Control experiments in AH.

α -amino ketone with 92% ee and 11% β -amino alcohol, implying a rapid reduction of the C=C bond compared to the C=O bond. These results suggested that asymmetric hydrogenation of the C=C bond occurred before C=O bond reduction (Scheme 7).

4. C_1 -Symmetric ferrocene based diphosphorus ligands

Ferrocene-based diphosphine ligands were first introduced by Hayashi and Kumada by utilizing Ugi's amine.³⁰ After their pioneering work, the same group as well as various other groups have synthesized several ferrocene-based diphosphorus ligands starting from the readily accessible Ugi's amine. However, here we will discuss only the C_1 -symmetric ferrocene-based chiral diphosphorus ligands and their application in

asymmetric hydrogenation. Togni and Spindler³¹ synthesized Josiphos type ligands³² which saw excellent industrial success in the synthesis of (+)-biotin as well as the herbicide (*S*)-metolachlor.³³ In addition to this, Weissensteiner and Spindler introduced the Walphos³⁴ class of ligands whereas Knochel introduced the Taniaphos ligand class³⁵ which has been successfully applied in the asymmetric hydrogenation of several olefins and ketone substrates (Fig. 7). Boaz developed a new class of phosphine-aminophosphine-based ligand Bophoz³⁶ whereas Chen and coworkers developed ChenPhos from Ugi's amine and applied it successfully in the AH of several functionalized olefins. Only recent applications of such ligands in asymmetric hydrogenation is presented below.

Sitagliptin has been approved by the FDA for the treatment of type 2 diabetes. Asymmetric hydrogenation has been successfully utilized for the synthesis of sitagliptin by Hansen and coworkers where a *tert*-butyl variant of the Josiphos type diphosphorus

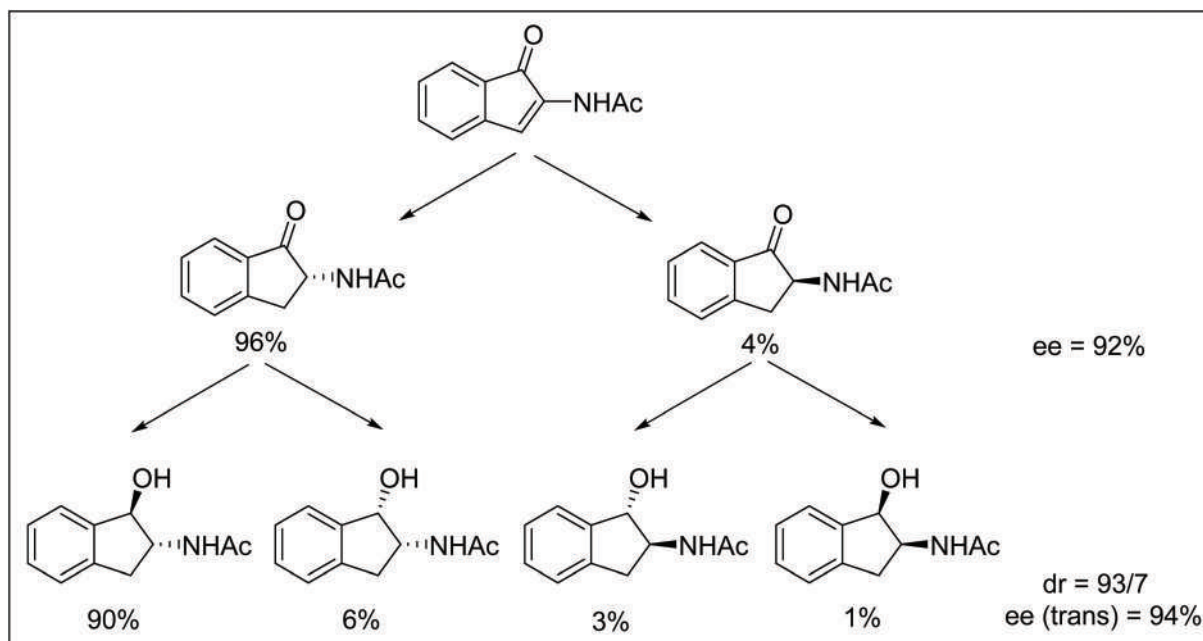
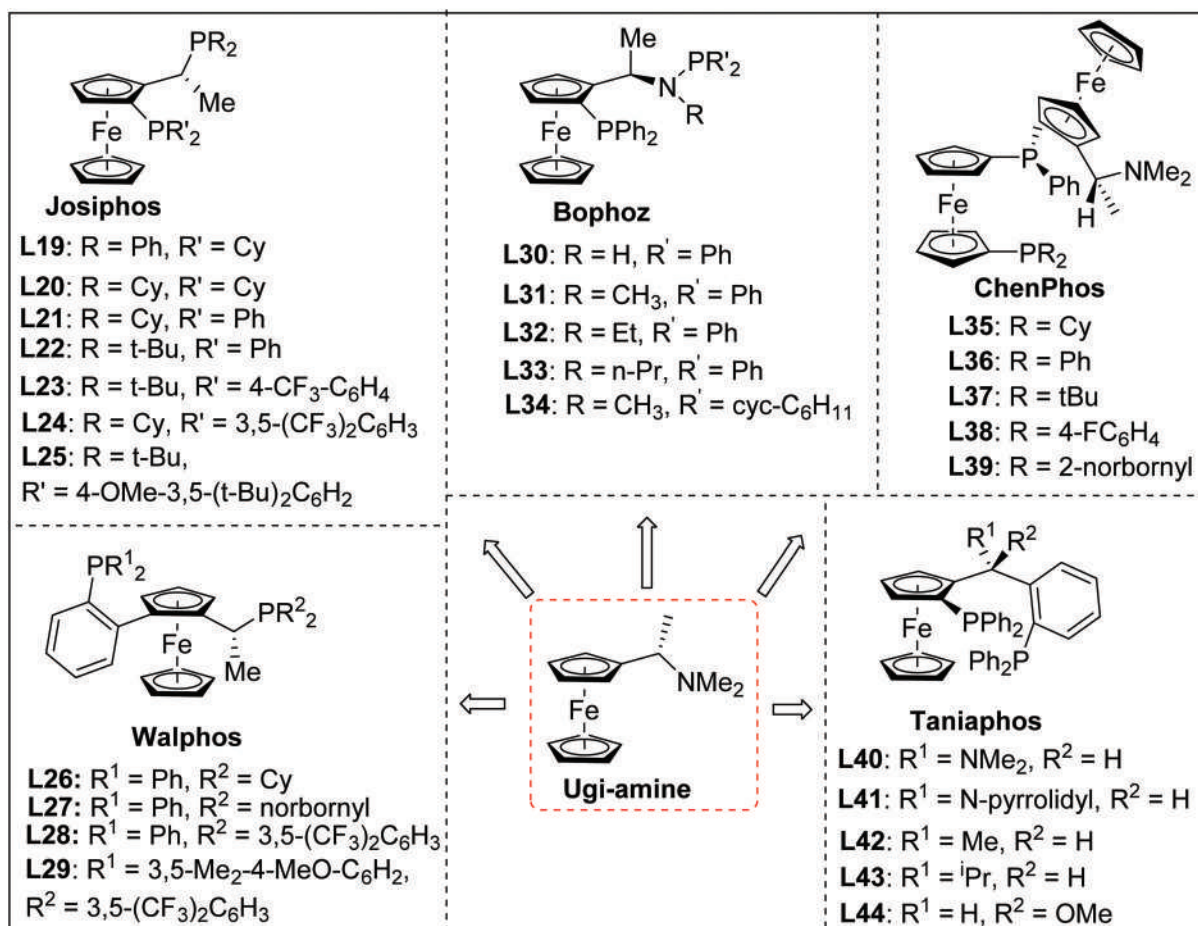
Scheme 7 Detailed conversion process for four isomers of β -amino alcohols.

Fig. 7 Different chiral ferrocenyl phosphines derived from the Ugi-amine.

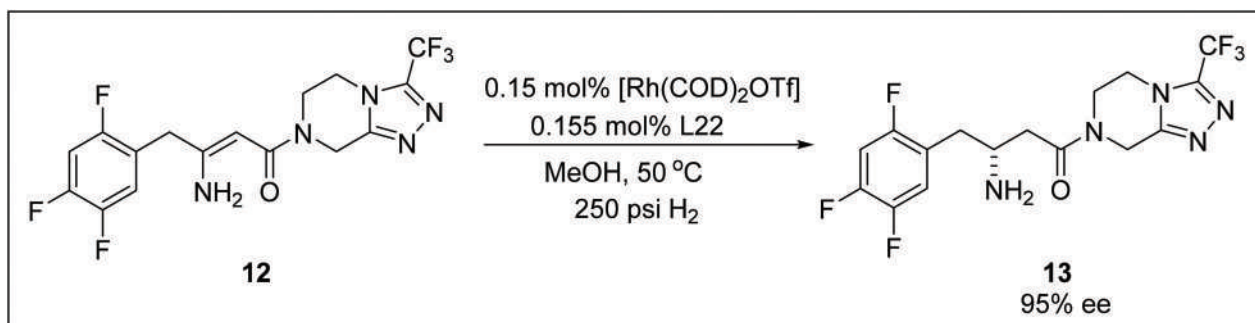
sphorus ligand afforded 95% ee, outperforming other commercially available bidentate chiral phosphine ligands. They also screened several additives during the optimization and found that a small amount of the acidic additive NH_4Cl (0.15–0.3 mol%) had a beneficial effect on the hydrogenation reaction in terms of both reactivity and selectivity. In addition to this, increasing the hydrogen pressure from 100 to 250 psi further helped to reduce the catalyst loading from 0.3 to 0.15 mol% without affecting the ee, making the process more cost-effective. At 50 °C, 8 L of methanol was found to be sufficient for full conversion of 1 kg of dehydro-sitagliptin into the product in 16 h. When the reaction was performed in the presence of deuterium instead of hydrogen, deuterium was incorporated at the β -position which suggested that the reaction might have proceeded through the involvement of the imine tautomer. Screening of several solid adsorbents revealed that 10 wt% Ecosorb C-941 was sufficient to remove almost all the dissolved rhodium from the crude hydrogenation product. The final conversion of the free base sitagliptin 12 to the pharmaceutically desired phosphate monohydrate salt further enhanced the ee to a nearly perfect level (>99.9% ee) (Scheme 8).³⁷

Chiral nitroalkanes are important building blocks found in many bioactive molecules and natural products like the muscle relaxant baclofen, the asthma agent NK5807, and Catramilast, a drug used for the treatment of atopic dermatitis. It is also a very important intermediate that can easily be converted into different structural motifs like amines, carboxylic acids, aldehydes, nitrile oxides, and denitrated compounds. In the literature, chiral β -branched nitroalkanes have been prepared in many different ways, such as (i) the bio-catalytic reduction of nitroalkenes by using baker's yeast and reductases, (ii) the asymmetric transfer hydrogenation of β,β -disubstituted nitroalkenes by transition metal catalysts and organocatalysts, and (iii) enantioselective conjugate additions of carbon or phosphorus nucleophiles. However, a more practical method could be the direct asymmetric hydrogenation of nitroalkenes. It is particularly attractive because the substrates can be easily synthesized through the nitration of olefins (nitration of α -methyl styrenes by N_2O_4 , CAN, or HNO_3) or by the Henry reaction.

With this idea, Zhang and coworkers first attempted the asymmetric hydrogenation of β,β -disubstituted nitroalkenes

with a series of bidentate symmetrical phosphine ligands. But in all cases, they obtained poor enantioselectivity with good conversion. In some cases, isomerization was a problem. Finally, they got a modest ee of 56% with 87% conversion and no isomerization when they used the ferrocene-based unsymmetrical ligand Josiphos L20. After that, the authors changed the substituents on phosphorus to tune the sterics and electronics. Finally, with the Josiphos L23 ligand, full conversion with 85% ee was achieved without isomerization. After optimizing the ligand, other parameters like the metal precursor, solvent, pressure, temperature, and catalyst loading were screened. Under the final optimized conditions, full conversion with 94% ee was obtained. A broad substrate scope where the reaction tolerates EWGs, as well as EDGs, was demonstrated. However, when the substituent was at the *ortho* position, the conversion was low (Scheme 9).³⁸

Trifluoromethyl groups containing chiral secondary alcohols are ubiquitous structural motifs found in many bioactive molecules, such as the tryptophan hydroxylase inhibitor LX1301. To access this class of compounds, several strategies have been developed such as the enantioselective trifluoromethylation of aldehydes, the kinetic resolution of racemic 1-aryl-2,2,2-trifluoroethanol, the enantioselective Hiyama cross-coupling, enzymatic bio-catalysis as well as asymmetric transfer hydrogenation. However, asymmetric hydrogenation could be a more direct approach to access this class of compounds. Catalytic methods that were developed for acetophenones did not work well for trifluoroacetophenone due to the different stereoelectronic properties. Noyori reported a chiral ruthenium catalyst for the asymmetric hydrogenation of ketones in the presence of a strong base whereas Iseki and coworkers reported a chiral rhodium-amidophosphine-phosphinite catalyst for the asymmetric hydrogenation of trifluoromethyl ketones which gave excellent results for many substrates but was not efficient for trifluoromethyl acetophenone.^{39,40} To address this challenge, Togni and coworkers prepared a series of rhodium(III) complexes bearing Josiphos type ligands by following a procedure that was earlier reported by Mashima *et al.* (Table 2).⁴¹ These were successfully implemented in the asymmetric hydrogenation of a series of trifluoro acetophenones with excellent yield and enantioselectivity (Scheme 10). However, in the case of the dimethyl-



Scheme 8 AH of dehydro-sitagliptin.

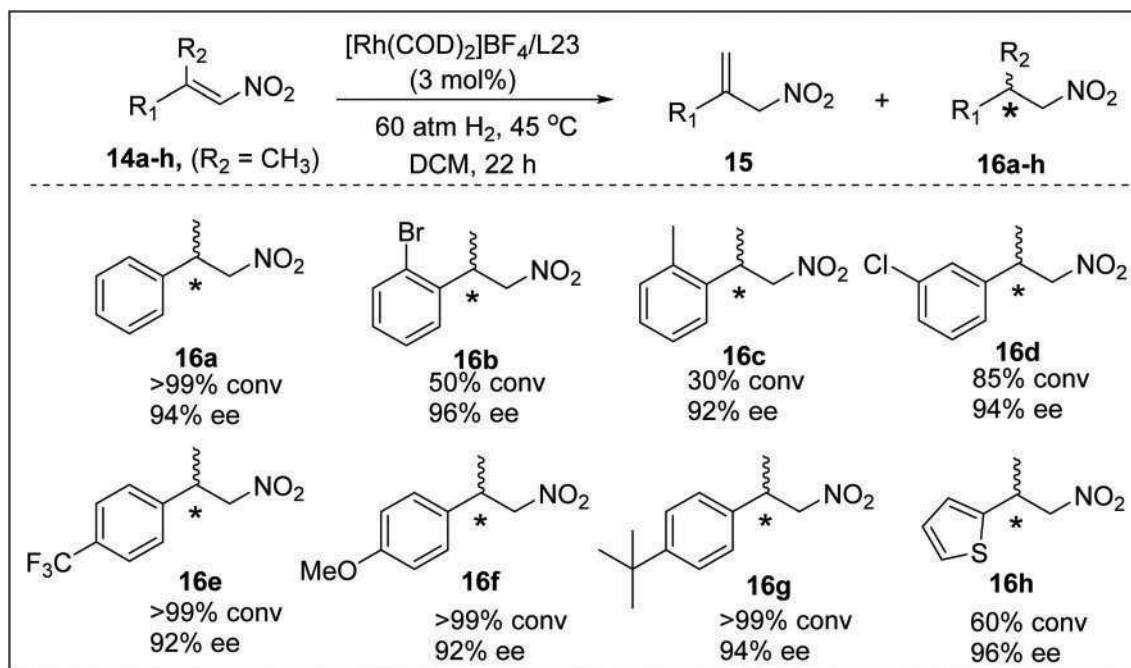
Scheme 9 AH of β,β -disubstituted nitroalkene.

Table 2 Synthesis of chloride bridged dinuclear Rh(III) complexes

1) ligand (2.05 equiv) toluene, rt, 3 h

2) HCl in Et_2O (10 equiv), rt, 3 h

$[\text{Rh}(\text{H})(\text{P}-\text{P}^*)]_2(\mu\text{-Cl})_3\text{Cl}$ (**17**)

Ligand	Catalyst	Yield (%)
L21	Rh-L21	74
L22	Rh-L22	64
L24	Rh-L24	86
L25	Rh-L25	65

amino group, a lower ee was obtained (66%). Fluorinated ketones bearing the CF_2Cl , C_2F_5 moiety afforded higher enantioselectivity, which may be due to the increased steric demand, whereas perfluorophenyl ketones afforded a lower yield and lower ee. A control experiment with acetophenone afforded no product, suggesting the critical role of the trifluoroalkyl groups for the success of the reaction (Scheme 11).⁴²

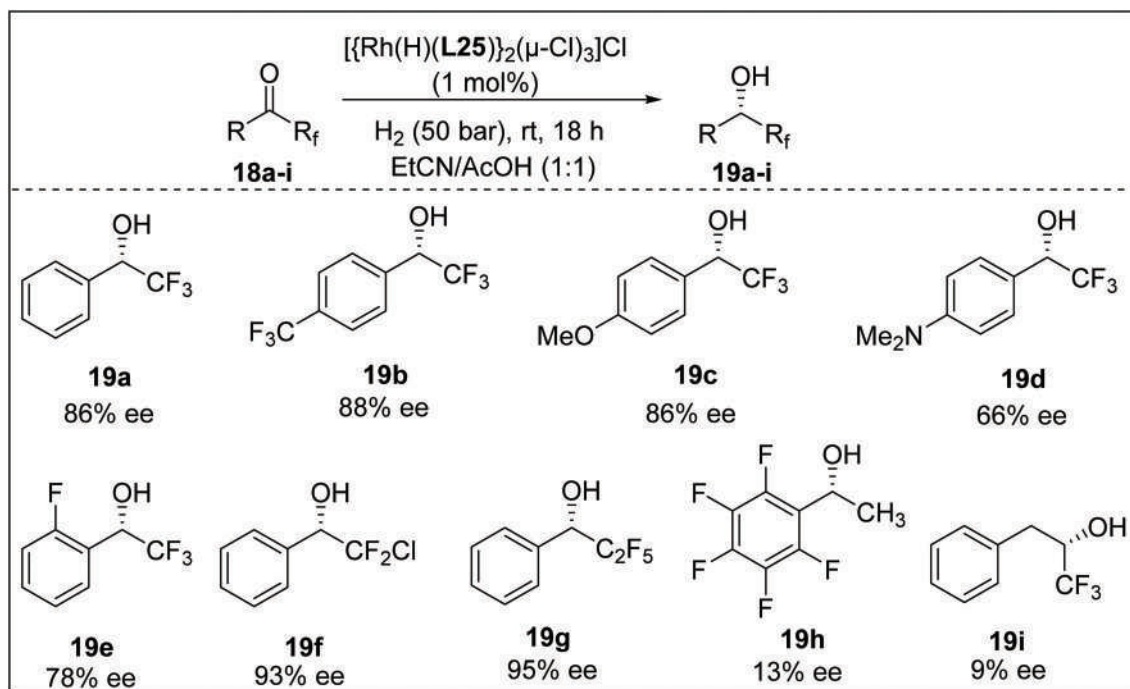
They further extended their methodology to 3-substituted-2-phenylindoles (Scheme 12), which have shown biological activity for G protein-coupled receptor modulation. In Et_3CN , 2 mol% catalyst afforded excellent yield and enantioselectivity. However, the 2-substituted phenyl or *t*-butyl group was crucial for a higher ee. The sterically more demanding $-\text{C}_2\text{F}_5$, $-\text{C}_3\text{F}_7$ fragments also afforded a higher ee. The dinuclear rhodium (III) monohydride species showed different reactivities compared to the conventional rhodium(I) complex involved in the

asymmetric hydrogenation of $\text{C}=\text{C}$ double bonds with a coordinating functional group which in turn increases the repertoire.

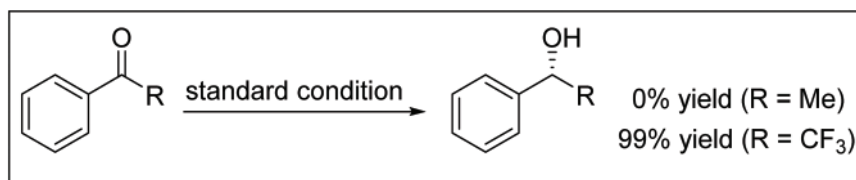
Chiral 3,4-disubstituted piperidines are widely occurring scaffolds in many natural products and bioactive molecules such as Roche-1, (-)-paroxetine, and (+)-femoxetine, and are well known for their important pharmacological activity. Although there are reports on the asymmetric hydrogenation of 2-substituted pyridines and related disubstituted and trisubstituted pyridines, usually 3-substituted pyridines are hydrogenated with low enantioselectivity.^{43,44} Thus 3,4-disubstituted pyridines are quite challenging substrates for asymmetric hydrogenation mainly because of the reactivity and enantioselectivity issue. To solve this problem, Zhang and coworkers adopted a strategy of kinetic resolution of 1,4-dihydropyridines and 1,4,5,6-tetrahydropyridines *via* asymmetric hydrogenation to efficiently synthesize chiral piperidine and tetrahydropyridines (Scheme 13). They successfully explored the kinetic resolution of a diverse array of racemic 3,4-disubstituted 1,4,5,6-tetrahydropyridines as well as 1,4-dihydropyridines *via* Rh-catalyzed asymmetric hydrogenation using the (*R*)-*t*-Bu-Josiphos (L22) ligand and obtained tetrahydropyridines and piperidines with excellent enantioselectivity. However, heteroaryl-substituted substrates cannot be well resolved. In the case of the *N*-methyl group protected *rac*-22f, no kinetic resolution was observed, giving *rac*-23f which shows the crucial role of the protecting group of the amine in this transformation.⁴⁵

This methodology was successfully applied in the synthesis of paroxetine, as shown in Scheme 14.

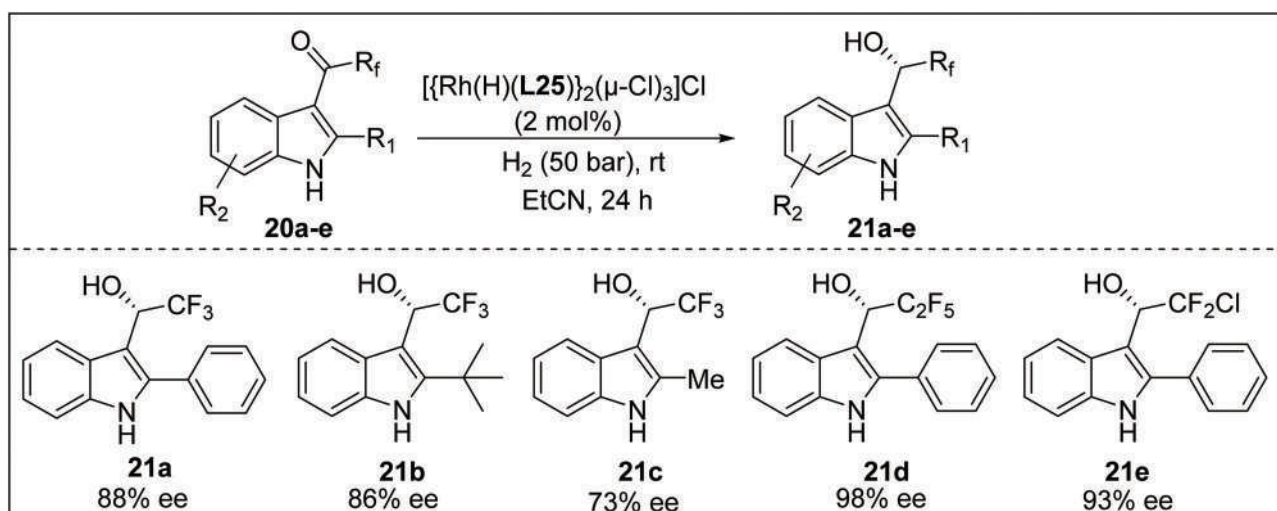
The benzodiazepine motif has attracted a lot of attention from the scientific community as well as pharmaceutical com-



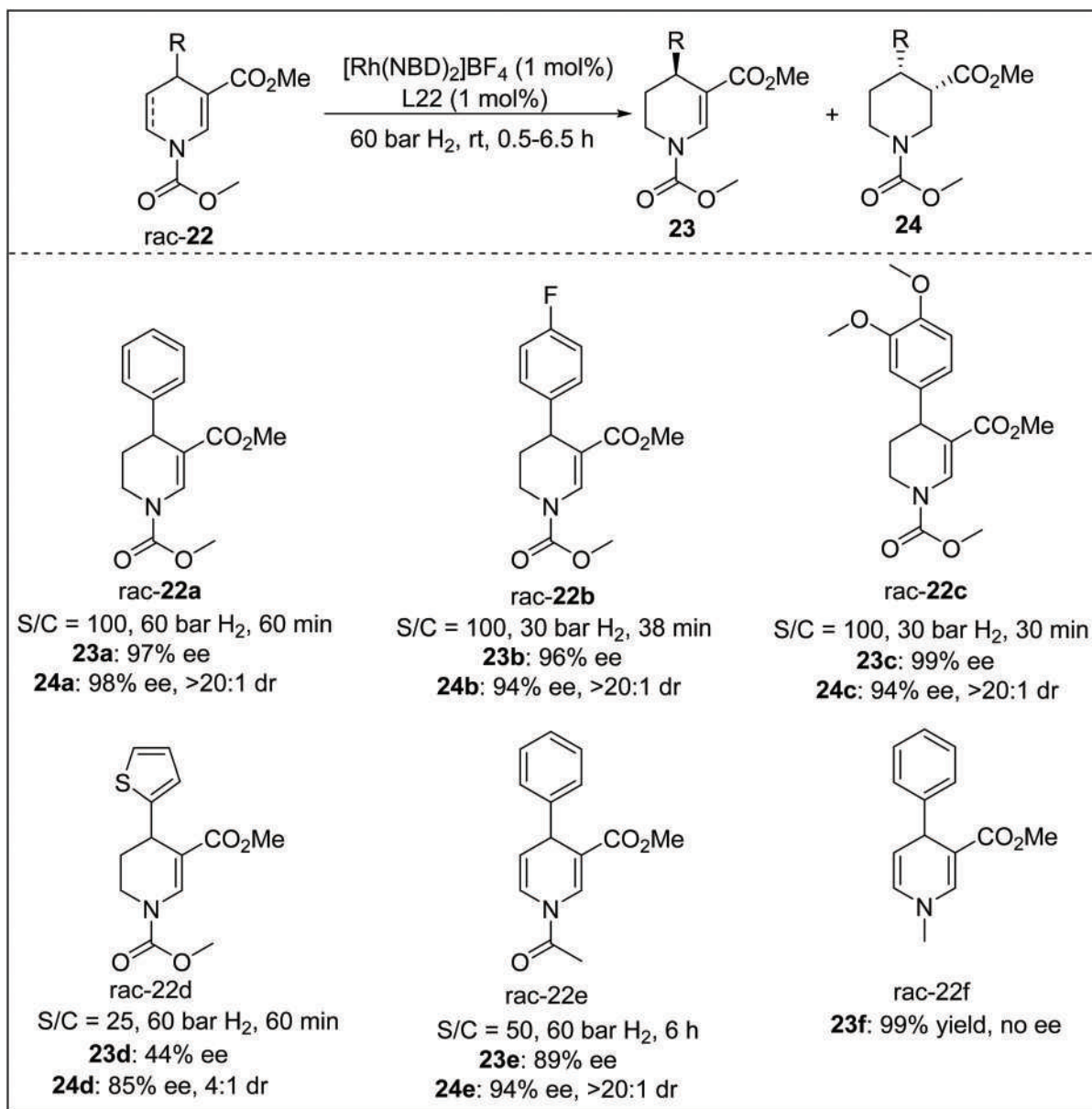
Scheme 10 AH of aryl perfluoroalkyl ketones.



Scheme 11 Comparison of reactivity between trifluoroacetophenone and acetophenone.



Scheme 12 AH of 3-(trifluoroacetyl)-2-arylimidoles and related substrates.



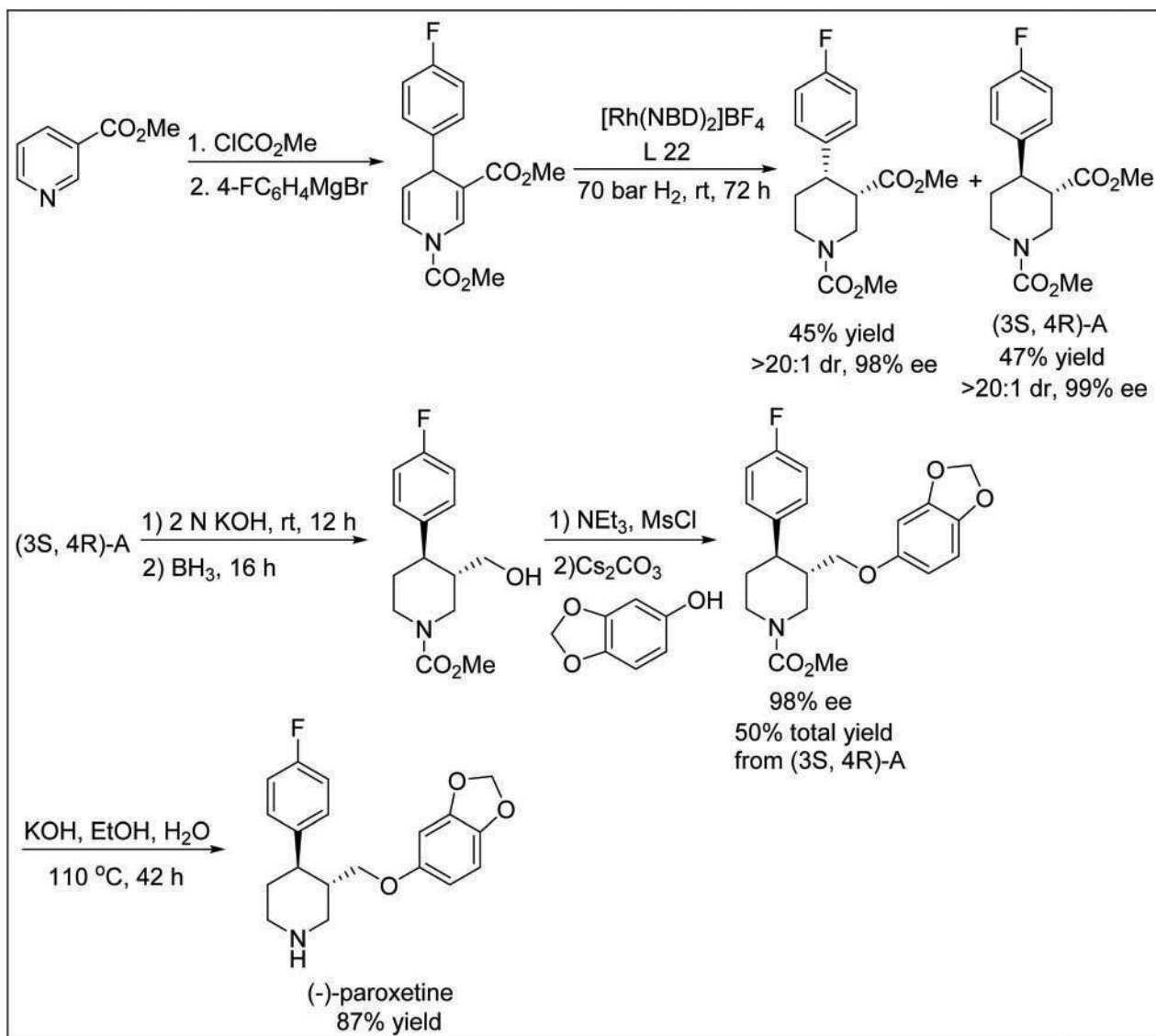
Scheme 13 Kinetic resolution of different 3,4-disubstituted 1,4,5,6-dihydropyridines.

panies since its discovery due to its effectiveness in the treatment of various pathologies related to the central nervous system. In addition, this class of compounds was shown to inhibit BET proteins, making it a potential medicine for the treatment of cancer and other inflammatory diseases. Eli Lilly has developed a practical enantioselective route for the synthesis of the drug candidate LY300164 using oxidoreductase for the introduction of a chiral center.⁴⁶ Along the same lines, Bayer Pharma identified BAY-1238097 (Scheme 15), a new member of this class of compounds with the aim to develop a cost-efficient robust process for the synthesis of the chiral intermediate **S-26**.

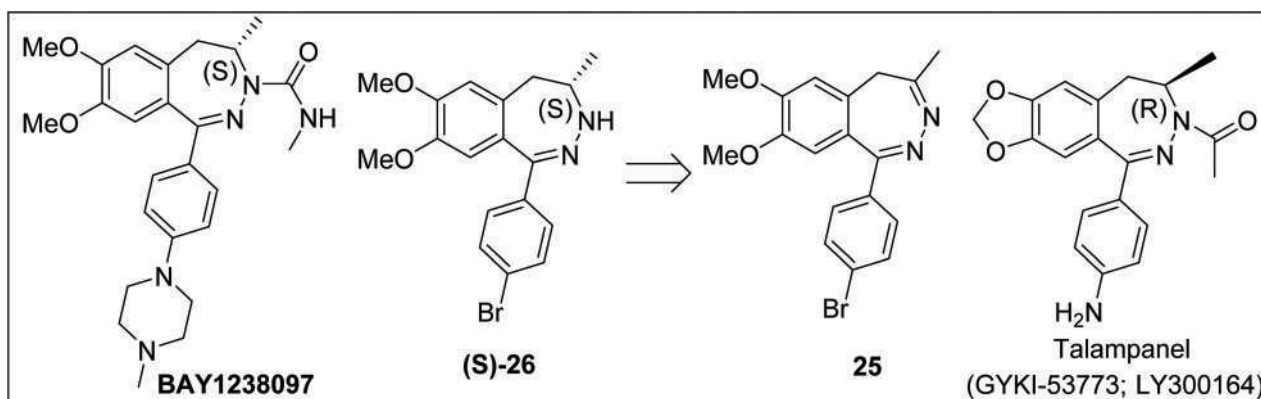
They carried out asymmetric hydrogenation using a high throughput experiment in an A96 parallel hydrogen reactor to

screen 48 different chiral ligands with and without an iodine additive in the presence of $[\text{Ir}(\text{COD})\text{Cl}]_2$ in DCM solvent (Scheme 16). Out of these 96 reaction mixtures, only in 13 cases they got above 50% ee.

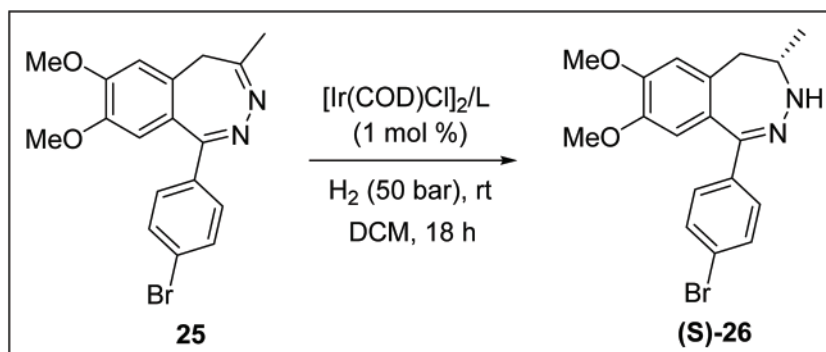
After further optimization of ligands, temperature, solvent, pressure and time, they found that WalPhos-L26 was the most enantioselective ligand. At room temperature, this catalyst gave 96% ee in THF with incomplete conversion (64% at S/C = 100). When the reaction was performed at 60 °C with a higher substrate to catalyst ratio (S/C = 1000), the enantiomeric excess decreased sharply (3% ee in THF, 9% ee in toluene) although the yield was acceptable (65% in THF, 81% in toluene). These results suggested that may be the Lewis basic product is displacing the chiral ligand, thus leading to product inhibition.



Scheme 14 Synthesis of (-)-paroxetine.



Scheme 15 Structures of BAY1230897, Talampanel, and a possible route to prepare (S)-26 from 25 via AH.



Scheme 16 AH of 25.

To solve this problem, several Lewis and Brønsted acids and acetic anhydrides were screened in stoichiometric amounts since the amine product will react with such additives *in situ* to form an acid–base adduct or an *N*-acyl derivative. With acetic anhydride, they obtained the acetylated product quantitatively at room temperature with 94% ee. At a lower catalyst loading, the conversion decreased although the enantiomeric excess was maintained. However, in the presence of 2.5 equivalents of (Boc)₂O with respect to the Ir-catalyst, a high turnover number as well as ee were obtained without any Boc-protected product formation which suggested that (Boc)₂O might be reacting with the Ir metal to form a more active and/or robust catalyst (Table 3). Finally, the asymmetric hydrogenation reaction was performed at 50 °C under 80 bar hydrogen pressure in kilogram scale with 1.2 kg substrate, 1.5 mol% ligand, 0.75 mol% [Ir(COD)Cl]₂ in THF for 16 hours which resulted in 94% conversion to the product with 92% ee. A final workup followed by crystallization gave almost 70% yield of the product with 99% ee.⁴⁷

In 2013 Chen and coworkers prepared a series of ferrocene-based *C*₁-symmetric modular diphosphine ligands, known as ChenPhos, starting from Ugi's amine.⁴⁸ These ligands were found to be air-stable and could be easily synthesized in one pot. In fact, they synthesized ligand L35 at a kilogram scale.

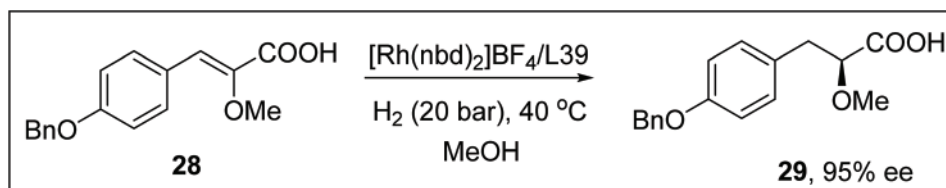
Finally, they used this ligand class for the asymmetric hydrogenation of (*E*)-3-(4-benzyloxyphenyl)-2-methoxyacrylic acid and achieved excellent enantiomeric excess with the ligand L39 (Scheme 17). In this regard, it is worth mentioning that these ligands were found to be inactive for the asymmetric hydrogenation of the corresponding ester substrates. This suggests that the electrostatic secondary interaction between the dimethylamino group of the ligand and carboxylic acid group of the substrate plays a crucial role in the success of the reaction.

5. Phosphine–phosphite and phosphine–phosphonite ligands

The phosphine–phosphite ligands are another important class of *C*₁-symmetric ligands that have found several applications in a wide variety of different catalytic reactions such as asymmetric hydroformylation,⁴⁹ allylic alkylation, asymmetric hydrogenation, conjugate addition and olefin hydrocyanation. There are reviews that have discussed their application in asymmetric catalysis thoroughly up to 2016.^{50,51} Therefore, this review presents only the more recent examples where these classes of ligands have been used in asymmetric hydro-

Table 3 AH in the presence of acetic-anhydride and Boc-anhydride

Entry	S/C	Temp (°C)	(RCO) ₂ O (equiv./1)	Conv. (%)	27-PG (%)	ee (%)
1	100	rt	None	61	0	96
2	100	rt	Ac ₂ O (1.5 equiv.)	100	100	94
3	500	rt	Ac ₂ O (1.5 equiv.)	70	100	94
4	1000	rt	Ac ₂ O (1.5 equiv.)	6	100	90
5	500	60	(Boc) ₂ O (0.005 equiv.)	91	0	89



Scheme 17 AH of (*E*)-3-(4-benzyloxyphenyl)-2-methoxyacrylic acid.

generation (Fig. 8). Optically active homobenzylic alcohols and alkanols are very important building blocks for synthesis. In 2017, Pizzano and coworkers successfully carried out the asymmetric hydrogenation of trisubstituted enol esters comprising of α,β -dialkyl, α -alkyl- β -aryl and α,β -diarylvinyl esters to prepare synthetically relevant chiral non-functionalized alcohols. They used Rh catalysts bearing phosphine–phosphite ligands to achieve high selectivity.⁵² In the case of α,β -dialkyl vinyl esters,

the reaction tolerated different lengths of alkyl chains. In the case of α -alkyl- β -arylvinyl esters and α,β -diarylvinyl esters, the reaction tolerated EWGs as well as EDGs on the aromatic ring (Scheme 18). However, in the case of (*Z*)-1-phenyl-2-(thiophen-3-yl)vinyl acetate, the enantiomeric excess was a little lower (79%). Interestingly, it was found that α,β -dialkyl substrates showed greater reactivity than the α -alkyl- β -aryl substrates which in turn showed greater reactivity than α,β -diaryl substrates.

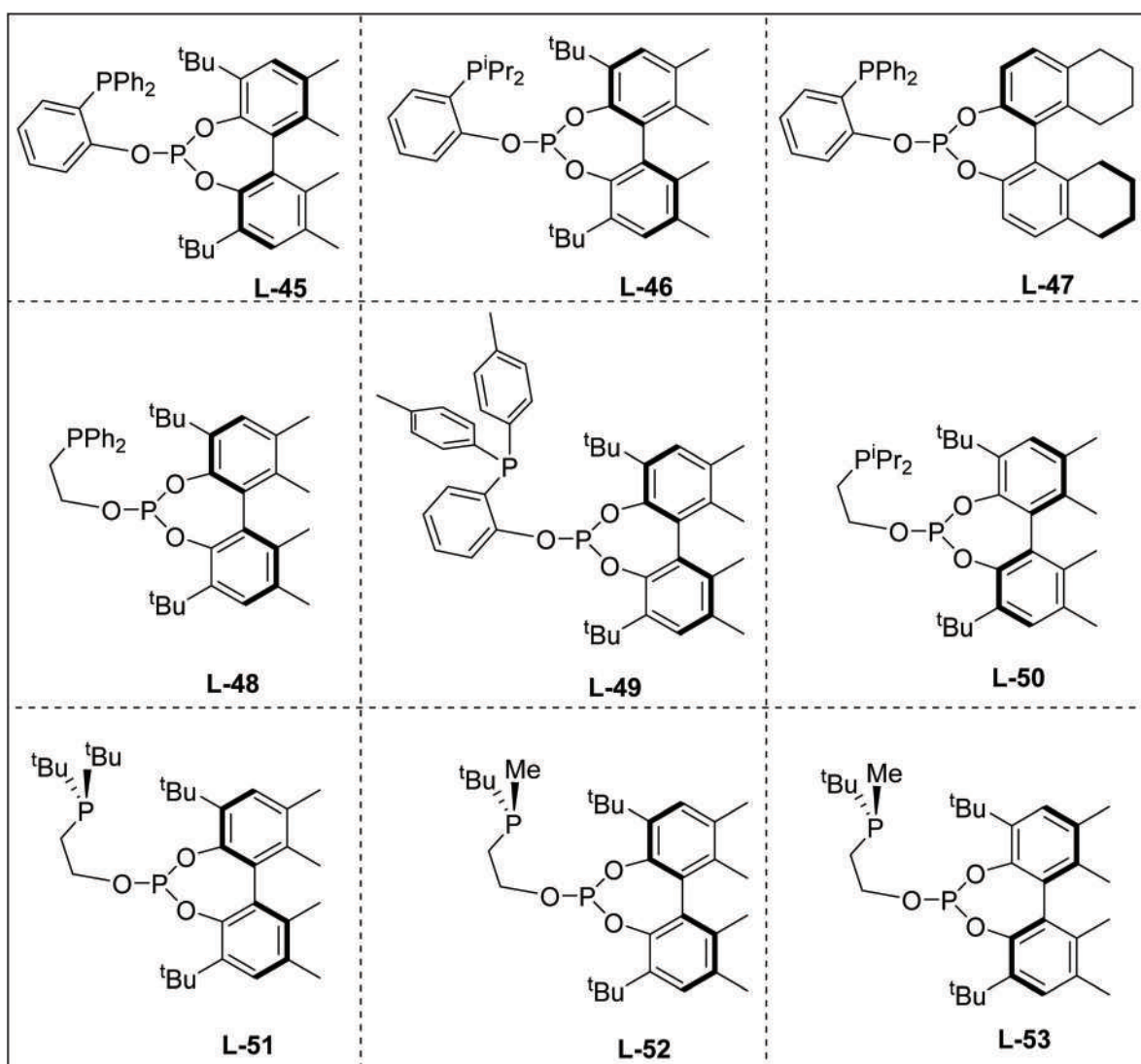


Fig. 8 Structure of phosphine–phosphite ligands L45–L53.

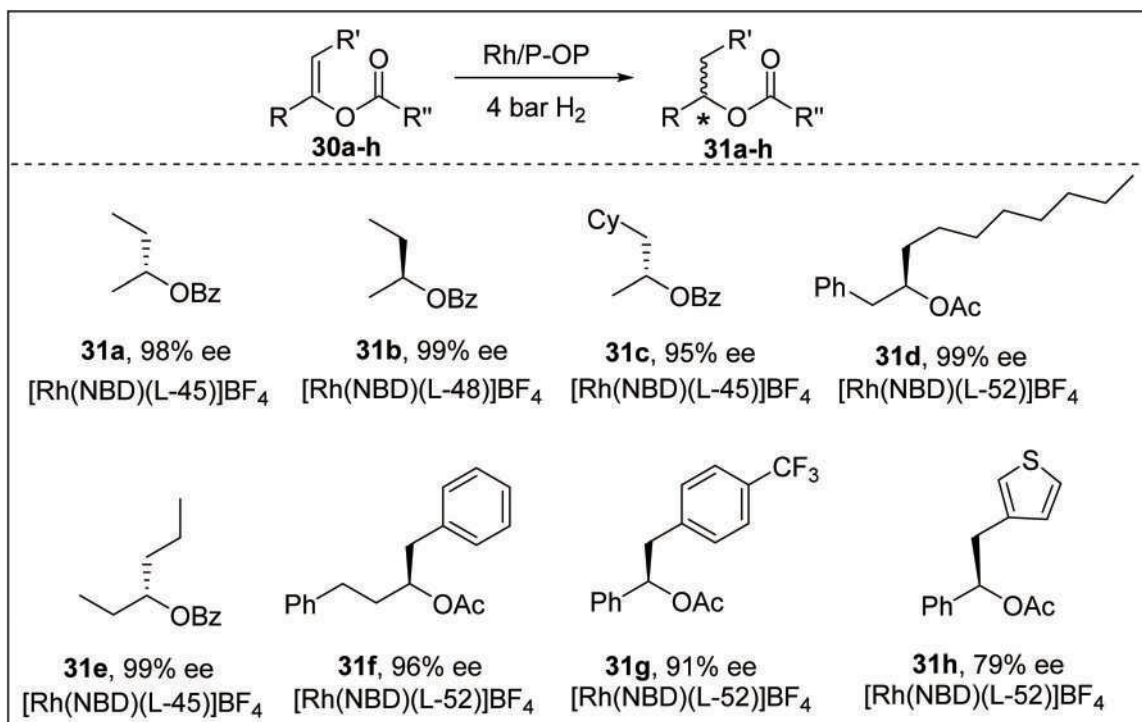
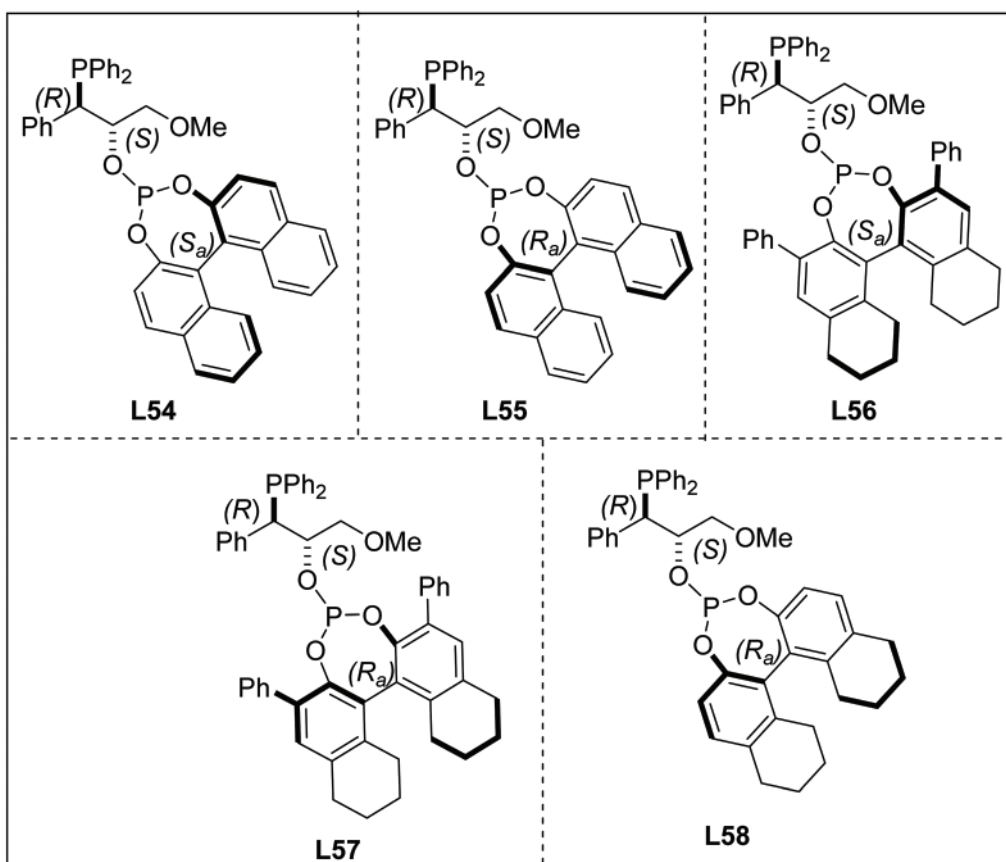
Scheme 18 AH of α,β -diaryl; α,β -dialkyl; and α -alkyl- β -aryl vinyl esters.

Fig. 9 Structure of phosphine–phosphite ligands L54–L58.

Ferran and coworkers synthesized a new family of modular P-OP ligands starting from enantiopure epoxides. Phosphine functionality was introduced in the chiral skeleton by epoxide ring opening with nucleophilic trivalent phosphorus derivatives. Further derivatization of hydroxy phosphines with trivalent phosphorus electrophiles afforded the targeted P-OP ligands (Fig. 9).^{53,54}

The asymmetric hydrogenation of some model substrates was performed with these ligands in THF solvent under 20 bar

Table 4 AH of model substrates **9b**, **9d**, and **9h** catalyzed by rhodium complexes of **L54**–**L58**

Entry	Ligand	9b ee (%)	9h ee (%)	9d ee (%)
1	L54	99	99	98
2	L55	86	97	94
3	L56	99	99	99
4	L57	96	99	98
5	L58	93	92	88

H₂ pressure at room temperature for 18 hours (Table 4). In each case, excellent enantiomeric excess was achieved. However, **L56** with substituents at the 3 and 3'-position outperformed others in enantioselectivity. Finally, they used **L56** in the asymmetric hydrogenation of structurally diverse challenging functionalized olefins. Full conversion with excellent enantioselectivity was obtained in most cases (Fig. 10).

Although several bidentate phosphine ligands have been synthesized for asymmetric hydrogenation, most of them involve tedious multiple-step synthesis and often give a very low yield. To overcome this synthetic bottleneck, Pringle and coworkers developed a series of C₁ backbone chiral diphosphorus ligands *via* a Si–P exchange reaction which generates a volatile by-product, thus making the purification step much easier (Fig. 11). The crude ligands were directly utilized in complexation with [Rh(diene)₂]BF₄ without further purification (where diene is norbornadiene or 1,5-cyclooctadiene) and finally evaluated in the asymmetric hydrogenation of three benchmark substrates, DMI, MAA and MAC. The results

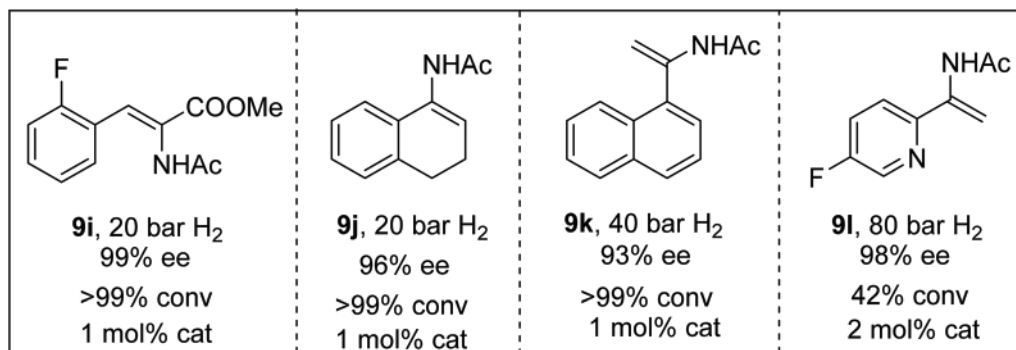


Fig. 10 AH of functionalized olefins catalyzed by [Rh(**L56**)(nbd)BF₄].

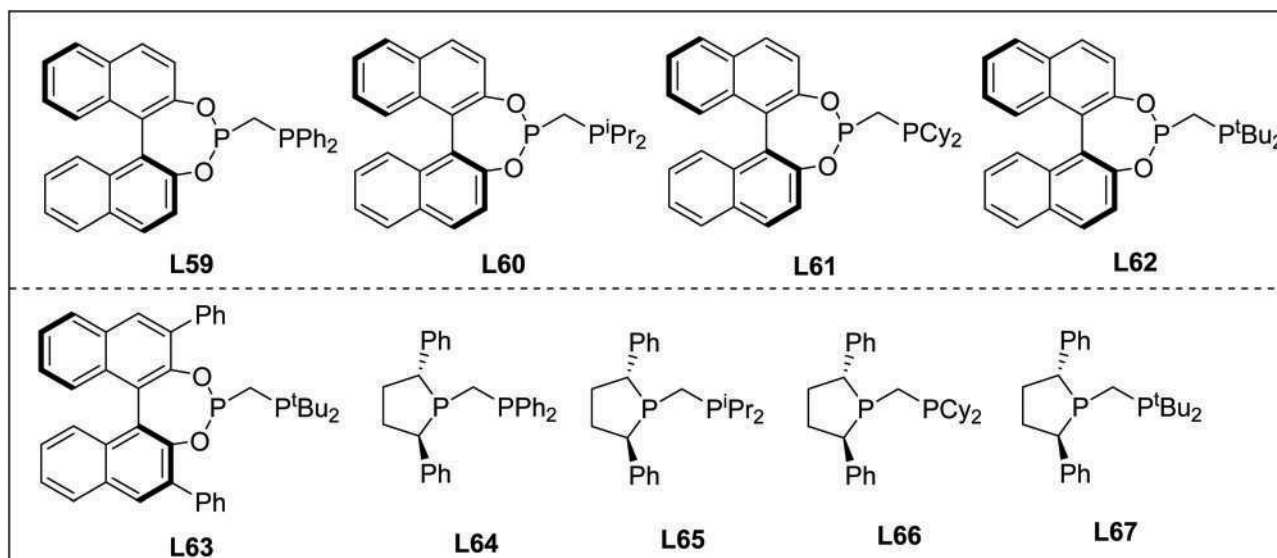


Fig. 11 Structure of ligands **L59**–**L67**.

Table 5 Asymmetric hydrogenation of **9a**, **9b**, and **9h**

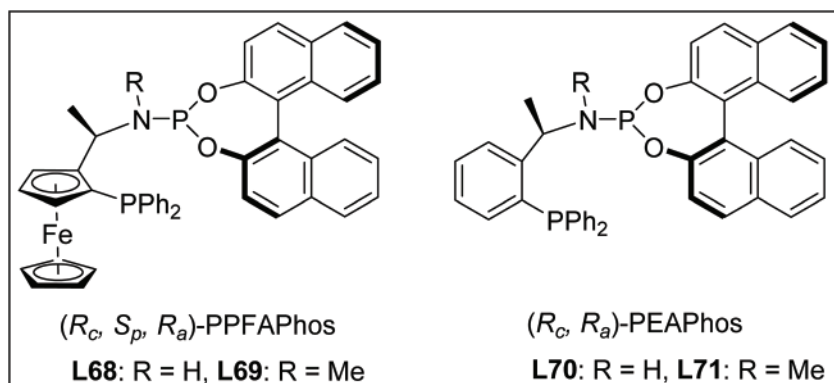
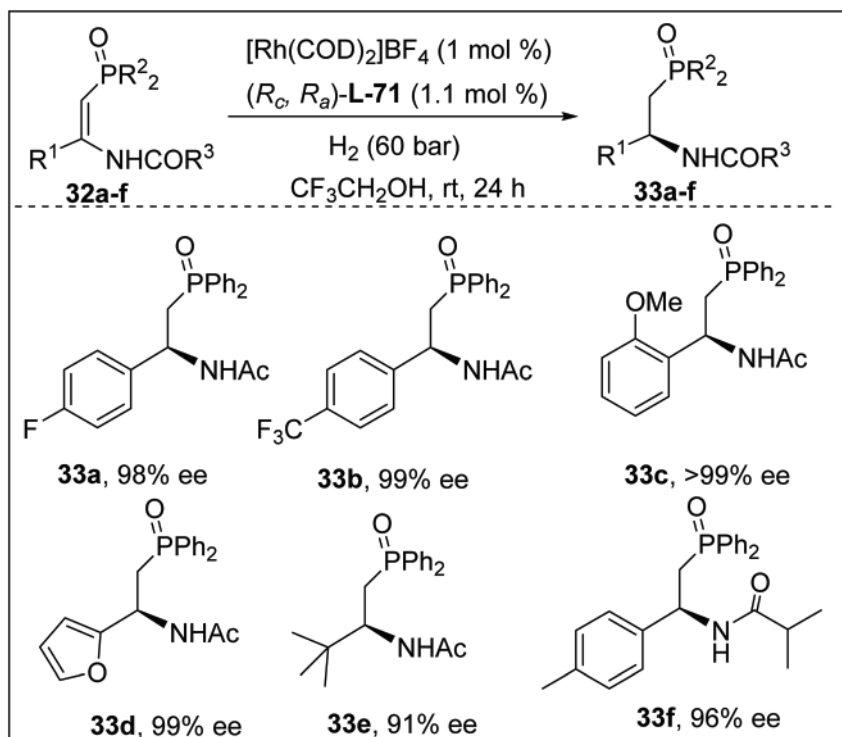
Entry	Ligand	9h (% ee)	9a (% ee)	9b (% ee)
1.	L61	95		
2.	L63		98	
3.	L65	97		
4.	L66		96	
5.	L67	99		
6.	L67		98	
7.	L67			99

Reaction conditions: S/C = 100 : 1, 20 °C, 1 h, 5 bar H₂, DCM.

showed that the enantioselectivity strongly depends on the ligand structure and in some cases the ligands afforded excellent (>95%) ee (Table 5).⁵⁵

6. Phosphine–phosphoramidite ligands

Phosphine–phosphoramidite ligands are another important class of hybrid diphosphorus ligands that have found wide application in asymmetric catalysis. The application of these ligands in asymmetric catalysis up to 2016 is thoroughly discussed elsewhere.^{56,57} This review will discuss only the more recent examples where these classes of ligands have been used

**Fig. 12** Unsymmetrical chiral ferrocenylphosphine-phosphoramidite ligands **L68** to **L71**.**Scheme 19** AH of (*Z*)-β-phosphorylated enamides.

in asymmetric hydrogenation. Optically active β -aminophosphines are well-known chiral motifs for the construction of diverse chiral ligands or organocatalysts. In 2019, Hu and co-workers first successfully achieved the asymmetric hydrogenation of β -phosphorylated enamides to synthesize chiral β -aminophosphine derivatives (Fig. 12). They achieved success by using hybrid chiral phosphine-phosphoramidite ligands developed by their group while commercially available BINAP showed poor activity and DuPHOS exhibited good activity but moderate enantioselectivity.⁵⁸ The reaction tolerated EWGs as well as EDGs irrespective of their position on the phenyl ring. To show the synthetic utility of this method-

ology, they carried out the reaction at the gram scale with the substrate **32c** under the standard condition with excellent ee (99%) and yield (99%) which upon hydrolysis followed by reduction could readily produce the optically active β -amino phosphine (Scheme 19).

Enantiomerically pure α -amino acids and their derivatives have found wide applications in the synthesis of several drugs such as cardiovascular drugs, anti-bacterial agents, glycopeptide antibiotics, and β -lactam antibiotics. Transition metal-catalyzed asymmetric hydrogenation of α -imino esters could be the most convenient and straightforward pathway to prepare such compounds. Hu and coworkers have successfully

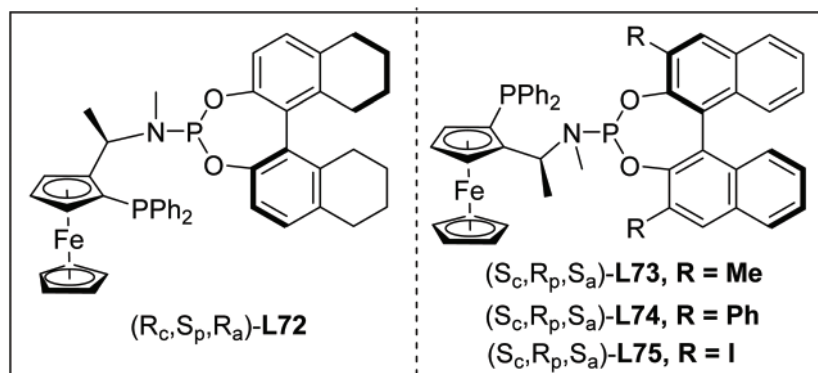
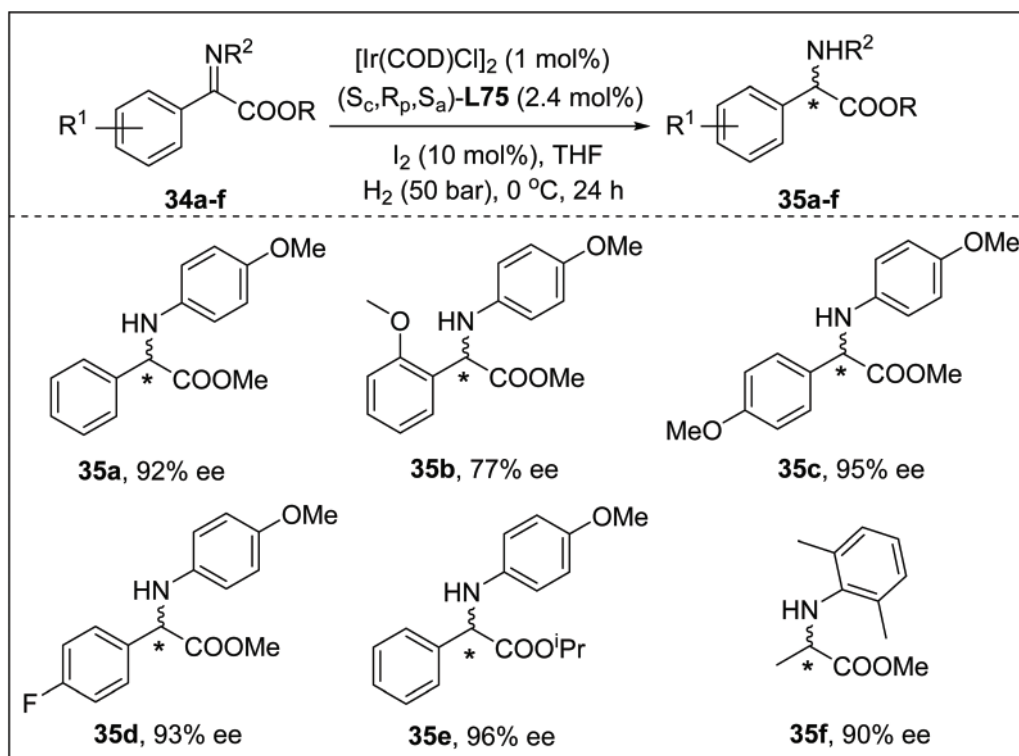


Fig. 13 Unsymmetrical chiral ferrocenylphosphine-phosphoramidite ligands.



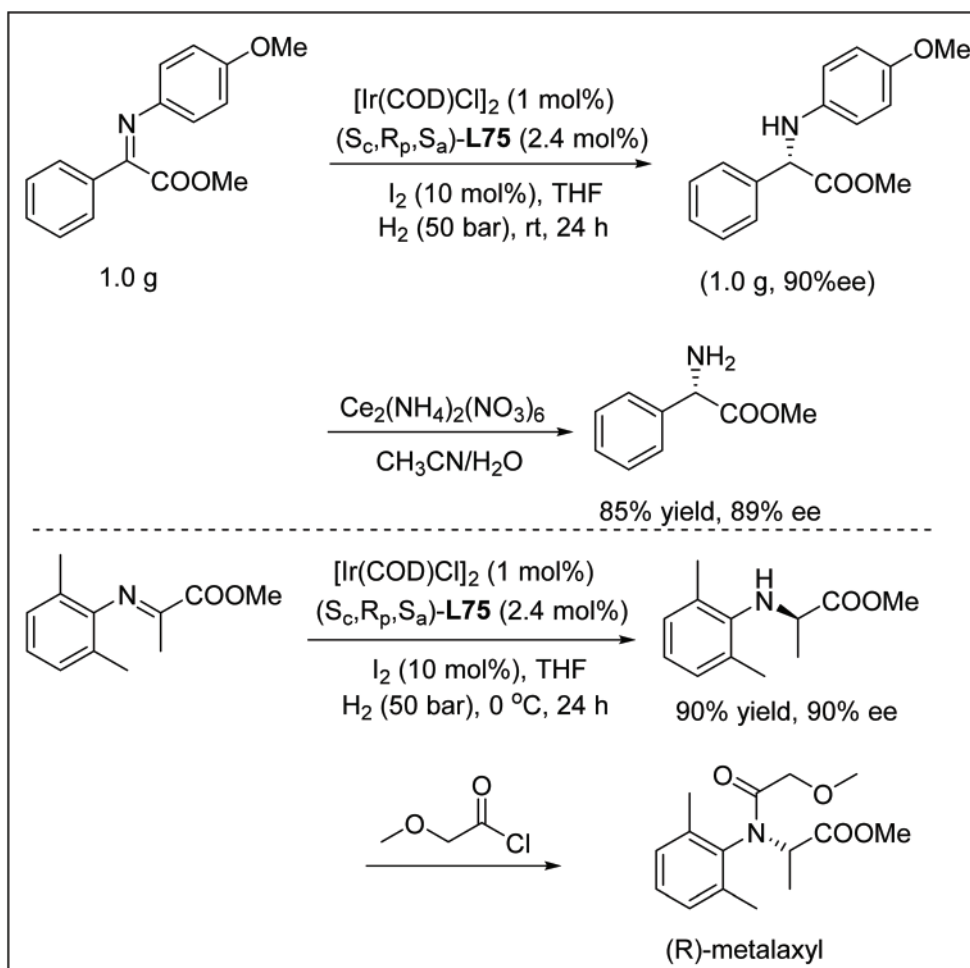
Scheme 20 AH of α -iminoesters.

utilized their hybrid phosphine phosphoramidite ligand for the asymmetric hydrogenation of α -imino esters (Fig. 13). EDGs, as well as EWGs, were well tolerated (Scheme 20). However, for the *ortho*-substituted substrate, the enantioselectivity is slightly lower, presumably due to the steric effect.⁵⁹

This methodology was successfully utilized to carry out the reaction at the gram scale and the protecting group could be

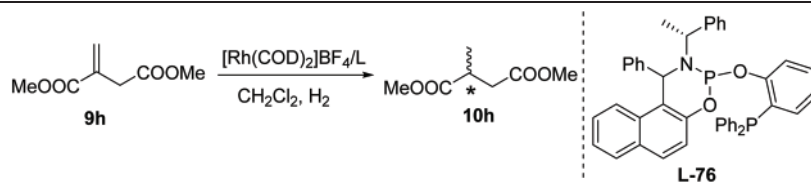
removed easily by using cerium ammonium nitrate with excellent yield and ee. Finally, (*R*)-metalaxyl, a fungicide, was successfully synthesized by applying this methodology (Scheme 21).

In 2017, Leitner and coworkers reported the synthesis of diastereomeric phosphine–phosphoramidite ligands by using a chiral amino alcohol, where the phosphorus atom at the phosphoramidite moiety was stereogenic (Table 6).⁶⁰ These



Scheme 21 Gram scale synthesis and application.

Table 6 AH of DMI with different diastereomers of L-76



Ligand	Conv. (%)	ee (%)
(<i>R</i> _C , <i>R</i> _C , <i>S</i> _P)-L76	85	96 (<i>S</i>)
(<i>R</i> _C , <i>S</i> _C , <i>R</i> _P)-L76	>99	73 (<i>R</i>)
(<i>R</i> _C , <i>R</i> _C , <i>S</i> _P)-L76	18	82 (<i>S</i>)

diastereomeric ligands were screened in the asymmetric hydrogenation of the benchmark substrate dimethyl itaconate in dichloromethane solvent at room temperature for 1 hour under 40 bar H_2 pressure. The results showed that the chirality of the P atom was responsible for the enantioselectivity whereas the chirality of the backbone amino alcohol was responsible for the activity. After that, several functionalized olefins were successfully hydrogenated by using a preformed metal–ligand complex $[Rh(cod)\{(R_C, R_C, S_P)\text{-L76}\}]$ with excellent enantioselectivity (Fig. 14). The reactions were performed at room temperature with 0.1 mol% catalyst loading for 3 hours under 15 bar hydrogen pressure. For the free acid substrates, methanol was found to be the choice of solvent whereas for other substrates, the reaction was carried out in dichloromethane.

7. Ferrocene based hybrid ligand with a covalent linker

In traditional homogeneous catalysis, the ligands are involved only to shape the microenvironment of the metal center by tuning the sterics and electronics around the metal center. The reaction occurs only at the metal center, the ligands act only as a mere spectator, they do not interact with the substrate directly. Researchers have always taken inspiration from “Mother Nature”. Nature’s catalyst, enzymes are really important in this context. Many natural enzymes, such as $[FeFe]$ -hydrogenase, lactate racemase, $[NiFe]$ -hydrogenase and alcohol dehydrogenase, are well known to take advantage of both

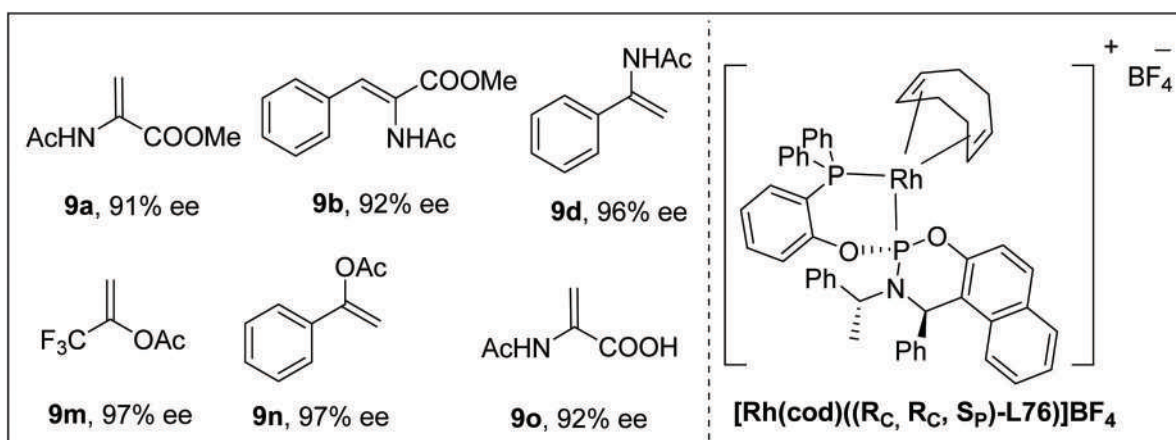


Fig. 14 AH of functionalized olefins by the L76 ligated Rh-complex.

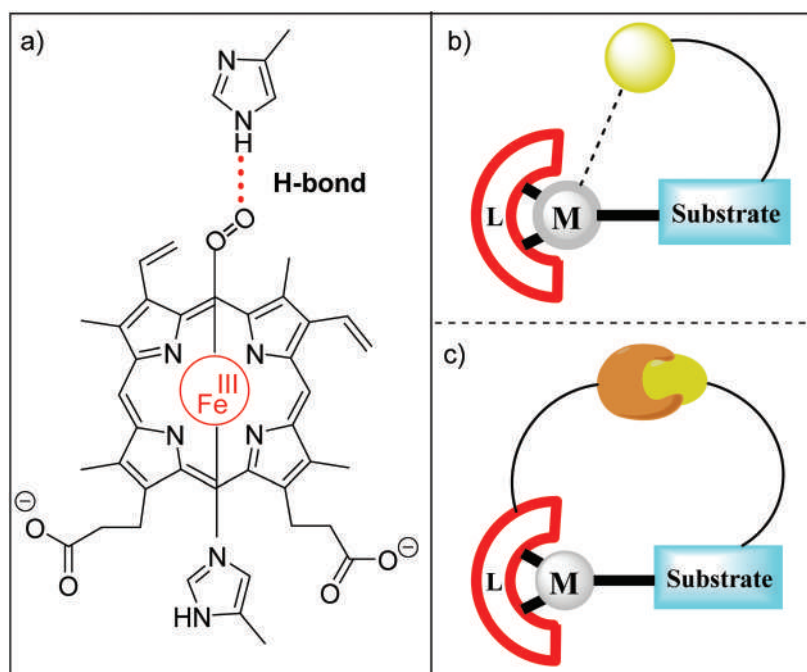


Fig. 15 (a) Hydrogen bonding in oxymyoglobin, (b) metal–substrate interaction, and (c) interaction of the substrate with the metal and ligand.

metals and the surrounding ligand environment to perform catalysis, known as cooperative catalysis.⁶¹ In fact, metal–ligand cooperation has also been found to play a crucial role in the function of metalloproteins (Fig. 15). One example is that of oxygen binding in myoglobin, where the hydrogen bonding interaction between the distal histidine residue and the Fe-coordinated oxygen is believed to be the driving force for the oxygenation process. In cooperative catalysis, both the metal and the ligand are involved in catalyzing the reaction which might involve a hydrogen bonding interaction, an ion-pair interaction, or a dative bonding interaction with the substrate. This makes the reaction more favorable than if the reaction were to occur solely at the metal center. There are many reviews on this topic.^{62–66} In this review, only recent examples where cooperative catalysis has been judiciously utilized in asymmetric hydrogenation have been presented. To do so, we have divided the following discussion into two parts, (i) hydrogen bonding catalysis and (ii) ion pair catalysis.

(i) Hydrogen bonding catalysis:

In the recent past, the concept of combining transition metal catalysis with organocatalysis has attracted considerable attention.⁶⁷ Owing to the unique activation mode of organocatalysts as compared to transition metal catalysts, the combined catalysis might lead to the discovery of unprecedented reactions that are not possible by either type of catalyst alone.⁶⁸ Catalyst compatibility is one of the key issues in this field. To solve this problem, one way out could be the synthesis of a single catalyst combining the property of a transition metal catalyst as well as an organocatalyst. With this idea, Zhang and coworkers synthesized a series of ferrocene-based bisphosphines with a covalent urea/thiourea linker (L8 and L77–L81), which will act as an activating and directing group to the substrate in asymmetric hydrogenation (Fig. 16).

Since thioureas are used to activate the nitro group in organocatalysis, with this idea they selected nitroalkenes as substrates

to test the activity of their catalysts (Scheme 22). By using ligand L8, first, they optimized the metal precursor and solvent. [Rh(COD)Cl]₂ afforded the best result in a protic solvent, especially *i*-PrOH with full conversion and 99% ee. Then a series of chiral ligands were tested as a control experiment. They found that the ligands (L82, L83, and L84) without a urea/thiourea moiety showed very low activity (Fig. 17). The more acidic and less self-assembling thiourea L8 performed much better than urea L81. Ligands L78, L79, and L80 showed low conversion and selectivity compared to L8 which suggests that the CF₃ group in L8 played a crucial role in the reaction. Under the optimized condition with Zhaophos (L8), a variety of substrates were successfully hydrogenated with excellent yield and selectivity irrespective of EDG or EWG except for *ortho*-OMe, which resulted in a slightly lower conversion and enantioselectivity (Scheme 22).⁶⁹

Chiral β-amino nitroalkanes are important structural motifs found in many pharmaceuticals such as GR-205171A, osetlamivir, asimadoline, and (+)-CP-99994, *etc.* For this reason, chiral β-amino nitroalkanes have been prepared in many ways such as (i) asymmetric aza-Henry reactions, (ii) asymmetric aza-Michael addition of amines to nitroalkenes, (iii) asymmetric hydrosilylation of oxy myoglobin and (iv) asymmetric hydrogenation of β-amino nitroalkenes. After successful asym-

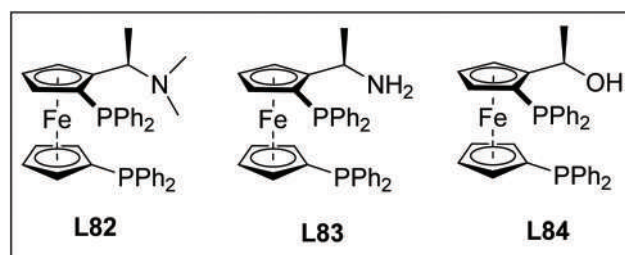


Fig. 17 Ligands without a urea or thiourea moiety.

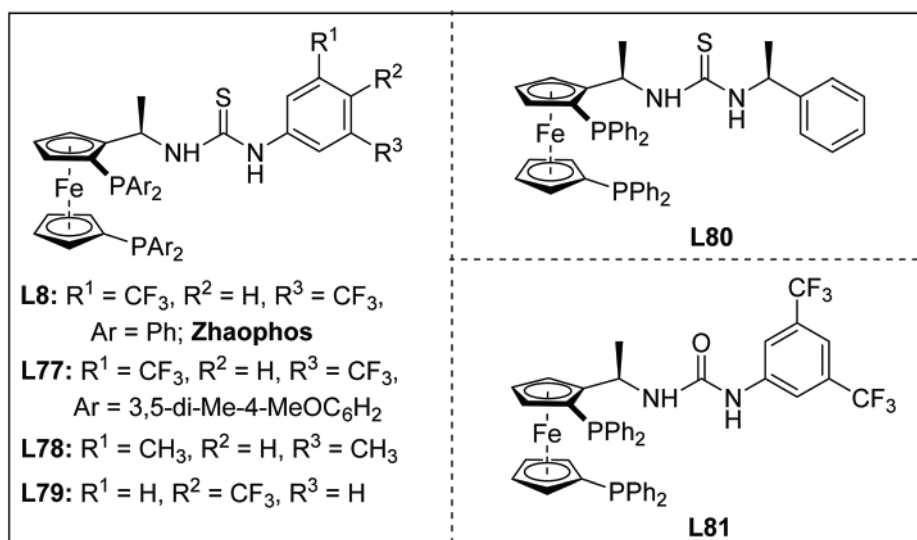
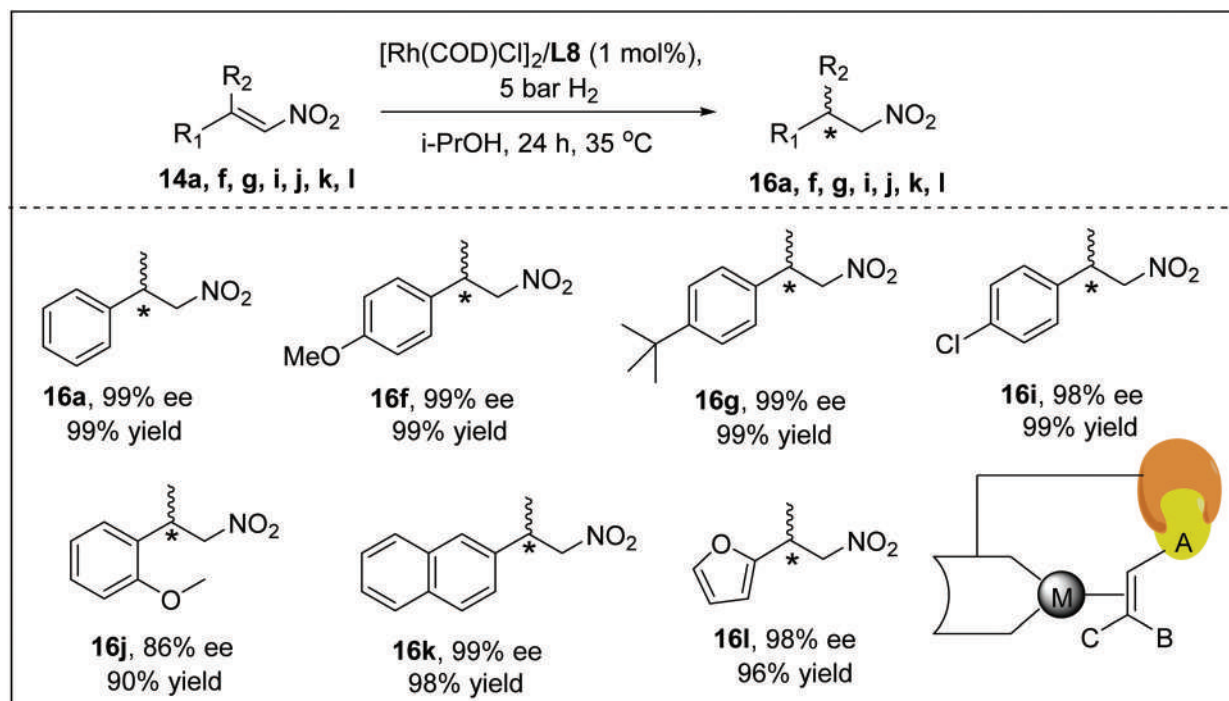
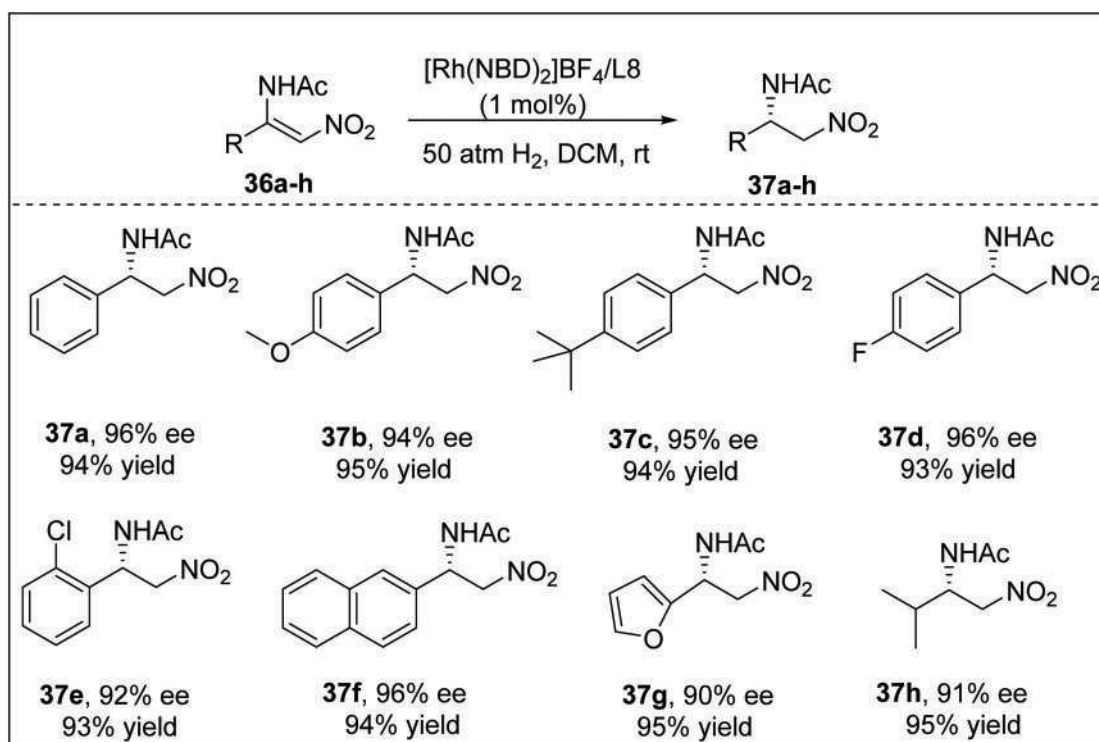


Fig. 16 Ferrocene-based diphosphorus ligands with a covalent linker.

Scheme 22 AH of β,β -disubstituted nitroalkenes.

metric hydrogenation of β,β -disubstituted nitroalkenes with their thiourea-based bifunctional ligand, the authors applied the same strategy with β -amino nitroalkenes. A variety of

β -acylamino nitroolefins with EDGs as well as EWGs were successfully hydrogenated with excellent enantioselectivity and yields (Scheme 23).⁷⁰

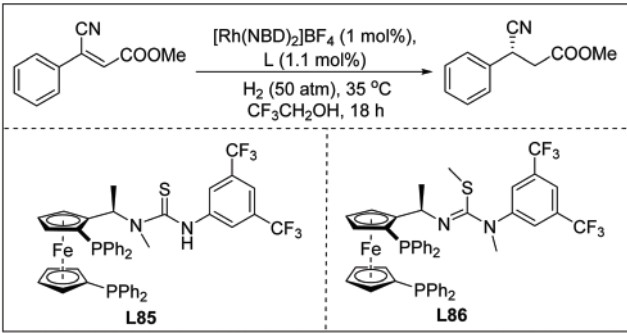
Scheme 23 AH of β -aminonitroolefins.

Chiral γ -aminobutyric acids are important building blocks found in numerous drugs, such as Rolipram, Brivaracetam, Vernakalant, Enblex, *etc.* In neuroscience, many of them show potential biological activity such as Pregabalin, Phenibut, and Baclofen. Due to their ubiquitous prevalence in pharmaceuticals, the synthesis of chiral GABA derivatives has attracted intense attention and many methods have been developed for their syntheses like biocatalytic asymmetric reduction, enzymatic kinetic resolution, asymmetric conjugate reduction, and Michael addition. However, the asymmetric hydrogenation of β -cyanocinnamic esters could be a more practical and direct way to synthesize chiral GABA derivatives.

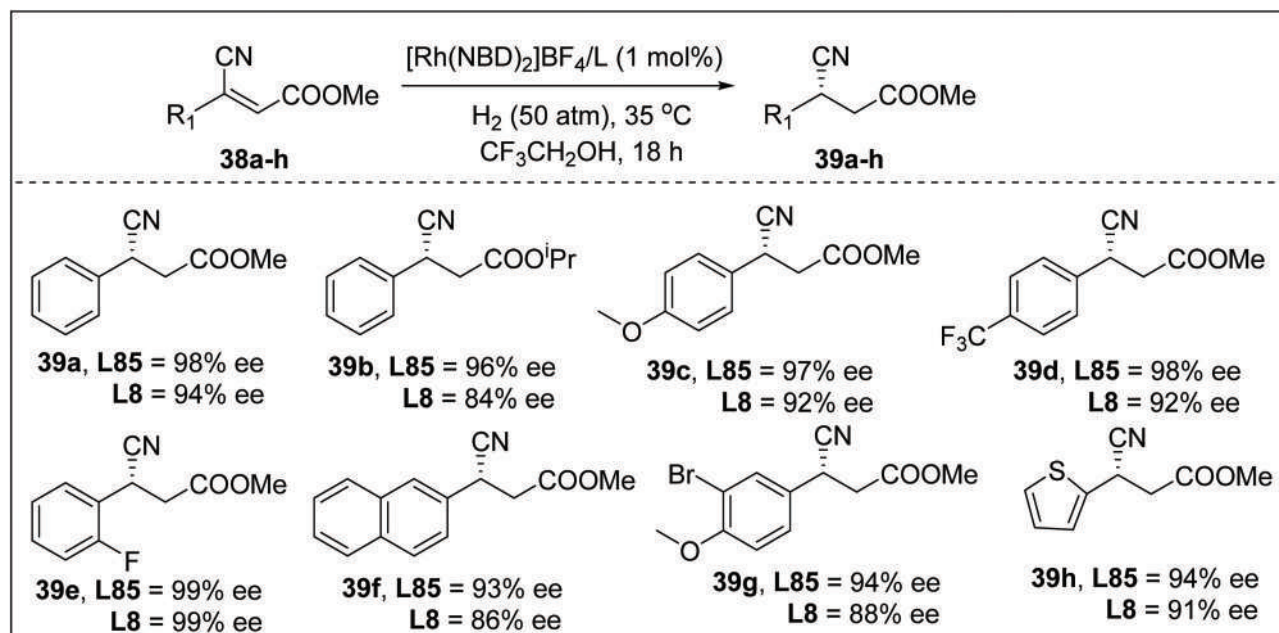
These substrates are quite challenging for asymmetric hydrogenation mainly due to two reasons: first, the presence of the electron-withdrawing cyano and ester group reduces the electron density of C=C, thus reducing its coordination ability with the metal, which in turn reduces the activity. Second, the linear nitrile group poses a problem for the suitable coordination of the C=C with the metal, leading to great difficulty in achieving high enantioselectivity. This difficulty was obvious when methyl (*Z*)-3-cyano-3-phenyl acrylate was used as a model substrate for the asymmetric hydrogenation. Several bidentate phosphine ligands were tested with no success, giving low to trace conversion with almost racemic products. The failure of the classical bidentate phosphine ligands led Zhang and co-workers to utilize their newly developed bifunctional ligands in this reaction. First, they selected Zhaophos (**L8**) for this reaction, since it has a covalently attached thiourea linker; they thought it could make a H-bond with the ester group of the substrate which might be helpful for the reaction. Indeed, after optimizing other reaction parameters, they achieved full conversion with 95% ee in $\text{CF}_3\text{CH}_2\text{OH}$ with 50 atm H_2 pressure at 35 °C (Table 7). To check the effect of the thiourea linker, they used three structurally related ligands **L82**, **L85**, and **L86** in the asymmetric hydrogenation of the aforementioned substrate. Ligand **L85** where one -NH is replaced with -NMe surprisingly gave better results with 98% ee compared to Zhaophos (**L8**). However, ligand **L86** without the -NH group and ligand **L82** without any thiourea showed low conversion and ee. After this, a series of substrates, containing EDG's as well as EWGs, were examined and in all cases, **L85** gave better enantioselectivity than Zhaophos (**L8**) (Scheme 24).⁷¹

From the substrate scope, it was found that **L85**, which can act as a single H-bond donor, outperformed **L8** in every case.

Table 7 Screening of different bisphosphine-thiourea ligands



Entry	Ligand	Conv. (%)	ee (%)
1	L8	99	95
2	L85	99	98
3	L86	Trace	—
4	L82	5	7



Scheme 24 AH of β -cyanocinnamic esters.

To shed light on the performance of **L85** and Zhaophos (**L8**), they used the B3LYP-GD3BJ/6-31G method to calculate the free energies of hydrogen bonds between different ligands with **38a** (ΔG_{HB}). Surprisingly, the authors found that even at different temperatures, the free energy for the hydrogen bond occurring between **38a** and Zhaophos was smaller compared to that of the hydrogen bond occurring between **38a** and **L85**. Thus, a stronger hydrogen bond between **38a** and **L85** made **L85** a more selective catalyst which was in agreement with the experimental results (Table 8).

Chiral succinic anhydrides and their derivatives are important synthetic intermediates as well as ubiquitous building blocks found in many metalloprotease inhibitors and bioactive molecules such as caspase 1 inhibitor, mupirocin H, and mitigli-nide. Zhang and coworkers successfully hydrogenated a series of 3-substituted maleic anhydrides with excellent enantioselectivity by using the chiral bifunctional bisphosphine-thiourea ligand Zhaophos (**L8**) by foreseeing that the hydrogen bond donor thiourea motif might be able to activate the carbonyl group of

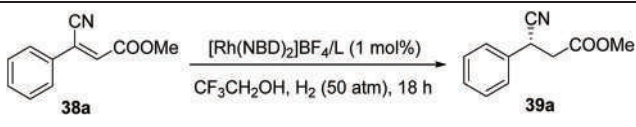
the substrate through hydrogen bonding interaction.⁷² The reaction tolerates EDGs as well as EWGs (Scheme 25).

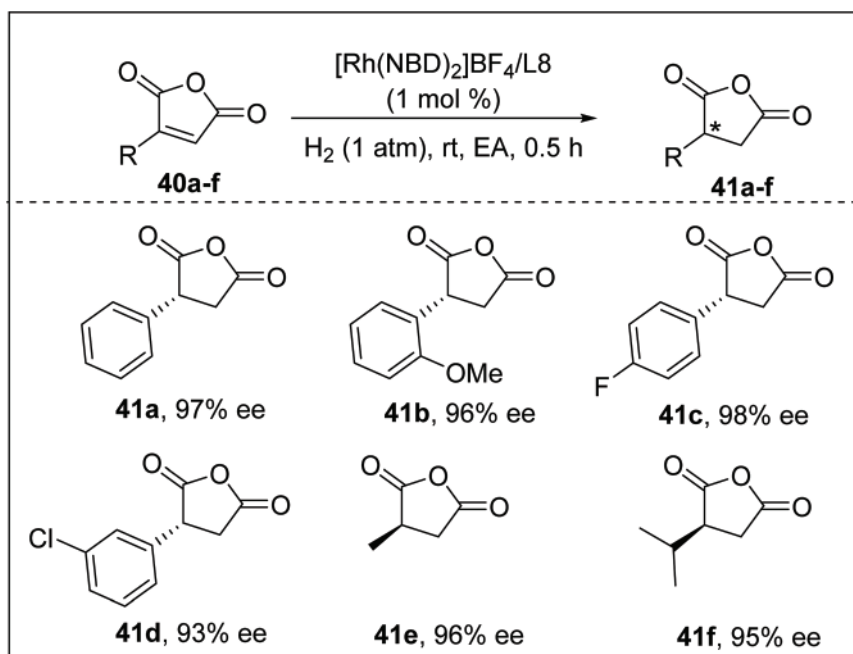
Finally, they successfully applied their methodology for the synthesis of 3-benzyl succinic anhydride which is a key intermediate for constructing mitigli-nide, a hypoglycemic drug (Scheme 26).

Optically pure β,β -disubstituted ketones are fundamentally important building blocks found in many pharmaceuticals, agrochemicals, and fragrances, such as the well-known anti-coagulant (*S*)-warfarin commonly used to prevent a heart attack. Carvone is very important for the flavor industry. Zhang and coworkers successfully utilized the bifunctional Zhaophos (**L8**) ligand for the asymmetric hydrogenation of a series of β,β -disubstituted conjugated enones with high chemo-selectivity and enantioselectivity (Scheme 27).⁷³ The reaction tolerates EDGs and EWGs on the β -substituted phenyl ring. However, enantiomeric excess was found to decrease when R^1 or R^3 groups were changed to alkyl groups.

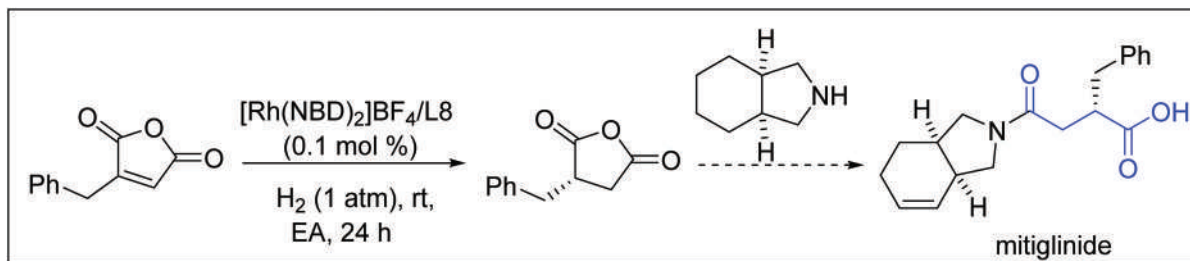
Chiral γ -lactams are ubiquitous building blocks found in many bioactive molecules and pharmaceuticals such as the antiepilepsy drug Brivaracetam and the antidepressant drug (*R*)-rolipram. After ring-opening, γ -amino acids are obtained which are key intermediates for a variety of chiral drugs and natural products, such as Pregabalin and Baclofen. For the first time, Zhang and coworkers successfully reported the asymmetric hydrogenation of α,β -unsaturated lactams having a substitution at the β -position. These are quite promising substrates, with the Zhaophos ligand assuming a possible hydrogen bonding interaction between the amide group of the substrate and the thiourea linker in the Zhaophos (**L8**) ligand. Several β -aryl-substituted α,β -unsaturated lactams with free NH as well as various substituents at the N-atom (Boc, Me, Bn, PMP, and Ph) were investigated. Almost in every case, the

Table 8 Comparison of Zhaophos (**L8**) and **L85**

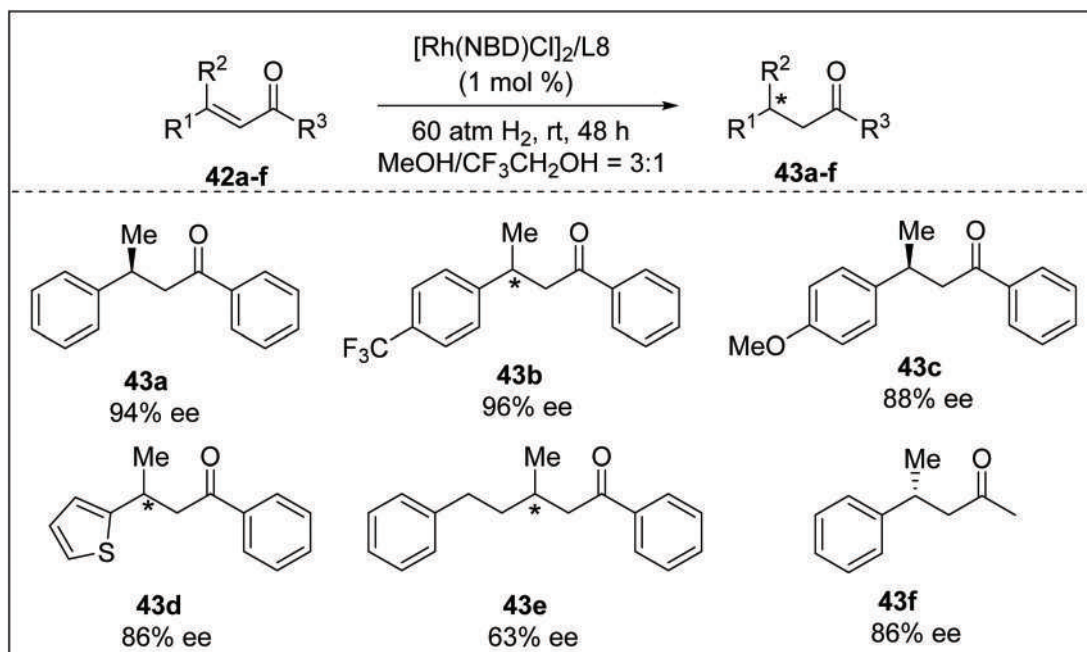
		0 °C	20 °C	35 °C	60 °C
					
Ligand					
L8	ΔG_{HB} (kcal mol ⁻¹)	-13.4	-12.2	-11.4	-10.0
	ee/conv.	97/20	95/94	95/99	92/99
L85	ΔG_{HB} (kcal mol ⁻¹)	-16.4	-15.3	-14.5	-13.2
	ee/conv.	99/60	98/99	98/99	93/99



Scheme 25 AH of different 3-substituted maleic anhydrides.



Scheme 26 Synthesis of mitiglinide.

Scheme 27 AH of β,β -disubstituted α,β -unsaturated ketones.

hydrogenation afforded the desired chiral γ -lactam with excellent yield and enantioselectivity, tolerating EWGs as well as EDGs on the aryl ring at different positions (Scheme 28).⁷⁴

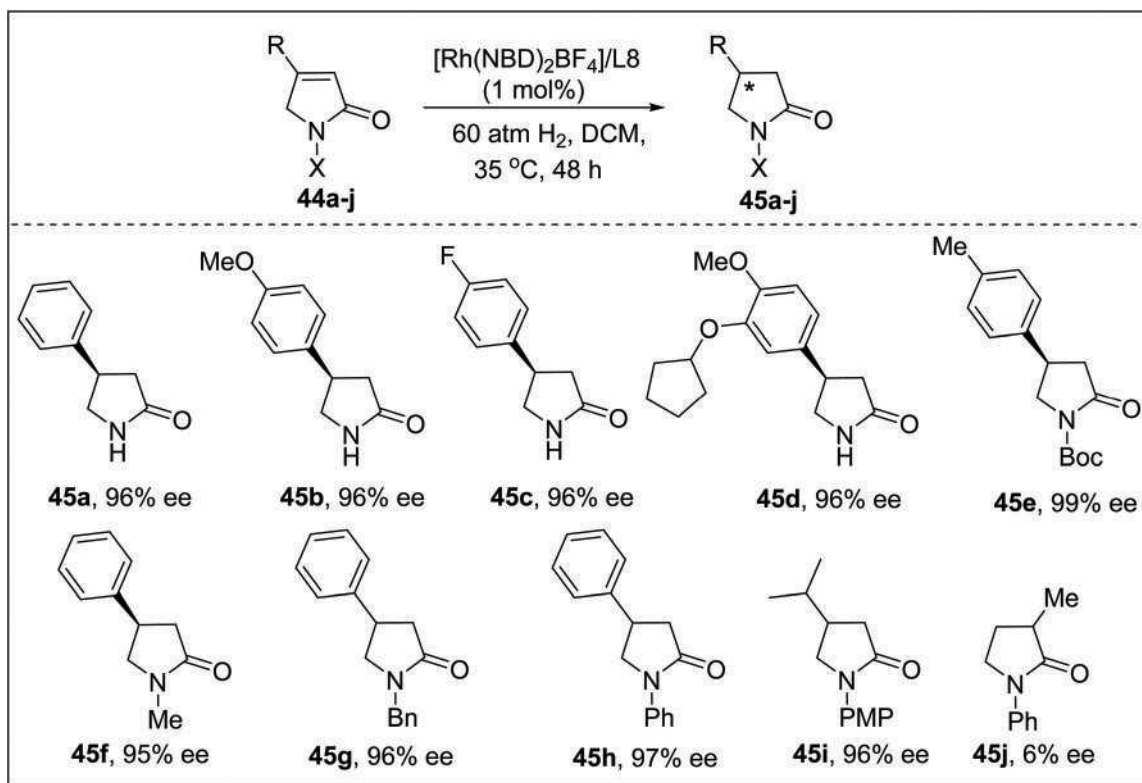
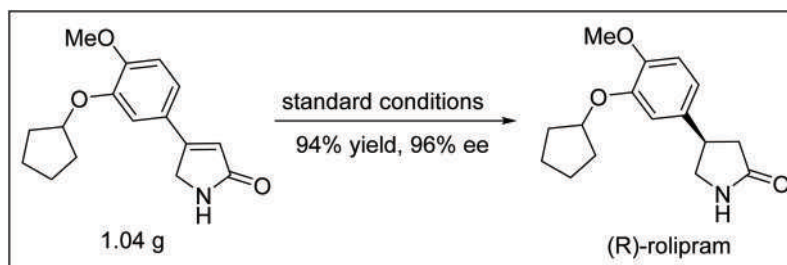
(*R*)-Rolipram, an antidepressant drug, was synthesized on a gram scale under the standard conditions with 94% yield and 96% ee, which demonstrates the utility of this methodology (Scheme 29).

1,5-Benzothiazepines are fundamentally important heterocyclic building blocks found in many bioactive molecules and pharmaceuticals such as the antihypertension drug diltiazem and the antidepressant drug thiazesim. Zhang and coworkers utilized their bifunctional Zhaophos (**L8**) ligand for the asymmetric hydrogenation of medium size unsaturated cyclic NH lactams having various substituents, obtaining excellent yield and enantioselectivity. It is worth mentioning that several commercial ligands such as SegPhos, DuanPhos, BINAP, f-BINAPHANE, JosiPhos, and MeO-BIPHEP did not show any activity during the optimization of the reaction.⁷⁵ Different substituents, EDGs as well as EWGs, are well tolerated in this reaction (Scheme 30).

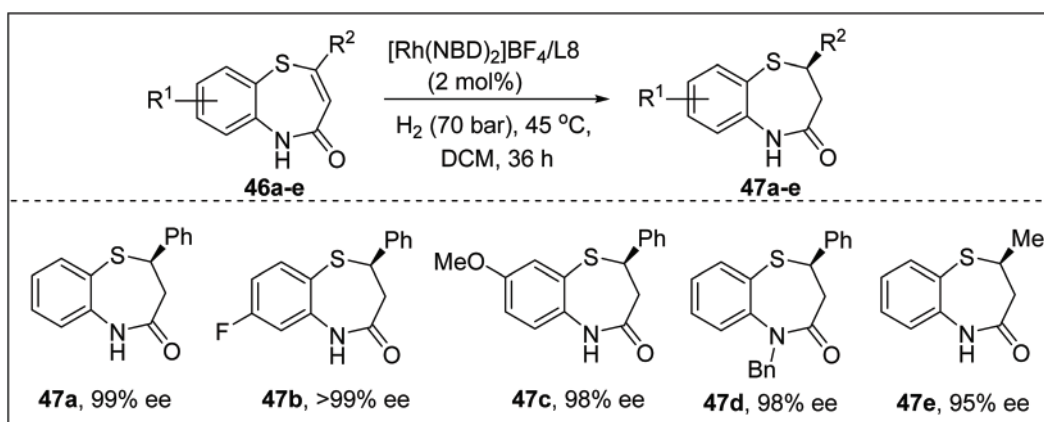
The synthetic utility of this methodology was demonstrated by performing a gram scale asymmetric hydrogenation of **46a** with 99% yield and 99% ee, which could easily be converted to (*R*)-thiazesim, an antidepressant drug (Scheme 31).

Chiral 2-substituted 2,3-dihydro-1,4-benzodioxane units are ubiquitous pharmacophores found in many bioactive molecules and pharmaceuticals such as the antihypertensive drug (*R*)-doxazosin, the antidepressant MKC-242, the antihypertensive agent IDR-16084 and the anticonvulsant JNJ-26489112. Zhang and coworkers successfully used their bifunctional bisphosphine-thiourea ligand **L8** (ZhaoPhos) and **L85** for the asymmetric hydrogenation of several 2-substituted benzo[*b*][1,4]dioxane derivatives having various substituents on the phenyl ring with excellent yield and enantioselectivity (Scheme 32). In fact, for methyl benzo[*b*][1,4]-dioxane-2-carboxylate (**48a**), asymmetric hydrogenation could be successfully carried out with *S/C* = 24 000, affording excellent results (Table 9).⁷⁶

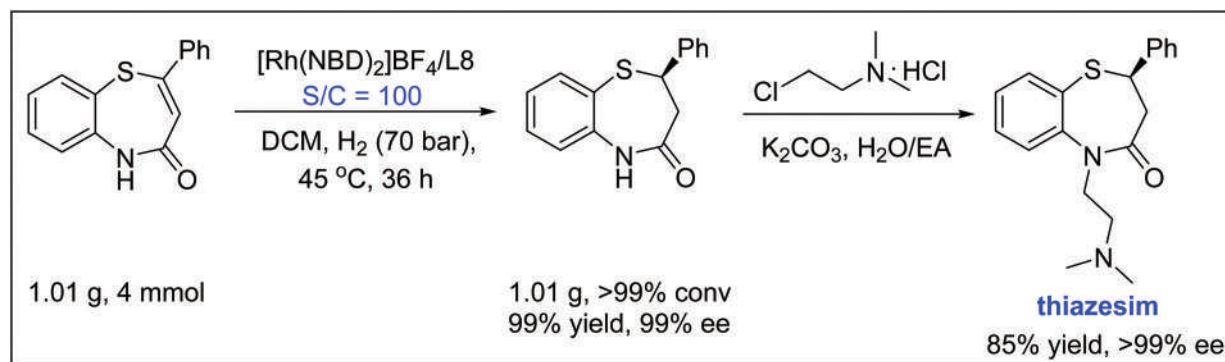
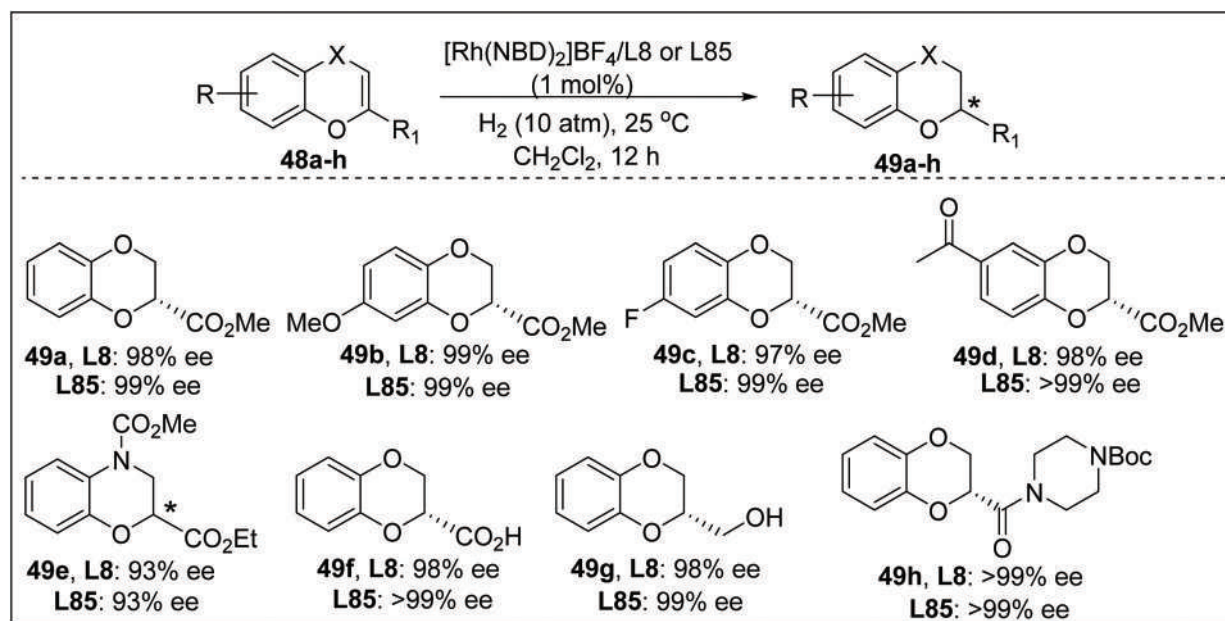
The synthetic utility of this methodology was demonstrated by synthesizing the antidepressant MKC-242 and the potent

Scheme 28 AH of α,β -unsaturated lactams.

Scheme 29 (R)-Rolipram synthesis in a gram scale.



Scheme 30 AH of unsaturated medium ring NH lactams.

Scheme 31 Gram scale synthesis of the antidepressant drug (*R*)-thiazesim.Scheme 32 AH of benzo[*b*][1,4]dioxine derivatives.Table 9 TON experiment with methyl benzo[*b*][1,4]dioxine 2-carboxylate

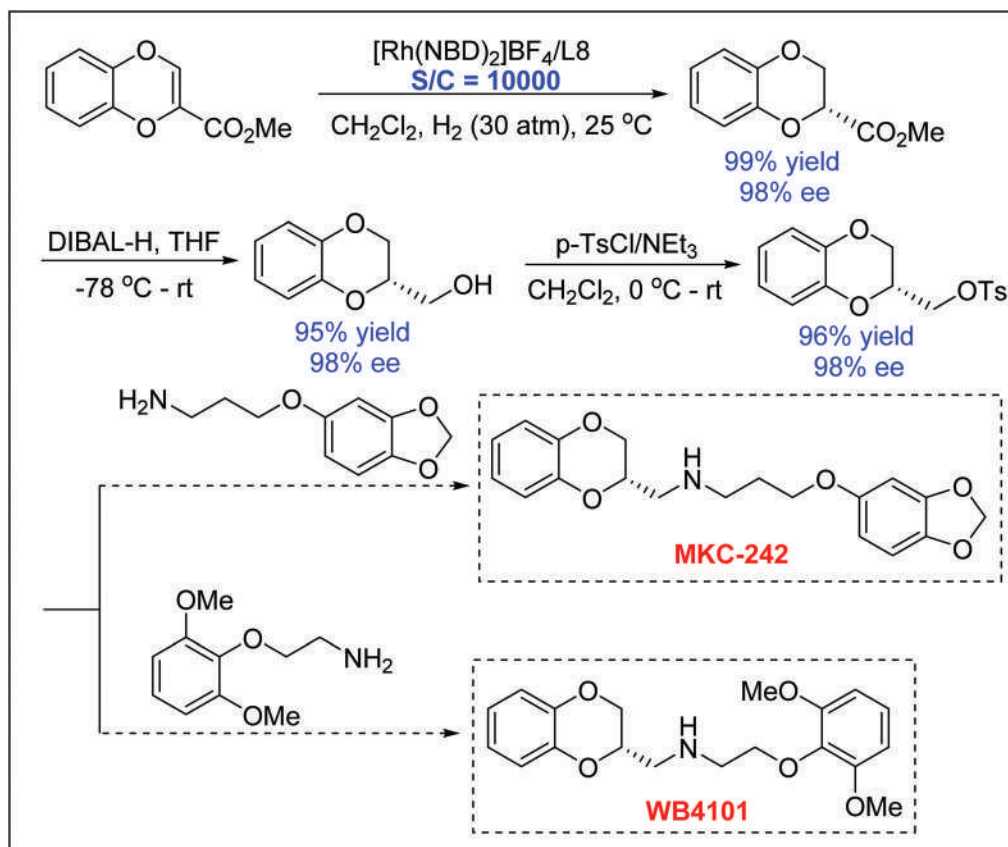
Entry	S/C	H ₂ (atm)	Time (h)	Conv. (%)	Yield (%)	ee (%)
1	2000	30	36	>99	98	98
2	5000	30	48	>99	98	98
3	10 000	30	52	>99	99	98
4 ^a	24 000	60	72	>99	99	97
5 ^b	24 000	60	72	>99	99	98

^a Reaction temperature = 40 °C. ^b Using ligand L85.

α_{1D} -adrenergic antagonist WB4101 in a gram scale with 0.01 mol% catalyst loading with excellent enantioselectivity and yield (Scheme 33).⁷⁷

(ii) Ion-pair catalysis

Chiral amines are important pharmacophores found in many bioactive molecules and agrochemicals such as the calci-



Scheme 33 Synthesis of the antidepressant MKC-242 and the antagonist WB4101.

mimetic agent Sensipar, and the elastase inhibitor DMP777. Unprotected -NH imines are challenging substrates compared to olefins and ketones for asymmetric hydrogenation as they often exist as a complex mixture of imine–enamine tautomers and E/Z isomers. Inspired by their earlier success in the thiourea-assisted asymmetric hydrogenation of nitroalkenes, Zhang and coworkers anticipated that anion binding catalysis assisted by thiourea might be helpful for the asymmetric hydrogenation of unprotected imines (Fig. 18).

Indeed, for several substrates having EWGs as well as EDGs, the authors achieved good to excellent enantio-

selectivity. However, in the case of the *ortho* -OMe group on the phenyl ring, the yield was significantly low (34%) (Scheme 34).⁷⁸

To check the effect of the counterion, several control experiments were performed by varying the counter ion and the additives which suggested that the chloride ion played a crucial role during the catalysis (Table 10).

Chiral dihydrobenzoxazinones and their derivatives are important structural motifs found in many biologically active molecules. In 2012, Zhou and coworkers first realized the asymmetric hydrogenation of prochiral benzoxazinones using

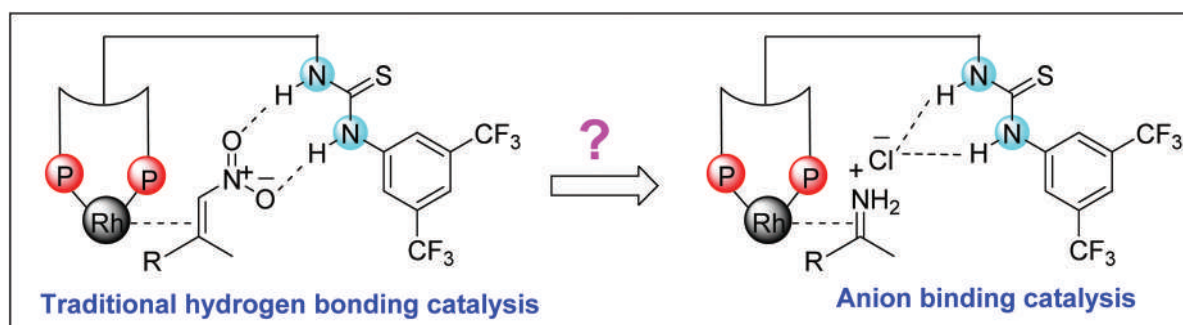
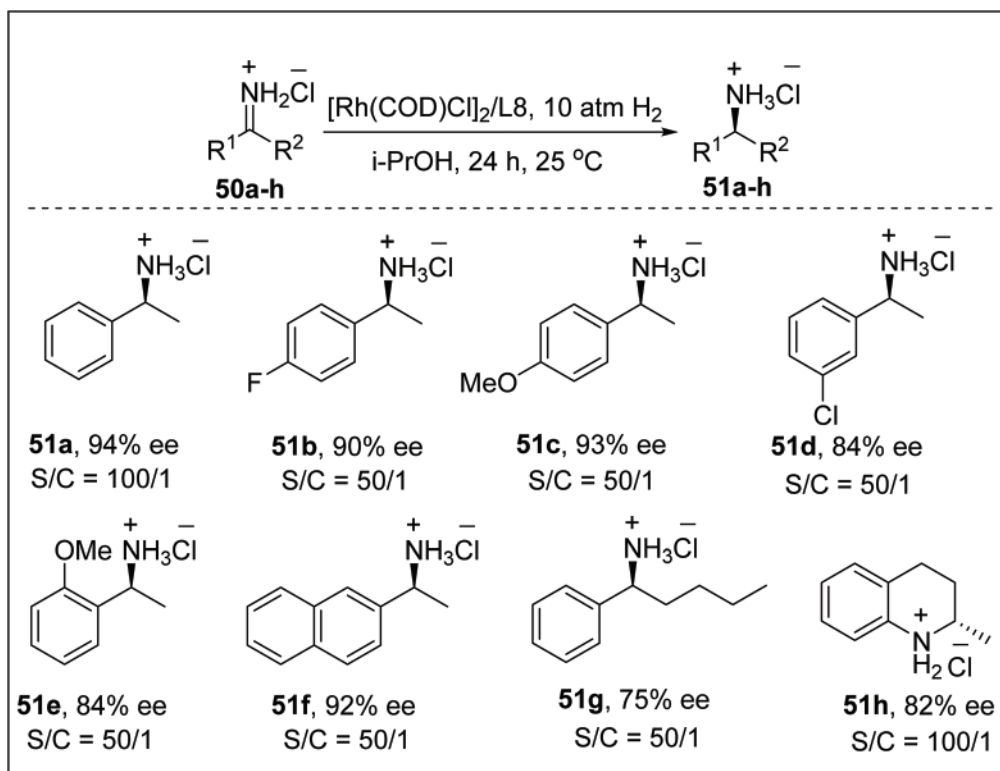


Fig. 18 Traditional hydrogen bonding catalysis vs. anion binding catalysis.



Scheme 34 AH of unprotected NH imines.

Table 10 Control experiments with different additives

Entry	50	Additive	Conv. (%)	ee (%)
1	50i	—	20	53
2	50i	Bu_4NCl	86	94
3	50i	LiCl	71	93
4	50a	—	99	94
5	50a	Bu_4NBr	77	90
6	50a	Bu_4NI	32	89

the Ru-catalyzed bio-mimetic approach in the presence of chiral phosphoric acid, while in 2015, Beller and coworkers achieved the same *via* relay catalysis by using $[\text{Fe}_3(\text{CO})_{12}]$ along with a chiral Brønsted acid.^{79,80} However, in both cases, the reactivity was not very high (TON < 2000). Zhang and co-workers thought their newly developed bifunctional bisphosphine-thiourea ligands might lead to a better catalyst by using an anion binding strategy assisted by thiourea. The authors screened several ligands, metal precursors, solvents, and additives and optimized the reaction conditions to achieve high reactivity and selectivity. They found that in the absence of the Brønsted acid HCl, there was no reaction. They general-

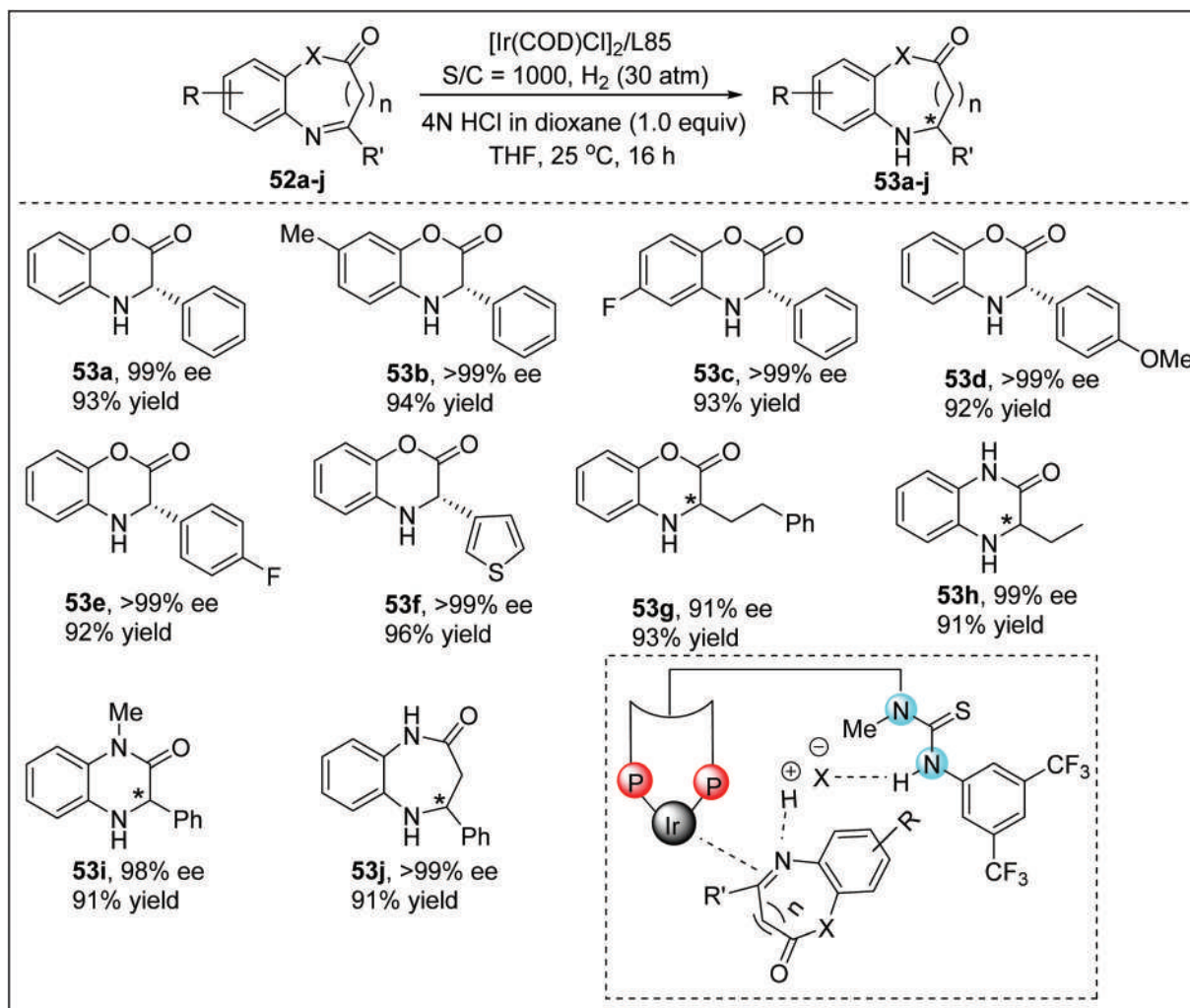
ized their methodology with a broad range of substrates with excellent enantioselectivity irrespective of EDGs or EWGs (Scheme 35).⁸¹

The authors selected 52a as a model substrate to investigate the upper limit of the catalytic activity in asymmetric hydrogenation. The catalytic system exhibited excellent reactivity and selectivity under 40 atm H_2 even with 0.0025 mol% (S/C = 40 000) catalyst loading, affording full conversion with 89% yield and 99% ee. Further lowering of the catalyst loading to 0.002 mol% resulted in 81% conversion with 72% yield and 99% ee (Table 11).

When the asymmetric hydrogenation of 52a was carried out in the presence of DCl in D_2O , there was no deuterium incorporation in the product which suggested that the H atom in the product mostly came from the hydrogen gas (Scheme 36).

Finally, the authors have shown the synthetic utility of this methodology by synthesizing the key intermediate which is useful for making potential IgE/IgG receptor modulators that are used to treat autoimmune diseases (Scheme 37).

The asymmetric hydrogenation of N-heteroarenes is highly attractive mainly due to their prevalence in many pharmaceuticals, agrochemicals, and natural alkaloids. However, resonance stabilization, as well as coordination of the heteroatom to the metal make these substrates extremely difficult to hydrogenate. Zhou and co-workers reported the asymmetric hydrogenation of isoquinolines by using the iridium-bisphosphine catalyst after activating the substrate using chloroformate or by the addition of BCDMH, whereas Mashima and co-workers



Scheme 35 AH of various benzoxazinones and the possible activation mode.

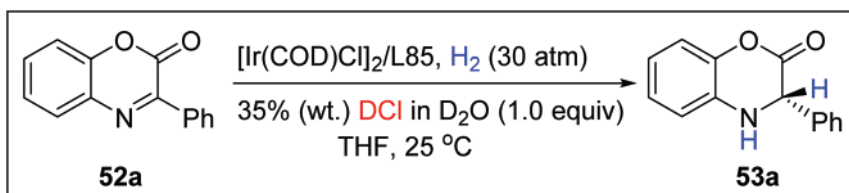
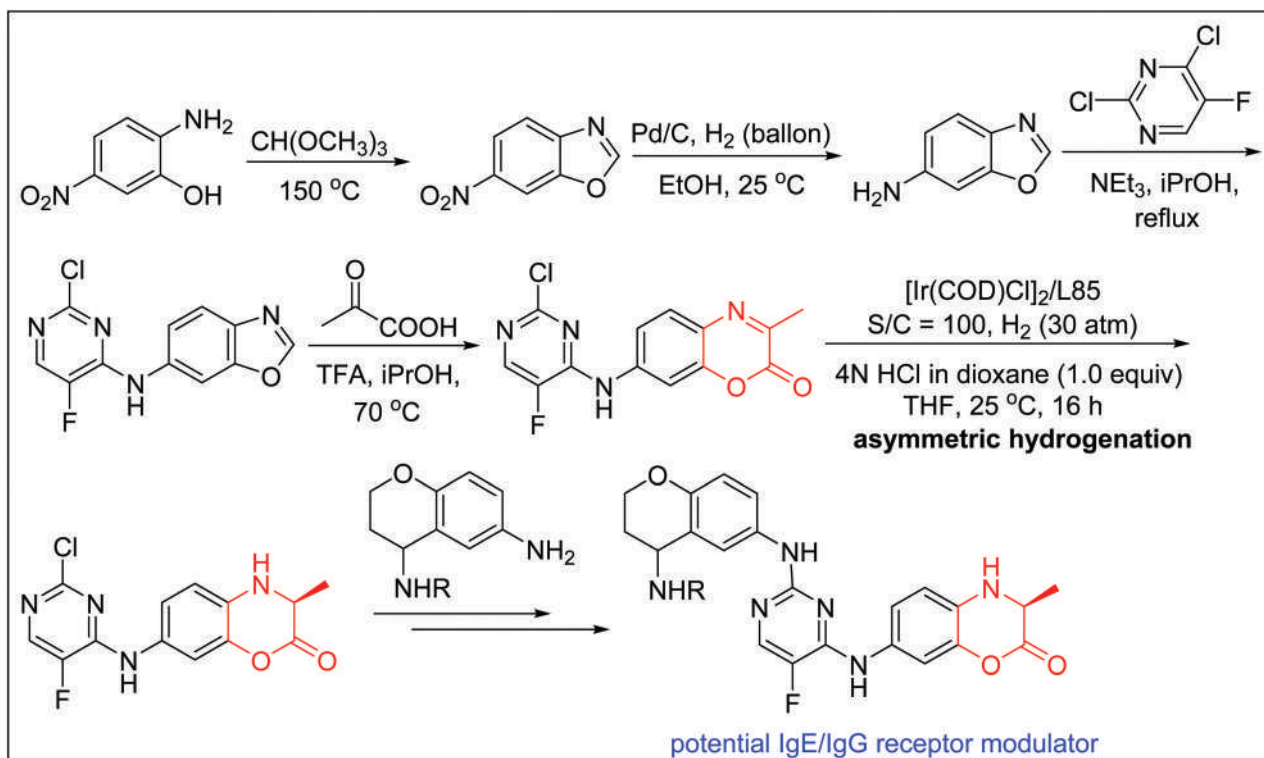
Table 11 High TON experiment

Entry	S/C	Time (h)	Conv. (%)	Yield (%)	ee (%)
1	1000	16	>99	93	99
2	10 000	48	>99	91	99
3	40 000	72	>99	89	99
4	50 000	72	81	72	99

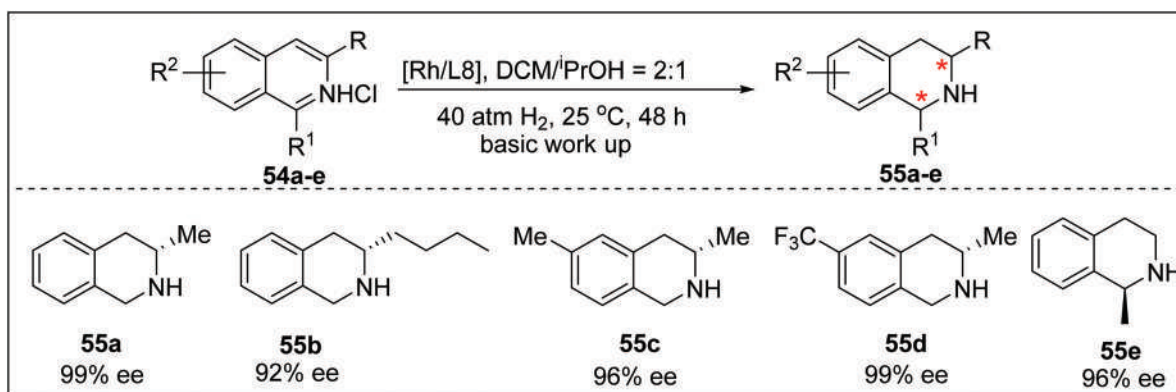
reported the use of the di-nuclear iridium(III)-bisphosphine complex for the same.^{82,83} Zhang and co-workers anticipated that activating such N-heteroarenes with a strong Brønsted acid such as HCl might be helpful to establish a salt bridge between the substrate and their newly developed bifunctional ligand with a covalent urea/thiourea tether and thus could be a successful strategy for the asymmetric hydrogenation of such

substrates.⁸⁴ With this idea, they successfully used the Zhaophos ligand (**L8**) for the asymmetric hydrogenation of several isoquinolines (Scheme 38). A solvent mixture of dichloromethane and isopropanol in a 2 : 1 ratio was found to be optimal to obtain excellent enantioselectivity. The reaction tolerates EWGs and EDGs on the phenyl ring. Different alkyl substituents at both the 1 and 3 positions were hydrogenated with high enantioselectivity. Later, they found out that under the same optimized conditions, several quinoline derivatives can also be successfully hydrogenated with high enantioselectivity (Scheme 39). Another advantage was that the reaction can be easily scaled up to the gram scale.

To probe the secondary interaction between the ligand and the chloride anion of the substrates, they mixed **L8** with 3 equivalents of substrate **54a** in CDCl_3 . The N-H peaks of thiourea, which were earlier hidden in the aromatic region within 7.3–7.0 ppm, shifted downfield to 9.10 and 7.62. Also, the three protons present on the 3,5-bis(trifluoromethyl) phenyl group of **L8** shifted downfield by 0.19 ppm, suggesting the anion binding between the ligand and substrates. To shed

Scheme 36 AH in the presence of DCI in D_2O .

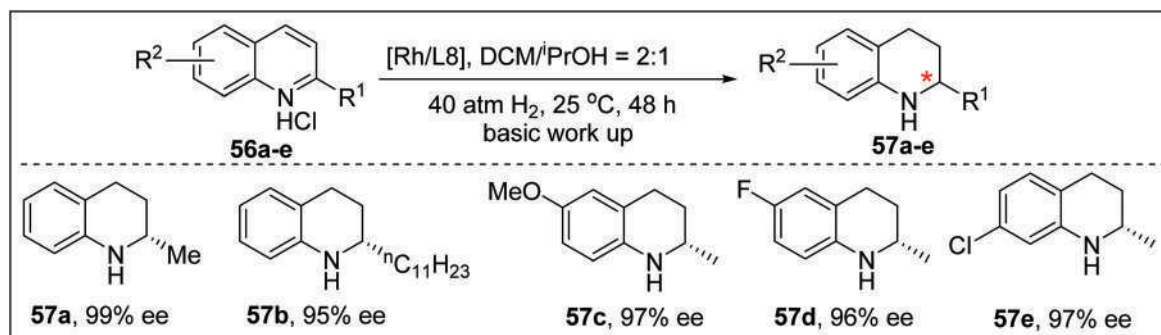
Scheme 37 Synthetic utility to construct the potential IgE/IgG receptor modulator.



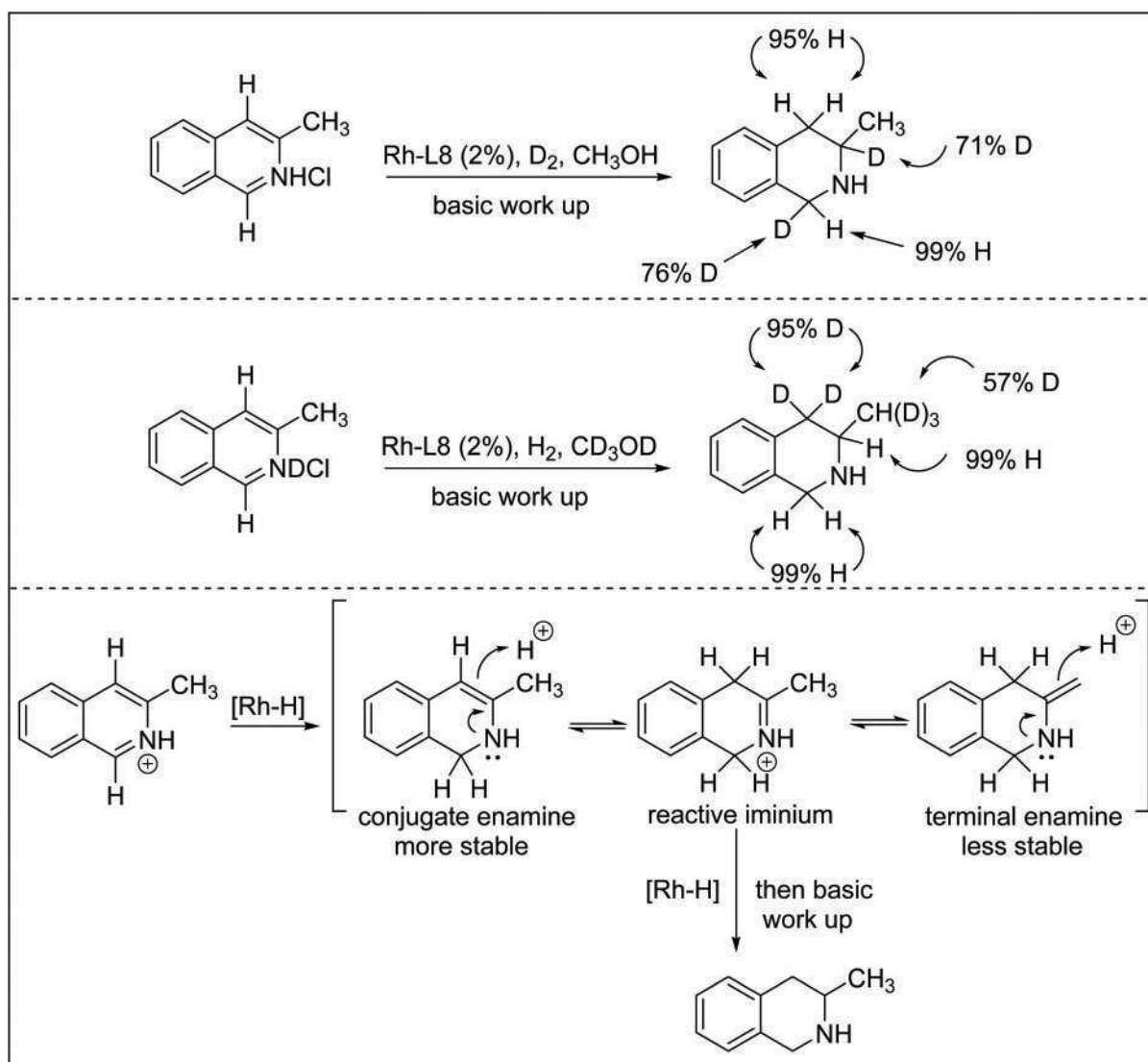
Scheme 38 AH of isoquinolines.

light on this reaction, deuterium labeling experiments were carried out (Scheme 40). The treatment of 3-methyl-isoquinoline hydrochloride with deuterium gas in methanol afforded D

atoms at the 1 and 3 positions which indicated that the H atom at the 4 position of the product must have come from the methanol solvent. Again, the treatment of 3-methyl-



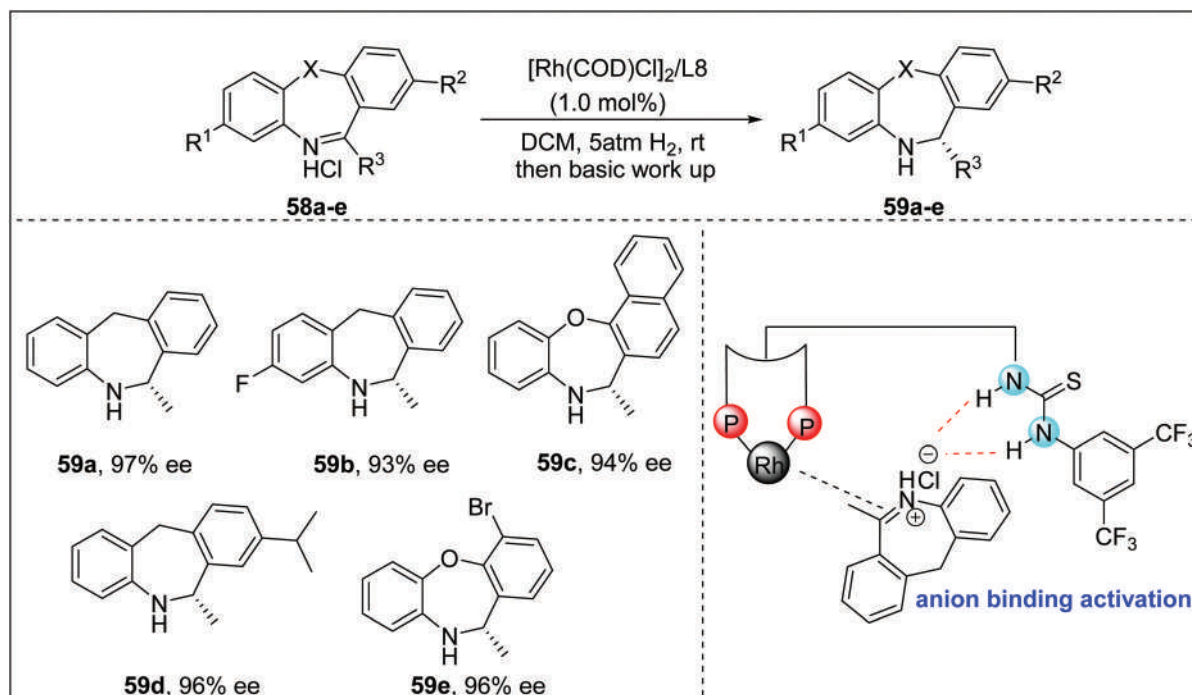
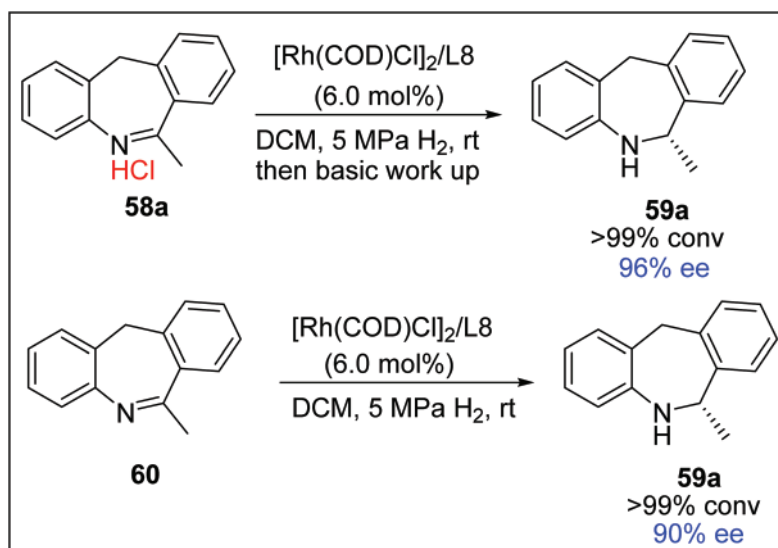
Scheme 39 AH of quinolines.



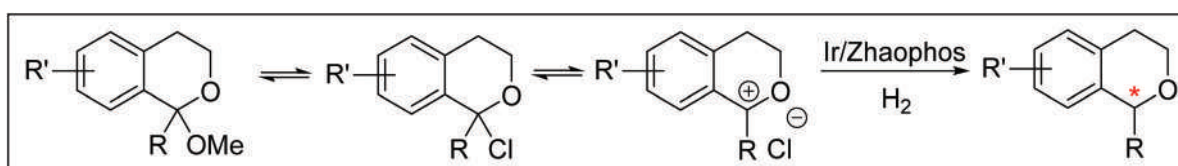
Scheme 40 Deuterium labeling experiment and proposed transformation path.

isoquinoline deuterium-chloride with hydrogen gas in methanol- d_4 incorporated hydrogen atoms at the 1 and 3 positions. However, at the 4 position, the original H atom was exchanged

with deuterium, resulting in two deuterium atoms at the 4 position which must have come from the methanol- d_4 solvent. Interestingly, the H-D exchange was also found in the methyl

Scheme 41 AH of 1*H*-dibenzo[*b,e*]azepine/oxazepine hydrochlorides.

Scheme 42 Control experiment.



Scheme 43 Strategy for the generation of the oxocarbenium ion and ionic hydrogenation.

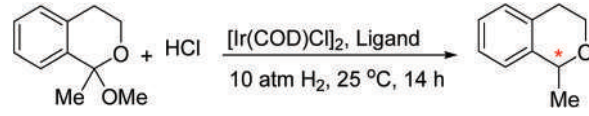
group. These observations suggested that after the addition of H at the 1 position, a conjugate enamine is formed which undergoes tautomerization, giving a reactive iminium intermediate that could easily be hydrogenated.

Chiral seven-membered cyclic amines are widely found in numerous natural products, bioactive molecules, and pharmaceuticals such as Cephalotaxine that shows excellent anticancer activity, Stemonine that displayed a potent antitubercular effect, and (*R*)-Mianserin that acted as an antidepressant and antiulcer drug. Zhang and co-workers successfully used their recently developed bifunctional chiral bisphosphine-thiourea ligand Zhaophos (**L8**) for the asymmetric hydrogenation of azepine/oxazepine hydrochlorides with high reactivity and excellent selectivity through an anion binding activation strategy (Scheme 41).⁸⁵

To probe the anion binding activation, the asymmetric hydrogenation of dibenzo[*b,e*]azepine was performed as a control experiment which showed lower enantioselectivity. This result suggested that the chloride anion played a crucial role in this reaction to achieve excellent enantioselectivity (Scheme 42).

In 2020, Zhang and coworkers successfully used the Zhaophos ligand in the iridium catalyzed asymmetric hydrogenation of oxocarbenium ions (Scheme 43), resulting in chiral isochromans with excellent enantioselectivity (Scheme 44).⁸⁶ The reaction tolerates different functional groups as well as C–C triple bonds. They anticipated that the thiourea moiety of the Zhaophos ligand could assist in the formation of the oxocarbenium ion by anion binding which can be subsequently reduced by the metal hydride *via* an ionic hydrogenation pathway.

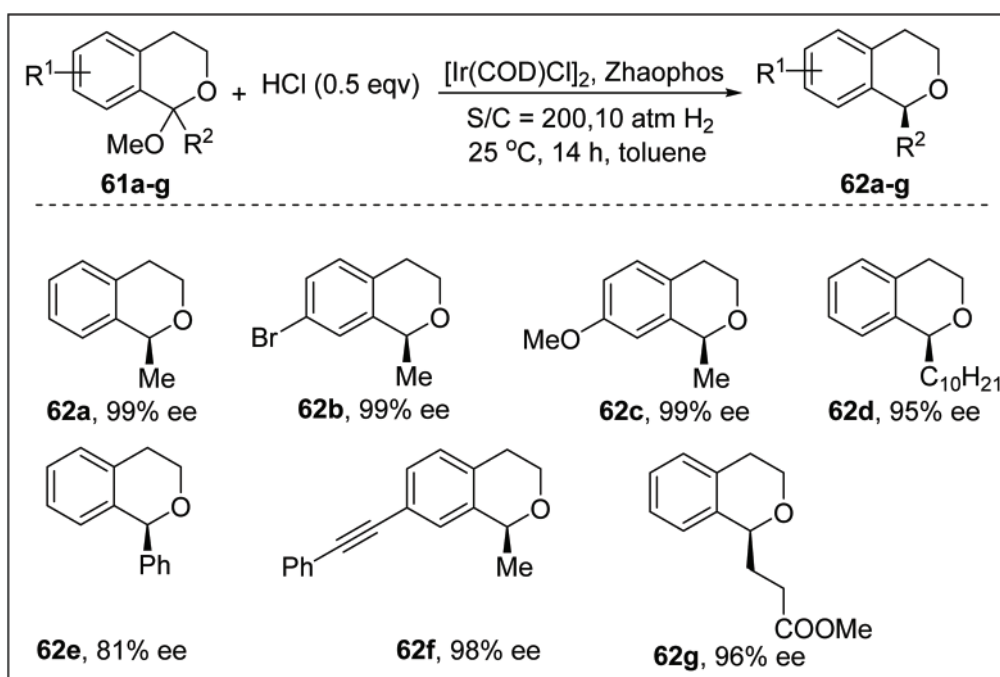
Table 12 Control experiments with different ferrocene based bisphosphine ligands

			
Zhaophos	dppf	L85	L86
98% yield 99% ee	No reaction	65% yield 40% ee	11% yield 36% ee

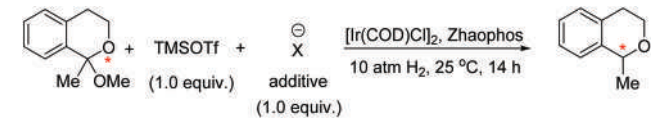
Several control experiments were performed to probe the anion binding interaction between the thiourea moiety and the chloride ion (Table 12). In the presence of the dppf ligand, there was no reaction whereas the yield and enantioselectivity were dramatically reduced when thiourea was methylated. To probe the role of the counterion, they used TMSOTf as a Lewis acid and different anions were added in the reaction where maximum enantioselectivity was achieved by chloride, demonstrating its superiority over other counter ions (Table 13). The ionic hydrogenation route was supported by DFT simulations.

In 2020, Zhang and coworkers reported the asymmetric hydrogenation of *N* and *O*-acetyl salicylamides using a variant of the Zhaophos ligand under acidic conditions involving cationic intermediates which were then reduced by an Ir or a Rh hydride complex (Scheme 45).⁸⁷ Substituents with different steric and electronic properties were well tolerated under the reaction condition.

When the reaction was performed in the presence of deuterium gas, deuterium was incorporated on the chiral carbon,



Scheme 44 AH of isochroman ketals.

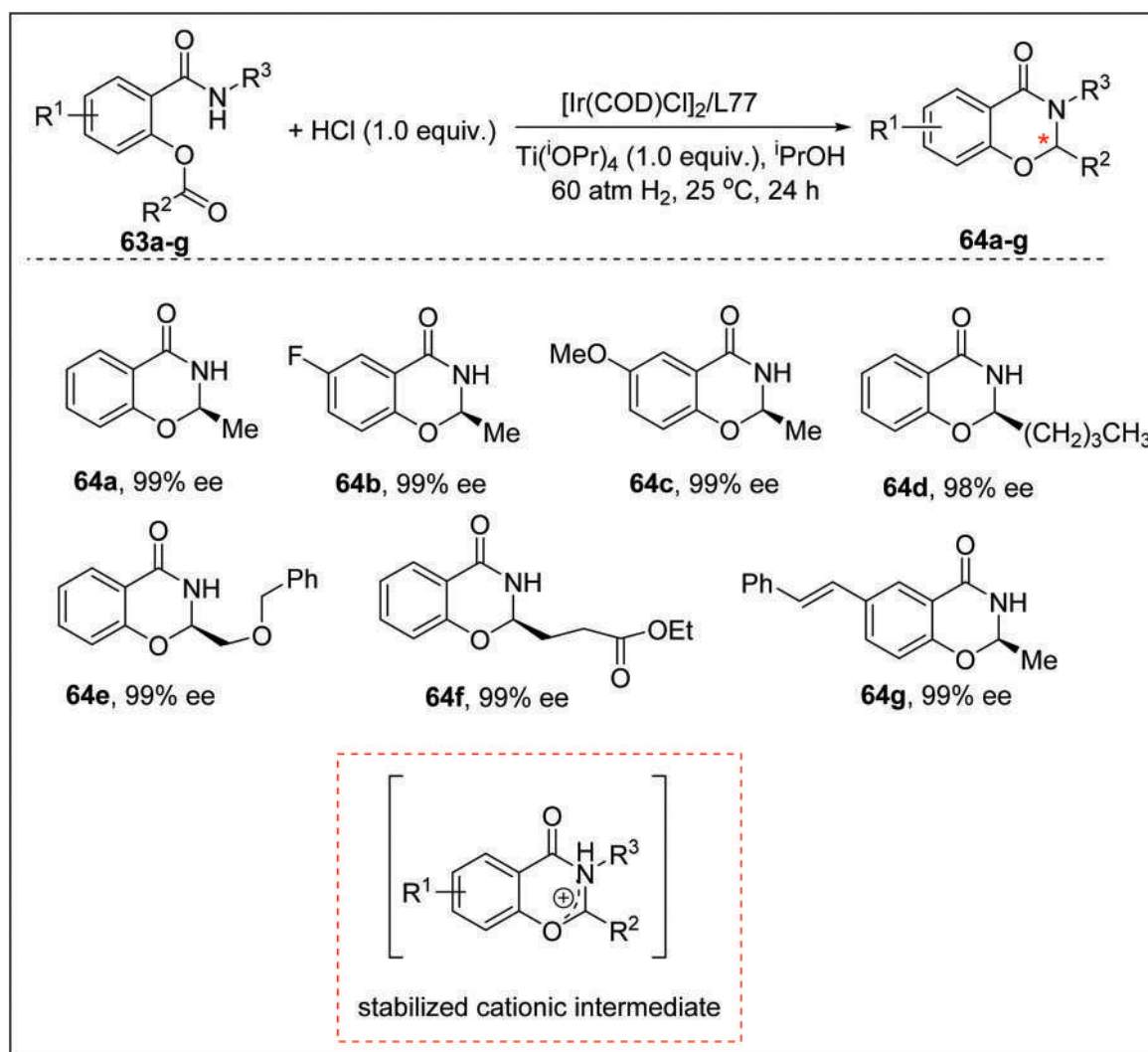
Table 13 Control experiments with different additives


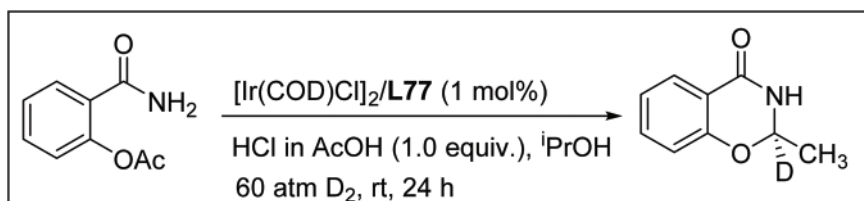
X ⁻	None	F ⁻	Cl ⁻	Br ⁻	I ⁻	HSO ₄ ⁻
Conv.	>95%	60%	>95%	<5%	<5%	>95%
ee	63%	72%	92%	60%	78%	48%

suggesting direct hydride transfer from the metal hydride complex to the cationic intermediate (Scheme 46). The structure of the reactive iridium hydride species was revealed by DFT, where the sulfur atom of the thiourea linker was coordinated to the metal, forming a chiral pocket. Steric maps were created using the percentage buried volume as a steric descriptor and utilized to discuss the enantiomeric induction in the catalytic process.

Similar to enzyme catalysis, attractive non-covalent interactions play a key role in the development of a new efficient catalytic system by reducing the degrees of freedom as well as the kinetic barrier in the transition state. With this idea, Zhang and coworkers synthesized a series of diphosphorus ligands (**L87–L91**) based on Ugi's amine motif, where the dimethylamine moiety could act as a proton acceptor which might be helpful for the non-covalent ion pair interaction with the acid substrates (Fig. 19).⁸⁸

Chiral α -substituted propanoic acids are fundamentally important building blocks that are ubiquitous in many pharmaceuticals and fine chemicals, such as in the non-steroidal anti-inflammatory and analgesic drugs naproxen and ibuprofen and in the anti-malarial drug artemisinin, are also useful to prepare the synthetically important synthon Roche ester. Although the asymmetric hydrogenation of 2-substituted acrylic acids has also been realized with chiral Ru, Rh and Ir catalysts, these methodologies are limited by the use of either high pressure or the use of an equivalent base to neutralize

**Scheme 45** Ir catalyzed AH to synthesize *N,O*-acetals.



Scheme 46 AH under the standard conditions with deuterium gas.

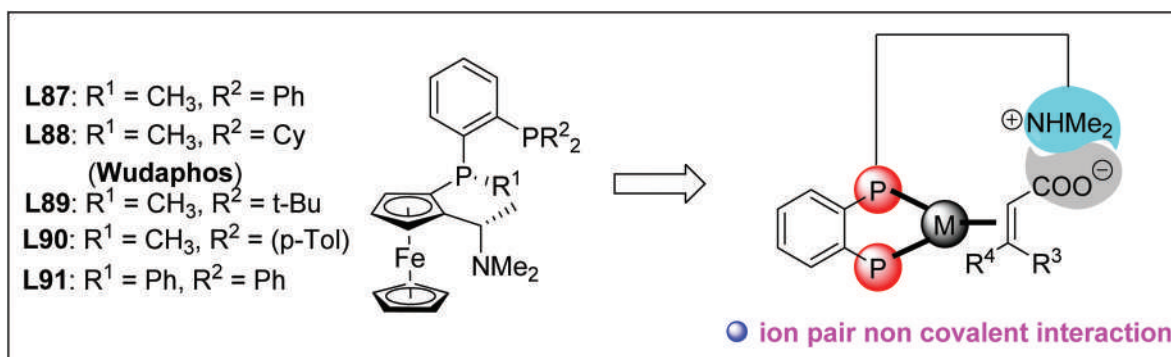
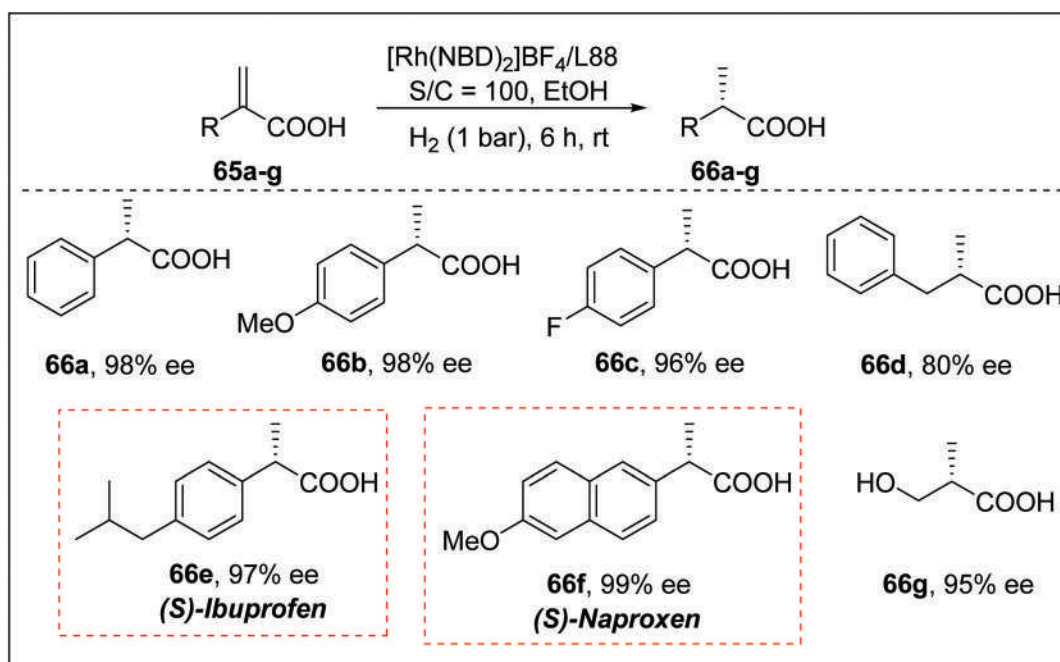


Fig. 19 Synthesis of new ferrocenyl bisphosphorus ligands.

the free acid. Zhang and coworkers successfully used the Wudaphos ligand (L88) for the asymmetric hydrogenation of a series of 2-aryl acrylic acids with EDGs as well as EWGs with excellent enantioselectivity under mild conditions (Scheme 47). The asymmetric hydrogenation of 2-substituted aryl acrylic acid was successfully carried out at catalyst loading

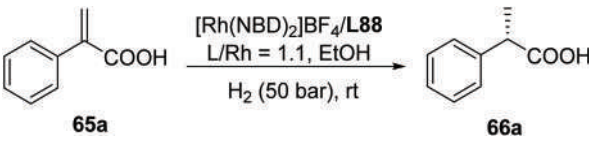
as low as 0.005 mol% under 50 bar hydrogen atmosphere with a very slight drop in the ee (Table 14).

To probe the non-covalent ion pair interaction, several control experiments were carried out. As the chain length was changed, although full conversion was obtained, enantiomeric excess dropped down dramatically (Scheme 48). Surprisingly,



Scheme 47 AH of 2-aryl acrylic acids.

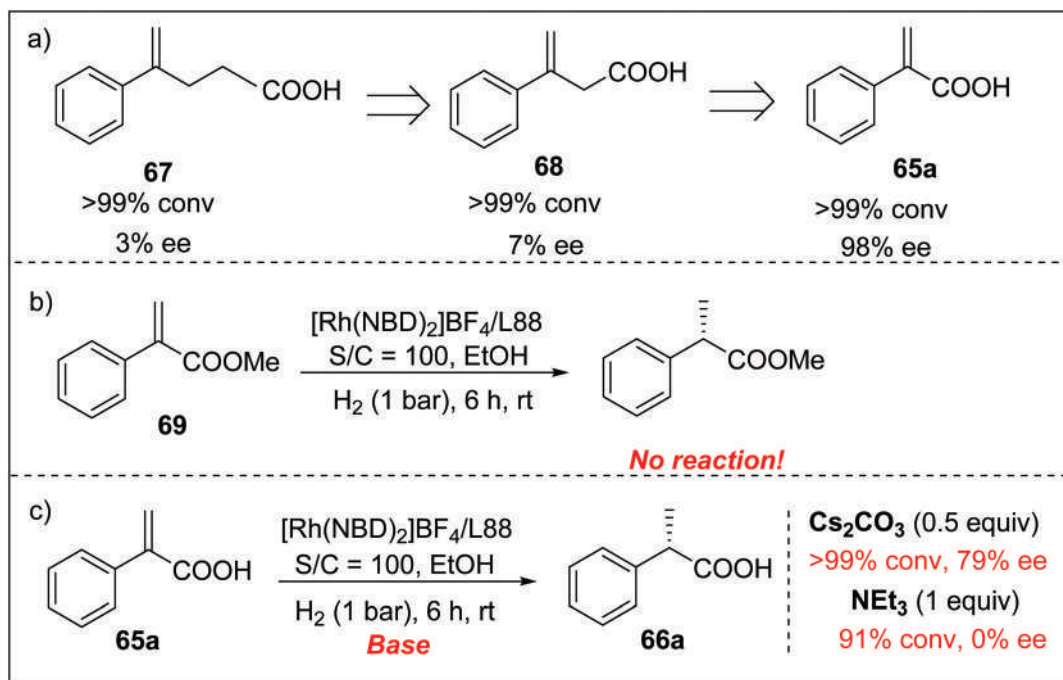
Table 14 High TON experiment with the Wudaphos ligand



Entry	S/C	Time (h)	Conv. (%)	ee (%)
1	5000	6	>99	98
2	10 000	12	>99	97
3	20 000	24	>99	96

no reaction occurred when the ester substrate was employed for the hydrogenation reaction. In the presence of one equivalent of triethyl amine, the racemic product was obtained whereas in the presence of 0.5 equivalents of Cs_2CO_3 , the ee dropped drastically. These experiments proved that ion-pair interaction was crucial for the success of this reaction.

The three-hindered quadrant ligand, trichickenfootphos (TCFP), developed by Hoge *et al.* has found wide applications in asymmetric hydrogenation. However, its highly air-sensitive oily appearance as well as the involvement of the chiral HPLC resolution during the ligand synthesis limit its practical use. To address these limitations as well as to incorporate the advantages of the non-covalent interaction, Zhang and co-



Scheme 48 Control experiments to investigate the effects of chain length and non-covalent ion pair interaction.

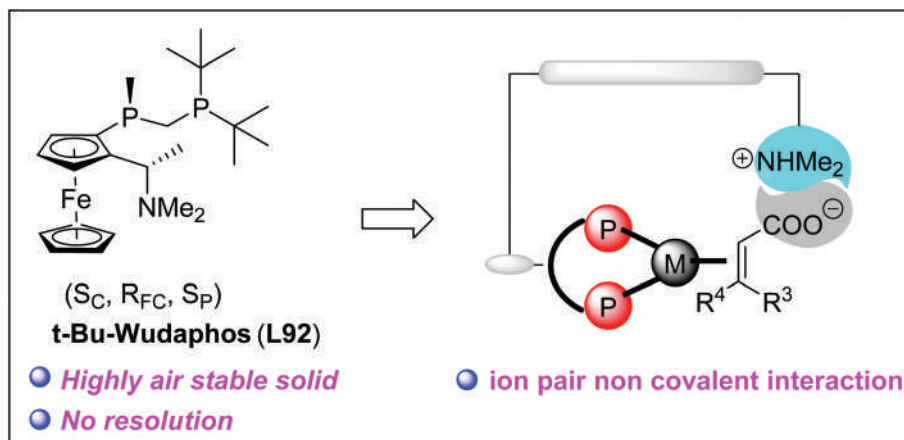
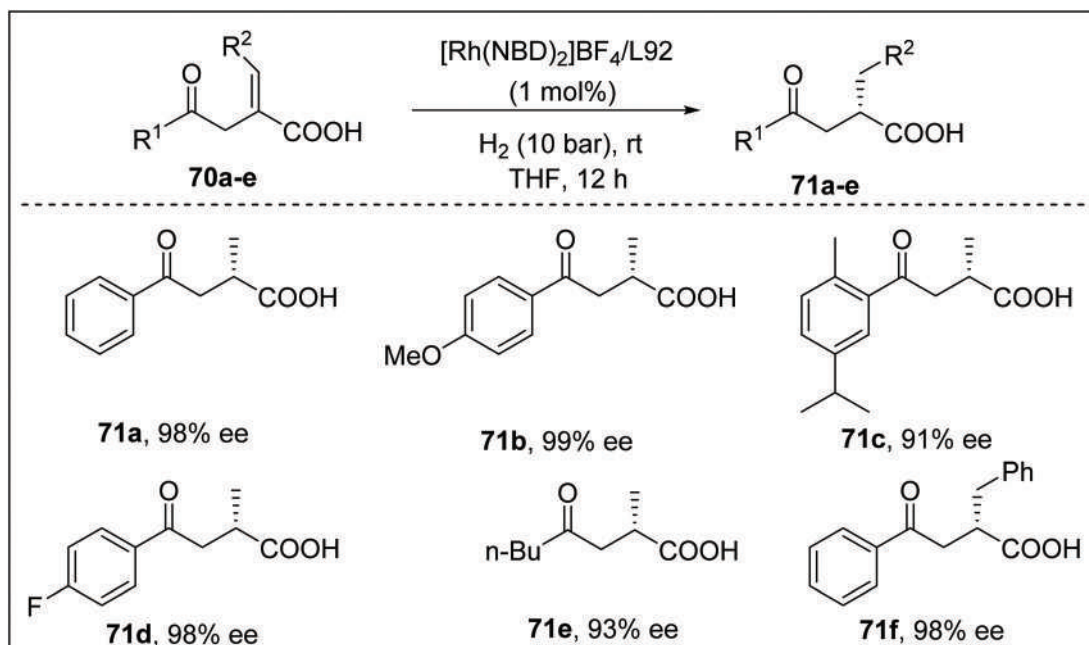


Fig. 20 Structure of t-Bu-Wudaphos.

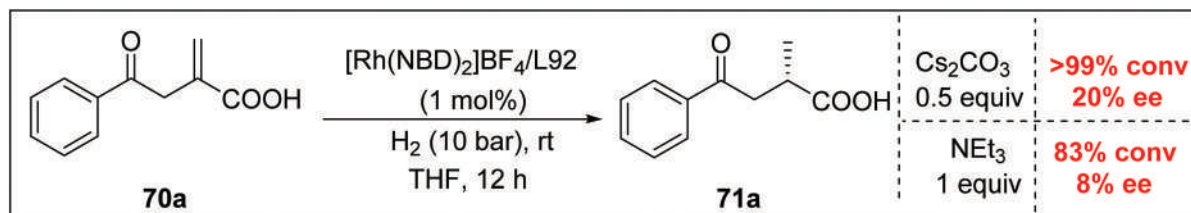
workers synthesized the *tert*-Bu-Wudaphos ligand as a yellow air-stable solid, which might exhibit excellent reactivity and enantioselectivity in the asymmetric hydrogenation of unsaturated acids through a non-covalent ion pair interaction (Fig. 20).⁸⁹

To test their hypothesis, α -methylene- γ -keto carboxylic acids were chosen as a model substrate (Scheme 49). In this regard, it is worth mentioning that the product chiral γ -keto

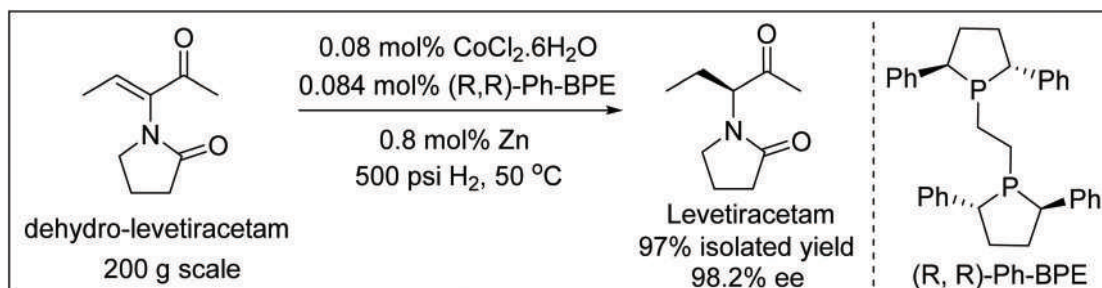
acids, obtained after the hydrogenation, are ubiquitous building blocks in natural products and pharmaceuticals. As anticipated, this class of substrates was successfully hydrogenated with the *t*Bu-Wudaphos ligand with excellent yield and enantioselectivity, tolerating many functional groups (EDGs and EWGs) under mild, base free conditions. Challenging alkyl-substituted substrates and trisubstituted unsaturated carboxylic acids were also well tolerated.



Scheme 49 AH of α -methylene- γ -keto carboxylic acids.



Scheme 50 Base effect in AH.



Scheme 51 Cobalt catalyzed AH of dehydro-levetiracetam.

The reaction can be performed on a gram scale with lower catalyst loading ($S/C = 1000$) under 50 bar H_2 pressure without reduced enantioselectivity, demonstrating its practical significance. To probe the ion-pair interaction, control experiments were conducted in the presence of a base that might be harmful for the ion-pair interaction. Indeed, in the presence of 0.5 equivalent of Cs_2CO_3 , 20% ee was obtained whereas in the presence of 1 equivalent of NEt_3 , an even further lower 8% ee was observed, suggesting the crucial role of the ion-pair interaction between the ligand and substrate to achieve a higher enantioselectivity (Scheme 50).

8. Conclusions and perspective

In asymmetric hydrogenation, a chiral pocket is created by the catalytically active metal center and ligands in the immediate vicinity, which induces enantioselectivity by restricting the movement of molecules around the coordinated substrate. The modification of this chiral pocket, either by changing the shape and size of the ligand or by changing the coordination of a metal, is the most obvious way to modify enantioselectivity. Because the accommodation of the substrate in the chiral pocket and the efficient shielding of one of its prochiral faces are conditioned by the global geometry of this environment, ligands and metal must be regarded as a whole when searching for the best chiral pocket for a certain reaction. C_2 -Symmetric ligands are usually chosen over C_1 -symmetric ligands for catalytic enantioselective transformations, although there are several notable exceptions. There are several obvious benefits of utilizing C_2 -symmetric ligands: perhaps most importantly, the reaction has fewer reaction channels, making chiral induction prediction easier. Furthermore, ligand synthesis is often easier. Often simple quadrant diagrams have been used to explain the primary factor of enantioselectivity in asymmetric hydrogenation. However, many times, it has been observed that the use of C_1 -symmetric ligands results in enantioselectivities that are comparable to or even higher than those obtained with the corresponding C_2 -symmetric analogs. These findings show that once the stereo-selection mechanism is fully known and the chiral pocket is defined, C_2 -symmetry is no longer essential, allowing for greater choice in ligand design for specific applications. As demonstrated in this review, metal complexes consisting of rationally designed C_1 -symmetric diphosphorus ligands can be utilized to produce chiral compounds with exceptional enantiomeric excess.

In addition to rational ligand design, asymmetric hydrogenations are typically performed with precious metals such as rhodium, ruthenium, and iridium. These precious metal catalysts have several advantages, such as ready availability and easy to handle synthetic precursors, broad substrate scope, high reactivity and predictable selectivity. Besides this, a well-studied mechanism, involving two-electron redox processes, has made precious metals the undisputed champion in this field. However, these precious metals (Rh, Ru, Ir, Pd, and Pt)

are the least abundant transition metals on the Earth's crust and are in the danger zone of being depleted within the next 50 years, which poses a serious threat from a sustainability perspective.^{90,91} It is due to their scarcity that the extraction of these metals is highly tedious and is thus associated with a higher cost, a higher global warming potential and a higher risk in ensuring their continuous supply.⁹² To combat these difficulties, enough attention has been paid to the development of catalysts based on 3d transition metals such as Mn, Fe, Co, Ni and Cu, mainly because of their greater earth abundance, lower cost, lower toxicity, and environmentally benign nature as compared to noble metals.^{93,94} However, base metals show unique reactivity as compared to noble metals. They exhibit variable coordination geometries, single-electron redox processes, facile ligand exchange, and multiple spin states. In addition to this, the facile change of the oxidation state as well as the presence of a radical intermediate make it difficult to carry out mechanistic studies, thus impeding catalyst development. To address these challenges, mainly three strategies have been adopted. First, the use of the redox-active ligand having energetically accessible levels. This often helps in electron flow between the metal and ligand, thus two-electron redox events are promoted as a whole.^{95,96} Second, the presence of strong-field ligands such as phosphines, carbon monoxide, and carbenes increase the crystal field stabilization energy for base metals, thus facilitate a two-electron redox event.⁹⁷ Third, low oxidation state catalysts for base metals can be generated *in situ* from metal(II/III) salts by using organometallic and non-organometallic reagents.^{98,99} Applying these strategies, significant progress has been made in the field of asymmetric hydrogenation in recent times by using base metals.^{100–115} Chirik and coworkers successfully carried out the asymmetric synthesis of Levetiracetam, a drug used to treat epilepsy, at the 200 gram scale with only 0.08 mol% cobalt catalyst loading with excellent enantioselectivity. These initial results are quite promising and show the competence of base/earth abundant metals with noble metals (Scheme 51).¹¹⁶

The above discussion clearly explains that base metals cannot be used as a direct drop-in replacement for noble metals which in turn creates a new chemical space for C_1 -symmetric diphosphorus ligands, where different arms taking care of different properties of the metal might be advantageous. Also, many existing ligands involve multiple synthetic steps and show poor scalability. This leads to increased cost which makes them impractical for use in large-scale processes, thereby enlarging the chemical space required for "rational ligand design". Finally, the presence of a versatile ligand toolbox will find application in other catalytic transformations beyond asymmetric hydrogenation.

Conflicts of interest

There are no conflicts to declare.

Acknowledgements

AS is thankful to CSIR for the fellowship (JRF and SRF). We are indebted to DST-SERB (EMR/2016/005120), CSIR-National Chemical Laboratory (HCP0011), India, and the AvH Foundation Bonn, Germany, for financial support. We thank Mr Kishor Khopade for helping us with the table of content figure.

Notes and references

- 1 T. P. Dang and H. B. Kagan, *J. Chem. Soc. D*, 1971, 481–481.
- 2 W. S. Knowles, M. J. Sabacky, B. D. Vineyard and D. J. Weinkauff, *J. Am. Chem. Soc.*, 1975, **97**, 2567–2568.
- 3 A. Miyashita, A. Yasuda, H. Takaya, K. Toriumi, T. Ito, T. Souchi and R. Noyori, *J. Am. Chem. Soc.*, 1980, **102**, 7932–7934.
- 4 R. Noyori, *Angew. Chem., Int. Ed.*, 2002, **41**, 2008–2022.
- 5 M. J. Burk, *J. Am. Chem. Soc.*, 1991, **113**, 8518–8519.
- 6 M. J. Burk, *Acc. Chem. Res.*, 2000, **33**, 363–372.
- 7 K. Inoguchi, S. Sakuraba and K. Achiwa, *Synlett*, 1992, 169–178.
- 8 T. V. RajanBabu and A. L. Casalnuovo, *J. Am. Chem. Soc.*, 1996, **118**, 6325–6326.
- 9 A. Togni, *Angew. Chem., Int. Ed. Engl.*, 1996, **35**, 1475–1477.
- 10 W. S. Knowles, *Acc. Chem. Res.*, 1983, **16**, 106–112.
- 11 W. Tang and X. Zhang, *Chem. Rev.*, 2003, **103**, 3029–3070.
- 12 W. Zhang, Y. Chi and X. Zhang, *Acc. Chem. Res.*, 2007, **40**, 1278–1290.
- 13 T. P. Yoon and E. N. Jacobsen, *Science*, 2003, **299**, 1691–1693.
- 14 A. Pfaltz and W. J. Drury, *Proc. Natl. Acad. Sci. U. S. A.*, 2004, **101**, 5723–5726.
- 15 C. S. G. Seo and R. H. Morris, *Organometallics*, 2019, **38**, 47–65.
- 16 S. Kraft, K. Ryan and R. B. Kargbo, *J. Am. Chem. Soc.*, 2017, **139**, 11630–11641.
- 17 P. Etayo and A. Vidal-Ferran, *Chem. Soc. Rev.*, 2013, **42**, 728–754.
- 18 Z. Zhang, N. A. Butt and W. Zhang, *Chem. Rev.*, 2016, **116**, 14769–14827.
- 19 T. Tewari, R. Kumar, A. C. Chandanshive and S. H. Chikkali, *Chem. Rec.*, 2021, **21**, 1182–1198.
- 20 T. Imamoto, *Chem. Rec.*, 2016, **16**, 2659–2673.
- 21 A. Cabré, A. Riera and X. Verdager, *Acc. Chem. Res.*, 2020, **53**, 676–689.
- 22 G. Xu, C. H. Senanayake and W. Tang, *Acc. Chem. Res.*, 2019, **52**, 1101–1112.
- 23 G. Hoge, H.-P. Wu, W. S. Kissel, D. A. Pflum, D. J. Greene and J. Bao, *J. Am. Chem. Soc.*, 2004, **126**, 5966–5967.
- 24 Q. Dai, W. Li and X. Zhang, *Tetrahedron*, 2008, **64**, 6943–6948.
- 25 W. Tang, A. G. Capacci, A. White, S. Ma, S. Rodriguez, B. Qu, J. Savoie, N. D. Patel, X. Wei, N. Haddad, N. Grinberg, N. K. Yee, D. Krishnamurthy and C. H. Senanayake, *Org. Lett.*, 2010, **12**, 1104–1107.
- 26 K. Huang, X. Zhang, T. J. Emge, G. Hou, B. Cao and X. Zhang, *Chem. Commun.*, 2010, **46**, 8555–8557.
- 27 Z. Zhang, Q. Hu, Y. Wang, J. Chen and W. Zhang, *Org. Lett.*, 2015, **17**, 5380–5383.
- 28 Y. Sawatsugawa, K. Tamura, N. Sano and T. Imamoto, *Org. Lett.*, 2019, **21**, 8874–8878.
- 29 Q. Hu, J. Chen, Z. Zhang, Y. Liu and W. Zhang, *Org. Lett.*, 2016, **18**, 1290–1293.
- 30 E. Drent, *Recl. Trav. Chim. Pays-Bas*, 1996, **115**, 448–449.
- 31 A. Togni, C. Breutel, A. Schnyder, F. Spindler, H. Landert and A. Tijani, *J. Am. Chem. Soc.*, 1994, **116**, 4062–4066.
- 32 H.-U. Blaser, B. Pugin, F. Spindler, E. Mejía and A. Togni, in *Privileged Chiral Ligands and Catalysts*, 2011, pp. 93–136.
- 33 H.-U. Blaser, *Adv. Synth. Catal.*, 2002, **344**, 17–31.
- 34 T. Sturm, W. Weissensteiner and F. Spindler, *Adv. Synth. Catal.*, 2003, **345**, 160–164.
- 35 T. Ireland, G. Grossheimann, C. Wieser-Jeunesse and P. Knochel, *Angew. Chem., Int. Ed.*, 1999, **38**, 3212–3215.
- 36 N. W. Boaz, S. D. Debenham, E. B. Mackenzie and S. E. Large, *Org. Lett.*, 2002, **4**, 2421–2424.
- 37 (a) K. B. Hansen, Y. Hsiao, F. Xu, N. Rivera, A. Clausen, M. Kubryk, S. Krska, T. Rosner, B. Simmons, J. Balsells, N. Ikemoto, Y. Sun, F. Spindler, C. Malan, E. J. J. Grabowski and J. D. Armstrong, *J. Am. Chem. Soc.*, 2009, **131**, 8798–8804; (b) For recent publications on sitagliptin using the C₂ symmetric ligand, see: K. V. Khopade, A. Sen, R. S. Birajdar, U. P. Paulbudhe, D. S. Kavale, P. S. Shinde, S. B. Mhaske and S. H. Chikkali, *Asian J. Org. Chem.*, 2020, **9**, 189–191.
- 38 S. Li, K. Huang, B. Cao, J. Zhang, W. Wu and X. Zhang, *Angew. Chem., Int. Ed.*, 2012, **51**, 8573–8576.
- 39 Y. Kuroki, Y. Sakamaki and K. Iseki, *Org. Lett.*, 2001, **3**, 457–459.
- 40 T. Ohkuma, M. Koizumi, H. Doucet, T. Pham, M. Kozawa, K. Murata, E. Katayama, T. Yokozawa, T. Ikariya and R. Noyori, *J. Am. Chem. Soc.*, 1998, **120**, 13529–13530.
- 41 Y. Kita, S. Hida, K. Higashihara, H. S. Jena, K. Higashida and K. Mashima, *Angew. Chem., Int. Ed.*, 2016, **55**, 8138–8138.
- 42 F. Brüning, H. Nagae, D. Käch, K. Mashima and A. Togni, *Chem. – Eur. J.*, 2019, **25**, 10818–10822.
- 43 K. Yusuke, I. Atsuhiko, H. Shoji and M. Kazushi, *Chem. Lett.*, 2014, **43**, 284–286.
- 44 M. Renom-Carrasco, P. Gajewski, L. Pignataro, J. G. de Vries, U. Piarulli, C. Gennari and L. Lefort, *Chem. – Eur. J.*, 2016, **22**, 9528–9532.
- 45 W. Li, H. Yang, R. Li, H. Lv and X. Zhang, *ACS Catal.*, 2020, **10**, 2603–2608.
- 46 B. A. Anderson, M. M. Hansen, A. R. Harkness, C. L. Henry, J. T. Vicenzi and M. J. Zmijewski, *J. Am. Chem. Soc.*, 1995, **117**, 12358–12359.
- 47 G. K. M. Verzijl, J. Hassfeld, A. H. M. de Vries and L. Lefort, *Org. Process Res. Dev.*, 2020, **24**, 255–260.

- 48 W. Chen, F. Spindler, B. Pugin and U. Nettekoven, *Angew. Chem., Int. Ed.*, 2013, **52**, 8652–8656.
- 49 S. H. Chikkali, J. I. van der Vlugt and J. N. H. Reek, *Coord. Chem. Rev.*, 2014, **262**, 1–15.
- 50 H. Fernández-Pérez, P. Etayo, A. Panossian and A. Vidal-Ferran, *Chem. Rev.*, 2011, **111**, 2119–2176.
- 51 A. Pizzano, *Chem. Rec.*, 2016, **16**, 2599–2622.
- 52 F. León, P. J. González-Liste, S. E. García-Garrido, I. Arribas, M. Rubio, V. Cadierno and A. Pizzano, *J. Org. Chem.*, 2017, **82**, 5852–5867.
- 53 H. Fernández-Pérez, M. A. Pericàs and A. Vidal-Ferran, *Adv. Synth. Catal.*, 2008, **350**, 1984–1990.
- 54 H. Fernández-Pérez, B. Balakrishna and A. Vidal-Ferran, *Eur. J. Org. Chem.*, 2018, 1525–1532.
- 55 E. L. Hazeland, A. M. Chapman, P. G. Pringle and H. A. Sparkes, *Chem. Commun.*, 2015, **51**, 10206–10209.
- 56 J. Wassenaar and J. N. H. Reek, *Org. Biomol. Chem.*, 2011, **9**, 1704–1713.
- 57 X.-S. Chen, C.-J. Hou and X.-P. Hu, *Synth. Commun.*, 2016, **46**, 917–941.
- 58 H.-Q. Du and X.-P. Hu, *Org. Lett.*, 2019, **21**, 8921–8924.
- 59 X.-H. Hu and X.-P. Hu, *Adv. Synth. Catal.*, 2019, **361**, 5063–5068.
- 60 C. Schmitz, K. Holthusen, W. Leitner and G. Franció, *Eur. J. Org. Chem.*, 2017, 4111–4116.
- 61 M. D. Wodrich and X. Hu, *Nat. Rev. Chem.*, 2018, **2**, 0099.
- 62 J. R. Khusnutdinova and D. Milstein, *Angew. Chem., Int. Ed.*, 2015, **54**, 12236–12273.
- 63 H. J. Davis and R. J. Phipps, *Chem. Sci.*, 2017, **8**, 864–877.
- 64 P. Dydio and J. N. H. Reek, *Chem. Sci.*, 2014, **5**, 2135–2145.
- 65 N. R. Mote and S. H. Chikkali, *Chem. – Asian J.*, 2018, **13**, 3623–3646.
- 66 Q. Zhao, C. Chen, J. Wen, X. Q. Dong and X. Zhang, *Acc. Chem. Res.*, 2020, **53**, 1905–1921.
- 67 Z. Du and Z. Shao, *Chem. Soc. Rev.*, 2013, **42**, 1337–1378.
- 68 A. E. Allen and D. W. C. MacMillan, *Chem. Sci.*, 2012, **3**, 633–658.
- 69 Q. Zhao, S. Li, K. Huang, R. Wang and X. Zhang, *Org. Lett.*, 2013, **15**, 4014–4017.
- 70 P. Li, M. Zhou, Q. Zhao, W. Wu, X. Hu, X.-Q. Dong and X. Zhang, *Org. Lett.*, 2016, **18**, 40–43.
- 71 X. Li, C. You, Y. Yang, Y. Yang, P. Li, G. Gu, L. W. Chung, H. Lv and X. Zhang, *Chem. Sci.*, 2018, **9**, 1919–1924.
- 72 Z. Han, R. Wang, G. Gu, X.-Q. Dong and X. Zhang, *Chem. Commun.*, 2017, **53**, 4226–4229.
- 73 T. Zhang, J. Jiang, L. Yao, H. Geng and X. Zhang, *Chem. Commun.*, 2017, **53**, 9258–9261.
- 74 Q. Lang, G. Gu, Y. Cheng, Q. Yin and X. Zhang, *ACS Catal.*, 2018, **8**, 4824–4828.
- 75 C. Yin, T. Yang, Y. Pan, J. Wen and X. Zhang, *Org. Lett.*, 2020, **22**, 920–923.
- 76 X. Yin, Y. Huang, Z. Chen, Y. Hu, L. Tao, Q. Zhao, X.-Q. Dong and X. Zhang, *Org. Lett.*, 2018, **20**, 4173–4177.
- 77 J. Shi, T. Wang, Y. Huang, X. Zhang, Y.-D. Wu and Q. Cai, *Org. Lett.*, 2014, **17**, 840–843.
- 78 Q. Zhao, J. Wen, R. Tan, K. Huang, P. Metola, R. Wang, E. V. Anslyn and X. Zhang, *Angew. Chem., Int. Ed.*, 2014, **53**, 8467–8470.
- 79 Q.-A. Chen, K. Gao, Y. Duan, Z.-S. Ye, L. Shi, Y. Yang and Y.-G. Zhou, *J. Am. Chem. Soc.*, 2012, **134**, 2442–2448.
- 80 L.-Q. Lu, Y. Li, K. Junge and M. Beller, *J. Am. Chem. Soc.*, 2015, **137**, 2763–2768.
- 81 Z. Han, G. Liu, R. Wang, X.-Q. Dong and X. Zhang, *Chem. Sci.*, 2019, **10**, 4328–4333.
- 82 L. Shi, Z.-S. Ye, L.-L. Cao, R.-N. Guo, Y. Hu and Y.-G. Zhou, *Angew. Chem., Int. Ed.*, 2012, **51**, 8286–8289.
- 83 A. Iimuro, K. Yamaji, S. Kandula, T. Nagano, Y. Kita and K. Mashima, *Angew. Chem., Int. Ed.*, 2013, **52**, 2046–2050.
- 84 J. Wen, R. Tan, S. Liu, Q. Zhao and X. Zhang, *Chem. Sci.*, 2016, **7**, 3047–3051.
- 85 P. Li, Y. Huang, X. Hu, X.-Q. Dong and X. Zhang, *Org. Lett.*, 2017, **19**, 3855–3858.
- 86 T. Yang, Y. Sun, H. Wang, Z. Lin, J. Wen and X. Zhang, *Angew. Chem.*, 2020, **59**, 6108–6114.
- 87 Y. Sun, Q. Zhao, H. Wang, T. Yang, J. Wen and X. Zhang, *Chem. – Eur. J.*, 2020, **26**, 11470–11477.
- 88 C. Chen, H. Wang, Z. Zhang, S. Jin, S. Wen, J. Ji, L. W. Chung, X.-Q. Dong and X. Zhang, *Chem. Sci.*, 2016, **7**, 6669–6673.
- 89 C. Chen, S. Wen, M. Geng, S. Jin, Z. Zhang, X.-Q. Dong and X. Zhang, *Chem. Commun.*, 2017, **53**, 9785–9788.
- 90 A. A. Yaroshevsky, *Geochem. Int.*, 2006, **44**, 48–55.
- 91 A. J. Hunt, T. J. Farmer and J. H. Clark, in *Element Recovery and Sustainability*, The Royal Society of Chemistry, 2013, pp. 1–28.
- 92 T. E. Graedel, E. M. Harper, N. T. Nassar, P. Nuss and B. K. Reck, *Proc. Natl. Acad. Sci. U. S. A.*, 2015, **112**, 4257–4262.
- 93 K. S. Egorova and V. P. Ananikov, *Angew. Chem., Int. Ed.*, 2016, **55**, 12150–12162.
- 94 K. S. Egorova and V. P. Ananikov, *Organometallics*, 2017, **36**, 4071–4090.
- 95 V. Lyaskovskyy and B. de Bruin, *ACS Catal.*, 2012, **2**, 270–279.
- 96 V. K. K. Praneeth, M. R. Ringenberg and T. R. Ward, *Angew. Chem., Int. Ed.*, 2012, **51**, 10228–10234.
- 97 P. J. Chirik, *Acc. Chem. Res.*, 2015, **48**, 1687–1695.
- 98 J. H. Docherty, J. Peng, A. P. Dominey and S. P. Thomas, *Nat. Chem.*, 2017, **9**, 595–600.
- 99 J. Peng and S. P. Thomas, *Synlett*, 2020, **31**, 1140–1146.
- 100 M. R. Friedfeld, M. Shevlin, J. M. Hoyt, S. W. Krska, M. T. Tudge and P. J. Chirik, *Science*, 2013, **342**, 1076–1080.
- 101 M. Shevlin, M. R. Friedfeld, H. Sheng, N. A. Pierson, J. M. Hoyt, L.-C. Campeau and P. J. Chirik, *J. Am. Chem. Soc.*, 2016, **138**, 3562–3569.
- 102 G. Liu, K. Tian, C. Li, C. You, X. Tan, H. Zhang, X. Zhang and X.-Q. Dong, *Org. Lett.*, 2021, **23**, 668–675.
- 103 Y. Liu, Z. Yi, X. Yang, H. Wang, C. Yin, M. Wang, X.-Q. Dong and X. Zhang, *ACS Catal.*, 2020, **10**, 11153–11161.
- 104 H. Zhong, M. Shevlin and P. J. Chirik, *J. Am. Chem. Soc.*, 2020, **142**, 5272–5281.

- 105 P. Viereck, S. Krautwald, T. P. Pabst and P. J. Chirik, *J. Am. Chem. Soc.*, 2020, **142**, 3923–3930.
- 106 X. Zhao, F. Zhang, K. Liu, X. Zhang and H. Lv, *Org. Lett.*, 2019, **21**, 8966–8969.
- 107 Z. Han, G. Liu, X. Zhang, A. Li, X.-Q. Dong and X. Zhang, *Org. Lett.*, 2019, **21**, 3923–3926.
- 108 J. F. Sonnenberg, K. Y. Wan, P. E. Sues and R. H. Morris, *ACS Catal.*, 2017, **7**, 316–326.
- 109 X. Li, C. You, S. Li, H. Lv and X. Zhang, *Org. Lett.*, 2017, **19**, 5130–5133.
- 110 J. Long, W. Gao, Y. Guan, H. Lv and X. Zhang, *Org. Lett.*, 2018, **20**, 5914–5917.
- 111 Y. Hu, Z. Zhang, J. Zhang, Y. Liu, I. D. Gridnev and W. Zhang, *Angew. Chem., Int. Ed.*, 2019, **58**, 15767–15771.
- 112 Y. Hu, J. Chen, B. Li, Z. Zhang, I. D. Gridnev and W. Zhang, *Angew. Chem.*, 2020, **59**, 5371–5375.
- 113 C. Liu, M. Wang, S. Liu, Y. Wang, Y. Peng, Y. Lan and Q. Liu, *Angew. Chem.*, 2020, **60**, 5108–5113.
- 114 S. Guo and J. Zhou, *Org. Lett.*, 2016, **18**, 5344–5347.
- 115 G. Liu, X. Zhang, H. Wang, H. Cong, X. Zhang and X.-Q. Dong, *Chem. Commun.*, 2020, **56**, 4934–4937.
- 116 M. R. Friedfeld, H. Zhong, R. T. Ruck, M. Shevlin and P. J. Chirik, *Science*, 2018, **360**, 888–893.

Erratum
